UPPER JURASSIC – LOWER CRETACEOUS CARBONATE PLATFORM MARGIN SUCCESSIONS OF THE EASTERN PONTIDES: CORRELATION OF THE PLATFORM AND BASIN, IMPLICATIONS FOR THE J/K BOUNDARY

A THESIS SUBMITTED TO
THE GRADUATE SCHOOL OF NATURAL AND APPLIED SCIENCES
OF
MIDDLE EAST TECHNICAL UNIVERSITY

BY

SERDAR GÖRKEM ATASOY

IN PARTIAL FULFILLMENT OF THE REQUIREMENTS
FOR
THE DEGREE OF DOCTOR OF PHILOSOPHY
IN
GEOLOGICAL ENGINEERING

AUGUST 2024

Approval of the thesis:

UPPER JURASSIC – LOWER CRETACEOUS CARBONATE PLATFORM MARGIN SUCCESSIONS OF THE EASTERN PONTIDES: CORRELATION OF THE PLATFORM AND BASIN, IMPLICATIONS FOR THE J/K BOUNDARY

submitted by **SERDAR GÖRKEM ATASOY** in partial fulfillment of the requirements for the degree of **Doctor of Philosophy** i**n Geological Engineering, Middle East Technical University** by,

Prof. Dr. Naci Emre Altun
Dean, **Graduate School of Natural and Applied Sciences** _____

Prof. Dr. Erdin Bozkurt
Head of the Department, **Geological Engineering** _____

Prof. Dr. Sevinç Özkan Altıner
Supervisor, **Geological Engineering, METU** _____

Examining Committee Members:

Prof. Dr. Bora Rojay
Geological Engineering, METU _____

Prof. Dr. Sevinç Özkan Altıner
Geological Engineering, METU _____

Prof. Dr. Muhittin Görmüş
Geological Engineering, Ankara University _____

Assoc. Prof. Dr. Fatma Toksoy Köksal
Geological Engineering, METU _____

Assoc. Prof. Dr. Ayşe Atakul Özdemir
Geophysical Engineering, Van Yüzüncü Yıl University _____

Date: 29.08.2024

I hereby declare that all information in this document has been obtained and presented in accordance with academic rules and ethical conduct. I also declare that, as required by these rules and conduct, I have fully cited and referenced all material and results that are not original to this work.

Name Last name : Serdar Görkem Atasoy

Signature :

ABSTRACT

UPPER JURASSIC – LOWER CRETACEOUS CARBONATE PLATFORM MARGIN SUCCESSIONS OF THE EASTERN PONTIDES: CORRELATION OF THE PLATFORM AND BASIN, IMPLICATIONS FOR THE J/K BOUNDARY

Atasoy, Serdar Görkem
Doctor of Philosophy, Geological Engineering
Supervisor: Prof. Dr. Sevinç Özkan Altıner

August 2024, 443 pages

The Upper Jurassic – Lower Cretaceous chronostratigraphic interval is characterized by unstandardized stages and includes the only Phanerozoic system boundary without a Global Boundary Stratotype Section and Point – the Jurassic/Cretaceous (J/K) boundary. Recent research has been mainly focused on deep marine continuous successions from the Tethyan region and provided important progress in calibration of pelagic bioevents. However, the correlation of these pelagic zonations with the schemes from shallow marine deposits is still obscure. Biostratigraphical data from marginal carbonates containing fossils both from the platform and basinal facies can provide the required links between these two distinct depositional environments. This kind of Upper Jurassic – Lower Cretaceous carbonates crop out in the Eastern Pontides in close association with the coeval shallow and deep marine successions.

Four stratigraphical sections were measured and logged in detail along the neritic and pelagic carbonates. Four biozones and two subzones were defined in the shallow marine successions by using benthic foraminifera and microencrusters that ranges the Kimmeridgian – Hauterivian interval. Six biozones and nine subzones were

differentiated in the slope to basin successions for the Kimmeridgian – Valanginian interval, based on calpionellids, benthic foraminifera, microencrusters and pelagic crinoids.

These successions were calibrated with a composite standard reference section through the application of the Graphic Correlation and Unitary Associations methods to overcome facies controlled biohorizons and calibrate fossil datums from unrelated phylogenies. Calibration of the Pontides Composite Reference Section with the Geological Time Scale (2020) reveals relative positions of both shallow and deep marine bioevents with respect to the Oxfordian – Hauterivian stage boundaries.

A depositional model with biofacies belts was produced for the Upper Jurassic – Lower Cretaceous successions of the Eastern Pontides.

Keywords: Upper Jurassic-Lower Cretaceous Carbonate Platforms, Calpionellid and Foraminifera Biostratigraphy, Eastern Pontides, Jurassic-Cretaceous Boundary, Quantitative Biostratigraphy

ÖZ

DOĞU PONTİD ÜST JURA - ALT KRETASE KARBONAT PLATFORM KENAR İSTİFLERİ: PLATFORM VE BASEN KORELASYONU, J/K SINIRI İÇİN ÇIKARIMLAR

Atasoy, Serdar Görkem
Doktora, Jeoloji Mühendisliği
Tez Yöneticisi: Prof. Dr. Sevinç Özkan Altıner

Ağustos 2024, 443 sayfa

Üst Jura – Alt Kretase kronostratigrafik aralığı Fanerozoyik'teki tek standardize edilmemiş Sistem sırını olan Jura/Kretase (J/K) sınırını içermektedir. Son çalışmalar, Tethys bölgesinde bulunan derin deniz çökellerine odaklanmış olup pelajik biyo-olayların kalibrasyonunda önemli ilerlemeler sağlanmıştır. Ancak, bu pelajik biyozonların sığ deniz istiflerden elde edilen biyozonlar ile korelasyonu hâlâ belirsizdir. Hem platform hem de havza fasiyeslerinden fosiller içeren platform kenarı karbonat çökellerinden elde edilecek biyostratigrafik veriler, bu iki farklı çökelme ortamı arasındaki gerekli bağlantıları sağlayabilir. Bu çeşit Üst Jura – Alt Kretase karbonatları, eş zamanlı sığ ve derin deniz istifleri ile yakın ilişki içinde Doğu Pontidlerde yüzlek vermektedir.

Neritik ve pelajik karbonatlar boyunca dört stratigrafik kesit detaylı olarak ölçülmüş ve kaydedilmiştir. Sığ deniz çökellerinde bentik foraminiferler ve mikrosarıcılar kullanılarak Kimmericiyen – Hotriviyen aralığını kapsayan dört biyozon ve iki asbiyozon tanımlanmıştır. Yamaç - havza istiflerinde, Kimmericiyen – Valanjiniyen aralığı için kalpionellidler, bentik foraminiferler, mikrosarıcılar ve pelajik krinoidler temel alınarak altı biyozon ve dokuz asbiyozon ayırt edilmiştir.

Bu istifler, fasiyes kontrollü biyo-olayların üstesinden gelmek ve farklı filojenilerden fosil verilerini kalibre etmek için Grafik Korelasyon ve Üniter Birlikler yöntemlerinin uygulanmasıyla bir kompozit standart referans kesit ile kalibre edilmiştir. Pontid Kompozit Referans Kesiti'nin Jeolojik Zaman Çizelgesi (2020) ile kalibrasyonu, hem sığ hem de derin deniz biyo-olaylarının Oksfordiyen – Hotriviyen kat sınırlarına göre konumlarını ortaya koymaktadır.

Doğu Pontidlerin Üst Jura – Alt Kretase çökelleri için biyo-fasiyes kuşaklarını içeren bir çökelme modeli üretilmiştir.

Anahtar Kelimeler: Üst Jura – Alt Kretase Karbonat Platformları, Kalpionellid ve Foraminifer Biyostratigrafisi, Doğu Pontidler, Jura – Kretase Sınırı, Kantitatif Biyostratigrafi

To my family…

ACKNOWLEDGMENTS

Foremost, I would like to express my gratitude to my advisor, Prof. Dr. Sevinç Altıner, for her guidance, support, encouragement, understanding, and endless patience throughout all the processes of this thesis. She stood by me during all the challenges I faced during the thesis period and ensured that I could overcome any setbacks by never withholding her support. She helped me channel my curiosity, which can easily expand and become scattered, into priority topics at the right time, ensuring the success of my thesis work. Thank you very much.

I would like to thank my mentor, Prof. Dr. Demir Altıner, for the support and guidance he has provided since the beginning of my master's thesis, as well as for the long conversations we had about geology and life, which have played an important role in shaping me as a person and as a geologist. I am especially grateful to him for introducing me to the critical role of paleontology in geology, for playing a significant role in helping me grasp the fundamentals of stratigraphy, for teaching me how microfossils can be used to solve geological problems, and for familiarizing me with the challenges of the geology of Turkey, all while consistently treating me as a colleague.

I am deeply grateful to the late Prof. Dr. Aral Okay, whom we recently lost, for his guidance on the Geology of the Pontides, for facilitating me to participate in fieldwork in key regions regarding geological problems, for his help in the face of difficulties during the TÜBİTAK project application process that coincided with the pandemic, and for his always positive and supportive attitude.

I would like to express my gratitude to Prof. Dr. Bora Rojay, one of the people I have had the most conversations with about geology in my department, knowing that his door is always open whenever I have a problem, even though he is not my advisor. I appreciate his long discussions and guidance on the geological problems of the Pontides, his constructive criticisms, support, and encouragement, as well as the time

he dedicated to the thesis monitoring committees and his insightful feedback. Additionally, I would like to thank him for not withholding his advice on life and career matters.

I would like to express my heartfelt thanks to Assoc. Prof. Dr. Ayşe Atakul Özdemir for her unwavering mental and scientific support, as well as for the time she dedicated to the thesis monitoring committees and her valuable feedback. I am also grateful for her always cheerful, understanding, and patient demeanor, which has guided me throughout this process.

I would like to extend my sincere gratitude to Prof. Dr. Muhittin Görmüş and Assoc. Prof. Dr. Fatma Toksoy Köksal for their valuable critiques and suggestions that contributed to the final form of the thesis.

I would like to thank Dr. Mustafa Yücel Kaya for his encouragement, for not hesitating to share his experiences, for his guidance, and for being like an older brother.

I would like to express my sincere gratitude to Sinan Yılmazer, a research assistant from Istanbul Technical University and the late Prof. Dr. Aral Okay's assistant, for providing e-signature access during a critical time in the pandemic. Without his support, the TÜBİTAK project application could not have been completed.

I would also like to extend my thanks to Zafer Kaplan for his dedicated assistance in preparing thin sections. Truly, the quality of Zafer Kaplan's thin sections is unmatched.

I would like to thank Ezgi Ünal İmer, for always encouraging me and never withholding her support.

I would like to express my thanks to Sadık Onat for his positive support throughout the thesis writing process.

I wish to express my sincere appreciation to Cumhur Özcan Kılıç and the thin section laboratory staff at the Mineral Research and Exploration Institute (MTA) for their

significant help and support in continuing thin section preparation after Zafer Kaplan's retirement from the department.

I am thankful to Dr. Robert William Scott for his assistance in supplying documents on the computer application of the graphical correlation method

I would like to express my gratitude to TÜBİTAK Scientific Programs Assistant Specialist Hacer Selin Öztürk for her continuous support in the execution of the TÜBİTAK project and for promptly resolving any issues that arose.

I extend my heartfelt thanks to İsmet Purutoğlu and the staff at Maydanoz Restaurant (Bayburt) for their hospitality, for saving my meals each day after returning from the field, and for their invaluable assistance in delivering the large number of collected samples to Ankara.

I wish to extend my thanks to Lionel Cavin from the Geneva Natural History Museum for his help in obtaining access to old paleontology articles.

I am very grateful to my roommate, Dr. Alican Aktağ, for his constant support and guidance. I’m glad we met!

I would like to thank my colleagues and friends Gamze Tanık, Dr. Hatice Kılıç Germeç, Dr. Arzu Arslan Kelam, Dr. Timur Ersöz and Batuhan Soyugür for their mental support, positive attitudes, and guidance.

I would also like to thank my family for all their support throughout my academic journey.

Finally, I would like to express my deepest gratitude to my beloved life partner, Damla Üstünel, for her patience with me during this process and for the love and support I have always felt from her. Her support and encouragement have never wavered at any stage. I’m so grateful to have you in my life.

This study was partially funded by Scientific and Technological Research Council of Turkey under grant number TÜBİTAK 120Y095 and by the Middle East

Technical University under grant numbers BAP-07-02-2014-007-404 and DKT-309-2018-3500.

TABLE OF CONTENTS

ABSTRACT v

ÖZ vii

ACKNOWLEDGMENTS x

TABLE OF CONTENTS xiv

LIST OF TABLES xvii

LIST OF FIGURES xviii

1 INTRODUCTION 1

1.1 Purpose and Scope 7

1.2 Geographical Setting 12

1.3 Materials and Methods 12

1.4 Previous Works on the Upper Jurassic – Lower Cretaceous Carbonates of the Eastern Pontides 15

1.5 Geological Setting 40

2 STRATIGRAPHY 55

2.1 Lithostratigraphy 56

2.1.1 Slope to Basin Pelagic Successions 56

2.1.2 Carbonate Platform Neritic Successions 85

2.2 Biostratigraphy 103

2.2.1 Pelagic Biozonation (Ağören & Ozansu Sections) 113

2.2.2 Neritic Biozonation (Nazlıçayır Section) 127

2.3 Quantitative Biostratigraphy 133

2.3.1 Correlation Tools versus Incomplete Rock Record and Need for Quantitative Biostratigraphy 138

2.3.2 Graphic Correlation Method (GCM) 153
2.3.3 Unitary Association Method (UAM) 167
2.3.4 Correlations by the GCM and the UAM: A comparison 175
2.3.5 Correlations of the PCP-CSRS with the Eastern Pontides Successions 191
2.3.6 Local Fossil Datums vs GCM 203
3 DISCUSSION on FOSSIL RANGES and STAGE BOUNDARIES 205
3.1 Kimmeridgian 206
3.2 Kimmeridgian/ Tithonian Boundary 207
3.3 Late Tithonian 208
3.4 Tithonian/ Berriasian Boundary 210
3.5 Berriasian/ Valanginian Boundary 214
3.6 Valanginian/ Hauterivian Boundary 215
3.7 Jurassic/ Cretaceous (J/K) Boundary 217
4 MICROFACIES ANALYSES 229
4.1 Slope to Basin Facies (Ağören and Ozansu measured sections) 232
4.2 Platform Facies (Nazlıçayır measured section) 239
5 MICROPALEONTOLOGY 247
5.1 Calpionellid Taxonomy 248
5.2 Foraminiferal Taxonomy 273
5.3 4.3. Taxonomy of *Incertae sedis*, annelids and crinoids..... 303
6 DISCUSSION AND CONCLUSION.....315
REFERENCES 325
APPENDICES

A. Measured Stratigraphic Sections 409

B. Sample-by-Sample Fossil Assemblages and Microfacies Types 410

C. Simplified Biostratigraphic Range Charts 411

D. CSRS Cycles and Section Dataiostratigraphic Range Charts 412

E. Graphic Correlations_Building the Pontides CSRS 413

F. Calibration Points, Biostratigraphic Literature,Calibrated Fossil Datums and CSRS Ranges 414

G. Unitary Association Matrix 415

H. Graphic Correlation of the sections with the Pontides CSRS 416

I. Fossil Plates 417

CURRICULUM VITAE 443

LIST OF TABLES

TABLES

Table 1.1. References of previous studies focused on the Jurassic – Cretaceous carbonate successions in the regions shown in Figure 1.4..... 11

Table 2.1 Summary of the main characteristics of the analyzed stratigraphical sections from the Western and Central Pontides for quantitative biostratigraphical analyses. 139

Table 2.2 Data points used in the absolute age calibration of the PCP-CSRS and related references. See also Appendix F. 160

LIST OF FIGURES

FIGURES

Figure 1.1. Facies distribution of important taxa along the Pontides Carbonate Platform. 4
Figure 1.2. A) Early Berriasian paleogeographical reconstruction of the western Tethyan region (modified after Stampfli & Hochard, 2009 and Cattò et al., 2018). **B)** Schematic paleogeographical map of the southern margin of Laurasia and the general facies distribution on the Pontides Carbonate Platform (PCP) for the Late Jurassic – Early Cretaceous interval. 5
Figure 1.3. Distribution of the Upper Jurassic – Lower Cretaceous carbonate successions in the Pontitdes. 6
Figure 1.4. Jurassic – Cretaceous outcrops and basement rocks of the Eastern Pontides. 9
Figure 1.5. Location map of the study areas. 12
Figure 1.6. Simplified tectonic map of the Europe and Mediterranean and Black Sea regions, showing main Phanerozoic sutures. 41
Figure 1.7. Simplified cross- and columnar-sections of the thrust sheets and allochthonous unit in the Pulur (Bayburt region). 47
Figure 1.8. Geological map of the study area and locations of the measured sections. 49
Figure 1.9. Geological map of the Ağören - Akyazı region and location of the Ağören measured section. 51
Figure 1.10. Geological map of the Ozansu (Bayburt) region and the location of the Ozansu (OA & OB) measured sections. 52
Figure 1.11. Geological map of the Nazlıçayır (Lörikas) region and the location of the Nazlıçayır measured section. 53
Figure 2.1. The bottom levels of the Ağören measure section. 57
Figure 2.2. The general view of the middle and upper levels of the Ağören measured section. 59

Figure 2.3. Ağören measured section. The legend is common to all measured sections. 61
Figure 2.4. Field photographs of the OA section. 74
Figure 2.5. Field photographs of the Hozbirikyayla Formation of the Ozansu section. 75
Figure 2.6. Ozansu-OA measured section. 77
Figure 2.7. Ozansu-OB measured section. 79
Figure 2.8. A) A general view of the studied outcrops from the Nazlıçayır Village. **B)** Google Earth image of the studied succession. 86
Figure 2.9. Field photographs from the lower levels of the Nazlıçayır section. 87
Figure 2.10. Field photographs from the middle part of the Nazlıçayır section. ... 89
Figure 2.11. Field photographs from the upper part of the Nazlıçayır section. 91
Figure 2.12. Nazlıçayır measured section. 93
Figure 2.13. Comparison chart of the pelagic biostratigraphical zonations used in this study and the proposed scheme for the Eastern Pontides pelagic Ağören and Ozansu successions. 104
Figure 2.14. Comparison chart of the neritic biostratigraphical zonations used in this study and the proposed scheme for the Eastern Pontides neritic Nazlıçayır successions. 105
Figure 2.15. Fossil distribution of the Ağören measured section. 115
Figure 2.16. Fossil distribution of the OA measured section. 117
Figure 2.17. Fossil distribution of the OB measured section. 119
Figure 2.18. Fossil distribution of the Nazlıçayır measured section (below the unconformity). 128
Figure 2.19. Fossil distribution of the Nazlıçayır measured section (above the unconformity. 129
Figure 2.20. A) Schematic paleogeographical map of the southern margin of Laurasia for the Late Jurassic–Early Cretaceous interval and the approximate locations of the analyzed successions. **B)** Distribution of the Upper Jurassic–Lower Cretaceous Carbonates in the Pontides. **C)** Clustering of the analyzed stratigraphic

sections based on presence/absence fossil data to provide simple visualization of the paleoenvironments of the measured sections in the dataset. 134
Figure 2.21. Relationship between the rock record and time. 142
Figure 2.22. Pitfalls commonly present in marginal carbonate biostratigraphy and importance of synthesizing large data from varieties of depositional environments. 147
Figure 2.23. Summary chart for the transition from raw biostratigraphic data to chronostratigraphy by application of quantitative biostratigraphic methods. 149
Figure 2.24. A comparison chart for bizonation types. 150
Figure 2.25. A graphic correlation sample from the first correlation round; KEL vs "evolving" CSRS. 155
Figure 2.26. Calibration of the PCP-CSRS (y-axis) with the GTS 2020 datums (x-axis). 161
Figure 2.27. The Pontides CSRS with absolute age calibrations. 165
Figure 2.28. A) Illustration of the "maximal horizon" concept for a section. **B)** A cyclic superpositional contradiction example. **C)** An example of superpositional contradiction between two cliques. 168
Figure 2.29. The G* graph from the UAM. 170
Figure 2.30. Steps in building unitary association zones (UAZs) from the unitary associations (UAs). 173
Figure 2.31. Correlation of the AÇ section with the PCP-CSRS. 177
Figure 2.32. Correlation of the STG section with the PCP-CSRS. 181
Figure 2.33. Correlation of the Alçılar section with the PCP-CSRS. 185
Figure 2.34. Correlation of the measured sections. 187
Figure 2.35. Correlation of the Ağören section with the PCP-CSRS. Purple bold line is the LOC. 193
Figure 2.36. Correlation of the Ozansu (OA and OB) sections with the PCP-CSRS. 195
Figure 2.37. Correlation of the Nazlıçayır section with the PCP-CSRS. 197

Figure 2.38. Correlation of the measured sections from the Eastern Pontides with the Western and Central Pontides successions and the PCP-CSRS. 201
Figure 2.39. Chronostratigraphic range chart of the analyzed stratigraphic sections from the GCM. 204
Figure 3.1. Late Jurassic – Early Cretaceous species richness and turnover rates from the Pontides Carbonate Platform. 221
Figure 3.2. Benthonic foraminiferal provinces and calpionellid subzone localities. 225
Figure 4.1. Original carbonate rock classification by Dunham (1962) and the expanded version by Embry and Klovan (1971). 230
Figure 4.2. The facies zones (FZ) of the rimmed carbonate platform model and the distribution of the standard microfacies types (SMF). 231
Figure 4.3. Microfacies from the lower levels of the Ağören section (Kelkit Formation). 233
Figure 4.4. Microfacies from the middle (Kelkit Formation, A-C) and upper (Hozbirikyayla Formation, D-L) levels of the Ağören section. The scale for the A is 1 mm and for the rest is 400µm. **A)** Sandy, lithoclastic floatstone (MF4/SMF5/FZ4). Sample A81. **B, C)** Litharenite with plane. 234
Figure 4.5. Microfacies photographs from the Ozansu sections. 236
Figure 4.6. Microfacies photographs from the OB section. 237
Figure 4.7. A slope depositional environment facies association example from the OB section. 238
Figure 4.8. Main microfacies types observed in the Nazlıçayır measured section. Berdiga Formation. 241
Figure 4.9. Main microfacies types observed in the Nazlıçayır measured section. Berdiga Formation. 242
Figure 4.10. A schematic depositional model for the studied region. 244
Figure 4.11. Microfacies distribution of the southern platform margin and slope environments of the Eastern Pontides Carbonate Platform during Kimmeridgian – Valanginian interval. 245

Figure 6.1. Summary of the important benthonic and planktonic fossil ranges in the PCP-CSRS. 319

CHAPTER 1

INTRODUCTION

The primary distinction that sets geology apart from other scientific disciplines (except history and evolutionary biology) is the fundamental and unavoidable interference of the time concept. Since Georges Cuvier's realization in 1796 that fossils have chronological significance (as he attempted to explain the “exclusive” presence of mammoth remains by a catastrophic disappearance of a world prior to humans) and William Smith's first use of fossils in 1815 to map strata according to their stratigraphic order, the fossil record has been recognized as the main tool for relative age assignment and correlation and consequently has become the basis of the construction of the Phanerozoic Geologic Time Scale. Biostratigraphical concepts, like many other concepts of stratigraphy, were developed on the Jurassic strata of western Europe and Britain (e.g., Callomon, 1995; Miall, 2004; Page, 2017; Hesselbo et al., 2020 for overview). Introduction of the stage concept and division of the Jurassic and Cretaceous strata accordingly by d’Orbigny (1840, 1842-1851, 1852) was followed by the development of the (bio-)zone concept by Oppel (1856-1858) who further subdivided those Jurassic strata (and stages) into ammonite zones. Historically, stages are packages of biozones (Arkell, 1956; Teichert, 1958; Monty, 1968; Murphy, 1977; Birkelund et al., 1984; Calloman, 1995, 2001; Remane, 2003; Miall, 2004; Page, 2017). Despite this early start and long history of study, the Upper Jurassic and, along with the age-old question of "where does the Jurassic end?", the Lower Cretaceous chronostratigraphy are still not standardized. This interval also includes the only system boundary without a Global Boundary Stratotype Section and Point (GSSP) in the Phanerozoic; the Jurassic – Cretaceous (J/K) boundary (e.g.,

Birkelund et al., 1984; Remane, 1991; Wimbledon, 1997; Énay, 2020; Wimbledon et al., 2020a; Granier et al., 2020a, 2020b; Hesselbo et al., 2020).

In accordance with the widely accepted catastrophist view of the 19th century, without being aware, stage (and zonal) boundaries were placed at unconformities within shallow marine, generally condensed successions where stratigraphical breaks create apparent faunal turnovers and "natural" boundaries (e.g., Remane, 2003; Cope, 2008). Shuffling of stage nomenclatures (e.g., Arkell, in 1956, listed 126 stage names that had been proposed only for Jurassic until his work), common provincialism among the traditional prime marker group of ammonites of this interval (e.g., Zeiss, 2003; Page, 2008), hiatuses present in the original "stratotypes" (e.g., Hesselbo et al., 2020) and other motivations, i.e., geopolitics (e.g., see Sarjeant & Wimbledon, 2000, and Granier, 2020a, for overview), have resulted in the erection of local chronostratigraphic schemes, correlation problems among paleogeographic realms and unstandardized chronostratigraphy.

Recent focus has shifted toward "complete" deep marine Tethyan successions. Calpionellids, with their rapid evolving lineages, have become an important group for the upper (upper case initial letters are used only for the ratified stages) Tithonian – Hauterivian interval with widely correlatable (over both margins of the Tethys from Himalaya to Mexico; see Wimbledon et al., 2020a, and the extensive list of references therein; and Atasoy et al. 2022) and stable biozonations (see Lakova & Petrova, 2013, and Benzaggagh, 2020, for a detailed overview). Calibration of calpionellid zones with other calcareous pelagic groups (e.g., calcareous nannofossils, dinoflagellates) is more or less successful (e.g., Özkan,1993; Lakova et al., 1999, 2017; Casellato, 2010; Benzaggagh et al., 2015a; Bakhmutov et al., 2018; Elbra et al., 2018; Grabowski, et al., 2019; Svobodová et al., 2019; Casellato & Erba, 2021; Wimbledon et al., 2020b; Michalík et al., 2021), although problems still exist in calibration with more endemic ammonites (e.g., Le Hégarat & Remane, 1968; Hoedemaeker et al., 1993; Bulot et al., 1996; Énay, 1997; Zeiss, 2003; Houša et al., 2007; Page, 2008; Frau et al., 2016; Reboulet et al., 2018) and radiolarians (e.g., Baumgartner et al., 1995; Mekik et al., 1997; Ślączka et al. 2018) and

sporadically occurring early planktonic foraminifers (e.g., Banner & Desai, 1988; Hudson et al., 2009; Gradstein et al., 2017, 2018, 2021). These developments have mostly led to proposals of stage boundary definitions based on pelagic bioevents and deep open marine sections (especially for the Lower Cretaceous).

Although there are important progress and refinements among the pelagic biozonations, relative positions of the shallow marine bioevents with respect to these pelagic schemes are still obscure, hindering common reference system for discussions about geological and biological events. At this stage of the problem, shelf-margin dwelling organisms have been proved critical (e.g., Altıner, 1991; Peybernès, 1998; Celestino et al., 2017; Atasoy et al., 2018; Bakhmutov et al., 2018; Atasoy et al., 2022). They have the property of being readily transportable down to the slope and into the inner platform facies or better still having wider range of habitat covering the upper slope to back-margin environments (Figure 1.1). This provides intercalation of biofacies and shedding of fossils that can near-synchronously intercalate into these two apart depositional environments. Fossil rich platform margin and slope carbonates in close association with their contemporaneous shallow marine successions are good targets for research on these key relationships.

The Late Jurassic – Early Cretaceous interval is characterized by wide carbonate platforms flanking the margins of the Tethys Ocean (e.g., Bernoulli & Jenkyns, 1974; Kiessling et al., 2003; Basilone & Sulli, 2016; Barrier et al., 2018). Turkey mainland has rock records of two main Jurassic – Cretaceous carbonate platforms developed on the opposite margins of the Tethys; namely the Tauride carbonate platform to the south (e.g., Özgül, 1976; Monod, 1977; Altiner et al., 1999; Altiner et al., 2000; Yılmaz & Altiner, 2001) and the Pontides Carbonate Platform (PCP) to the north (e.g., Saner, 1980; Görür et. al., 1983; Okay et. al.., 1990; Altıner et. al.., 1991; Koçyiğit & Altıner, 2002; Kalvoda & Bábek, 2010; Okay & Nikishin, 2015; Barrier et al., 2018; van Hinsbergen et al., 2020; Fig. 1.2) which were today separated along the Tethyan İzmir-Ankara-Erzincan (İAE) suture (Ketin, 1966; Şengör & Yılmaz,

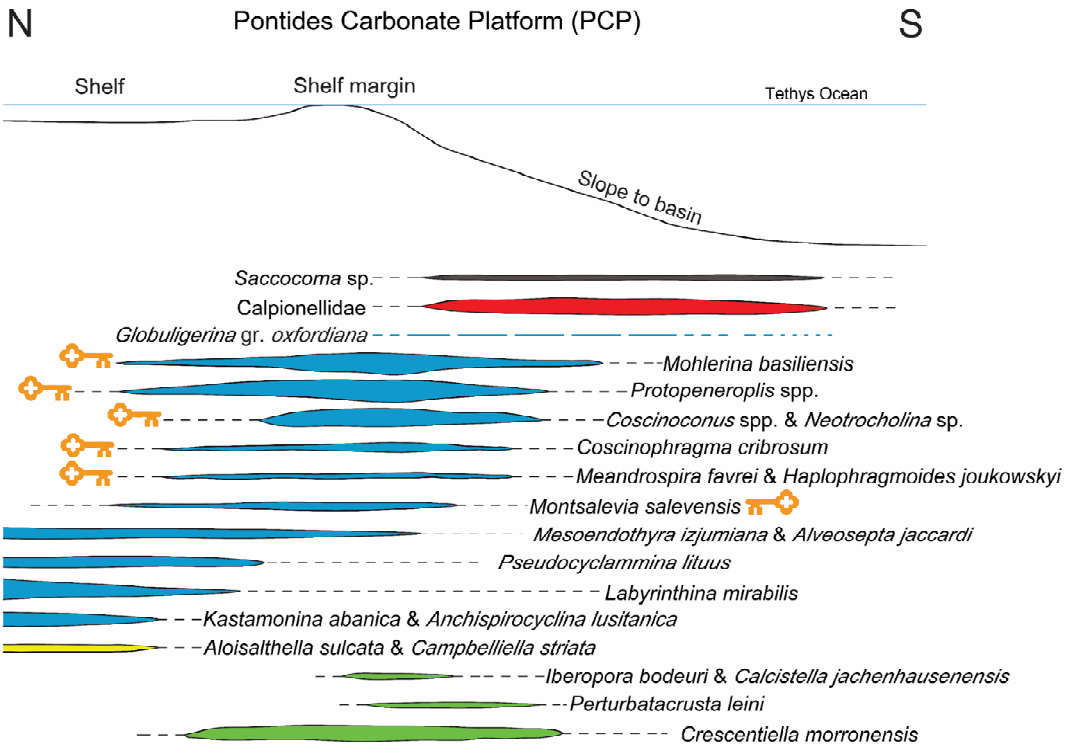

Figure 1.1. Facies distribution of important taxa along the Pontides Carbonate Platform. The golden "key" symbol indicates the critical taxa having wider range of occurrence, providing the link for calibration of the shallow and deep marine bioevents (modified from Atasoy et al., 2022). Brown: pelagic crinoids; red: calpionellids; blue: foraminifers; yellow: algae; green: microencrusters.

1981; Okay & Tüysüz, 1999). The Upper Jurassic – Lower Cretaceous carbonate rocks of this PCP form the most distinctive and laterally traceable succession in the Pontides (Fig. 1.3). The Upper Jurassic – Lower Cretaceous marginal successions seem to be missing in the Western and Central Pontides (Fig. 1.3; Altiner et al., 1991; Okay & Tüysüz, 1999; Okay & Altiner, 2016; Okay et al. 2018). The Kimmeridgian – Hauterivian carbonate outcrops of the Western Sakarya Zone in areas very close to the İAE suture (e.g., Bursa region) still display shallow marine facies (e.g., Altiner et al., 1991; Okay & Tüysüz, 1999; Fig. 1.3). Similarly, Tithonian – Berriasian carbonate rocks cropping out at the core of the Haymana anticline also have shallow marine characteristics (Fig. 1.3; Okay & Altiner, 2016). Only the intervening Mudurnu trough succession between the Central Sakarya Basin and Gerede shows

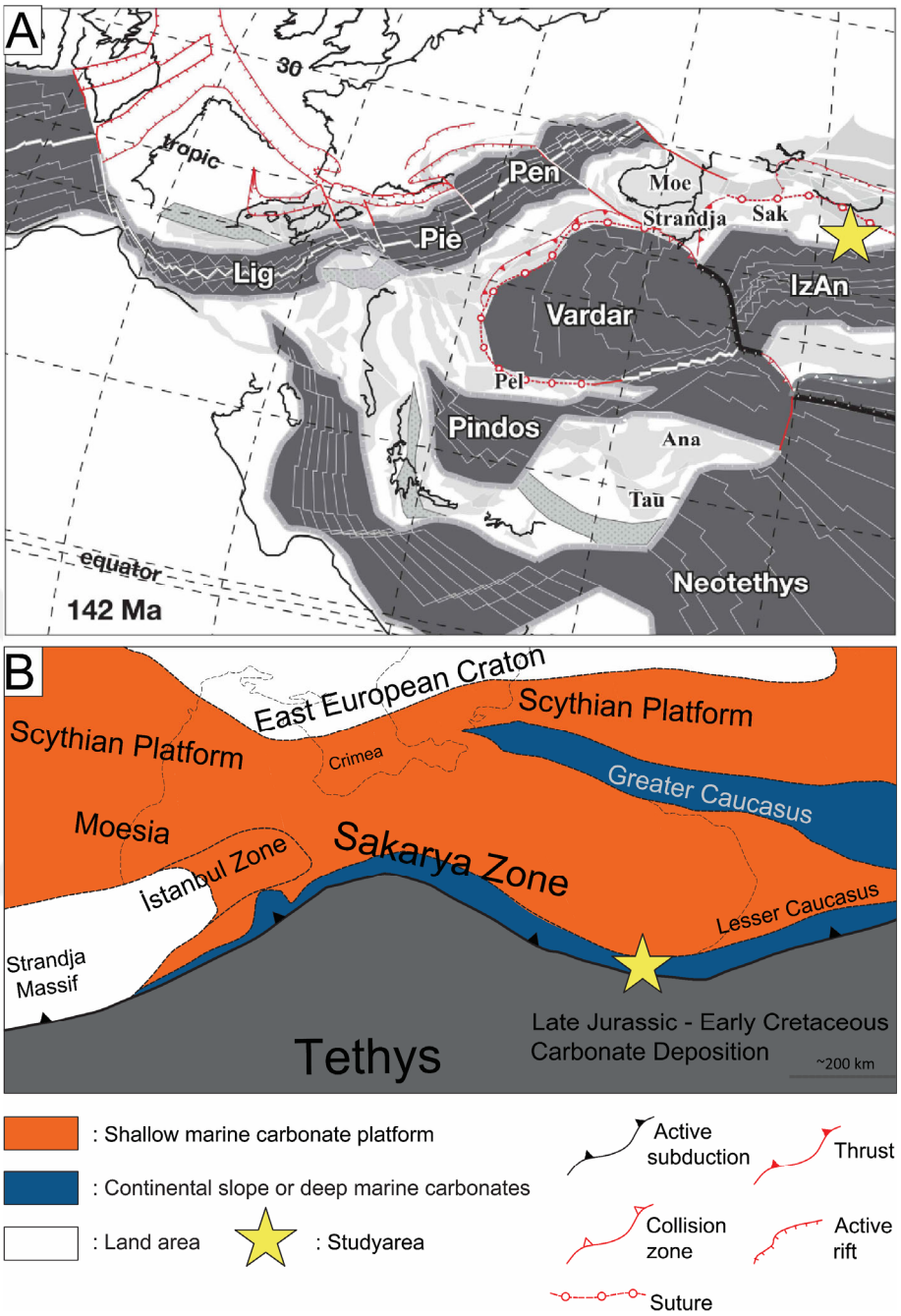

Figure 1.2. A) Early Berriasian paleogeographical reconstruction of the western Tethyan region (modified after Stampfli & Hochard, 2009 and Cattò et al., 2018). Ana: Anatolides; IzAn: İzmir–Ankara Ocean; Lig: Ligurian Ocean; Moe: Moesia: Pen: Penninic; Pie: Piedmont; Sak: Sakarya; Tau: Taurus. Gray color indicates elevated areas (terrestrial or erosional regions). **B)** Schematic paleogeographical map of the southern margin of Laurasia and the general facies distribution on the Pontides Carbonate Platform (PCP) for the Late Jurassic – Early Cretaceous interval (modified from Okay et al., 2013; Nikishin et al., 2015). The yellow star, common to both figures, roughly indicates the paleogeographic location of the study area.

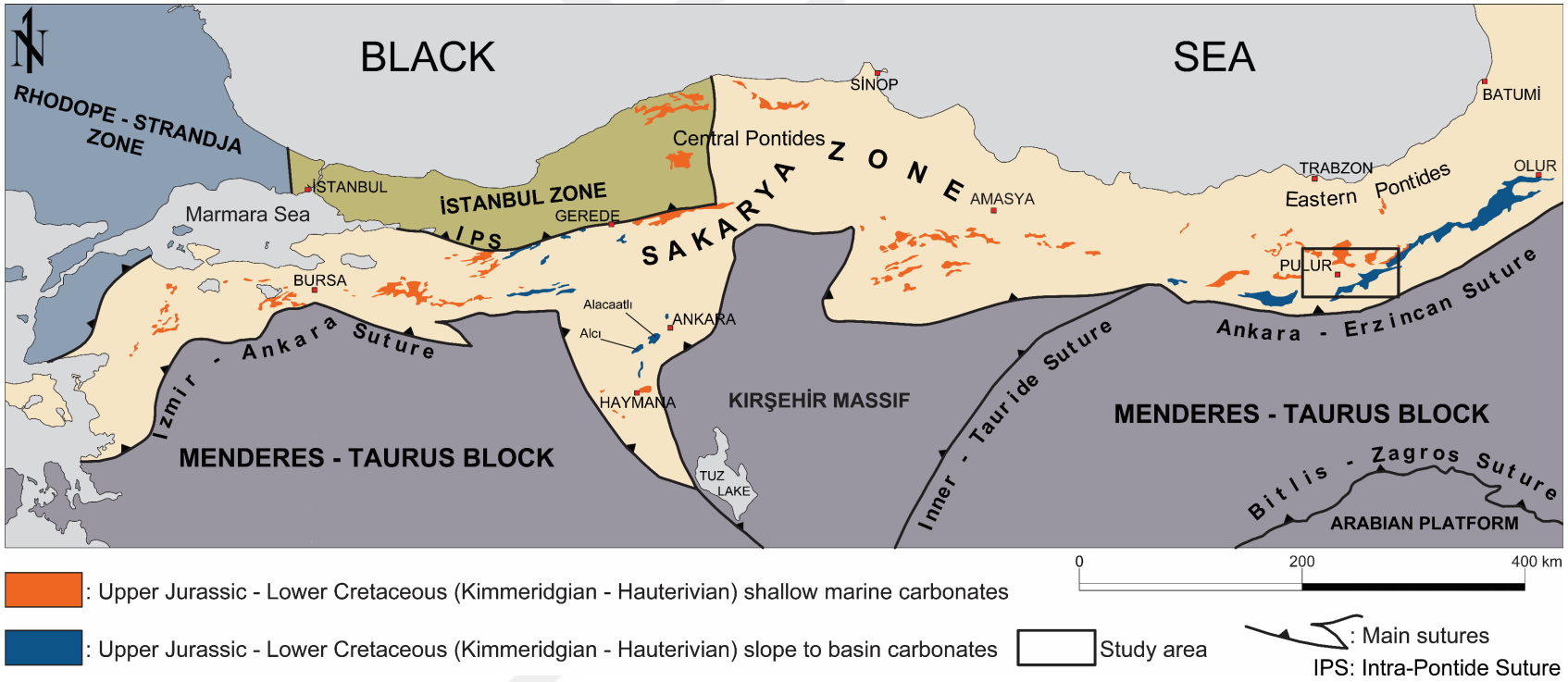

Figure 1.3. Distribution of the Upper Jurassic – Lower Cretaceous carbonate successions in the Pontitdes (modified from Okay & Altiner, 2016).

in-situ Upper Jurassic – Lower Cretaceous carbonate margin – slope to basin deposits (Fig., 1.3; Fourquin, 1975; Toker, 1976; Saner, 1980; Yılmaz et al., 1981; Önal et al., 1988; Altiner et al., 1991; Yılmaz et al., 2016). However, they represent a kind of embayment deposits of the Tethys between two paleohighs (the Biga-Bursa-Bilecik Carbonate Platform and the Aktaş-Sekinindoruk High; see Altiner et al., 1991) for the Kimmeridgian – Hauterivian interval rather than south-facing platform margin carbonates. Further, allochthonous blocks belonging to the marginal deposits of this Upper Jurassic – Lower Cretaceous PCP crop out in an olistostrome belt that extends from the northeast of Haymana through the Alçı – Alacaatlı line to the north of Ankara (Fig. 1.3; Koçyiğit, 1991; Rojay & Süzen, 1997; Okay et al., 2019). Similar limestone blocks and tectonic slices of carbonate deposits within imbricated zones crop out along the İAE suture belt (e.g., Bergougnan, 1987; Koçyiğit et al., 1988; Koçyiğit, 1991; Okay & Tüysüz, 1999; Rojay, 2013; Atasoy et al., 2018).

On the other hand, in the Eastern Pontides, the Upper Jurassic – Lower Cretaceous shallow marine carbonates crop out in close proximity to their coeval deep marine equivalents (Fig. 1.3 & 1.4). These neritic carbonates pass southward into pelagic limestones, indicating the presence of a south-facing platform margin (Fig. 1.3 & 1.4; Görür, 1988; Burşuk, 1992; Robinson et al., 1995; Okay et al., 1997; Timur, 2000; Ustaömer & Robertson, 2010). Both types of carbonates crop out in a wide region just to the north of the İAE suture zone as north-vergent thrust sheets (e.g., Bergougnan, 1976; Okay et al., 1997; Ustaömer & Robertson, 2010). This close relationship of these two types of Upper Jurassic – Lower Cretaceous carbonates in the Eastern Pontides provide promising geological configuration to study these successions in terms of the Upper Jurassic – Lower Cretaceous chronostratigraphical problems. This is the reason the research area is located in this region.

1.1 Purpose and Scope

The aim and extent of this study, which addresses the Upper Jurassic – Lower Cretaceous chronostratigraphic problems, can be listed as follows:

- Detailed stratigraphical analysis of the Upper Jurassic – Lower Cretaceous pelagic and neritic successions in the Gümüşhane – Bayburt region,
- Detailed documentation of microfossil assemblages,
- Construction of a composite biozonation scheme based on variety of fossil groups (e.g., calpionellids, foraminifers, calcareous algae, microencrusters and pelagic crinoids),
- Correlation of the Upper Jurassic – Lower Cretaceous neritic and pelagic successions,
- Calibration of the basinal and shallow marine Late Jurassic – Early Cretaceous bioevents through the application of quantitative biostratigraphical methods,
- Determination of the possible shallow marine benthic biohorizons for the delineation of the Upper Jurassic – Lower Cretaceous stages in neritic deposits and their relative position with respect to well-established pelagic biozonation schemes,
- Testing the proposed two alternative criteria and suggestions for the determination of the J/K boundary and evaluating the utility and practicality of both levels (the base of the Berriasian, e.g., Wimbledon, 2017; or the base of the Valanginian, e.g., Granier, 2019),
- Contribution to solution of the unstandardized and problematic Upper Jurassic – Lower Cretaceous chronostratigraphy problems,
- Detailed microfacies analysis and determination of depositional environments,
- Documentation of the Eastern Pontides Carbonate Platform evolution during the Late Jurassic – Early Cretaceous interval,
- Production of depositional model for the Upper Jurassic – Lower Cretaceous Eastern Pontides carbonates.

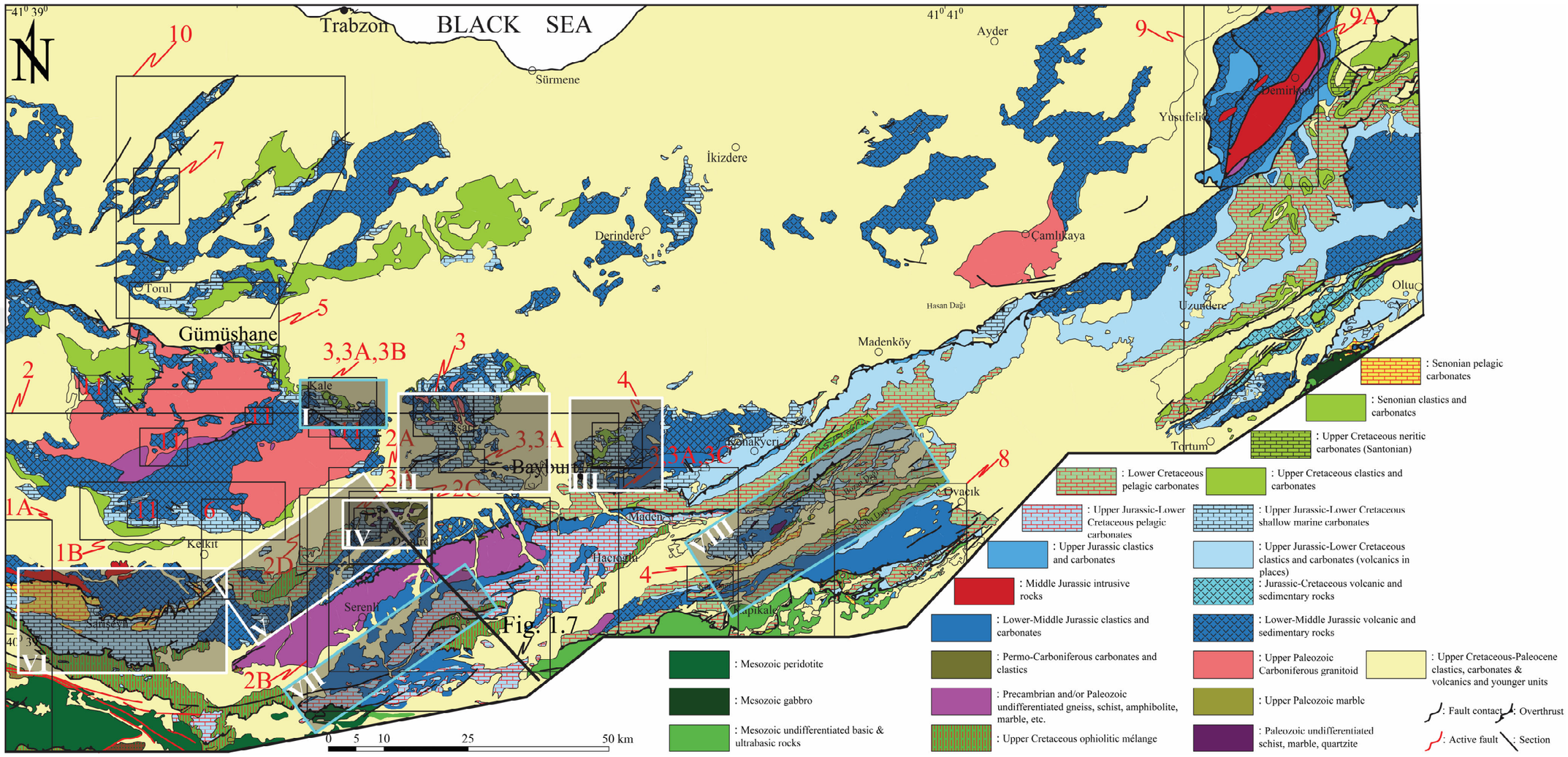

Figure 1.4. Jurassic – Cretaceous outcrops and basement rocks of the Eastern Pontides (simplified from MTA, 2002; 2015). The thin black boxes with red Arabic numerals show the locations of the previous studies on the J-K carbonates (see Table 1.1 for references). The shaded boxes with Roman numerals are the target study areas. I: Gümüşhane (Nazlıçayır); II: Bayburt (Balkaynak); III: Bayburt (Uluçayır); IV: Cebre Relative Autochthon (Okay et al., 1997); V: Hamurkesen thrust sheet and the outcrops to the east of Demirözü (Okay et al., 1997); VI: Çimendağı thrust sheet (Bergougnan, 1976; 1987); VII: Aşutka thrust sheet (Okay et al., 1997); VIII: İmalıdağ thrust sheet and the Kapıkale – Ovacık line (Burşuk, 1992; Okay et al., 1997; Timur, 2000). Upper Jurassic – Lower Cretaceous carbonate successions that provide well-exposed and continuous outcrops suitable for the study's purpose have only been observed in the regions I, VII and VIII (boxes with cyan border). A cross section along the thick black line is provided in the Figure 1.7.

Table 1.1. References of previous studies focused on the Jurassic – Cretaceous carbonate successions in the regions shown in Figure 1.4.

1A) Siran-Refahiye	**5) Gümüşhane-Torul**
Nebert (1964)	Yılmaz (1997), Yılmaz & Kandemir (2006)
1B) Kelkit (north)	**6) Southern Regions of Kelkit**
Wedding (1963)	Yılmaz (1992)
1C) Giresun-Alucra-Ağvanis-Refahiye	**6A) Gümüşhane**
Nerbert (1961), Pelin (1977)	Özyurt et al. 2018
Okay (1983), Rojay (1985)	**7) Başoba and Ayralaksa Plateaus (Trabzon)**
2) Alucra-Gümüşhane-Bayburt and Southern Regions	Taslı et al. (1999), Kırmacı et al. (2018)
Bergougnan (1976, 1987)	Özyurt et al. (2022), Özyurt et al. (2024)
2A) Bayburt and Southern Regions	**8) Ovacık-Aşkale (Erzurum)**
Ketin (1951)	Timur (1997, 2000)
2B) Bayburt and Southern Regions	**9) Oltu-Olur-Şenkaya-Narman-Tortum-Uzundere-Yusufeli**
Okay et al. (1997)	Dokuz (2000)
2C) Southern Regions of Bayburt-Demirözü Line	Konak et al. (2001, 2009)
Akdeniz (1988), Okay & Leven (1996)	**9A) Artvin-Demirkent**
Çapkınoğlu (2003)	Ustaömer & Robertson (2010)
2D) Demirözü (Bayburt)-Köse (Kelkit)	**9B) Olur**
Ağar (1977)	Yılmaz (1985), Tunç (1992)
3) Kale (Gümüşhane) - Bayburt	Bozkuş (1992)
Taslı (1990)	**10) Torul-Maçka (Trabzon)**
3A) Alucra-Gümüşhane-Bayburt	Şen (2007)
Kırmacı (1992)	**11) Gümüşhane-Kelkit**
3B) Kale (Gümüşhane)	Kandemir & Yılmaz (2009)
Taslı (1993), Kırmacı et al. (1996)	**Eastern Pontides (GENERAL)**
Bucur et al. (2000), Bektaş et al. (2001)	Akın (1978), Şengör et al. (1980)
Eren & Taslı, 2002, Bucur et al. (2004)	Bergougnan & Fourquin (1982)
Koch et al. (2008), Vincent et al. (2018)	Bergougnan (1987)
Schlagintweit et al. (2019)	Görür et al. (1983), Görür (1988)
Granier (2020b), Özyurt et al. (2023)	Yılmaz (1989), Robinson et al. (1995)
Özyurt & Kırmacı (2024)	Yılmaz et al. (1997)
3C) Bayburt (Uluçayır)	Okay & Şahintürk (1997)
Kırmacı (2000)	Yılmaz et al. (2000)
4) Bayburt-Kop Dağı	Koçyiğit & Altıner (2002)
Burşuk (1992)	Okay & Nikishin (2015)

1.2 Geographical Setting

The study area is composed of 3 main locations (Fig. 1.5) located on different tectonic units broadly representing different depositional environments on the eastern part of the PCP (see Chapter 1.5 for details). Studied regions cover 1:25k-scaled Trabzon quadrangles of H45d2 (location 1), H44d4 (location 2) and H43a3 (location 3). Study area 1 is located just to the south of the Ağören village at the Bayburt – Erzurum border. Location 2 is at the northern flank of the Otlukbeli Mountains to the south of the Ozansu village. Location 3 is situated at the Nazlıçayır (Lörikas) village to the southeast of Gümüşhane.

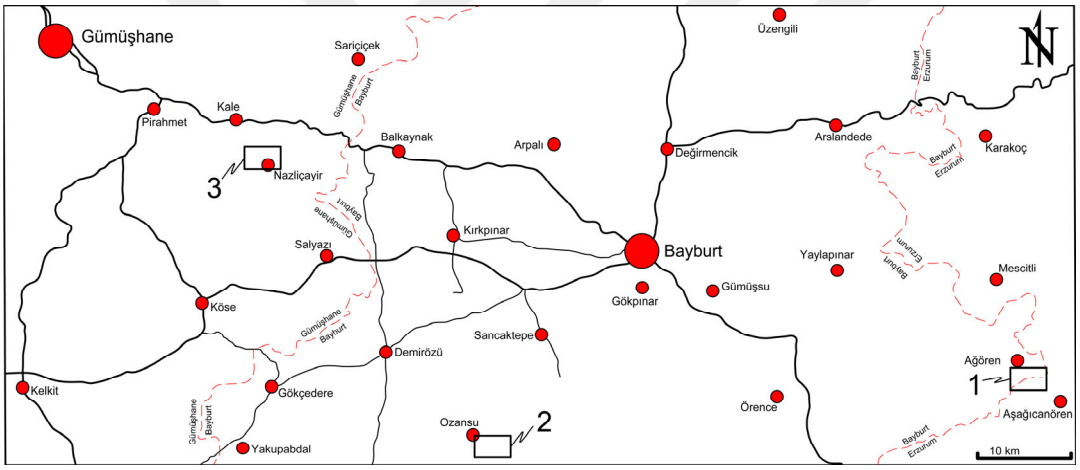

Figure 1.5. Location map of the study areas. 1: Ağören measured section; 2: Ozansu measured sections; 3: Nazlıçayır measured sections.

1.3 Materials and Methods

Field and laboratory work form the basis of this study. Since the Upper Jurassic – Lower Cretaceous pelagic successions are understudied and there is no recent research on them in the Eastern Pontides, first one and a half week of the 2 months-fieldwork dedicated to search for well-exposed and continuous outcrops suitable for the research purpose (shaded regions in Fig. 1.4). Regions I, VII and VIII (with cyan

borders in Fig. 1.4) offer well-exposed and rather continuous outcrops qualified for detailed analysis.

A stratigraphic section was measured and sampled at regular intervals along the outcrops just to the south of Ağören village (north of Akyazı village; location 1 in Fig.1.5), located in the İmalıdağ thrust sheet. A total of 294 samples were taken along the 589-meter-long Ağören measured section. In the Ozansu region (location 2 in Fig. 1.5), located in the Aşutka thrust sheet, two stratigraphic sections were logged (OA & OB measured sections). The OA section measures 65 meters in length, and a total of 33 samples were collected. The OB section is 236 meters long, with 201 samples taken along the section. These successions are located on the slope to basin depositional environment of the PCP.

Another section was measured in the Nazlıçayır village (location 3 in Fig 1.5). Throughout this shallow marine sequence of the PCP, a total of 6 stratigraphic sections were measured. Abundant key beds (e.g., basalt levels, counting layers above and below this basalt and checking facies for lateral shifts, tracking thick characteristic dolomitic intervals or distinctive limestone layers laterally), which allow for lateral shifts at levels where outcrop conditions worsen in the region, thereby facilitating reliable correlation and continuous measurements in more accessible outcrop areas, have enabled the production of a composite stratigraphic section with a total thickness of 350 meters. Along this section, a total of 161 rock samples were collected. Among these samples, 11 were collected from the basalt level for use in subsequent research. The remaining 150 samples were collected from carbonate, dolomite, and sandstone beds.

Thin sections were obtained from the collected samples for micropaleontological and microfacies analyses. 495 thin sections from the pelagic successions were prepared in the thin section preparation laboratory of the Department of Geological Engineering, METU. The 161 shallow marine rock samples were thin sectioned in the laboratories of the General Directorate of Mineral Research and Exploration (MTA) in Ankara.

Fossil content and constituent composition of each sample were documented and in the light of obtained data, microfacies types and depositional environments were determined. Microfacies analyses of the carbonate rocks followed the updated version of Dunham's (1962) carbonate rock classification, revised by Embry & Klovan (1971), and the facies analysis methodology developed by Flügel (2004, 2010) with considering the remarks of Lokier and Junaibi (2016). The Pettijohn's (1975) scheme was used for the classification of the clastic levels under the microscope. For the percentage estimations of the rock constituents and the relative abundance estimation of the fossil contents, visual comparison charts were used (Baccelle & Bosellini, 1965).

A variety of fossil groups (e.g., foraminifers, calpionellids, microencrusters, crinoids) were used for biostratigraphical analysis. The zonal boundaries were positioned between the two closest samples with contrasting fossil content. The chronostratigraphical position of the studied successions was determined by the correlation of the established biozonations with the previously published schemes.

Additionally, for calibration of the bioevents from the neritic and pelagic successions and determination of the relative position of these bioevents with respect to the Upper Jurassic – Lower Cretaceous stage boundaries (Oxfordian – Hauterivian), quantitative biostratigraphical methods of graphical correlation (Shaw, 1964; Edwards, 1984) and the unitary associations (Guex, 1977, 1991), corresponding to two classical biostratigraphical approaches; the zonations based on first occurrence (FO)/ last occurrence (LO) events (i.e., interval zones) and the zonations based on assemblages (i.e., Oppel zones), respectively, are used for data treatment. Correlations obtained by conventional biostratigraphy and quantitative methods are compared and implications for biozonations and age assignments are discussed. A composite standard reference section for the Upper Jurassic – Lower Cretaceous PCP strata is constructed as a working hypothesis that accounts for both pelagic and neritic deposits by calibrating shallow and deep marine bioevents with respect to the Oxfordian – Hauterivian stage boundaries through the application of quantitative

biostratigraphical methods while providing new insights into the chronostratigraphical problems summarized previously.

1.4 Previous Works on the Upper Jurassic – Lower Cretaceous Carbonates of the Eastern Pontides

The Upper Jurassic – Lower Cretaceous carbonate rocks of the Pontides (Fig. 1.3) are studied under the general name of Bilecik Limestone in the Western Pontides (e.g., Granit & Tintant, 1960; Altınlı, 1973a, b; Okay et al., 1990; Altıner et al., 1991). In the northern part of the Central Pontides, they are called the İnaltı Formation (e.g., Ketin & Gümüş, 1963; Saner et al., 1980; Yılmaz & Tüysüz, 1984; Tüysüz et al., 1990; Derman & Sayılı, 1995) and in the southern part of the Central Pontides, they are known as the carbonates of the Amasya Group (e.g., Blumenthal, 1950; Alp, 1972; Özcan et al., 1980; Rojay, 1993, 1995; Rojay & Altıner, 1998). Their contemporaneous carbonates in the Eastern Pontides are named as the Berdiga Limestone (e.g., Pelin, 1977; Taslı, 1984; Rojay, 1985; Taslı, 1990; Kırmacı, 1992).

There are valuable studies on the facies (Taslı, 1990; Kırmacı, 1992; Kırmacı et al., 1996; Yılmaz, 1997; Kırmacı, 2000; Eren & Taslı, 2002; Koch et al., 2008; Vincent et al., 2018; Özyurt & Kırmacı, 2024), diagenesis (Kırmacı, 1992; Kırmacı et al., 1996; Koch et al., 2008; Özyurt et al., 2018; Kırmacı et al., 2018; Vincent et al., 2018; Özyurt et al., 2024), and benthic foraminifera-algae micropaleontology and biostratigraphy (Taslı, 1990; Taslı, 1993; Kırmacı et al., 1996; Taslı et al., 1999; Bucur et al., 2000, 2004; Koch et al., 2008; Vincent et al., 2018; Granier, 2019; Schlagintweit et al., 2019) of the Upper Jurassic – Lower Cretaceous shallow marine carbonates in the region. However, despite well-studied stratigraphic sequences, there are contrasting opinions on the chronostratigraphic position of the successions, largely due to the difficulty of age determination caused by the dolomitization, which is common in the neritic carbonates of the region that obscures the original depositional texture (Taslı, 1990; Taslı, 1993; Bucur et al., 2000, 2004; Koch et al., 2008; Vincent et al., 2018; Granier, 2019). Compared to these rather abundant

studies on shallow marine carbonates, studies on the contemporaneous slope to basin deposits are very few (Tunç, 1992; Burşuk, 1992; Timur, 1997; Okay et al., 1997, Timur, 2000). The studies by Tunç (1992) and Burşuk (1992) are on calpionellid biostratigraphy but were conducted using generalized vertical sections for the region rather than detailed measured sections. Neither these studies nor the others that cover a wider area including deep marine carbonate sequences (i.e., Robinson et al., 1995; Okay et al., 1997; Ustaömer & Robertson, 2010) detail the age interval and depositional environments of these successions.

Berdiga Formation (*s.l.*) was introduced by Pelin (1977) in Alucra (Giresun) region that encompasses not only the Upper Jurassic – Lower Cretaceous shallow marine carbonates but also the part of the underlying Lias – Dogger volcaniclastics and carbonates and the overlying Aptian – Albian pelagic limestones. This integration of different lithologies from wide chronostratigraphic levels as members into the formation definition is probably the root of miscommunication and misinterpretation that still preclude the discussions on the stratigraphical range of the neritic carbonate successions (Berdiga Limestone *s.s.*) of the Berdiga Formation in the Eastern Pontides to this day. Even the Aptian – Albian age assignment was not based on the faunal assemblage present (there was no age-diagnostic fauna at the uppermost 70 m of the Berdiga Formation in its type locality; beggie colored, thin-bedded ammonitic micrites of the Kıcılı Yayla Limestone Member of Pelin, 1977; probably an equivalent of the well-known Soğukçam Limestone from the Western Pontides, Altınlı, 1973a; Altıner et al., 1991), but was interpreted from the stratigraphic relation with the immediately overlying Turonian red pelagics of Elmalıdere Formation (an equivalent of the Kapanboğazı Formation) that made Pelin (1977) to assign this wider age range to the Berdiga Formation. The presumed presence of post–Hauterivian neritic strata was found itself well-established in the literature with the erroneous attribution of age data in the pioneering studies (e.g., Bergougnan, 1976, 1987; Robinson et al., 1995; Okay et al., 1997) from basinal carbonates to shallow marine successions by the following researchers that have given rise to illustrations of generalized stratigraphic sections with shallow marine carbonate

deposition continuous from Oxfordian to well into Albian without any documentation of post-Hauterivian neritic fossil assemblages (e.g., Kırmacı et al., 1996; Taslı et al., 1999; Dokuz, 2000; Eren & Taslı, 2002; Koçyiğit & Altıner 2002; Özyurt et al., 2018; Kırmacı et al., 2018; Vincent et al., 2018; Özyurt et al., 2022; Özyurt et al., 2024).

The first studies were dealing with much larger area and wider stratigraphical intervals, in which the Upper Jurassic – Lower Cretaceous carbonate successions formed just a minor part. Ketin (1951) conducted a pioneering study in the Bayburt region that introduced the Permo – Carboniferous sedimentary successions. He described the major Liassic transgression in the region similar to the Jurassic of Ankara and Amasya successions and claimed the presence of widespread intra-Jurassic discontinuity in the Bayburt area which eroded the Dogger strata. He also recognized the existence of north-vergent tectonic slices but did not detail them.

Nebert (1961) introduced the Ağvanis Schists and defined these metamorphics as the basement rocks of the Mesozoic cover of the Eastern Pontides. Wedding (1963) focused on the Jurassic successions and argued against the absence of Dogger strata for which the definitive proof came from Ağralı et al. (1965) by the study of palynology of the Bayburt Jurassic successions that reveal Dogger palynomorphs at the uppermost levels of strata previously claimed as Liassic deposits. Nebert (1964) expands his work in 1961 to further east, Alucra – Refahiye line, and described Lias – Dogger flysch and overlying Malm – Lower Cretaceous siliceous carbonates that passes up into Turonian – Campanian red pelagic micrites with lists of fossil occurrences.

The first in-depth work in the Eastern Pontides came from Bergougnan in 1976 which forms a major part of his later published PhD thesis (Bergougnan, 1987). He considered the Pontic Range to belong to the southern margin of Eurasia (based on fossil assemblages; details are present in his PhD thesis but not in the 1976 paper). He differentiated two nappes originated from south (with respect to autochthonous Alucra-Bayburt successions); tectonic ophiolitic mélange forming the lower nappe

which is in turn overthrust by the Çimendağı nappe (whose carbonates were interpreted to be linked to the autochthonous Alucra-Bayburt successions) while the carbonates of the Munzur Mountain was decided to belong the southern margin of Tethys based on divergence in fossil fauna and stratigraphy that is previously documented by Bergougnan (1975), Adamia (1975), Bassoullet et al. (1975), Biju-Duval et al. (1977) and Bassoullet and Bergougnan (1981). Depending on the taxa list (e.g., *Protopeneroplis* sp., *Labyrinthina mirabilis*, "*Conicospirillina*" *basiliensis*, "*Trocholina*" *elongata*, "*Trocholina*" *alpina*, *Nautiloculina* sp., *Pseudocyclammina lituus*, *Salpingoporella pygmaea*, *Bacinella irregularis, Calpionella alpina*, *C. elliptica*, *Calpinellopsis oblonga*, *Tintinnopsella carpathica*: a combination of benthic foraminifera and algae characterizing shelf margin settings and co-occurrence of pelagic calpinellids with upper slope dwelling microencrusters) and microphotographs (typical of slope grainstone – packstone facies) provided by Bergougnan (1987) from the Çimendağ measured sections, a shelf margin, slope to basin depositional setting can be interpreted for this carbonate nappe. Bergougnan (1976, 1987) agreed with the presence of intra-Jurassic disconformity which formed the base of the Malm transgression in the region. Bergougnan also detected another disconformity at the base of the Upper Cretaceous deposits. Although Bergougnan (1976, 1987) distinguished pelagic and neritic Upper Jurassic – Lower Cretaceous carbonates from each other by fossil assemblages, he did not formalize these distinct units into separate formations. He introduced the Kelkit Formation (which can be considered as the equivalent of the Mudurnu Formation from the western Pontides; e.g., Saner, 1980; Altıner et al., 1991) for the Liassic volcaniclastics that underly the Upper Jurassic – Lower Cretaceous carbonates.

Following the introduction of the Berdiga Formation (*s.l.*) by Pelin (1977) as mentioned above, the first attempt to differentiate neritic and pelagic Upper Jurassic – Lower Cretaceous carbonates came from Ağar (1977) who introduced the Çaltepe Limestone for the shallow marine carbonates and the Hozbirikyayla Limestone for the pelagic carbonates in the Bayburt-Kelkit region.

Şengör et al. (1980) tried to synthesize the accumulated data in the Eastern Pontides to propose a tectonic model for the geological evolution of the region in terms of its place within the trinity of the Paleotethys and Neotethys Oceans and the Cimmerian Continent of Şengör (1979) that predicts completely different tectonic order and sense of movement for the tectonic slices in the region and Gondwana affinity for the Pontides. They proposed the closure of the Paleotethys Ocean as the reason for the cessation of sedimentation during the late Early Jurassic to early mid-Jurassic interval (the mid-Jurassic disconformity of Ketin, 1951) and overriding of oceanic assemblage by the continental assemblage from south to north. Consequently, a contrasting province for the ophiolites (northern derived) was interpreted in comparison to the work of Bergougnan (1976). Bergougnan and Fourquin (1982; submitted before the publication of Şengör and Yılmaz, 1981 but published later in 1982) pointed out the inconsistencies and conflicting inferences of the model that contradicts with the well-established data from the field observations and that forced Şengör et al. (1980) to suggest unlikely subduction polarity, tectonic transportation distances and erosional rates to explain the presence of supposedly northern-derived-ophiolitic material (Paleotethyan origin) to the south of the continental series of the Bayburt-Kelkit region with *a priori* assumption that any pre-Liassic ophiolite should be Paleotethyan oceanic assemblage.

Şengör and Yılmaz (1981) framed the Upper Jurassic – Lower Cretaceous carbonates of the Eastern Pontides as the passive margin successions developed on the southern margin of Laurasia during a rifting phase continuing since the beginning of Lias following the complete closure of the Paleotethys in the Middle Jurassic that amalgamated the Eastern Pontides and the Scythian Platform. The same Liassic rifting interpretation was detailed by Görür et al. (1983) based on sedimentological data from the Pontides.

Okay (1983), as opposed to Şengör et al. (1980, 1982), demonstrated relative autochthonous character of the Ağvanis metamorphics, composed of metabasics, marbles and phyllites, that formed the basement rocks of the Eastern Pontides overlain by the Liassic transgressive volcaniclastics (the Hacıören Formation,

equivalent of the Kelkit Formation) and categorized them under the Ağvanis Group. He emphasized the similarities between the Ağvanis Group and the Tokat Massif (Blumenthal, 1950; Alp, 1972; Seymen, 1975; Koçyiğit, 1979; Özcan et al., 1980) and defined the Ağvanis metamorphics as the easternmost elongation of the previously described Karakaya Formation (Bingöl et al., 1973; Tekeli, 1981; with equivalent units in the Ankara region, Bailey & McCallien, 1950; Erol, 1956; Akyürek et al., 1979; Özkaya, 1982) which later paved the way the introduction of the Sakarya Zone by Okay (1984). This Sakarya Zone grouped the Sakarya Continent of Şengör and Yılmaz (1981) and the Central and the Eastern Pontides based on the recognition of that the Karakaya Complex forms the pre-Jurassic basement of stratigraphically similar Mesozoic and younger cover rocks. Okay (1983) introduced the Boynuktepe Group for the Middle Jurassic – Upper Cretaceous carbonates cropping out as a *rétrocharriage* nappe over a Paleocene olistostrome (the Taşdemir Formation; probably an equivalent of the Sipikör Formation of Bergougnan, 1987) to the north of the Ağvanis metamorphics without differentiating them into formations. These carbonates show a variety of facies and age intervals like the original definition of the Berdiga Formation (*s.l.*) of Pelin (1977). Similarly, these shallow marine to deep marine carbonate succession is overlain by the Upper Cretaceous red pelagic micrites. Depending on the similar facies, stratigraphic order and depositional ages, this carbonate nappe is thought as the western elongation of the Çimendağı Nappe (Bergougnan, 1975) by Okay (1983).

Rojay (1985) defined the tectono-stratigraphic characteristics of the Kelkit Valley subzone of the North Anatolian Fault. He differentiated a Kelkit Group that unconformably overlies the Permian – Triassic metamorphics of the Tokat Group. This Kelkit Group includes the Liassic volcaniclastics, volcanics and clastics (with *rosso ammonitico* lenses) of the Kayabaşı Formation (an equivalent of the Kelkit Formation) at the bottom and the overlying carbonates of the Dogger(?) - Neocomian Berdiga Formation (*s.l.*). Although the nomenclature of Pelin (1977) was followed for the Berdiga Formation that incorporates also a part of the underlying Lias – Dogger volcaniclastics, Rojay (1985) was able to differentiate the Upper Jurassic –

Lower Cretaceous dolomites and carbonates of the Berdiga Formation into Çaltaş and Kıcılıyayla Members, respectively. Especially the carbonates of the Kıcılıyayla Member overlying the dolomites of the Çaltaş Member revealed a striking stratigraphy with transition from platform carbonates at the bottom into the overlying Berriasian calciturbiditic slope deposits. He also recognized rather rarely observed *in-situ* reefal shelf-margin deposits in the region that intercalate with the platform carbonates of the Çaltaş Member. Additionally, Rojay (1985) showed the presence of an angular unconformity between the Kelkit Group and the overlying volcano-sedimentary sequence of the Upper Cretaceous Akçağıl Group.

Akdeniz (1988) focused on the Permo-Carboniferous sedimentary succession in the Demirözü region (SW Bayburt) while providing detailed map of the region that also differentiates the outcrops of the Upper Jurassic – Lower Cretaceous carbonates in the lithostratigraphic framework of Ağar (1977) which gives importance on facies types. He also illustrated the north-vergent tectonic slices defined previously by Ketin (1951) in several cross sections.

Yılmaz (1989) compares and shows the similarities between NE Turkey and Caucasus basement rocks. He correlated the Eastern Pontides with the Somecheti-Kafan (Karabakh) belt of the Transcaucasia and the Tauride Platfrom with the Iranian Platform of the Lesser Caucasus with the intervening North Anatolian – Lesser Caucasus ophiolitic belt.

Okay (1989) delineated the tectonic units and sutures in the Pontides and use the common Upper Jurassic – Lower Cretaceous carbonate cover successions over both the Istanbul and Sakarya Zones as the evidence for the closure of the Intra-Pontide Suture between these two tectonic units in pre-Late Jurassic times at least for the Central Pontides segment.

The first comprehensive research on the Upper Jurassic – Lower Cretaceous carbonate successions in the Eastern Pontides is the PhD thesis of Taslı (1990) that focused on the neritic carbonates of the Gümüşhane – Bayburt region. He differentiated 9 lithofacies types and 7 biozones for the Callovian? – Lower

Barremian strata. This biozonation is based on benthic foraminifers that defines "*Archaeosepta*" *basiliensis* interval zone, *Alveosepta jaccardi* range zone, unfossiliferous interval zone (for a dolomitic interval), "*Pseudotextulariella*" *salevensis* range zone, *Barkerina barkerensis* range subzone, *Pseudotextulariella keciensis* range zone and *Cuneolina hensoni – Everticyclammina hedbergi* concurrent range zone. A depositional model for the Gümüşhane – Bayburt region was proposed in W-E oriented cross section sketches that do not regard the slope to basinal deposits in the south. Taslı (1990) is the first study to recognize the post-Early Kimmeridgian unconformity and the "Oxfordian" basalt flows within the shallow marine carbonates in the Gümüşhane region. These basalt flows were later named as the Keçidere Basalt by Taslı (1997).

Kırmacı (1992) conducted PhD research in the Alucra-Gümüşhane-Bayburt region that focused on the sedimentology of the Upper Jurassic – Lower Cretaceous carbonate succession. This study shares common localities with Taslı (1990). Kırmacı (1992) modified the original Berdiga Formation (*s.l.*) of Pelin (1977) by excluding the basal volcaniclastics and named the rest of the carbonate succession as the Berdiga Limestone. He carried out detailed microfacies analyses on those successions and documented the diagenetic history of these carbonates.

The first biostratigraphic studies on the pelagic successions after the work of Bergougnan (1987) were performed by Tunç (1992) in Olur (Erzurum region) and by Burşuk (1992) in Bayburt and Kop Mountains (NW Erzurum). Instead of regularly sampled measured sections, these studies provide generalized stratigraphical columns with approximate total thicknesses of units on which the calpionellid zone boundaries were tentatively placed along with calpionellid assemblage lists.

Bozkuş (1992) mapped the Olur region and documented the stratigraphical relationships. He studied the Upper Jurassic – Lower Cretaceous deep marine carbonates under the name of Yeşilbağlar Formation (Yılmaz, 1985) and provided a measured strtatigraphical section with list of fossil assemblages.

Taslı (1993) published only the Jurassic part of his PhD thesis (Taslı, 1990) that focused on the micropaleontology of the foraminifer assemblages of the "*Archaesepta*" *baisliensis* and *Alveosepta jaccardi* zones (Callovian – Lower Kimmeridgian).

Robinson et al. (1995) tried to describe stratigraphic and tectonic development of the Eastern Pontides based on sections logged at 8 localities, 1 seismic profile, K-Ar and Sr-isotope dating and biostratigraphical data. The samples are very sparsely distributed (e.g., 3 or 5 spot samples for 6 km thick succession and even no sampling for the Upper Jurassic – Lower Cretaceous carbonate intervals like the Bayburt section, and in any of the sections there are no samples from the bottom or top of the carbonate strata); however, they attempted to construct a chronostratigraphical chart for the region and suggest Oxfordian – Barremian continuous neritic and pelagic sedimentation without any documented post-Hauterivian fauna.

Bektaş et al. (1995) analyzed Late Cretaceous carbonate platform drowning in the Eastern Pontides by proposing continuous southward subduction of the Paleotethys to the north underneath the Eastern Pontides for the Liassic – Dogger and Late Cretaceous intervals that created two different phases of rifting. The last one leads to the drowning of the Upper Jurassic – Lower Cretaceous carbonate platforms. This research did not emphasize the southern margin of the platform where there is clear evidence for pelagic deposition and without any age data they speculate continuous shallow marine deposition until Cenomanian in their columnar sections.

Kırmacı et al. (1996) revisited the Lower Cretaceous part of the Nazlıçayır (Gümüşhane) carbonate successions which had been previously studied by Taslı (1990) and Kırmacı (1992) in their PhD research. In contrary to these previous works, Kırmacı et al (1996) interpreted completely different chronostratigraphic positions for the upper part of the successions. Based on foraminifera and algae data, they suggested Barremian to Late Aptian shallow marine deposition for the succession and tried to draw a similarity with the Urgonian facies of Europe, although there were no typical post-Hauterivian taxa. They also noted that "without

orbitolinids, which are missing in the section, it is very difficult to give a precise age determination of the Berdiga Limestone section." Their inferred Aptian age was based on the occurrence of *Novalesia producta*, a species described from the uppermost Aptian – lowermost Albian of Spain (Magniez, 1974). However, those illustrated forms are actually longitudinal sections of *Vercorsella* common in Valanginian strata (see biostratigraphary section for further discussions). Additionally, *Haplophragmoides globulus* individual from the so-called Aptian strata illustrated by them is an equatorial section of a *Meandrospira favraei*, a taxon which is again common in Valanginian – Hauterivian strata. In any case, stage boundaries in their study were defined loosely by giving only ranges for certain parts of the succession like Barremian to Early Aptian or Late Barremian to Early Aptian, which was also the case for the previous studies on these shallow marine successions.

Okay and Leven (1996) re-examined the previously defined Upper Paleozoic sequences exposed in the Cebre autochthoun and Hamurkesen thrust sheet (characteristics of these thrust sheets were later detailed in Okay et al., 1997) in Bayburt region that formed the basement of Mesozoic cover in these tectonic units. They realized tectonic repetition of the Paleozoic sequence in Bayburt and restricted the depositional age to latest Carbonifereous to earliest Permian based on fusulinid foraminifers and stated the similarity of these Pontide sequences with the Lower Permian sequences from the Greater Caucasus. Based on this similarty and Euramerican affinities of the plant fossil in the Paleozoic sequences of Bayburt (Şengör, 1990), they concluded that the Eastern Pontides were located along the southern margin of Laurasia.

Yılmaz (1997) studied the Cretaceous platform-basin transition in the Gümüşhane region, although the platform and basin deposits in this study are not synchronous. Instead of contemporaneous platform-basin deposits, he investigated the Upper Jurassic – Lower Cretaceous neritic carbonates and the overlying Upper Cretaceous pelagic sediments marking a platform drowning. An Aptian – Albian age is assigned to the uppermost level of this "neritic" Berdiga Formation based on "pelagic" foraminifers like *Hedbergella* sp., and *Globigerinelloides* sp., which again clearly

shows the confusion that had been introduced by the original Berdiga Formation (*s.l.*) description of Pelin (1977).

Yılmaz et al. (1997) reviewed geology and tectonic evolution of the Pontides. They used homogenizing lithostratigraphical nomenclature that assign well-established formation names from the Western Pontides (e.g., Altıner et al., 1991) to the Eastern Pontides Mesozoic successions by equating the Mudurnu Formation, the Bilecik Limestone and the Soğukçam Limestone from the Western Pontides with the Kelkit Formation, the Berdiga Limestone (*s.s.*) and the Lower Cretaceous pelagic carbonates of the Eastern Pontides, respectively. They continued to use the tectonic model of Şengör and Yılmaz (1981) with minor modification that suggest the Paleotethys Ocean was open in the western part as a remnant basin between the Istanbul Zone and the Sakarya Continent until the latest Cretaceous, closure of which would create the Intra-Pontide suture in that segment. They still suggested a position on the northern margin of the Gondwanaland for the Pontides during Permian.

Okay et al. (1997) gave detailed account of the stratigraphy and tectonic history of the Pulur (Bayburt) region. They differentiated a relative autochthon and three north-vergent thrust sheets, which from the lowermost tectonic position to the top (from north to south) are Cebre relative autochthon and Hamurkesen, Aşutka and İmalıdağ thrust sheets. The Cebre relative autochthon is composed of low-grade metamorphics (fine-grained schists and phyllites) at the base and the overlying Upper Carboniferous sandstone, limestones, conglomerate, quartzite and black shale with thin coal seams (the Çatalçeşme Formation), the Upper Carboniferous – Lower Permian red sandstones (the Hardişi Formation), the Jurassic neritic limestones (the Çaltepe Limestone) and the Upper Cretaceous hemipelagic clastic and carbonate rocks (the Gevenli Formation). The widespread Jurassic volcaniclastic Kelkit Formation is missing in the Cebre unit. Although they did not suggest any depositional setting, the Çaltepe Limestone seems to represent a platform margin in this unit depending on the listed foraminifer assemblages by Okay et al. (1997; e.g., *Protopeneroplis* sp., "*Trocholina*" sp., *Lithocodium aggregatum*, *Bacinella irregularis*, *Saccocoma* sp., *Globochaete* sp., *Ophthalmidium* sp. at the lower parts

and *Pseudocyclammina lituus*, *Neotrocholina* sp., "*Cladocoropsis*" *mirabilis*, "*Tubiphytes*" *morronensis* from the uppermost levels). They interpreted Late Jurassic – Berriasian age for these carbonates. However, the presence of Berriasian would be questionable depending on the listed taxa. The Hamurkesen thrust sheet includes low-grade metamorphics (phyllite and metatuffs) at the base and the overlying Çatalçeşme Formation (more recrystallized and more strongly deformed compared to the Cebre unit), the Jurassic volcaniclastic rocks (the Kelkit Formation), newly defined Kimmeridgian "neritic" carbonates (the Kazalı Limestone) and the overlying Tithonian – Berriasian pelagic biomicrite with intercalations of calciturbidites, marly siltstones and green, fine-grained volcanogenic sandstones at the lower parts (the Hozbirikyayla Limestone; can be viewed as an equivalent formation of the combination of the Yosunlukbayırı Formation and the Sogukçam Limestone of Altıner et al., 1991). They could not observe *in-situ* fossils within the Kelkit Formation. There are several limestone olistoliths within these Jurassic volcaniclastics. They identified a Late Jurassic fossil assemblage similar to the Çaltepe Limestone from the Cebre unit (e.g., "*Cladocoropsis*" *mirabilis*, "*Tubiphytes*" *morronensis*, *Protopeneroplis striata*, *Protopeneroplis* "*trochangulata*", "*Trocholina*" sp., *Bacinella irregularis*, *Koskinobullina socialis*). The Kazalı Limestone revealed similar taxa associaton with the Çaltepe Limestone (e.g., *Nautiloculina* sp., *Protopeneroplis* "*trohangulata*", "*Conicospirillina*" *basiliensis*, "*Trocholina*" *alpina*, "*Tubipyhtes*" *morronensis*, *Bacinella irregularis*) whose outcrop characteristics (thickly bedded, oolitic black limestone) led the mapping as a separate formation. This Kazalı Limestone corresponds to the lower parts of the Hozbirikyayla Limestone of Ağar (1977). Although its age was interpreted as Kimmeridgian, the fossil content suggests a Tithonian stratigraphical position. Okay et al. (1997) constrained the upper age limit of the Kelkit Formation as Kimmeridgian by these age data. Typical slope to basin taxa association was listed by Okay et al. (1997) from the Hozbirikyayla Limestone (e.g., "*Trocholina*" sp., "*Tubiphytes*" *morronensis*, *Charentia* sp., *Nautiloculina* sp., *Mesoendotyhra* cf. *izjumiana*, "*Conicospirillina*" *basiliensis*, *Koskinobullina socialis*, *Bacinella*

irregularis, *Saccocoma* sp., "*Cadosina*" sp., *Calpionella alpina*, *Tintinnopsella carpathica*, *Crassicollaria parvula*, *Tintinnopsella longa*, *Calpionellopsis simplex*, *C. oblonga*). A Tithonian – Berriasian age was assigned based on calpinellid and benthic foraminiferal assemblages (Okay et al., 1997). The Hamurkesen sheet is tectonically overlain by the Aşutka thrust sheet along the Pulur thrust (of Ketin, 1951). The Aşutka sheet consists of strongly deformed micashist, cordierite-sillimanite-garnet schist, amphibolite, gneiss, metagranite and exceedingly rare marble (the Pulur metamorphic complex) as the basement rocks and the overlying Jurassic volcanoclastics (the Kelkit Formation) and pelagic biomicrites (the Hozbirikyayla Limestone). Slices of ophiolitic mélange lie with a thrust contact over the Cretaceous palegics of the Hozbirikyayla Limestone, both are unconformably overlain by Maastrichtian rudist-bearing carbonates (the Kapıkaya Limestone of Keskin et al., 1989; to the south of the study area of Okay et al., 1997) and/or by the Paleocene – Lower Eocene flysch with olistostromal levels (the Sipikör Formation and Işkılör-Tütenli Olilstostrome of Bergougnan, 1987). This flysch and olistostromes are overthrust by the Çimendağı Nappe of Bergougnan (1976, 1987) to the southwest of the study area of Okay et al. (1997). The Kelkit Formation in this tectonic unit is much finer-grained (also with no olistoliths) than the equivalent successions in the Hamurkesen sheet. The Hozbirikyayla Limestone, in the Aşutka thrust sheet, has a folded structure and is made up of thinly to medium bedded, light beggie radiolarian biomicrites with rare intercalations of medium bedded calciturbidites. They obtained Berriasian fauna in the middle part of the carbonates (e.g., *Calpionella alpina*, *C. elliptica*, *Tintinnopsella carpathica*, "*Trocholina*" *sagittaria*, *Neotrocholina* sp., *Protopeneroplis* "*trochangulata*"). A sample from the uppermost part of the succession, just below the ophiolitic mélange, revealed Aptian – Albian taxa (e.g., *Hedbergella planispira*, *H. gorbachikae*). The ophiolitic mélange is made up of radiolarian chert, pelagic and neritic limestone, spilitized basalt, serpentinite, sandstone, shale and siltstone blocks and slices. Samples collected from the carbonate blocks within the mélange yields Aptian – Albian age interval (e.g., *Hedbergella trochoidea*, *H. gorbachikae*, *H. delrioensis*, *H. sigali*, *H. planispira*, *H.*

planispira, *Globigerinelloides blowi* and *Ticinella bejaouensis*). These planktonic foraminifer data together with the age of the unconformably overlying Upper Campanian – Maastrichtian Kapıkaya Limestone (ages from Bergougnan, 1987) constrain the age of mélange formation and emplacement to the Aptian – Upper Campanian interval. The Upper Paleocene – Lower Eocene Sipikör Formation was interpreted by Okay et al. (1997) as a clastic wedge deposited in a foreland basin in front of the northward advancing İmalıdağ thrust sheet. Norman (1976) showed the paleo-currents were largely parallel to the axis of the basin and were flowing from the southwest towards the northeast. Along the region between Ağvanis and Erzurum, to the north of the İAE suture zone, allochthonous Mesozoic carbonates crop out extensively. These carbonates were named by Yılmaz (1985) and Bergougnan (1987) as the Çimendağı nappe in the west and İmalıdağ nappe in the east. Both nappes tectonically overly the Sipikör Formation in the north and the ultramafic rocks in the south. The main difference between these two thrust sheets is that the Jurassic – Lower Cretaceous sequence in the İmalıdağ unit developed in deeper facies. Okay et al. (1997) observed only a limited portion of the İmalıdağ sequence and defined them as composed of a sandstone – shale series at the base and stratigraphically overlying pelagic micrites of Tithonian – Berriasian age. A remarkably similar succession on the İmalıdağ nappe was also defined by Bergougnan (1987). Okay et al. (1997) again emphasized the similarity between the Ağvanis Massif and the Nilüfer unit of the Karakaya Complex and proposed similar tectonostratigraphic position for both of these units while correlating the Pulur metamorphics and the Kazdağ Group (composed of gneiss, marble and amphibolite). By this way, the basement rock relationships of the Sakarya Zone of the Pontides had been established. To help in visualization of this complex tectonostratigraphic configuration, a cross section, simplified columnar sections from each thrust sheets and the autochthonous unit have been provided in the Figure 1.7 (Chapter 1.5) with a sketch cross-section that explain the proposed configuration for the basement rocks. They explained the absence of the Kelkit Formation in the Cebre autochthon, and differentiation in facies of the Jurassic deposits within different thrust sheets as

the result of differentiation in paleotopography; e.g. fault bounded high-standing areas record shallow marine deposition while the rest of the basin received volcaniclastic deposition that show deepening towards south. This initial rifting phase (Görür et al., 1983) followed by the deposition of the Upper Jurassic – Lower Cretaceous shallow marine (in the north) to deep marine (in the south) carbonates in the region. They proposed an attempted subduction of the Eastern Pontides continental margin in a south-dipping intra-oceanic subduction zone as the mechanism for the Cenomanian – Turonian ophiolitic mélange obduction northward over the south-facing continental margin. The immediately following Senonian volcanic arc development in the northern Eastern Pontides was explained by the change of polarity of the subduction towards north under the continental margin of the Eastern Pontides after this ophiolitic mélange obduction that finally led to opening of the Black Sea (e,g., Görür, 1988; Okay et al., 1994; Hippolyte et al., 2010, 2017, 2018) . The development of the thrust stack described above was attributed to the Late Paleocene – Early Eocene collision between the Eastern Pontides and the Anatolide – Tauride continents. This age constraint was interpreted from the observation that the post-collisional Middle Eocene marine carbonates and clastics unconformably overlie the various thrust sheets and the ophiolitic mélange in the region.

Okay and Şahintürk (1997) published basically the same paper in AAPG Memoir with additions of paleogeographical maps and stratigraphic columns that compare the Eastern Pontides and the Munzur Mountains. In that column, they show a strange chronostratigraphic level for the neritic carbonates of the Eastern Pontides that is continuous from Pliensbachian to Aptian; a regression from the data previously published by Okay et al. (1997) in the same year and also contradicts with the paragraphs within the same paper (Okay & Şahintürk, 1997) where they clearly indicated that the youngest shallow marine deposits preserved are the Upper Barremian strata in the north (Pelin, 1997; Bergougnan, 1987) and the youngest pelagic carbonates preserved are the Aptian limestones in the south (Burşuk, 1981, Okay et al., 1997) with Albian ages are obtained only from the Maden region near

the suture zone (Elmas, 1994; Robinson et al., 1995). They also mentioned the difficulty of drawing a single tectonic line to delineate Tethyan suture like in the regions farther west due to the mushroom-type structure of the accretionary complex and peridotite that lie both on the Pontides and Anatolide-Tauride units.

Taslı et al. (1999) described a shallow marine sequence unconformably overlain by Upper Cretaceous – Paleocene olistostromal flysch deposits. They misinterpreted the pelagic carbonate deposits as the continuation of the neritic Berdiga Limestone and assigned the uppermost levels of their "neritic" carbonates an Aptian – Albian age based on planktonic foraminifera. All stage boundaries are fuzzy and general time intervals were assigned to strata (e.g., Hauterivian – Barremian – Aptian etc.) without any post – Hauterivian taxa.

Timur (2000 based on his PhD study in 1997) mapped the Yesirçöl Mountain (Aşkale, Erzurum) and described Jurassic – Tertiary geological evolution of the region. He illustrated an Upper Jurassic – Lower Cretaceous succession remarkably similar to the descriptions by Bergougnan (1987) from the same region. For this interval, Timur (2000) defined an Upper Jurassic clastic deposit (the Rizekent Formation, an equivalent of the Kelkit Formation from the Bayburt region with less volcaniclastic material) and overlying cherty pelagic carbonates (with calpionellids; the Yesilçör Formation, an equivalent of the Hozbirikyayla Limestone) through a transitional interval of intercalated pelagic carbonates and deep marine clastics (that revealed mixed neritic and pelagic fauna; the Büyükgüney Formation, an equivalent of the uppermost parts of the Kelkit Formation). Although he proposed a conformable contact between the Yesilçör Formation and the overlying Başkurtdere Formation (pelagic clastics and carbonates), the fauna provided indicates a time gap between the calpionellid-bearing Yesilçör Formation and the *Globotruncana*-bearing Başkurtdere Formation. This last formation is tectonically overlain by an ophiolitic mélange.

Kırmacı (2000) defined an Oxfordian – Portlandian shallow marine succession to the north of Bayburt (Uluçayır) and carried out a microfacies analysis. Benthic

foraminifer assemblage listed (e.g. *Protopeneroplis striata*, "*Archaeosepta*" *basiliensis*, *Everyicyclammina* sp., *Labyrinthina mirabilis*) suggests only the presence of Kimmeridgian without characteristic Tithonian taxa. His Oxfordian assignment to the lowermost part of the succession is also questionable.

Bucur et al. (2000) revisited the Nazlıçayır succession (Gümüşhane) and documented its dasyclade algae assemblages. They revised the previously assigned Late Aptian age for the uppermost parts of the Berdiga Limestone in the region by Kırmacı et al. (1996) and restricted the age span to Berriasian – Barremian for the carbonates overlying the dolomitic interval.

Yılmaz et al. (2000) provided further data supporting the paleogeographical configuration that the Eastern Pontides and Transcaucasus belong to the same geological belt representing an active southern margin of Eurasia.

Bektaş et al. (2001) described Liassic neptunian dikes in Variscan granites, and Albian and Campanian neptunian dikes in the Malm – Lower Cretaceous platform carbonates from the Amasya, Gümüşhane (Kale) and Kilop (Gümüşhane) regions. They interpreted these dikes to correspond to extensional tectonic regimes during Mesozoic. However, chronostratigraphic positions of those dikes were not documented in detail. Additionally, there are some strange interpretations like the following sentence: "The extensional cracks, filled with red pelagic, Albian limestones on the Malm – Lower Cretaceous carbonate platform, imply that the original contact between platform carbonates and overlying ophiolitic mélange was sedimentary, not tectonic."

Dokuz (2000) in his PhD study measured 3 sections, in the Yusufeli (Artvin) region, logging the Berdiga Formation. He preferred to use Berdiga Formation (sensu Pelin, 1977) over the Hozbirikyayla Limestone (of Ağar, 1977) since there are clastic deposits at the base of the carbonates (his explanation) overlying the Jurassic volcaniclastic Hamurkesen Formation (an equivalent of the Kelkit Formation). However, these carbonate rocks should belong to the calciturbiditic and pelagic carbonates of the Hozbirikyayla Limestone depending on the fossil lists provided by

Dokuz (2000; e.g., *Protopeneroplis striata*, *Pseudocyclammina lituus*, *Alveosepta jaccardi*, "*Conicosprillina*" *basiliensis*, *Protopeneroplis* "*trochangulata*", "*Tubiphytes*" *morronensis*, *Saccocoma* sp., *Tintinnopsella* sp., *Calpionellites darderi*, *Globigerina hoterivica*, "*Cadosina*" sp., *Meandrospira favrei*; a typical slope to basin fossil association). These carbonates pass upward into Upper Cretaceous turbidites (the Yusufeli Formation, an equivalent of the Gevenli Formation). This incorporation of the pelagic Lower Cretaceous carbonates into Berdiga Formation (*s. l.*) further introduced confusion on the upper age limit of the carbonate platform deposition in the Eastern Pontides (e.g., Dokuz et al., 2017).

Konak et al. (2001) reported the continuation of the north-vergent imbricated tectonic slices of the Bayburt region to the northeast into the Yusufeli – Olur region. The age interpretations on these tectonic units; however, is problematic. For example, they assigned a Barremian – Aptian depositional age for the carbonates present in their Öğdem Unit based on the fossil list including only *Microsolena* sp., *Stylosmilia* sp., radiolaria, pelecypod bivalves, sponge spuicules, echinoid plates and bryozoa as evidence. This age interpretation is a total fabrication that introduced only confusion to the age span of carbonate platform deposition in the Eastern Pontides.

Eren and Taslı (2002) examined the hardground surface on the uppermost strata of the Berdiga Limestone below the overlying Upper Cretaceous (Santonian) pelagic red limestones and marls (middle part of the Kermutdere Formation, an equivalent of the Kapanboğazı Formation). They documented detailed descriptions of this Kilop Hardground and Neptunian dikes. They interpreted the formation of this hardground as the result of break-up and subsidence of the Eastern Pontides carbonate platform during the formation of the Black Sea back-arc basin. However, they assigned again an improbable age to the uppermost portion; Early Aptian without demonstrable post-Hauterivian taxa (their *Praechrysalidina* sp. specimens should belong to *Redmondoides lugeoni*).

Koçyiğit and Altıner (2002) synthesized the previously published data from the Sakarya Zone with a newly introduced Ankara (İneköy) section to document the

tectonostratigraphic evolution of the North Anatolian Paleorift during the Hettangian – Aptian interval. They also erroneously suggested Kimmeridgian – Aptian age for the carbonate platform development over the Sakarya Zone.

Bucur et al. (2004) revisited the Nazlıçayır (Gümüşhane) section third time. In this study, they also included the strata below the dolomitic interval. They studied the benthic foraminifer assemblage and produced a picture very similar to the original work of Taslı (1990). They interpreted an Oxfordian – ?Barremian interval for these shallow marine carbonates. No zonation was suggested.

Yılmaz and Kandemir (2006) re-examined the extensional phases in the Eastern Pontides. They suggested Upper Jurassic – Cenomanian depositional age for the platform carbonates of the Berdiga Formation without any age data.

Şen (2007) demonstrated the subduction related geochemistry for the Jurassic volcanism in the Eastern Pontides that had been previously attributed to extensional regime since Şengör and Yılmaz (1981).

Koch et al. (2008) also carried out a study in the Nazlıçayır (Gümüşhane) succession. They mostly focused on the diagenetic features of the carbonates while proposed Oxfordian – Barremian depositional age. They interpreted the Jurassic basaltic level as a diabase sill, although, Taslı (1990) demonstrated gradational transition from volcaniclastics that intercalated with the basalt flow and the overlying neritic carbonates into the overlying pure carbonates. They revised the age of this level as Kimmeridgian (previously Oxfordian). Although, they showed all the stage boundaries clearly delineated in their log, no details on taxa were provided. They did not mention the disconformity described by Taslı (1990) on the same outcrop. Additionally, they noted that detailed biostratigraphy of the Berdiga Limestone is very problematic in the absence of orbitolinids which makes the presence of Barremian questionable.

Konak et al. (2009) revised the questionable age interpretations of Konak et al. (2001) and used well known lithostratigraphic units from the Western Pontides (e.g., Soğukçam Limestone of Altıner et al., 1991).

Kandemir and Yılmaz (2009) examined the *rosso ammonitico* facies of the Şenköy Formation (equivalent of the Kelkit Formation) and interpreted them as products of transgressive phases during the Early Jurassic rifting.

Ustaömer and Robertson (2010) tried to overcome an enormous task of revealing the Late Paleozoic – Early Cenozoic tectonic development of the Eastern Pontides (Artvin region). The Artvin Basin was interpreted as a supra-subduction rift associated with incipient arc magmatism which was inverted during the Late Middle Jurassic, partially eroded and covered by Upper Jurassic shallow marine deposits together with localized eruption of enriched basalts. The Late Jurassic – Early Cretaceous interval was characterized as the interval of pelagic carbonate deposition mixed with clastic influxes. The rest of the evolutionary history interpreted was similar to Okay et al. (1997). They also defined seven north-vergent tectonic slices. They proposed northward subduction of an oceanic lithosphere that created a back-arc rifting in the region that led to deposition of the Jurassic volcaniclastic series. Then, during the early Late Jurassic a topographic edifice collided with the Pontides that uplifted the region which immediately followed by the Late Jurassic – Early Cretaceous extensional collapse, after the consumption of this hypothetical crustal edifice, during which the Upper Jurassic – Lower Cretaceous carbonates deposited.

Vörös and Kandemir (2011) reported a Pleinsbachian brachiopod fauna (160 specimens, 13 species) from the *rosso ammonitico* facies of the Şenköy Formation (an equivalent of the Kelkit Formation) in the Gümüşhane region that shows Eurasian affinity and suggested that the Eastern Pontides was far from the Gondwana and close to the Eurasian margin of Tethys during the Early Jurassic.

Okay and Nikishin (2015) evaluated tectonic evolution of the southern margin of Laurasia in the Black Sea region and suggested presence of a single Tethys Ocean. They differentiated Avalonia- and Armorica-type terranes in the region. They

proposed Late Carboniferous amalgamation of the Sakarya Zone to Laurasia during the Variscan orogeny. Following the Cimmeride orogeny an extensional magmatic arc was established as a result of northward subduction of the Tethys Ocean. They proposed deposition of the Upper Jurassic – Lower Cretaceous neritic to pelagic carbonates over the southern margin of Laurasia during a break in subduction.

Dokuz et al. (2017) interpreted the Late Jurassic lava flows as submarine planar flows parallel to the bedding planes of the Upper Jurassic carbonates (the Berdiga Limestone) or the volcanoclastic deposits (the Kelkit Formation). They interpreted this Late Jurassic magmatism with subduction-related geochemical signatures as the product of the southward subduction of the Paleotethys oceanic lithosphere. The slab breakoff of this lithosphere would led to ascending up of the intraplate-type mafic lavas to the shelf surface during the Kimmeridgian (e,g., creating the Keçidere Basalt of Taslı 1997) followed by the formation of disconformity surfaces (Taslı, 1990) and the deposition of clastic sediments during an epirogenic movement. They still followed the model of Şengör and Yılmaz (1981) and still illustrate Albian – Cenomanian age for the uppermost level of the Berdiga Formation.

Soycan (2017) carried out a PhD study focusing on the biostratigraphy and systematics of radiolarian fauna in the Middle Jurassic and Upper Cretaceous volcaniclastic successions around Trabzon, Artvin, Bayburt and Erzurum regions of the Eastern Pontides. They assigned the observed Late Bajocian – Early Bathonian radiolaria assemblages to the unitary association zones (UAZs) of Baumgartner et al. (1995). The Late Cretaceous (Coniacian – Campanian) part of this thesis was later published by Soycan and Hakyemez (2018) that dealt with the calibration of radiolarian and planktonic foraminifera biochronology.

Kırmacı et al. (2018) studied the dolomitization history of the Upper Jurassic – Lower Cretaceous neritic carbonate succession introduced by Taslı et al. (1999) in the Başoba Yayla (Trabzon) and revealed two stages of dolomitization; the first one took place during the burial stage and the last dolomitization stage occurred during the Late Cretaceous when the region became a magmatic arc.

Özyurt et al. (2018) analyzed the geochemical characteristics of the Upper Jurassic – Lower Cretaceous platform carbonates in the Hazine Mağara (Gümüşhane) in terms of dolomitization and recrystallization history. They documented three types of replacive dolomites (i.e., microcrystalline dolomites, fabric-preserving dolomites and fabric-destructive dolomites) and a history of diagenetic processes including dolomitization, recrystallization, dissolution, silicification and pyrite mineralization (associated with the emplacement of the polymetallic mineralization at the top of the succession) that were highly affected by hydrothermal alteration.

Akdoğan et al. (2018) revealed the presence of Triassic magmatic activity in addition to the Late Jurassic volcanic arc episode in the Eastern Pontides through the study of the detrital zircons collected from the bottom and the top levels of the Jurassic volcanoclastic deposits (the Şenköy Formation) in Gümüşhane region. They proposed episodic northward subduction of the Tethys under the southern margin of Laurasia that hosted these volcanic arcs.

Vincent et al. (2018) tried to constrain the age spans of the discontinuities present in the Upper Jurassic – Lower Cretaceous shallow marine carbonates of the Eastern Pontides (Nazlıçayır section) by using Sr-isotopes and benthic foraminifera assemblages. They interpreted two major hiatuses that span the latest Kimmeridgian to Tithonian or Berriasian and the Hauterivian to Barremian, respectively. They correlated the measured section and the recorded hiatal events with the successions around the Black Sea. They realized that these unconformities do not coincide with eustatic lowstands, instead they correlate with Late Tithonian to Berriasian and Hauterivian to Early Aptian episodes of rifting in the Greater Caucasus and concluded that these subaerial exposures were caused by rift flank uplift during periods of regional extension. They disregarded the previously suggested mechanism of slab break-off (e.g., Dokuz et al., 2017) since the uplift would occur before the surface magmatism as suggested by lithospheric models (e.g., Davies & von Blanckenburg, 1995) not in the reverse order observed in the Gümüşhane succession. They suggested tracing of these unconformity surfaces into the offshore Black Sea to evaluate the exploration targets since subaerial exposure is often associated with

karstification and secondary porosity creation. Although the post-Kimmeridgian unconformity was first recognized by Taslı (1990), they set "documenting the presence of a major erosional disconformity within the lower part of the section not recognized by Koch et al. (2008)" as one of their aims. They used the same lithofacies units of Koch et al. (2008) with modifications at the exposure surfaces "newly" recognized. They did not propose a new biostratigraphical framework nor followed the schemes of Taslı (1990, 1993). They reported unusual benthic foraminifera associations with poor illustrations (i.e., not satisfying the identifications in most cases). They interpreted ?Late Callovian (or Oxfordian) to Latest Barremian (or earliest Aptian) depositional age span for the succession that was punctuated with the above-mentioned discontinuities depending on the combination of Sr-isotope ages and foraminifer assemblages.

Schlagintweit et al. (2019) documented the presence of *Barkerina dobrogiaca*, a Valanginian marker with Laurasian affinity from the Nazlıçayır (Gümüşhane) section. This foraminifer had been recorded under the name *Barkerina barkeriensis* or *Barkerina* sp. (e.g., Bergougnan, 1987; Taslı, 1990; Bucur et al.,2004; Koch et al., 2008; Eren & Taslı, 2002; Granier 2020b submitted in 2019 but published later).

Granier (2020b) revised the material of Vincent et al. (2018) and add calcareous algae data. He proposed completely contrasting age interpretations based on completely different benthic foraminifera (similar to well-documented Western Pontide assemblages) identifications from the same samples. He made the following conclusions: i. Kimmeridgian strata below the discontinuity, no record of Callovian and Oxfordian, ii. Valanginian to ?Lower Hauterivian strata above the unconformity, and iii. No Upper Hauterivian or Barremian strata at the top of the section. This revised picture is in accordance with successions and history of the Pontides carbonate platforms well-documented from the Western (e.g., Altıner et al., 1991) and Central (Rojay & Altıner, 1998; Kaya, 2014) Pontides. He went over picture-by-picture fossil identifications of Vincent et al. (2018; in which Boudagher-Fadel was responsible for micropaleontology) and demonstrated and corrected misidentifications. He suggested that the stratigraphic gap possibly corresponds to

the Berriasian and most, if not all, the Tithonian in the Nazlıçayır succession. He criticized the poor application of geochemical tools without solid biostratigraphy. Finally, Granier proposed this unconformity to mark the Jurassic – Cretaceous boundary in the area (*sensu* d'Orbigny and Oppel, cf. Granier, 2019).

Dokuz and Sünnetçi (2019) discovered Early Jurassic acidic magmatism in the Olur region, an interval dominated by basic magmatism in the Eastern Pontides. As a result, in accordance with Dokuz's earlier studies, they suggested that these Early Jurassic bimodal magmatic rocks developed in a back-arc setting during the southward subduction of the Paleotethys oceanic lithosphere.

Kandemir et al. (2022) carried out analysis of petrography and whole-rock major, trace and rare earth elements on the Jurassic Şenköy Formation and interpreted similar source areas and depositonal environment with the previous works; a deposition under well-oxygenated water column over a rift paleotopography fed by a volcanic arc to the north (over a south subducting Paleotethys oceanic crust) and exposed basement rocks. The subduction polarity in this study contradicts with the previous studies of the first author of this paper.

Akkemik et al. (2022) recorded the first fossil wood flora from the Şenköy Formation of the Eastern Pontides that suggests an abundant water supply under a relatively cool/humid climate. Although these floras show similarities with the contemporaneous records from Iran and Georgia, they do not allow sounding paleogeographical interpretations.

Özyurt et al. (2022) studied a Lower Cretaceous carbonate platform to slope successions of the Ayralaksa plateau (Trabzon). Paleotemperature analysis was carried out on belemnite samples from the overlying slope deposits that gave a temperature range of f 18.30–26.77 °C with an average of 23.13 °C during Albian. The stage boundaries are fuzzy and general time intervals were assigned to strata (e.g., Kimmeridgian - Hauterivian – Barremian – Aptian etc.) without any post – Hauterivian taxa similar to the age interpretation of Taslı et al. (1999) from the same region.

Eker and Arı (2023) analyzed geochemical characteristics of the Upper Jurassic – Lower Cretaceous carbonates from Gümüşhane region. They compiled samples from different levels of these carbonates from five different successions without age data. They provide average total organic carbon, types of kerogens and thermal maturity of the samples.

Kandemir et al. (2024) introduced large Fe-Mn oncoids from the Lower Jurassic *rosso ammonitico* strata of Gümüşhane region. The trace element data show hydrothermally introduced signatures. A rift-related volcanism during the deposition of these *rosso ammonitico* facies was put forward as the mechanism that introduced Fe, Mn, trace and rare earth elements into the seawater. Similar depositional settings are proposed as in the previous studies (e.g., Altıner et al., 1991; Varol & Gökten 1994; Kandemir & Yılmaz, 2009; Kandemir et al., 2022).

Özyurt and Kırmacı (2024) restudied the Kimmeridgian strata of the Nazlıçayır section in terms of microfacies and geochemical analysis to reveal paleoclimatic and paleoenvironmental conditions. They analyzed the trace and rare earth elements and stable isotope signatures of these peritidal carbonates. Organic chemistry data, to evaluate their hydrocarbon potential, was also obtained. These Kimmeridgian strata were interpreted to deposit in a shallow subtidal lagoon environment or a partly protected interior ramp depositional setting. They suggested an aridification event that controlled the (low) weathering input, organic matter source, productivity, evaporation and salinity enhancement. The over-maturation of organic matter has reduced the hydrocarbon potential.

In the current state summarized in this section, there are no detailed biostratigraphic and microfacies analyses of the Upper Jurassic - Lower Cretaceous platform margin-slope to basin carbonate deposits in the region. On a broader scale, looking at the biostratigraphic studies covering the Late Jurassic - Early Cretaceous interval in the Pontides, studies on shallow marine biozonation include Altıner (1991) in the western Sakarya Zone, Koçyiğit and Altıner (2002) in the Ankara region, Kaya and Altıner (2015) in the Central Pontides, Okay et al., (2017) and Rojay and Altıner

(1998) in the Amasya region, and Taslı (1990, 1993), Taslı et al. (1999), Bucur et al. (2000, 2004), Koch et al. (2008), Vincent et al. (2018) and Granier (2020b) in the Eastern Pontides. Biostratigraphic studies on deep marine deposits include Altıner and Özkan (1991), Özkan (1993, 1999), Mekik et al. (1999) in the western Sakarya Zone, and Bergougnan (1987), Tunç (1992) and Burşuk (1992) in the Eastern Pontides. Studies linking deep marine and shallow marine platform depositional environments using variety of fossil groups in platform margin-slope facies are relatively few (e,g,, Altıner, 1991; Atasoy et al., 2018). Worldwide, biostratigraphic studies conducted on slope deposits containing both pelagic and shallow marine fossil assemblages are quite few, but their importance has begun to be recognized (e.g., Bakhmutov et al. 2018). Although studies on the Upper Jurassic - Lower Cretaceous chronostratigraphy and especially the J-K boundary have accelerated recently, calibration of pelagic biotic events with shallow marine benthic biotic events has not yet been achieved.

1.5 Geological Setting

Turkey mainland has two major Gondwanaland-derived tectonic units, positioned on the opposite margins of the Tethys during most of the Paleozoic–Mesozoic interval, namely the Pontides to the north (on the southern continental margin of Laurasia) and the Anatolide-Tauride Block (*s.l.*, including the Menderes–Taurus Block and the Kırşehir Massif) to the south (on the northern margin of Gondwanaland) (Okay & Nikishin, 2015; Okay & Topuz, 2017; Kuznetsov et al., 2019). The Tethys Ocean was consumed by northward subduction under Laurasia and these two continents finally came together during the Alpine orogeny in the latest Cretaceous to Eocene continent-continent collision (Şengör & Yılmaz, 1981; Okay & Şahintürk, 1997; Ocakoğlu et al., 2019; Okay et al., 2020a, 2020b). Today, the İzmir–Ankara–Erzincan (İAE) Suture zone separates these two units and represents the boundary between Laurasia and Gondwanaland in Anatolia (Okay & Tüysüz, 1999; Fig. 1.3 & 1.6).

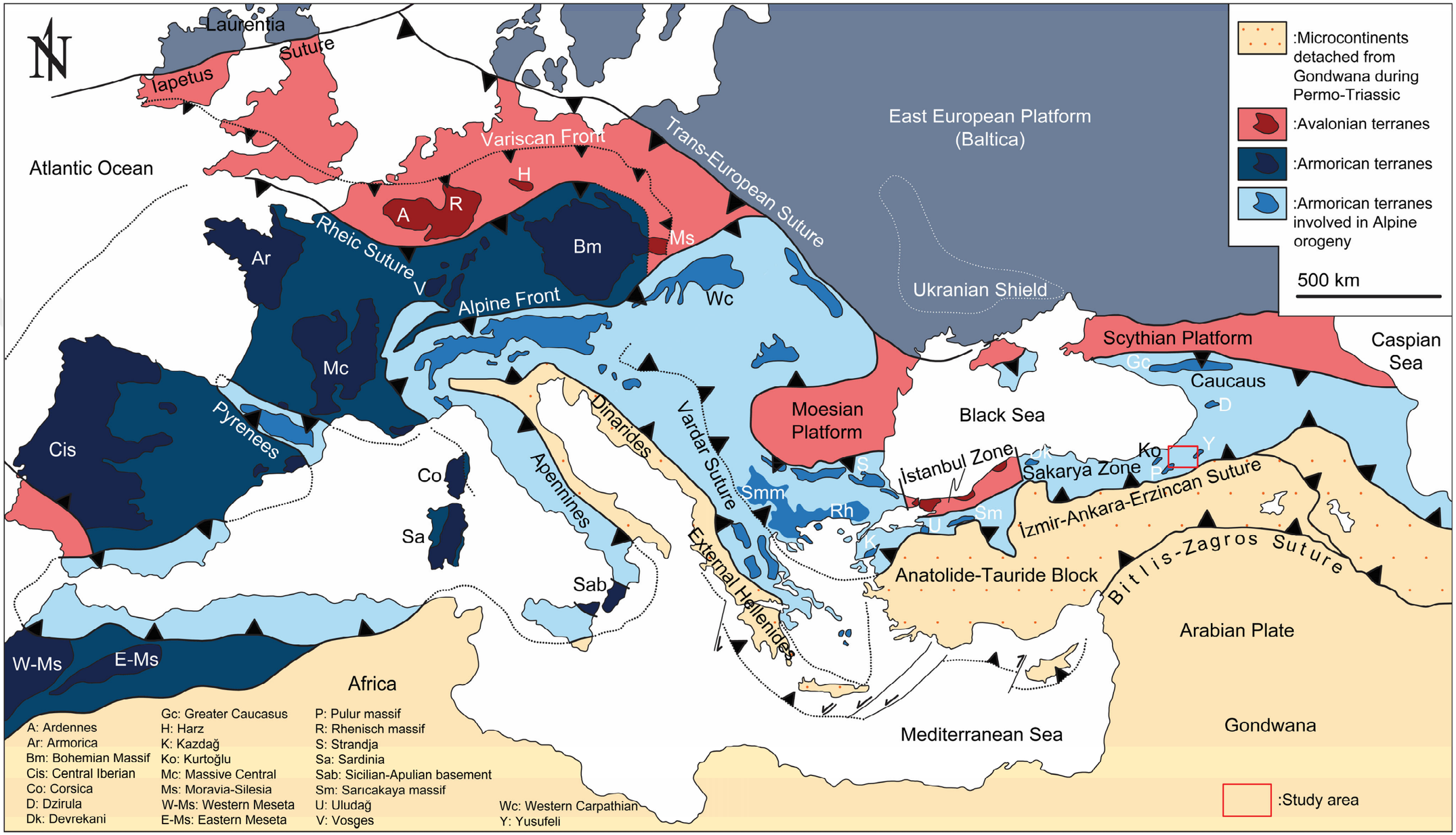

Figure 1.6. Simplified tectonic map of the Europe and Mediterranean and Black Sea regions, showing main Phanerozoic sutures (modified after Neubauer, 2002; Okay et al., 2008; von Raumer et al., 2013; Schmidt et al., 2019, Topuz et al., 2020; Akdoğan et al., 2021; Topuz et al., 2024). Triangles indicate subduction polarities.

The Pontides consist of three tectonic entities: the Sakarya and İstanbul Zones and the Strandja Massif (Okay & Tüysüz, 1999). The main difference between the İstanbul and the Sakarya Zones, separated by the Intra-Pontide Suture, lies in their pre-Jurassic stratigraphy. The İstanbul Zone is an Avalonia-type terrain that is characterized by an upper Neoproterozoic crystalline basement (Ustaömer et al., 2005; Bozkurt et al., 2008; Okay et al., 2008; Okay & Nikishin, 2015) and an overlying Paleozoic sedimentary succession (e.g., Görür et al, 1997; Özgül, 2012; Fig. 1.6). On the other hand, the Sakarya Zone shows affinity to Armorican terrains with its Carboniferous plutonism (and related high temperature metamorphism) and metamorphosed Lower Paleozoic sequences (Okay & Nikishin et al., 2015; Okay & Topuz, 2017; Topuz et al., 2019; 2023; Fig. 1.6; 1.8). The Strandja Massif has dissimilar Jurassic – early Late Cretaceous evolution with Late Jurassic deformation and metamorphism and lack of carbonate deposits of this interval (Okay et al., 2001; Sunal et al., 2011).

The carbonates of the Upper Jurassic – Lower Cretaceous PCP deposited over both the Sakarya and İstanbul Zones in the Central Pontides (Tüysüz, 1999; Okay et al., 2018). These two tectonic units seem to have come together before the Kimmeridgian at least in the Central Pontides transect of the Intra-Pontide Suture (e.g., Okay et al., 2018; Akdoğan et al., 2021; Okay et al., 2024; Fig. 1.3 & 1.6).

In the Sakarya Zone, the PCP developed over a structural basement shaped by the Carboniferous Variscan orogeny (e.g., Göncüoğlu et al., 2000; Topuz et al., 2007; Dokuz et al., 2011; Okay & Topuz, 2017; Topuz et al., 2023) and the Late Triassic to (?Late) Jurassic subduction-accretion of the Karakaya Complex (*s.l*) and related oceanic edifices (e.g., Okay & Göncüoğlu, 2004; Robertson & Ustaömer, 2012; Göncüoğlu et al., 2012; Sayit & Göncüoğlu, 2013; Okay et al., 2015; Çimen et al., 2018; Okay et al., 2020b; Marroni et al., 2020). The Eastern Pontides form the easternmost part of this geological unit, sharing the similar basement rocks, in the Turkey mainland.

Geographically, the Eastern Pontides is a loosely defined term used for the region skirting the Eastern Black Sea coast of Turkey. Its western boundary is taken arbitrarily either as the Yeşilırmak or Kızılırmak river near Samsun. Tectonically, it forms the eastern part of the Sakarya Zone of the Pontides. It is bounded in the south by the Ankara-Erzincan Tethyan suture belt and in the north by the East Black Sea Basin; in the east, it extends without a break into the Lesser Caucasus, where it can be correlated with Achara-Trialet and Artvin-Karabakh zones (e.g., Yılmaz et al., 2000). Its western geological boundary with the Central Pontides is stratigraphic and corresponds to facies change in the Cretaceous sequence (e.g., Okay et al., 2018; the Çağlayan Formation).

The Eastern Pontides is commonly divided into an inner/ southern and an outer/ northern part (e.g., Akın, 1978; Okay & Şahintürk, 1997; Konak et al., 2001, 2009). The outer Eastern Pontides are dominated by Senonian and middle Eocene volcanic and volcanoclastic rocks, which hide much of the pre-Senonain geology. On the other hand, pre-Senonian rocks are widely exposed in the inner Eastern Pontides, which occupied a fore-arc position during the Senonian and underwent much more intensive deformation than did the outer Eastern Pontides during the Early Tertiary continental collision (e.g., Şengör & Yılmaz, 1981; Okay & Şahintürk, 1997). The transitional boundary between these two parts follows approximately the Niksar-Gümüşhane-Ardunç line (Fig. 1.4).

The pre-Jurassic basement of the Eastern Pontides consists of the Early Carboniferous high temperature metamorphics (the Pulur Massif; e,g., Okay, 1996: Topuz et al., 2004; Dokuz et al., 2011; Topuz et al., 2023), the Carboniferous Gümüşhane and Köse Granotoids (e.g., Yılmaz, 1976; Topuz et al., 2007, 2023), the Upper Carboniferous – ?Lower Permian sedimentary successions with coal intercalations (the Çatalçeşme and Hardişi Formations; e.g., Ketin, 1951; Akdeniz, 1988; Okay & Leven, 1996; Çapkınoğlu, 2003; Kandemir & Lerosey-Aubril, 2011) and the Permian – Triassic metamorphics (metabasite – marble -phyllite of the Ağvanis Massif; e.g., Nebert, 1961; Okay, 1983; Rojay, 1985; Topuz et al., 2014; Fig. 1.4, 1.7 & 1.8).

Transgressive Liassic deposits unconformably overly these basement rocks. The Jurassic successions are mainly characterized by widespread volcaniclastics with coal levels and intervals of *rosso ammonitico* – type condensed deposits. This Kelkit Formation shows deepening in its facies towards the south with increasing occurrence of deeper turbidites and limestone olitoliths (Ketin, 1951; Nebert, 1961; Wedding, 1963; Pelin, 1977; Bergougnan, 1987; Görür et al., 1983; Robinson et al., 1995; Okay & Şahintürk, 1997). *Rosso ammonitico* deposits can directly overlie basement rocks without intervening clastics (e.g., southern and eastern regions of Gümüşhane – Kale line; Taslı, 1990; Kandemir & Yılmaz, 2009; Fig. 1.4 & 1.8). These volcaniclastics were previously assumed to be products of a rifting phase (e.g., Şengör et al., 1980; Görür et al., 1983; Yılmaz et al., 1997). Recent studies interpret them as the products of subduction that characterized the southern margin of Laurasia during Toarcian – Oxfordian interval (e.g., Şen, 2007; Meijer et al., 2010; Okay et al., 2014; Dokuz et al., 2017; Akdoğan et al., 2018).

The Kelkit Formation is overlain by the carbonates of the Berdiga Limestone *s.l.* (Pelin, 1977; Rojay, 1985; Taslı, 1990; Kırmacı, 1992; Robinson et al., 1995; Okay et al., 1997; Kırmacı, 2000; Koch et al., 2008; Fig 1.4 & 1.8). These carbonates show a major differentiation in facies in the Late Jurassic (Okay et al., 1997). The northern regions are characterized by the shallow marine carbonates started to deposit in the Oxfordian – Tithonian interval (Fig. 1.4; Pelin, 1977; Rojay, 1985; Yılmaz, 1989; Taslı, 1990; Kırmacı, 1992; Yılmaz, 1992; Taslı, 1993; Robinson et al., 1995; Yılmaz, 1997; Taslı et al., 1999; Timur, 2000; Kırmacı, 2000; Bucur et al., 2000; Bektaş et al., 2001; Eren & Taslı, 2000; Bucur et al., 2004; Koch et al., 2008; Kandemir & Yılmaz, 2009; Özyurt et al., 2018; Kırmacı et al., 2018; Vincent et al., 2018; Granier, 2020b; the Berdiga Limestone *s.s.* and the Çaltepe Limestone). In contrast, pelagic calciturbidite and biomicrite deposition, started in the Tithonian, characterized the southern regions (Fig. 1.4 & 1.8; Ketin, 1951; Burşuk, 1975, 1981,1992; Tunç, 1992; Okay et al., 1997; the Hozbirikyayla Limestone). The emplacement of an ophiolitic mélange in the southern Eastern Pontides during the Cenomanian – Turonian interval disrupted the carbonate deposition (Okay et al.,

1997). The following uplift and erosion phase completely eroded these carbonate deposits in places (e.g. Alucra region, Pelin, 1977). The Campanian carbonates can directly overly the Jurassic successions (e.g., Pelin, 1977; Bergougnan, 1987; Robinson et al., 1995; Eren & Taslı, 2002) or Carboniferous granitoid basement rocks, as in the Gümüşhane region (Yılmaz, 1972; Fig 1.4 & 1.8). The youngest known age of the northern shallow marine carbonates is Hauterivian or ?Barremian (Pelin, 1977; Bergougnan, 1987; Koch et al., 2008; Vincent et al., 2018; Granier, 2020b). The upper age of the southern deep marine carbonates has been reported as Aptian – Albian (Burşuk, 1981; Okay et al., 1997; Taslı & Özsayar, 1997). In the Maden region (near the contact with the ophiolitic mélange) Albian ages have been reported (Elmas, 1994; Robinson et al., 1995). The inner Eastern Pontides were deformed during the Paleocene – Eocene continent-continent collision and shortening compensated by the north-vergent thrust stacks that thrust over the para-autochthon shallow marine successions of Cebre unit (Fig.1,4, 1.7 & 1.8; e.g., Bergougnan, 1976; Okay et al., 1997). The tectonic relationships and stratigraphy of these units with a simplified cross section and stratigraphic columns are summarized in Figure 1.7.

The measured sections are located in the İmalıdağ and Aşutka Thrust Sheets and in the Gümüşhane region which can be thought as the northern equivalent of the Cebre relative autochthon (Fig. 1.8). This distribution of the study areas enabled recording of both shallow marine and slope to basin deposits of the PCP. The geological maps of the study areas are given in the following figures (Fig. 1.8, 1.9, 1.10 & 1.11).

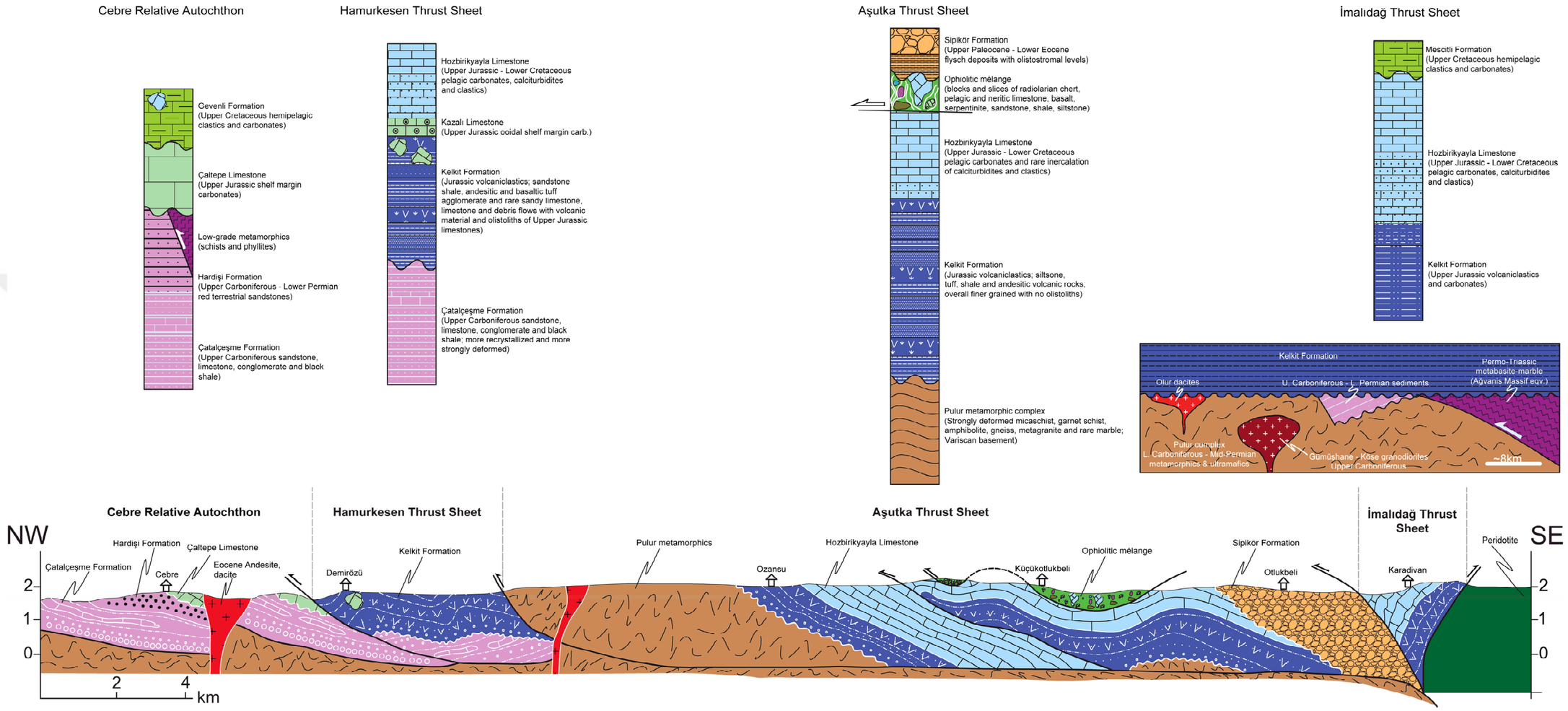

Figure 1.7. Simplified cross- and columnar-sections of the thrust sheets and allochthonous unit in the Pulur (Bayburt region). The smaller sketch cross-section summarizes the relationship of the basement rocks and the basal deposits of the unconformably overlying Mesozoic cover (modified from Bergougnan, 1987; Akdeniz, 2011; Okay et al., 1997; Dokuz et al., 2011; Karslı et al., 2012; Topuz et al.,2023; and personal observations. For cross section line see Figure 1.4.

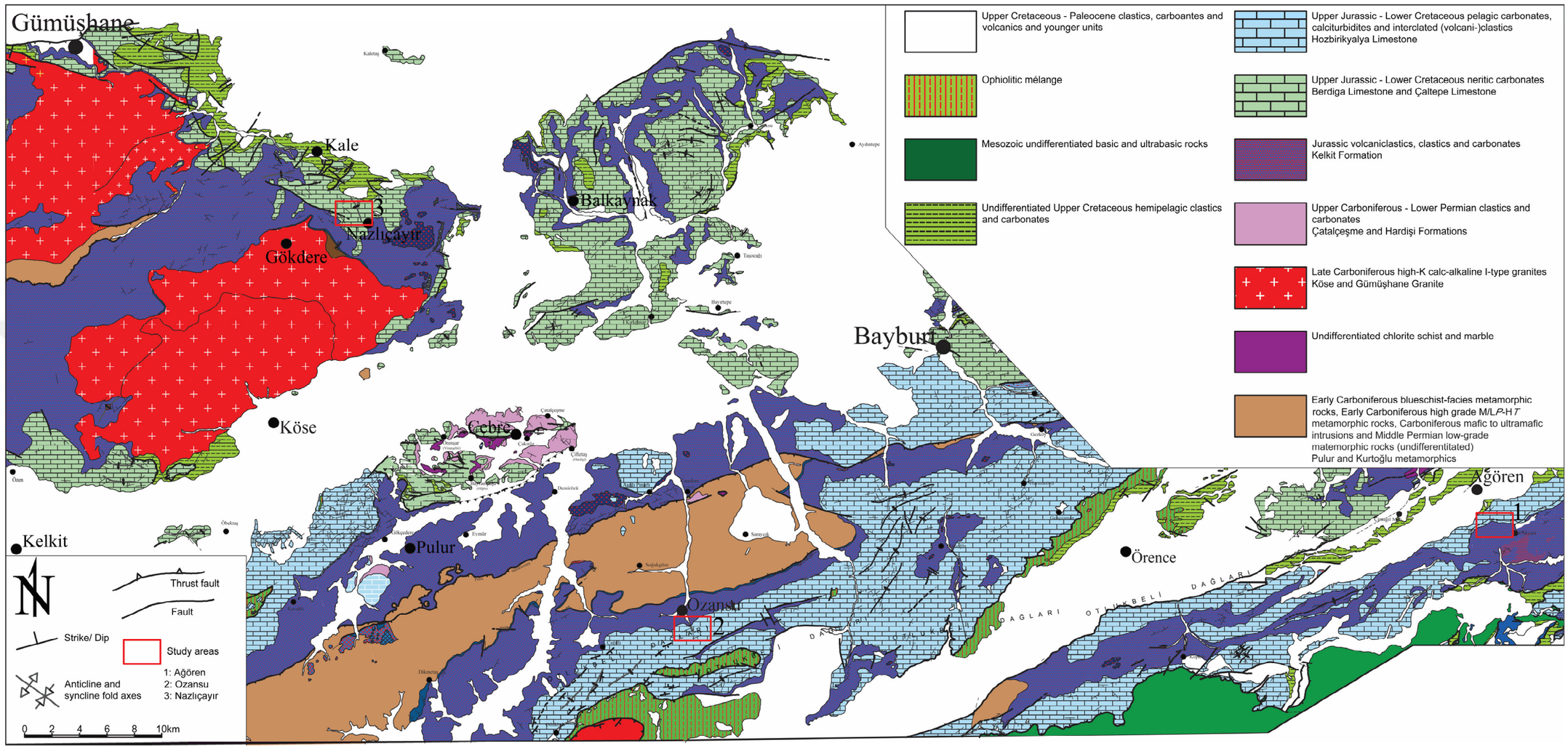

Figure 1.8. Geological map of the study area and locations of the measured sections (modified from Okay et al., 1997: Topuz et al., 2023 and MTA, 2011, 2016a, b, c, 2018).

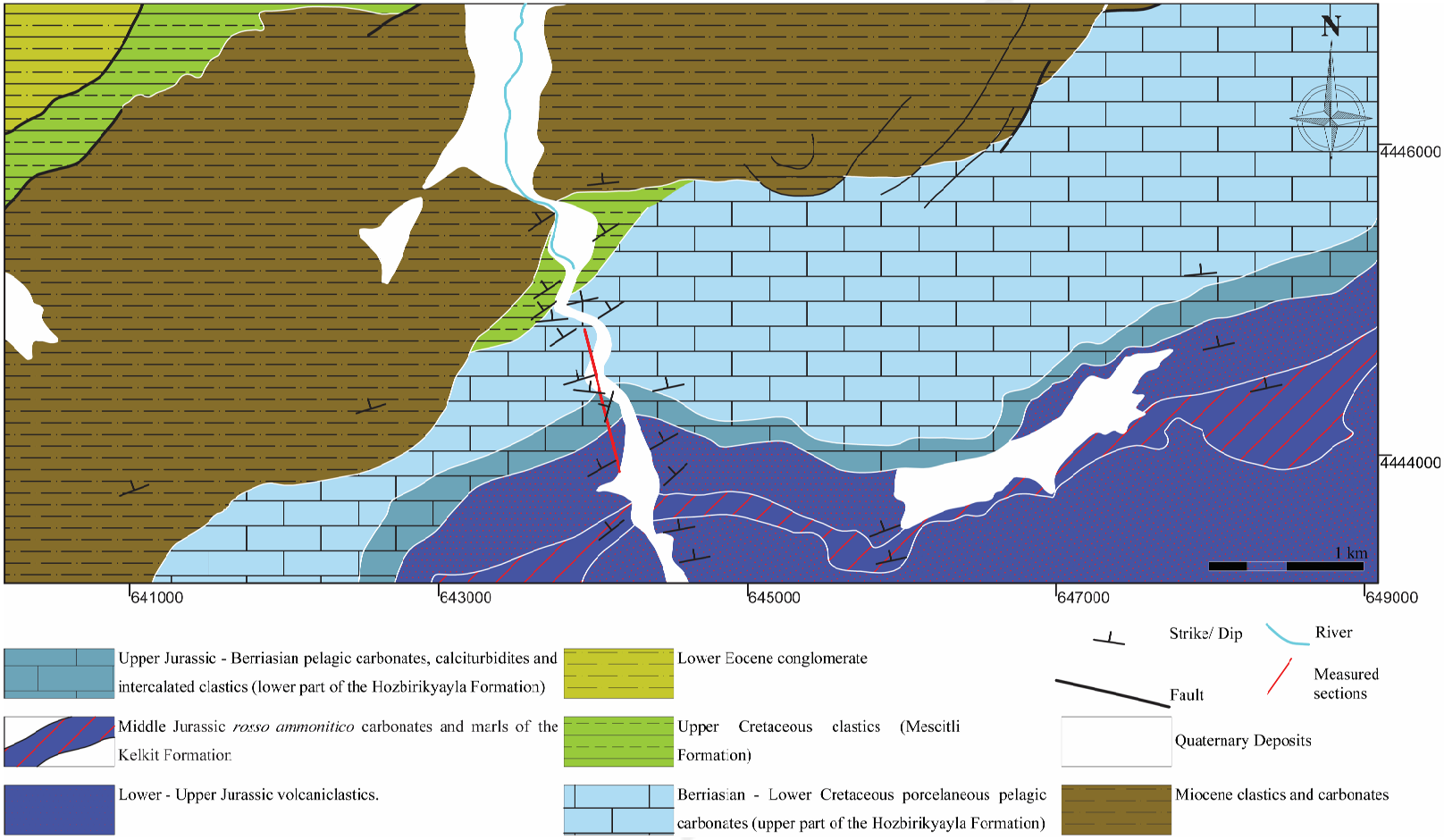

Figure 1.9. Geological map of the Ağören - Akyazı region and location of the Ağören measured section (modified from Akdeniz, 1989).

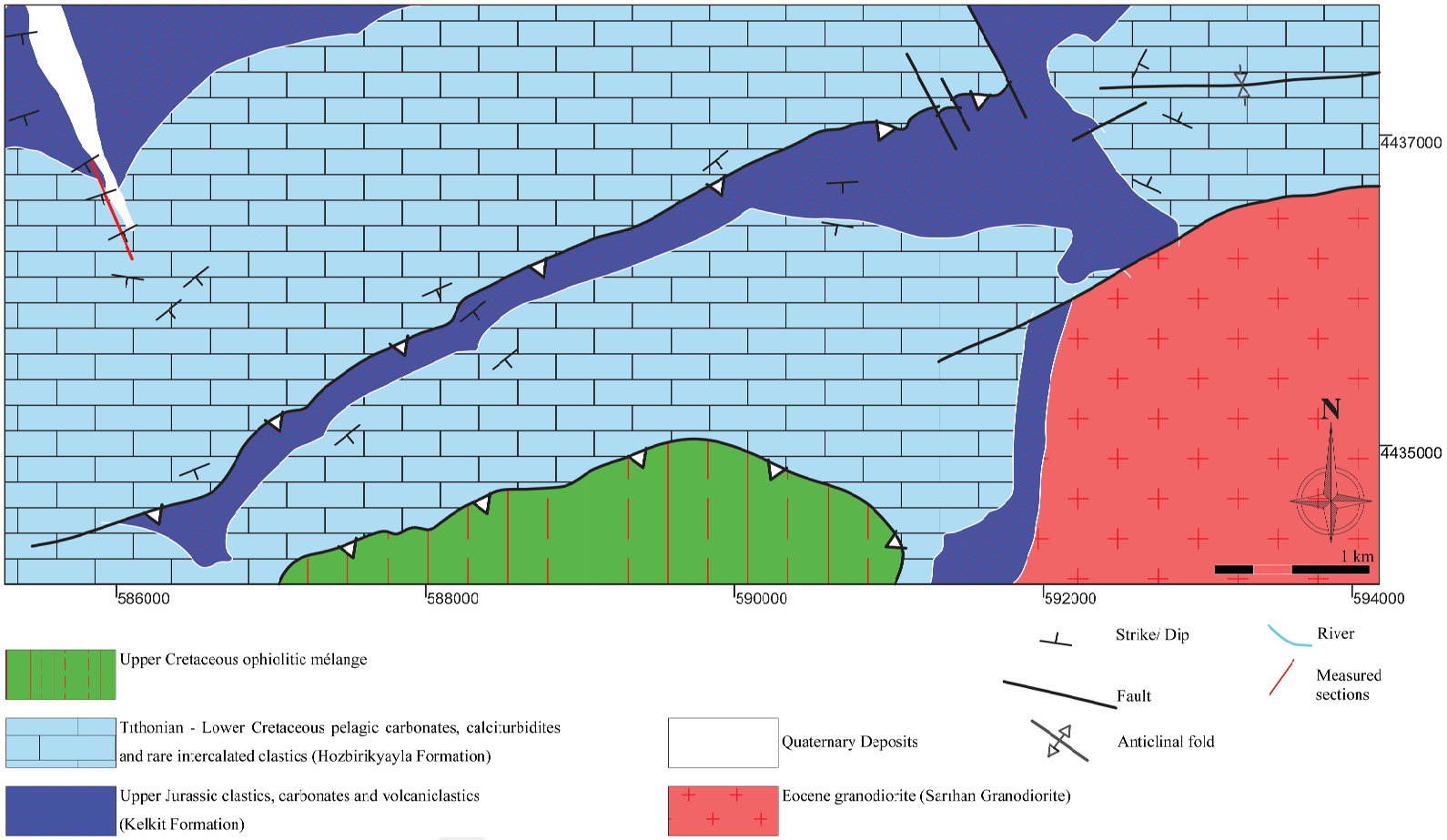

Figure 1.10. Geological map of the Ozansu (Bayburt) region and the location of the Ozansu (OA & OB) measured sections (modified from Korkmaz, 1984).

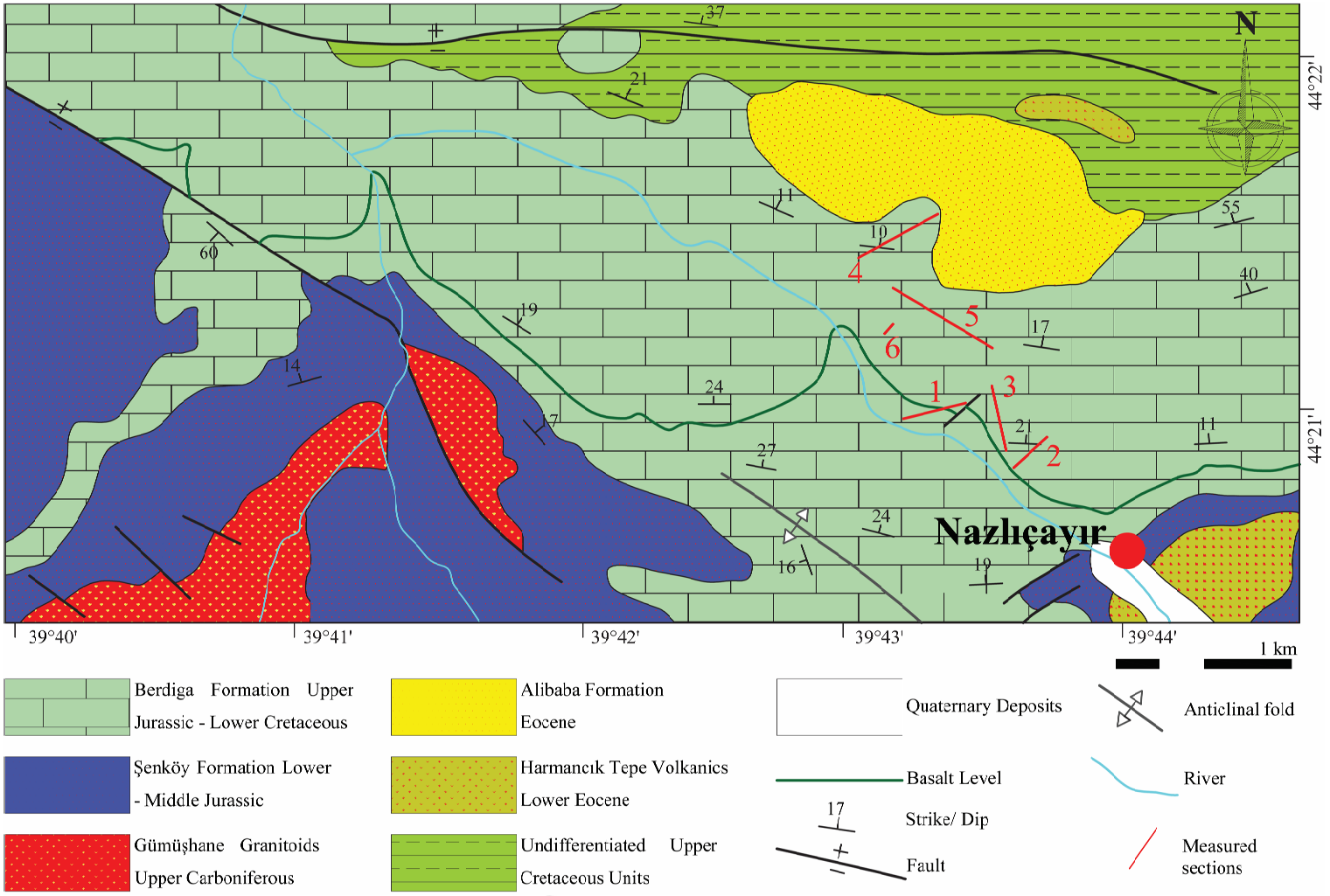

Figure 1.11. Geological map of the Nazlıçayır (Lörikas) region and the location of the Nazlıçayır measured section (modified from Kırmacı et al., 1996; Vincent et al., 2018). The stratigraphic section produced by correlating and combining six short detailed measured sections shown on the map.

CHAPTER 2

STRATIGRAPHY

In this chapter, stratigraphic details of each measured section are given in order from southernmost tectonic units towards the northern ones: i.e., details from pelagic deposits to slope deposits will be reported then the shallow marine platform successions are documented. Firstly, lithostratigraphy of each succession will be detailed and then biostratigraphy and age interpretations will be discussed. The studied Upper Jurassic – Lower Cretaceous neritic and pelagic successions will be correlated by both classical biozonation concepts and quantitative biostratigraphy methods. The basinal and shallow marine Late Jurassic – Early Cretaceous bioevents will be calibrated through the application of Graphic Correlation and Unitary Association Zone methods. The possible shallow marine benthic biohorizons for the delineation of the Upper Jurassic – Lower Cretaceous stages in neritic deposits and their relative positions with respect to well-established pelagic biozonation schemes will be determined. The proposed two alternatives (the base of the Berriasian, e.g., Wimbledon, 2017; or the base of the Valanginian, e.g., Granier, 2019) for the determination of the unstandardized J/K system boundary will be tested and the utility and practicality of both levels will be explored. The chronostratigraphic positions of the neritic and pelagic bioevents with respect to the Upper Jurassic – Lower Cretaceous stage boundaries will be documented and discussed.

2.1 Lithostratigraphy

Studied successions characterize slope to basin and shallow marine deposits of the Upper Jurassic – Lower Cretaceous PCP. Accordingly, slope to basin pelagic succession will be documented first, then shallow marine deposits will be detailed.

2.1.1 Slope to Basin Pelagic Successions

The Ağören and Ozansu measured sections represent the slope to basin depositional settings of the eastern part of the PCP. The lithostratigraphy of each succession is detailed below.

2.1.1.1 Ağören Measured Section

The Ağören section is located on the northern flank of the Otlukbeli Mountains to the south of Ağören village (north of Akyazı village; Fig, 1,5, 1.8 & 1.9). Tectonically, it belongs to the Imalıdağ thrust sheet (Yılmaz, 1985; Bergougnan, 1987 and Okay et al., 1997; Fig. 1.7). A total of 294 samples were collected along the 589-meter-long Ağören section. The field logging was carried out by bed-by-bed measurements and descriptions. The Ağören section is given in Figure 2.3 (a high-resolution version can be found in Appendix A). Microfacies types, interpreted depositional environments and fossil content for each sample are given in Appendix B.

The bottom levels of the section are characterized by the deep marine clastic turbidites of the Kelkit Formation (Fig. 2.1 & 2.3). The thickness and frequency of the marl and limestone intervals increase towards the middle parts of the succession. The sandstone beds commonly show sole marks and fining upward trends (Fig. 2.1C, D, H). These polygenetic sandstone beds include rock fragments (mudstone, limestone, metamorphic and volcanic rock fragments), ooids, minor microfossils and variety of minerals (quartz, feldspar, glauconite and mica minerals). The limestone

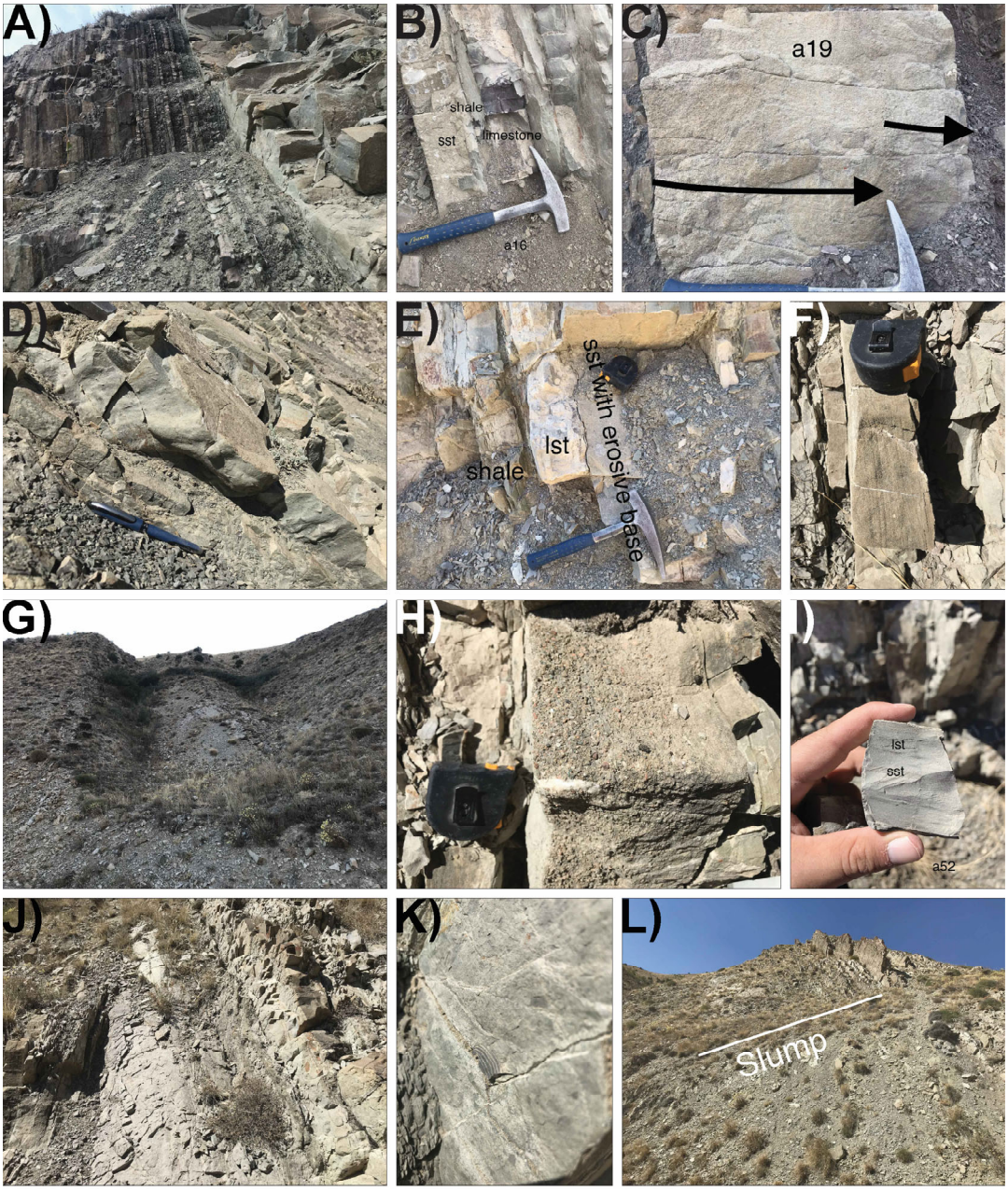

Figure 2.1. The bottom levels of the Ağören measure section. **A)** The view of the clastic turbidites at the bottom levels of the section. Shale, mudstone, siltstone alternations dominate these levels with minor marl and limestone intercalations (AP1). **B)** A close-up view of a sandstone, shale and limestone alternation (AP6). **C)** A sandstone bed with two upward-fining cycles (AP7). **D)** Sole mark at the bottom surface of the sandstone beds (AP9). **E)** Shale, limestone and sandstone alternation. Sandstones have erosional bottom surfaces (AP12). **F)** Sandstone bed with cross laminations (AP18). **G)** Slump interval between two undeformed levels (AP16). **H)** Fining upward polygenetic sandstone bed, conglomeratic at the base (AP18). **I)** Very

Figure 2.1 (*continued*) thin clastic laminations within limestone bed (AP23). **J)** Another short slump interval between two undisturbed bedded levels (AP19). **K)** An aptyhcus at the bottom of a sandstone bed (AP29). **L)** Another slump interval (AP21). Towards the middle and upper parts of the succession, the thickness and frequency of the slump intervals increase. The "AP" label with numbers indicates the levels of the photographs on the measured section (Fig. 2.3). Each photograph level is shown on the measured sections. lst: limestone, sst: sandstone, w: with.

beds that intercalate with these clastics are rarely pure carbonate rocks. They commonly have clastic inputs as thin laminae (Fig. 2.1I). The thickness and frequency of the slumped intervals increase towards the middle part of the section (Fig. 2.1G, J, L & 2.3). The Kelkit Formation passes into the overlying Hozbirikyayla Formation at the 193 m level (Fig. 2.3).

The Hozbirikyayla Formation is composed of deep marine deposits dominated by carbonates with minor clastic intercalations (Fig. 2.2 & 2.3). The most distinctive feature of this formation is the porcelaneous carbonates (Fig. 2.2) that form laterally traceable stratigraphic level in the Eastern Pontides. These pelagic carbonates commonly show intercalations of shale at the lower parts (Fig. 2.2A). Some coarse-grained sandstone intercalations are also present (Fig. 2.2B). These observations indicate that even these carbonate-dominated levels still received clastic input from the shelf environment. These sandstone beds commonly show erosional basal contact (Fig. 2.2B, D). The Jurassic/Cretaceous System boundary is delineated within this formation (Fig. 2.2C & 2.3, Appendix B). Thick slumped intervals are common features of the Hozbirikyayla Formation. While the thickness of these intervals can reach 100 m (Fig. 2.2J & 2.3), the lower and upper contacts of the slumped intervals are easily recognizable and traceable (Fig. 2.2E, I). The uppermost part of the section is characterized by the porcelaneous pure pelagic limestones with chert nodules and laminae (Fig. 2.2K). These levels show rare shale intercalations. The Hozbirikyayla Formation is unconformably overlain by the Upper Cretaceous flysch deposits to the north of the measured section (Fig. 1.9 & 2.2L).

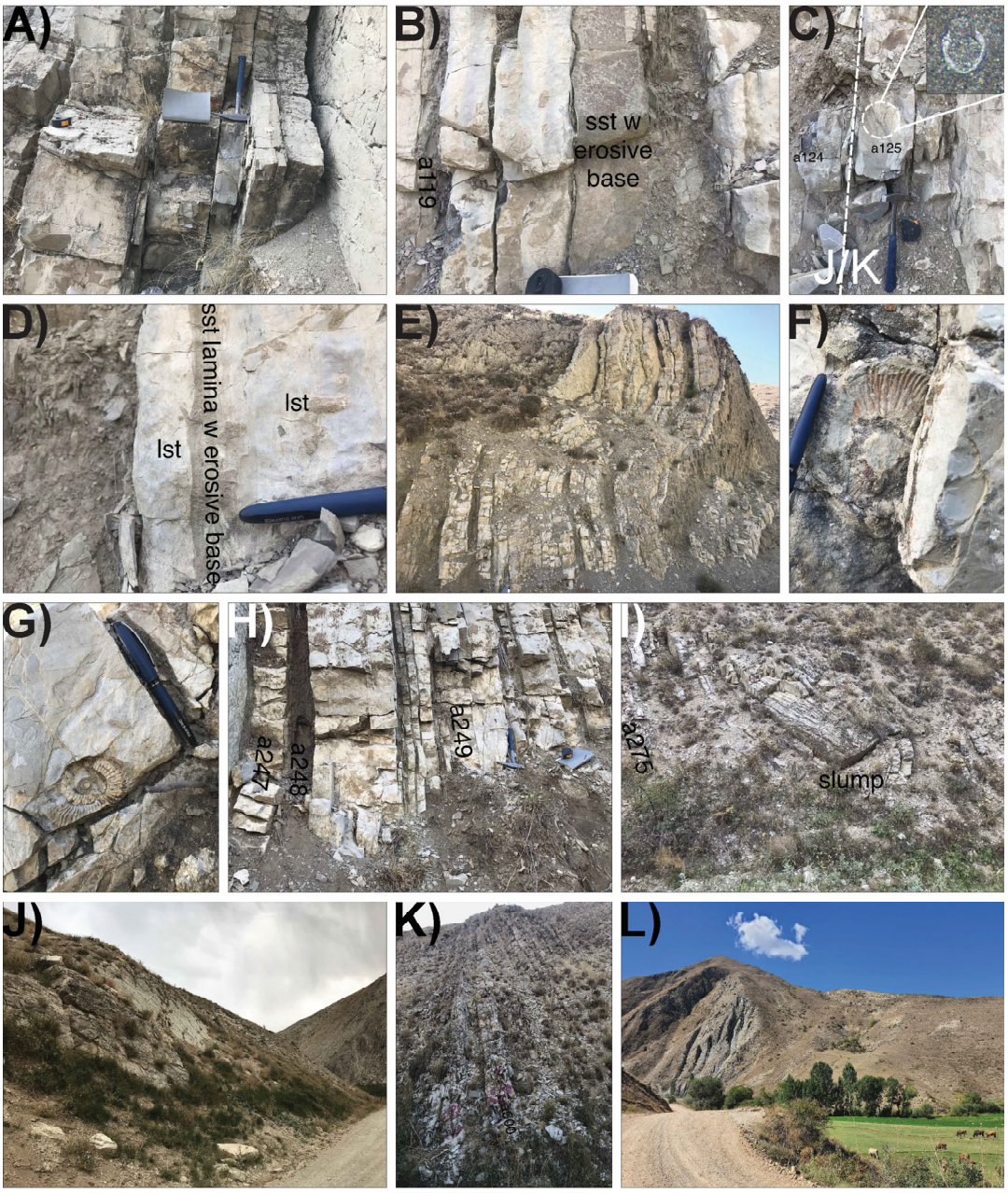

Figure 2.2. The general view of the middle and upper levels of the Ağören measured section. **A)** Porcelaneous limestone beds of the Hozbirikyayla Formation with shale intercalations (AP34). **B)** Limestone, sandstone and shale intercalations. The sandstone beds commonly show erosive bases (AP36). **C)** Field view of the Jurassic/Cretaceous (Tithonian/Berriasian) boundary. The boundary is between the samples A-124 and A-125 (AP38). The boundary is delineated by the acme of *Calpionella alpina* calpionellid species. The inlet shows a microphotograph of a *C. alpina* individual in sample A-125. **D)** An intercalated sandstone lamina with erosive base within a limestone bed (AP37). **E, I, J)** The slump intervals get thicker and their frequencies also increase toward the middle and upper parts of the succession (AP44,

Figure 2.2 (*continued*) AP64). **F, G)** Ammonites at the limestone bedding planes (AP55, 56). **H)** A view of the shale intercalated levels (AP61). **K)** The uppermost level of the section is characterized by the porcelaneous pure pelagic carbonates. **L)** The general view of the angular unconformity between the Hozbirikyayla Formation and the overlying flysch deposits. lst: limestone, sst: sandstone, w: with.

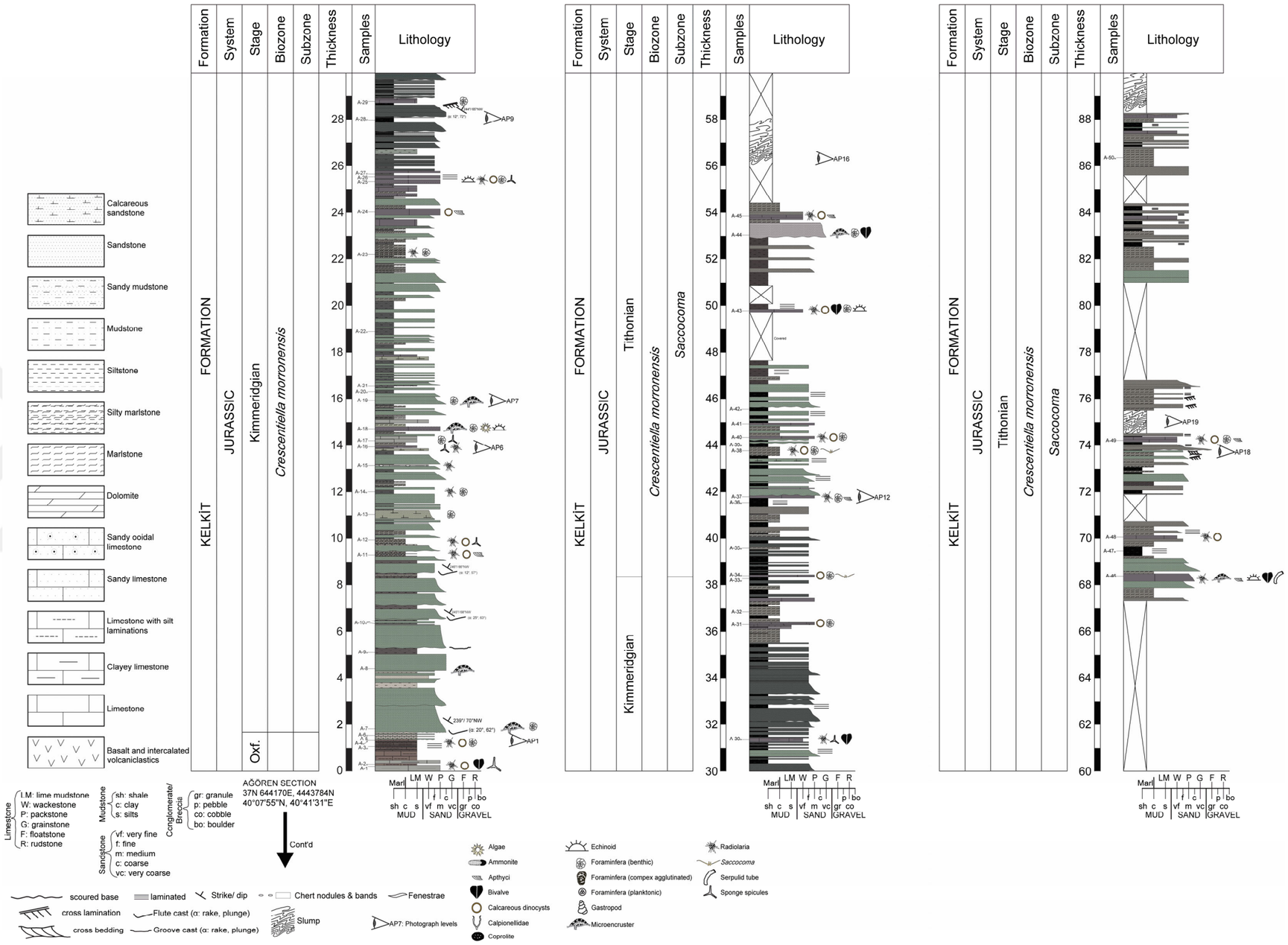

Figure 2.3. Ağören measured section. The legend is common to all measured sections.

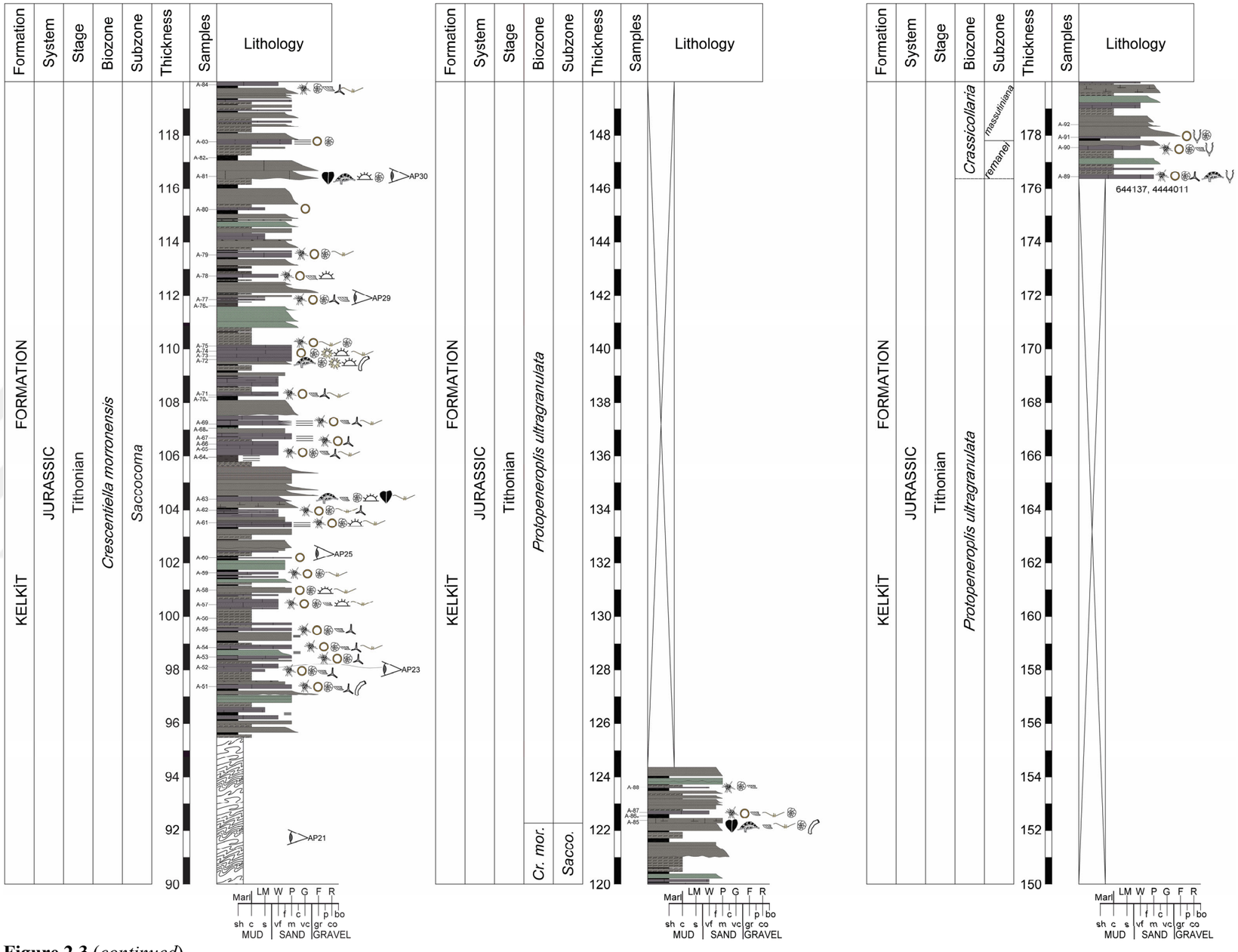

Figure 2.3 (*continued*)

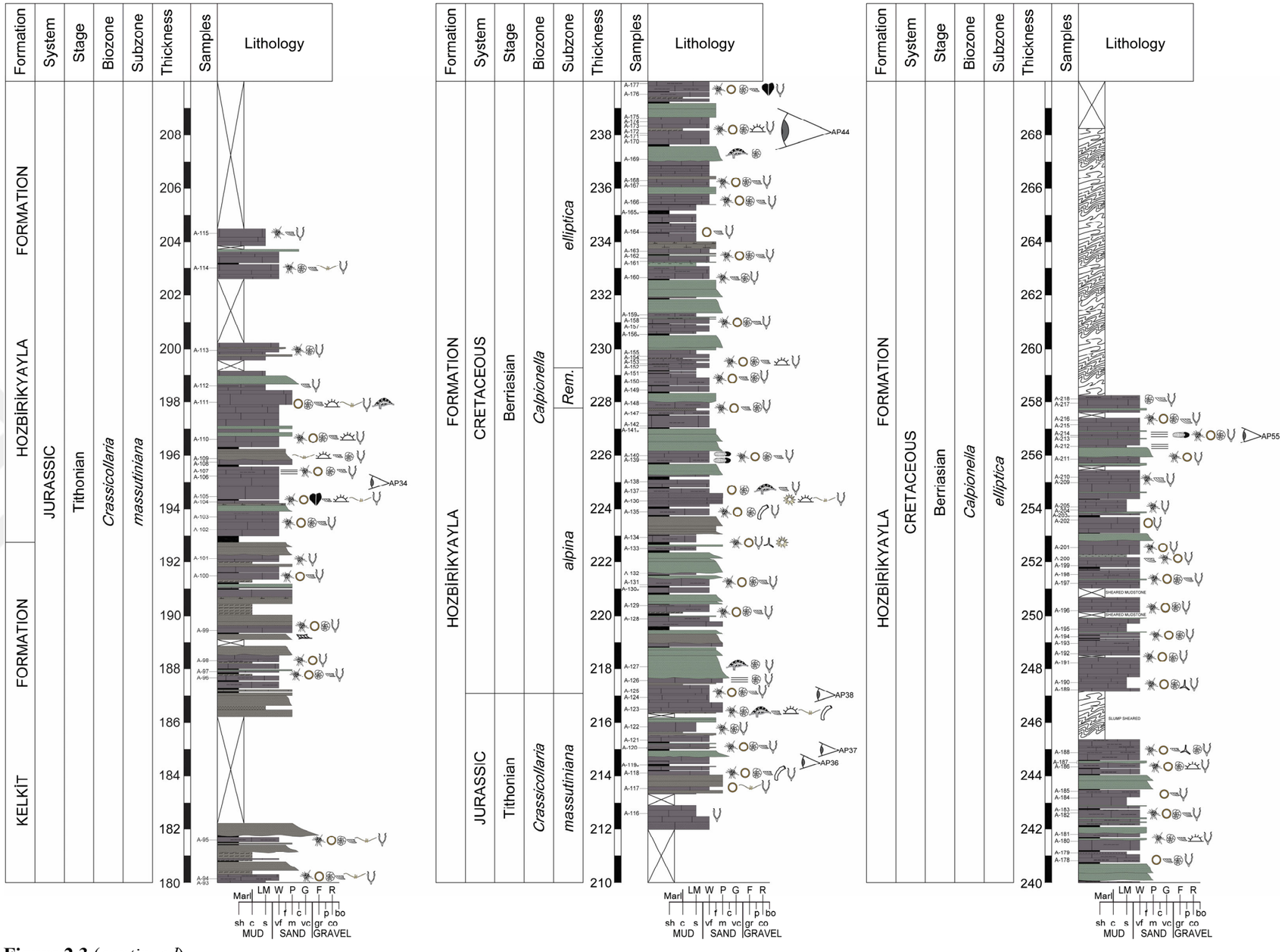

Figure 2.3 (*continued*)

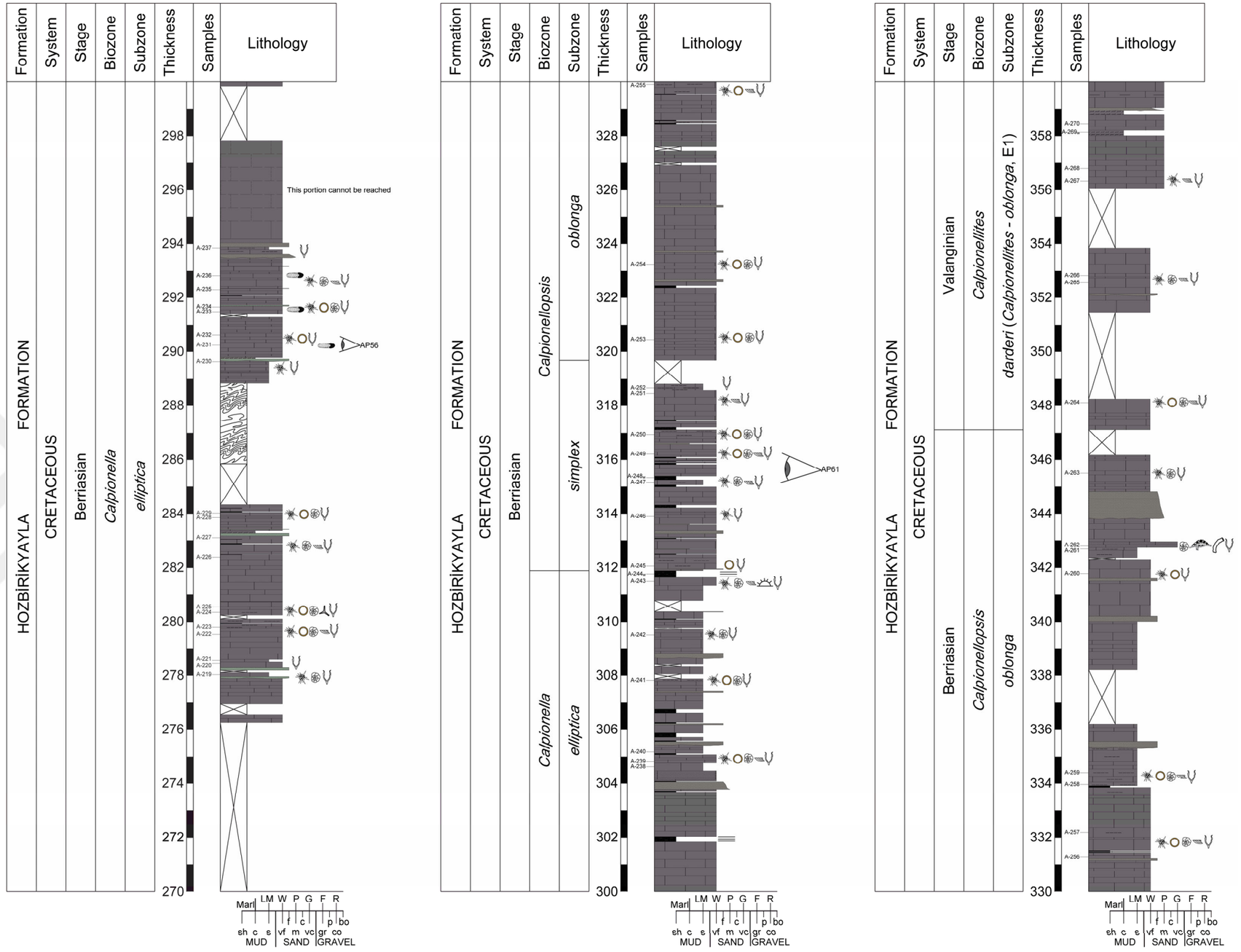

Figure 2.3 (*continued*)

Figure 2.3 (*continued*)

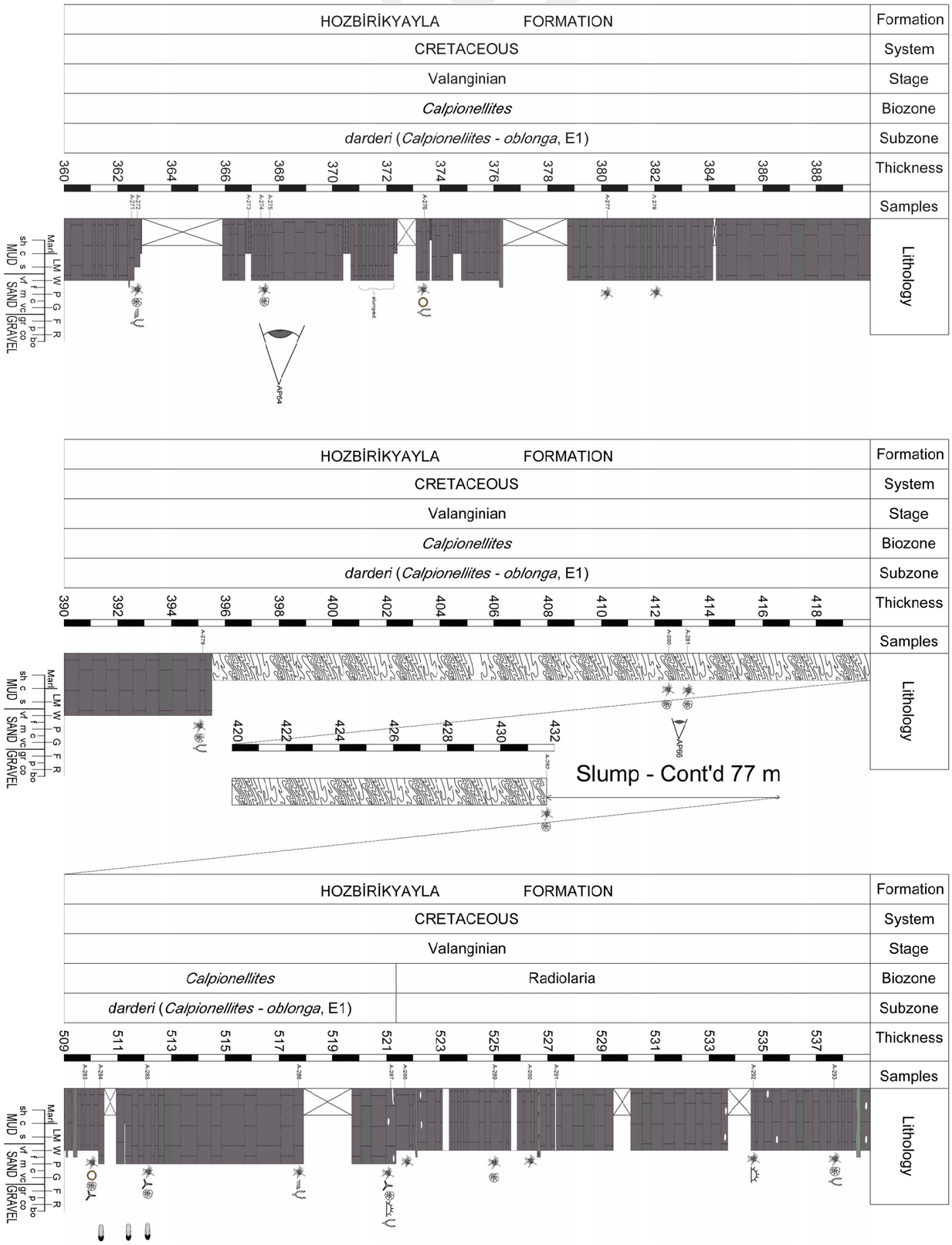

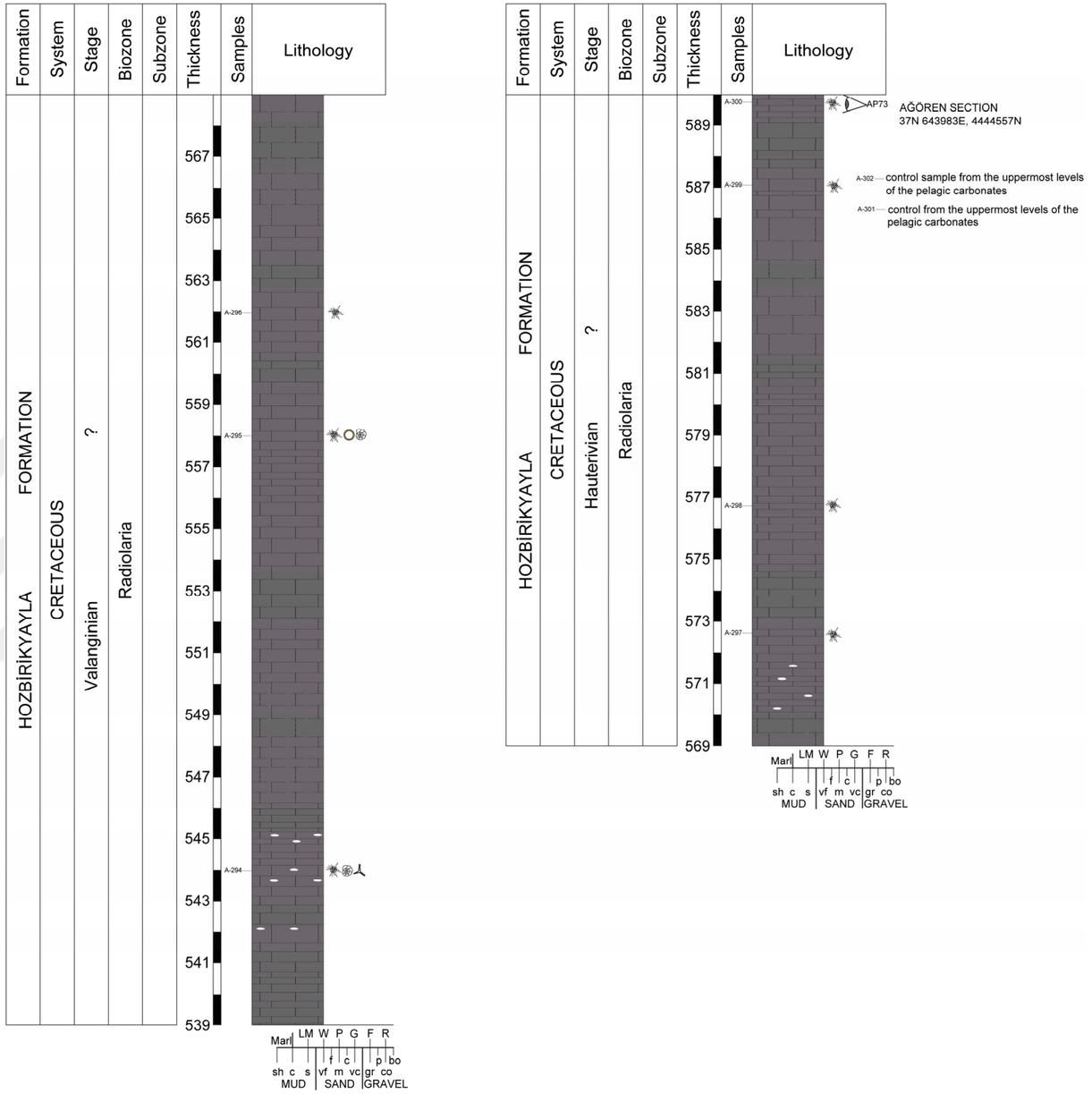

Figure 2.3 (*continued*)

2.1.1.2 Ozansu Measured Section

The Ozansu measured section is located in the Aşutka thrust sheet, 55 km west of the Ağören section, just to the south of the Ozansu village (Fig. 1.5, 1.8 & 1.10). Two stratigraphical sections were measured (OA and OB sections; Fig. 2.6, 2.7 and Appendix B). OA section is 65 m in thickness and a total of 33 samples were collected along the succession. The OB section is 236 m in length. Along the section a total of 201 samples were collected. Bed-by-bed measured logs of the successions are given in Figures 2.6 and 2.7. Sample-by-sample microfacies types, interpreted depositional environments and fossil contents can be found in Appendix B.

Similar to the lower levels of the Ağören section, the bottom part of the Ozansu measured section is characterized by the clastic turbiditic deposits of the Kelkit Formation (Fig. 2.4 & 2.6). The bottom of the succession is dominated by the sandstone-shale alternations (Fig. 2.4A, B). The overlying middle parts are characterized by shale dominated intervals (Fig. 2.4C, D). There are thick ooidal limestone lenses within this interval (Fig. 2.4C & 2.6). In the overlying levels, thin intercalations of limestones are present within shale dominated intervals (Fig. 2.4E). Towards the upper middle part of the section, sandstones start to dominate the deposition (Fig. 2.4D). Following this level, the frequency of marl beds increases that intercalate with shales (Fig. 2.4F). Just above this interval, limestone beds start to dominate and mark the transition from the Kelkit Formation into the overlying Hozbirikyayla Formation (Fig. 2.4G & 2.6). This bottom level of the Hozbirikyayla Formation shows intercalations of marl and minor sandstone levels with carbonates (Fig. 2.4H). The upper boundary of the OA section is faulted, and the rest of the outcrop is poorly exposed (Fig. 2.4I). The OB section was measured to the south of the OA section by shifting to a well-exposed outcrop (Fig. 1.10 & 2.7).

The OB section is characterized by the limestones of the Hozbirikyayla Formation. In comparison to the Ağören section, the Hozbirikyayla Formation in the OB section shows thicker carbonate gravity flow deposits with higher frequency (Fig. 2.5A, C, D, G-N, P-S & 2.7) and rare clastic intercalations (Fig. 2.5B, E, F, H, K & 2.7). To-

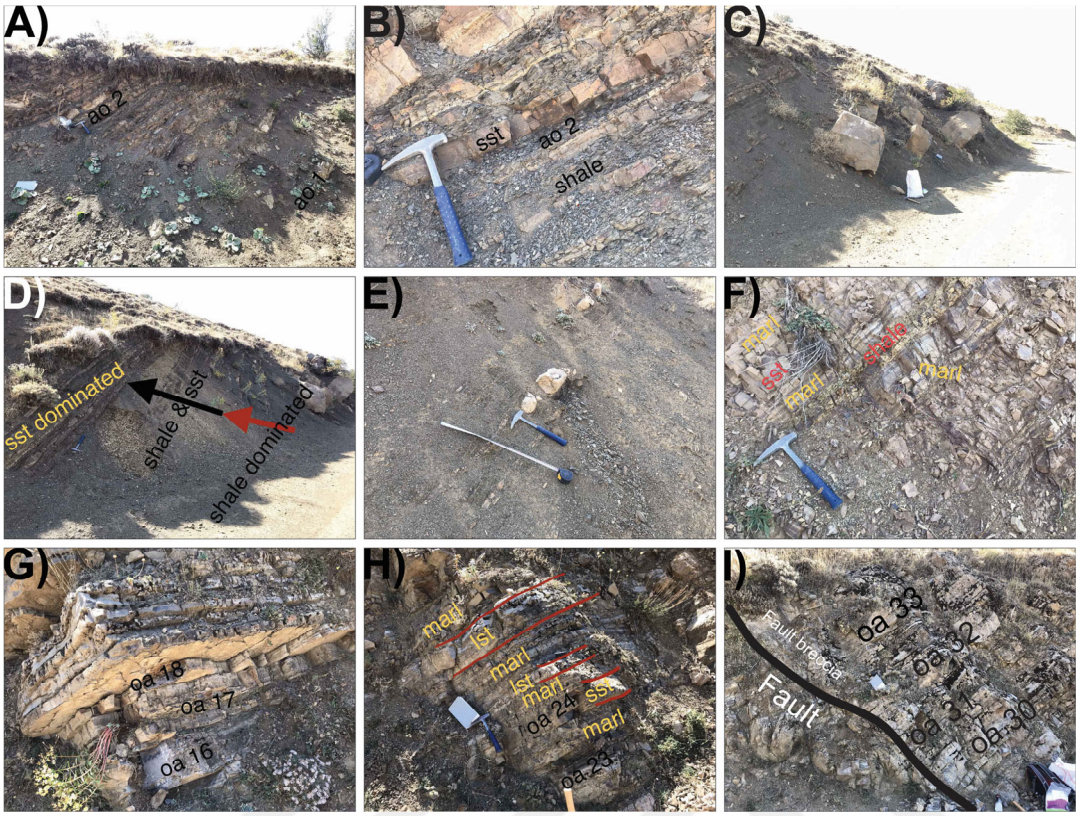

Figure 2.4. Field photograph of the OA section. A-F) Kelkit Formation, G-I) Hozbirikyayla Formation. **A)** General view of the bottom levels showing sandstone, siltstone and shale alternations (OAP1). **B)** Close-up view of the sandstone and shale alternation (OAP1). **C)** Intercalation of the thick bedded sandy ooidal grainstones and the volcanogenic sandstones within the shale dominated interval (OAP4). **D)** Transition from the shale dominated interval (overlying the ooidal grainstone beds) into the sandstone dominated level through a shale and sandstone alternation (OAP6). **E)** Intercalated limestone lenses within shale (OAP7). **F)** Close-up view of the marl, shale and sandstone alternation (OAP8). **G)** The base of the Hozbirikyayla Formation (OAP9). **H)** Intercalation of shale and sandstone beds with the carbonates of the Hozbirikyayla Formation (OAP12). **I)** The faulted upper boundary of the OA section (OAP13). lst: limestone, sst: sandstone. The "OAP" labels with number indicates the levels of the photographs on the measured section (Fig. 2.6). Each photograph level is shown on the measured sections.

wards the uppermost level of the section outcrop conditions get poor. Thick slump intervals occur in a nearby hill at nearly the same stratigraphical level. Since the beds cannot be traced, the OB section ends at this point (at 234 m; Fig. 2.7).

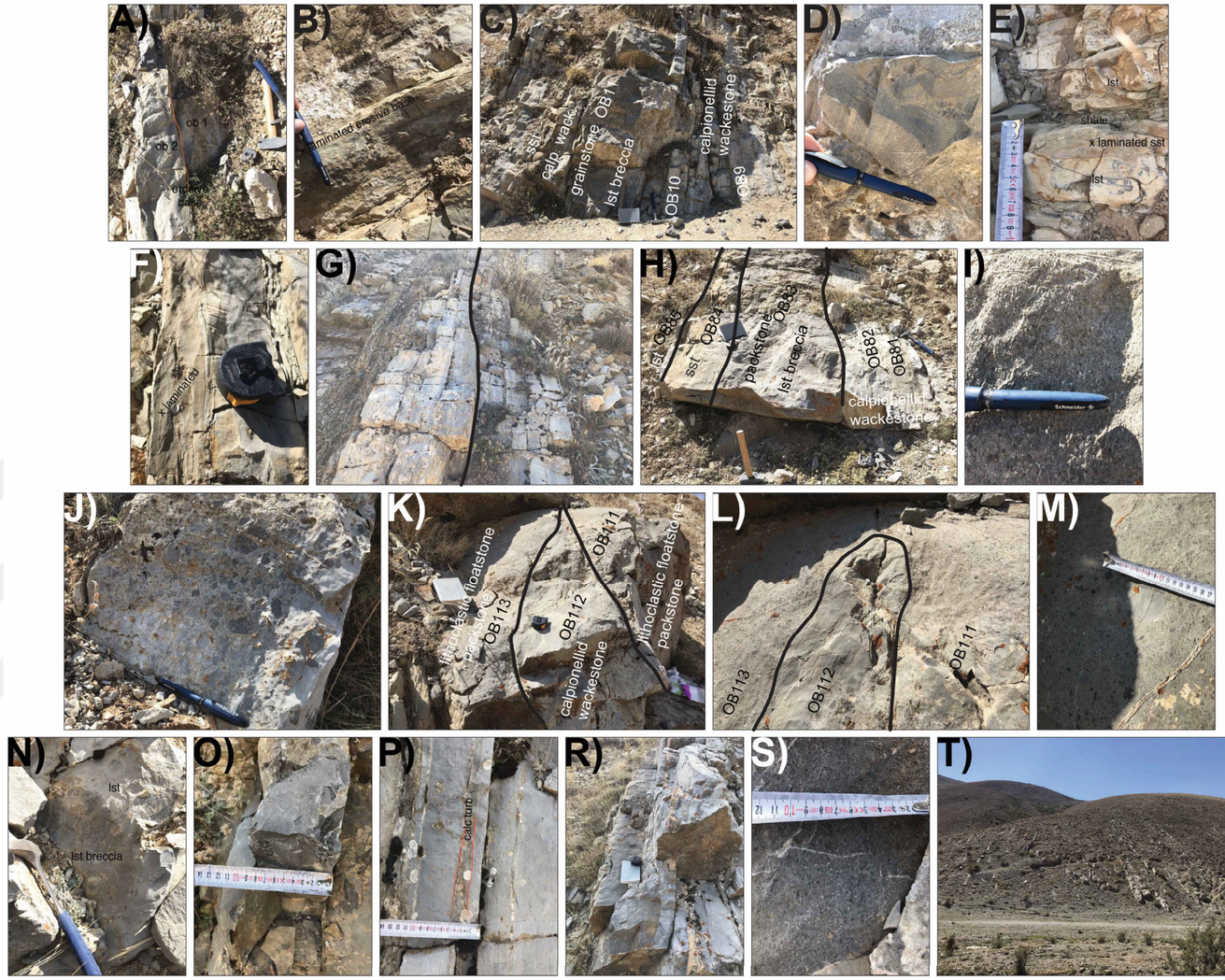

Figure 2.5. Field photographs of the Hozbirikyayla Formation of the Ozansu section. **A)** The erosional contact between two limestone beds, a very common sedimentary structure of this gravity-flow-deposits-dominated succession (OBP1). **B)** Cross-laminated sandstone lense (OBP3). **C)** Thick calciturbiditic bed between calpionellid wackestone beds. This gravity flow deposit shows fining upward character from limestone breccia at the base to grainstone facies at the top. A sandstone level intercalates towards the left of the photograph (OBP4). **D)** Close-up view of grainstone facies (OBP4). **E, F)** Cross-laminated sandstone bed intercalated between limestone beds (OBP8 & 15). **G)** Cross-bedded limestone with erosional basal contact. Towards the top of the bed, facies passes into calpionellid wackestone (OBP9). **H)** Thick gravity flow deposit lense between calpionellid wackestones. Facies change from floatstone at the bottom to packstone towards top (OBP13). **I)** Close-up view of floatstone facies (OBP13). **J)** Close-up view of a limestone breccia level, floatstone facies (OBP16). **K, L)** Intercalated calpionellid wackestone facies between two gravity flow floatstone levels (OBP17). **M)** Close-up view of a breccia level (OBP17). **N)** Carbonate breccia with floatstone facies intercalated between calpionellid wackestones (OBP18). **O)** Limestones with chert nodules and laminae with increasing frequency towards the top of the succession (OBP21). **P)** The thickness and frequency of the gravity flow deposits decreases towards the top of the section. There are rare intercalated calciturbiditic laminae at upper part of the section (OBP22). **R, S)** The last calciturbiditic bed of the section. The bed has floatstone-packstone facies with erosional base (OBP23). **T)** The general view of the OB measured section. The “OBP” labels indicates the photograph levels on the measured section (Fig. 2.7).

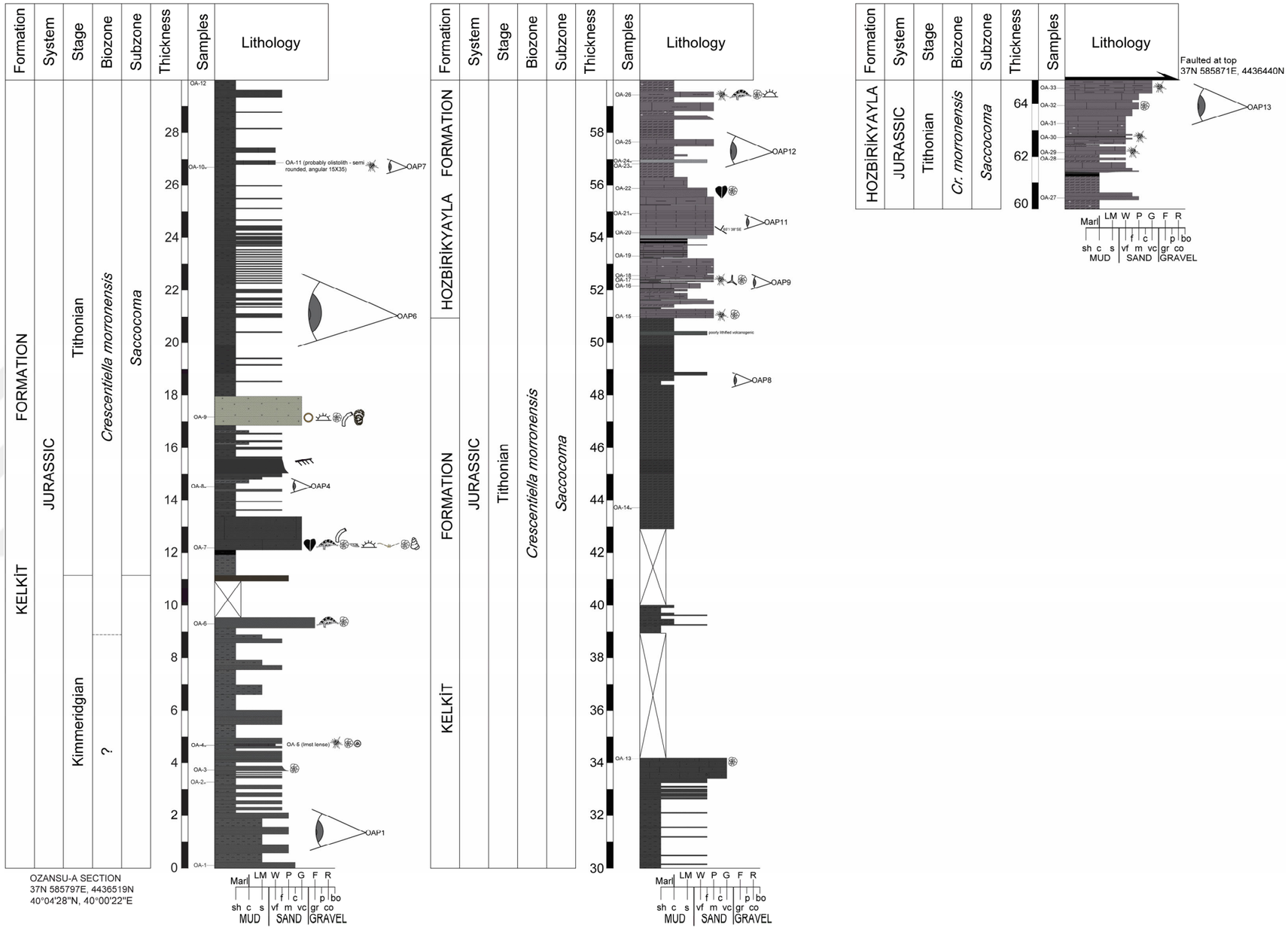

Figure 2.6. Ozansu-OA measured section. For symbols see Fig. 2.3.

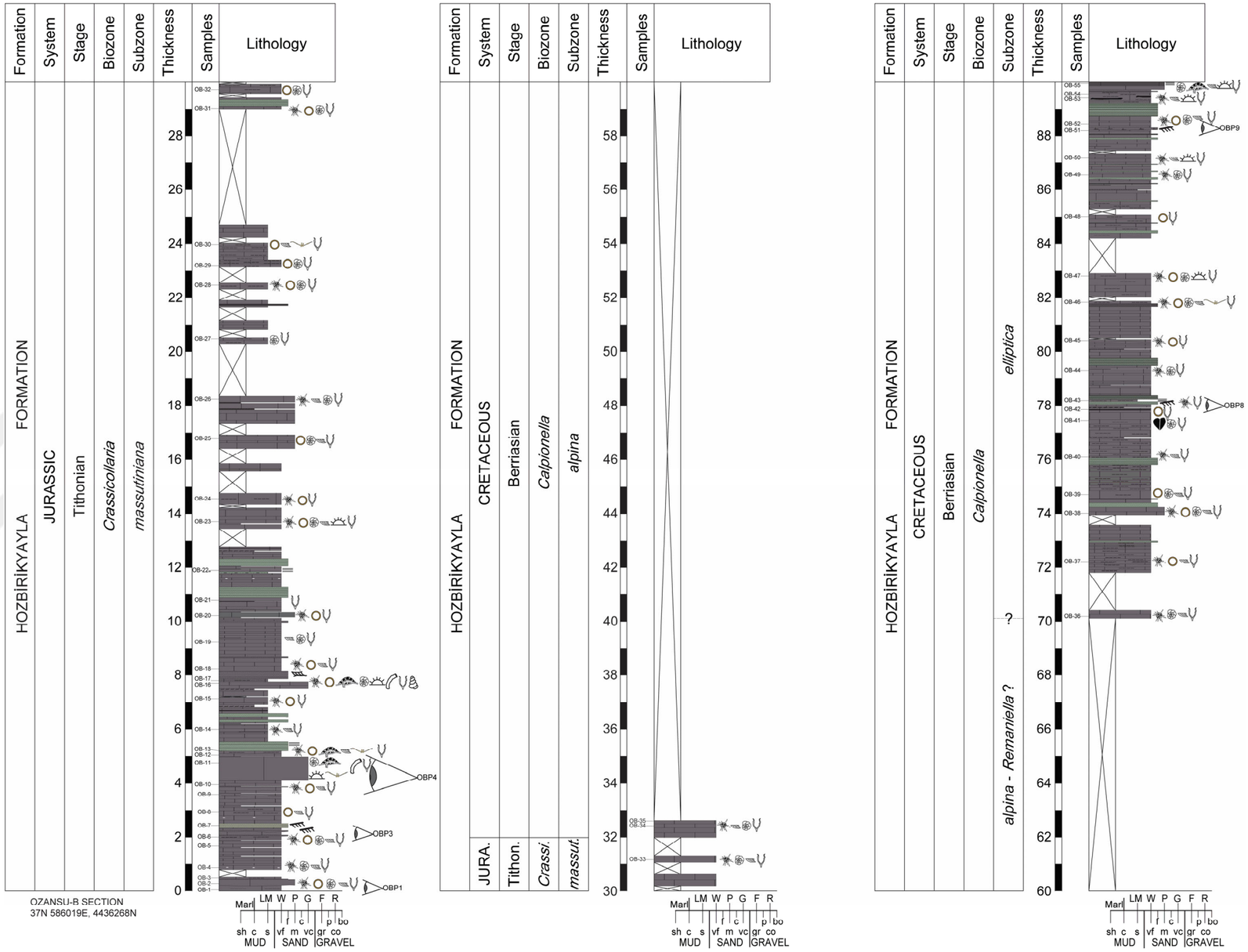

Figure 2.7. Ozansu-OB measured section. For symbols see Fig. 2.3.

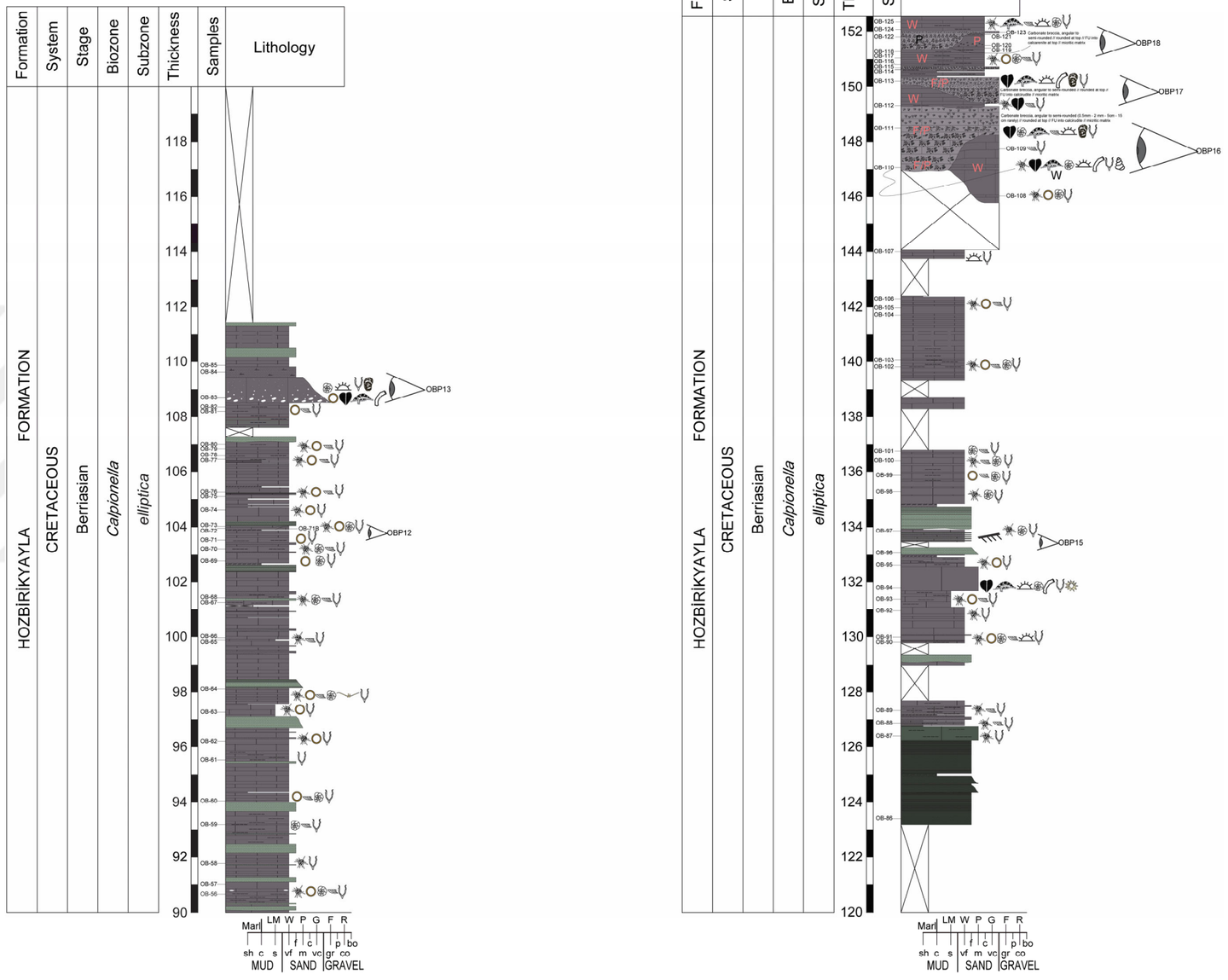

Figure 2.7 (*continued*)

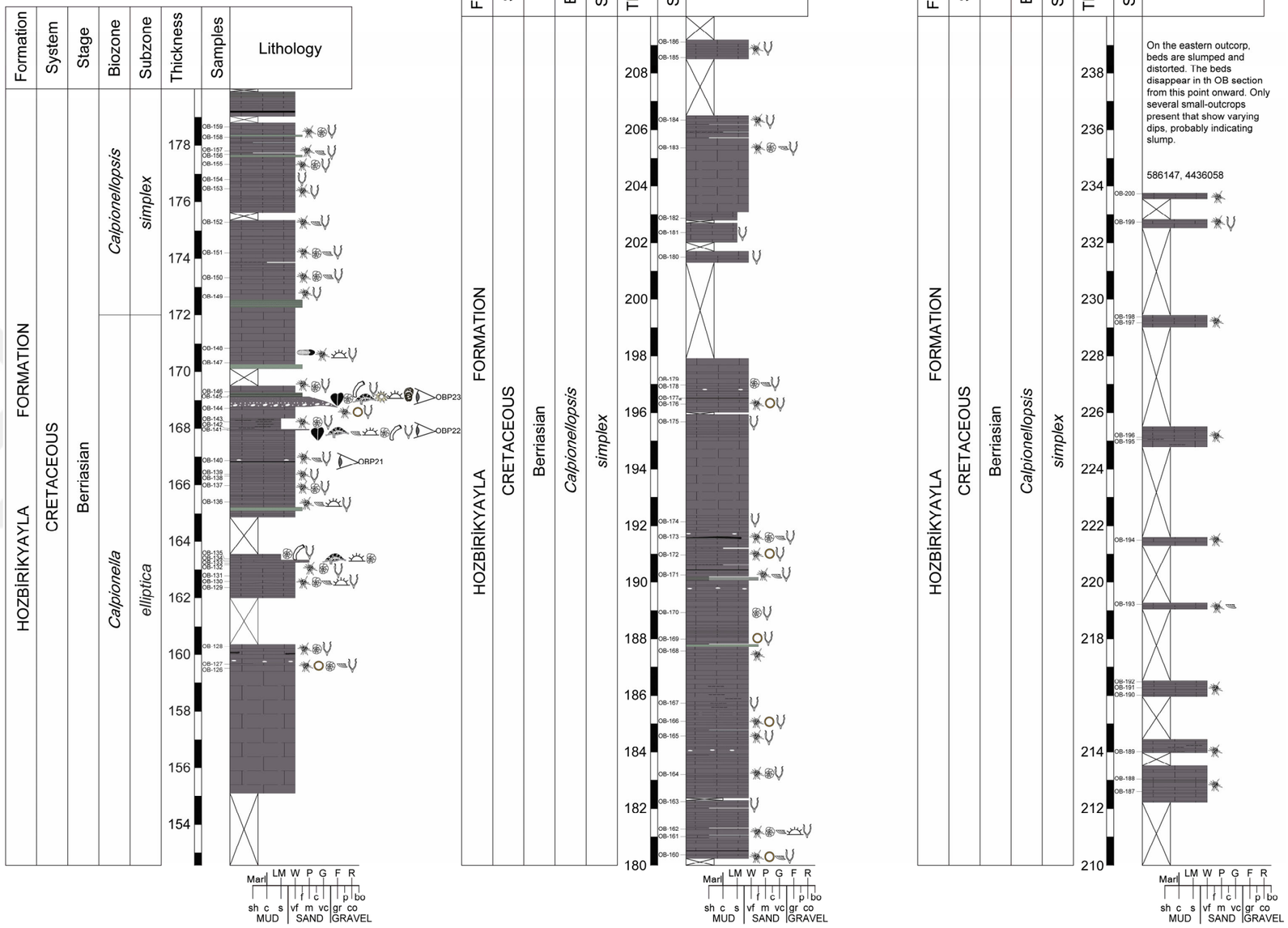

Figure 2.7 (*continued*)

2.1.2 Carbonate Platform Neritic Successions

The Nazlıçayır measured section characterizes the shallow marine deposits of the eastern part of the PCP. The details of the lithostratigraphic properties of the succession are given below.

2.1.2.1 Nazlıçayır Measured Section

Nazlıçayır measured section is located near the Nazlıçayır (Lorikas) Village to the southeast of Gümüşhane (Fig. 1.5, 1.8, 1.11, 2.8). Tectonically, the Nazlıçayır successions can be viewed as the northern continuation of the para-autochthon units previously described. A total of 6 stratigraphic sections were measured along the shallow marine carbonates. The stratigraphical section routes were shifted at the levels where the outcrop conditions worsen by detecting and correlating key stratigraphical horizons (e.g., basalt levels, key beds with unique microfacies, thick dolomitic levels etc.). By these solid correlations, a composite measured stratigraphical section was produced with a total thickness of 350 m (Fig. 2.8, 2.12). The succession was logged bed-by-bed with measurements and descriptions (Fig. 2.12, Appendix B). A total of 161 rock samples were collected. Among these samples, 11 were collected from the basalt level for use in following studies. The remaining 150 samples were collected from carbonate, dolomite, and sandstone beds.

The Upper Jurassic – Lower Cretaceous carbonate rocks are well-exposed in the Nazlıçayır region in a deeply eroded valley and present laterally traceable outcrops (Fig. 2.8). The lower part of the succession is characterized by dark grey massive lagoonal micrites with wackestone facies that show intercalations with back-margin intraclastic packstones, fenestral micrites and rare dolomites (Fig. 2.9, 2.12, Appendix B). At the base, the succession starts with dark micritic limestone (Fig. 2.9A). Rare intercalation of shale, marl and volcaniclastic levels are also present (Fig. 2.9A). Some levels show intercalations of intraclastic floatstones (Fig. 2.9B,C).

Figure 2.8. A) A general view of the studied outcrops from the Nazlıçayır Village. The location of the photograph is shown in Fig. 2.8B. For biozone descriptions see Chapter 2.2. **B)** Google Earth image of the studied succession. The first and last samples of each measured sections are labelled on the image with separate coloring unique to individual sections. The "eye" symbol marks the location where the photograph shown in Fig. 2.8A was taken. The turquoise and yellow continuous lines indicate the key levels used for shifting and correlation of the stratigraphical sections.

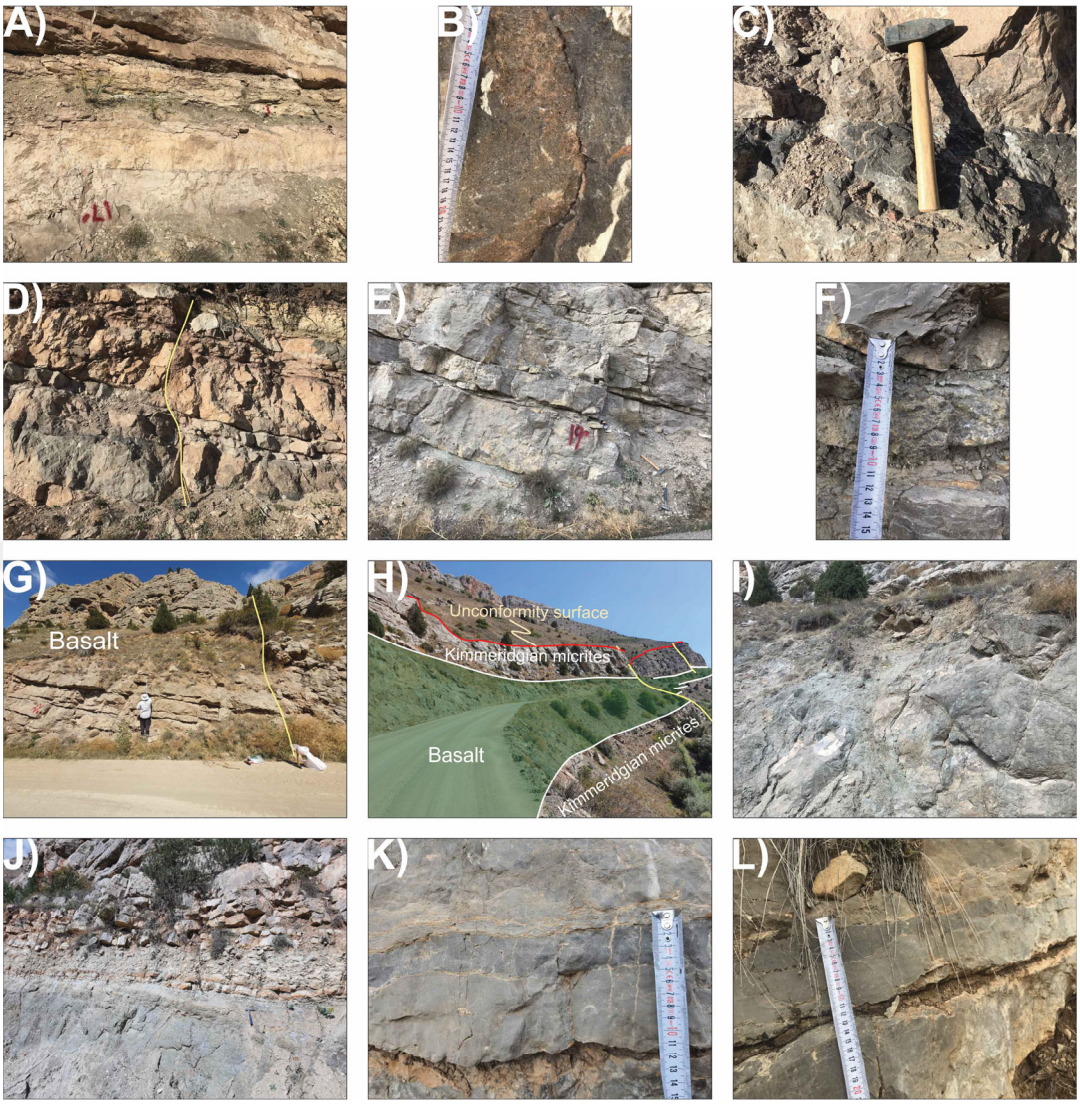

Figure 2.9. Field photographs from the lower levels of the Nazlıçayır section. **A)** Dark grey packstone-wackestone beds at the basal levels of the Berdiga Limestone. Rarely shale, marl and volcaniclastic interbeds are present (LP1). **B)** Intraclastic floatstone bed (LP2). **C)** Black micritic carbonates (LP3). **D)** Synsedimentary fault (yellow line; LP4). **E)** Micritic beds start to stack and thicken toward the younger levels (LP8). **F)** Microbreccia (LP9). **G)** Basalt flow sandwiched between micritic carbonates. The yellow line marks another fault (LP10). **H)** The general view of the basalt level (green hatch) and confining carbonates. The yellow lines indicate the faults. The red line shows the erosional relief of the incised valley. East is to the right (LP12). **I)** Closer view of the basalt (LP12). **J)** The upper contact of the basalt flow is characterized by intercalation with volcaniclastics that show transition into micritic carbonates (LP13). **K)** Dark grey intraclastic carbonate key bed intercalated within grey calcitic mudstone beds overlying the basalt level (LP14). **L)** The same key level at the base of the second section located to the east of the first section (LP

Figure 2.9 (*continued*) 15). The "LP" labels with number indicates the levels of the photographs on the measured section (Fig. 2.12).

Synsedimentary faults offset the strata at this lower part of the succession (Fig. 2.9D). Towards the upper levels of the lower part, the thickness of the beds increases (Fig. 2.9E). Rare thin breccia levels occur from time to time (Fig. 2.9F). A 25 m-thick basalt level interrupts these thick micritic carbonates (Fig. 2.9G-J). Although the lower contact of the basalt is not clearly exposed in the region, its sandwiched position between the underlying and overlying neritic carbonates (Fig. 2.9G, H), the presence of intercalated volcaniclastic deposits and the observation that these volcaniclastic deposits pass into overlying micritic carbonates through an interval of intercalation (Fig. 2.9J) indicate that the emplacement of the lava flow was contemporaneous with the carbonate deposition and it is a product of submarine volcanism developed on a shallow marine shelf. There is no consensus on the age of this basaltic level. The age interpretations range from Late Oxfordian (Taslı, 1997) to Early Tithonian (Koch et al., 2008; Dokuz et al., 2017). In this study, the age of this basalt is interpreted as Kimmeridgian (within the *Mesoendothyra izjumiana – Alveosepta jaccardi* subzone; see Chapter 2.2 for biostratigraphy). The older carbonates underlying the basalt flow have *Mohlerina basiliensis* and *Crescentiella morronensis* taxa, indicating back-margin depositional environments. In contrast, the neighbouring carbonates immediately below and above the basalt have fossil assemblages indicative of lagoonal environments (e.g., *Alveosepta jaccardi*, *Streptocyclammina pravula – muluchenensis*, *Pseudocyclammina lituus*). These observations demonstrate that there is a regressive trend towards the basalt level, and the shallower lagoonal deposits dominate the aftermath of the volcanic event (Fig. 2.12; Appendix B).

In the middle part of the succession, carbonate deposition was interrupted, and this event was recorded as a pronounced erosional relief; an incised valley (Fig. 2.8A, 2.9H and 2.10B, D, E). The erosional relief changes across the outcrop and reaches maximum depth of 31 m. Oxidation coatings and brecciated beds support the interp-

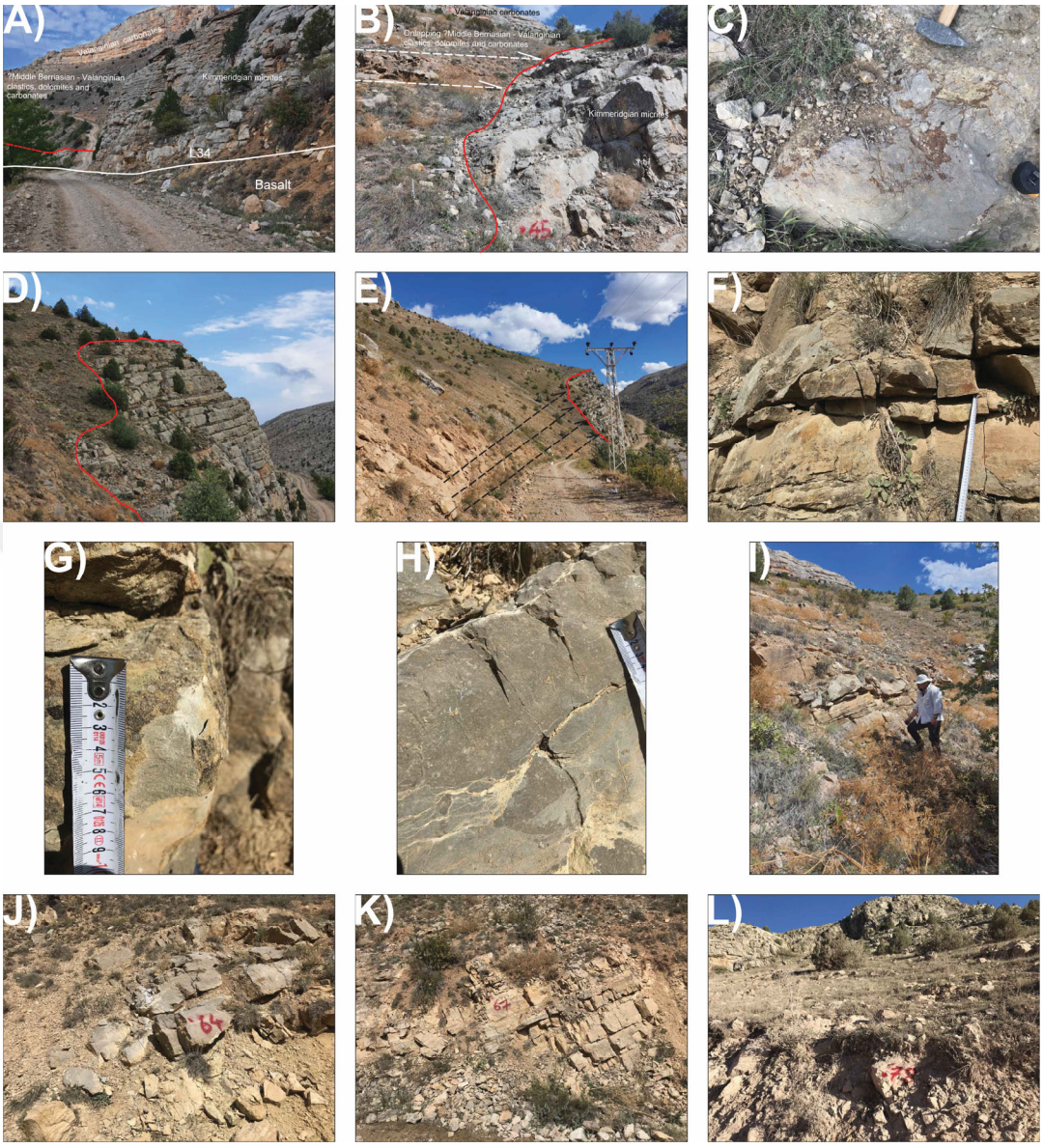

Figure 2.10. Field photographs from the middle part of the Nazlıçayır section. **A)** The base of the second measured section in the eastern part of the outcrop. Red line indicates the erosional surface. Sample L34 is labelled. Northwest is to the left (LP15). **B)** Close-up view of the incised valley walls (LP17). **C)** Oxidized coatings on the bed surfaces at the incised valley walls (LP17). **D, E)** Onlapping transgressive infill deposits. A view towards east. **F, G)** Close-up view of the first levels of the sandstone infill deposits (LP20). **H)** Close-up view of the intercalated carbonate infill deposits (LP21). **I)** A general view of the infill deposits (LP22). **J)** Carbonate deposition starts to dominate towards the upper levels of the infill deposits (LP23). **K)** Uppermost infill deposits, characterized by dolomitization (LP24). **L)** The basal level of the third measured section. Section was shifted to the north (LP25).

retation of exposure due to a relative sea-level drop (Fig. 2.10C). The presence of much thicker carbonates at the incised valley walls and at the levels close to the erosional surface is also in accordance with the position of these beds within the sequence stratigraphic framework, representing a high-stand systems tract (HST) deposits (Fig. 2.10A, B, D and 2.12). The first transgressive lithologies filling the incised valley are characterized by intercalation of sandstone and shale (Fig. 2.10F, G, I). Limestones rarely intercalate with the clastics (Fig. 2.10H). Towards the middle portion of the infill deposits, deposition starts to be dominated by the carbonates (Fig. 2.10J). These carbonates onlap onto the incised valley walls (Fig. 2.10B, E). The uppermost levels of the infill succession are characterized by dolomitization and thick dolomites (Fig. 2.10K). These dolomite beds give poor outcrops and show weak lateral continuity. By detecting the same stratigraphy and the first level of the transition from dolomites to micrites to the north, another (fourth) section was measured (Fig. 2.8, 2.10L, 2.12).

The same stratigraphy with incised valley infill deposits is present at the basal levels of the fourth section. It starts with greenish sandstones and is followed by dolomitic levels. These levels are overlain by medium to thickly bedded carbonates and rare dolomitic levels (Fig. 2.11A, B). These carbonates mostly have micritic texture and show intercalations with wackestone – packstone and grainstone facies (Fig. 2.11A-K and 2.12). Rare dolomitic intervals are also present (Fig. 2.11I). Some levels are rich in macrofossils (e.g., bivalves, corals, microencrusters and gastropods: Fig. 2.11C, D). Laminated micritic beds start to intercalate towards the middle part of the fifth section (Fig. 2.11E and 2.12), indicating a very shallow depositional setting. The uppermost level of the succession is characterized by the intercalation of thick- to very thick-bedded (maximum 2 m-thick) and thin- to medium-bedded carbonates (Fig. 2.11F-K). The succession ends with a recent erosional surface with varying relief (Fig. 2.8 and 2.11K).

Figure 2.11. Field photographs from the upper part of the Nazlıçayır section. **A)** A view from the middle part of the quary road (fourth) section (LP26). **B)** A view from the upper levels of the quary road section. West is to the right (LP27). **C, D)** Thin to medium bedded fossiliferous carbonates from the fifth section (LP28, LP29). **E)** Laminated micrites (LP29). **F, H)** Thickness of the beds increases towards the upper levels (LP30). **G)** Intercalated thin bedded micrites (LP30). **I)** A dolomitic level (LP32). **J)** Claret ret micrites at the uppermost levels of the succession (LP33). **K)** A general view from the uppermost part of the succession. The section ends with a recent erosional surface. **L)** A general view of the extra (sixth) section measured on the incised valley wall and basal infill deposits in the western part of the region. The red line shows the erosional surface of the incised valley. The inlet shows a close-up view of the brecciated beds at the highest level of the incised valley walls (LP36).

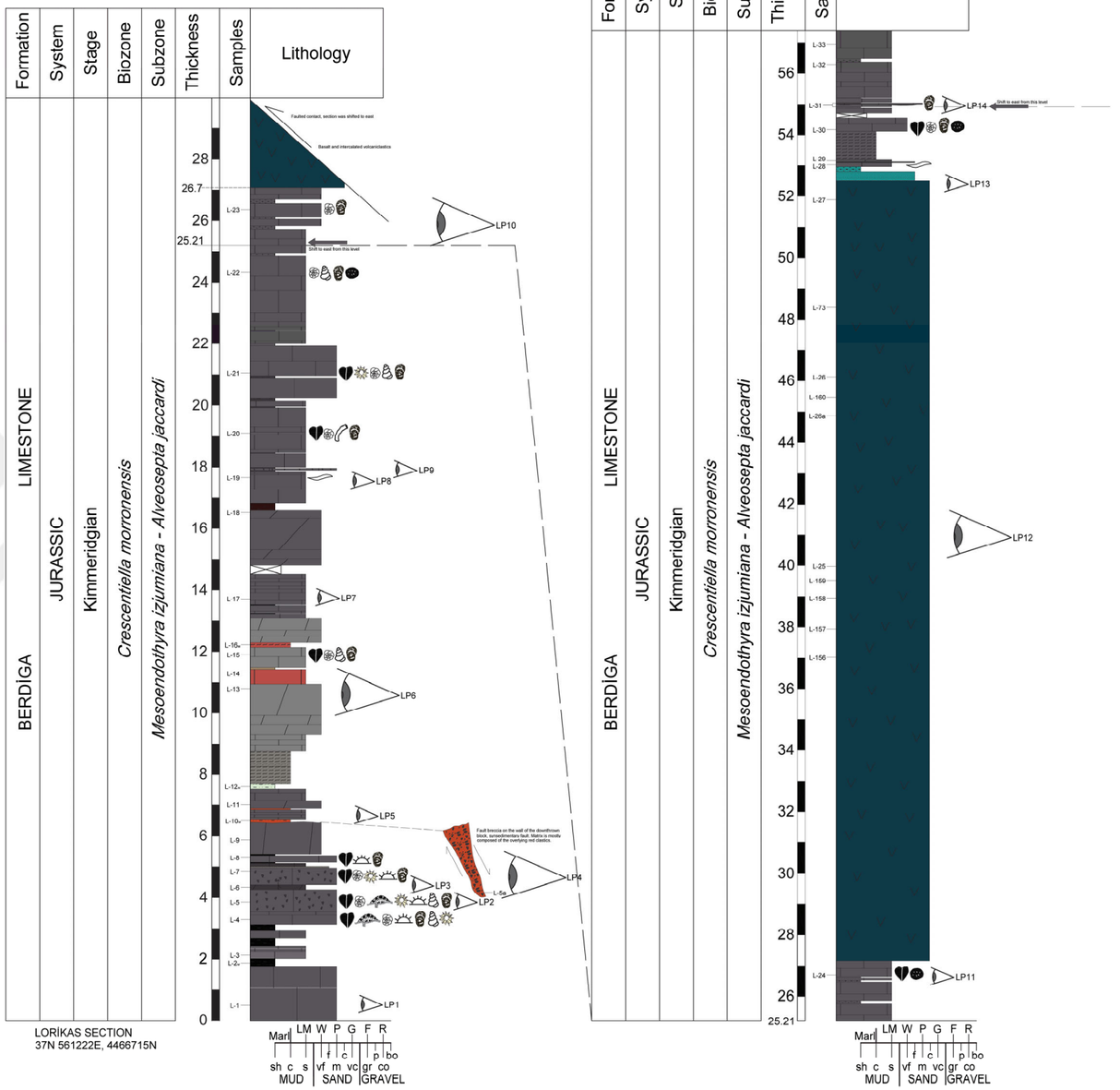

Figure 2.12. Nazlıçayır measured section. For symbols see Fig. 2.3.

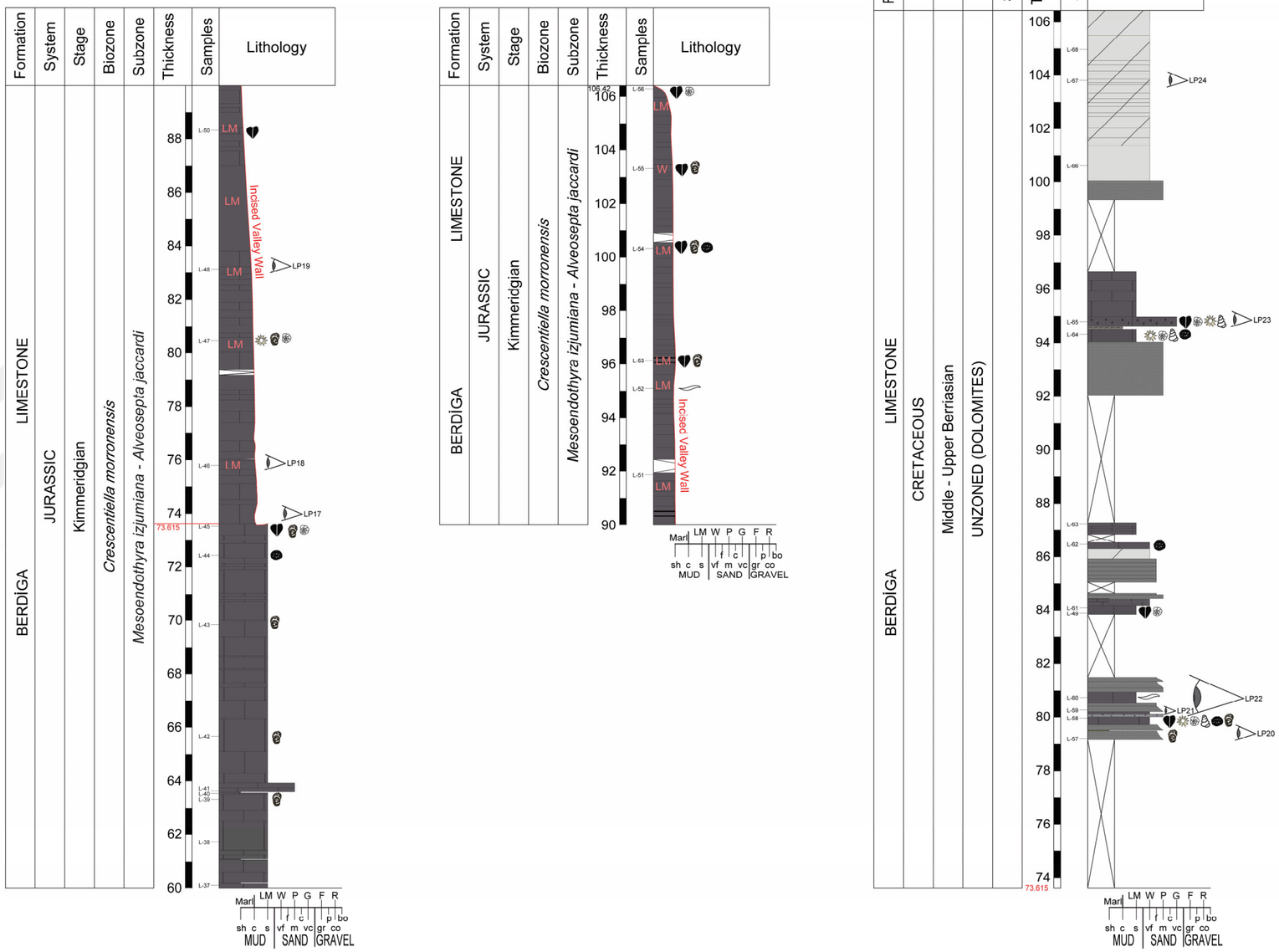

Figure 2.12 (*continued*)

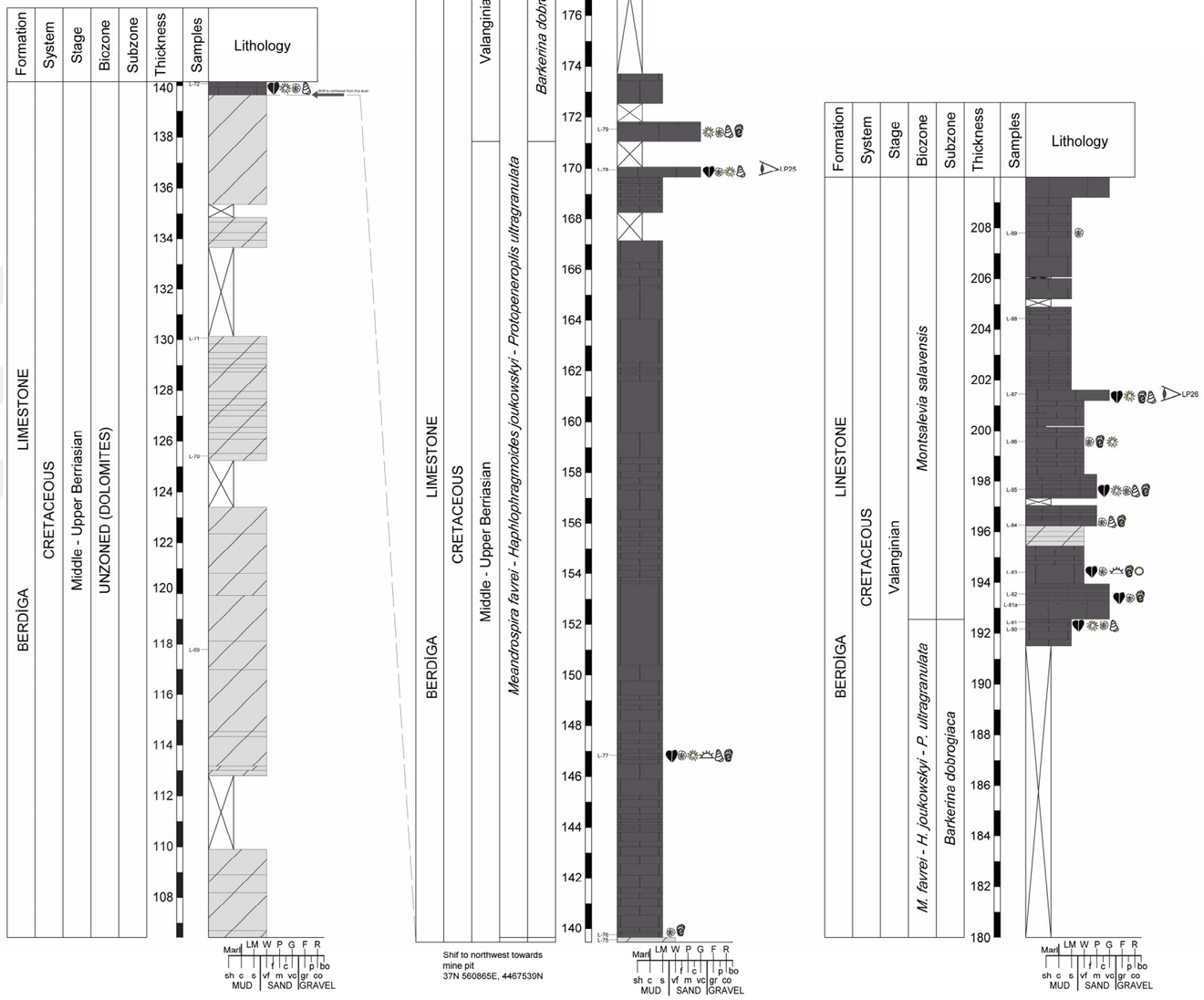

Figure 2.12 (*continued*)

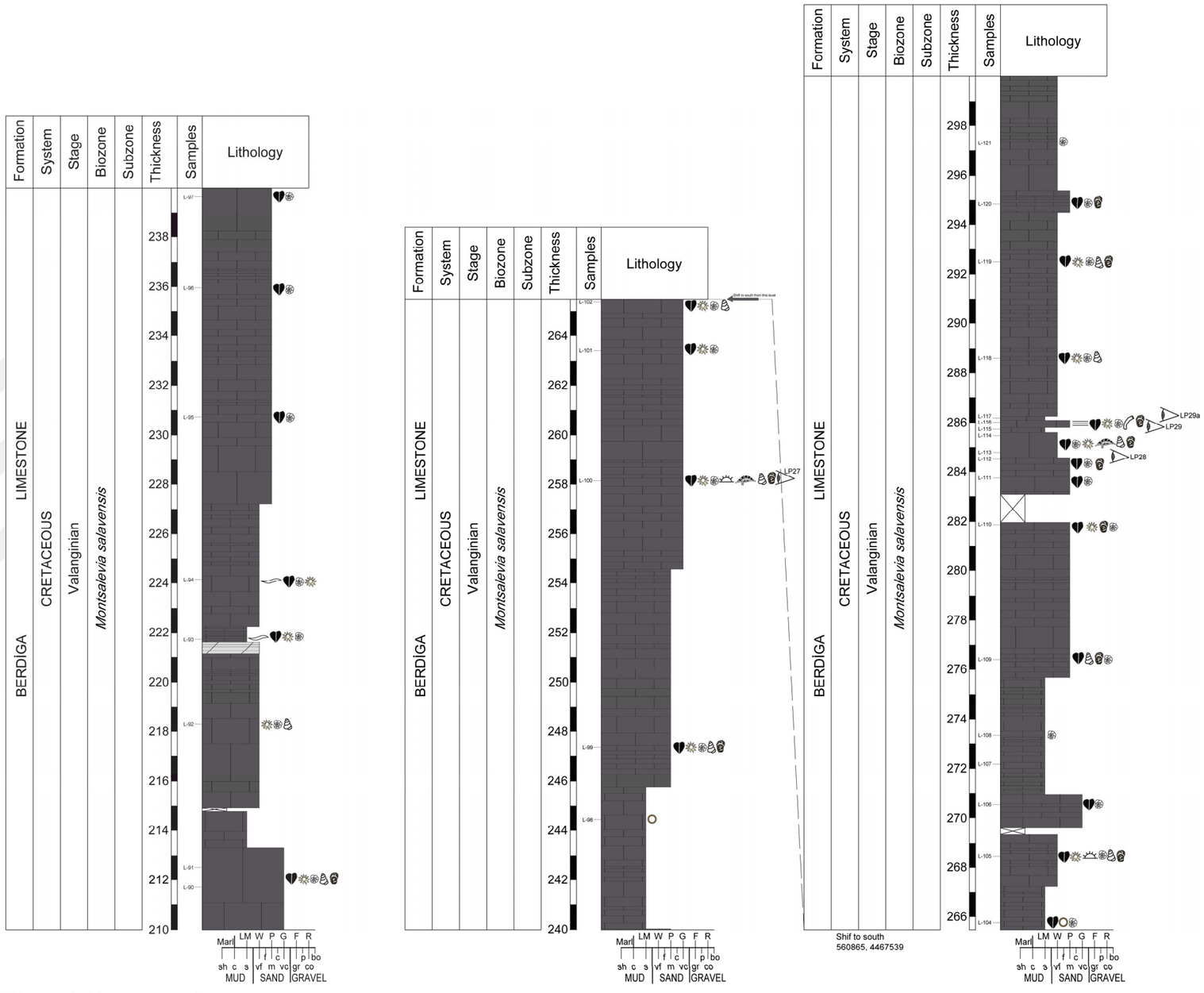

Figure 2.12 (*continued*)

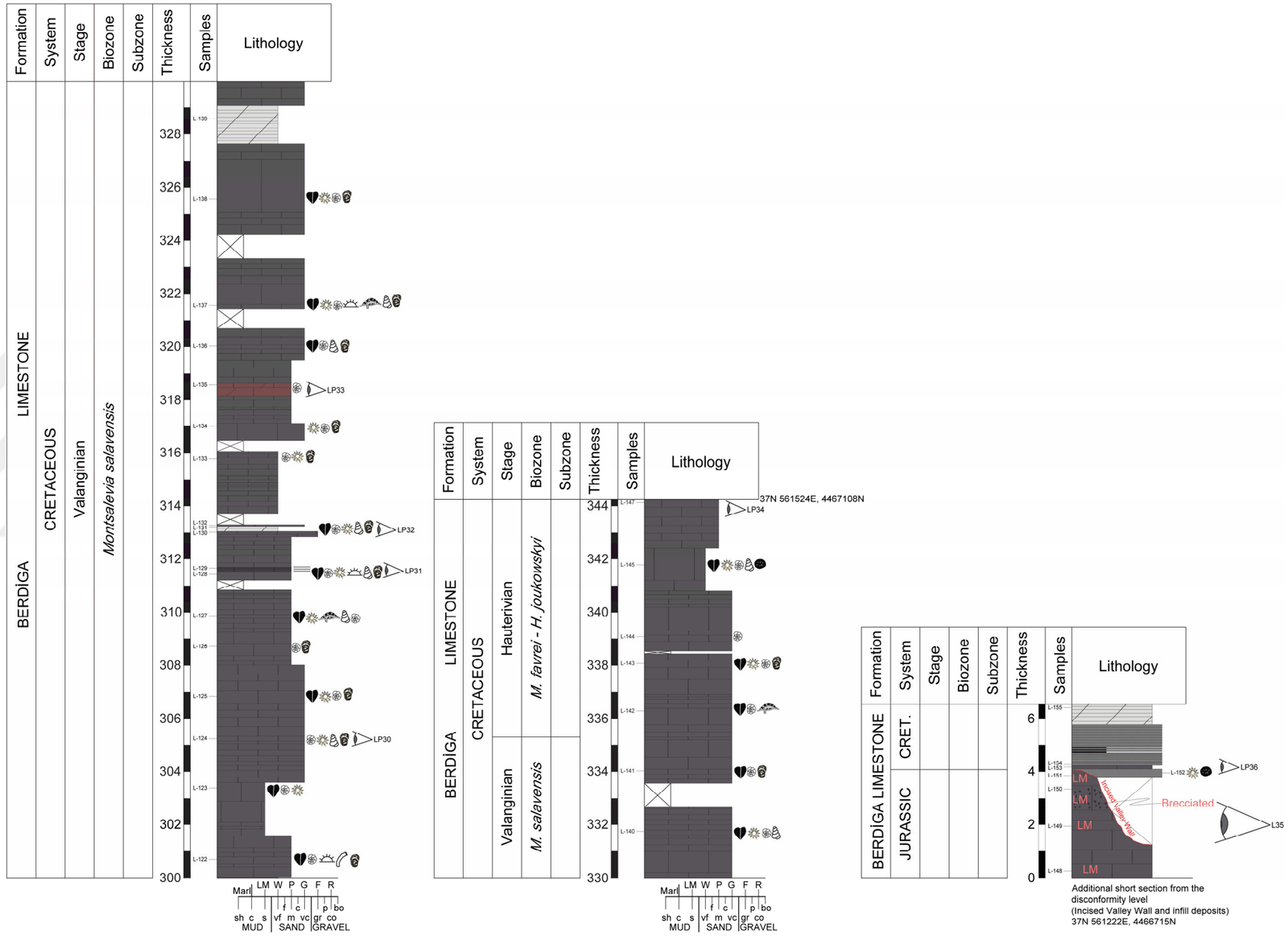

Figure 2.12 (*continued*)

2.2 Biostratigraphy

The presence of two different depositional domains led to construction of two separate biozonation schemes based on foraminifers, calpionellids, pelagic crinoid *Saccocoma* and microencruster *Crescentiella morronensis* for pelagic (Ağören and Ozansu sections) and neritic (Nazlıçayır section) successions.

Figures 2.13 and 2.14 provide comparison charts of the previously published biozonation schemes that were used in the construction of the biostratigraphical framework in this study. In the light of these biostratigraphical schemes, interpreted ages were assigned to biozones proposed in this study.

The first agreed standard quardripartite calpionellid biozonation scheme was introduced by Alleman et al. (1971; Fig. 2.13). Since there was not enough data on the ordering of the evolutionary calpionellid bioevents, assemblage zones and successive acme intervals were used in previous schemes (Remane, 1963). As the data on calpionellid assemblages accumulated with new species recognized, higher resolution had started to be achieved that gave rise to finer subzonations (Fig. 2.13). The most famous and widely applicable scheme was proposed by Remane (1971; Fig. 2.13). His Zone A (corresponding to the base of the standard *Crassicollaria* Zone) was defined by the first occurrence of calpionellids with fully hyaline lorica. A1, A2 and A3 subzones were introduced within his Zone A. The base of the A1 subzone is at the base of the Zone A. The following subzone A2 is delineated by the first occurrence (FO) of the large variety of *Calpionella alpina* (*Calpinella grandalpina*). The A3 subzone is characterized by the predominance of *Crassicollaria brevis* over *Crassicollaria intermedia*. Remane (1971) differentiated two subzones within the *Calpionella* standard zone. The B Zone is defined at its base by the acme of spherical forms of *Calpionella alpina*, corresponding to the base of the standard *Calpionella* Zone. The FO of the large variety of *Tintinnopsella carpathica* marks the base of the Zone C. Subzone D1 is defined at the base by the first occurrence of *Calpionellopsis simplex*. This also defines the base of the Zone D

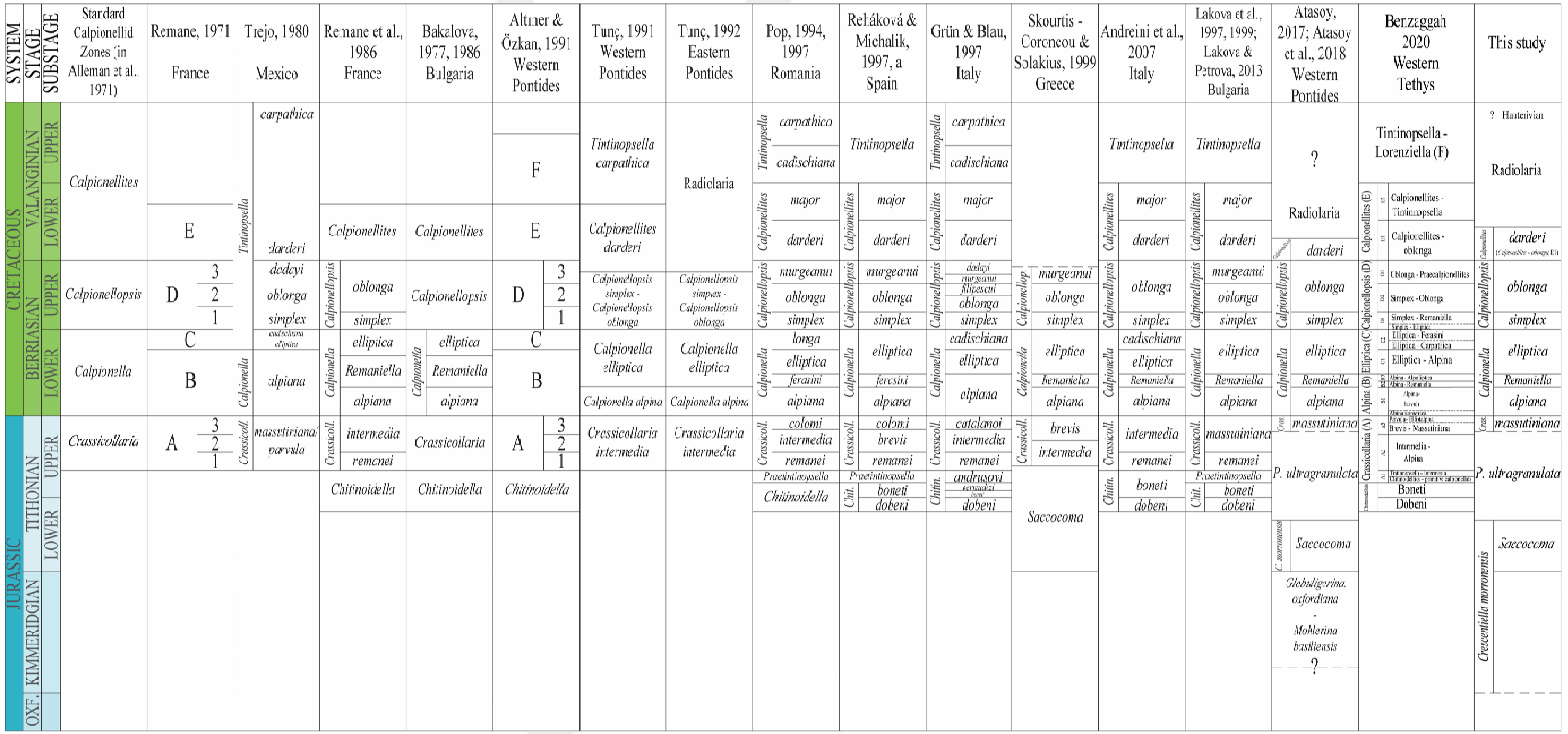

Figure 2.13. Comparison chart of the pelagic biostratigraphical zonations used in this study and the proposed scheme for the Eastern Pontides pelagic Ağören and Ozansu successions.

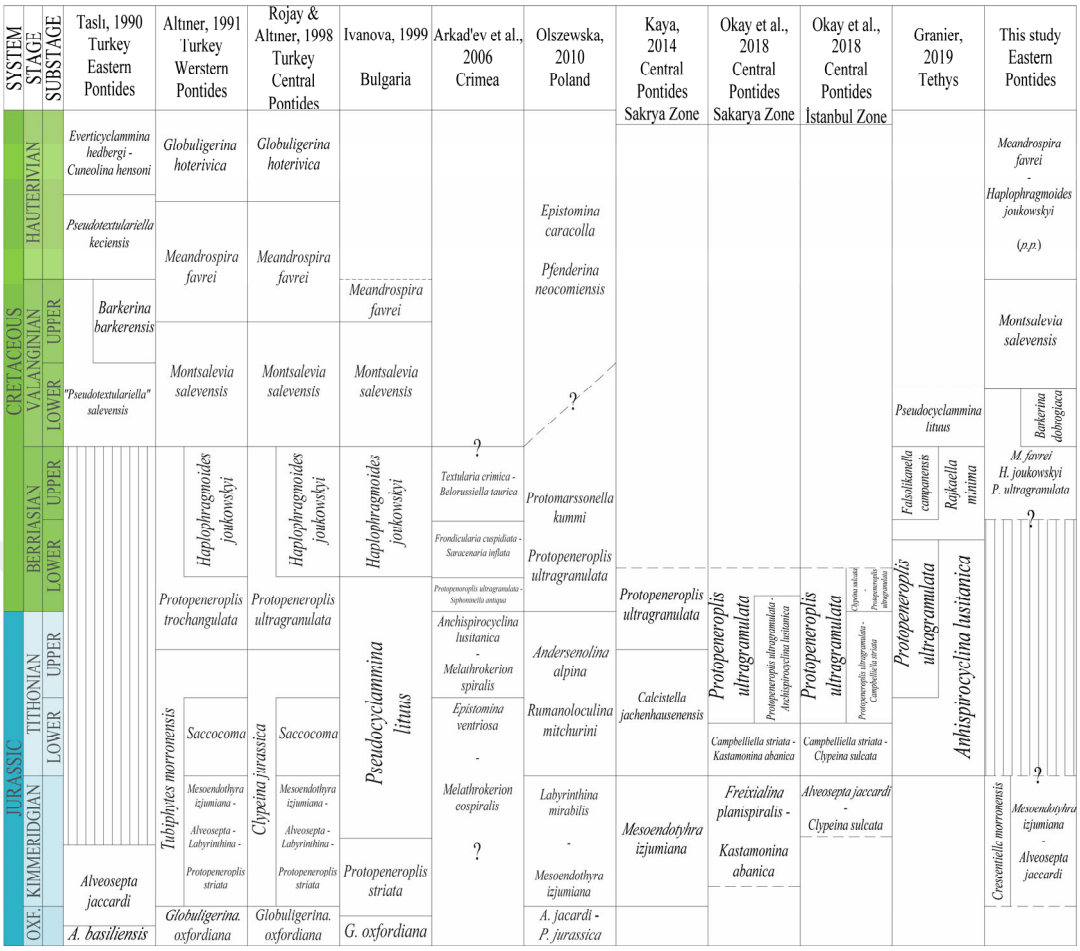

Figure 2.14. Comparison chart of the neritic biostratigraphical zonations used in this study and the proposed scheme for the Eastern Pontides neritic Nazlıçayır successions.

that corresponds to the base of the standard *Calpionellopsis* Zone (Alleman et al., 1971; Remane, 1971). Subzone D2 is characterized by the predominance of *Calpionellopsis oblonga* over *Calpionellopsis simplex*. The FOs of *Lorenziella hungarica* and *Calpionellites darderi* define the bases of the D3 subzone and Zone E, respectively.

Remane et al. (1986) modified the 1971 scheme. They defined *remanei* and *intermedia* subzones within the *Crassicollaria* Zone characterized by the dominance of the name giving taxa and correspond to the bases of the previously defined A1 and A2 subzones (Fig. 2.13). An additional *Remaniella* subzone was also introduced

within the *Calpionella* Zone, defined by the FO of remaniellid calpionellids. Remane's previous C Zone was discarded and replaced with the *elliptica* subzone defined by Pop (1974). This subzone is characterized at its base by the FO *Calpionella elliptica* (Remane et al., 1986). For the *Calpionellopsis* Zone, two subzones were defined: namely, the *simplex* and *oblonga* subzones. Their basal boundaries were placed at the successive FOs of *Calpionellopsis simplex* and *Calpionellopsis oblonga*, respectively. The definition of the Zone E was kept the same; only a new name was introduced (*Calpionellites* Zone). They also introduced a *Chitinoidella* Zone for the lower portion of the upper Tithonian (Fig. 2.13). This zone is characterized by the FO of chitinoidellids (the proposed ancestors of calpionellids with microgranular or double layered lorica walls).

A similar biozonation scheme was produced from Bulgaria by Ivanova-Bakalova (1977, 1986). In her scheme, the *Crassicollaria* and *Calpionellopsis* Zones were used without any subzonal division (Fig. 2.13).

In the following years, the general outline of the Remane et al. (1986)'s scheme was kept. Altıner and Özkan (1991) introduced an additional F zone that completed the Remane's 1971 scheme (Fig. 2.13). The boundaries of this F Zone were defined by the successive last occurrences of *Calpionellites darderi* and *Tintinnopsella carpathica*, respectively. This occurrence of *T. carpathica* after the extinction of *Cpts. darderi* had also been observed previously by Trejo (1980) in Mexico but he did not attempt to define a formal zone with well-defined boundaries. In the following years, other calpionellid zonations from Turkey came from the works of Tunç (1991, 1992) and Burşuk (1992). In their schemes, mainly the standard zones were used over generalized stratigraphical columns without specific ordering of bioevents. Tunç (1991, 1992) defined assemblage zones like "*Calpionellopsis simplex – Calpionellopsis oblonga* Zone".

Especially following the emendations on the genus *Remaniella* by Pop (1994) and Grün and Blau (1996), revisions have been made to the previously published biozonation schemes with introduction of more subdivisions (Pop, 1994, 1997;

Reháková & Michalik, 1997, 1997a; Grün & Blau, 1997; Lakova et al., 1997, 1999; Skourtis-Coroneou & Solakius, 1999), although the main zonal boundaries have remained the same with the Remane's (1971) scheme (Fig. 2.13). Among them, Grün and Blau (1997) proposed an unusual FO for the *Remaniella catalanoi* in the *Crassicollaria* Zone. They introduced a *catalanoi* subzone as the equivalent of the previously defined *colomi* subzone (Fig. 2.13). Then it was realized that the upper Tithonian *Crassicollaria* Zone is missing and *elliptica* subzone (of *Calpionella* Zone) is in direct contact with the *remanei* subzone (of *Crassicollaria* Zone) in the Rau Stau section on which Grün and Blau (1997) constructed their biozonation (e.g., Reháková, 1998).

Skourtis-Coroneou and Solakius (1999) established a bizonation from Greece similar to the scheme of Reháková and Michalik (1997, 1997a). They did not recognize any specimen of chitinoidellids and instead they defined a *Saccocoma* Zone similar to Altıner (1991) whose base was interpreted to be at the base of Tithonian (Fig. 2.13 & 2.14). Their *brevis* subzone was placed rather higher than previously established zonations (Fig. 2.13).

Lakova and Petrova (2012, 2013) tried to synthesize previously published biozonation schemes and proposed a standard global calpionellid zonation. To achieve wide geographical applicability, they discarded taxon with controversial vertical ranges and morphologies and subzones that are not recognized globally. Their biozonations dismissed the *colomi* subzone (in *Crassicollaria* Standard Zone), *cadischiana* subzone (in *Calpionella* Zone), Zone C (based on the predominance of *Tintinnopsella carpathcia*) and Zone D3 (characterized by the FO of *Lorenziella hungarica*; Fig. 2.13). They only utilized first occurrence bioevents for the determination of the zones and subzones which are globally recognized. The only exception is the usage of the last occurrence (LO) of *Calpionellites* to define the base of the *Tintinnopsella* Zone, since there is no evolutionary event among calpionellids in this interval. The following bioevents were used in their biozonation in ascending order; FOs of chitinoidellids, *Chitinoidella boneti*, *Praetintinnopsella andrusovi*, hyaline-walled calpionellids (*Tintinnopsella carpathica*, *T. ramenei*), *Calpionella*

grandalpina and *C. alpina*, explosion of *Calpionella alpina* (and coeval decline of the genus *Crassicollaria* and LO of *Calpionella elliptalpina*), FO *Remaniella* (*Remaniella ferasini* and *R. duranddelgai*), *Calpionella elliptica*, *Calpionellopsis simplex*, *Calpionellopsis oblonga*, *Praecalpionellites murgeanui*, *Calpionellites darderi*, *Calpionellite major* and the LO of *Calpionellites* (Lakova & Petrova 2012, 2013). The Tithonian/ Berriasian boundary is placed at the base of the *alpina* subzone (base of the *Calpionella* Zone), characterized by the acme of *Calpionella alpina* (spherical forms; Fig. 2.13). The boundary between the lower and upper Berriasin is defined by the base of the *simplex* subzone (base of the *Calpionellopsis* Zone). The base of the *Calpionellites* Zone (base of the *darder* subzone) delineates the base of the Valanginian (Fig. 2.13).

Atasoy (2017) and Atasoy et al. (2018) proposed a biozonation scheme that utilized both pelagic and shelf-margin-dwelling benthic fauna for the Upper Jurassic – Lower Cretaceous carbonate successions of the Sivrihisar (Eskişehir) region. They proposed a scheme based on planktonic and benthic foraminifers, pelagic crinoids, microencrusters and calpionellids (Fig. 2.13). They proposed a *Globuligerina oxfordiana – Mohlerina basiliensis* Zone for the Kimmeridgian interval. This biozone is overlain by their *Saccocoma* subzone of the partially developed *Crescentiella morronensis* Zone. The reason for this partial development of the microencruster-based zone is the unsuitable facies present at the lower levels of their succession. However, the pelagic facies present in those intervals ensure confident record of the FO datum for the pelagic crinoid *Saccocoma*. The chitinoidellids are not abundant in the Pontides. Similar to the lower part of the scheme of Skourtis-Coroneou and Solakius (1999), this interval was dominated by *Saccocoma* (Fig. 2.13). The following *Protopeneroplis ultragranulata* Zone was delineated by the FO of the name-landing benthic foraminifer. This foraminifer, being easily transportable down to the slope and into the back-margin lagoonal environments, provides a link for both depositional environments. Higher in this zone, *Crassicollaria* sp. and *Calpionella alpina* appears simply as a result of biofacies change (shift from a calciturbiditic slope deposition to pelagic deposition dominated interval) that define

the base of the *massutiniana* Zone (*pro parte*; Fig. 2.13). The rest of their scheme is in accordance with the previously published calpionellid biostratigraphy (Fig. 2.13). Another peculiar characteristic of the Sivrihisar region is the dominance of radiolarian wackestone facies in the early Valanginian and local disappearances of calpionellids (also the case in the Eastern Pontides; Fig. 2.13).

Although there are many studies confirming the well-established calpionellid biozonations, recently Benzaggah (2020) proposed a scheme with finer divisions. Being a splitter paleontologist and inspired by the biohorizon concept of ammonite biostratigraphers (Page, 1995), he introduced many new taxa and further subdivisions into a scheme with high resolution already. These new subdivisions are based on concurrent range zones of newly proposed calpionellids (Fig. 2.13). As in the case for most of the ammonite biohorizons, although they provide finest divisions of strata a geologist can get on paper, they are not traceable outside the outcrop on which they are established (see Chapter 2.3 for further discussion on biozonation concepts). This should be the reason he used capital letters (non-italized) in the zonation names as it is the case for the ammonite standard chronozones.

In contrast to these pelagic schemes applicable globally there is no consensus on the shallow marine zonation of the Upper Jurassic - Lower Cretaceous strata due to the effects of biofacies, paleogeographic realms, common presence of hiatal surfaces, dolomitization etc. (see Chapter 2.3 for further details on these factors). These limiitations mostly have resulted in local biostratigraphical schemes (Fig. 2.14).

Taslı (1990) proposed a zonation based on benthic foraminifers for the Nazlıçayır succession of the Eastern Pontides (Gümüşhane). He defined 7 biozones including an interval of unfosiliferous strata also (Fig. 2.14). He defined an "*Archaeosepta*" *basiliensis* zone at the base that is limited from the top by the base of the overlying *Alveosepta jaccardi* Zone. This *A. jaccardi* Zone is delineated by the FO of the name-giving taxon. He noted that this zone is hard to trace laterally outside the Nazlıçayır region due to facies change. The strata of this zone are overlain by thick dolomites that inhibit biozonation for this interval. As a result, Taslı (1990) left this interval

unzoned (Fig. 2.14). For the overlying biointraspratic carbonates and intercalated dolomitic intervals, he defined a "*Pseudotextulariella*" *salevensis* Range Zone (Fig. 2.14). In the upper portion of this zone, Taslı (1990) differentiated a *Barkerina barkerensis* subzone (Fig. 2.14) delineated by the FO of this taxon (correct taxon is *Barkerina dobrogiaca*). This is one of the first documentation of this genus from the Pontides (second to Bergougnan, 1987) which became critical for the delineation of the Valanginian Stage in the following years (see Chapter 2.2.2, 2.3 and 3 for further details). He differentiated *Pseudotextulariella keciensis* and *Everticyclammina hedbergi – Cuneolina hensoni* Zones for the overlying strata and suggested a Hauterivian – Barremian age. The individuals grouped under his new species *P. keciensis* actually belong to *Vercorsella* genera (also abundant in Valanginian). This species is unaccepted and dismissed in the following years. *Buccicrenata* ("*Everticyclammina*") *hedbergi* is also present in Valanginian strata. His *Cuneolina hensoni* specimens should also belong to the large flabelliform *Vercorsella* species (probably *V. camposaurii*). These remarks should recall the age data questioned in Chapter 1.4.

Altıner (1991) proposed a biozonation for the western part of the PCP that accounts for both platform and adjacent slope to basin deposits. The easily transportable nature of the utilized fossil groups (e.g., "*Tubiphytes*" *morronensis*, *Protopeneroplis* "*trochangulata*", *Montsalevia salevensis* and *Meandrospira favrei*) which are present at the platform margin environments. This property of the fossil assemblages made direct calibration of them with ammonites and calpionellids of basinal associations possible (e.g., Altıner, 1991; Cope, 1991; Altıner & Özkan, 1991). Altıner (1991) introduced the "*Tubiphytes*" *morronensis* interval zone defined at its base by the FO of the microencruster "*Tubiphytes*" *morronensis* and at its upper boundary by the FO of *Protopeneroplis* "*trochangulata*". It has two subzones; namely, the *Mesoendotyhra izjumiana – Alveosepta jaccardi – Labyrinthina – Protopeneroplis striata* assemblage subzone, indicating a Kimmeridgian age and the *Saccocoma* range subzone whose base corresponds to the base of Tithonian. His *Protopeneroplis* "*trochangulata*" zone was defined between the successive FOs of

P. "*trochangulata*" and *Montsalevia salevensis* and the base of this zone is considered to be in the upper Tithonian (Fig. 2.14). This zone has *Haplophragmoides joukowskyi* subzone marked at its base by the FO of *H. joukowskyi*. The following *M. salevensis* and *M. favrei* Zones were defined by the successive FO of the name-delivering taxa, respectively.

A similar biozone scheme was proposed by Rojay and Altıner (1998) for the Amasya region with the only difference of the "*Clypeina jurassica*" Zone (defined at the base by the FO of *Aloisalthella sulcata*). This zone is identical with respect to its chronostratigraphic position of the "*Tubiphytes*" *morronensis* Zone of Altıner (1991; Fig. 2.14).

Ivanova (1999) established another zonal scheme from Bulgaria. While she kept the general outline of Altıner (1991)'s zonation, *Protopeneroplis striata* and *Pseudocyclammina lituus* Zones were introduced (Fig. 2.14). The basal boundaries of these zones were delineated by the successive FOs of *P. striata* and *P. lituus*.

Arkad'ev et al. (2006) carried out a detailed study from Crimea and described biostratigraphic units based on ammonites, foraminifers and ostracods. They introduced a foraminiferal scheme that mainly utilizes assemblage zones of the name-delivering taxa (Fig. 2.14).

Olszewska (2010) defined four assemblage biozones from Poland for the Kimmeridgian – Valanginian interval, calibrated by ammonites. Her *Labyrinthina mirabilis – Mesoendothyra izjumiana* Zone is comparable with the *M. izjumiana – Alveospeta – Labyrinthina – P. striata* subzone of Altıner (1991; Fig. 2.14). The base of the *Protopeneroplis ultragranulata – Protomarssonella kummi* assemblage zone is correlated with the base of Berriasian.

Kaya (2014), with a pioneering study on the microencrusters of the Upper Jurassic – Lower Cretaceous İnaltı Limestone, proposed a biozonation scheme for the Tithonian – earliest Berriasian with three zones that also incorporates *Calcistella jachenhausenensis* encruster as a zone marker for the Tithonian Stage (Fig. 2.14).

He differentiated a *Mesoendothyra izjumiana* Zone for Kimmeridgian and *P. ultragranulata* Zone for the upper Tithonian – lowermost Berriasian (Fig. 2.14).

Okay et al. (2018) published two biozonation for the İnaltı Limestone deposited over both the Sakarya and İstanbul Zones in the Central Pontides (Fig. 2.14). For the succession cropped out in the Sakarya Zone they proposed a biozonation scheme for the Kimmeridgian – lowermost Berriasian strata that is based on benthic foraminifer and dascyladacean algae. They defined a *Freixialina planispiralis – Kastamonina abonica* Zone for the Kimmeridgian interval (*pro parte*; Fig. 2.14). The base of the Tithonian is defined by the base of the following concurrent range zone of *Campbelliella striata* - *Kastamonina abanica* (Fig. 2.14). The middle – upper Tithonian and lowermost Berriasian strata are characterized by the *Protopeneroplis ultragranulata* Zone and *P. ultragranulata – Anchispirocyclina lusitanica* subzone (Fig. 2.14). For the synchronous strata deposited on the İstanbul Zone, they defined the *Alveosepta jaccardi* – "*Clypeina*" *sulcata* Zone for the Kimmeridgian (*pro parte*) whose basal contact is faulted. The base of the Tithonian Stage is delineated by the base of the following concurrent range zone of *Campbelliella striata* – "*Clypeina*" *sulcata* (Fig. 2.14). The overlying part is very similar to the Sakarya Zone zonation with only differences in subzonation (Fig. 2.14). The middle – upper Tithonian and the lowermost Berriasian are characterized by the *P. ultragranulata* Zone with two subzones. The *P. ultragranulata – Campbelliella striata* Zone represents the middle – upper Tithonian strata while the overlying concurrent range zone of "*Clypeina*" *sulcata – Protopeneroplis ultragranulata* delineates the lowermost Berriasian (Fig. 2.14).

Recently, for the upper Tithonian – upper Valanginian strata, unconformity bounded assemblage zones (mostly coinciding with formation boundaries) have been proposed by Granier (2019; Fig. 2.14). The *Anchispirocyclina lusitanica* assemblage zone is defined at the base by the FO of *A. lusitanica* for the Tithonian – lower Berriasian strata. The algae of "*Clypeina*" *sulcata* and *Otternstella lemmensis* form important constituents while the Kimmeridgian species are either missing (e.g., *Alveosepta jaccardi*, *Alveosepta powersi*) or restricted to the lower part of the zone

(e.g., *Kurnubia palastiniensis* and *Campbelliella striata*). The *Protopeneroplis ultragranulata* assemblage subzone's base is defined by the first appearance datum (FAD) of the name-giving taxon. This zone represents the upper Tithonian – lower Berriasian. The overlying *Rajkaella minima* assemblage zone characterizes the middle – upper Berriasian with a subzone of *Falsolikanella campanensis* for the upper Berriasian (Fig. 2.14). The base of the *Rajkaella minima* Zone, which is at or near a disconformity, is defined by the FAD of *Rajkaella minima* or alternatively by the FAD of *Triploporella*? *Paturloni* or of *Montsalevia* gr. *Salevensis*, or by the absence of *Anchispirocyclina lusitanica* (Fig. 2.14). The FAD of *Falsolikanella campanensis* defines the base of the *Falsolikanlle campanensis* subzone that spans the upper Berriasian (Fig. 2.14). Alternative bioevents include the FAD of *Pfenderina neocomiensis*, *Valdanchella miliani* and *Pseudocymopolia pluricellata*. The absence of *Zergabriella embergeri* or environmentally related algae (e.g., *Falsolikanella campanensis*, *Clypeina catinula*, *Cly. isabellae*, *Cly. zumetae*) defines the lower boundary of his last biozon of *Pseudocyclammina lituus* Zone spanning the lower Valanginian (*pro parte*; Fig. 2.14). The top of this zone is defined by the LO of the *P. lituus*.

In the following parts proposed bioznations for the Eastern Pontides Upper Jurassic – Lower Cretaceous successions will be introduced.

2.2.1 Pelagic Biozonation (Ağören & Ozansu Sections)

7 zones and 9 subzones were differentiated for the deep marine succsessions of the Ağören and Ozansu measured sections sections (Fig. 2.15, 2.16 & 2.17).

***Crescentiella morronensis* Zone**

This zone represents the lowermost levels of the Ağören section (Fig. 2.15). It is also recognized partially in the OA measured section (Fig. 2.16). The lower boundary of this zone is defined by the FO of *Crescentiella morronensis* microencruster. The upper boundary is delineated by the FO *Protopeneroplis ultragranulata* that defines

the lower boundary of the overlying biozone (Fig. 2.13 & 2.15). Altıner (1991) introduced this "*Tubiphytes*" *morronensis* Zone above his *Globuligerina oxfordiana* Zone. The recognition of this zone in a basinal setting is dependent on the suitable biofacies to record shelf margin-dwelling microencruster. Altıner (1991)'s zonal succession resulted from the development of a pelagic plateau type sedimentation (the Taşçıbayırı Formation of NW Turkey) into a carbonate platform type (the Günören Limestone of NW Turkey; Altıner, 1991; Altıner et al., 1991). Its calibration with Jurassic ammonites suggested a Kimmeridgian age for the base of this zone at least for the PCP (see Chapter 2.3 and 3 for further discussions on bioevent datums with respect to the stage boundaries).

Radiolaria, calcareous dinocysts, microencrusters (*Radiomura cautica*, rare *Lithocodium aggregatum, Iberopora bodeuri*, *Perturbatacrusta leini*, *Koskonobullina socialis*), very rare algae, serpulid tubes (*Terebella lapilloides*, *Carpathiella triangulate*, *Carpathiella perforata*, *Carpathiella plassenensis*), pelagic crinoid *Saccocoma* sp., other *incertae sedis* (*Cayeuxia* sp., *Globochaete* sp., *Mercierella*? *dacica*) and benthic forminifers (*Textularia* spp., *Glomospira* sp., *Meandrospira* sp., *Nautiloculina* sp., very rare *Pseudocyclammina lituus*, *Mohlerina basiliensis*, *Belorussiella* sp., *Quinqueloculina* spp., rare *Haghimashella* sp., *Mesoendotyhra*? sp., *Protomarsonella* sp., *Lenticulina* spp., *Troglotella incrustans*, *Neotrocholina* sp., *Ophthalmidium* sp., *Spirillina* sp., very rare *Coscinophragma cribrosum*) constitute the accompanying taxa in this zone.

***Saccocoma* subzone**

The bottom of this subzone is at the FO datum and acme of *Saccocoma* sp. which has been considered to mark the base of Tithonian (Nicosia & Parisi, 1979; Altıner, 1991; Skourtis-Coroneou & Solakius, 1999; Fig. 2.14; see Chapter 2.3 and 3 for further discussion). This subzone is recognized in both Ağören and OA sections (Fig. 2.15 & 2.16). The fossil assemblage is similar to the *Crescentiella morronensis* Zone (Fig. 2.15, 2.16 & Appendix B).

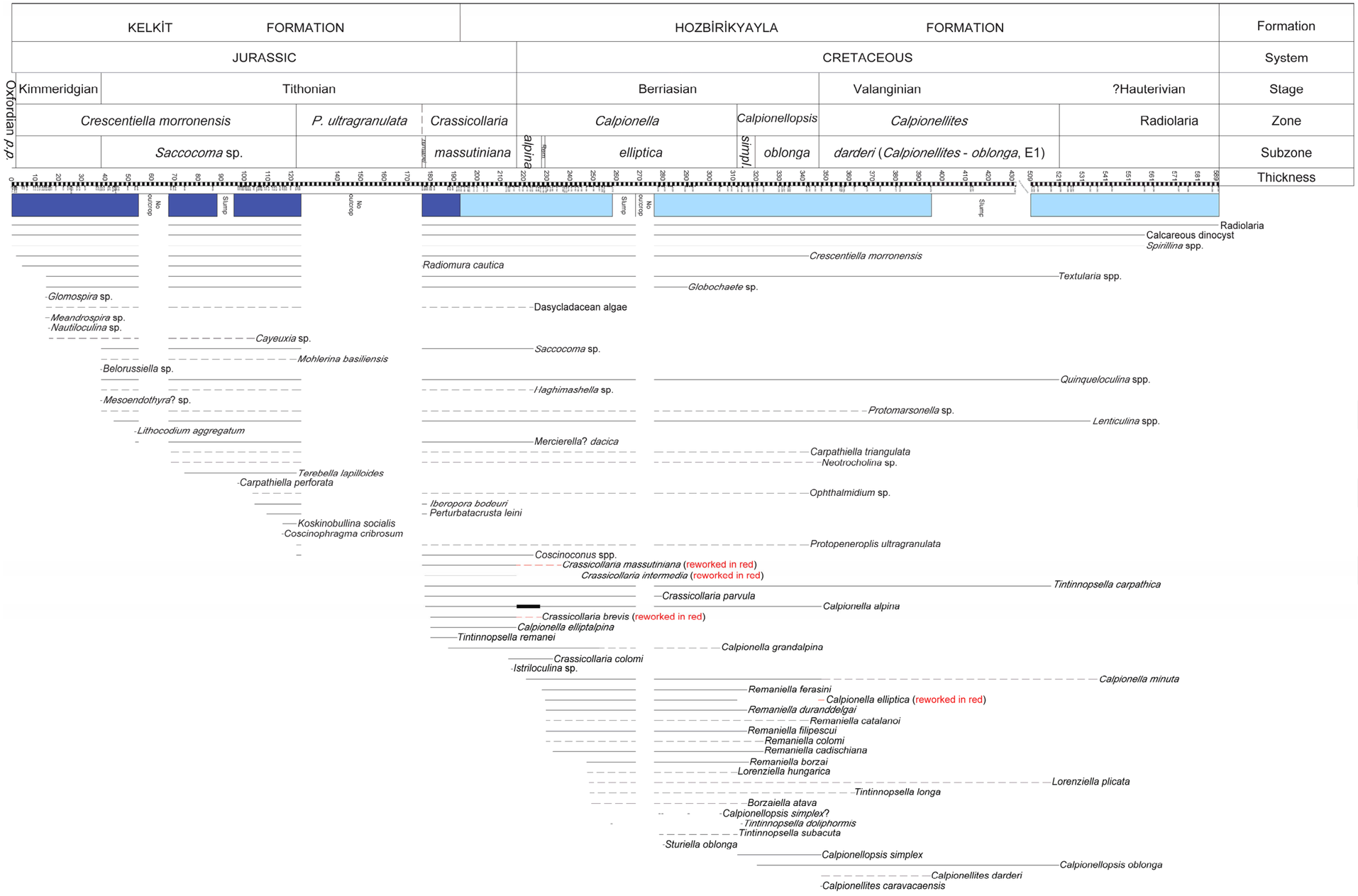

Figure 2.15. Fossil distribution of the Ağören measured section (see also Appendix B for sample-by-sample documentation and Appendix C for high resolution version).

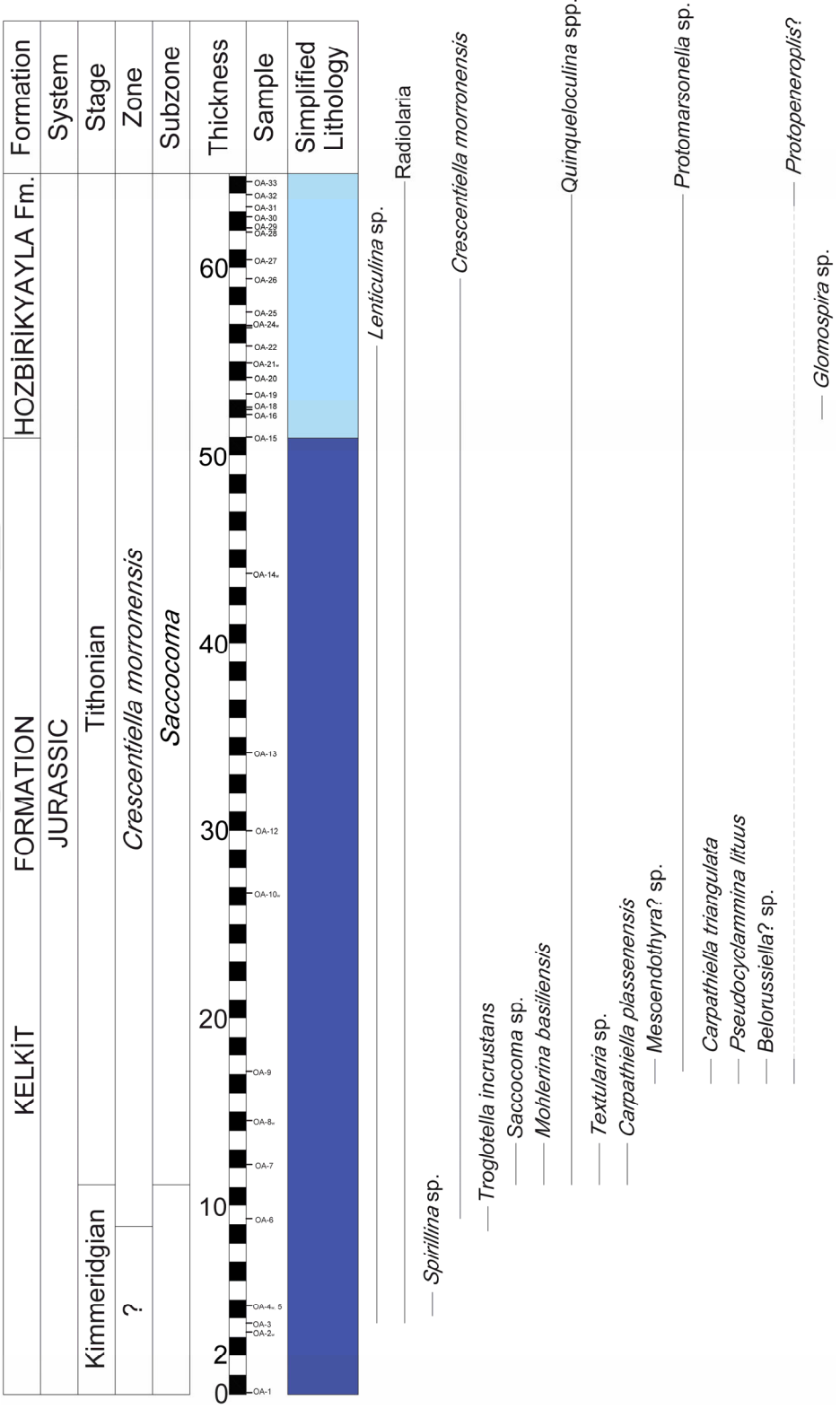

Figure 2.16. Fossil distribution of the OA measured section (see also Appendix B for sample-by-sample documentation and Appendix C for high resolution version).

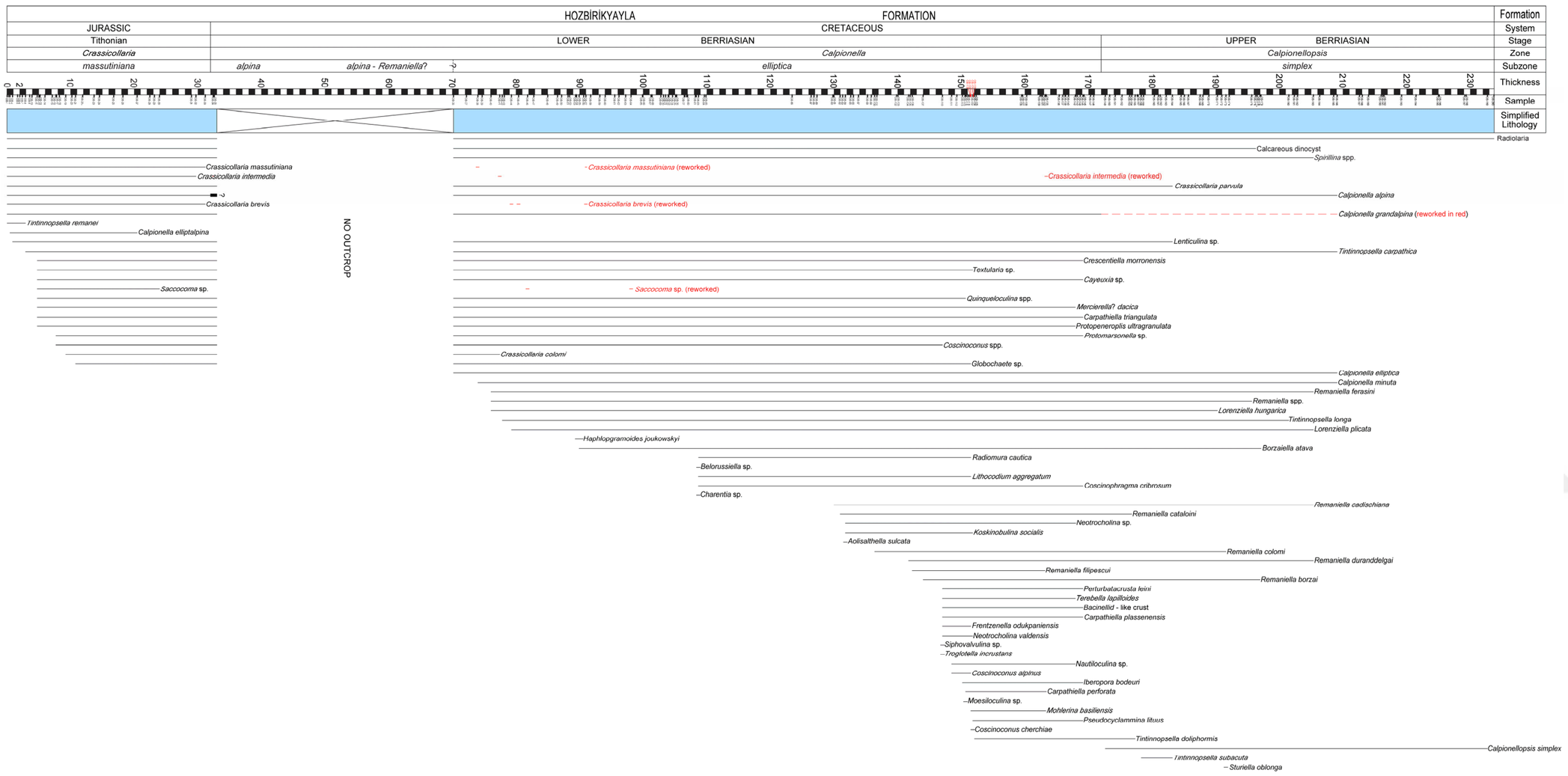

Figure 2.17. Fossil distribution of the OB measured section (see also Appendix B for sample-by-sample documentation and Appendix C for high resolution version).

Protopeneroplis ultragranulata Zone

The FO of *Protopeneroplis ultragranulata* marks the lower boundary of this zone following the *Crescentiella morronensis* Zone. This zone is only recognized in the Ağören section within the Kelkit Formation (Fig. 2.15). Most of the zone is represented by an outcrop gap (Fig. 2.15). Just below this gap, the FO of *P. ultragranulata* made differentiation of the basal boundary possible (Fig. 2.15 & Appendix B). The upper boundary of this zone is drawn with dashed line in Figure 2.15, since the following zone partly developed, and the basal boundary of the overlying zone coincides with the first strata following the outcrop gap. In accordance with the previous studies (Fig. 2.13 & 2.14) middle - upper Tithonian chronostratigraphic position is assigned to this zone.

Most of the taxa present in the underlying *Crescentiella morronensis* Zone still exist in the *P. ultragranulata* Zone with addition of *Coscinocnus* spp (Fig. 2.15).

Crassicollaria Zone

At the end of the previously explained covered interval in the Ağören section, the first beds reveal calpionellid fossils of *Crassicollaria* group (Fig. 2.15 & Appendix B). The direct transition from the *P. ultragranulata* Zone to the *Crassicollaria* Zone without the record of intervening chitnioids indicates the sample-bias resulted from this covered interval. As a result, the lower boundary of this *Crassicollaria* Zone must be diachronic in the Ağören section. This same zone is also recorded in the lower part of the OB measured section (Fig. 2.17).

Fossil assemblages include calpionellids (*Tintinnopsella remanei*, *T. carpathica*, *Crassicollaria massutiniana*, *Cr. intermedia*, *Cr. parvula*, *Cr. brevis*, *Cr. colomi*, *Calpionella. alpina*, *C. grandalpina*, *C. elliptalpina*), pelagic crinoid *Saccocoma* sp., radiolaria, calcareous dinocysts, benthic foraminifers (*Spirillina* sp., *Lenticulina* sp., *Textularia* spp., *Coscinoconus* spp., *Protomarsonella* sp., *P. ultragranulata*, *Quinqueloculina* spp., *Ophthalmidium* sp., *Istriloculina* sp., *Neotrocholina* sp.), microencruster (*Crescentiella morronensis*, *Radiomura cautica*, *Iberopora bodeuri*,

Perturbatacrusta leini), serpulid tube *Carpathiella triangulata*, *incertae sedis* (*Cayeuxia* sp., *Globochaete* sp., *Mercierella*? *dacica*) and rare algae (Fig. 2.15, 2.17 & Appendix B).

***Tintinnopsella remanei* subzone**

The evolution from the double-walled *Praetintinnopsella* to the first hyaline-walled calpionellids (e.g., *T. remanei*, *Cr. brevis*, *Cr. intermedia*) marks the base of this subzone and also the base of the *Crassicollaria* Zone.

This subzone is only partially observed in the Nazlıçayır section (Fig. 2.15) due to the above-explained covered interval. This subzone is recognized by the presence of *Cr. massutiniana*, *Cr. intermedia*, *Cr. parvula*, *T. carpathica* and the absence of *C. alpina* although *T. remanei* first occurred in the Nazlıçayır section within the *massutiniana* subzone (Fig. 2.15 and Appendix B).

Since *C. alpina* and *C. grandalpina* are already present in the first sample from the OB section *remanei* subzone is not differentiated in the Ozansu succession.

***Crassicollaria massutiniana* subzone**

This subzone is recorded in both pelagic successions (Ağören & OB sections; Fig. 2.15 & 2.17). The lower boundary (only present in the Ağören section) of this subzone is defined by the synchronous FOs of *C. alpina* and *C. grandalpina* (Fig. 2.15 & Appendix B).

***Calpionella* Zone**

The acme of *Calpionella alpina* defines the lower boundary of this calpionellid zone (Fig. 2.13, 2.15, 2.17 & Appendix B). As previously mentioned in Chapter 1, this level is the most globally recognized bioevent that is proposed as the marker of the Tithonian/ Berriasian and the Jurassic/ Cretaceous (J/K) boundary (see Chapter 2.3 and 3 for further discussion). *Crassicollaria* assemblages show important decline in abundance through the basal boundary of this zone and *C. elliptalpina* disappears at (Nazlıçayır section) or below (OB section) this level (Fig. 2.15, 2.17 & Appendix

B). *C. alpina* becomes the dominant species. Some reworked (with deformed loricae) specimens of *Cr. massutiniana*, *Cr. intermedia* and *Cr. brevis are* also observed within this zone (see Chapter 2.3 and 3 for further discussion on the boundary). The upper boundary is defined by the FO of *Calpionellopsis simplex* which also marks the lower boundary of the overlying *Calpionellopsis* Zone.

Fossil assemblage of this zone includes calpionellids (*Cr. parvula*, *Cr. colomi*, *T. carpathica*, *T. longa*, *T. subacuta*, *T. doliphormis*, *C. alpina*, *C. grandalpina*, *C. minuta*, *C. elliptica*, *Remaniella ferasini*, *R. duranddelgai*, *R. catalanio*, *R, filipescui*, *R. colomi*, *R. cadischiana*, *R. borzai*, *Lorenziella hungarica*, *L. plicata*, *Borzaiella atava*, *Sturiella oblonga*), microencrueters (*Crescentiella morronensis*, *Lithocoduim aggregatum*, *Koskinobullina socialis*, *Radiomura cautica*, *Perturbatacrusta leini*, *Iberopora bodeuri*), benthic foraminifers (*Haplophragmoides joukowskyi*, *Spirillina* sp., *Textularia* spp., *Belorussiella* sp., *Haghimashella* sp., *Quinqueloculina* spp., *Ophthalmidium* sp., *Moesiloculina sp*., *Protomarsonella* sp., *Lenticulina* sp., *Neotrocholina* sp., *Nautilicoluna* sp., *Charentia* sp., *Protopeneroplis ultragranulata*, *Mohlerina basiliensis*, *Pseudocyclammina lituus*, *Coscinoconus* spp., *Coscinophragma cribrosum*, *Troglotella incrustans*), calcaresous dinocysts, radiolaria, *incertae sedis* (Globochaete sp., *Mercierella*? *dacica*), algae (*Aloisalthella sulcata*), pelagic crionid *Saccocoma* sp. (disappears below the boundary in the OB section; Fig. 2.17) and serpulid tubes (*Carpathiella triangulata*, *Car. plassenensis*, *Car. perforota*, *Terebella lapilloides*,

***Calpionella alpina* subzone**

This is the lowermost zone of the *Calpionella* Zone. The base is defined by the acme of *C. alpina* (Fig. 2.15, 2.17 & Appendix B). *Crassicollaria brevis*, *Cr. intermedia*, *C. grandalpina* assemblages show important decline. *C. elliptalpina*, dominating the uppermost level of the underlying Crassicollaria Zone, disappears at the Tithonian/ Berriasian boundary. *Cr. brevis* and *Cr. intemedia* disappear within the alpina subzone (see Chapter 2.3 and 3 for further discussions). *Crassicollaria parvula* is

the most dominant Crassicollaria species in this subzone. The upper boundary is at the base of the overlying *Remaniella* subzone.

***Remaniella* subzone**

The base of this zone is defined by the FO of the remaniellid calpionellids (with bipartite collars). The order of origination of the *Remaniella* species is still not clear, however, *Remaniella ferasini* is thought to be the ancestor of this stock and widely used as the marker of the base of this zone (Fig. 2.15 & AppendixB). Accordingly, the base of this zone is delineated by the FO of *R. ferasini* in Ağören section (Fir. 2.15 & Appendix B). *C. alpina* loses its dominance within this subzone. Only several reworked individuals of *Cr. brevis* and *Cr. intermedia* were observed in this zone (Fig. 2.15 & Appendix B). *Remaniella* zone could not be recognized in the OB section due to an outcrop gap (Fig. 2.17).

The upper boundary is defined by the base of the overlying *elliptica* subzone.

***Calpionella elliptica* subzone**

The FO of *Calpionella elliptica* marks the lower boundary of this subzone (Fig. 2.13, 2.15 & Appendix B). This zone is limited from above by the following *Calpionellopsis* Zone (Fig. 2.15 & 2.17). The basal boundary of this zone is only recognized in the Ağören measured section (Fig. 2.15). The lower part of this zone is unfortunately within a covered interval in the OB section (Fig. 2.17). *Remaniella* thrives within this subzone with evolution of *R. filipescui*, *R. cadischiana*, *R. borzai*, *R. duranddelgai*, *R. catalanoi*, and *R. colomi* (Fig. 2.15 & 2.17). However, the relative abundance of remaniellid calpionellids never reaches a dominant level. *Lorenziella plicata* and *L. hungarica* show FOs within this subzone (Fig. 2.15 & 2.17). *C. grandalpina* is relatively abundant. *Haplophragmoides joukowkyi* is also recorded within a short interval of this subzone in the OB section (Fig. 2.17); a taxon whose FO is important for the delineation of the middle Berriasian (see Chapter 2.3 and 3 for further discussion).

Calpionellopsis Zone

The base of this zone is differentiated by the FO of *Calpionellopsis simplex*. The base of the overlying *Calpionellites* Zone defines the upper boundary in the Ağören section (Fig. 2.15). The uppermost part of the OB section is still in the *Calpionellopsis* Zone (Fig. 2.17). The base of this zone is proposed to be at the boundary of the lower and upper Berriasian (Fig. 2.13). The fossil assemblage is similar to the underlying *elliptica* subzone. (Fig. 2.15 & 2.17). As the number of calciturbiditic intervals decreases middle Berriasian onward shelf margin-dwelling taxa decreases in abundance that create local disappearances (Fig. 2.15 & 2.17).

Calpionellopsis simplex subzone

The base of this subzone is at the base of the *Calpionellopsis* Zone. *C. elliptica* shows major decline in abundance in the lower level of and disappears within this zone (Fig. 2.15 & 2.17). *Remaniella* species are still diversified. *C. grandalpina* could not survive into the *simplex* subzone in the Ağören section (Fig. 2.15) as suggested by Benzaggagh (2020), while it is still sporadically present in the OB section. These taxa in the OB section should be reworked specimens (Fig. 2.17). When compared to the thickness in the OB section, *simplex* subzone is represented by a short interval of strata in the Ağören section. As can be seen in Appendix B that A-201 sample with "red hatch" records a questionable presence of *Calpionellopsis simplex* which is followed by several questionable records (A-224, A-232, A-233, A-239). If these were true *C. simplex* individuals, it would place the lower boundary of the *simplex* subzone and the *Calpionellopsis* Zone 30 m lower in the Ağören section. This datum actually will be suggested by the quantitative biostratigraphical analyses in Chapter 2.3 as the FO level of *C. simplex* in the Ağören section.

The following zones and subzones are only recorded in the Ağören section.

Calpionellopsis oblonga subzone

The lower boundary is delineated by the FO of *Calpionellopsis oblonga* (Fig, 2.15). *T. carpathica* and *T. longa* are abundant (Fig. 2.15 & Appendix B). *R. cadischiana*

is the dominant remaniellid within this subzone accompanied by *R. colomi*. Other remaniellids disappeared within the *simplex* subzone. The base of the overlying *Calpionellites* Zone is constrained by the *oblonga* subzone above.

***Calpionellites* Zone**

The FO of *Calpionellites darderi* (Fig. 2.15 & Appnedix B) defines the base of this zone and the Berriasian/ Valanginian boundary (see Chapter 2.3 and 3 for further details). This zone is partially observed in the Ağören section. The upper boundary of the zone is a facies controlled local level, characterized by the arrival of radiolara-rich facies (Fig. 2.15). *C. simplex* disappears within the *oblonga* subzone. *C. oblonga*, *T. oblonga* and *T. longa* are abundant. *Calpionellites caravacaensis* is firstly reported from the Pontides in this study from this *Calpionellite* Zone (Fig. 215 & Appendix B).

***Calpionellites – Calpionellopsis oblonga* E1 subzone**

This subzone is differentiated by the co-occurrence of *Calpionellites darderi* and *Calpionellopsis oblonga* (Fig. 2.15 & Appendix B). It corresponds to the E1 subzone of Benzaggagh (2020: Fig. 2.13).

"Radiolaria" Zone

Radiolaria – rich facies strats to dominate the deposition in the early Valanginian (Fig. 2.15). The sporadic presence of *C. minuta* (Fig. 2.15 & Appendix B) indicates the lower portion of this Zone could be still in the *darderi* subzone (Fig. 2.13, 2.15 and also see Chapter 2.3 and 3 for further discussion). Unfortunately, there is no index fossils in the rest of the section to provide solid constraints on the age interpretations (Fig. 2.15). The thickness of the measured portion may suggest the presence of Hauterivian strata. Accordingly, without labelling a solid boundary, Hauterivian age with question mark is placed on the log (Fig. 2.15).

2.2.2 Neritic Biozonation (Nazlıçayır Section)

4 zones and 2 subzones were differentiated in the shallow marine strata of the Nazlıçayır Section (Fig. 2.18, 2.19 & Appendix B).

***Crescentiella morronensis* Zone**

This zone represents the lowermost part of the Nazlıçayır section (Fig. 2.18). The lower boundary of this zone is delineated by the FO of the *Crescentiella morronensis* microencruster. This zone is identical to the lower part of the "*Tubiphytes*" *moronensis* Zone of Altıner (1991; Fig. 2.14).

The fossil assemblage of this zone includes benthic foraminifers (*Mesoendothyra izjumiana*, *Mesoendotyhra* cf. *croatica*, *Alveosepta jaccardi*, *Mohlerina basiliensis*, *Coscinophragma cribrosum*, *Pseudocyclammina lituus*, *Pseudocyclammina sphaeroidalis*, *Streptocyclammina hottingeri*, *Streptocyclammina* gr. *parvula-muluchensis*, *Protopeneroplis striata*, *Nautiloculina* sp, *Charentia* cf. *cuvilieri*, *Charentia* sp., *Everticyclammina* sp., *Kurnubia*? sp., cf. *Bramkampella arabica*, *Ammobaculites* sp., *Textularia* sp., *Meandrospira* sp., *Istriloculina* spp., *Quinqueloculina* sp., *Glomospira* sp., *Moesiloculina* sp., *Coscinoconus* spp., *Trogrotella incrustans*, *Spirillina* sp.), algae (*Campbelliella striata*, *Aloisalthella sulcata*), rare microencrusters (*Lithocodium aggregatum*), crustacean microcoprolites (*Favreina* spp.), *incertase sedis* (*Cayeuxia* sp., *Mercierella*? *dacica*) very rare calcareous dinocyst (in the sample L41).

The upper boundary of this zone is truncated by a prominent unconformity in the region which brought the Kimmaridgian and middle – upper Berriasian strata in direct contact (Fig. 2.8, 2.10, 2.12, 2.18 & 2.19).

***Mesoendothyra izjumiana – Alveosepta jaccardi* subzone**

This zone is identified by the presence of some complex foraminifers including *Mesoendothtyra izjumiana*, *Alveosepta jaccardi* and sporadically occurring *Protopeneroplis striata* (Fig. 2.18). The encrusting foraminifer *Mohlerina basilien-*

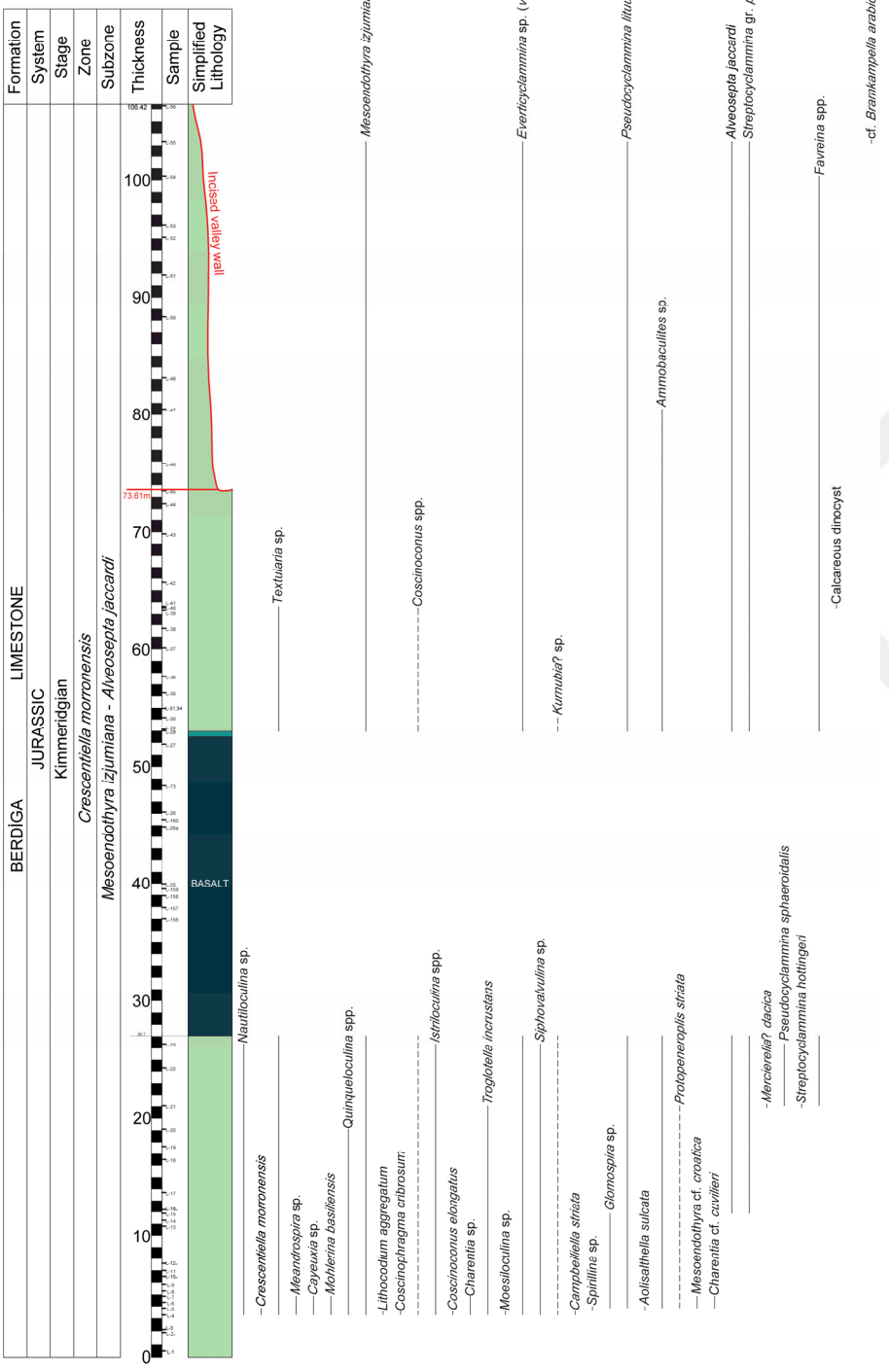

Figure 2.18. Fossil distribution of the Nazlıçayır measured section (below the unconformity; see also Appendix B for sample-by-sample documentation and Appendix C for high resolution version).

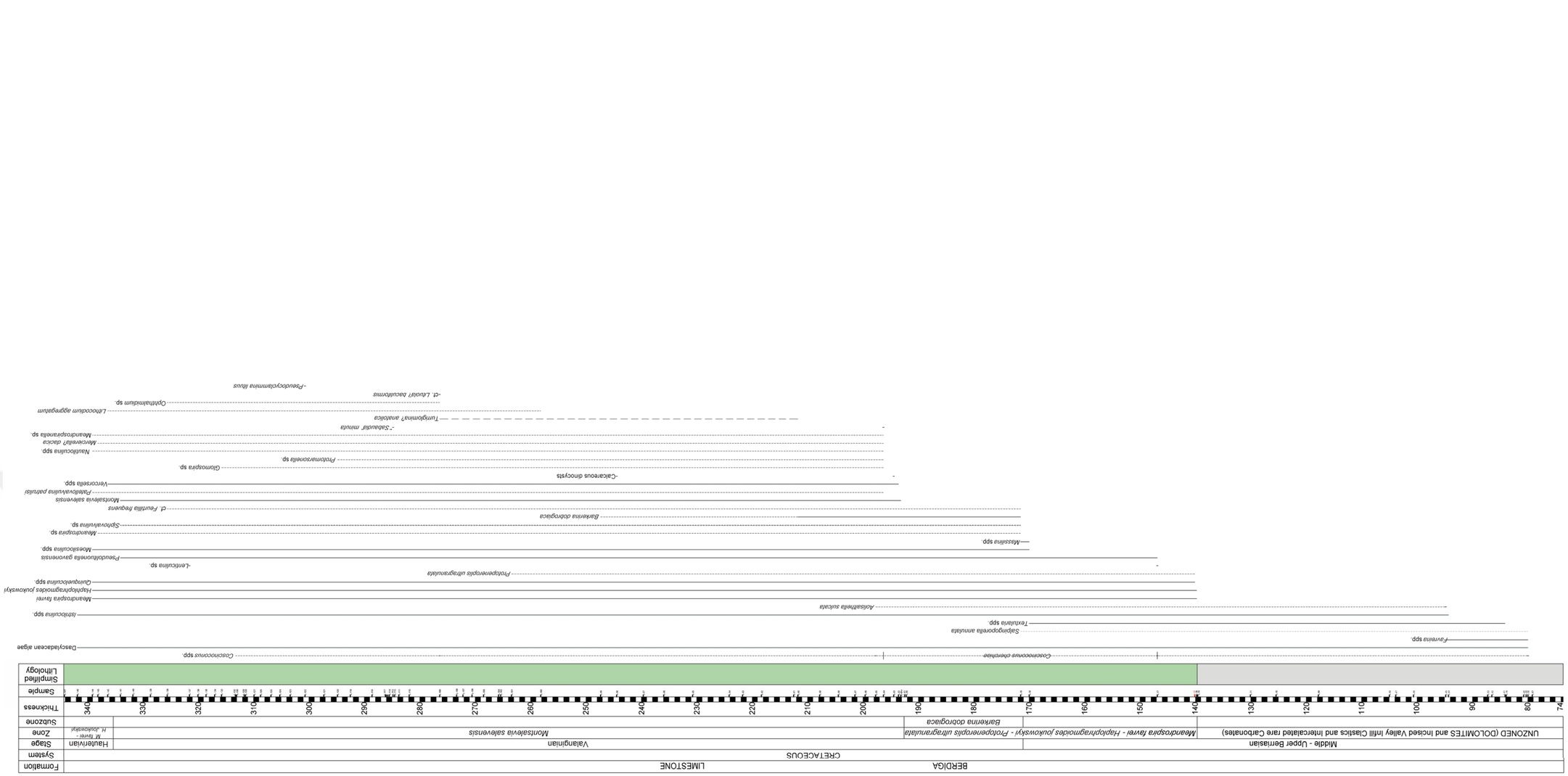

Figure 2.19. Fossil distribution of the Nazlıçayır measured section (above the unconformity; see also Appendix B for sample-by-sample documentation and Appendix C for high resolution version).

sis form another prominent constituent. *Pseudocyclammina lituus* is also another member of this subzone. *Pseudocyclammina sphaeroidalis* is recorded in the strata just below the basalt level (Fig. 2.18). While *Streptocyclammina hottingeri* is rare, *S.* gr. *parvula – muluchensis* continuously recorded in this zone (Fig. 2.18 & Appendix B). The algae of *Aloisalthella sulcata* and *Campbelliella striata* only occurs at the lowermost portion of this zone (Fig. 2.18 & Appendix B).

Unzoned Dolomitic Interval

Thick dolomites and incised valley infill clastics and intercalated rare carbonates following the unconformity in the Ağören section do not yield index taxa and any continuous record of fossil to delineate a biozone and depositional age for this interval. Consequently, this part is left unzoned (Fig. 2.19 & Appendix B).

Rare foraminifers (*Coscinoconus* spp., *Textularia* spp.), algae (*Aloisalthella sulcata* and cf. *Salpingopoerlla annulata*) and microcoprolites (*Favreina* spp.) were observed in the intercalated carbonate strata (Fig. 2.19 & Appendix B).

***Meandrospira favrei – Haphlophragmoides joukowskyi – Protopeneroplis ultragranulata* Zone**

The carbonates following the dolomitic intervals yield diversified fossil assebmlages that lead to differentiation of *Meandrospira favrei – Haphlophragmoides joukowskyi – Protopeneroplis ultragranulata* Zone. The lower boundary is delineated by the local FOs of the name-landing taxa (Fig. 2.19 & Appendix B). The lower boundary of this zone is obviously a local datum marking a transition from dolomitic interval to neritic carbonates (Fig. 2.19).

Fossil assemblage includes foraminifers (*M. favrei*, *H. joukowskyi*, *P. ultragranulata*, *Pseudolituonella gavonensis*, *Moesiloculina* spp., *Meandrospira* sp., *Massilina* sp., *Quinqueloculina* spp., *Lenticulina* sp., *Siphovalvulina* sp., cf. *Feurtillia frequens*, *Barkerina dobrogiaca*, *Coscinoconus* spp., *Textularia* spp,), and algae (*Aloisalthella sulcata* and cf. *Salpingopoerlla annulata* and other undetermined taxa).

Barkerina dobrogiaca subzone

This subzone is differentiated at the upper part of the *M. favrei – H. joukowskyi – P. ultragranulata* Zone. The lower boundary of this subzone is determined by the FO of *Barkerina dobrogiaca* (Fig. 2.19 & Appendix B). This species is proposed as a Valanginian marker (e.g., Schlagintweit et al., 2019) confined to the northern Tethys margin. Accordingly, it is used as the Valanginian-base marker in this study (Fig. 2. 19 & Appendix B).

Montsalevia salevenesis Zone

The base of the *Montsalevia salevensis* Zone is defined by the FO of the name-giving taxon and the upper boundary is delineated by the last occurrence (LO) this foraminifer (Fig. 2.19 & Appendix B). When compared to the previously published schemes (Fig. 2.14) the FO datum of *M. salevensis* recorded in this study seems to be a local elevated bottom. Taslı (1990) recorded this foraminifer before the FO of *B.* "*barkeriensis*" (Fig. 2.14). However, on the same Nazlıçayır succession, Granier (2020b) recorded *B. dobrogiaca* below the FO of *M. salevensis* as in this study (Fig. 2.19 & Appendix B). This could be the real FO of *M. salevensis* in this succession. In this case the lower boundary of this zone should be facies controlled. The second option would be again a local FO datum due to sample bias introduced by the sample intensity immediately following the dolomitic interval, an interval in which the outcrop conditions are poor. In any case, this bioevent in the Nazlıçayır section represents a local datum (see Chapter 2.3 and 3 for further discussion).

The accompanying fossil assemblages include foraminifers (*Meandrospira favrei*, *Haplophragmoides joukowksyi*, *Protopeneroplis ultragranulata*, *Pseudolituolina gavonensis*, rare cf. *Feurtillia frequens*, *Barkerine dobrogiaca*, *Patellovalvulina patrulisi*, *Vercorsella* spp., very rare "*Sabaudia*" *minuta*, rare *Turriglomina*? *anatolica*, rare *Lenticulina* spp., rare *Coscinoconus* spp., *Siphovalvulina* sp., *Glomospira* sp., *Meandrospira* sp., *Meandrospirinella* sp., *Moesiloculina* spp., *Quinqueloculina* spp., *Ophthalmidium* sp., *Istriloculina* spp., *Protomarsonella* sp., *Nautiloculina* spp., very rare *Lituola*? cf. *baculiformis* and *Pseudocyclammina*

lituus), rare *incertae sedis* (*Mercierella*? *dacica*), algae (*Aloisalthella sulcata* at the lower portion and undetermined algae), very rare calcareous dinocysts (only in the sample L96) and rare microencrusters (*Lithocodium aggregatum*).

***Meandrospira favrei – Haplophragmoides joukowskyi* Zone**

The lower boundary of this biozone is delineated by the LOW of *M. salevensis* and does not coincide with an evolutionary bioevent (Fig. 2.19). This biozone represents an assemblage zone of the name-landing taxa. The upper boundary is at a recent erosional surface in the study area. It is proposed to represent lowermost Hauterivian (see Chapter 2.3 and 3 for further discussion). The fossil assemblage is similar to the underlying biozone (Fig. 2.19 & Appendix B).

When the pelagic and neritic biozonation schemes are compared, it can be realized that there is no single bioevent that defines the stage boundaries nor synchronous fossil datums that guarantee solid correlation. In the following chapter stage boundaries and fossil bioevents will be discussed further with quantitative biostratigraphical analyses.

2.3 Quantitative Biostratigraphy

In this chapter, a dataset coming from 17 localities on the PCP and its related basinal associations will be analyzed (Fig. 2.20). The aim of this chapter is to construct a composite stratigraphic standard as a working hypothesis that accounts for both the pelagic and neritic deposits of this Upper Jurassic – Lower Cretaceous carbonate platform by calibrating shallow marine and deep marine bioevents through the application of quantitative biostratigraphical methods while providing new insights into the chronostratigraphical problems summarized in the introduction part. Quantitative methods, namely the graphic correlation (Shaw, 1964; Edwards, 1984) and the unitary associations (Guex, 1977; 1991), corresponding to two classical biostratigraphical approaches; the zonations based on first occurrence (FO)/ last occurrence (LO) events (i.e., interval zones) and the zonations based on assemblages

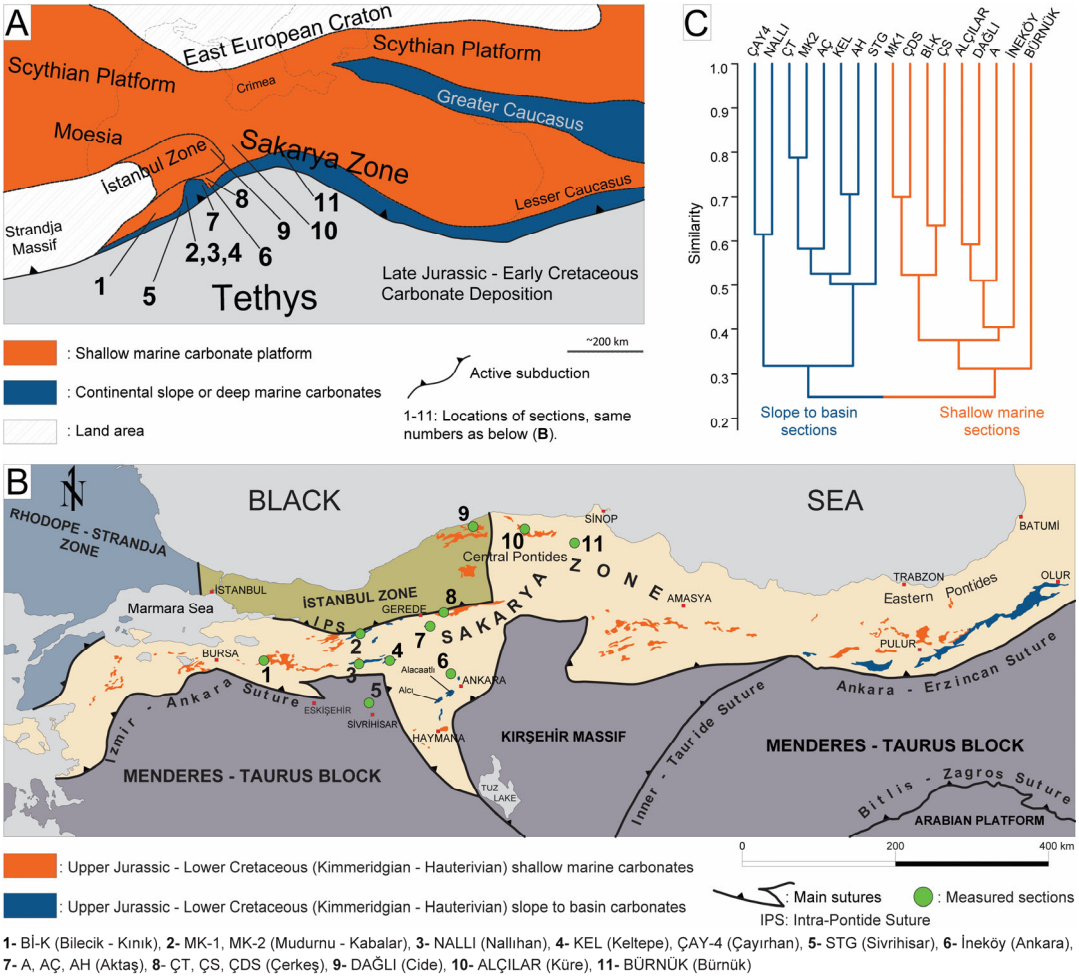

Figure 2.20. A) Schematic paleogeographical map of the southern margin of Laurasia for the Late Jurassic–Early Cretaceous interval and the approximate locations (1-11) of the analyzed successions (modified from Okay et al., 2013 and Nikishin et al., 2015). **B)** Distribution of the Upper Jurassic–Lower Cretaceous Carbonates in the Pontides (modified from Okay & Altiner, 2016). The numbers (1-11) show the locations of the stratigraphic sections. **C)** Clustering of the analyzed stratigraphic sections based on presence/absence fossil data (unweighted paired group with arithmetic mean (UPGMA), Bray-Curtis similarity index, cophenetic correlation with Cophen. corr. 0.7446) to provide simple visualization of the paleoenvironments of the measured sections in the dataset (from Atasoy et al., 2022).

(i.e., Oppel zones), respectively, are used for data treatment. Correlations obtained by conventional biostratigraphy and quantitative methods are compared and implications for biozonations and age assignments are discussed.

In the Sakarya Zone, the PCP developed over a structural basement shaped by the Carboniferous Variscan orogeny (e.g., Göncüoğlu et al., 2000; Topuz et al., 2007; Dokuz et al., 2011; Okay & Topuz, 2017) and the Late Triassic to (?Late) Jurassic subduction – accretion of the Karakaya Complex (*s.l.*) and related oceanic edifices (e.g., Okay & Göncüoğlu, 2004; Robertson & Ustaömer, 2012; Göncüoğlu et al., 2012; Sayit & Göncüoğlu, 2013; Okay et al., 2015; Çimen et al., 2018; Okay et al., 2020b; Marroni et al., 2020). The Jurassic transgression over this basement laid down fluviatile to shallow marine sediments with *rosso ammonitico* lenses in the Western Pontides (Görür et al., 1983; Altiner et al., 1991; Varol & Gökten, 1994; Alkaya & Meister, 1995; Kuznetsova et al., 2003; Delikan & Orhan, 2020; section locations 1 and 6 in Fig. 2.20B), known as the Lower–Middle Jurassic Bayırköy Formation, while a widespread Toarcian–Oxfordian volcanic arc and related volcaniclastic sedimentation characterized the Central and Eastern Pontides (Şen, 2007; Meijer et al., 2010; Okay et al., 2014; Akdoğan et al., 2018). Middle Jurassic metamorphism accompanied this volcanism in the northern Central Pontides (Okay et al., 2014; section locations 10 and 11 in Fig. 2.20B). In the Mudurnu region (section locations 2, 3, 4 and 7 in Fig. 2.20B), contemporaneous deposits are characterized by volcanics and volcaniclastics of the Middle Jurassic Mudurnu Formation (Saner, 1980; Altiner et al., 1991; Koçyiğit & Altiner, 2002; Genç & Tüysüz, 2010).

The main phase of carbonate platform development started with starved pelagic plateau–type deposits; the Callovian–Oxfordian Taşçıbayırı Formation, overlying the Bayırköy Formation in the Western Pontides and Ankara region (Altiner et al., 1991; Koçyiğit & Altiner, 2002; section locations 1 and 6 in Fig. 2.20B). The carbonates of this formation are made up of condensed deposits of pelagic oolites and bioclastic wackestones–grainstones containing traces of volcanic activity and nodular *rosso ammonitico* limestone levels (Altiner et al., 1991; Kuznetsova & Bragin, 1999; Kuznetsova et al., 2003; Delikan & Orhan, 2020). A similar facies association also marks the onset of carbonate deposition in the Aktaş region (section location 7 in Fig. 2.20B), known as the Dedeninseti Formation, overlying the

Mudurnu volcanics (Altiner et al., 1991). In the intervening Mudurnu Trough (section locations 2, 3, 4 and 7 in Fig. 2.20B), the Mudurnu Formation is overlain by a sequence of deep marine carbonates and calciturbidites with limestone blocks and breccia levels containing intercalated volcanics and volcaniclastics. This Callovian–Tithonian Kurcalıkdere Formation deposited within a rapidly subsiding unstable basin and forms transitional facies between the Mudurnu volcanics and the overlying pelagic carbonates (Altiner et al., 1991). The condensed pelagic plateau–type deposits on the paleo–highs surrounding the Mudurnu trough are overlain by the shallow marine carbonates of the Kimmeridgian–Valanginian Günören Limestone (Altiner et al., 1991) in the Western Pontides (section locations 1 and 6 in Fig. 2.20B). The Aktaş Formation is the equivalent shallow marine deposits in the Aktaş–Gerede region (sections ÇDS and ÇS at the location 8 and the marginal section A at the location 7 in the Fig. 2.20B). These shallow marine carbonate factories shedded carbonate grains into the intervening deep marine sequences of the Mudurnu region, forming the slope facies of the Oxfordian–Valanginian calciturbiditic Yosunlukbayırı Formation (Altiner et al., 1991; section locations 2, 3, 4, 5 and 7 in Fig. 2.20B). This facies represents the transitional deposits between the shallow marine limestones and the pure pelagic porcelaneous Maiolica–type carbonates of the Tithonian–Aptian Soğukçam Limestone (Altiner et al., 1991; Yilmaz et al., 2016) which covers the shallow marine carbonates in the Western Pontides with a drowning unconformity in the Hauterivian (Altiner et al., 1991).

The Kimmeridgian–Berriasian shallow marine carbonates are named as the İnaltı Formation in the Central Pontides (section locations 9, 10 and 11 in Fig. 2.20B). These carbonates directly overlie the Permo-Triassic red beds (section location 9 in Fig. 2.20B) or the Middle Jurassic continental to shallow marine clastics in the eastern part of the İstanbul Zone (Tüysüz, 1999; Okay et al., 2018). In the Sakarya Zone segment of the Central Pontides, the İnaltı Formation rests on the Upper Triassic Flysch deposits (Okay et al., 2015) and the Middle Jurassic metamorphics of the subduction–accretion complexes (Aygül et al., 2016) with basal clastics of the

Bürnük Formation (Tüysüz, 1999; Kaya & Altiner, 2015; Okay et el., 2018; section locations 10 and 11 in Fig. 2.20B).

These Upper Jurassic–Lower Cretaceous shallow marine carbonates, ranging in facies from tidal flat deposits to lagoonal and reefal limestones, form the most distinctive and laterally traceable stratigraphic succession over the Pontides (Fig. 2.20B). In the Eastern Pontides, these shallow marine carbonates (known as the Berdiga Limestone) pass southward into deep marine deposits, cropping out in several north–vergent thrust sheets just to the north of the İAE suture (Fig. 2.20B; Bergougnan, 1976; Görür, 1988; Burşuk, 1992; Robinson et al., 1995; Okay et al., 1997; Timur, 2000; Ustaömer & Robertson, 2010). In contrast, in the northern (e.g., Okay et al., 2018) and southern (Rojay, 1995; Rojay & Altıner, 1998) Central Pontides and similarly in the western Pontides (Altıner et al., 1991; Okay & Tüysüz, 1999), these slope to basin marginal carbonates are missing. The Upper Jurassic–Lower Cretaceous outcrops still reveal shallow marine facies in areas very close to the İAE suture (see Bursa region in Fig. 2.20B). The southernmost Upper Jurassic–Lower Cretaceous carbonate outcrops of the Pontides in the Haymana region (Fig. 2.20B) are mainly shallow marine, with the only difference that the carbonate platform in that segment was drowned in the Berriasian (Okay & Altıner, 2016), earlier than other areas. As mentioned previously, *in-situ* slope to basin carbonates are present in the Mudurnu region (section locations 2, 3, 4 and 7 in Fig. 2.20B). Further, allochthonous blocks belonging to the marginal deposits of this Upper Jurassic–Lower Cretaceous PCP crop out in an olistostrome belt that extends from the northeast of Haymana through the Alçı–Alacaatlı line to the north of Ankara (Fig. 1B; Koçyiğit, 1991; Rojay & Süzen, 1997; Okay et al., 2019). Similar limestone blocks and tectonic slices of carbonate deposits within imbricated zones crop out along the İAE suture (e.g., Koçyiğit et al., 1988; Koçyiğit, 1991; Okay & Tüysüz, 1999; Rojay, 2013).

A tectonic slice belonging to this PCP crops out to the north of Sivrihisar (Gautier, 1984; Okay & Tüysüz, 1999; Atasoy et al., 2018; section location 5 in Fig. 2.20B). The carbonate sequence in this slice is characterized by imbricated shallow marine

and slope to basin carbonates. This succession includes deposits from the Kimmeridgian–Berriasian calciturbiditic slope to basin carbonates of the Yosunlukbayırı Formation and the overlying Valanginian Soğukçam Limestone (Atasoy et al., 2018; section location 5 in Fig. 2.20B).

In the post-Hauterivian times, the pelagic deposition dominated over most of the Pontides (Altıner et al., 1991; Rojay, 1995; Okay & Nikishin, 2015; Okay & Altıner, 2016). As far as known there is no documented post-Hauterivian continuous shallow marine carbonate deposition (e.g., Altiner et al., 1991; Okay et al., 2018; Granier, 2020b) as the region became tectonically active (e.g., Okay et al., 2013; Okay & Nikishin, 2015). For this reason, the Hauterivian is selected as the upper limit for data analysis.

The studied 17 stratigraphical sections from this Upper Jurassic–Lower Cretaceous PCP can be broadly assigned to two major depositional environments for the analyzed Callovian–Early Hauterivian interval (Fig. 2.20C). A simple objective cluster analysis divides the measured sections into two main groups with similarity indices indicating closer relationships within subgroups according to the presence/ absence fossil data (Fig. 2.20C and Appendix D). This dendrogram is in accordance with the biofacies and microfacies analyses and provides a simple general visualization. A detailed summary of the main characteristics of the successions analyzed is given in Table 2.1 with related references.

2.3.1 Correlation Tools versus Incomplete Rock Record and Need for Quantitative Biostratigraphy

2.3.1.1 Nature of sedimentary record

The most obvious drawback complicating temporal correlation and calibration is the incompleteness of the rock record. Since the pioneering studies that speculated on fragmentary character of the geologic record (e.g., Buckman, 1893; Barrell, 1917),

Table 2.1 Summary of the main characteristics of the analyzed stratigraphical sections from the Western and Central Pontides for quantitative biostratigraphical analyses.

Section (in compositing order)	Location	Lithostratigraphy*	Succession Characteristics	Biofacies	(Sub-) Zones**	References
AÇ	Aktaş (location 7 in Fig. 1B)	Yosunlukbayırı Formation (1070 m)	Pelgic carbonates with calciturbiditic intervals (Slope Facies)	Pelagic & Neritic Taxa	I, II†, (IIa, IIb), III†, (IIIa), IV A3, B, C, D1, D2, D3, E, F	Altiner (1991) Altiner & Özkan (1991) Altiner et al. (1991)
KEL	Kozağaç - Keltepe (Çayırhan) (location 4 in Fig. 1B)	Yosunklukbayırı Formation (400 m) Soğukçam Limestone (280 m)	Pelgic carbonates with calciturbiditic and breccia intervals (Slope Facies) ***pass into*** pure pelagic carbonates (Basinal Facies)	Pelagic & Neritic Taxa	II, (IIb†), III Ch, A1, A2, A3, B, C	Altiner (1991) Altiner & Özkan (1991) Altiner et al. (1991) Mekik et al. (1999)
AH	Aktaş (location 7 in Fig. 1B)	Yosunlukbayırı Formation (416 m)	Pelgic carbonates with calciturbiditic intervals (Slope Facies)	Pelagic & Neritic Taxa	II, (IIb), III, (IIIa) A3, B, C, D1	Altiner (1991) Altiner & Özkan (1991) Altiner et al. (1991)
STG	Sivrihisar (Eskişehir) (location 5 in Fig. 1B)	Yosunklukbayırı Formation (407 m) Soğukçam Limestone (43 m)	Pelgic carbonates with calciturbiditic intervals (Slope Facies) ***pass into*** pure pelagic carbonates (Basinal Facies)	Pelagic & Neritic Taxa	*G.oxfordiana* - *M. basiliensis*, *C. morronensis* (*Saccocoma*), *P. ultragranulata*, *Crassicollaria* (*massutiniana*), *Calpionella* (*alpina, Remaniella, elliptica*), *Calpionellopsis* (*simplex, oblonga*), *Calpionellites* (*darderi*) Zones	Atasoy et al. (2018)
ÇT	Türbedağ (Çerkeş) (location 8 in Fig. 1B)	Yosunlukbayırı Formation (534 m)	Pelgic carbonates with calciturbiditic intervals (Slope Facies)	Pelagic & Neritic Taxa	III, (IIIa), IV D2, E, F	Altiner (1991) Altiner & Özkan (1991) Altiner et al. (1991)
MK-2	Karapınarkayağı (Mudurnu) (location 2 in Fig. 1B)	Yosunklukbayırı Formation (191 m) Soğukçam Limestone (>124m)	Pelgic carbonates with calciturbiditic intervals (Slope Facies) ***pass into*** pure pelagic carbonates (Basinal Facies)	Pelagic & Neritic Taxa	III, (IIIa†), IV, V A3, C, D1, E, F	Altiner (1991) Altiner & Özkan (1991) Altiner et al. (1991)
MK-1	Kabalar (Mudurnu) (location 2 in Fig. 1B)	Mudurnu Formation (341 m) Kurcalıkdere Formation (88 m) Yosunlukbayırı Formation (211 m)	Volcanics arc ***overlain by*** olistostromal carbonates that ***pass into*** pelgic carbonates with calciturbiditic intervals (Slope Facies)	Pelagic & Neritic Taxa	II, (IIa), (IIIa) B, C	Altiner (1991) Altiner & Özkan (1991) Altiner et al. (1991)
ÇAY-4	Çayırhan (Beypazarı) (location 4 in Fig. 1B)	Yosunlukbayırı Formation (220 m)	Pelgic carbonates with calciturbiditic intervals (Slope Facies)	Pelagic & Neritic Taxa	II, (IIb) Ch, A1, A2	Altiner (1991) Altiner & Özkan (1991) Altiner et al. (1991)
NALLI	Nallıhan (location 3 in Fig. 1B)	Yosunklukbayırı Formation (755 m) Soğukçam Limestone (50 m)	Pelgic carbonates with calciturbiditic and breccia intervals (Slope Facies) ***pass into*** pure pelagic carbonates (Basinal Facies)	Pelagic & Neritic Taxa	(IIb), V A, C	Altiner (1991) Altiner & Özkan (1991) Altiner et al. (1991)
ÇDS	Deresoplan (Çerkeş) (location 8 in Fig. 1B)	Aktaş Formation (357 m) Yosunklukbayırı Formation (127 m)	Shallow marine carbonates (Platform Facies) ***pass into*** pelagic carbonates with calciturbiditic intervals (Slope Facies)	Neritic & Pelagic Taxa	II, (IIa), (IIIa) C	Altiner (1991) Altiner et al. (1991)
Bi-K	Kınık (Bilecik) (location 1 in Fig. 1B)	Bayırköy Formation (25 m) Taşçıbayırı Formation (25 m) Günören Limestone (436 m) Soğukçam Limestone (>240 m)	Basal clastics are unconformably ***overlain by*** pelagic plateau-type carbonates that ***pass into*** shallow marine carbonates (Platform Facies) ***were drowned by*** pure pelagic carbonates (Basinal	Neritic (mainly) & Pelagic Taxa	I, II, (IIa†), IV†, V	Altiner (1991) Altiner et al. (1991)
ÇS	Sekinindoruk (Çerkeş) (location 8 in Fig. 1B)	Aktaş Formation (902 m) Soğukçam Limestone (>20 m)	Shallow marine carbonates (Platform Facies) ***were drowned by*** pure pelagic carbonates (Basinal Facies)	Neritic Taxa	(IIa), III, (IIIa), IV	Altiner (1991) Altiner et al. (1991)
Bürnük	Bürnük (location 11 in Fig. 1B)	Bürnük Formation (>23 m) İnaltı Formation (385 m)	Basal clastics are unconformably ***overlain by*** shallow marine carbonates (mainly Reefal and Lagoonal Facies) (***ended with an unconformity***)	Neritic Taxa	*Mesoendothyra izjumiana*, *Calcistella jachenhausenensis* and *Protopeneroplis ultragranulata* Zones	Kaya (2014) Kaya & Altiner (2015)
Alçılar	Alçılar (Küre) (location 10 in Fig. 1B)	Bürnük Formation (>10 m) İnaltı Formation (605 m)	Basal clastics are unconformably ***overlain by*** shallow marine carbonates (Platform Facies; Pelagic incursion in the uppermost part) (***ended with an unconformity***)	Neritic Taxa	*Freixialina planispiralis* - *Kastamonina abanica*, *Campbelliella striata* - *Kastamonina abanica*, *Protopeneroplis ultragranulata* (*Protopeneroplts ultragranulata* - *Anchispirocyclina lusitanica*) Zones	Okay et al. (2018)
Dağlı	Dağlı (Cide) (location 9 in Fig. 1B)	İnaltı Formation (1392 m)	Shallow marine carbonates (Platform Facies) (***fault bounded***)	Neritic Taxa	*Alveosepta jaccardi* - *Clypeina sulcata*, *Campbelliella striata* - *Clypeina sulcata*, *Protopeneroplis ultragranulata* (*P. ultragranulata* - *C. striata, C. sulcata* - *P. ultragranulata*) Zones	Okay et al. (2018)
İncköy	İncköy (Ankara) (location 6 in Fig. 1B)	Bayırköy Formation (102 m) Taşçıbayırı Formation (73 m) Günören Limestone (910 m)	Basal clastics are unconformably ***overlain by*** pelagic plateau-type carbonates that ***pass into*** shallow marine carbonates (Platform Facies) (***ended with an unconformity***)	Neritic (mainly) & Pelagic Taxa	Not Zoned (Kimmeridgian - Berriasian?)	Koçyiğit & Altiner (2002)
A	Aktaş (location 7 in Fig. 1B)	Dedeninsecti Formation (77 m) Aktaş Formation (1090 m)	Pelagic plateaut-type carbonates are ***overlain by*** shallow marine carbonates (Platform Facies)	Neritic Taxa	II, III, (IIIa)	Altiner (1991) Altiner et al. (1991)

* Deposits above drowning unconformities (e.g. Bi-K, ÇS sections) and unconformity bounded basal clastics (e.g. Bi-K, Alçılar sections) are not included in analysis. First line is the bottom, last line is the top of the section.

** Biozones of Altiner (1991); **I:** *Globuligerina* gr. *oxfordiana* Zone; **II:** *"Tubiphytes" morronensis* Zone; **IIa:** *Mesoendothyra izjumiana - Alveosepta - Labyrinthina - Protopeneroplis striata* subzone; **IIb:** *Saccocoma* subzone; **III:** *Protopeneroplis ultragranulata* Zone; **IIIa:** *Haplophragmoides joukowskyi* subzone; **IV:** *Montsalevia salevensis* Zone; **V:** *Meandrospira favrei* Zone. ***Chitinoidella*, A1, A2, A3, B, C, D1, D2, D3*** and **E** Zones are the Vocontian Trough calpionellid biozones of Remane (1985); **F:** last calpionellid zone introduced by Altiner & Özkan (1991) between the successive last occurences of *Calpionellites darderi* and *Tintinnopsella carpathica*.

†: Zones and subzones in the biozone-type sections.

different perspectives have been proposed on sedimentation trends. The concepts range from classical continuous sedimentation in pelagic environment on one hand to minor sedimentation between dominant episodes of removal and nondeposition (e.g., "catastrophic uniformitarianism" of Ager, 1973). Between these two extreme ends, sedimentation models accounting wider observations have been proposed by Strauss & Sadler (1989) and an improved statis model by Tipper (2015), putting importance also on nondepositional intervals. The common consensus in these later models is that sedimentation rates vary significantly, and the rock record is incomplete even at finer scales (e.g., Dott, 1983; Aubry, 1995; Calloman, 1995; Miall, 2015, 2016). This is evident from the negative power law relationship between the rock accumulation rates and the time span of measurement as documented by Sadler (1981), Tipper (1983), Plotnick (1986), Schlager et al. (1998), Sadler (1999) and Kemp (2012): as the time span of the measurement increases, calculated sedimentation rate decreases, indicating increasing number of intervening cryptic hiatal surfaces (apart from obvious unconformities) punctuating the sedimentary record. The study of recent deposits demonstrates that even pelagic domains are dynamic (e.g., Hollister et al., 1984) and underwater vast regions can be full of hiatuses (e.g., Keller et al., 1987; Rea et al., 2006; Erdem et al., 2016). In fact, many stratification planes at all scale represent nondepositional and/or erosional surfaces (e.g., Campbell, 1967; Macquaker & Howell, 1999; Kowalewski & Bambach, 2008; Trabucho-Alexandre, 2015; Gani, 2017). Preserved stratal thicknesses are closely related to time; unrecorded intervals are confined to the stratal surfaces and the rest is trapped within the rock record. Figure 2.21 illustrates a simple hypothetical succession, with intervals of net sedimentation, nondeposition and erosion, and its relationship with time, represented by the rock record. As clearly seen, stratal thickness closely mimics the time record, however they differ significantly; unrecorded interval can be more than the recorded geologic time (Fig. 2.21).

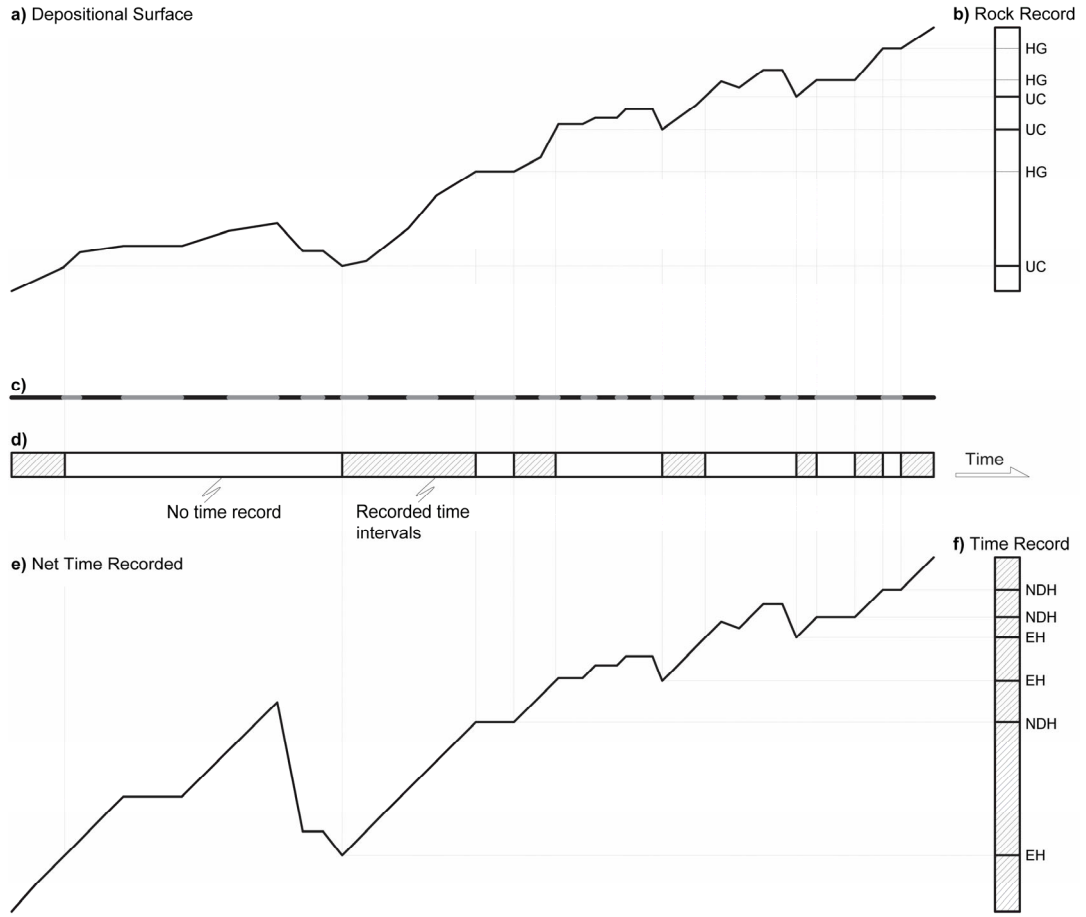

Figure 2.21. Relationship between the rock record and time. **a)** The changes of the depositional surface elevation (from an initial sediment – water interface) with respect to time (d). Effects of compaction and dissolution are not considered. Net sedimentation increases the elevation of the depositional surface, nondepositional periods create hardgrounds with no (or minor) elevation change. Erosional periods remove a certain thickness of the previously deposited sediments; removed thickness depends on the intensity of the erosive action. **b)** "Rock Record" column represents the final stratigraphical record. HG: hardground surface; UC: unconformity surface. **c)** The ends of the alternating black and gray lines represent the changes in the trend of deposition (i.e., increasing and decreasing rates of deposition and erosion). **d)** The time axis common to both graphs (a) and (e). Hatched boxes indicate recorded time intervals. Blank boxes represent the unrecorded time intervals confined to the stratal surfaces (i.e., HG and UC surfaces). **e)** Net time recorded vs time graph. Each increment of time on both axes will draw a 1:1 trend line independent from the rate of deposition. Erosive periods represented by decreasing trend lines with slopes depending on the rate of erosion. Nondepositional intervals will draw horizontal lines. **f)** "Time Record" column shows the net recorded geologic time by the rock record (b). Note that the total time passed (d) is more than twice of the recorded geologic time. NDH: nondepositional hiatus; EH: erosional hiatus. Dashed thin lines between the graphs are the traces of hiatal intervals and surfaces. Note that in depo-

Figure 2.21 (*continued*) sitional environments dominated by cross stratification, time – thickness relationship will be more complicated as the bedding planes bounding cross stratified bedforms will be time transgressive composite surfaces. (from Atasoy et al., 2022)

2.3.1.2 Correlation tools and their pitfalls

All correlation tools at our disposal suffer from the fragmentary character of the geologic record. Only the radiometric dating provides direct timelines (with error margins – a correlation canal), however volcanics are rarely found intercalated within sedimentary rocks and do not provide continuous data points along a succession. Other main correlation methods; biostratigraphy, isotope stratigraphy and magnetostratigraphy, depend on recognition of contrast between samples along a succession (Salvador, 1994). These contrasting criteria are presence, absence and acme of certain fossils or fossil groups for biostratigraphy, shifts in isotope patterns for chemostratigraphy and magnetic reversals for magnetostratigraphy; all marking changes across a datum. Then these horizons are used as correlation lines between sections and as means of age assignment by correlation with standard chronostratigraphic scales. Each of these methods has its deficiencies. Bioevents are biofacies dependent and can be diachronic even under good preservation conditions (e.g., Monnet & Bucher, 2002; Hilgen et al. 2005; Cody et al., 2008; Kowalewski & Bambach, 2008; Wade et al. 2011; Lucas, 2018). Measured isotope patterns can be greatly modified by the sedimentation rates; a gradual signal change in a succession with high sedimentation rates can be recorded as a sharp jump in a succession where condensed intervals or gaps are present, disturbing the original isotope pattern (e.g., Loutit et al., 1988; Miall, 2010; Trabucho-Alexandre, 2015; Strasser, 2016 and see Price et al., 2016 for compilation of data through the Late Jurassic–Early Cretaceous interval and greatly varying curves). Let alone isotope values can show variance in today's oceans, depending on the circulation patterns (e.g., Ravizza & Zachos, 2003; Smith et al., 2015) and diagenesis is another problem. Similarly, for magnetostratigraphy, the space between recorded reversals is subjected to

sedimentation rates and the completeness of the successions. Burial diagenesis, low grade metamorphism and remagnetizations can overprint the original signal (e.g., Aubry et al., 2007; Smith et al., 2015) and missing intervals can lead to miscorrelation, the "bar-code effect" (Torrens, 2002).

Besides these main tools, model dependent correlation and calibration methods are present. Sequence stratigraphy is a powerful method, depending on correlation of cyclic stratal surfaces induced by eustasy. Because of the character of unconformities which obviously include hiatuses of varying magnitude, sequence boundaries are not always easy to locate chronostratigraphically (e.g., amalgamation of closely spaced sequence boundaries) and demonstration of global synchroneity is not straightforward due to the overprint of allocyclic and autocyclic processes (e.g., Aubry, 1991; Miall, 1992; Schlager, 2010; Strasser, 2016; Holbrook & Bhattacharya, 2012; Miall, 2016; Catuneanu, 2019). Astrochronology provides fine scale resolution to estimate duration of successions, zones and stages; especially for Neogene chronostratigraphy which is astronomically calibrated and tied to the present time. For the rest of the geologic time scale, "floating" orbital time scales with lower resolution have been established (for review see Huang, 2018). This method may be the most sensitive correlation tool to the incomplete rock record and varying sedimentation rates as continuous sedimentation of the succession under analysis is one of the main assumptions of the method for transformation from thickness to time domain. The possibility of artificial signal production by the tuning processes, the uncertainties in the retrodiction of past orbital frequencies and the assumption of linear response of the climatic system to the orbital changes and its direct influence on the sedimentary system are adding volume to the error margins for older geologic time intervals (e.g., Miall & Miall, 2004; Bailey, 2009; Vaughan et al., 2011; Sinnesael et al., 2019).

Except from radiometric dating and biostratigraphy, all other correlation tools are based on pattern matching of repetitive proxies that require independent age control. If temporal correlation attempts are solely based on those physical tools and model dependent methods, the output will be excessively prone to subjective judgement

(e.g., Zeller, 1964; Miall, 1992; Torrens, 2002) and mostly a kind of lithostratigraphic correlation will be achieved (Miall & Miall, 2004; what is called "tyranny of strata" by Şengör, 2016).

2.3.1.3 Biostratigraphic correlations and their limits

Biostratigraphy stands alone as the only method that independently provides nonrepetitive, unique datums for correlation of strata (e.g., Teichert, 1958, Eldredge & Gould, 1977; Miall, 2004) due to the irreversible character of evolution (Dollo's [1893] law). That is why the main structure of the Geological Time Scale had been constructed long before the development of modern physical correlation methods and radiometric dating. However, biostratigraphic correlation also includes many difficulties. Biostratigraphy is a never-ending practice, always having room for refinement and improvement. Biostratigraphic raw data from a succession provide local, stratal bioevents and ranges less than or equal to the true total stratigraphic range of taxa (biozone vs biochronozone). Each new sampled stratigraphical section (or even resampling of previously documented sections) provides data that confirms or challenges the already existed biostratigraphical frameworks. Both kinds of observation are important, but the contradicting ones are especially valuable, given that there are no erroneous identifications, since they generally expand our knowledge toward the true ranges of taxa and their relative positions with respect to each other. As data are synthesized from different localities, a global picture approximating the true geographical and stratigraphical distributions of taxa will be produced. Then, age assignment to rocks by fossils becomes the interpretation of the local biozones in the light of these global (or regional) syntheses.

Nevertheless, this inductive approach does not provide linear progress as interpretation tends to get complicated in calibration of taxa from different lineages and different biofacies. This difficulty is particularly prominent in the correlation and calibration of the pelagic and shallow marine bioevents among different fossil groups, which forms one of the main targets of this study. Marginal carbonates can

provide the link between these two distinctly separated depositional environments since they generally contain mixed fauna including both pelagic and shallow marine fossils. Figure 2.22 illustrates some pitfalls that may be present in this kind of carbonates where quantitative methods can be useful for calibration and correlation problems. Figure 2.22A shows a hypothetical stratigraphic section with a facies evolution from pelagic limestones to shelf margin and shallow marine carbonates through an interval of calciturbiditic slope deposits. An unconformity is present toward the top of the section represented by an exposure surface with dissolution. The section ends with transgressive pelagic carbonates. Three index fossils are observed whose total local distributions are given within the succession. The bottom of the succession is characterized by a shallow aragonite compensation depth (ACD) interval, hindering preservation of the Fossil C with aragonitic test in these deep marine deposits. Up in the section, calciturbiditic intervals start to dominate. Some of them have prominent erosive bases, removing unknown amounts of the data (Fig. 2.22A). These calciturbiditic deposits bring with themselves shelf margin dwelling shallow marine taxa, the Fossil D. However, we cannot be sure about the synchroneity of its FO level. Along the section stylolites are present (Fig. 2.22A) and an important amount of the previously deposited carbonates were probably dissolved along the stylolite planes. Like erosive bases, unconformities and condensed intervals, these stylolites also contribute to the ordering and scaling problems of the bioevents. Then, up in the section regressive shelf margin carbonates are overlain by lagoonal limestones. Just below the shelf margin carbonates, the LO of the Fossil C is located, probably a facies-controlled datum (Fig. 2.22A). The shallow marine carbonates are truncated by an unconformity surface that also probably truncated the top of the Fossil D's range. The LOs of the Fossils A and B occur within the overlying pelagics. This section was logged by two different geologists with different sampling densities (Fig. 2.22A; Log A & B), creating sampling bias and diachronic biohorizons even between these two logs (Fig. 2.22B). None of the logs could record the global horizons since local ranges are present in that region (Fig. 2.22A & B). Direct assignment of a chronostratigraphic level via correlation to global schemes

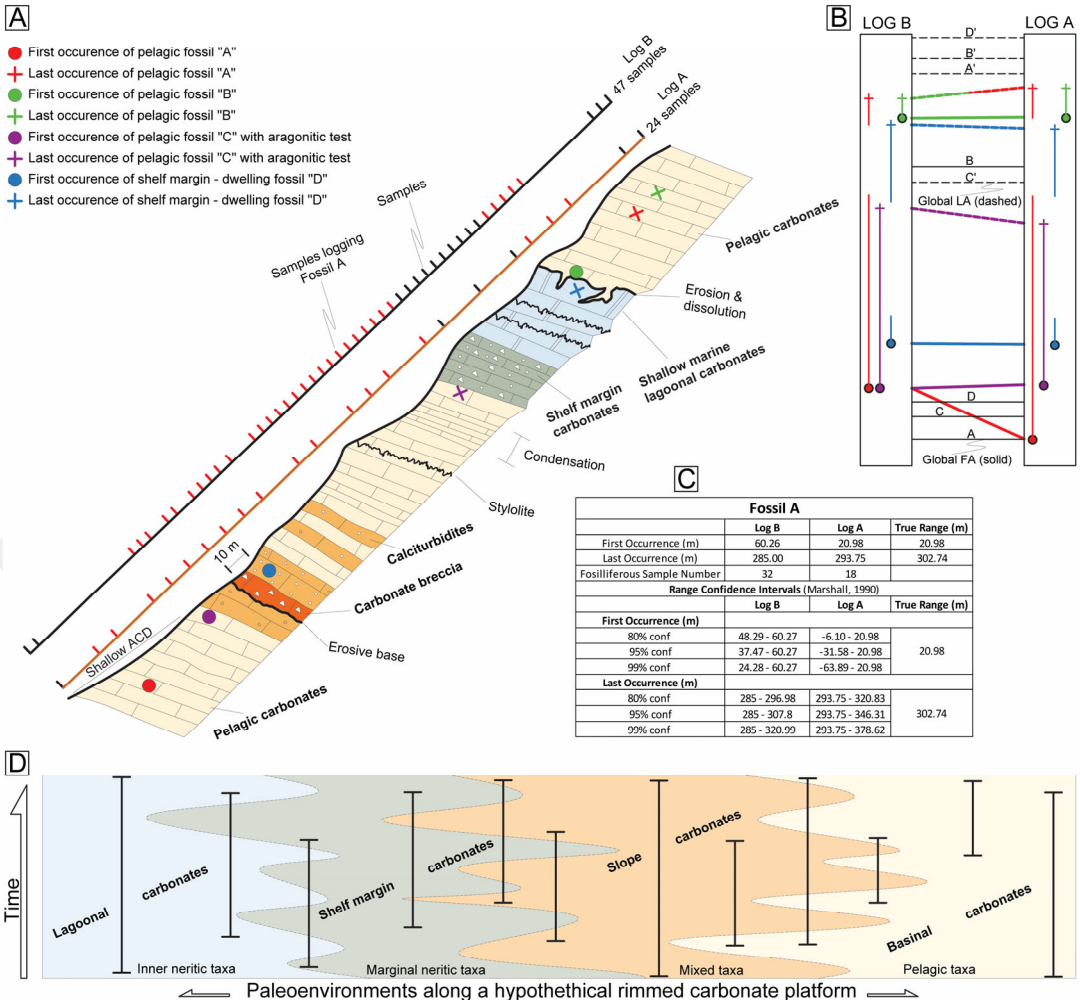

Fossil A

	Log B	Log A	True Range (m)
First Occurrence (m)	60.26	20.98	20.98
Last Occurrence (m)	285.00	293.75	302.74
Fosilliferous Sample Number	32	18	
Range Confidence Intervals (Marshall, 1990)			
	Log B	**Log A**	**True Range (m)**
First Occurrence (m)			
80% conf	48.29 - 60.27	-6.10 - 20.98	20.98
95% conf	37.47 - 60.27	-31.58 - 20.98	
99% conf	24.28 - 60.27	-63.89 - 20.98	
Last Occurrence (m)			
80% conf	285 - 296.98	293.75 - 320.83	302.74
95% conf	285 - 307.8	293.75 - 346.31	
99% conf	285 - 320.99	293.75 - 378.62	

Figure 2.22. Pitfalls commonly present in marginal carbonate biostratigraphy and importance of synthesizing large data from varieties of depositional environments. **A)** A hypothetical stratigraphic section showing changes in facies. The section was logged at different times by different researchers with different sampling plan (24 samples for Log A & 47 samples for Log B). Three index species were recorded. Individual characters of these fossils are given at top left. Circles are local FOs, crosses are local LOs. ACD: aragonite compensation depth. Short lines along the logs represent sampling levels. Red sample lines are the ones recording the Fossil A. **B)** Correlation of the logs A & B. Interpreted stratigraphic distributions of the fossils are shown with related colors within the log columns. Colored solid lines between the logs are the correlation lines of the FO horizons with related fossil color code. The dashed colored lines are the tie lines of the LOs. Global first appearance (FA) synchronous datums are represented by the thin solid black lines between the logs with related fossil letters. Global last appearance (LA) synchronous datums are represented by the thin dashed black lines labelled by letters with apostrophe. Note the diachroneity of the observed local ranges within the same succession due to sampling bias and the major differentiation from the global chronostratigraphic surf-

Figure 2.22 (*continued*) aces. **C)** Range confidence interval comparison for the Fossil A between the two logging sessions. FO and LO levels of the Fossil A are given in meters for Log A & B. Number of samples recording the Fossil A is given in the "Fossiliferous Sample Number" line. The true stratigraphic levels corresponding to the FA and LA global datums of the Fossil A are provided in the "True Range" column. Below these data, calculated range confidence intervals are given (according to Marshall, 1990). Although logger B collected nearly twice sample, only the range confidence interval for Log A covers the true FA datum and only the logger A manage to observe the FO of Fossil A synchronous with its global FA datum. For last occurrences both loggers observed depressed tops even older than local true LO level. **D)** Paleoenvironment change with time along a cross section of a hypothetical carbonate platform with a rimmed margin. Several stratigraphic sections were measured on outcrops belonging to different facies of this platform instead of limited number of observations from a section (A). Vertical solid lines in the illustration represent the distribution of these measured sections in paleoenvironments and time. Each section has its own characteristic facies and fossil content and represents varying time duration with major overlaps. Slope carbonates including mixed fauna provide the key facies linking shallow marine marginal and open marine pelagic fauna. Quantitative methods can evaluate all fossil data at the same time regardless of facies types and can help in eliminating biased correlations solely based on index fossils. For discussion see the text (from Atasoy et al., 2022).

with a priori synchroneity assumption can create miscorrelation (Fig. 2.22B; Huxley's [1862] homotaxis). Increased number of samples may not improve the situation (Fig. 2.22C).

The most reliable fossil datum should be provided by the observed phyletic first occurrence from an ancestor if the evolutionary lineage is well established (not reversible morphological responses to local ecological variations but true speciation; e.g., Murphy, 1977; Remane, 1991; Murphy & Salvador, 1999; Pignatti & Papazzoni, 2017). On the other hand, in biostratigraphic studies synthesizing several fossil groups with unrelated lineages from varieties of depositional environments, the phyletic control cannot be always ensured. Index fossil based conventional correlations give more importance on several species specific to a certain depositional environment and correlation upon them generally provide non-contradictory tie lines in the expense of the complete use of biostratigraphical data and higher resolution. The stratigraphical distribution of accompanying fossils with

respect to these index species mostly show contradicting orders, e.g., species A above index species B in one section and in another section species A below index species B, then in another section species C appears just below the LO of species B: What can be the relative positions of species A and C and all the other fossils observed? That is the main difficulty in the ordering and scaling of bioevents from unrelated lineages recorded in several measured sections overlapping in time and located on different depositional environments (Fig. 2.22D). In this kind of correlation problems, quantitative biostratigraphical methods can liberate biostratigraphers from the vagaries of incomplete rock record exemplified in the Figure 2.22 by incorporating large volume of paleontological data (e.g., Hammer & Harper, 2006, 2024). Instead of separately dealing with each of these subenvironments, quantitative methods can provide a helpful tool in sequencing of all kinds of bioevents and for the determination of relative distances between these biohorizons by analyzing datasets including the mixed fauna provided by the marginal carbonate deposits in addition to data from solely shallow marine and deep marine successions (Fig. 2.23).

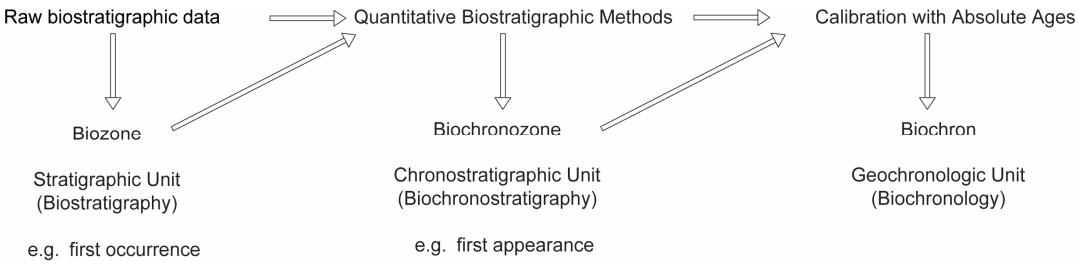

Figure 2.23. Summary chart for the transition from raw biostratigraphic data to chronostratigraphy by application of quantitative biostratigraphic methods. If absolute age data is incorporated, biochronology will be achieved at the end.

2.3.1.4 Biozonation types and their corresponding quantitative methods

Speciation concepts (e.g., phyletic gradualism vs. punctuated equilibrium, Eldredge & Gould, 1977; allopatric speciation, Mayr, 1963), taxonomic approaches (e.g., typological vs biometric, Less, 1998; Less & Kovács, 2009; phenetic vs cladistic,

Ansety & Pachut, 2004) and nature of the fossil record (e.g., discrete distribution of radiolarian rich outcrops within mélanges, Baumgartner et al., 1995; discontinuous terrestrial biostratigraphy, Woodburne & Swisher, 1995) all have influence over the preferred biozonation type (e.g., Pignatti, 1998; Fig. 2.24).

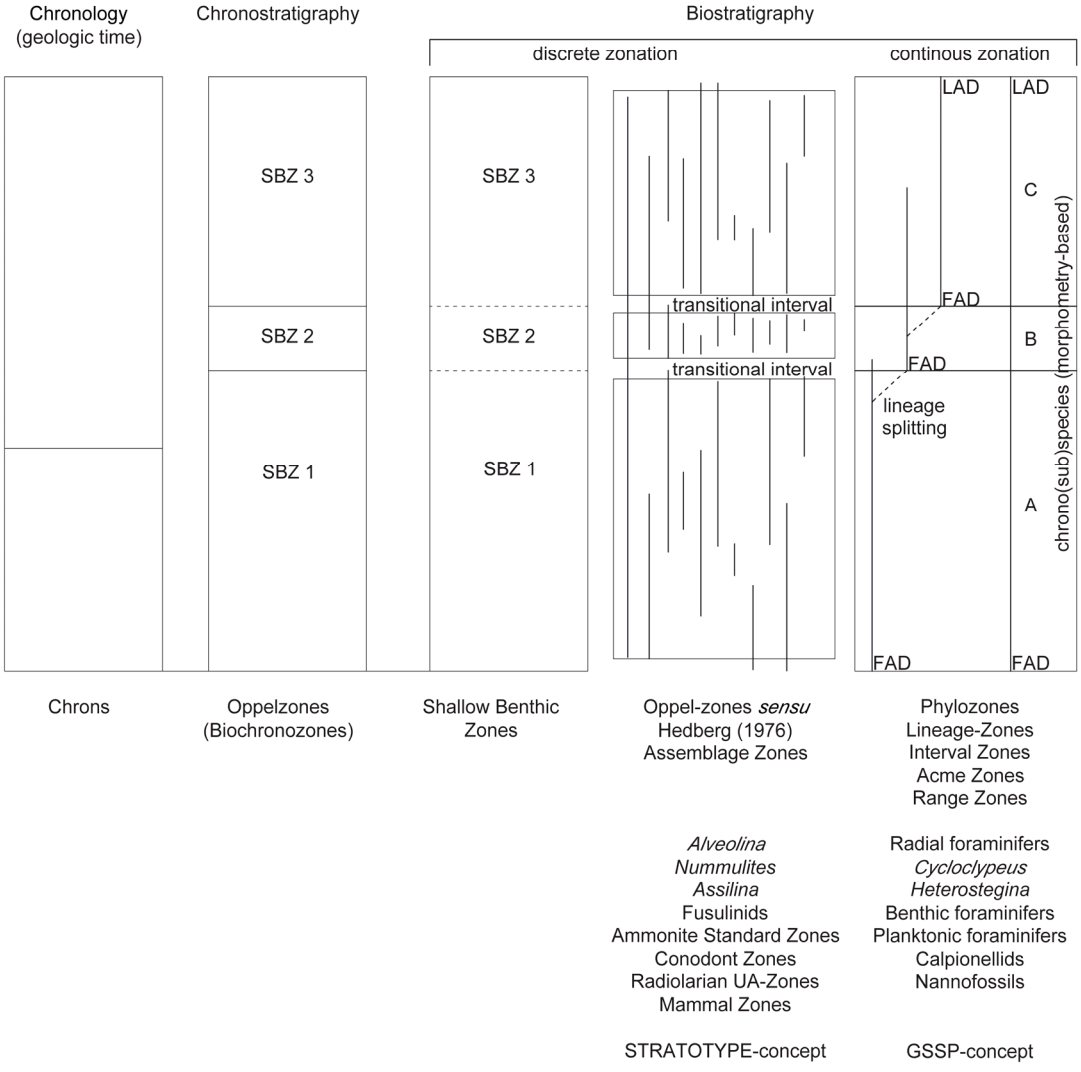

Figure 2.24. A comparison chart for biozonation types. SBZ: shallow benthic zonation (modified from Pignatti & Papazzoni, 2017).

There are mainly two kinds of biozonation: (i) continuous and (ii) discrete (Fig. 2.24). The continuous schemes include the commonly used zonation types whose boundaries are defined by the specified FO/LO datums such as interval zones, range zones and lineage zones (e.g., Murphy & Salvador, 1999). The acme zone can be regarded as a sub-type of this category; instead of evolutionary datum, prominent population increase of a species is used for the definition of the lower boundary. These continuous schemes are favored by the modern GSSP methodology (McLaren, 1977; Cowie et al., 1986; Remane et al., 1996) and mostly includes the pelagic biostratigraphic zones.

The discrete zonation includes the Oppel zones (or assemblage zones; the difference between them has often been considered non-existent; e.g., Johnson, 1979), which are defined on the recognition of the co-occurrence of a distinctive assemblage of taxa that differentiate an interval from the overlying and underlying strata (e.g., Remane, 1991; Page, 1995; Scott, 2013; Page, 2017; Fig. 2.24). In the absence of the index species, correlative vicariants can be used, providing flexibility in application for wide paleogeographic and paleoenvironmental ranges (e.g., Serra-Kiel et al., 1998; Pignatti & Papazzoni, 2017). They are discrete zonations, that is, successive Oppel zones are separated by intervals of unknown duration that do not belong to any of the adjacent zones (e.g., Page, 1995; Pignatti, 1998; Guex et al., 2016; Speijer et al., 2020). These intervals sandwiched between successive Oppel zones are also correlatable (e.g., intervals between the Jurassic ammonite biohorizons – sub-subzone, Page, 2017).

When compared to the pelagic zonation schemes, the shallow marine fossil zonations are regarded discrete and Oppelian due to the discontinuities commonly induced by the sea level changes, preventing recognition of reliable FO/LO datums (Pignatti, 1998; Guex et al., 2016; Septfontaine, 2020). In addition to the Cenozoic shallow marine benthic zonations (SBZ – nummulitids and alveolinids, Serra-Kiel et al., 1998), the NW Europe Jurassic ammonite standard zones from the shallow marine successions (e.g., Page, 1995) are discrete and Oppelian. Other examples include some benthic foraminiferal schemes (e.g., Septfontaine, 1991), conodont zonations

(e.g., Paul, 1983) and well-known radiolarian unitary associations for the Tethys Ocean (e.g., Baumgartner et al., 1995). Recently, for the upper Tithonian–upper Valanginian strata, unconformity bounded assemblage zones (mostly coinciding with formation boundaries) with similar concepts has been proposed by Granier (2019) based on benthic foraminiferal and algal assemblages.

In that sense, Oppel zones should have roots in stage stratotype concept where stages are defined both at their bottoms and tops and characterized by their fossil content and separated from adjacent stages by natural breaks (i.e., unconformities); species turnover marks the boundaries (Fig. 2.24). Whereas the interval zones, in accordance with GSSP methodology, are defined at their bases by bioevent datums (Fig. 2.24). This duality is underlined by Hottinger (2013, p.327): "H.M. Bolli had 'invented' the zonation of planktonic foraminifera in and for the Caribbean, and he and his students took a leading part in the Deep Sea Drilling Project (DSDP). I had two reasons to welcome this division. On one hand, I felt that the planktonic way of life restricts the morphology of the foraminifera to a degree that does not allow many conclusions as to its function and significance beyond taxonomy. On the other hand, I have been (and still am) opposed to Hedberg (1976)'s concepts of biostratigraphy: I realize the significance of stage and zone boundaries in an oilfield of limited geographical extension and reasonably uniform sedimentation, but refuse to extend this system with its 'boundary stratotypes' to a worldwide 'chronostratigrapy' based on fossils and their evolution. A boundary has no material basis; it is an abstraction and therefore cannot be correlated. Only the fossil content of a pile of sediments above and below a so-called boundary can be correlated and used to measure time in geological dimensions."

Quantitative biostratigraphical methods are commonly used in calibration of all sorts of data in the construction of geologic time scales (e.g., Sadler, 2020 – GTS 2020). For biostratigraphy there are 4 main quantitative methods; namely the constrained optimization (CONOP; Kemple et al., 1989, 1995), the ranking and scaling (RASC; Agterberg & Nel, 1982a, 1982b; Agterberg & Gradstein, 1999), the graphic correlation (Shaw, 1964; Edwards, 1984; Carney & Pierce, 1995) and the unitary

associations (Guex, 1977, 1991). The first three of these methods are based on FO/LO data and produce continuous schemes. Only the unitary associations method provide assemblage based, discrete zonations (i.e., Oppelian zones).

The RASC method is a probabilistic analysis that produces the most likely solution by computing average taxa ranges whereas the rest of the methods try to maximize observed ranges (Hammer & Harper, 2006). The algorithm of this method, being written mainly for petroleum well applications, gives importance to the LOs and not necessarily preserves the observed co-occurrences (Guex et al., 2016). The program firstly orders the bioevents (ranking) and then determines the spaces between these datums (scaling). Although it eliminates reworked tops, there can be shortcomings due to the nature of its design in correlating and scaling bioevents from different environments.

The CONOP method is a multi-dimensional graphic correlation that simultaneously correlate all sections by finding best fit to all sections and automatically draw a multidimensional line of correlation (LOC), producing composite charts very fast even with large numbers of data when compared to time consuming, labor intensive graphic correlation method. Although it is widely used in the construction of the GTS 2020 (Sadler et al., 2009; Smith et al., 2015; Sadler, 2020), it seems to create arbitrary extension and truncation of ranges (Glaster et al. 2010) and artificial condensation intervals (Guex et al. 2016). So, instead of these two methods, the graphical correlation and the unitary associations methods, corresponding to previously discussed two classic biostratigraphical approaches (i.e, continuous and discrete schemes, respectively), are used for data treatment. The details of each method are given in the following part.

2.3.2 Graphic Correlation Method (GCM)

Graphic Correlation (Shaw, 1964; Edwards, 1984; Carney & Pierce, 1995) is a semi-quantitative method based on correlation of section pairs on a x-y graph through a

line of correlation (LOC) positioned with respect to the bioevents common to both sections. Taxa FO and LO datums (metric stratigraphic levels) are required for the analysis. Firstly, a standard reference section (SRS) is selected. The SRS should be the most complete section with greatest sampled intervals and should be the section representing the longest estimated chronostratigraphical interval without condensed intervals since the scale of the composite standard reference section (CSRS) will be proportional to the thickness of the SRS. The facies of the SRS should be suitable for reliable fossil datums. In the first correlation, the section qualified second according to these criteria mentioned above will be correlated with the SRS. SRS is positioned on the x-axis and the section to be correlated is located on the y-axis. Common fossil datums are plotted on the graph. A LOC (or a segmented LOC) is located according to the following rules: Tops in the highest sample and bottoms in the lowest sample should be avoided if possible. Most of the tops will draw to the right, and most of the bottoms to the left of a reasonably placed LOC (or better still lying on the LOC) due to the assumed relatively complete ranges of taxa in the SRS (Fig. 2.25). This LOC will extend the fewest possible events in the SRS. In addition to fossil datums, common physical horizons i.e., radiometric dating, key beds, ash horizons, isotope shift datums, paleomagnetic reversal horizons etc., can be used as data points (e.g., Ellwood et al., 2017; Scott, 2019). If synchroneity is guaranteed, the LOC should be forced to pass through those data points. A regression line can be calculated, but this method will assign equal weight to all fossil datums. As it has been suggested (e.g., Miller, 1977; Simmons, 1994; Carney & Pierce, 1995), placing a LOC manually is mostly preferred while taking into account of validity and significance of each data point. This point is both the power and the weakness of this methodology, where interpretation can introduce subjectivity while the manual placement forces the biostratigrapher to consider each biohorizon in terms of pitfalls illustrated in Figure 2.22. Fossil datums that lie far off the LOC indicate facies controlled higher bottoms or depressed tops, reworking or misidentification (Fig. 2.25). The trend of the LOC depends on the accumulation rates between the sections. The term “rock accumulation rate”, instead of sedimentation rate. is used to emph-

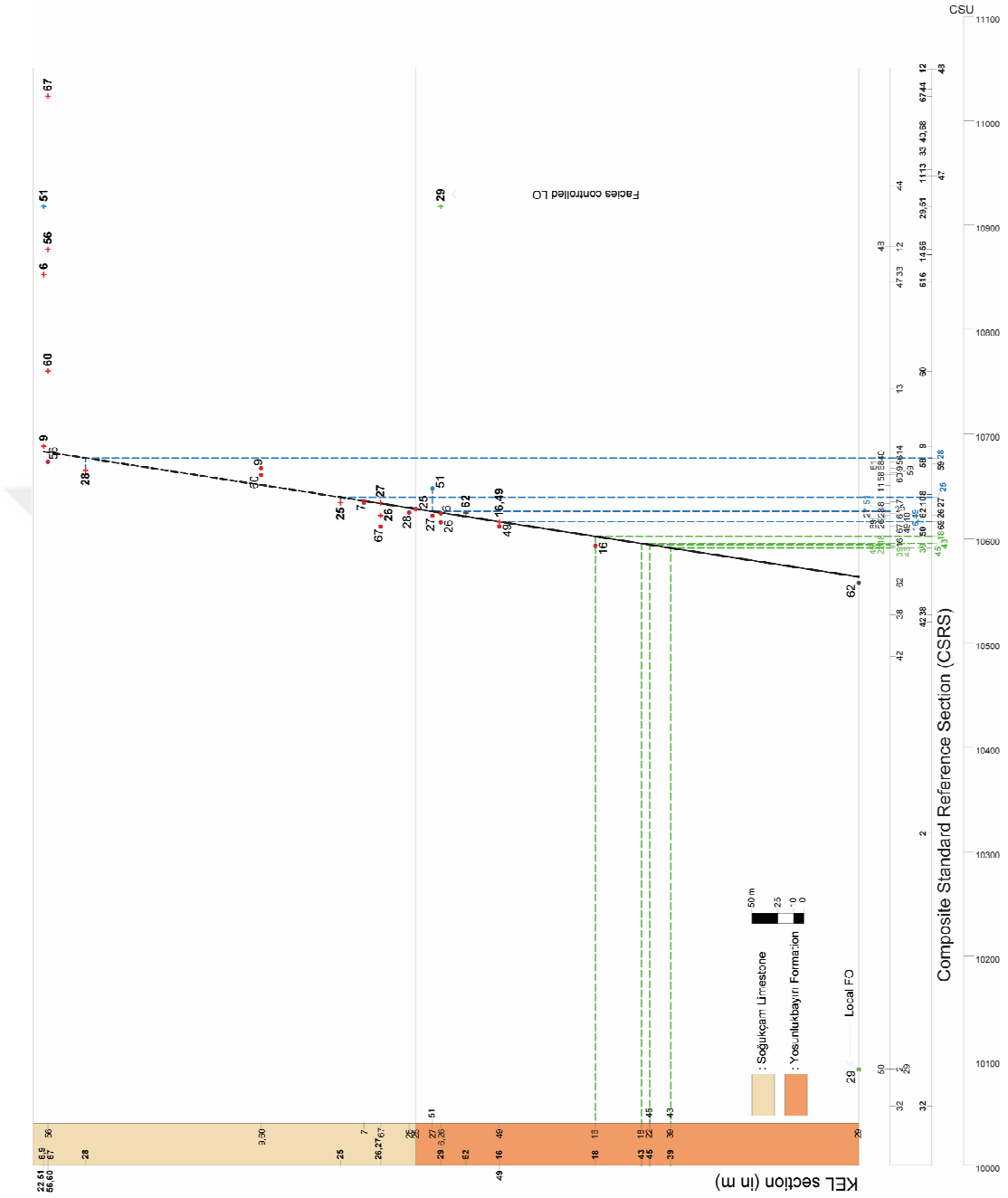

Figure 2.25. A graphic correlation sample from the first correlation round; KEL vs "evolving" CSRS. Common fossil datums are plotted. A LOC is manually placed according to the constraints discussed in Chapter 2.3.2. Tops (crosses) plotted to the left of the LOC (indicating early LOs in the CSRS) is extended in the CSRS by projecting across the LOC to their new positions (e.g., LO of taxon 25, red cross; taxon codes and names with related datum information are given in Appendix D and in the inlet of Figure 2.27). Similarly, the bottoms (filled circles) plotted to the right

Figure 2.25 (*continued*) of this LOC (meaning late FO in the CSRS) are extended by projecting through the LOC to their new positions (e.g., FO of taxon 51). These adjustments are indicated by blue dashed lines. Fossil information that are not present in the CSRS but recorded in the correlated section can also be projected through the LOC by drawing a horizontal line from the related datum to meet the LOC, and then projecting that horizon down along a vertical line to the CSRS (green dotted lines). Bold numbers listed to the left of the KEL section and at the bottom of the CSRS are the LOs with related taxa codes. The numbers at the right side of the KEL section and the ones on the upper side of the CSRS are the FOs. The arbitrary scale from units 10000 to 11100 are the composite standard units (CSU, see Chapter 2.3.2 for discussion). For succession data see Table 2.1. Circles are FOs. Crosses are LOs. Colors and taxa codes are the same as Fig. 2.27. For high resolution figure see Appendix E (from Atasoy et al., 2022).

asize that the final thickness of rock record is determined by the sedimentation rates, erosion, differential mechanical compaction, stylolitization (chemical compaction) etc. (Fig. 2.21). Similarly, the distance between the bioevents is a product of rock accumulation rate.

Terraces drawn by the LOC can indicate fault, unconformity or facies change. A straight LOC should be considered as the average rate of rock accumulation within the related interval, not an indication of constant rock sedimentation.

Incomplete fossil ranges are indicated by the tops plotted to the left of the LOC and the bottoms plotted to the right of the LOC. They can be placed to their calibrated places by projecting through the LOC as illustrated in Figure 2.25. Fossil ranges are maximized with successive correlation to other sections. Fossil data that are not present in the SRS (or in the evolving CSRS; SRS is called CSRS after the first correlation) but occur in the section graphed against it can be projected through the LOC to their correlative positions in the CSRS (Fig. 2.25). This may be the most important feature of the methodology that allows the calibration of fossils from unrelated lineages and varieties of depositional environments. The only requirement is that the “evolving” CSRS and the section graphed against it should have enough common fossil datums to allow a reliable placement of the LOC. This is why the

graphic correlation method is a useful method for our purpose in this study that aims the correlation of bioevents from shallow marine and deep marine Upper Jurassic–Lower Cretaceous successions. The connecting data including common taxa from these distinctly separated environments are provided by the platform margin–slope to basin successions (i.e., AÇ, KEL, AH, STG, ÇT, MK-2, MK-1, ÇAY-4, NALLI and ÇDS sections, Fig. 2.20 and Table 2.1; see also Appendix D for detailed presence/absence data). As the range data from more and more sections, characterized by different depositional environments and by diversity of ages, are composited, the CSRS becomes applicable to deposits from shallow marine to deep marine environments and the ranges within the CSRS approximate maximum ranges of the taxa. By this way, all fossil bioevents within the CSRS are ordered and scaled with respect to each other.

At least 3 rounds of correlation and calibration are suggested (e.g., Carney & Pierce, 1995) for stabilization of the LOC as the CSRS matures. In the following correlation rounds, the datums directly obtained from the section graphed against the "evolving" CSRS should be removed from the composite to avoid artificial self-correlation.

Equal subdivisions of the mature CSRS (equal thickness) are named as composite standard units (CSU); an arbitrary scale having common properties with chronostratigraphic units (Fig. 2.25; Carney & Pierce, 1995). Successive CSUs within the CSRS do not necessarily have the same time duration. CSUs common to both sections are like chronostratigraphic units having varying thicknesses among sections and bounded by synchronous surfaces known as composite standard time equivalents (CSTE, Carney & Pierce, 1995). They simply provide correlation lines projected from the related CSTE in the CSRS and transferred to the section graphed against it through the LOC (see the following sections for examples).

The Pontides data matrix is provided in Appendix D. All fossil data were generated by the same working group, Marine Micropaleontology Research Unit, in the Geological Engineering Department of METU; to some extent ensuring consistent taxonomic identifications and strong familiarity with the local facies and local

geology. All the sections are located within a genetically related geological setting (Fig. 2.20).

For this study, the AÇ section (section location 7 in Fig. 2.20A, B and Table 2.1) providing those requirements discussed above is chosen as the SRS. The AÇ section is also the type section of two critical biozones defined by Altiner (1991) applicable to both platform and slope environments; namely the "*Tubiphytes*" *morronensis* Zone (Zone II) and the *Protopeneroplis ultragranulata* Zone (Zone III, Table 2.1). The first correlation round is where the ranges in the SRS are most prone to artificial expansions as noted by Edwards (1984) and MacLeod & Keller (1991). So, additionally a methodology similar to MacLeod & Keller (1991) is followed; within the first correlation round well-established sequences of biohorizons was maintained (see Appendix F–Biostratigraphy References).

Three rounds of correlation have been carried out. The compositing order is as given in Table 2.1 and details of compositing are reported in Appendix D. Individual graphic correlations for each section within each 3 rounds are given in Appendix E.

Within the lower parts of most of the deep marine sections from the Pontides, elevated ACD position is suggested by the presence of *aptychi* without the aragonitic ammonite shells (mostly moulds are present) and the presence of aragonitic *Globuligerina* gr. *oxfordiana* as the nuclei of pelagic oncoids in a protected position. This observation is also in accordance with the previously suggested shallow ACD for Tethys until the Late Kimmeridgian (e.g., Winterer & Bosellini, 1981; Roth 1983; Vulpius & Kiessling, 2018). With combination of rare occurrence of Jurassic planktonic foraminifers and difficulties of species determination on thin sections (e.g., Wernli 1988; Gradstein et al., 2017; Gradstein et al., 2021), we simply grouped Jurassic planktonic foraminifers recorded in the successions under the catch-all name *G.* gr. *oxfordiana*. So, the related ranges within the CSRS should be considered as a group range. Similarly, chitinoidellids are not abundant in the Pontides. Following the systematic revisions of the family Chitinoidellidae by Pop (1997), Sallouhi et al. (2011) and Benzaggah (2021) and the related zonation nomenclature (Chitinoidellids

Zone instead of *Chitinoidella* Zone) by Benzaggah (2020) we grouped all microgranular forms under the general term chitinoidellids with the exception of double walled *Praetintinnopsella*. So, when we refer to the ranges of this chitinoidellid group we simply imply the total range of the family. Chitinoidellids were recorded in only three sections; KEL, ÇAY-4 and NALLI (with only one sample) sections. Due to the lack of abundant chitinoidellid records within the Pontides, the well-studied Barlya section (Lakova & Petrova, 2013) from Bulgaria was used as the first correlated section with the SRS (AÇ section) to ensure better control for this critical interval to which all other uppermost Jurassic fossils will be calibrated (Appendix D & E).

At the end of the last round a CSRS, calibrated to CSUs, is obtained. Biozones and stage boundaries (if defined by the present taxa) already exist in the CSRS by definition. The analyses can be ended at this point, because the CSU and CSTE provide correlation among the CSRS and all individual sections. Additionally, this scheme can be calibrated with absolute time scales. There are two options for absolute age calibration; (i) correlating a contemporaneous section with age data to the CSRS (ii) or directly assigning the related absolute ages to these bioevent datums and then interpolate between them which is actually the same procedure with the first one if the interpreter forces the LOC to pass from all common data points. We have opted to correlate the Pontides Carbonate Platform CSRS (PCP-CSRS) with the Geological Time Scale (GTS 2020). The details of the absolute age calibration points and related references are given in the Table 2.2 and Appendix F (Calibration Points). Figure 2.26 illustrates this calibration process. Similar to the previous correlation, common reliable datums are plotted on a x-y graph and a LOC is plotted. Several types of regression have been performed (Fig. 2.26). Although the FOs of *Alveosepta jaccardi*, *Pseudocyclammina lituus* and *Anchispirocyclina lusitanica* (blue circles 2, 3 and 52) clearly represent elevated FOs in the PCP-CSRS (overall facies controlled local bottom levels), even a simple linear regression to all data points in the graph fits well (orange regression line in Fig. 2.26). The FOs of the calpionellids *Calpionella elliptica*, *Calpionellopsis simplex* and *Calpionellopsis obl-*

Table 2.2 Data points used in the absolute age calibration of the PCP-CSRS and related references. See also Appendix F.

Chitinoidellids	FO	146.58	Base Chitiroidellids Zone (Base of dobeni subzone)	Benzaggagh (2020)	Chitiniodellids instead of *Chitinoidella* due to systematic revisions of the dobeni group
Chitinoidellids of *boneti* group - *Praetintinnopsella* -primitive *Crassicollaria* - *Tintinnopsella*	Co-occurence	-	AO assemblage sub-subzone of the *remanei* subzone	Benzaggagh (2020) (partially eqv. of *Praetintinnopsella* Zone of Grandesso, 1977)	Instead of Lakova & Petrova (2013)'s *Praetintinnopsella* Zone. Although not observed in the Pontides, our CSRS suggests the occurence of this sub-subzone. Lakaova & Petrova (2013) differentiated *remanie* subzone with the FOs of *T.remanei* and *T. carpathica*. In their columns, FO of *T. carpathica* are consistently below FO of *T. remanei*. In their *Praetintinnopsella* subzone *Chitinoidella boneti*, *T. carpathica*, *Praetintinnopsella andrusovi* and some other chitinoidellids co-occur; then the base of the Crassicollaria Zone is defined by the base of the remanei subzone which corresponds to the FO of *T. remanei*, which is not consistent since the hyaline lorica-calpionellids already present in the subzone *Praetintinnopsella*. On the ohter hand AO sub-subzone of Benzaggah (2020) also record similiar assemblage of chitinoidellids, *T. remanei*, *T. carpathica* and affinities of *C. intermedia* and *C. alpina*. So instead of separating this interval as *Praetintinnopsella* Zone like Lakova & Petrova (2013, which also includes the hyaline walled calpionellids) below *Crassicollaria* Zone (which corresponds to the FOs of the hyaline walled calpionellids), we differentiated an AO "subzone" like Benzaggah (2020)'s AO sub-subzone under the *remanie* subzone.
Tintinnopsella carpathica & *T. remanei*, first hyaline walled calpionellids	FO	144.56	Base remanei subzone// Crassicollari Zone (first calpionelids)	Remane et al. (1986)	
Calpionella grandalpina & *C. alpina*	FO	-	Base massutiniana subzone	Lakova (1993), Lakova & Petrova (2013)	Since *C. intermedia* occurs at the latest part of the underlying *remanei* subzone of Remane et al. (1986, eqv. of A1 subzone), *massutiniana* subzone is used. *Crassicollari colomi* has not been identified and *colomi* subzone of Pop (1994) and Rehakova & Michalik (1997) are not used.
Calpionella alpina	Acme base	143.1	Base Berriasian// Base alpina subzone// Base Calpionella Zone	Pop (1974), Remane et al. (1986)	
Remaniella ferasini or first remaniellid	FO	142.63	Base Remaniella subzone	Remane et al. (1986)	
Calpionella elliptica	FO	141.63	Base elliptica subzone	Catalano-Liguori (1971), Remane et al. (1986)	
Calpionellopsis simplex	FO	139.92	Base simplex subzone	Remane et al. (1986)	
Calpionellopsis oblonga	FO	138.77	Base oblonga subzone	Remane et al. (1986)	
Praecalpionellites murgeauni	FO	138.48	Base murgeauni subzone	Pop (1986)	Not good control in the Pontides; STG, ÇT sections only
Calpionellites darderi	FO	137.7	Base Valanginian// Base darderi Zone	Trejo (1980), Borza (1984), Altiner & Özkan (1991)	Defiened as the total range of the genus *Calpionellites* by Trejo (1980). *Calpionellites major* and consequently a *major* subzone has not been recorded from the Pontides however synchornous extinctions with *C. darderi* have been reported; Lakova et al. (1997), Benzaggah (2020).
	LO	-	Base *Tintinnopsella carpathica* Zone// within late Valanginian		
Tintinnopsella carpathica	LO	-	Top *Tintinnopsella carpathica* Zone// within Hauterivian	Trejo (1975, 1980), as an extended F Zone of Altiner & Özkan (1991) and Reháková & Michalik (1997)	
Mohlerina basiliensis	FO	165.79	latest Bathonian	Peybernes (1998) scaled in TSC 8.0	
Alveosepta jaccardi	FO	161.53	base Oxfordian	Peybernes (1998) scaled in TSC 8.0	
Pseudocyclammina lituus	FO	155.51	latest Oxfordian	Bassoullet (1997) scaled in TSC 8.0	
Labyrinthina mirabilis	FO	153.62	early Kimmeridgian	Bassoullet (1997) scaled in TSC 8.0	
Globuligerina oxfordiana	LCO	-	late Kimmeridgian	Last consistent occurrence, scaled form Gradstein et al. (2017, 2018); within lowest Beckeri Zone (TSC 8.0)	
Alveosepta jaccardi	LO	149.24	base Tithonian	Peybernes (1998) scaled in TSC 8.0	
Anchispirocyclina lusitanica	FO	148.12	early Tithonian	Bassoullet (1997) scaled in TSC 8.0	
Labyrinthina mirabilis	LO	148.12	early Tithonian	Bassoullet (1997) scaled in TSC 8.0	
Protopeneroplis ultragranulata	FO	147.6	late early Tithonian	Peybernes (1998) scaled in TSC 8.0	
Protopeneroplis striata	LO	143.1	base Berriasian	Bassoullet (1997) scaled in TSC 8.0	
Anchispirocyclina lusitanica	LO	142.19	early Berriasian	Arnaud-Vanneau (1998) scaled in TSC 8.0	
Protopeneroplis ultragranulata	LO	138.92	late Berriasian	Arnaud-Vanneau (1998) scaled in TSC 8.0	
Montsalevia salevensis	LO	132.6	base Hauterivian	Arnaud-Vanneau (1998) scaled in TSC 8.0	
Meandrospira favrei	LO	127.99	late Hauterivian	Arnaud-Vanneau (1998) scaled in TSC 8.0	

Stages	Datum	Age (ma)	References
Bajocian	Base	170.9	GTS 2020
Bathonian	Base	168.17	GTS 2020
Callovain	Base	165.29	GTS 2020
Oxfordian	Base	161.53	GTS 2020
Kimmeridgian	Base	154.78	GTS 2020
Tithonian	Base	149.24	GTS 2020
Berriasian	Base	143.1	GTS 2020
Valanginian	Base	137.7	GTS 2020
Hauterivian	Base	132.6	GTS 2020
Barremian	Base	126.5	GTS 2020
Aptian	Base	121.4	GTS 2020

GTS2020: Geological Time Scale 2020
TSC 8.0: Time Scale Creator Program version 8.0 (calibrated to GTS2020)
LO: Last Occurrence
LCO: Last Consistence Occurrence
FO: First Occurrence

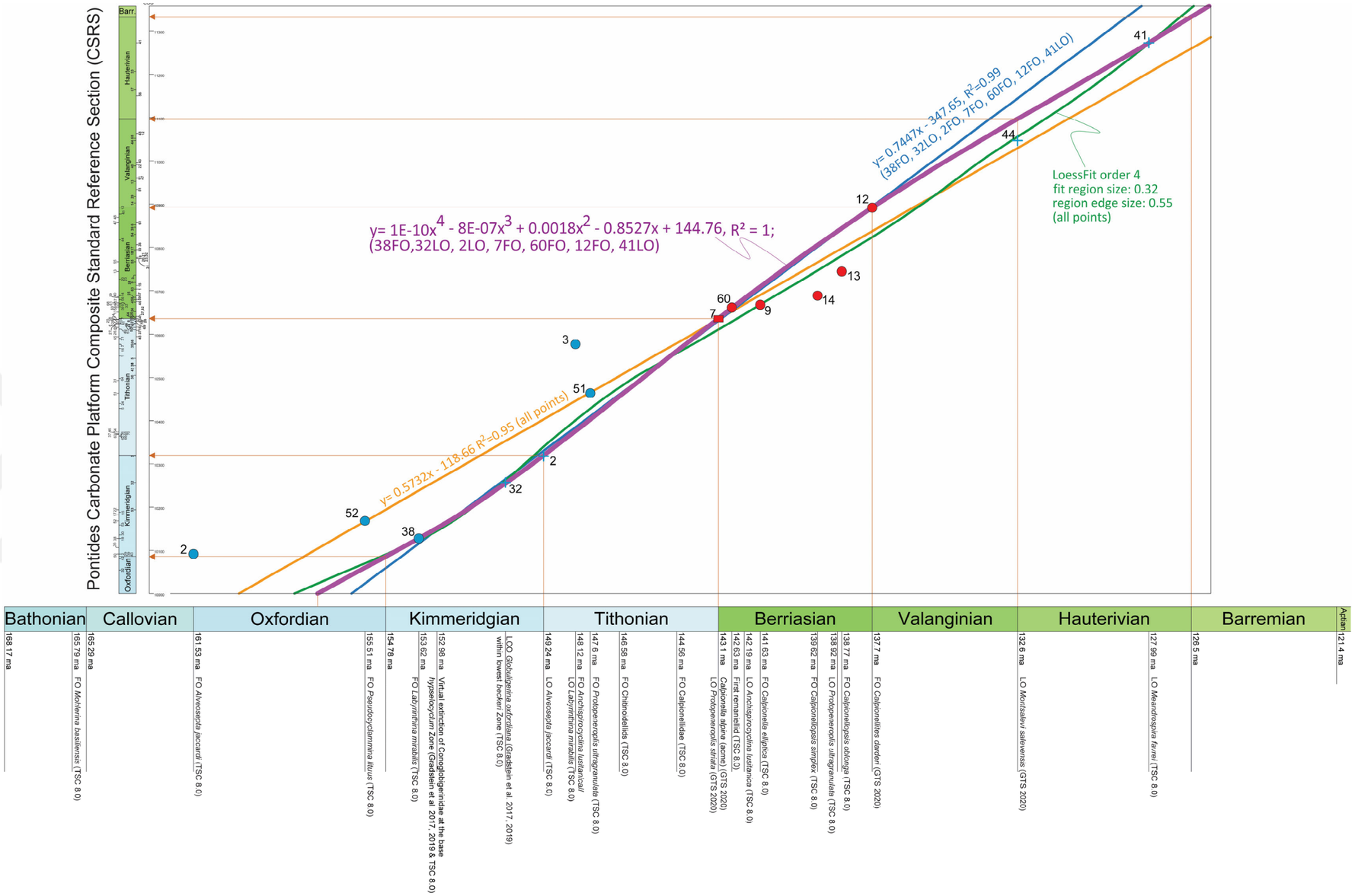

Figure 2.26. Calibration of the PCP-CSRS (y-axis) with the GTS 2020 datums (x-axis). Several types of regressions are tested with varying data points. Related equations and correlation coefficients are given on the graph with related colors. The data points used for individual regression are given within parentheses next to the related regression equation. The fourth order polynomial regression over the FOs of 38, 60, 12 and LOs of 32, 2, 41, and the acme of 7, marked by bold purple line, was chosen for the absolute age calibration. Circles are FOs. Crosses are LOs. Colors and taxa codes are the same as Fig. 2.27. See the text for discussion (from Atasoy et al., 2022).

onga seem to be affected by condensation for the related time interval over the Pontides (close spacing of the datums in the PCP-CSRS in contrast to the spacing between those events in the GTS 2020). So, these points are disregarded for the calibration. The apparently more reliable datums are characterized by the FOs of *Labyrinthina mirabilis*, *Remaniella ferasini* and *Calpionellites darderi* (blue circle 38, and red circles of 60 and 12), LOs of *Alveosepta jaccardi* and *Meandrospira favrei* and the last consistent occurrence (LCO) of *Globuligerina oxfordiana* (blue crosses of 2, 41 and 32), and the lower boundary of the *Calpionella alpina* acme (red square 7). The fourth order polynomial regression (purple colored line in Fig. 2.26) is chosen as the LOC (a LOC placement nearly corresponding to direct age assignments to those datums; instead of segmented linear LOC, a 4th order polynomial is fitted that smooths the calibration of the intervals between datums). Absolute ages and the positions of the stage boundaries have been projected to the PCP-CSRS through this LOC (Fig. 2.26). At the end, the Pontides CSRS with numerical age calibration has been obtained (Figure 2.27). The list of the numerically calibrated fossil datums is given in Appendix F (CSRS Calibrated Fossil Datums).

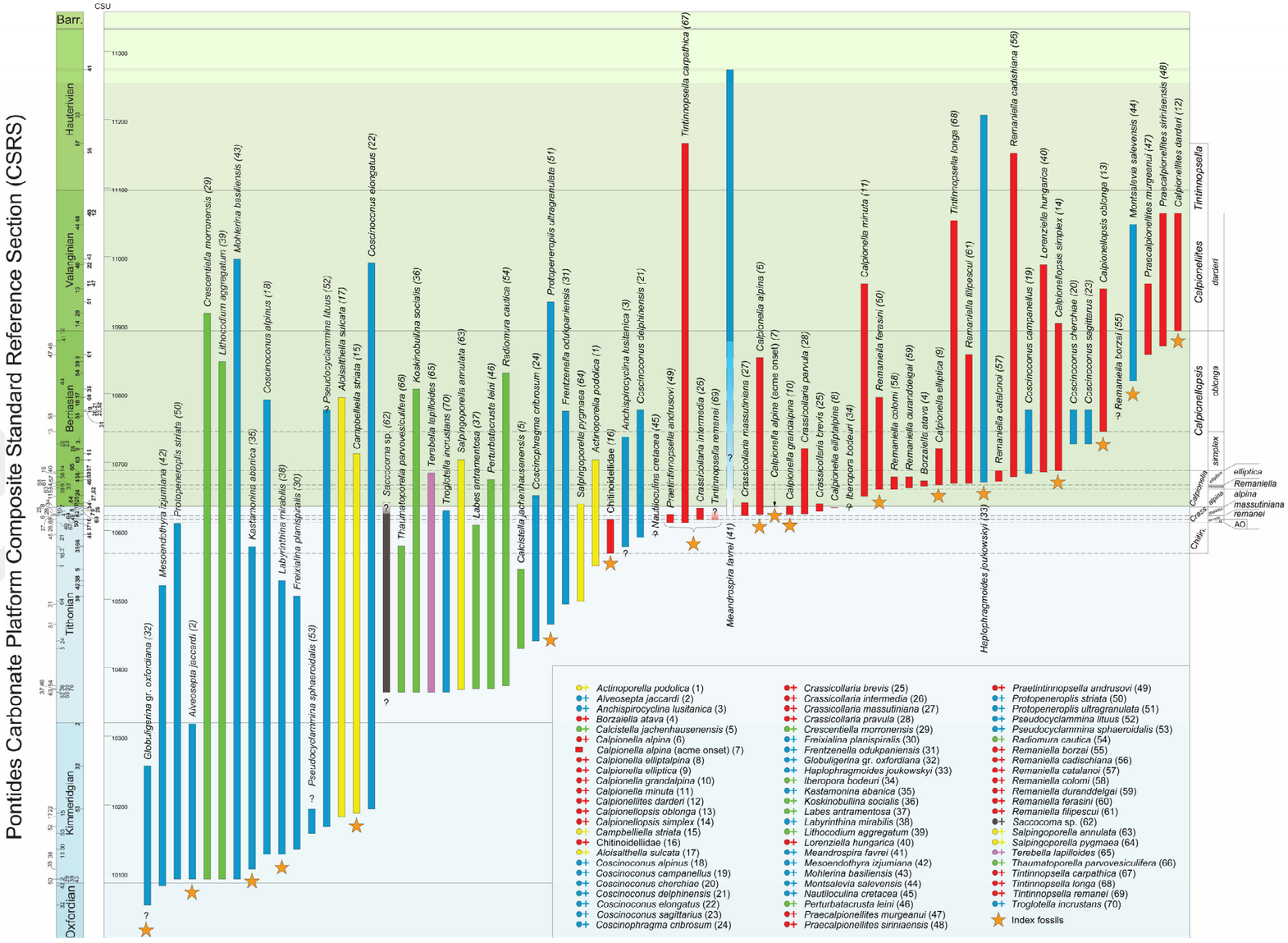

Figure 2.27. The Pontides CSRS with absolute age calibrations. The column on the left is the CSRS with bioevent datums. Similar to the previous graphics, the bold numbers lined up on the right wall of the CSRS are the LOs while the ones on the left wall are the FOs datum: all are scaled and calibrated to absolute time. Individual fossil ranges are presented. Blue bars: foraminifers. Yellow bars: algae. Green bars: microencrusters. Red bars: calpionellids. Brown bars: crinoids. Stars below the range bars indicate index fossils used in the previous shallow and deep marine zonations. CSU: Composite standard units (the vertical scale on the left side of the range chart). Calpionellid zonations inserted next to the range chart based on calpionellid datums. Information on zones can be found in Appendix F (Calibration Points). Age calibrations for each datum are given in Appendix F (CSRS Calibrated Fossil Datums). A high-resolution version of this chart can be also found in Appendix F (from Atasoy et al., 2022).

2.3.3 Unitary Association Method (UAM)

The unitary associations method (UAM; Guex, 1977, 1991; Guex et al., 2016) is a deterministic approach to the biostratigraphical problems which gives importance on observed co-occurrences (not bioevent datums) while preserving maximum number of observed and reproducible superpositions and produces discrete sequence of assemblage zones like Oppel zones. The free UAGgraph (0.45) program by Hammer et al. (2015) was used for analyses (the PAST software by Hammer et al., 2001 can also carry out UA analyses). Sample by sample fossil data or fossil FO/LO datums within each section are required. For the second data input type, the UAGraph makes range through occurrence assumption. Most of the sections from the Pontides only provide LO/FOs data (Appendix D). Accordingly, we opted for the second type of data input. The UAGraph input matrix is provided in Appendix G ('Pontides J-K UA.txt' file, it can also run on the PAST).

The method (and the UAGraph program) progresses through the following data treatment steps. Firstly, the method searches for samples with the maximal set of fossil assemblages which are not a subset of other samples – maximal horizons (Fig. 2.28A). Then samples with fossil content included in another sample are discarded. The remaining maximized fossil assemblages that are strictly distinct from each other in all sections are called residual maximal horizons. Following that, superpositional relationship of taxa pairs are investigated. If taxa A occurs above taxa B in one section and vice versa in another section, this common type of contradiction is solved by considering these taxa to be "virtually" co-occurring. It means that although they have been never recorded together, they should co-exist in time. All other methods try to figure out a ranking in this kind of contradictions (that is the one of the main reasons in some situations CONOP create artificial condensation intervals, Guex et al., 2016), while UAM does not enforce a superposition. Graph theory notations are used to illustrate relationships among taxa, samples and cliques. Arrows indicate superpositions (Fig. 2.28B, i.e., 'a' below 'c') and solid lines (edges) are used for co-occurrences (Fig. 2.28B, i.e., 'c' co-exists with

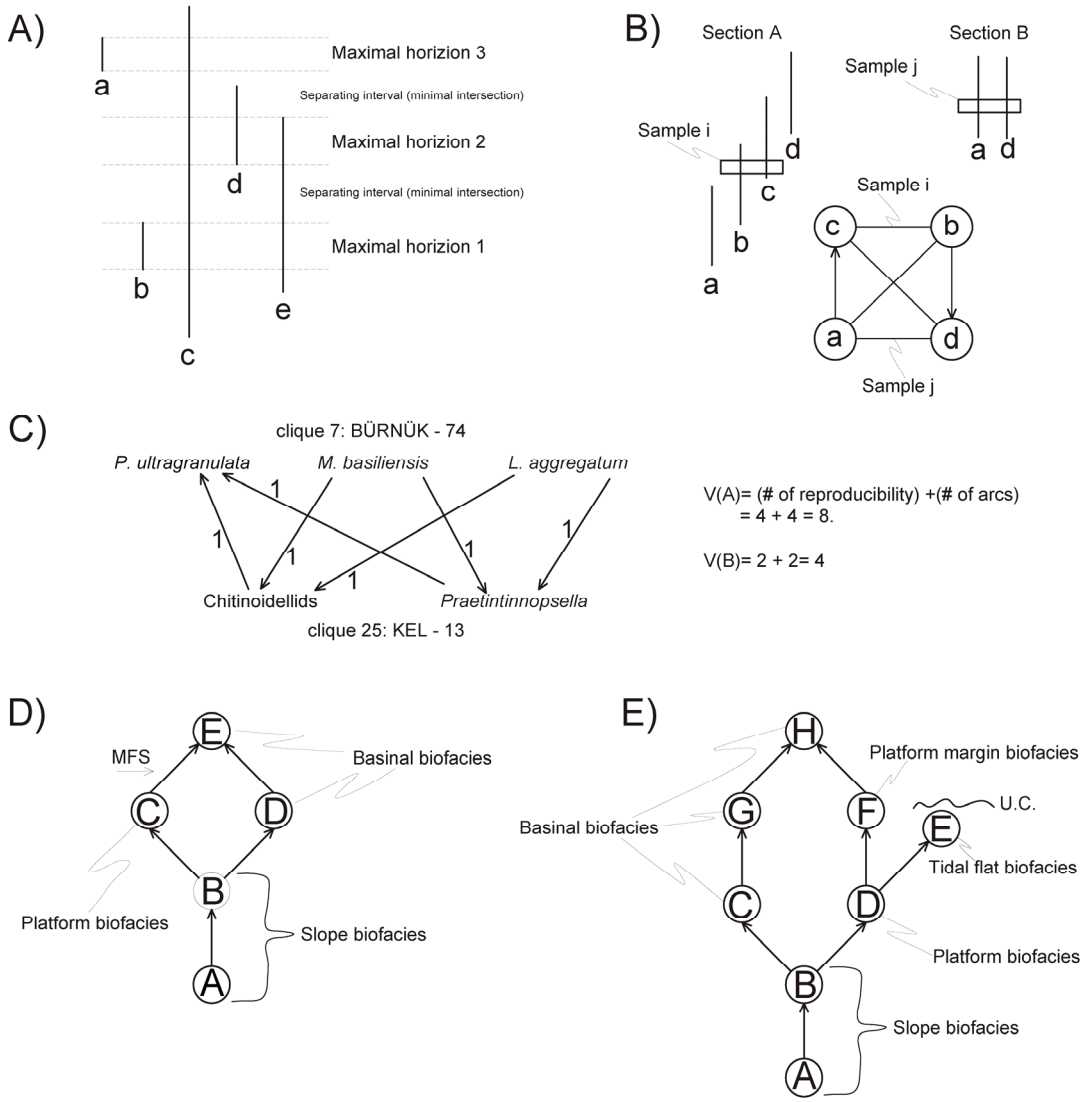

Figure 2.28. A) Illustration of the "maximal horizon" concept for a section. They are the beds or samples that have taxa showing maximal development of diversity which are not a subset of any other sample (or bed) and strictly different from each other. They are separated from each other by intervals of "minimal intersection" of taxa which are subsets of other samples, that is where the concept "discrete" notion comes from. **B)** A cyclic superpositional contradiction example. Sample 'i' records the co-existence of the taxa 'b' and 'c' while the sample 'j' includes the taxa 'a' and 'd'. When all other superpositional and co-occurrence observations from the samples are taken account, a cyclic relationship of the kind illustrated by the edges and arrows (just below the sections) are obtained. Note that the sample 'i' can be both above and below the sample 'j'. Such contradictions are destroyed by replacing one of the superpositional relationships with an edge (co-existence). Modified from Galster et al. (2010). **C)** An example of superpositional contradiction between two cliques. A: set of arcs that links the taxa of the clique 7 (sample BÜRNÜK-74) to the clique 25 (sample KEL-13) in the direction clique 7 → clique 25. B: set of arcs in the opposite

Figure 2.28 (*continued*) direction. V(A) and V(B) are values calculated as shown in the figure. The numbers on the arrows indicate the reproducibilities of related relation (e.g., number of times Chitinoidellids occur below *P. ultragranulata*). The number of arcs is the total number of arcs going from the related clique to the other one. If V(A)>V(B) the clique 7 is located below the clique 24 (can be seen in the graph of cliques with contradicting superposition option in the UAGraph program). If V(A)=V(B) the stratigraphic relationship between the pair of cliques is undetermined. **D, E)** Branching in the longest path of the maximal cliques. The facies types and their relative order within all sections can give rise to intervals within successions with characteristic fossil assemblages (pelagic vs neritic or mixed fauna) and this kind of parallel path formations. The letters within circles represent maximal cliques. **D)** Illustration of a path configuration that can result from the varying facies evolution present within sections that share a common underlying facies (biofacies) type. A common slope facies and related fossil assemblages characterizes the oldest samples within all sections. Then, later in time, some sections passed into shallow marine facies while others evolved into basinal associations. The uppermost levels of the sections are represented by the basinal deposits. Shift from maximal clique D to E should be related to evolution of the common basinal taxa since both share the same facies. The sections that gave rise to the branching of C (shallowing upward in the related successions) must later experience a deepening trend into a pelagic environment that resulted in the superpositional relationship of C → E. MFS: maximum flooding surface. **E)** Additionally, some branches may not connect to any of the cliques, clique E. This may result from the unique facies occurrence in the uppermost levels of some of the sections that do not allow the taxa in the "dead-end" maximal clique to be followed by biofacies which shares a common fossil assemblage with other maximal cliques in a suitable superpositional relationship (G, F, H) which in return would permit the clique E to join the main path. The branch D → E may result from a major regressive trend ending with an unconformity (U.C.) in some of the sections that share a common biofacies in their lower levels. Setting Gk merge threshold to zero in the UAGraph program allows merging of this kind of cliques and preservation of data from unrelated facies (from Atasoy et al., 2022).

'b'). Cyclic superpositions, i.e., "A above B, B above C, and C above A" or "A co-occurring with B, C above A, and C below B" type contradictions are also solved by replacing a superpositional relationship (arrow) with a "virtual" co-occurrence (edge). UAM tries to minimize this kind of replacements, while virtual edges strengthen lateral reproducibility. All relationships between taxa are summarized in a G* graph (Fig. 2.29). This biostratigraphic graph gets so crowded with 69 taxa (which basically shows superpositional and co-existence relationship by arrows and

edges). By using the UAGraph input matrix provided in Appendix G, the graph can be obtained via the “Biostratigraphical graph” analysis option.

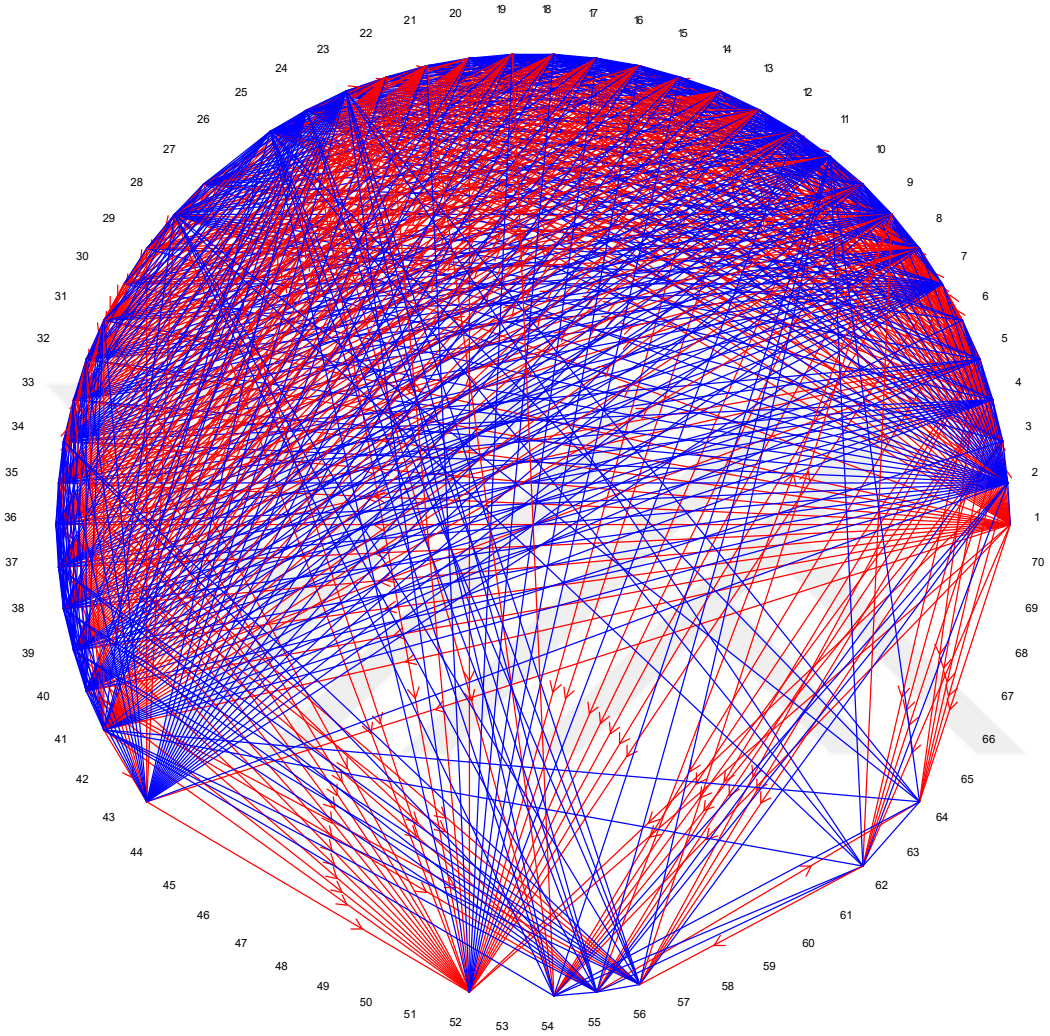

Figure 2.29. The G* graph from the UAM. Blue edges indicate co-occurrences. Red arrows show superpositional relationships. Taxa codes are the same as Fig. 2.27.

Following these initial analyses, the UAM seeks for “maximal cliques” which are co-occurring fossil assemblages that are not included in any larger group of co-existing assemblages. The maximal cliques are initial unitary associations requiring

further analyses. Maximal cliques have only real edges (observed co-occurrences) while unitary association, which is also a maximal clique, may have virtual edges. Then, the UAM tries to rank these maximal cliques according to the relationships documented in the graph G* (Fig.2.29). This ordering is carried out by inspecting the superpositional relationships between the fossil assemblages of the related clique pairs (Fig. 2.28C). Contradictions are solved by majority vote as explained in the Figure 2.28C over an example of the contradiction between the clique 7 (BÜRNÜK section, sample 74 from a shallow marine succession) and the clique 25 (KEL section, sample 13 from a basinal succession), then the weakest link (least observed relationship) is destroyed.

Some empirical and statistical manipulation of the original data is suggested (e.g., Monnet et al., 2011; Chen et al., 2019; Wu et al., 2020) through bootstrapping, resampling and discarding to eliminate contradictory superpositional relationships. These approaches are not followed in this study (see Guex, 2011; Guex et al. 2016 for discussion) since the exact relationships among the fossils from different lineages and different facies are not known and that is exactly what we are after for. So, such contradictions are left to the program algorithm that solves them with majority vote or as explained by inducing virtual co-existence (Fig. 2.28B, C).

After all the superpositional relationships between the maximal cliques have been resolved, the maximal cliques should be ordered along a unique path. However, facies types present in the studied sections with their unique biofacies can gave rise to branching in the longest path (Fig. 2.28D, E). In that case, the merging of cliques is carried out by the method according to the faunal similarity. The option “Gk merge threshold” controls the percentage of taxa shared to be considered for the merging process. If it sets to ‘100’, this step will be suppressed, and the cliques outside the longest path will be lost, meaning a loss in data. This is not desired since our aim is to calibrate fossils from distinct environments that co-existed in time but not occur together in space. So, we set the value to ‘0’ to always allow merging. Most problematic taxa are the ones that occur only in a single section, significantly increasing the number of conflicting superpositions. So, to overcome this problem,

the “null endemic taxa” option present in the UAM is used which simply removes the singletons (they are not useful for correlation, e.g., Mailliot et al., 2006). The “hard superposition” option forces the UAM to preserve a dictated superpositional relationship by refusing transformation of the taxa relationship into a virtual co-existence in the final unitary associations. No hard superposition was applied in our analysis.

At the end, unitary associations, maximal distinct sets of mutually co-existing species (assemblage zones), are obtained (Fig. 2.30A). The original samples from individual sections are automatically assigned to the related unitary associations (Appendix G – UAs Correlation Tables; “correlation table” option in the UAGraph), providing a mean for correlation. A sample may have a fossil assemblage that uniquely assigns it to a unitary association or when the sample includes taxa that do not allow differentiation between the unitary associations, a range of UA is assigned. Depending on the lateral reproducibility (the number of sections/regions in which the given UA is observed; “UA reproducibility” option in the UAGraph), the number of arcs between the UAs (frequency of arcs; “Real arcs between UAs” option in the UAGraph), the dissimilarity index D (an index to measure faunal similarity between successive UAs, ranges from 0 to 2; “Unitary associations” option in the UAGraph) and the suggested merges (“Reproducibility graph” in the UAGraph), the UAs can be merged with their adjacent ones to strengthen lateral reproducibility and correlation (Figs. 2.30B & C). This merging will produce the unitary association zones (UAZs) with wide lateral traceability and superpositional control in the expense of resolution. The order of bioevents within each UAs (and UAZs) is indeterminate since the UAM do not force superposition for previously discussed stratigraphical contradictions, instead virtual co-existence is induced. The UAM tries to optimize this tradeoff between the resolution and lateral traceability while providing strong superpositional control among the UAs.

The original samples are now assigned to UAZs (see Appendix G – UAs Correlation Tables), that is they are correlated. The lower and upper boundaries of strictly defined UAZ provide reliable correlation lines between sections. In the case of samp-

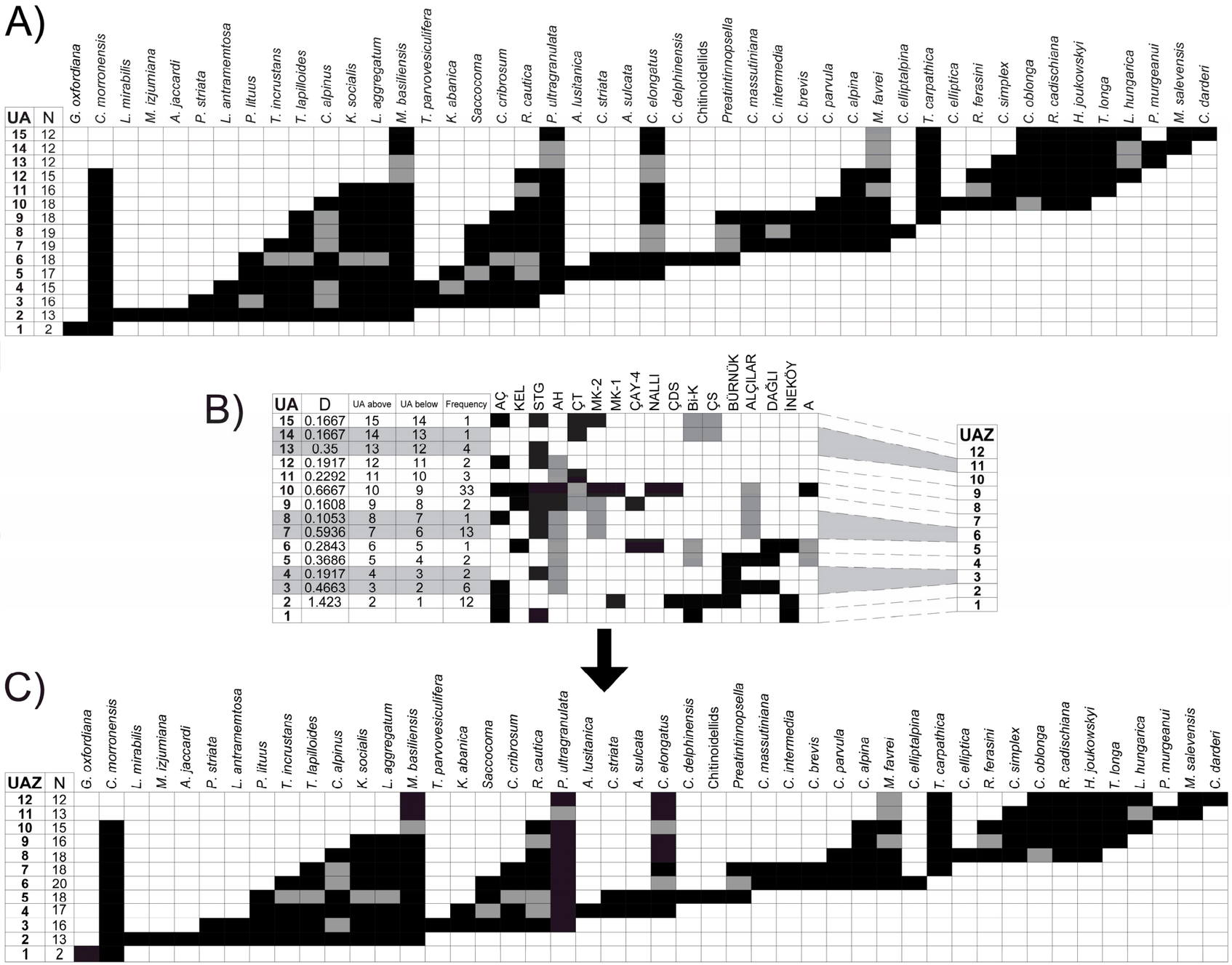

Figure 2.30. Steps in building unitary association zones (UAZs) from the unitary associations (UAs). **A)** UAs obtained at the end of the data treatment. Each UA is characterized by distinct assemblage of taxa that differentiate the unit from immediate assemblages. All individual samples are assigned to these UAs, i.e., they are correlated (see Appendix G). If a sample does not have characteristic taxa of a given UA or it has taxa characteristics of several UAs, a range of potential UAs will be assigned to that sample. Black boxes real occurrences. Grey boxes virtual co-occurrences. **B)** The reproducibility table of the UAs. Black boxes are strictly defined UAs, gray boxes are coalescence of UAs. D: dissimilarity index; ranges between 0-2, lower values indicate close similarity between successive UAs. Frequency is the number of real arcs (observed superpositions) between successive UAs. Successive UAs with low dissimilarity index, lower number of arcs and limited lateral reproducibility are merged to obtain 12 UAZs from the initial 15 UAs. **C)** Distribution of taxa within the obtained UAZs after merging of UAs in the previous step. This merging strengthens the lateral reproducibility of the related UAs in the expense of resolution (from Atasoy et al., 2022).

les assigned to a range of UAs, superpositional relationships within individual section samples and related UAs can be evaluated to further restrict the UA assignment. For example, the sample BiK-5 (from the Bilecik section) is assigned to a range of UAs 2-10 since it has no characteristic fauna to be uniquely identified (Appendix G – UAs Correlation Tables). However, overlaying series of samples (BiK-6 to BiK-14) are distinctly assigned to UA 2 and the underlying samples of BiK- 3 and BiK-4 have UA 1 assemblage. So, this superpositional relation will force the sample BiK-5 to be assigned to UA 2 uniquely. In addition to the previously explained merging step, this kind of restrictions from examination of superpositional relationships among successive UAs will further refine the UA (and UAZ) assignments and lateral reproducibility. A reliable correlation is not possible for indeterminate intervals and intervals with ranges of UAs between two uniquely defined nonconsecutive different UAs. The singletons discarded in the initial steps of the analysis can be reintroduced by dating the related sample levels via the UAZ and inserting these taxa to their dated unitary associations. Since documenting the UAZs of total number of 868 samples will require unnecessary space, the correlation table of samples to related UAs and UAZs are provided in the Appendix G (UAs Correlation Tables).

2.3.4 Correlations by the GCM and the UAM: A comparison

2.3.4.1 GCM correlations

We have obtained two means of correlation with completely different approaches. The GCM has provided bioevent-datum-based composite section that integrates shallow and deep marine fauna calibrated to CSUs and absolute ages (Fig. 2.27). This composite section now can be used for correlating among sections regardless of the biofacies types present in individual successions.

Similar to the CSRS compositing steps, individual sections are graphed against the PCP-CSRS. Figures 2.31, 2.32 and 2.33 illustrate three correlation examples (all

individual correlation graphs are provided in Appendix E). The first example is the correlation of the AÇ section characterized by calciturbiditic pelagic carbonates of the Yosunklukbayırı Formation (Altiner et al., 1991; Table 2.1, Fig. 2.31). The plot of the common taxa on the graph suggests a relatively well-constrained linear LOC (bold purple line in Fig. 2.31). The bottom of the succession is characterized by shallow marine fauna transported down to the slope and intercalated with pelagic taxa. The correlation line is constrained by the FOs of *Alveosepta jaccardi*, *Protopeneroplis striata*, *Crescentiella morronensis* and *Globuligerina* gr. *oxfordiana* (circles 2, 50, 29 and 32 respectively in Fig. 2.31) in the lower part of the graph. Toward the middle part, LOs of *Alveosepta jaccardi*, *Mesoendothyra izjumiana*, *Labyrinthina mirabilis* and *Protopeneroplis ultragranulata* provide appropriate datums that nearly lie on the LOC (crosses 2, 42, 38 and 50, respectively in Fig. 2.31). The FOs of *Mesoendothyra izjumiana*, *Labyrinthina mirabilis*, *Protopeneroplis ultragranulata* and *Saccocoma* sp, (circles 42, 38, 51, and 60, respectively) lie far off the LOC indicating facies controlled, local elevated bioevent datums (Fig. 2.31). In the middle levels, the evolution of calpionellids provides closely spaced data points and good constraints. The FOs of *Crassicollaria parvula*, *Calpionella alpina*, *C. elliptalpina*, *C. elliptica*, *Remaniella ferasini*, and *Calpionellopsis simplex* (red circles 28, 6, 9, 60, and 14) and the acme of *Calpionella alpina* (red square 7) lie on or very close to the LOC. The upper level of the LOC is constrained by the successive LOs of *C. alpina*, *Calpionellopsis oblonga*, *Lorenziella hungarica*, *Coscinoconus elongatus*, *Protopeneroplis ultragranulata*, and *Montsalevia salevensis* (Fig. 2.31; crosses 6, 13, 40, 22, 51, and 44 with related fossil-group colors as in the Fig. 2.27). The FOs of *Lorenziella hungarica*, *Remaniella cadischiana*, *Haplophragmoides joukowskyi*, and *M. salevensis* (circles 40, 56, 33, and 44) and the LOs of *Remaniella cadischiana*, *Tintinnopsella carpathica*, *T. longa*, *Calpionellites darderi*, *Haplophragmoides joukowskyi* (crosses 56, 67, 68, 12, 33) represent elevated bottoms and truncated local tops, respectively. An alternative LOC for the upper part of the graph is indicated by a dashed line (Fig. 2.31). This LOC is constrained by the FOs of *Calpionellopsis oblonga* and *Calpione-*

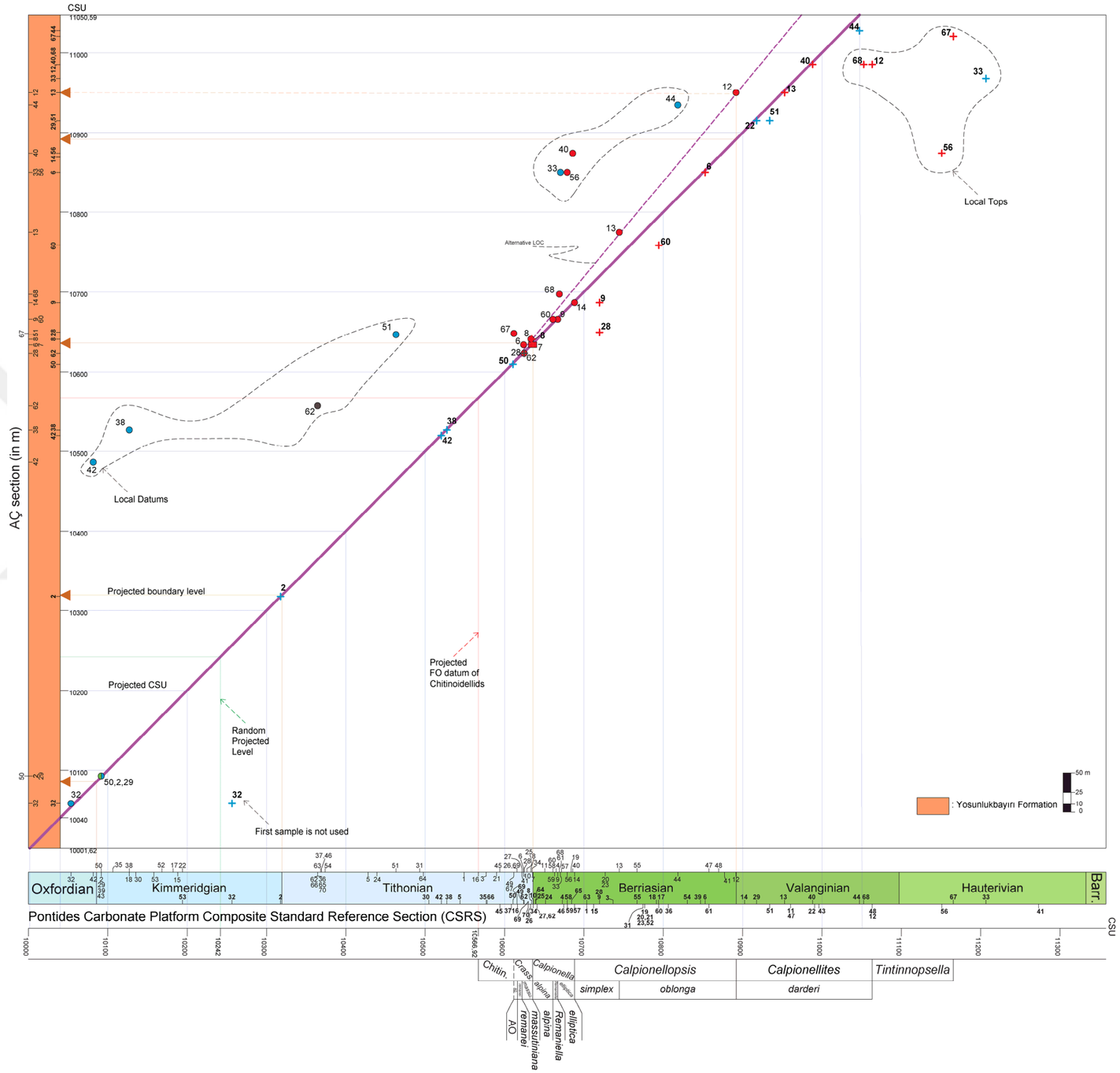

Figure 2.31. Correlation of the AÇ section with the PCP-CSRS. Purple bold line is the LOC. Dotted purple line is an alternative correlation line. Orange lines with arrow heads are the projected boundary levels. Blue lines are the projected CSTEs. Taxa codes are the same as Fig. 2.27. A high-resolution version is present in Appendix H. For discussion see the text (from Atasoy et al., 2022).

llites darderi (red circles 13 and 12). However, this alternative requires a change in the slope of the LOC, indicating an increase in the rate of rock accumulation toward the top of the AÇ section, which is not suggested by the facies present (in contrast numbers of calciturbiditic intervals decreases toward top, Altiner et al., 1991). Additionally, the top of the LOC is well constrained by the successive LOs of taxa that nearly lie on the correlation line. So, an unsegmented simple LOC with constant slope has been chosen for correlation (Fig. 2.31). This also suggests slight late FOs of *Tintinnopsella longa*, *Calpionellopsis oblonga* and *Calpionellites darderi* in the AÇ section (red circles 68. 13. and 12), may be a result of sample bias. After a reasonable LOC is placed the correlation procedure is straightforward.

Any kind of data present in the PCP-CSRS can be projected through this LOC to their related levels in the correlated AÇ section. The orange lines with arrow heads on the AÇ section are the projected stage boundaries (Fig. 2.31). The blue lines are the projection of the CSTEs. Even if the CSRS was not calibrated with absolute ages, the correlation via the CSUs and the CSTEs would still be possible, only the scale will be a random chronostratigraphic scale. In Figure 2.31, only the major divisions of the CSTE are drawn (e.g., 10500, 10600, etc.). Finer equal divisions on the CSRS can be also projected if finer scale correlation is desired. The green line in Figure 2.31 represents a random level (CSTE of 10242) projected from the PCP-CSRS to its corresponding level in the AÇ section. Similarly, the corresponding levels of bioevent datums not recorded in the correlated section but present in the CSRS can be projected. For example, although the taxa characteristic of the Chitinoidellids and AO Zones (sensu Benzaggah, 2020) are missing, and calpionellids of the *remanei* (sensu Remane et al., 1986) and *massutiniana* (sensu Lakova, 1993: Lakova & Petrova, 2013) subzones of the *Crassicollaria* Zone are not diversified in the AÇ section (only represented by the FO of *C. parvula* – red circle 28 and the elevated bottom of *T. carpathica* – red circle 67), bases of these zones and subzones can be correlated. An example for the base of the Chitinoidellid Zone is given in Figure 2.31, which is not recorded in the AÇ section. The base can be correlated by the

projection of the related CSTE in the PCP-CSRS (CSTE of 10566.92, red line in Fig. 2.31) through the LOC.

The next correlation example illustrates a succession with facies changes (black arrows and related facies information in Fig. 2.32). Similar to the previous AÇ section, the lower levels of the STG section are characterized by the calciturbiditic Yosunlukbayırı Formation. Toward the top of the succession, Maiolica-type pure pelagic, radiolarian rich carbonates of the Soğukçam Limestone overlie these calciturbiditic carbonates with a transitional interval showing changes from coarse grained grain-, float-, rud- stone facies to fine grained wackestone interval with intercalated packstone levels. A LOC is placed according to the positions of the FOs and LOs as explained in the methodology section. When the common taxa are plotted on the graph, a major change in the rock accumulation rates for the STG section is forced by the bioevents clustered toward the top of the graph that suggest major slow down phase in the upper part of the STG section that is in consensus with the observed facies changes (Atasoy et al., 2018; Fig. 2.32). For the lower part, there is an alternative LOC (dashed line) suggesting two additional segments and changes in rock accumulation rates. Although this is also supported by the facies changes at related levels (black arrows and related facies information in the Fig. 2.32; Atasoy et al., 2018), the constraining data points of this alternative LOC position seem to be not reliable as they do not fully develop in the studied Pontides successions. For example, the FO of *Saccocoma* sp. (brown circle 62) recorded with the FO of *Crescentialla morronensis* (green circle 29) at the same level (Fig. 2.32). In the literature, oldest documented FO of Saccocoma is from Oxfordian (Heinz & Isenschmid, 1988; Olszewska et al., 2012; Benzaggagh et al., 2015b) with two acme levels: first in the Early Kimmeridgian (Heinz & Isenschmid, 1988; Benzaggah et al., 2015b) and the second, more intense acme, at the base (Altiner, 1991) or in the earliest (Heinz & Isenschmid, 1988; Benzaggagh et al., 2015b, see also Appendix F – Biostratigraphy References) Tithonian. The oldest *Crescentiella morronensis* levels are recorded within the Oxfordian (e.g., Pleş et al., 2013) and at the base of Kimmeridgian (Altiner, 1991; Chiocchini et al., 2008). For a better calibration of the

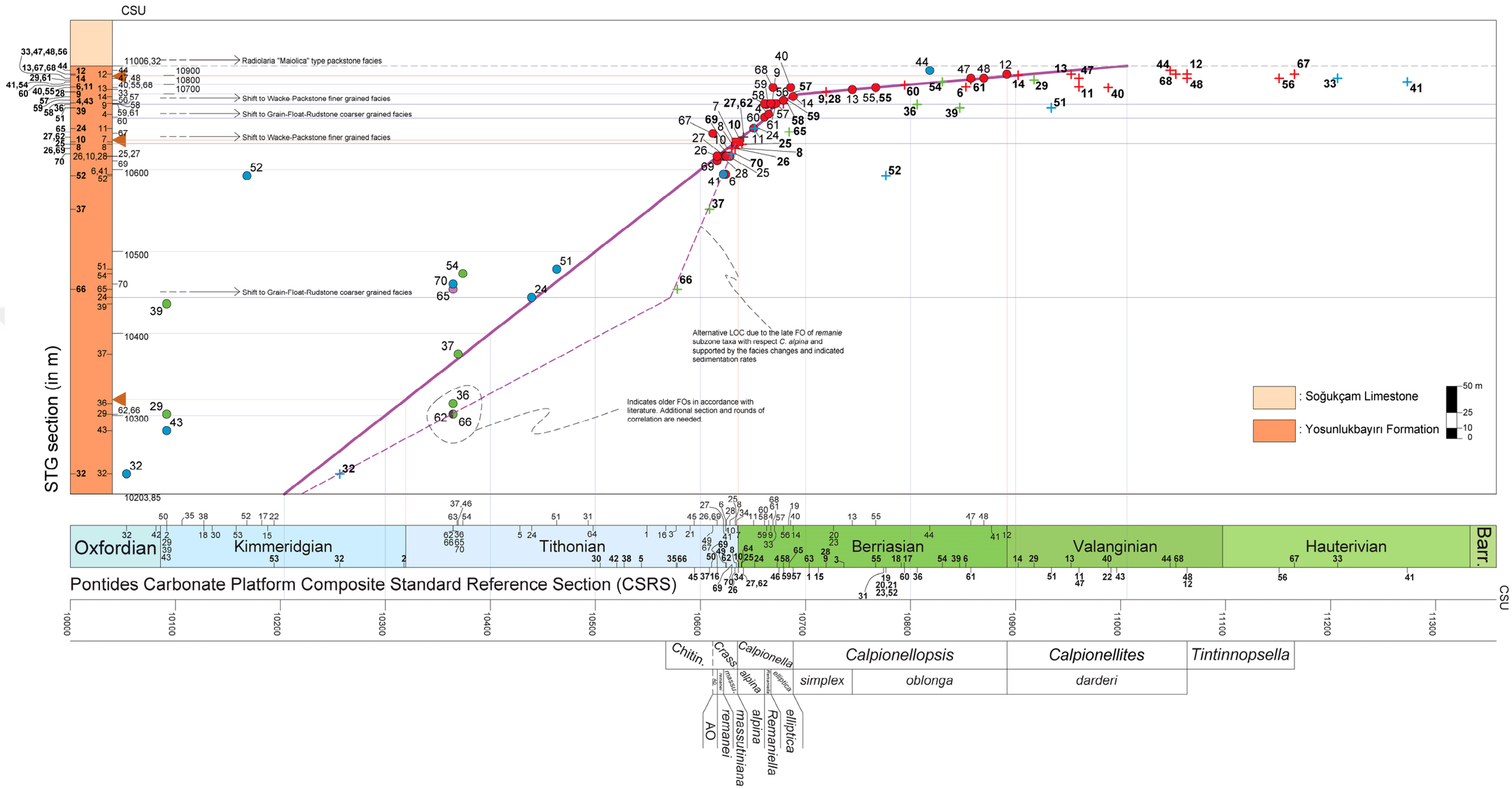

Figure 2.32. Correlation of the STG section with the PCP-CSRS. Purple bold line is the LOC. A segmented LOC reflecting facies changes in the STG succession is placed. Dashed lines are the alternative correlation lines. Facies shifts are indicated by the black arrows. Facies information next to them is also provided. Orange lines with arrow heads are the projected boundary levels. Blue lines are the projected CSTEs. Taxa codes are the same as Fig. 2.27. A high-resolution version is present in Appendix H. For discussion see the text (from Atasoy et al., 2022).

Saccocoma levels additional data is clearly required (Fig. 2.27). The FO of Crescentiella morronensis seems to be near the base of Kimmeridgian for the PCP (Fig. 2.27; Altiner, 1991). The late FO of this microencruster can be due to the lack of data from older deposits or may be related to tectonically induced shallowing of the basement in the Pontides that can provide suitable water depth for thriving of shallow marine fauna, marking the onset of carbonate platform development only Kimmeridgian onward (Altiner et al., 1991).

A linear LOC, well constrained by the calpionellids in the upper parts, and passes very close to the FOs of *Protopeneroplis ultragranulata* and *Coscinophragma cribrosum* (circles 51 and 24), that is not requiring segmentation, is chosen (bold purple LOC in the Fig. 2.32). The FO of *P. ultragranulata* was calibrated by Peybernès (1998, based on the data by Heinz & Isenschmid, 1988) at the base of the middle Tithonian and *Coscinophragma cribrosum* was reported from the Upper Jurassic (Bucur et al., 1996). These data are in consensus with our observations and calibration (Fig. 2.27). Accordingly, the CSTEs and the stage boundaries present in the PCP-CSRS are projected through the LOC to their related levels in the STG section. The FOs of *G.* gr. *oxfordiana* is sample-biased and not reliable in the STG section. The FOs of foraminifers *Mohlerina basiliensis* and *Pseudocyclammina lituus* show clear diachronism and facies controlled late appearances in the STG section (Fig. 2.32).

The final correlation example is from the shallow marine Alçılar section (Okay et al., 2018; Table 2.1, Fig. 2.33). Platform carbonates of the İnaltı Limestone unconformably overlie the clastics of the Bürnük Formation and the section ends with an unconformable contact with the overlying Lower Cretaceous flysch deposits of the Çağlayan Formation (Okay et al., 2018; Table 2.1, Fig. 2.33). Toward the top of the succession pelagic incursions are present (Okay et al., 2018). The plot of common fossils on a graph provides well constrained LOC (Fig. 2.32) when compared to other shallow marine sections which generally illustrate scattered bioevent datums (Appendix H). The linear LOC is constrained by the FOs of *Freixialina planispiralis*, *Pseudocyclammina lituus*, *Campbelliella striata*,

Coscinoconus elongatus, *Protopeneroplis ultragranulata*, *Frentzenella odukpaniensis* (circles 30, 52, 15 and 22, respectively; Fig. 2.33) and the LOs of *Freixialina planispiralis*, *Kastamonina abanica*, *Anchispirocyclina lusitanica* (crosses 30, 35 and 3, respectively; Fig. 2.33). The far-off lying FOs of *Crescentiella morronensis*, *Coscinoconus alpinus*, *Mohlerina basiliensis*, *A. lusitanica* and *Calpionella alpina* (circles 29, 18, 43, 3 and 6; Fig. 2.33) represent local elevated bottoms. Similarly, the LOs of *A. jaccardi*, *C. striata*, *P. lituus*, *C. elongatus*, *M. basiliensis* and *C. morronensis* (crosses 2, 15, 52, 22, 43 and 29; Fig.2.33) are depressed local tops. Again, the related CSTEs are correlated to corresponding datums in the Alçılar section (Fig. 2.33).

Similar detailed analyses and correlations were carried out for the rest of the measured stratigraphic sections from the Jurassic–Cretaceous of the Pontides. The individual graphic correlations are given in Appendix H. Finally, all of the sections have become correlated to the PCP-CSRS and to each other (Fig. 2.24).

2.3.4.2 UAM correlations

The UAM provides 15 UAs, 53 residual horizons, 34 maximal cliques, 156 contradictions, 7 cliques in cycles and 0 residual virtual edges. As previously mentioned, to eliminate contradictions, some authors suggest using additional statistical methods; we did not apply any additional data manipulation and left the UAM (and UAGraph program) to come up with a solution directly obtained from the original raw data. From this data, 15 initial UAs, via merging (as explained in detail previously), 12 UAZs are established (Fig. 2.30) and the individual samples are directly assigned to unique UAZs or range of them (Appendix G). The samples within each section are correlated by using this strictly defined UAZs (Fig. 2.34).

In contrast to the correlation datums obtained from the GCM, the UAZs are defined by fossil assemblages (Fig. 2.30) and having philosophy of the Oppel zones in its core, it provides units defined at both their bases and tops (Fig. 2.28 & 2.30). The dr-

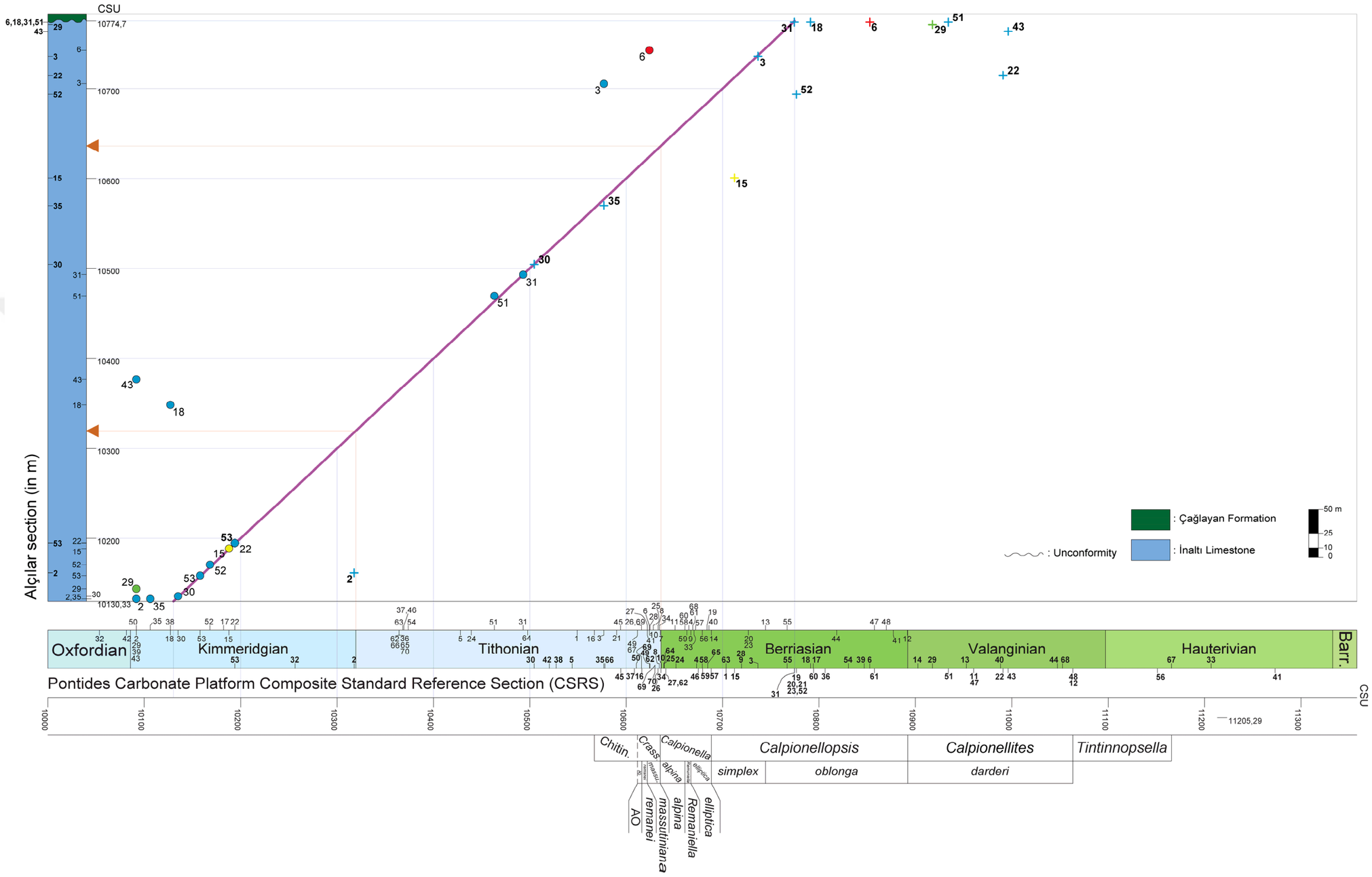

Figure 2.33. Correlation of the Alçılar section with the PCP-CSRS. Purple bold line is the LOC. A simple linear correlation line is well constrained by the taxa. Orange lines with arrow heads are the projected boundary levels. Blue lines are the projected CSTEs. Taxa codes are the same as Fig. 2.27. A high-resolution version is present in Appendix H. For discussion see the text (from Atasoy et al., 2022).

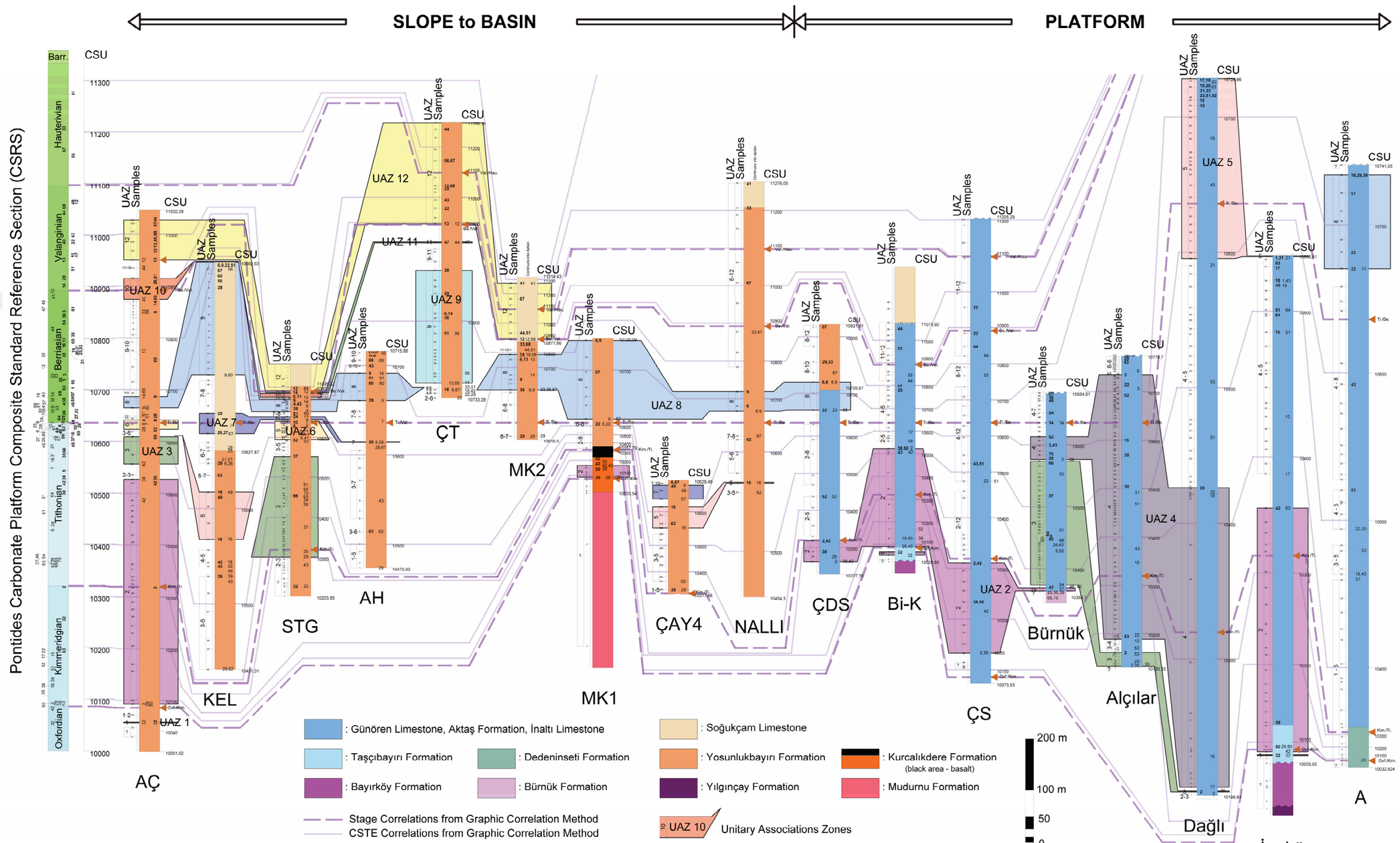

Figure 2.34. (*caption on next page*).

Figure 2.34. Correlation of the measured sections. The scale on the left is the PCP-CSRS obtained from the GCM. The common vertical thickness scale for the sections is given below next to the lithologies. The sections are plotted in the order of compositing from left to right. All sections are correlated to the PCP-CSRS and to each other via the CSTE. All CSTEs have been calibrated to absolute ages. Related CSTUs are given next to each section. The thick dashed purple lines are the stage boundary correlation lines by the GCM. The thin solid purple lines are the correlation lines of the CSTEs from the GCM. GCM provides datum correlations. UAZs obtained from the UAM are superimposed on the same graph. Uniquely defined UAZs are illustrated as colored transparent, background clouds correlating related individual samples from each succession. Same color belongs to the same UAZ. The numbers of the UAZs are given within individual clouds. Next to each section, uniquely defined UAZs and UAZ ranges are given in boxes besides sample numbers. Note that there is no one to one correspondence of these UAZs to the PCP-CSRS scale and geological stages on the left. It correlates distinct maximal taxa assemblages. UAM provides units (assemblages instead of biohorizons) for correlation. The UAZs with the highest lateral reproducibility are the ones that include taxa occupying platform margins. Note the contradictions they show. The Tithonian/ Berriasian boundary correlated by the GCM is placed within the UAZ 4 for the Alçılar section whereas it is located within the UAZ 5 for the Dağlı section and within the UAZ 7 for the KEL section. High resolution version of this figure is also given in Appendix H. See the text for discussion (from Atasoy et al., 2022).

awback of the UAM in applications with mixed fauna clearly appears when the UAZ correlations are superposed on the section correlations obtained from the GCM (Fig. 2.34): the UAZs are correlatable as long as the related fossil assemblage is present in the sections. As we previously explained that the GCM can provide correlation datums (CSTEs) for intervals that do not share common fossils or even in intervals that completely lack correlatable biohorizons if there is enough common fossil datums for placement of the LOC confidently in correlation with the CSRS (Fig. 2.31 & 2.34). In the correlation of stratigraphic sections with varieties of biofacies and calibration of bioevents of unrelated lineages, UAM is limited by the depositional environment distribution of the individual UA fossil assemblages. The determination of individual UAZs in larger numbers of sections is enhanced by the presence of fossils having wide facies extend. These kinds of fossils are the ones present at the shelf margin that are prone to transportation down to the slope facies and into the lagoonal environments (Fig. 1.1). These key fossils for the Late Jurassic–

Early Cretaceous interval mainly include *Alveosepta jaccardi*, *Coscinoconus alpinus*, *C. campanellus*, *C. cherchiae*, *C. delphinensis*, *C. elongatus*, *C. sagittarius*, *Coscinophragma cribrosum*, *Haplophragmoides joukowskyi*, *Labyrinthina mirabilis*, *Meandrospira favrei*, *Mesoendothyra izjumiana*, *Mohlerina basiliensis*, *Montsalevia salevensis*, *Protopeneroplis striata*, *P. ultragranulata*, and *Pseudocyclammina lituus* among benthic foraminifers and the microencruster *Crescentiella morronensis* (Altiner, 1991; Atasoy et al., 2018; Atasoy et al., 2022). The most laterally reproducible UAZ are the UAZ 2, 3, 5 and 8 which are mainly characterized by the assemblages of above listed taxa (Figs. 2.30 & 2.34).

2.3.4.3 GCM vs UAM

There are important contradictions between the correlation datums suggested by the GCM and the UAZs. For example, the stage boundaries and the CSTEs from the GCM are correlated with different UAZs in different sections (Fig. 2.34). The Tithonian/ Berriasian boundary (calibrated to the CSTE of 10635.29, Appendix F – CSRS Calibrated Fossil Datums) falls within UAZ 6 in AÇ and STG sections, UAZ 7 in the KEL section, UAZ 4 in the Alçılar and UAZ 5 in the Dağlı sections (Fig. 2.34). This has resulted from the different biostratigraphical approaches the two methods based on (Fig. 2.24). The bioevent order within individual UAZs are indeterminate as previously explained. The UAM does not force superposition for each stratigraphical contradiction (instead induces virtual co-existence), while the GCM seeks for the ordering of bioevents. The effect of this approach can be also seen, for example, in the assemblage of the UAZ 6 (Fig. 2.30). The taxa of the *Crassicollaria* Zone have well-established FO order and related subzones (Table 2.2), although they are used as elements of the UAZ 6 without any superpositional relationship (Fig. 2.30). So, the base of a subzone of the *Crassicollaria* Zone provided by the GCM will contradict with the UAZ assignments of the corresponding levels in the sections. The UAGraph program allows the users to force superpositions in the initial stages of analyses. Although this option will result in

proliferation in numbers of UAs obtained (due to forced superpositions, the number of induced virtual co-existence will be reduced), the lateral traceability of these zones will be greatly limited. It can be considered that the UAM is not the best choice for applications in assemblages from different facies, since the method is greatly limited by the number of common taxa present in each section. This method should be useful for the successions with similar biofacies that will provide common fossil assemblages enabling detection of UAZs in most of the correlated sections. Then the number of the UAs (UAZs) will be a function of taxa turnover rates.

2.3.5 Correlations of the PCP-CSRS with the Eastern Pontides Successions

In this chapter, the measured sections from the Eastern Pontides will be correlated with the PCP-CSRS by the GCM according to the rules and steps explained in detail above.

The first correlated succession is the pelagic Ağören measuered section (Fig. 2.35). The lower part of the section provides relatively few reliable bioevent datums. The FOs of *Protopeneroplis ultragranulata* and *Coscinophragma cribrosum* (blue circles 24 and 51, respectively) used for the LOC placement (Fig. 2.35). Slumped intervals create highly inclined LOC segments that represent intervals of higher rock accumulation rates (Fig. 2.35). The middle portion of the *Calpionella* Zone and the *oblonga* subzone has relatively lower rock accumulation rates which also suggested by the thickness of the related strata in the range chart (Fig. 2.15). The GC suggests that there is no Hauterivian strata in the uppermost part of the radiolarian rich succession (Fig. 2.35). For the Kimmeridgian/ Tithonian boundary, a higher position is suggested by the GCM (Fig. 2.35; first orange correlation line in a higher position than the FO of *Saccocoma* sp.; see Chapter 3 for further discussion). As it can be seen in the Appendix B there are several samples with questionable *Calpiopnellopsis simplex* occurrences (i.e., A-201, 224, 244 and 239) before the typical form recorded in the sample A-245 that delineates the lower boundary of the *simplex* subzone (Fig.

2.15). The GCM suggests that the first recorded questionable presence is the real first occurrence of the taxon, The thick dashed black line in Figure 2.35 that projects the FO datum of *C. simplex* (red circle 14) into the real stratigraphic position that coincides with the stratigraphic level of the sample A-201. This kind of controls allowed by the GCM is another powerful feature of the method in comparison to the UAM.

The first measured section in the Ozansu region (the OA section) does not yield enough bioevent for reliable correlation with the PCP-CSRS (Fig. 2.36). In the OB measured section benthic fossils show scattered elevated local FO and LO datums (Fig. 2.36). The calpionellids provide reliable bioevents. The first calpionellid bioevents are clustered at the lower boundary of the OB section due to sample-bias induced by the lower boundary limit of the section. The LOC is placed in that segment between the acme of *C. alpina* (red circle 7 in Fig. 2.36). Reworked tops proposed for *Cr. intermedia*, *Cr. intermedia*, *Cr. massutiniana* and *Saccocoma* sp in the range chart (Fig. 2.17) is confirmed by the GCM (Fig. 2.36, dark red crosses 25, 27, 62).

The most difficult succession to correlate is the Nazlıçayır measured section due to the presence of an unconformity and thick dolomitic interval (Fig. 2.37). The strata below the unconformity are again dated as Kimmeridgian (more precisely middle – upper Kimmeridgian with CSU 10200 & 10300 dated in the section; Fig. 2.37). Although the LO datum of *A. jaccardi* is obviously a local level, it provides upper depositional age limit for the uppermost strata in this part of the section that still fall into uppermost Kimmeridgian (Fig. 2.37). The first carbonate beds overlying the dolomitic interval provide local elevated FO datums of *P. ultragranulata*, *M. favrei*, *H. joukowskyi* and *C. cherchiae* (blue circles of 51, 41, 33 and 20 in Fig. 2.37). LO datums of *S. annulata*, *A. sulcata*, *C. cherchiae* and *P. lituus* seems to be not maximized in the PCP-CSRS (Fig. 2.37) that require further refinement by correlation with succession that has wider chronostratigraphic interval. In the second part overlying the unconformity surface the LOC is located with respect to the LOs of *P. ultragranulata* and *M. salevensis* and the FO of *M. salevensis* (blue crosses of

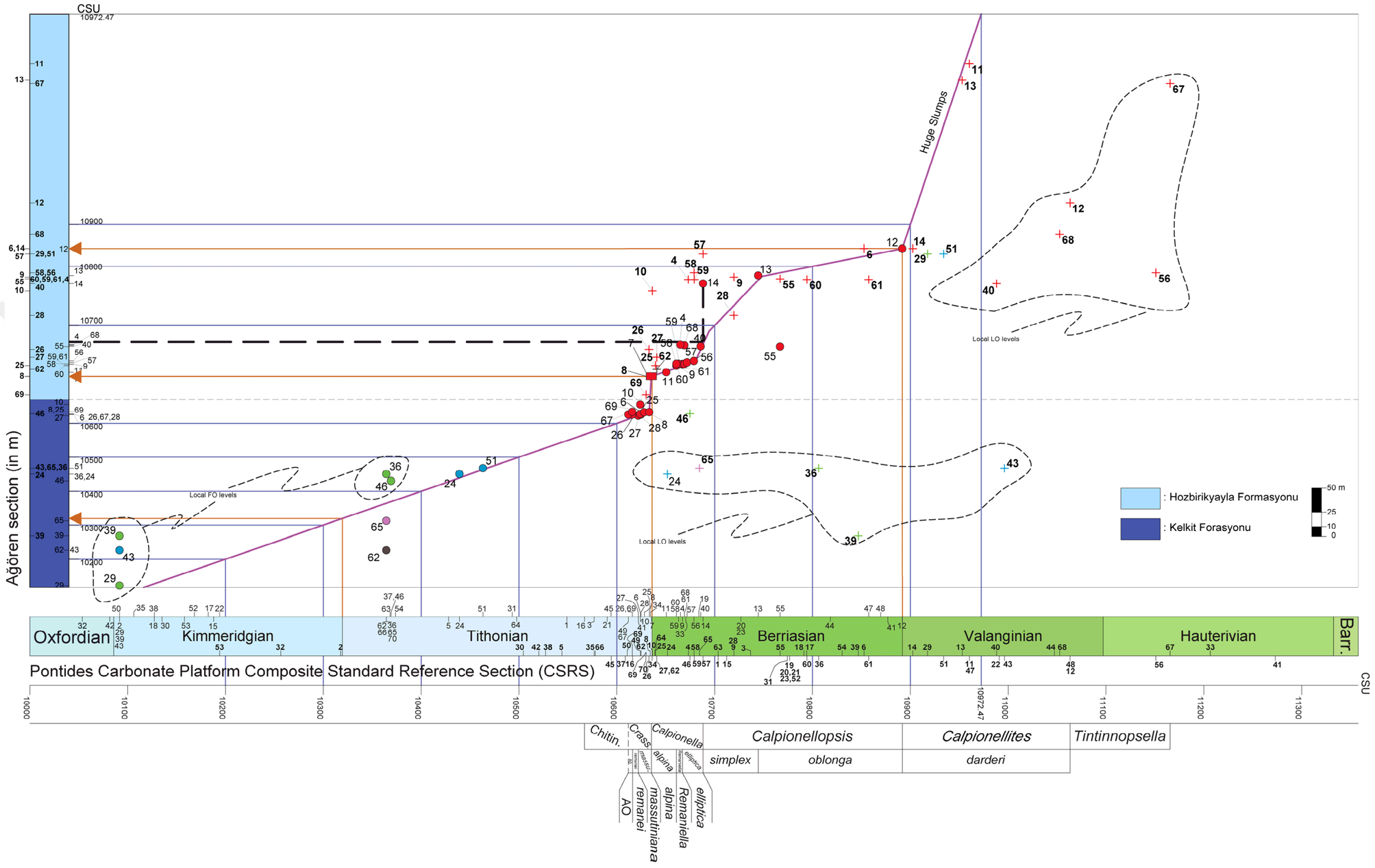

Figure 2.35. Correlation of the Ağören section with the PCP-CSRS. Purple bold line is the LOC. A segmented linear correlation line is well constrained by the taxa. Orange lines with arrow heads are the projected boundary levels. Blue lines are the projected CSTEs. Taxa codes are the same as Fig. 2.27. A high-resolution version is present in Appendix H. For discussion see the text.

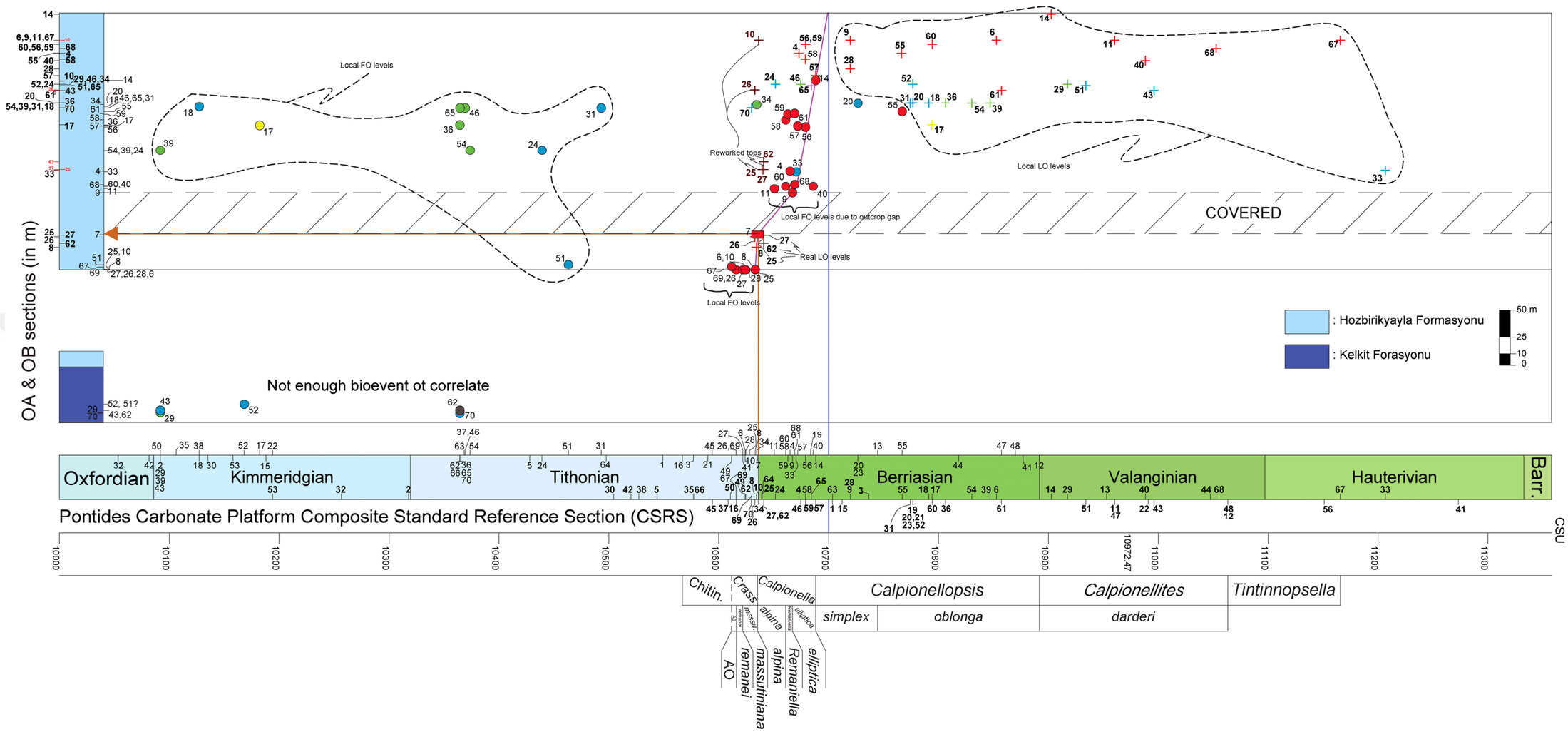

Figure 2.36. Correlation of the Ozansu (OA and OB) sections with the PCP-CSRS. Purple bold line is the LOC. A segmented linear correlation line is well constrained by the taxa. Orange lines with arrow heads are the projected boundary levels. Blue lines are the projected CSTEs. Taxa codes are the same as Fig. 2.27. A high-resolution version is present in Appendix H. For discussion see the text.

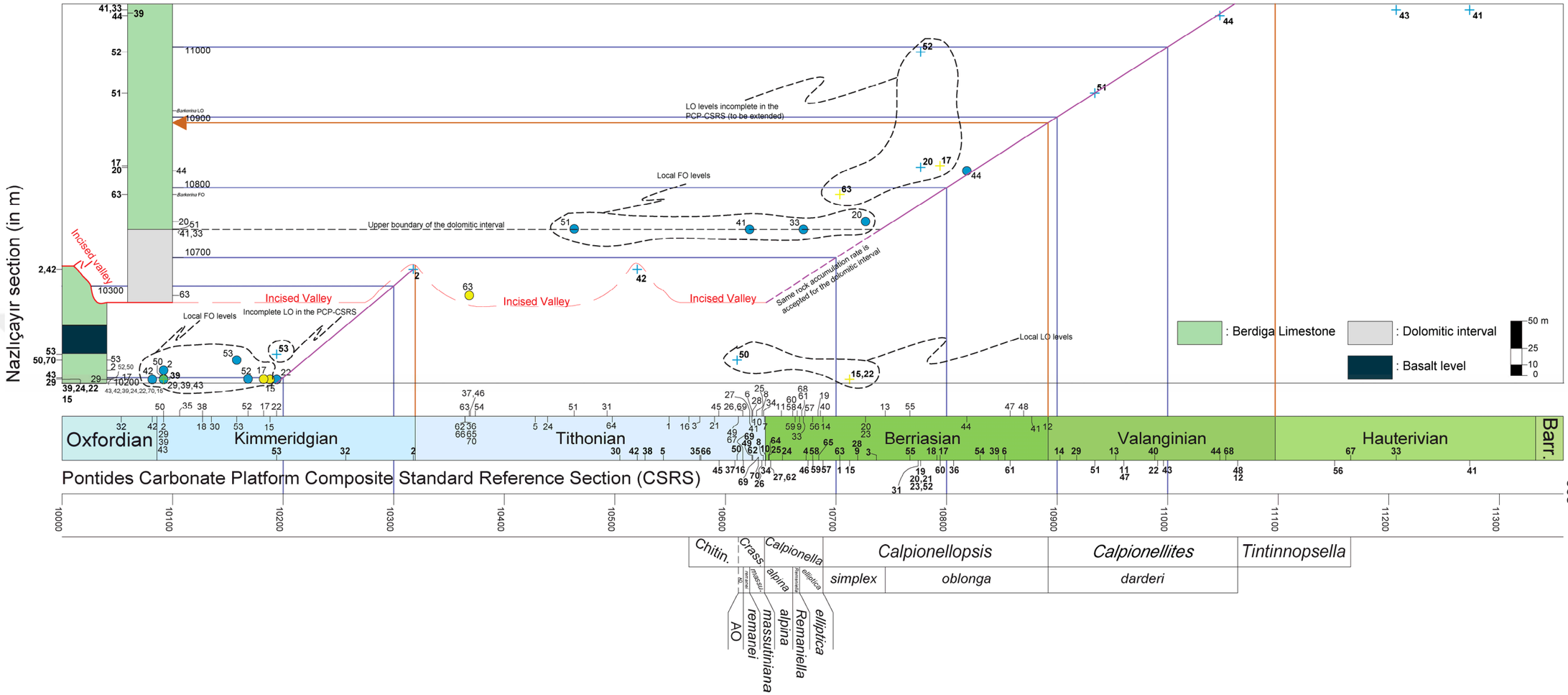

Figure 2.37. Correlation of the Nazlıçayır section with the PCP-CSRS. Purple bold line is the LOC. Two separate simple linear correlation lines for each segment of the succession are well constrained by the taxa. Orange lines with arrow heads are the projected boundary levels. Blue lines are the projected CSTEs. Taxa codes are the same as Fig. 2.27. A high-resolution version is present in Appendix H. For discussion see the text.

51 & 44 and blue circle of 44, respectively). The so-called Valanginian-marker *Barkerina dobrogiaca* (Schlagintweit et al., 2019) seems to have FO in the middle Berriasian (Fig. 2.37). This chronostratigraphic level should be further tested as there are contradicting records: from middle Berriasian (Ivanova et al., 2015 from Thrace Basin) before the FO of *M. salevensis* similar to the Nazlıçayır section (Fig. 2.19). Granier (2020b) also recorded *B. dobrogiaca* before the FO *M. salevensis* in the Nazlıçayır section. In contradiction from the same succession, Bucur et al. (2004) recorded the FO of *M. salevensis* before the FO *B. dobrogiaca*. A similar record has been documented by Taslı (1990). The chronostratigraphic significance of this benthic foraminifer should be further studied. The unconformity in the section is interpreted to represent Tithonian and the lowermost Berriasian (Fig. 2.37 & 2.38) in consensus with Vincent et al. (2018) and Granier (2020b). This time interval also corresponds to high clastic sediment influx to the basinal environments recorded as clastic turbidites in the Ağören and Ozansu successions (Fig. 2.3, 2.6, 2.7 & 2.12). Contrary to previous studies detailed in Chapter 1.4, there are no Upper Hauterivian and Barremian strata in the Nazlıçayır section.

The individual high resolution graphic correlations are given in Appendix H. Finally, the Eastern Pontides sections have become correlated to the Western and Central Pontides successions and the PCP-CSRS (Fig. 2.38).

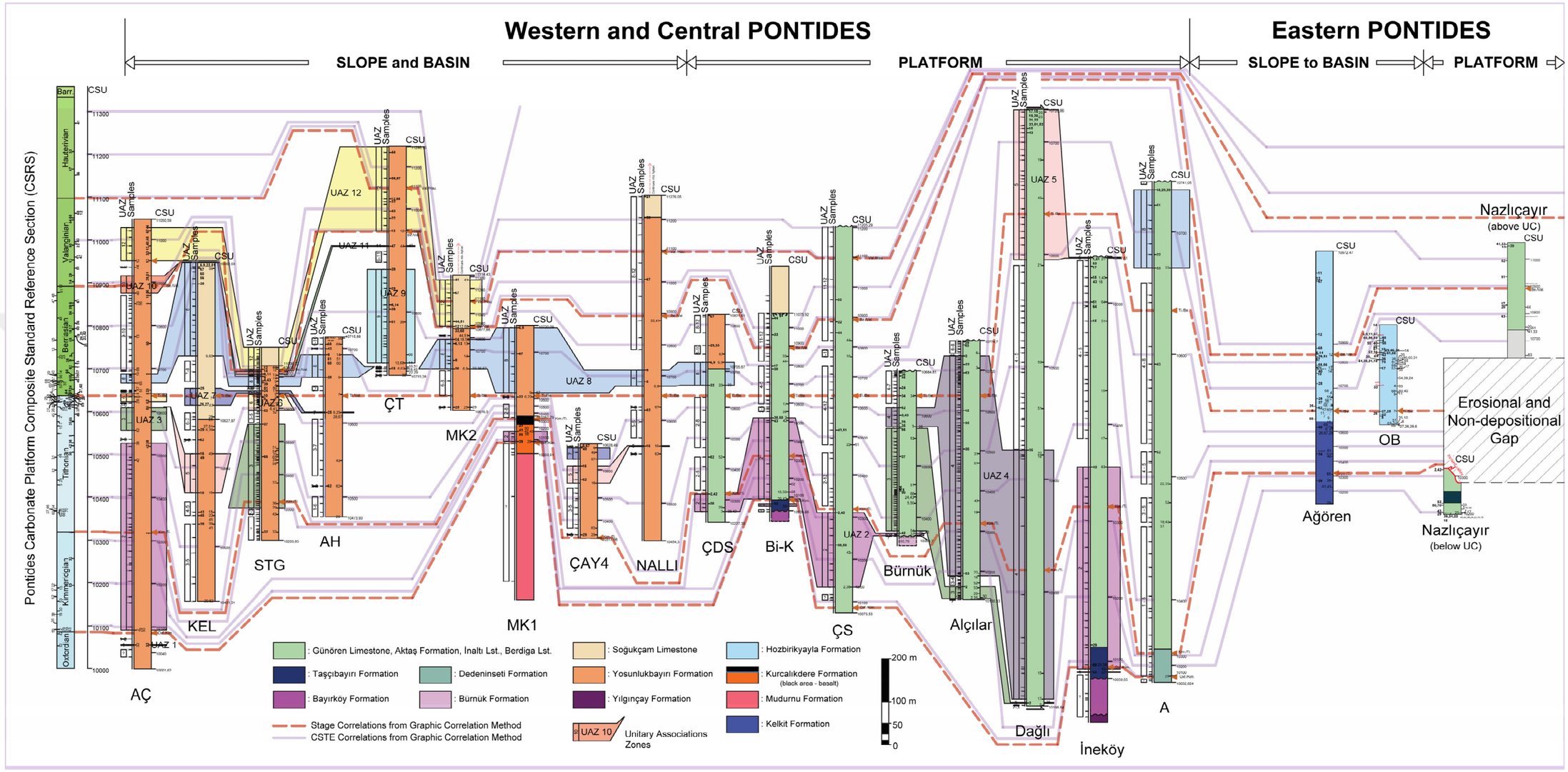

Figure 2.38. Correlation of the measured sections from the Eastern Pontides with the Western and Central Pontides successions and the PCP-CSRS. Symbols are the same as Figure 2.34.

2.3.6 Local Fossil Datums vs GCM

A chronostatigraphic chart of the analyzed sections is additionally prepared based on the GCM (Fig. 2.39). On this chart, the vertical scale of the sections corresponds to time. Note that depending on the rock accumulation tempo, the area each individual section covered in the vertical scales of Figures 2.38 and 2.39 are contrasting, e.g., the thick Kel section (Fig. 2.38) covers a very short time interval (Fig. 2.39). Similarly, although the Dağlı section is about twice the thickness of the Alçılar section, the latter represents a wider time interval (Figs. 2.38 & 2.39). This chronostratigraphic chart is also important for illustration of diachronism among the original fossil datums within each section (Fig. 2.39). The correlation lines solely based on the recognition of FO bioevent datums will cross timelines and stage boundaries (Fig. 2.39). Among the taxa illustrated in Figure 2.30, *P. ultragranulata* (51) seems to provide relatively reliable and consistent chronostratigraphic positions in the sections for correlations of shallow marine and deep marine succession.

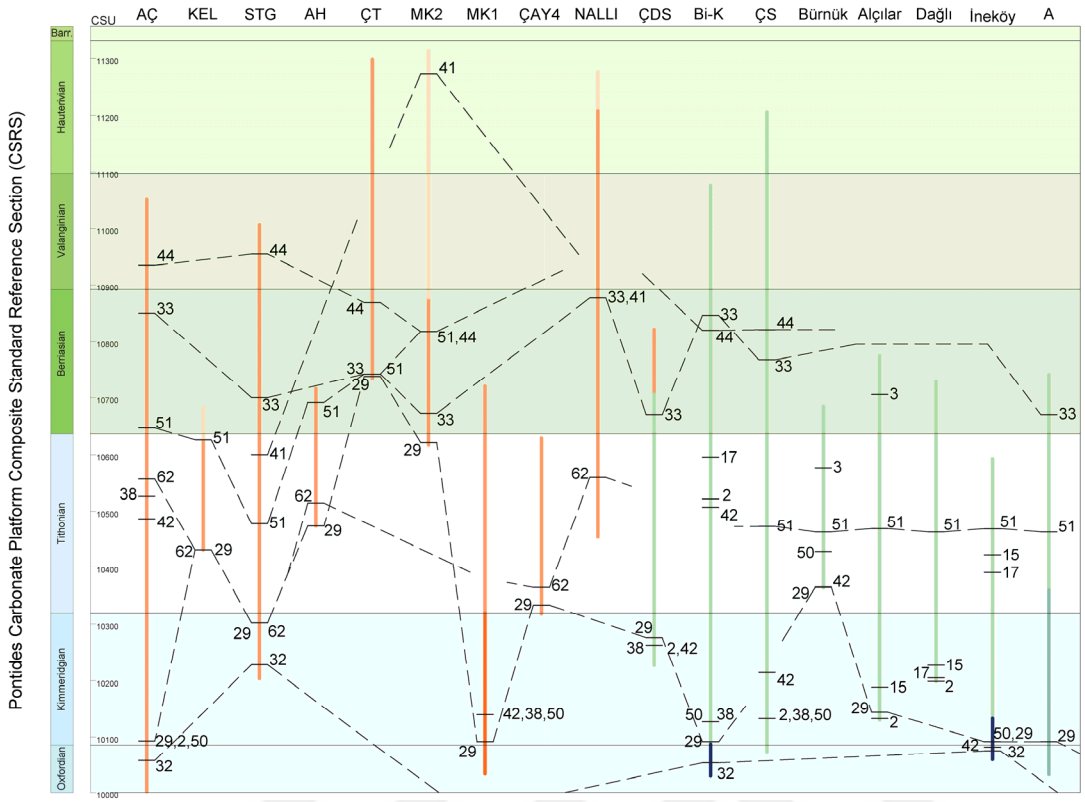

Figure 2.39. Chronostratigraphic range chart of the analyzed stratigraphic sections from the GCM. The FO datums of the index taxa, recorded in sections (original stratigraphic levels within each section), commonly used in biozonations of the previous studies are labelled with related taxa numbers (same as Fig. 2.27). These individual datums (and sections themselves) are calibrated to the PCP-CSRS to estimate the diachronism. Note the important diachroneity of the bases and tangling biohorizons. Direct correlations based on FO datums may lead to miscorrelations. Compared to their relative length in Figure 2.38, the KEL, STG, Bi-K, Dağlı, İnekoy and A sections cover contrasting space in the vertical scale (time). Color codes for the formations are the same as Fig. 2.27 (from Atasoy et al., 2022).

CHAPTER 3

DISCUSSION on FOSSIL RANGES and STAGE BOUNDARIES

The following discussion will focus on the implications of the PCP-CSRS (Fig. 2.27) obtained from the GCM on the ranges of taxa reported from the previous works. The chronostratigraphic range covered by any CSRS depends on the maximum stratigraphic range displayed by the composited sections. In this study, 17 measured sections from the J-K successions of the Pontides are used (Table 2.1), which produced a CSRS that ranges from Oxfordian to Hauterivian (Fig. 2.27). Stratigraphic sections with older intervals are present (Altiner et al., 1991). We only used the sections with well documented biohorizons and within the range of desired choronostratigraphic position to allow calibration of Late Jurassic–Early Cretaceous shallow and deep marine bioevents (Appendix D). So, it should not be interpreted that the Pontides Jurassic successions are limited to Oxfordian–Tithonian interval when Figure 2.27 is examined; the lower limit is completely determined by the oldest lower boundary present in the analyzed sections. Similarly, the upper limit is determined by the youngest level provided by the compiled sections, pelagic successions in the Pontides continue into the Aptian (Altıner et al., 1991). Additional good quality sections covering older and younger strata will extend the ranges in this PCP-CSRS; it is an evolving scheme. Reference lists for the FO/LO datums of benthic and planktonic foraminifers, algae, microencrusters, pelagic crinoids and calpionellids have been compiled. For space concern, the full content of these lists is given in Appendix F (Bisotratigraphy References).

3.1 Kimmeridgian

The last consistent occurrence of Jurassic planktonic foraminifers in the Pontides seems to be in the Upper Kimmeridgian (Fig. 2.27). This "bottleneck" interval is also suggested by Gradstein et al., (2017, 2018) from the lowest *beckeri* Zone onward until the Berriasian reappearance of planktonic foraminifers (Grandstein et al., 2018). Görög and Wernli (2004) provides the only documented rich Tithonian occurrence from the Hungarian section with ammonites and calpionellids (see also Gradstein & Waskowska, 2021). Other previous studies also suggest Early Kimmeridgian disappearance (e.g., Altıner, 1991; Benzaggagh et al., 2015a). This Kimmeridgian–Tithonian decline of aragonitic Jurassic planktonic foraminifers contrasts with the diversification of nannofossils and dinocysts (Gradstein et al., 2018) and can be related to changes in ocean chemistry.

Although the base of the Kimmeridgian is characterized by a cluster of FO events, much older records have been documented for those taxa (Fig. 2.27). An upper Oxfordian FO for the *Mesoendothyra izjumiana* has been reported (Krajewski & Olszewska, 2007). Aalenian evolution has been suggested for *Protopeneroplis striata* (Septfontaine, 1974; Bucur, 1997, Bassoullet, 1997). Peybernès (1998) calibrated the FO of *Alveosepta jaccardi* at the base of Oxfordian. Similarly, the Oxfordian seems to be a diversification time for *Crescentiella morronensis* (Pleş et al., 2013). *Lithocodium aggregatum*, a long ranging microencruster, also appears at the near base Kimmeridgian in the Pontides (Fig. 2.27). The FO of the encrusting *Mohlerina basiliensis* also has been reported from earlier ages; latest Bathonian–near base Callovian (Bassoullet, 1997; Peybernès, 1998). In contrast to these previous works, the sudden thriving of benthic fauna around the base of Kimmeridgian in the Pontides should be related to local tectonics and the facies change from the pelagic plateau type to shallow marine carbonates that only provide suitable environment for these taxa to thrive from Kimmeridgian onwards (Altiner et al., 1991). Although those datums are clearly local, they provide solid correlation datum at least over the Pontides given that no further elevated datums are dealt with (may result from

sample bias or diachronism of facies, etc.). However, even in the later situation, correlation of a section with the PCP-CSRS will reveal possible diachronism and sample biases and will provide sounding correlation.

Kastomonina abanica appears to first occur in the Lower Kimmeridgian in accordance with the type locality record (Sirel, 1993). The FO of this foraminifer seems to be a good indicator for Kimmeridgian; however, it is restricted to the platform facies only. *Labyrinthina mirabilis* was reported from the Oxfordian (Heinz & Isenschmid, 1988; Leinfelder, 1994; Pleş et al., 2015) and also from the uppermost Oxfordian–near base Kimmeridgian (Septfontaine, 1980-81; Bassoullet, 1997; Krajewski & Olszewska, 2007; Olzewska et al., 2012; Pleş et al., 2019), making the FO of this foraminifer an indicator for the near base Kimmeridgian interval (Fig. 2.27). Among the algae, *Campbelliella striata* provides good approximation for the Upper Kimmeridgian (Fig. 2.27; Heinz & Isenchmid, 1988; Bassoullet, 1997; Schlagintweit, 2011; Olszewska et al., 2012; Neamţu et al., 2019).

3.2 Kimmeridgian/ Tithonian Boundary

The LO of *A. jaccardi* is a good proxy for the base of Tithonian (Fig. 2.27). Base–Tithonian LO is also reported by previous studies (e.g., Bassoullet, 1997; Peybernès, 1998; Pleş et al., 2015; Olszeewska et al., 2012; Okay et al., 2018). The FO of the foraminifer *Anchispirocyclina lusitanica* is considered as a good marker for the base of the Tithonian with earliest Tithonian records (e.g., Ebli & Schlagintweit, 1998; Peybernès, 1998; Krajewski & Olszewska, 2007; Olszewska et al., 2012); however, this taxon seems to have elevated (younger) first appearance in the Pontides (Fig. 2.27; Kaya & Altiner, 2015; Okay et al., 2018). Since this taxon is only present in two Central Pontides sections (the Bürnük and Alçılar sections), additional data is required for more reliable calibration. The microencruster *Calcistella jachenhausenensis* is generally considered as a Tithonian marker (e.g., Pleş et al., 2013; Kaya & Altiner, 2015), although base Kimmeridgian FO (Pleş et al., 2019) and mid-Berriasian disappearance are also reported (Neamţu et al., 2019). This taxon

only occurs in the Bürnük section, and the base of the Tithonian seems to be missing in that succession as suggested by the PCP-CSRS correlations (Fig. 2.27 & 2.39; see Appendix H). The pelagic crinoid *Saccocoma* sp. is another taxon generally used as a Tithonian base marker in the Pontides (Altiner, 1991; Rojay & Altiner, 1998; Atasoy et al., 2018). Although the FO for that taxon is placed close to the base of Tithonian by the PCP-CSRS (Fig. 2.27), much earlier records have been reported with several acme levels in Kimmeridgian and Tithonian. Heinz and Isenschmid (1988), Olszeweska et al., (2012) and Benzaggagh et al. (2015a, 2015b) reported occurrences from Oxfordian. Additionally, Chiocchini et al., (2008) placed the FO of this taxon in the Middle Kimmeridgian. Two acme levels have been reported. The first acme is in the early–early Late Kimmeridgian (Heinz & Isenschmid; 1988; Benzaggagh et al., 2015a, 2015b). The second and more intense acme is considered to be around the base of Tithonian (Heinz & Isenschmid, 1988; Altiner, 1991; Benzaggagh et al., 2015a, 2015b). This second acme probably corresponds to the base of *Saccocoma* subzone from the Pontides (Altiner, 1991; Rojay & Altiner, 1998; Atasoy et al., 2018); however, the GCM places this bioevent in the earliest Tithonian, a little higher position than the previously suggested base of the *Saccocoma* subzone (Fig. 2.27).

3.3 Late Tithonian

In the late Tithonian an important datum is provided by the FO of the microgranular walled chitinoidellids, marking the base of the well-known Chitinoidellid Zone (sensu Benzaggagh, 2020; base of the dobeni subzone; Fig. 2.27). The benthic foraminifers *Coscinophragma cribrosum* and *Protopeneroplis ultragranulata* successively appear below the base of this zone (Fig. 2,27). Similar mid to late Tithonian FO is observed for *C. cribrosum* in previous studies (e.g., Bucur et al., 1996). Peybernès (1998), based on observation of Heinz & Isenschmid (1988), calibrated the FO of *P. ultragranulata* in the upper Tithonian below the Chitinoidellid Zone as suggested by the PCP-CSRS. *M. izjumiana* shows LO just

below the Chitinoidellid Zone (Fig. 2.27), however this datum requires further confirmation. Similar upper Tithonian LO is also observed by Krajewski and Olszewska (2007). *L. mirabilis* also has LO at the same level (Fig. 2.27). Relatively older levels for the LO of this taxon are suggested from the lower Tithonian (Krajewski & Olszewska, 2007; Chiocchini et al., 2008; Olszewska, 2012). *P. striata* disappears from the Pontides record in the highest level of the Chitinoidellid Zone (Fig. 2.27). This bioevent also provides a good approximation for the Tithonian/ Berriasian boundary both for peri-reefal and slope deposits. Late (Schlagintweit & Ebli, 1999; Bucur et al., 2004) and latest (Septfontaine, 1974; Bucur, 1997; Chiocchini et al., 2008) Tithonian extinction levels for this taxon are similarly reported in the literature. *K. abanica* also shows LO within the lowest part of this zone (Fig. 2.27). Tithonian LO for *K. abanica* is reported by Okay et al., (2018) whereas Kaya (2014) interpreted the LO of this foraminifer as earliest Berriasian. The correlation of the Bürnük section with the PCP-CSRS assigns Late Tithonian for this bioevent (Appendix H). Neamţu et al., (2019) suggest even higher LO in the latest Berriasian. The FO datum of the trocholinid foraminifer *Coscinoconus delphiniensis* is calibrated to the middle of the Chitinoidellid Zone in the latest Tithonian (Fig. 2.27). Similar latest Tithonian FO records are suggested by Ebli and Schlagitnweit (1998) and Dragastan et al. (2014).

Younger levels witnessed rapid evolution of calpionellid species that allow detailed division of the rock record. Benzaggagh (2020) defined an AO subzone within the lowest Crassicollaria Zone. This unit is characterized by the co-occurrence of chitinoidellids of *boneti* group, *Praetintinnopsella*, and primitive calpionellids with hyaline test. Although this unit has not been directly observed from the analyzed sections, the PCP-CSRS predicts the presence of this very short ranging unit at the lowest part of the *remanei* subzone. Accordingly, we differentiate an assemblage sub-subzone of AO within the lowest part of the *Crassicollaria* Zone/ *remanei* subzone on the PCP-CSRS (Fig. 2.27). The LO of the chitinoidellids marks the upper boundary of the AO sub-subzone (Fig. 2.27). The upper boundary of the *remanei* subzone is delimited by the FO of *Calpionella grandalpina* and *C. alpina*, also

defining the lower boundary of the *massutiniana* subzone (Lakova, 1993; Lakova & Petrova. 2013).

3.4 Tithonian/ Berriasian Boundary

The Tithonian/Berriasian (T/B) boundary is defined by the lower boundary of the *Calpionella alpina* acme in pelagic successions (i.e., working definition of the previous Berriasian Working Group, Wimbledon, 2017; Wimbledon et al., 2020a), characterizing the base of the *alpina* subzone (Pop, 1974; Remane et al., 1986; Kowal-Kasprzyk & Reháková, 2019). As noted by Remane et al. (1986), the *C. alpina* explosion event does not necessarily indicate a significant increase in the absolute frequency of this species, but it corresponds to a rapid increase in the relative abundance. Other calpionellid bioevents across the T/B boundary are the successive LOs of *Crassicollaria intermedia* and *Calpionella elliptalpina* below the boundary and prominent decrease in the *Calpionella grandalpina*, *Crassicollaria brevis* and *Crassicollari massutiniana* populations across the boundary who got extinct just above this level (Fig. 2.27). Benzaggagh (2020) suggests disappearance of *C. grandalpina* at the *Calpionellopsis* Zone as in the case for the OB section (Fig. 2.17). The range of this taxon should be further examined in the feature as reworked tops are suggested from the GCM (Fig. 2.36).

The algae *Aloisalthella sulcata* disappears in the middle Berriasian (Fig. 2.27). Similar within Berriasian LOs are reported in early studies (Granier & Deloffre, 1994; Bassoullet, 1997; Masse, 1998; Granier & Bucur, 2011; Granier, 2019a). The LO of the accompanying algae *C. striata* is in the early Berriasian (Fig. 2.27). Although some authors restrict the highest occurrence of this algae to Tithonian (e.g., Granier & Deloffre, 1994; Schlagintweit et al., 2005; Granier & Bucur, 2011; Granier, 2019), lowermost Berriasian occurrences have been reported (e.g., Bassoullet, 1997; Chiocchini et al., 2008; Mircescu et al., 2013; Bucur et al., 2014a). In both cases, this bioevent provides a datum near the T/B boundary and the LO of

this alga can provide signals in shallow marine successions about the approximate position of the T/B boundary.

The pelagic crinoid *Saccocoma* shows a major decline in abundance toward the T/B boundary as the saccocomid facies are replaced by calpionellid facies. This Tethys-wide shift in facies is generally considered as the combined effect of nannoconid bloom (nannofossil calcification event; e.g., Bornemann et al., 2003; Casellato, 2008; Grabowski et al., 2019) and tectonic organization of continents surrounding the Tethys that modified the oceanic circulation patterns and distribution of upwelling zones (effecting the biosiliceous factories, e.g., Muttoni et al., 2005). This combination resulted in deepening of carbonate compensation depth and general facies change from radiolarites to Maiolica–type pelagic limestones with micritic matrix, in some cases, full of nannofossils. This is an example of how biologic evolution influence sedimentation patterns and can trigger the formation of facies types specific to certain geologic time intervals. Previous research mostly reports the disappearance of the saccocomids before the *alpina* subzone (e.g., Skourtis-Coroneou & Solakius, 1999; Kroh & Lukeneder, 2009; Michalík et al., 2016; Svobová et al., 2019; Grabowski et al., 2019; Benzaggagh, 2020; Wimbledon et al., 2020b). The PCP-CSRS suggests the penetration of this crinoid into the lowest part of the *alpina* subzone (Fig. 2.27). Similar observations are documented by several studies (Reháková et al., 2011; Atasoy et al., 2018; Vaňková et al., 2019; Kowal-Kasprzyk et al., 2020).

Among the microencrusters, the LOs of *Perturbatacrusta leini* and *Iberopora bodeuri* seem to provide biohorizons close to the T/B boundary (Fig. 2.27). Top Tithonian (Pleş et al., 2013) and within Berriasian (Granier & Berthou, 2002; Schlagintweit, 2004; Schlagintweit et al., 2005) last occurrences are reported for *Iberopora bodeuri*. The data for this peri-reefal microencruster is only provided by the Bürnük section (Kaya & Altiner, 2015), requiring additional sections to further refine its range in the PCP-CSRS (Fig. 2.27). The LO datum of *P. leini* is documented from the earliest Berriasian (Schlagintweit & Gawlick, 2011; Kaya & Altiner, 2015; Atasoy et al., 2018; Pleş et al., 2019) and from the Berriasian top (Pleş

et al., 2013), providing additional criterion in marginal carbonates around the T/B boundary.

Another taxon indicating the proximity of the T/B with its LO in the early Berriasian is *A. lusitanica* from shallow marine environments (Fig. 2.27). In consensus with the PCP-CSRS suggestion, LO levels strictly constricted to the lower Berriasian are reported for this taxon (Arkad'ev et al., 2006; Bassoullet, 1997; Ebli & Schlagintweit, 1998; Arnaud-Vanneau, 1998; Granier & Bucur, 2011; Olszewska et al., 2012; Granier 2019; Neamţu et al., 2019). The FO of *Haplophragmoides joukowskyi* has been reported from the lowermost (Altıner, 1991) and middle (Chiocchini et al., 2008; Pleş et al., 2019) Berriasian. Similar choronostratigraphic position is suggested by the PCP-CSRS (Fig. 2.27).

Note that, although some other LO events near the T/B boundary are suggested by the PCP-CSRS, their ranges are clearly not fully developed in the studied successions. For example, the long-ranging taxa of incertae sedis *Thaumatoporella parvovesiculifera*, *Koskinobullina socialis* and *Labes antramentosa*, *Terebella lapilloides* worm tubes, and *Actinoporella podolica*, *Salpingoporella annulata* and *S. pygmaea* algae have partially developed local ranges limited by the data recorded in the composited sections. Similarly, *Pseudocyclammina lituus* seems to have lower tops in the studied successions (Fig. 2.27); much younger records have been reported from the lower Valanginian (e.g., Granier, 2019) and base Hauterivian levels (e.g., Chiocchini et al., 2008; Bucur et al., 2014b).

Another taxon that should be mentioned is *Meandrospira favrei*. This benthic foraminifer is reported from the middle Valanginian in the Pontides (*M. favrei* Zone of Altıner, 1991). In addition to similarly reported stratigraphic levels in the literature (e.g., Ivanova et al., 2008; Petrova et al., 2011), this taxon also documented from the lowermost Valanginian (Arnaud-Vanneau, 1988, calibrated at the same level with the FO of *Montsalevia salevensis*), base of Berriasian (Bucur et al., 2014b), upper Berriasian (Arnaud-Vanneau et al., 1987; Krajewski & Olszewska, 2007) and lowermost Berriasian (Bakhmutov et al., 2018). Atasoy et al. (2018) reported this

taxon from the *massutiniana* subzone (latest Tithonian). This observation from the Pontides need further confirmation since it is observed from two levels in the STG section assigned to *massutiniana* Zone with no record until another Berriasian level with *M. favrei* that hinders observation of well-presented population for healthy species level identification. Accordingly, the range of this taxon is illustrated with 2 options in the PCP-CSRS (Fig. 2.27). The dark blue column indicates the calibration without STG section data. This data already suggests extension of the FO level well into the upper Berriasian (below the *darderi* subzone, Fig. 2.27). If the STG data for *M. favrei* is integrated, the FO of this taxon is further extended into the latest Tithonian (within the *massutiniana* subzone).

Among trocholinids, the PCP-CSRS range of *Coscinoconus delphinensis* ends in the late Berriasian (Fig. 2.27). Although similar LO levels have been reported (e.g., Ebli & Schlagintweit, 1998), younger levels have also been documented from the middle (Dragastan et al., 2014) and the top Valanginian (Pleş et al., 2019). The LO of *Coscinoconus alpinus* is within the middle Berriasian (Fig. 2.27). Krajewski & Olszewska (2007) and Pleş et al. (2019) suggested within Valanginian and top Valanginian last occurrences, respectively. Additionally, *C. campanellus*, *C. cherchiae*, and *C. sagittarius* seem to have potential of providing good chronostratigraphic control in the lower Berriasian (Fig. 2.27). The FOs of *C. campanellus* have been noted from the base Berriasian (Dragastan et al., 2014; Neamţu et al., 2019) and within the early Berriasian (Altiner, 1991). Besides these studies confining this taxon to Berriasian, LO datum is also reported from the top Valanginian (Dragastan et al., 2014). *C. cherchiae* and *C. sagittarius* are confined to the middle Berriasian in the PCP-CSRS (Fig. 2.27). For the FO of these taxa, Berriasian datums are noted (Ebli & Schlagintweit, 1998; Dragastan et al., 2014; Pleş et al., 2019: Neamţu et al., 2019), however Valanginian disappearances, in contrast to the PCP-CSRS, are also reported (Chiocchini et al., 2008; Dragastan et al., 2014; Pleş et al., 2019). The LO for *C. elongatus* is also reported from the Valanginian (Altıner, 1991; Krajewski & Olsezwska, 2007). There is not much detailed

biostratigraphical work on this overlooked group and these forms still require further research and confirmation of their already reported datums.

3.5 Berriasian/ Valanginian Boundary

Taxonomic problems and endemism among the ammonites led the Valanginian Working Group to provisionally shift the base of Berriasian/ Valanginian (B/V) boundary to the base of *Calpionellites* Zone (Bulot et al., 1996; Hoedemaeker et al., 2003). The base of the *Calpionellites* Zone (base *darderi* subzone) is defined by the FO of *Calpionellites darderi* (Trejo, 1980; Pop, 1994). The benthic foraminifer *Montsalevia salevensis* appears just below the base of this well-known calpionellid zone in the PCP-CSRS (Fig. 2.27) in accordance with the Berriasian first appearances reported in previous studies (Zaninetti et al., 1987; Altıner, 1991; Bucur et al., 2004; Krajewski & Olszewska, 2007; Petrova et al., 2011; Pleş et al., 2019). Recently, *Barkerina dobrogiaca* is documented from the Eastern Pontides and elaborated as a Valanginian marker taxon by Schlagintweit et al. (2019). This benthic foraminifer was described from the lower Valanginian beds of SE Romania by Neagu (2000). The *Barkerina* genus in the Eastern Pontides is firstly recorded by Bergogunan (1987; as *B. barkerensis*) and *described* by Taslı (1990) from the Valanginian beds who assigned these individuals to *Barkerina barkerensis* (a closely related species with larger form and thought to be restricted to the Albian of southern America; e.g., Hamaoui, 1973). Bucur et al. (2004) from the same succession in the Eastern Pontides identified those assemblages as ?*Barkerina* sp. that occur in association with *M. salevensis*, *M. favrei* and *H. joukowskyi* and again interpreted a Valanginian age. There are several following studies on the same succession that aimed to restrict the age of discontinuity surfaces punctuating these shallow marine carbonates from the Gümüşhane region (Koch et al., 2008; Vincent et al., 2018). Following the revision of Granier (2020b) and synthesis of previous biostratigraphic work (Taslı, 1990; Eren & Tasli, 2002; Bucur et al., 2000, 2004), a Valanginian age is also assigned to the *B. dobrogiaca* assemblages of the Eastern Pontides

(Schlagintweit et al., 2019) in accordance with the record from the type locality in Romania (Neagu, 2000). This so-called Valanginian-marker *Barkerina dobrogiaca* (Schlagintweit et al., 2019) seems to have FO in the middle Berriasian in this study (Fig. 2.37). This chronostratigraphic level should be further tested as there are contradicting records: from middle Berriasian (Ivanova et al., 2015 from Thrace Basin) before the FO of *M. salevensis* similar to the Nazlıçayır section (Fig. 2.19). Granier (2020b) also recorded *B. dobrogiaca* before the FO *M. salevensis* in the Nazlıçayır section. In contradiction from the same succession, Bucur et al. (2004) recorded the FO of *M. salevensi*s before the FO *B. dobrogiaca*. A similar record has been documented by Taslı (1990). This taxon has not been reported from the western and Central Pontides. Successions with continuous record of *B. dobrogiaca* will enhance the Valanginian shallow marine and pelagic bioevent calibrations in the PCP-CSRS and will provide prediction on the bioevent datums of this taxon with respect to stage boundaries. The chronostratigraphic significance of this benthic foraminifer should be further studied.

Additionally, the microencruster *C. morronensis* also seems to have LO level within the early Valanginian (Fig. 2.27). Slightly higher levels from the mid-Valanginian (Altıner, 1991; Chiocchini et al., 2008) and the top Valanginian (Pleş et al., 2013) have been suggested in the literature.

3.6 Valanginian/ Hauterivian Boundary

The *Calpionellites* Zone is originally introduced by Alleman et al. (1971) that ranges from the FO of *C. darderi* to the disappearance of the calpionellids. Another division, the *major* subzone (Pop, 1994), within this *Calpionellites* Zone above the *darderi* subzone is defined at the base by the FO of *Calpionellites major*. This species and the associated subzone have not been reported from the Pontides (Fig. 2.27). As pointed out by Benzaggagh (2020), the collars of the *Calpionellites* species are fragile, sometimes limiting the identification. Consequently, the successive appearances of these two species are not well documented. The upper boundary of

the *Calpionellites* Zone is defined by the LO of genus *Calpionellites* (Pop, 1974) below the Valanginian/ Hauterivian (V/H) boundary.

The LO of *Montsalevia salevensis* seems to be confined to the *Calpionellites* Zone (Fig. 2.27). In addition to similar upper Valanginian LOs in previous studies (Altıner, 1991; Eren & Taslı, 2002; Krajewski & Olszewska, 2007), base Hauterivian (Septfontaine, 1980-81; Arnaud-Vanneau, 1988) and earliest Hauterivian (Bucur et al., 2004; Pleş et al., 2019) disappearances are also noted, providing a proximity marker for the V/H boundary in shallow marine deposits (Fig 2.27). Similarly, the LOs of *Coscinoconus elongatus*, *Mohlerina basiliensis* and *Protopeneroplis ultragranulata* are within the *darderi* subzone (Fig. 2.27). Mid-Valanginian disappearances have been reported for *C. elongatus* (Altıner, 1991; Krajewski & Olszewska, 2007). For *M. basiliensis*, LOs are noted from the lower Valanginian (Granier, 2019) and the upper Valanginian (Krajewski & Olszewska, 2007; Chiocchini et al., 2008). In contrast to the PCP-CSRS, the lower Barremian record for the top of *P. ultragranulata* is suggested (Bucur, 1997).

Trejo (1975, 1980) introduced *Tintinnopsella carpathica* subzone within the upper part of the original *Calpionellites* Zone (of Alleman et al., 1971), later differentiated as *Tintinnopsella* Zone by Borza (1984) and F Zone by Altıner and Özkan (1991). The top and base of this *Tintinnopsella* Zone is defined by the successive disappearances of the genus *Calpionellites* and calpionellids altogether, respectively. The chronostratigraphic position of the base of this zone is interpreted to be in the upper Valanginian as also suggested by the PCP-CSRS (Fig. 2.27). However, as already pointed out by Remane et al. (1986), the LO events of calpionellids are not so much reliable especially in this interval. Trejo (1975) firstly interpreted the range of this zone as late Valanginian – Early Hauterivian, however later restricted to the late Valanginian (Trejo, 1980). In the following years, Hauterivian records of *T. carpathica* have been documented (Borza & Michalík, 1986; Pop, 1994; Granier et al., 1995; Remane, 1998, Lakova & Petrova, 2013). The PCP-CSRS also predicts extension of this zone and survival of last calpinellids into the Hauterivian (Fig. 2.27). Similar extension is also suggested by the graphic correlation calibration of

calpionellid bioevents and magnetochrons by Scott (2019). These reported occurrences need further study due to possible reworking of upper Berriasian strata as pointed out by Granier (2020a). No solid bioevent horizion has been identified for the V/H boundary among the datums provided by studied taxa (Fig. 2.27). As previously discussed, LO of *Montsalevia salevensis* in the latest part of *Calpionellites* Zone can provide a hint about the approximating V/H boundary (Fig. 2.27) as it is used to delineate the V/H boundary in the neritic Nazlıçayır section in this study (Fig. 2.19). Two other benthic foraminifers, *Haphlophragmides joukowskyi* and *Meandrospira favrei*, also seem to successively disappear in the Middle and Upper Hauterivian, respectively (Fig, 2.27). Lower to Middle Hauterivian LO is reported for *H. joukowskyi* (Altıner, 1991; Chiocchini et al., 2008; Pleş et al., 2019). Additional to the LOs in the Lower Hauterivian (Bucur et al., 2014b), Late Hauterivian (Arnaud-Vanneau, 1998; Krajewski & Olszewska, 2007) disappearances are also noted for *M. favrei*.

Obviously, among calpionellids, the LO of the genus *Calpionellites* is a good approximation in pelagic deposits for the V/H boundary (Fig. 2.27). Besides the dominant *T. carpathica* (and accompanying *T. longa*), the presence of *Lorenziella hungarica*, *L. plicata* and *Remaniella cadischiana* is reported from the lowest part of the *Tintinnopsella* Zone (e.g., Lakova & Petrova, 2013). Benzaggagh (2020) noted scarce presence of the remaniellids of the *cadischiana* group within this zone. Similar distribution has also been predicted by the PCP-CSRS (Fig. 2.27), but the survival of the *R. cadischiana* needs further confirmation.

3.7 Jurassic/ Cretaceous (J/K) Boundary

Currently, there are two opposing views regarding the definition of the J/K boundary. The past (2008-2020) Berriasian Working Group supports the position of this last unstandardized Mesozoic stage boundary to be defined at the T/B boundary (Wimbledon. 2017; Wimbledon et al., 2020a), generally known as the Kilian's (or Mazenot's) view (see Énay, 2020 for a review). The second, known as the Oppel's

(or d'Orbigyn's) view, suggests shifting of the J/K system boundary to the B/V stage boundary (Granier, 2019, Énay, 2020, Granier et al., 2020a). They defend that the base Valanginian, corresponding a crisis that affected ammonites, vertebrates, larger foraminifers and calcareous algae is a better choice for a system boundary. If we evaluate the results of the PCP-CSRS in the light of these discussions, both boundaries can be confidently delineated within pelagic successions on the basis of calpionellid bioevents (Fig. 2.27). Although many bioevents cluster around the T/B boundary and it can be easily defined by the calpionellid bioevents, it is clear from the previous discussion that no direct shallow marine indicator is present for this boundary since the benthic assemblages of latest Tithonian and earliest Berriasian are similar as pointed out by Granier (2019). For the second choice, similar situation is also hindering the confident delineation of the base Valanginian in the shallow marine successions (Fig. 2.27). As discussed previously, further refinement on the range of *B. dobrogiaca* can provide solid FO datum for this boundary.

Instead of interval and acme zones, another approach is detailed by the biostratigraphy of benthic foraminifers and calcareous algae in a dual scheme of assemblage zones by Granier (2019). The boundaries of these assemblage zones mostly coincide with sequence boundaries (and formation boundaries), resulted in "natural" breaks in assemblages and providing discrete populations (within each individual unit the relative order of bioevents is not known "due to their scattered presence", Granier, 2019). This is very similar to the UAM philosophy (Figs. 2.28 & 2.30). The main problem with this kind of discrete biozonation, as in the case of Jurassic ammonites and Tertiary larger foraminifers, is that the schemes are discontinuous (e.g., delimited by 'natural' discontinuity boundaries) while promising correlation with continuous chronostratigraphical scales (see detailed discussion in Pignatti & Papazzoni, 2017 and Fig.2.24), resulting in commonly fuzzy and diachronic boundaries (Fig. 2.38). The bases of assemblage zones are mostly defined by the FO or LO events limiting discrete associations of populations, again making this approach prone to diachronism of the bioevent datums similar to the problems of interval zones (e.g., Wu et al., 2020). Additionally, the hiatuses present at the

unconformity surface will further complicate the correlations among regions with varying records of these eustatic signals when coupled with local tectonics as in the case for the unconformity surface in the Nazlıçayır succession which had promoted as the B/V and J/K boundary in the Pontides by Granier (2020b). There is still much more work to do for correlation of shallow marine and deep marine environments, clearly requiring integrated approaches additional to biostratigraphy instead of correlation solely based on bioevents and assemblages.

Besides that, the modern GSSP methodology is a pragmatical solution to the fuzzy boundaries of previous stratotype concept where boundaries commonly coincide with discontinuity surfaces. For example, A GSSP can be placed at a geochemical signal – K/Pg boundary (Molina et al., 2006), at a magnetic reversal – Paleogene/Neogene boundary (Steininger et al., 1997) or can be placed arbitrarily within a bundle of events – base Maastrichtian at the arithmetic mean of 12 biohorizons (Odin & Lamaurelle, 2001). At the end they are just reference points in the rock (Remane, 2003). The most important suggestion must be that GSSPs "should be defined wherever possible in an area where nothing happened" (McLaren, 1970) in order to avoid interpretation of any event that may have punctuated the rock record (Cowie et al., 1986; Remane, 2003; Miall, 2004). However, in the choice of the system boundaries that originally thought to delimit the important turnovers in evolution of organisms, Granier et al. (2020a)'s suggestion of separating the discussions on delineation of the T/B boundary and the choice of a J/K system boundary should be agreed upon.

The continuous zonations do not need major species turnovers to be recognized. For example, the calpionellid assemblages of the uppermost *Calpionella* Zone and the basal levels of the immediately overlying *Calpionellopsis* Zone (i.e., *simplex* subzone) are very similar (Fig. 2.27). Only a FO event, i.e., the evolution of *C. simplex*, is enough to differentiate another successive zone. In contrast, the UAZs (and Oppel Zones) are closely related to species turnover rates that enables recognition of unique maximal fossil assemblages that are strictly different from the bounding assemblages.

Diversity and turnover rate analyses are known to be very sensitive to the durations of time bins over which the calculations are carried out and equal time divisions are suggested whenever it is possible (e.g., Sepkoski & Koch, 1996, Purdy, 2008). UAZs, as time bins for such examinations, were shown to be suitable as the estimations are unaffected by the unknown durations of the UAZs (e.g., Escarguel & Bucher, 2004; Brosse et al., 2016). Figure 3.1A shows the species richness fluctuations over the 12 UAZs. Although the fossil assemblage in this study only forms a small subset of the total diversity (which is controlled by paleogeography, biofacies, preservation conditions and sampling biases) within the interested geological time interval, these species-based calculations can mimic the general trends. The stage boundaries are positioned between the UAZs (Fig. 3.1A & B) according to the biostratigraphic data of their fossil content in the PCP-CSRS (Fig. 2.27). As pointed out previously, UAM lumped calpionellids of latest Tithonian and earliest Berriasian into the same bins without their bioevent orders. Therefore, the position of the Tithonian/ Berriasian boundary cannot be precisely located (Fig. 3.1A & B). Overall, there is an increase in species richness from the Oxfordian into the Berriasian followed by a falling trend especially mid-Berriasian (UAZ9) onward. The big jump in the graph from the Oxfordian to the Kimmeridgian is related to the onset of carbonate platform development over the Pontides characterized by flourishing of shallow marine taxa. To overcome the biases induced by dealing with a subset of total diversity and removal of singletons from the calculation of the UAZs, the relationship between the cumulative last appearance datums (LADs) and the cumulative first appearance datums (FADs) within each UAZ are also examined (Fig. 3.1B). Preservation conditions would increase or decrease the total number of species observed and modify the numbers of recorded origination and extinction datums as well. However, the ratio of cumulative FAD and LAD would not change significantly (e.g., Guex et al., 2016: Brosse et al., 2016). The UAZ1 and UAZ12 at the borders of Figure 3.1B should be disregarded as they are biased by the truncated ranges, i.e., the lowest UAZ may range downward and the last UAZ may continue upward (Guex et al., 2016). The intervals between the UAZ6 – UAZ7 and the UAZ9

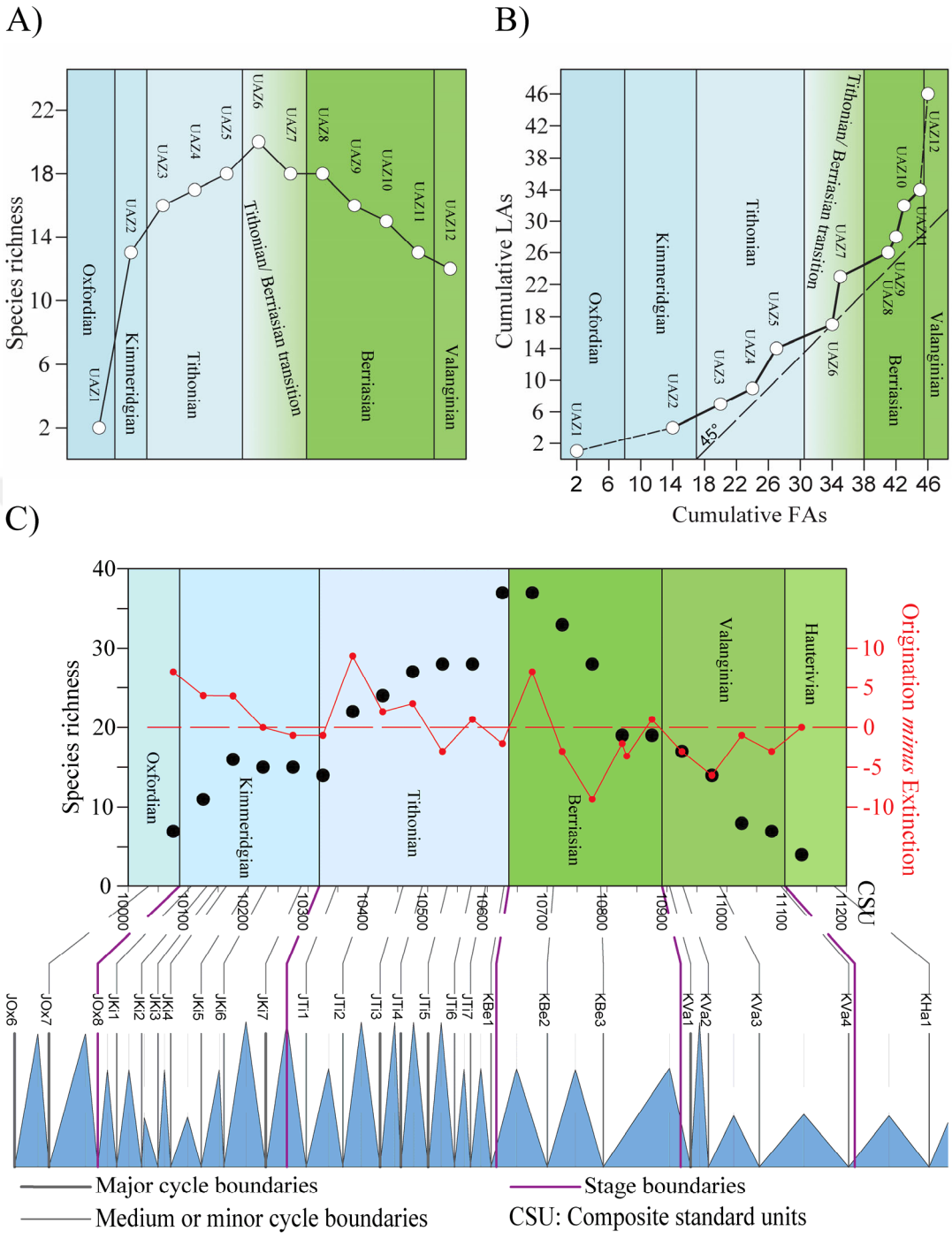

Figure 3.1. Late Jurassic – Early Cretaceous species richness and turnover rates from the Pontides Carbonate Platform. **A)** Species richness trend across the UAZs given in Fig. 2.30C. **B)** Species turnover rates calculated from the UAZs. Steep slopes indicate high extinction rates and vice versa. 1:1 slope indicates equal numbers of extinction and origination. **C)** Species richness and 'Origination minus Extinction' trends calculated from the GCM. Oxfordian–Hauterivian cycles are from the TSC 8.0 based on the calibration of Haq, 2014, 2017 and the GTS 2020. The peaks of the

Figure 3.1 (*continued*) blue triangles indicate maximum floodings dividing transgressive – regressive trends. (from Atasoy et al., 2022).

– UAZ10 in the Tithonian/ Berriasian transition and in the middle Berriasian, respectively are characterized by increased turnover rates (i.e., steep slopes in Fig. 3.1B) which is also suggested by increased numbers of bioevents clustering around these time intervals in the PCP-CSRS (Fig. 2.27). Most of those bioevents are characterized by originations and extinctions of the calpionellids, foraminifers and algae, and no major extinction event is present (only background extinctions).

Another diversity calculation is carried out over the PCP-CSRS obtained from the GCM (Fig. 3.1C). In contrast to the UAM, there is no need to remove singletons, i.e., all fossil data is used in calculations. The CSUs obtained by the equal subdivisions of the PCP-CSRS scale provide time bins with practically equal time durations. Any desired length of CSUs can be chosen. For the calculations in the Figure 3.1C, CSUs time bins with length of 50 CSU are used. There are two superimposed data on this figure; namely, the "Species Richness" and the "Origination minus Extinction" trends. The first one is the species counts for each of the time bins. The second one is a simple calculation of differences between the total origination and extinction numbers within the same time bins that signifies the number of taxa affecting the diversity trends (Purdy, 2008; M value of Şengör et al., 2008). When this value is positive it indicates diversity increase, when the value is negative it indicates diversity decline. Data points are calculated over the time bins and placed in the middle of related intervals (Fig. 3.1C). Again, the species richness increases toward the Berriasian and followed by a decline in the middle Berriasian (Fig. 3.1C). The Berriasian–Valanginian transition is also characterized by decrease in diversity, and this falling trend continued into the earliest Hauterivian, however the difference between origination and extinction converges to zero from the largest negative value in the middle Berriasian (Fig. 3.1C). This means that relatively minor extinction is enough for reducing the number of species in this interval because of low origination numbers.

These diversity drops calculated from the UA and GC methods are in consensus with the general trend toward lower sea levels through the late Tithonian into the Valanginian (Fig. 3.1C) which also greatly reduces the shallow marine areas of the Tethyan carbonate platforms (e.g., Flügel & Kiessling, 2002; Kiessling et al., 2003; Kocsis & Scotese, 2021). The Valanginian–Hauterivian interval also represents general platform drowning phase (Erba & Parente, 2024) both in the northern (e.g., Weissert et al., 1998; Föllmi et al., 2006; Morales et al., 2013; Grădinaru et al., 2016) and the southern (e.g., Amodio et al., 2008; Bodin et al., 2010; Basilone, 2021) margins of the Tethys Ocean that is also the case for the PCP (e.g., Altiner et al., 1991; Yilmaz et al., 2012). In this interval, disappearances dominate the shallow marine bioevents and this is why the lower and upper Valanginian in the shallow marine carbonates are mostly zoned by criteria based on last appearances and absence of certain taxa present in the underlying biozones (e.g., *Pseudocyclammina lituus* Zone of Granier, 2019) instead of cosmopolitan first appearance datums.

The base of the Granier's (2019) *Rajkaella minima* assemblage biozone (documented in a wide region from Jura Mountains to USA for middle Berriasian) can be roughly approximated by the FO of *Montsalevia salevensis* and the LO of *Anchispirocyclina lusitanica* in the in shallow marine deposits of the Pontides (Fig. 2.27). In the absence of accompanying algae reported by Granier (2019), the basal boundary remains elusive. The LOs of *Coscinoconus alpinus* and *C. delphiniensis* and the FOs of *C. cherchiae* and *C. sagittarius* may provide additional markers (Fig. 2.27). The *Pseudocyclammina lituus* biozone of Granier (2019), proposed for the lower Valanginian, cannot be traced into the Pontides. This zone is defined by the absence of *Zergabriella embergi* or related algae (*Falsolikanella campanensis*, *Clypeina catinula*, *Clyp. isabella* and *Clyp. zumetae*). Only one of these algae (*Falsolikanella campanensis*) has been reported from the Pontides (Bucur et al., 2000 from Eastern Pontides). The LOs of *Crescentiella morronensis* and *Protopeneroplis ultragranulata* and the FO of *Montsalevia salevensis* may provide approximations for the basal boundary of this assemblage biozone in the Pontides (Fig. 2.27).

In comparison to the Carpatho-Balkanides (e.g., Schalingtweit & Bucur, 2021) and European fossil assemblages (e.g., Granier, 2019), the Late Jurassic – Early Cretaceous Pontides fauna seem to be less divesified as already pointed out by Şengör et al. (1988) for the foraminiferal assemblages: The *Choffatella pyrenaica*, *Pfenderina neocomiensis*, *Valdanchella miliani*, and *Pseudotextulariella courtionensis* provinces are limited to the western European successions and the *Orbitolinopsis capuensis* and *Kurnubia* plexus provinces are limited to the southern margin of Tethys (Figure 3.2A). These differences in the foraminiferal and algal assemblages limit the tracibility of the proposed European shallow marine zonations into to the successions on the Laurasian margin of Tethys.,

Barkerına dobrogiaca seems to be confined to the northern Tetyhan margin with occurrences from ?Valanginian of Sierra del Valdancha, SE Spain (Shcroeder, 1968), Valanginian of Sardinia. Italy (Azema et al., 1977), Valanginian of Southern Dobrogea, SE Romania (Neagu, 2000), middle to upper Berriasian of Chalkodhili Peninsula and Thrace region, NE Greece (Ivanova et al., 2015) and ?Valanginian of Turkey (Taslı, 1990; Eren & Taslı, 2002, Bucur et al., 2004; Koch et al., 2008; Schlagintweit et al., 2019; Granier, 2020b and this study).

In contrast to shallow marine assemblages, calpionellids provide widely traceable biohorizons (Fig. 3.2B & C). The base of the *alpina* subzone (T/B boundary primary marker candidate) can be traced from Mexico to Arabian Gulf over both margins of the Tethys (Fig. 3.2B). Similarly, the base of the *darderi* subzone (B/V boundary primary marker candidate) has been defined in a wide region from Cuba to Oman (Fig. 3.2C). Calibration of shallow marine biohorizions with these calpionellid datums in individual regions will reveal relative positions of (sub-)endemic fossil bioevents with respect to the cosmopolitan shallow marine and deep marine fossil FO/ LO levels.

Composite (e.g., Altıner, 1991; Atasoy et al., 2018) and dual (e.g., Granier, 2019) biozonations incorporating varieties of fossil groups from unrelated lineages always have the risk of diachronic boundaries controlled by biofacies. These kinds of zonati-

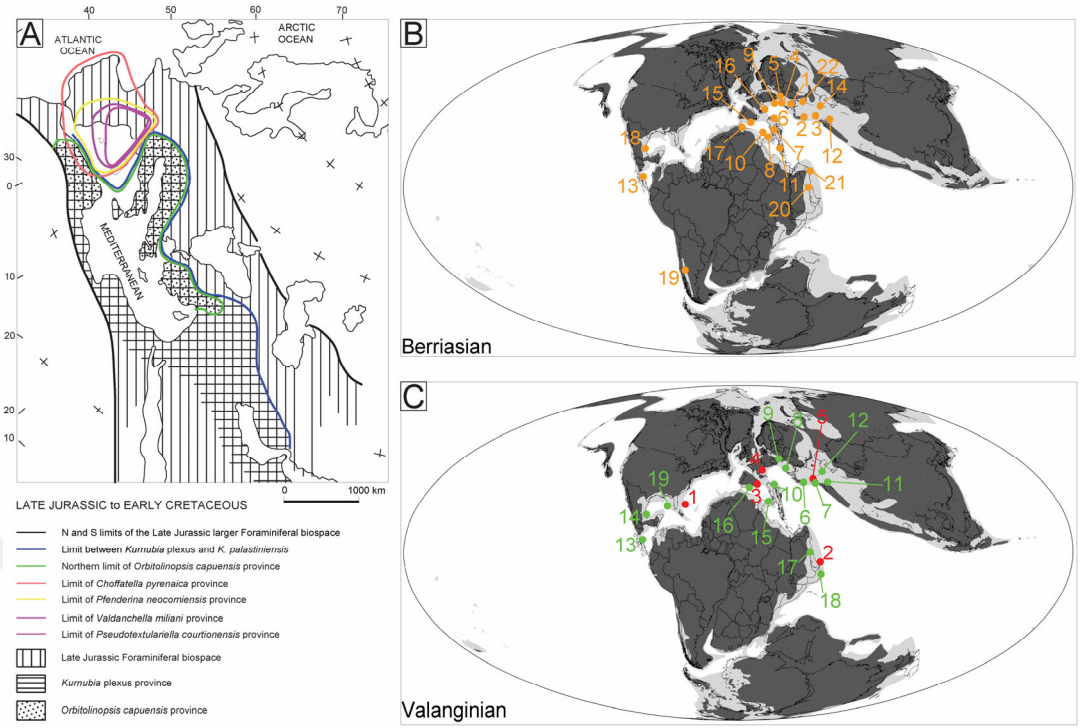

Figure 3.2. Benthonic foraminiferal provinces and calpionellid subzone localities. **A)** Late Jurassic to Early Cretaceous foraminiferal provinces in the Tethysides (from Şengör et al., 1988). **B)** Berriasian. Localities recording the *alpina* subzone basal boundary. For calpionellid zones, this and the following map (C) show localities where the bases of the related subzones have been clearly documented without a gap or partial record. Basemaps are from Kocsis & Scotese (2021). *1*- Pieniny Klippen Belt, Carpathians – Czech Republic, Slovakia, Western Ukraine, Poland, Romania, Bulgaria (Lakova, 1993; Ivanova, 1997; Lakova et al., 1999; Reháková et al., 2011; Lakova & Petrova, 2013; Michalík et al., 2016; Elbra et al., 2018; Petrova et al., 2019; Kowal-Kasprzyk & Reháková, 2019; Michalík et al., 2021), *2*- Western Sakarya Zone, Western Pontides – Turkey (Altiner & Özkan, 1991; Özkan, 1993; Atasoy et al., 2018), *3*- Eastern Sakarya Zone, Eastern Pontides – Turkey (this study), *4*- Western and Southern Carpathians – Southern Romania, Slovakia, Hungary, Eastern Serbia (Pop, 1974, 1986, 1994, 1998; Bucur, 1992; Reháková, 1995; Houša et al., 1999; Michalík et al., 2009; Grabowski et al., 2010a, b; Petrova et al., 2012), *5*- Western Carpathians – Poland (Pszczółkowski, 1996; Grabowski & Pszczółkowski, 2006), *6*- Eastern Alps – Northern Italy (Channell & Grandesso, 1987; Grün & Blau, 1997), *7*- Central Italy – Umbria (Houša et al., 2004), *8*- Sicily (Catalano & Liguori, 1971; Andreini et al., 2007), *9*- Austria (Reháková et al., 1996, 2009; Lukeneder et al., 2010), *10*- Tunisia (Memmi et al., 1989; Boughdiri et al., 2006; Maalaoui & Zargouni, 2017), *11*- Ionian Zone – Greece (Skourtis-Coroneou & Solakius, 1999), *12*- Northern Iran – Shal (Azimi et al., 2008), *13*- Cuba (Pop, 1976; Pszczółkowski & Myczyński, 2010; López-Martínez et al., 2013b), *14*- Chechnya – Russia (Makarieva, 1974), *15*- Iberian Peninsula – Southern Spain (Alle-

Figure 3.2 (*continued*) mann et al., 1975, Pruner et al., 2010; Hoedemaeker et al., 2016; Svobodová & Košťák, 2016), *16*- Southern France (Remane, 1963; Le Hégarat & Remane, 1968; Cecca et al., 1989; Wimbledon et al., 2020b), *17*- Northern Morocco (Benzaggagh & Atrops, 1995; Benzaggagh et al., 2010), *18*- Mexico (Trejo, 1980; López-Martínez et al., 2013a; López-Martínez et al., 2015), *19*- Argentina (López-Martínez et al., 2017a; Kietzmann et al., 2021), *20*- Arabian Gulf – Kuwait (Al-Rifaiy & Lemone, 1987), *21*- Northern Iraq (Wimbledon et al., 2016), *22*- Crimea (Platonov et al., 2014). **C)** Valanginian. 1-5) Shallow marine localities. 1-4) Granier (2019)'s shallow marine biozone locations. *1*- IODP 392A, *2*- Abu Dhabi, *3*- Alicante – Southern Spain, *4*- Jura – Eastern France, *5*- Eastern Pontides (Schlagintweit et al., 2019 and this study). *6-18)* Localities recording the *darderi* subzone basal boundary. *6*- Western Sakarya Zone, Western Pontides – Turkey (Altiner & Özkan, 1991; Özkan, 1993; Atasoy et al., 2018), *7*- Eastern Sakarya Zone, Eastern Pontides – Turkey (this study), *8*- Western and Southern Carpathians – Romania, Slovakia, Bulgaria, Hungary (Pop, 1986; 1994; Bucur, 1992; Reháková, 1995; Lakova et al., 1999; Főzy et al., 2010; Lakova & Petrova, 2013), *9*- Western Carpathians – Poland (Pszczółkowski, 1996; Pszczółkowski & Myczyński, 2004), *10*- Northern Italy (Channell & Grandesso, 1987; Grün & Blau, 1997), *11*- Northern Iran – Shal (Azimi et al., 2008; Benzaggagh et al., 2012), *12*- Chechnya – Russia (Makarieva, 1974), *13*- Cuba (Pszczółkowski & Myczyński, 2010), *14*- Mexico (Trejo, 1980; López-Martínez et al., 2017b; Jiménez-López et al., 2021), *15*- Sicily (Andreini et al., 2007), *16*- Iberian Peninsula - Southern Spain (Aguado et al., 2000), *17*- Arabian Gulf – Kuwait (Al-Rifaiy & Lemone, 1987), *18*- Oman (Celestino et al., 2017), *19*- DSDP 535 & 537 (Silva & McNulty, 1984). Modified from Atasoy et al., 2022.

ons do not have the resolution and stability of zonations based on phyletic first occurrences, i.e., the placement of zone boundary at an evolutionary event from an ancestor to a descendant. The other types of zonations mostly correspond to biofacies changes (sometimes boundaries are at formation boundaries, unconformities etc.). To overcome these difficulties in dealing with organisms from both shallow and deep marine environments and having unrelated lineages, quantitative biostratigraphical methods are opted to use in this study for calibration. Comparison of the graphical correlation based on FO/LO events (very similar to the GSSP methodology, Fig.2.27) and the unitary association zones (assemblage zones, Fig. 2.30) reveals important diachroneity and lack of lateral traceability of the latter (Fig. 2.38). Similarly, when the FO events do not represent a phyletic evolution, they also show major diachroneity (Fig. 2.39). This is also the reason for the dashed line boundaries

present in the Paleogene larger benthic foraminifera assemblage zones (SBZ) in the Geological Time Scale (2020).

GSSP criteria have been dominated by FAD of planktonic and nektonic fossils and several physical proxies. There are only 6 stage boundaries (out of total 77 ratified boundaries) delineated by last occurrence criterion (Gradstein et al., 2020): 1) the bases of Tortonian (last common occurrence of *Discoaster kugleri* as main criterion, a calcareous nannofossil), 2) the base of Serravallian (near LAD of *Sphenolithus heteromorphus* as secondary criterion, a calcareous nannofossil), 3) the base of Aquitanian (near LAD of *Reticulofenestra bisecta* as secondary criterion, a calcareous nannofossil), 4) the base of Rupelian (LAD of *Hantkenina* & *Cribrohantkenina* as main criterion, planktonic foraminifers), 5) the base of Priabonian (extinction of large acarininids and *Morozovelloides crassatus*, planktonic foraminifers and several accessory FAD of calcareous nannofossils), 6) base Lutetian (LO of *Blackites inflatus*, a calcareous nannofossil). Only two are from benthic foraminifers: base Hettangian (FO of *Praegubkinella turgescens* as a secondary criterion) and the base of Visean (FAD of *Eoparastafella simplex*, as the main criterion). Both are based on phyletic bioevents (from *Oberhauserella* lineage to *Praegubkinell turgescens* and *Eoparastafella ovalis* to *E. simplex*). Unconformity bounded and LO datum dominated criteria are hard to establish.

CHAPTER 4

MICROFACIES ANALYSES

Microfaceis analyses include both lithofacies analyses (determination of the depositional texture of rocks, composition of grains and background material) and biofacies analysis (examination of fossil associations). Since similar lithofacies can occur in variety of depositional environments and the diagenetic processes can greatly modify the original texture (e.g., compaction can transform a wackestone into a packstone or background micritic matrix can be replaced by sparite etc.), biofacies data are especially important to interpret the depositional settings.

Since the "X-Y-Z model" of Irwin (1965) for carbonate platform deposition, new concepts and several models has been introduced mainly based on the investigation of the analogous modern subtropical and tropical carbonates and their comparison with the ancient ones. It is obvious that each depositional time interval (determining type of the faunal and floral associations), latitudinal position (warm- vs cool-water carbonates), morphology of the shelf (ramp vs. platform with slope break), sedimentation rates (drowned vs rimmed platform), siliciclastic input, paleoceanographic conditions and many other parameters affect the microfacies types and their distribution.

One of the widely known models is the Wilson's Standard Facies Model (1975) that describes 9 Standard Facies Zones (FZ) with 24 Standard Microfacies Types (SMF) for a rimmed tropical carbonate platform. A revision of this model was introduced by Flügel (2004) that includes 26 SMF Types for a rimmed carbonate platform with 10 Facies Zones. Another model for the ramp type carbonate platforms was also proposed by him with 30 Ramp Microfacies Types (RMF).

In this study, the expanded version of Dunham (1962)'s classification of carbonate rocks by Embry and Klovan (1971) was used for the textural classification of each sample (Fig. 4.1 & Appendix B). This classification is chosen over the classification of Folk (1959, 1962), since it gives information about the depositional texture and conditions by default in contrary to descriptive scheme of Folk (e.g., there is no distinction between bioclastic floatstone, packstone and wackestone in Folk's scheme; they can all be classified as biomicrite).

CLASSIFICATION OF LIMESTONES (DUNHAM 1962)

DEPOSITION TEXTURE RECOGNIZABLE					DEPOSITIONAL TEXTURE NOT RECOGNIZABLE
Original components not bound together during deposition				Original components were bound together during deposition as shown by intergrown or lamination contrary to gravity, sediment-floored cavities that are roofed over by organic or questionable organic matter and are too large to be interstices	CRYSTALLINE CARBONATE (Subdivide according classification designed to bear on physical texture or diagenesis)
Contains mud (particles of clay and fine silt size)			Lacks mud and is grain-supported		
Mud-supported		Grain-supported			
less the 10% grains	more than 10% grains				
MUDSTONE	WACKESTONE	PACKSTONE	GRAINSTONE	BOUNDSTONE	

EXPANDED CLASSIFICATION (EMBRY and KLOVAN 1971)

ALLOCHTHONOUS LIMESTONE ORIGINAL COMPONENTS NOT ORGANICALLY ORIGINAL BOUND DURING DEPOSITION						AUTOCHTHONOUS LIMESTONE COMPONENTS ORGANICALLY BOUND DURING DEPOSITION		
Less than 10% > 2 mm components contains lime mud (< 0.03 mm)			no lime mud	Greater than 10% > 2 mm components		by organisms which		
Mud supported		Grain-supported		Matrix-supported	> 2 mm component supported	build a rigid framework	encrust and bind	act as bafflers
less than 10% grains (> 0.03 mm and < 2 mm)	greater than 10% grains					BOUNDSTONE		
MUDSTONE	WACKESTONE	PACKSTONE	GRAINSTONE	FLOATSTONE	RUDSTONE	FRAMESTONE	BINDSTONE	BAFFLESTONE

Figure 4.1. Original carbonate rock classification by Dunham (1962) and the expanded version by Embry and Klovan (1971; modified from Flügel, 2010).

By the integration of biofacies data with the textural classification of each sample, microfacies type were determined. The comparison of them with the SMF types and determination of the distribution of microfacies through the measured sections (to eliminate local energy changes that may hinder the original depositional texture) helped in the differentiation of the depositional environments of the Eastern Pontides Carbonate Platform. For comparison, SMF type of Flügel (2004) for a rimmed carbonate platform was used (Fig. 4.2). Although there is no direct observation on the reefal facies of the Eastern Pontides in this study, a rimmed platform model has been adopted. The PCP includes reefal belts (Altıner et al., 1991; Kırmacı, 1992; Ka-

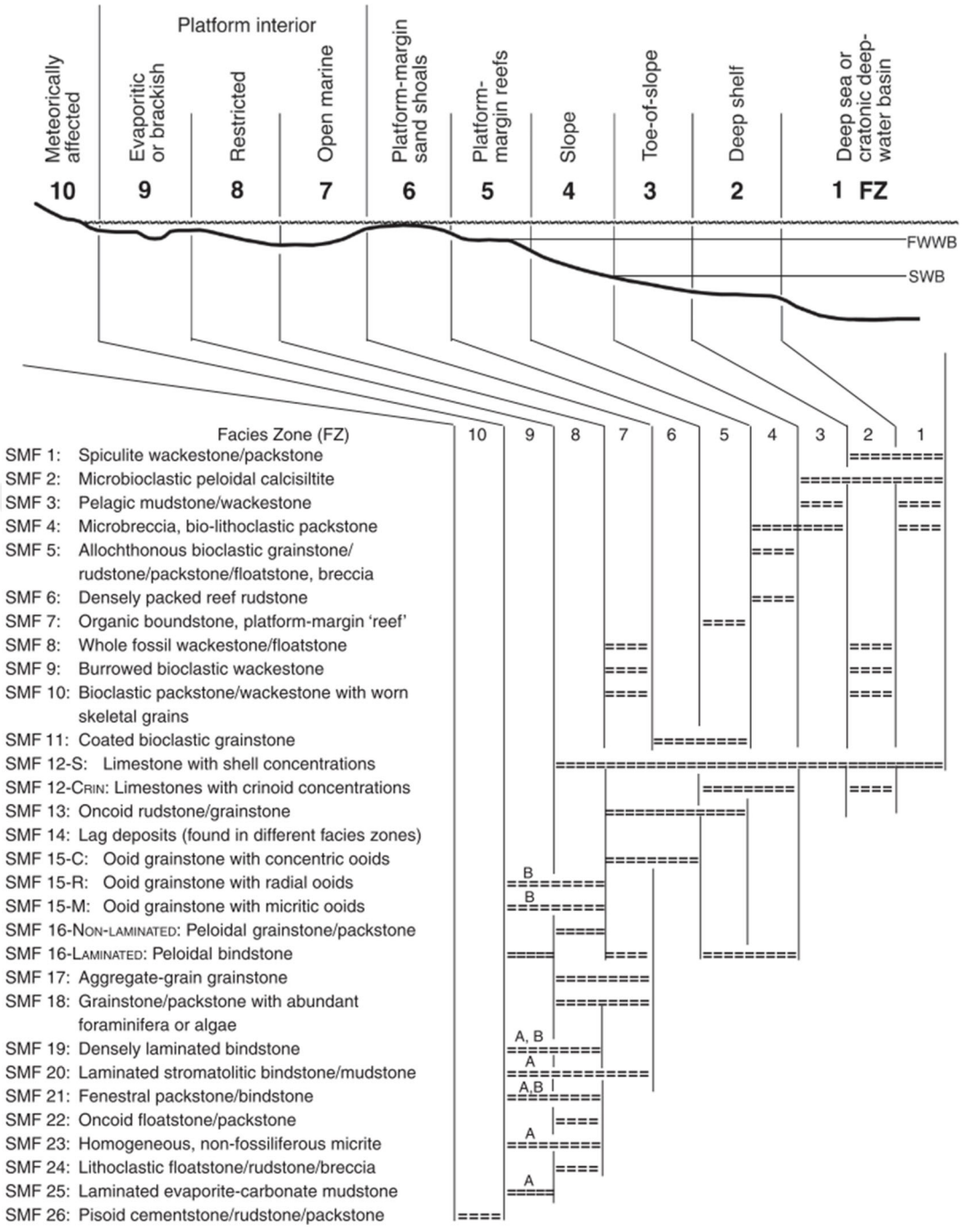

Figure 4.2. The facies zones (FZ) of the rimmed carbonate platform model and the distribution of the standard microfacies types (SMF). Note that the same SMF type can occur in several FZs which make the integration of biofacies data and the examination of microfacies distribution within a studied succession necessary for the determination of depositional environment (A: evaporitic, B: brackish) (Flügel, 2010).

ya, 2014; Kaya & Altıner, 2015). Additional support for this choice can be listed as follows; i) there are transported shallow marine bioclasts in the slope carbonates of this platform, ii) the presence of turbiditic clastic and carbonate deep marine deposits, iii) the presence of thick slumped intervals, and iv) the presence of incisions on the shallow marine platform. These observations suggest the presence of under-water relief with respect to the platform margin. Microfacies types for each of the measured sections will be detailed in the following sections.

4.1 Slope to Basin Facies (Ağören and Ozansu measured sections)

Slope to basin facies of the Eastern PCP are represented by the Ağören and Ozansu successions in the Ağören, OA and OB measured sections (Fig. 2.3, 2.6, 2.7).

6 main microfacies types were differentiated in the slope to basin succession.

MF1 Sandy calcimudstone – micritic sandstone/ Silty marlstone/ Calcimudstone with radiolaria (SMF3/ FZ3)

This is the rarest facies type found in the lower part of the Ağören succession (Fig.4.3D, E). There are no important grain types. Within the same thin section facies can change from calcimudstone to micritic sandstone and lamination of these two can be observed. Some calcimudstones with radiolaria show very thin calpionellid wackestone lenses in the OA section (Fig. 4.5F). This type lenses time to time have peloidal, lithoclastic packstone facies (Fig.4.6I). Quartz is the dominant grain type in the sandy parts. SMF3/ FZ3 are the assigned facies zones (Fig.4.2). Toe-of-slope depositional environment is interpreted for this microfacies type.

MF2 Radiolarian/ Calpionellid wackestone/ packstone (SMF3/ FZ3)

This microfacies is commonly intercalate with the clastic turbidites at the lower portion of the Ağören succession. Depending on probably the CCD level radiolaria or calpionellids become the main constituent of the facies. Some types of this facies also include clayey or silty content. They represent the toe-of-slope facies (SMF3/

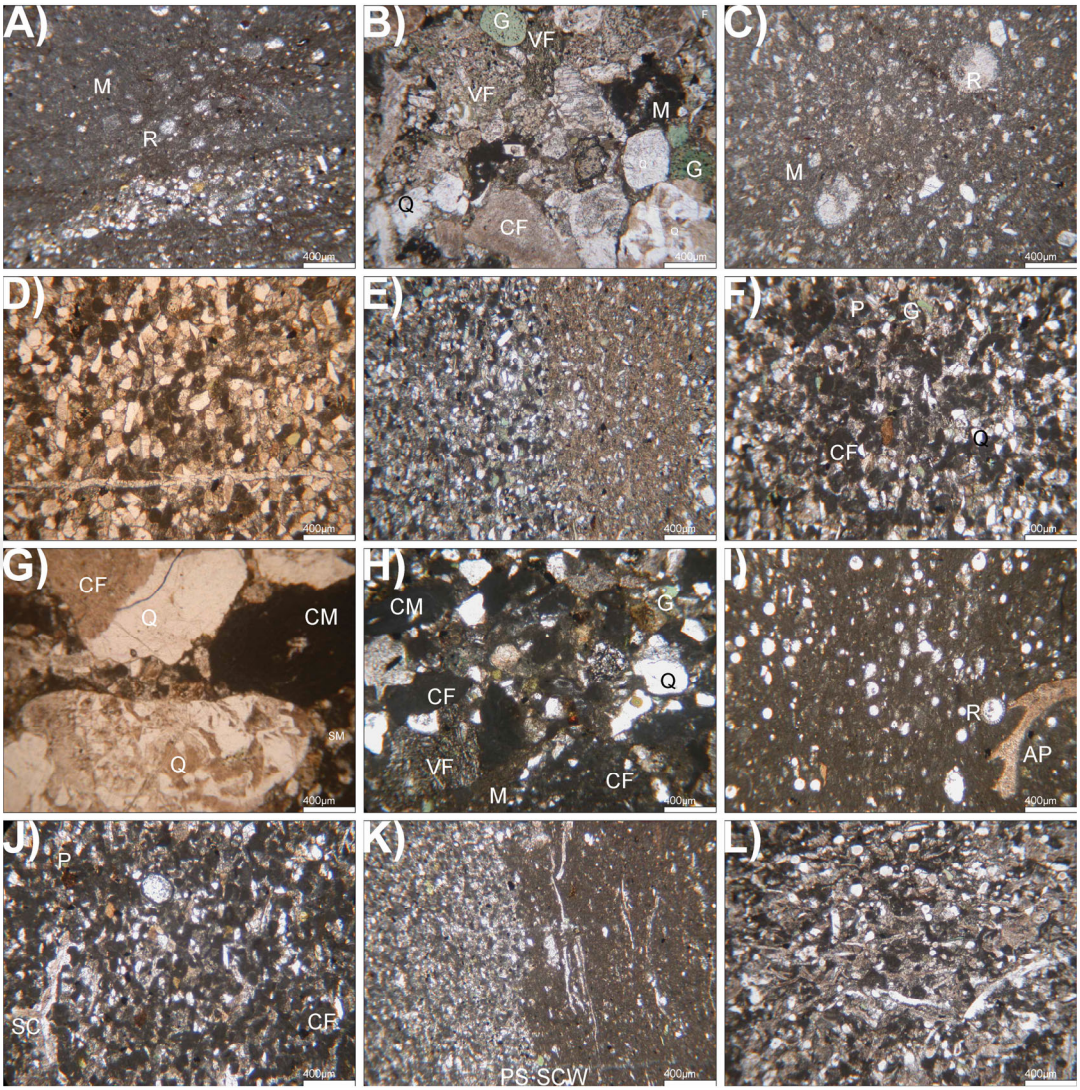

Figure 4.3. Microfacies from the lower levels of the Ağören section (Kelkit Formation). All scales are 400µm. **A)** Clayey radiolarian packstone with intercalations of calcite mudstone laminae. Slope to basin transition (MF2/SMF3/FZ3). Sample A1. **B)** Sublitharenitic-litharenitic sandstone (MFCD). Sample A8. **C)** Radiolarian wackestone with minor quartz grains (MF2/SMF3/FZ3). Sample A15. **D)** Sandy limestone – micritic sandstone (MF1/SMF3/FZ3). Sample A18. **E)** Laminated silty marlstone with minor sandstone laminae. This microphotograph shows the contact between sandy lamination and the marl (MF1/SMF3/FZ3). Sample A23. **F)** Sandy, peloidal lithoclastic packstone (MF3/SMF4/FZ4). Sample A34. **G)** Sublitharenit – greywacke (quartz-wacke; MFCD). Sample (A44). **H)** Lithoclastic packstone (MF3/SMF4/FZ4). Sample A46. **I)** Radiolarian wackestone – packstone (MF2/ SMF3/FZ3). Sample A51. **J)** Sandy peloidal packstone (MF3/SMF4/FZ4). Sample A61. **K)** Sandy (quartz grains) peloidal packstone – laminated saccocomid wackestone (MF3/SMF4/FZ4). Sample A69. **L)** Peloidal, sandy, saccocomid packstone (MF3/ SMF4/FZ4). Sample A 75.

Figure 4.3 (*continued*) Q: quartz, M: micrite, SM: silty micritic matrix, G: glauconite, CF: carbonate rock fragments, VF: volcanic rock fragments, P: peloid, R: radiolaria, CM: *Crescentiella morronensis*, AP: aptyhcus, SC: *Saccocoma*, PS: peloidal packstone, SCW: saccocomid wackestone.

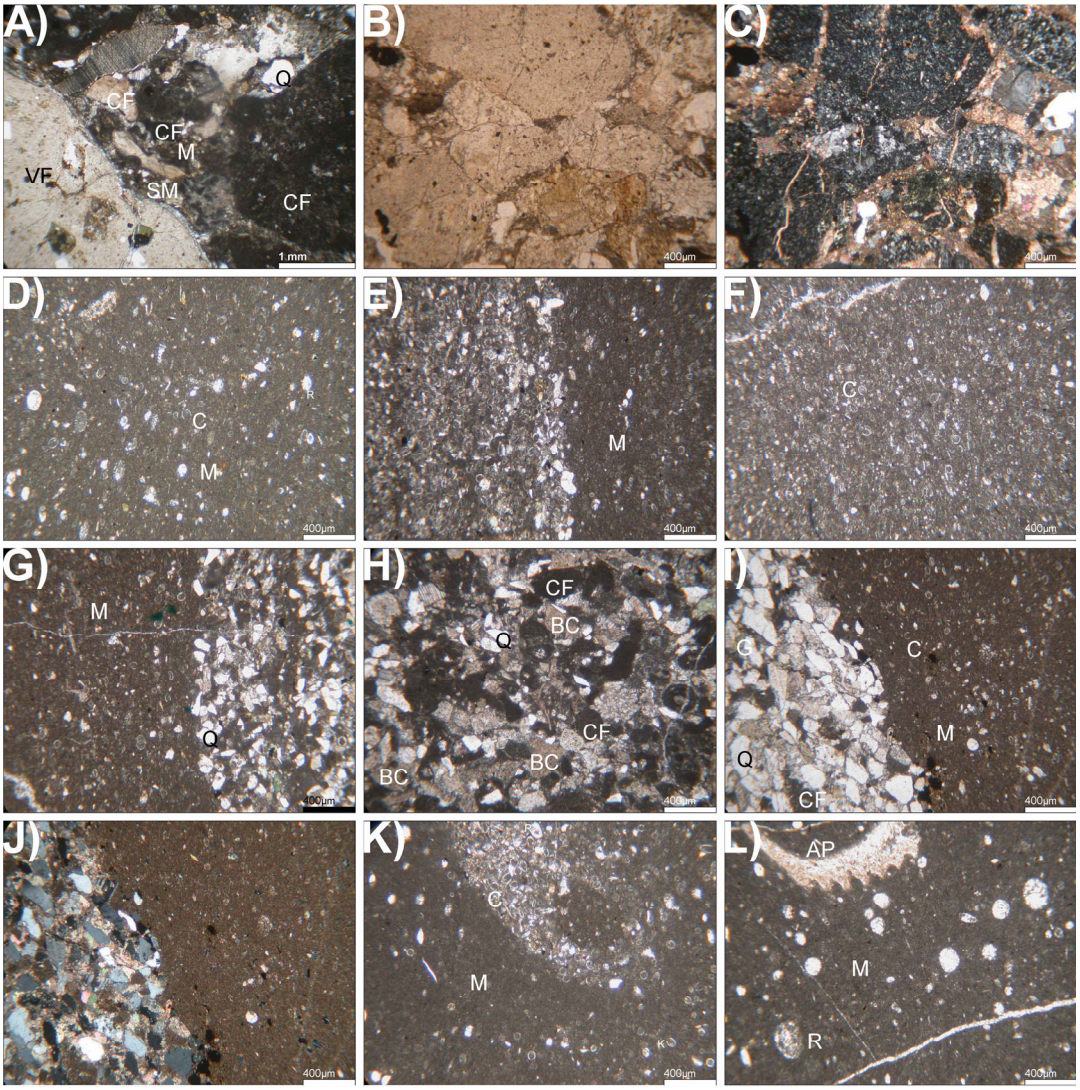

Figure 4.4. Microfacies from the middle (Kelkit Formation, A-C) and upper (Hozbirikyayla Formation, D-L) levels of the Ağören section. The scale for the A is 1 mm and for the rest is 400µm. **A)** Sandy, lithoclastic floatstone (MF4/SMF5/FZ4). Sample A81. **B, C)** Litharenite with plane- and cross-polarized views (MFCD). Sample A92. **D)** Silty calpionellid wackestone (MF2/SMF3/FZ3). Sampel A 96. **E)** Calpionellid wackestone with calpionellid packstone lenses with contrasting species diversity (MF2/SMF3/FZ3). Sample A101. **F)** Calpionellid wackestone-packstone (MF2/SMF3/FZ3). Sample A106. **G)** Calpionellid wackestone with sandy laminati-

Figure 4.4 (*continued*) ons (MF2/SMF3/FZ3). Sample A120. **H)** Sandy lithoclastic packstone with saccocomids (MF3/SMF4/FZ4). Sample A136. **I, J)** Calpionellid wackestone with sublitharenitic lenses. Plane- and cross-polarized views (MF2/SMF3/FZ3). Sample A187. **K)** Calpionellid wackestone with sandy calpionellid packstone lenses (MF2/SMF3/FZ3). Sample A 199. **L)** Radiolaria wackestone (MF2/SMF3/FZ3). Sample A270. Q: quartz, M: micrite, SM: silty micritic matrix, G: glauconite, CF: carbonate lithoclasts, VF: volcanic rock fragments, P: peloid, R: radiolaria, C: calpionellid, AP: aptyhcus, BC: bioclast.

FZ3; Fig.4.3A, C, I; 4.4D, E, F, G, I, J and K). Within some of the calpionellid wackestone facies, lenses of calpinellid packstones with monospesific assemblages are present (Fig. 4.4E, 4.5G), indicating species-type-dependent transportation they may raise some concern about the reliability of the acme zones of calpionellids as remarked by Granier et al. (2020b, cryptic mud turbidites). Intercalations of this facies type with coarse-grained floatstone – packstone facies is also observed in the OB section (Fig. 4.6F & 4.7). Some members of this facies type have clastic laminations (Fig. 4.5J).

MF3 (Sandy) Peloidal, lihoclastic packstone-wackestone with bioclasts/ Peloidal bioclastic packstone (SMF4/ FZ4)

Saccocoma sp. is an important constituent of this microfacies types (Fig. 4.3J. 4.4 K). In some samples they can become the main constituent (Fig. 4.3L). Some types of facies are dominated only by lithoclasts and peloids (Fig. 4.3H). This microfacies type is only observed in the Ağören measured section.

MF4 (Sandy) Peloidal, lihoclastic, bioclastic floatstone/ floatstone to packstone with bioclasts (SMF5/ FZ4)

This is the second most dominant facies type in the OB section (second to MF2). It represents calciturbiditic slope deposition that punctuated calpionellid/ radiolarian wackestone – packstone facies. The same type of facies association is also present in the Ağören section (Fig. 4.4A). In addition to pelagic fossil content of the matrix (Fig. 4.5L), this facies also includes platform derived benthic foraminifers, microen-

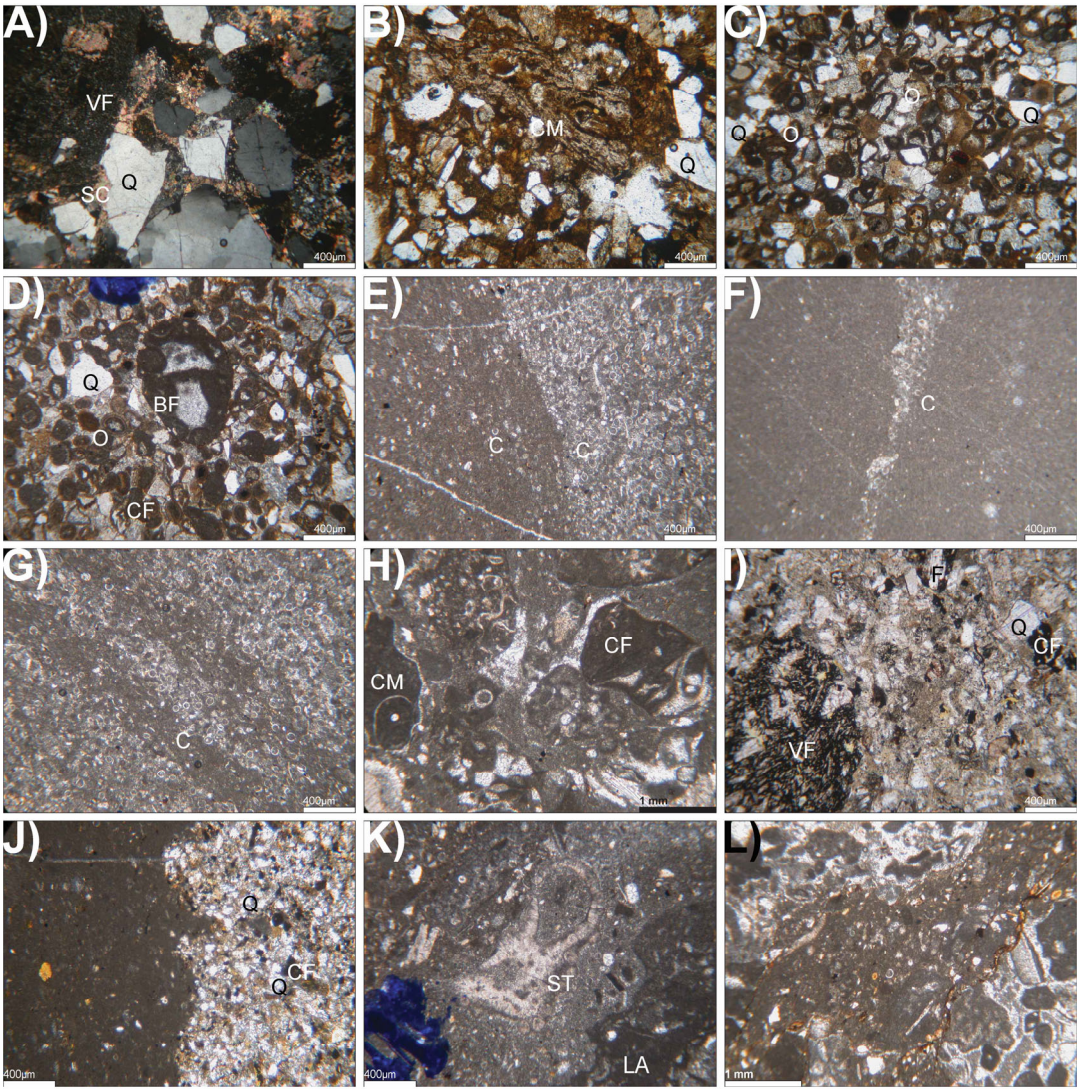

Figure 4.5. Microfacies photographs from the Ozansu sections. A-D) OA section, Kelkit Formation. E-L) OB section, Hozbirikyayla Formation. Scale for H and L is 1 mm. Scale for the rest is 400µm. **A)** Sublitharenite (MFCD). Sample OA1. **B)** Sublitharenite with *Crescentiella morronensis* (CM; the cortex is degraded; MFCD). Sample OA6. **C, D)** Sandy, ooidal grainstone with benthic foraminifera (MF5/SMF15-C/FZ6; BF: *Pseudocyclammina lituus*). Samples, OA7 and 9. **E)** Radiolarian wackestone with silty, peloidal calpionellid packstone lenses. This kind of micron-sized gravity flow laminae can be also seen in very fine-grained facies (MF2/SMF3/FZ3). Sample OB49. **F)** Calcimudstone with radiolaria with silty calpionellid wackestone lense (MF1/SMF3/FZ3). Sample OB63. **G)** Laminated silty peloidal calpionellid wackestone (MF2/SMF3/FZ3). OB71. **H)** Lithoclastic, bioclastic, peloidal packstone – floatstone (MF4/SMF5/FZ4). OB83. **I)** Lithic greywacke – sublitharenite (MFCD). Sample OB86. **J)** The contact between a litharenitic lense and the silty calpinellid wackestone facies (MF2/SMF3/FZ3). Sample OB88. **K)** Lithoclastic, bioclastic floatstone – packstone facies (MF4/SMF5/

Figure 4.5 (*continued*) FZ4). Sample OB110. **L)** Lithoclastic floatstone (MF4/SMF5/FZ4). Matrix has a sandy, calpionellid wackestone facies. Sample OB111. Q: quartz, F: feldspar, SC: spary calcite, CF: carbonate lithoclast, VF: volcanic rock fragment, P: peloid, R: radiolaria, C: calpionellid, CM: *Crecentiella morronensis*, ST: *Carpathiella plassenensis*, LA: *Lithocodium aggregatum*, BF: benthic foraminifera.

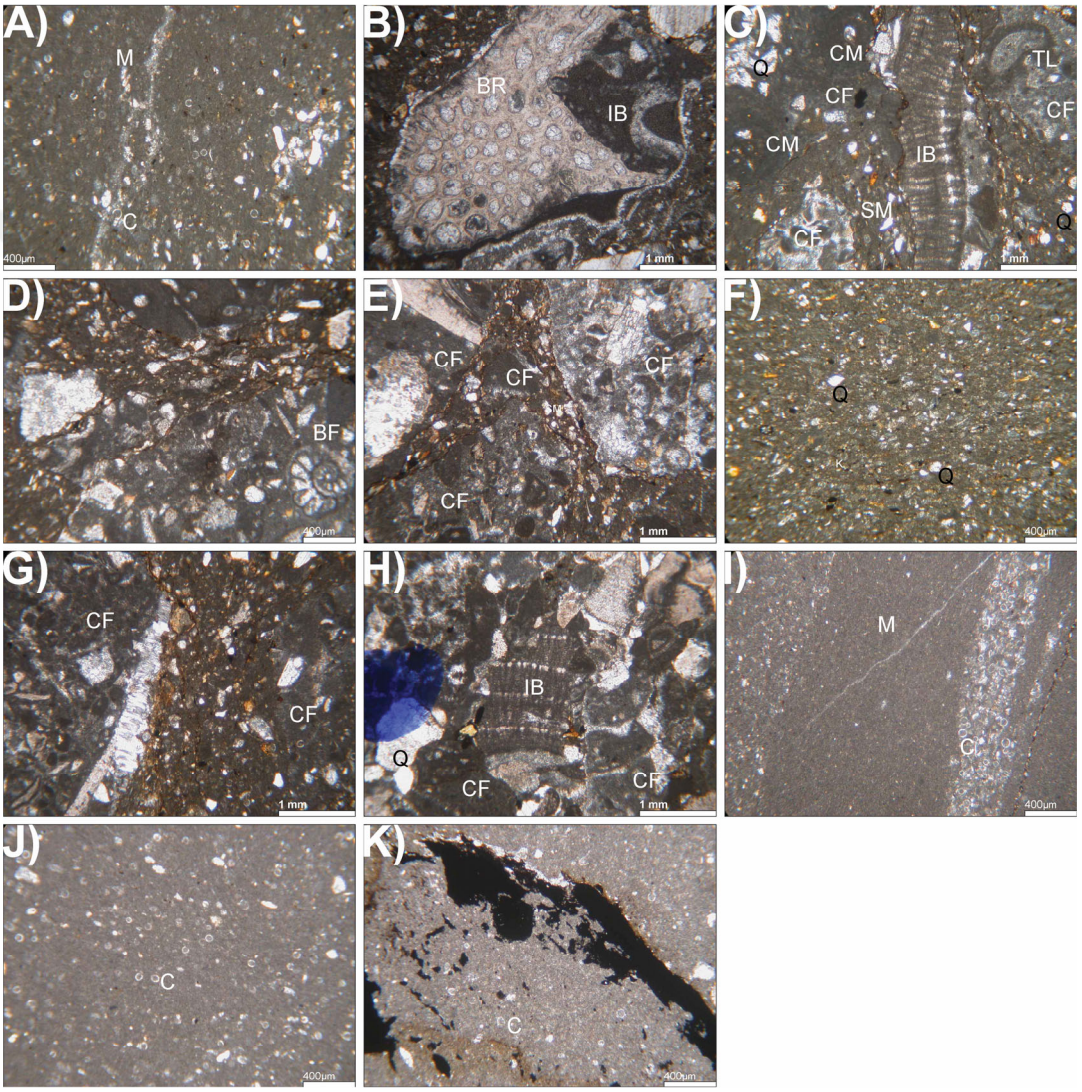

Figure 4.6. Microfacies photographs from the OB section. The scale for B, C, E, G, and H is 1 mm, for the rest is 400µm. **A)** Silty, calpionellid wackestone (MF2/SMF3/FZ3). Sample OB112. **B)** Lithoclastic, bioclastic floatstone – packstone (MF4/SMF5/FZ4). Sample OB113. **C, D, E)** Sandy, lithoclastic, bioclastic floatstone – packstone facies (MF4/SMF5/FZ4). Sample OB113. **F)** Bioclastic, silty, sandy, calcite mudstone (MF1/SMF3/FZ3). Sample OB114. **G)** Lithoclastic, bioclastic flo-

Figure 4.6 (*continued*) atstone facies (MF4/SMF5/FZ4). Sample OB115. **H)** Lithoclastic, bioclastic, peloidal packstone (MF4/SMF5/FZ4). Sample OB122. **I)** Calcimudstone with calpionellid, peloidal, lithoclastic packstone lenses (MF1/SMF3/FZ3). Sample OB135. **J)** Calpionellid wackestone (MF2/SMF3/FZ3). Sample OB171. **K)** Radiolarian, calpionellid wackestone with petroleum lenses (MF2/SMF3/FZ3). Sample OB172. Q: quartz, CF: carbonate lithoclast, P: peloid, R: radiolaria, M: micrite, SM: silty micrite, C: calpionellid, CM: *Crescentiella morronensis*, TL: *Terebella lapilloides*, BR: bryozoa, IB: *Iberopora bodeuri*, BF: benthic foraminifer (*Protopeneropolis ultragranulata*).

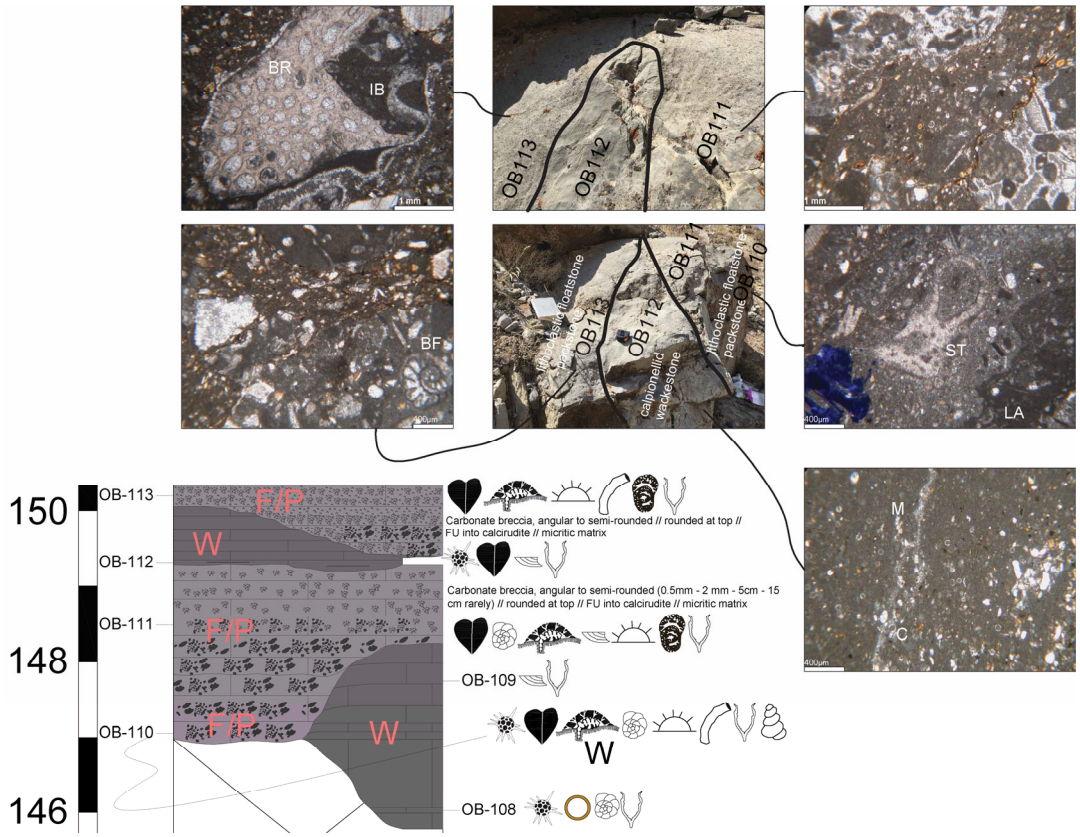

Figure 4.7. A slope depositional environment facies association example from the OB section. The related portion of the OB section is given in the left corner (symbols are the same with the Fig. 2.3). This interval is characterized by the pelagic deposits of MF2 (calpionellid wackestone; OB-112) that are distrubted by the calciturbiditic beds with facies type of MF4 (lithoclastic, bioclastic floatstones/ packstones; OB-110, OB-111 and OB-113) with field and micro-photographs. The erosive bases of the calciturbiditic intervals eroded important portion of the calpionellid wackestone facies. Although these types of facies bring with themselves shelf-margin dwelling taxa into to the basinal associations that provide calibration levels, they also add difficulties to ordering and scaling of bioevents in slope to basin facies as explained

Figure 4.7 (*continued*) in detail in Chapter 2.3. See also Figure 4.5 and 4.6 for thin section explanations.

crusters, rare algae, serpulid tubes (Fig. 4.5H, K, L & 4.6B, C, D, G, H). The lower boundary of MF4 facies with the underlying calpionellid/ radiolarian wackestone – packstone facies are mostly erosive (Fig. 4.7).

MF5 (Sandy) Ooidal grainstone with benthic foraminifer (SMF15-C/ FZ6)

This facies is only observed in the uppermost level of the OA section (Fig. 2.6, 4.5C, D). This facies corresponds to the SMF15-C division of Flügel (2010) with coated superficial coated grains. It is interpreted to represent platform margin sand shoals. When the presence of *Saccocoma*, calcareous dinocysts and apthycus with the platform derived benthic foraminifers, microencrusters and serpulid tubes is taken into account, it should represent the upper slope depositional environments for the Tithonian interval in the OB section.

MFCD Sublitharenite – litharenite. greywacke (SMF15-C/ FZ6)

The name of this facies stands for "microfacies clastic deep". All deep marine clastic deposits are grouped under the MFCD. They especially dominated the lower and lower middle portion of the Ağören succession and the OA section (Fig. 2.3, 2.6). They rarely occur in the lower portion of the OB section (Fig. 2.7). Carbonate and volcanic rock fragments are very common (Fig. 4.3B, G, H; 4.4, B, C; 4.5A, B). Glauconite is a common constituent (Fig. 4.3 B, F & H). Quartz, muscovite, biotite minerals and iron oxide coated grains are commonly present (Appendix B). Intercalation of these clastics with the pelagic carbonates suggests deep marine depositional settings.

4.2 Platform Facies (Nazlıçayır measured section)

7 main microfacies types were differentiated in shallow marine successions of the Nazlıçayır region.

MF6 Peloidal, ooidal, lithoclastic grainstone (SMF16/ FZ8)

This facies represents back margin lagoonal depositional setting on the carbonate platform. Shelf margin dwelling benthic foraminifers (e.g., *Mohlerina basiliensis*, *Coscinoconus* spp.) frequently present (Fig. 4.8A, B). Other constituent includes bivalve and echonoid fragments, gastropoda and rare algae). This facies is observed in the strata below the discontinuity surface at the lower portion of the section. Compared to the similar facies observed in the upper part of the section (MF9) the amount of bioclast is so much less in the MF6 and does not constitute the major grain type.

MF7 Calcimudstone/ Sandy micrite (SMF23/ FZ8)

This facies represents lagoonal depositional environments. It is both observed in the strata below the basalt level (Fig. 4.8D) and the strata above the unconformity surface (Fig. 4.8K, L). The facies above the unconformity also includes clastic content and represents incised valley infill restricted shallow marine environments.

MF8 Fenestral micrite (SMF21/ FZ8)

This facies represents restricted platform interior environments. It is observed below the basalt level (Fig. 4.8E). These strata below the basalt level show transition from back margin lagoonal facies MF6 below to fenestral micrites towards the basalt, indicating a shallowing upward trend for this portion.

MF9 Bioclastic, intraclastic/ ooidal packstone - grainstone (SMF18/ FZ7)

This facies represents a back margin high energy environment. It is one of the most common facies types present in the Nazlıçayır section. Main constitutes includes benthic foraminifera, algae, microencrusters, echinoid and bivalve fragments in addition to lithoclasts and peloids (Fig. 4.8F & 4.9A, D - H). Some samples have excessive amounts of *Favreina* spp. (Fig. 4.8F, 4.9A).

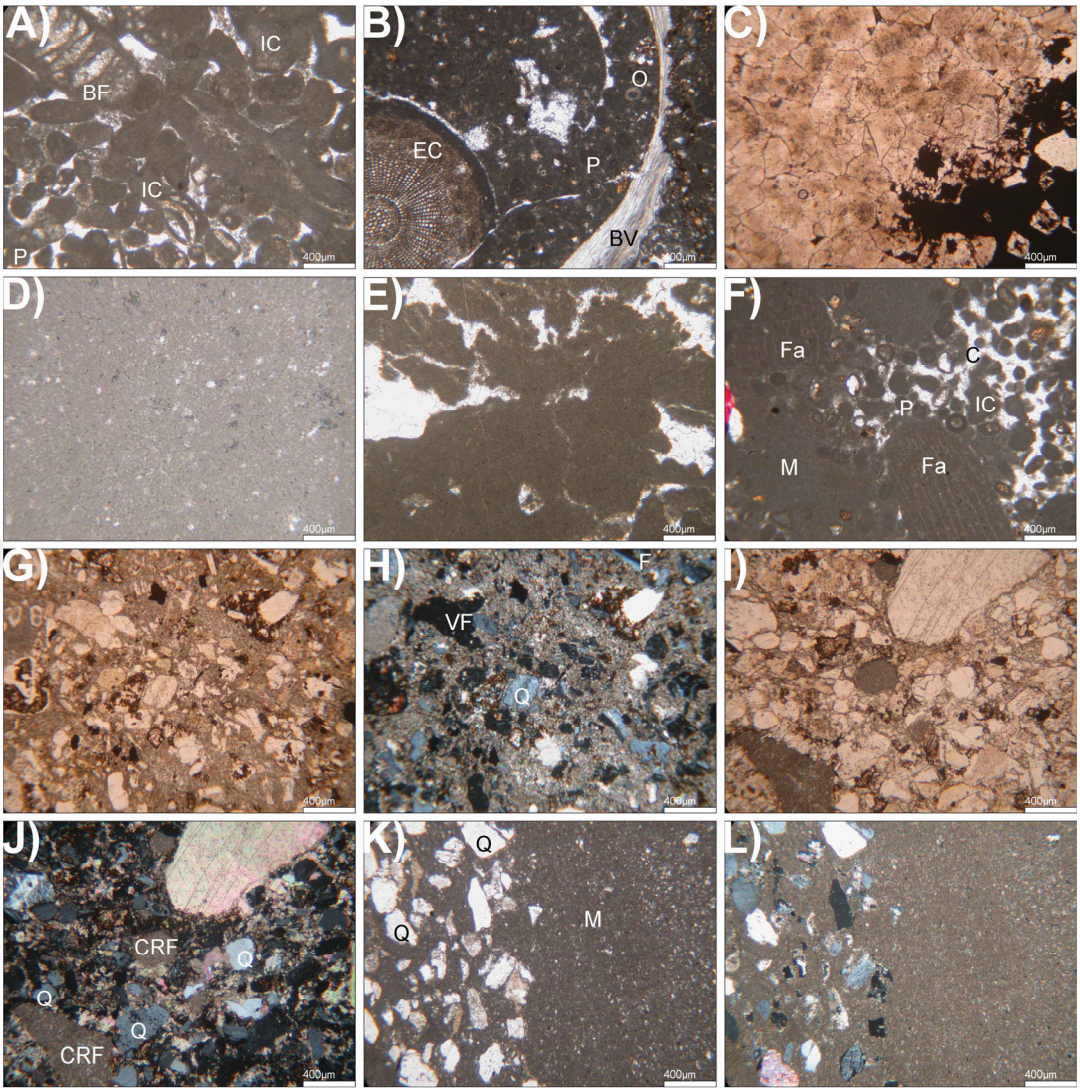

Figure 4.8. Main microfacies types observed in the Nazlıçayır measured section. Berdiga Formation. All scales 400µm. **A)** Peloidal, ooidal, lithoclastic grainstone (MF6/SMF16/FZ8). Sample L4. **B)** Peloidal, intraclastic, ooidal packstone (MF6/SMF16/FZ8). Sample L8. **C)** Dolostone (sieve, mosaic texture). Sample L13. **D)** Calcimudstone (MF7/SMF23/FZ8). Sample L15. **E)** Fenestral limestone (MF8/SMF21/FZ8). Sample L19. **F)** Bioclastic peloidal grainstone – packstone (MF9/SMF18/FZ7). Sample L22. **G, H)** Calcareous lithicwacke – sandy micrite, normal and cross polarized views (MFCS-incise valley infill). Sample L57. **I, J)** Coarse grained lithicwacke normal and cross polarized views (MFCS-incise valley infill). Sample L59. **K, L)** Micrite with sand laminations, normal and cross polarized views (MF7/SMF23/FZ8). Sample L61. BF: benthic foraminifera, IC: intraclast, EC: echinoid fragment, O: ooid, BV: bivalve fragments, M: micrite, Fa: Favreina sp., C: calcite cement, VF: volcanic rock fragment, Q: quartz, F: feldspar, CRF: carbonate rock fragment, P: peloid.

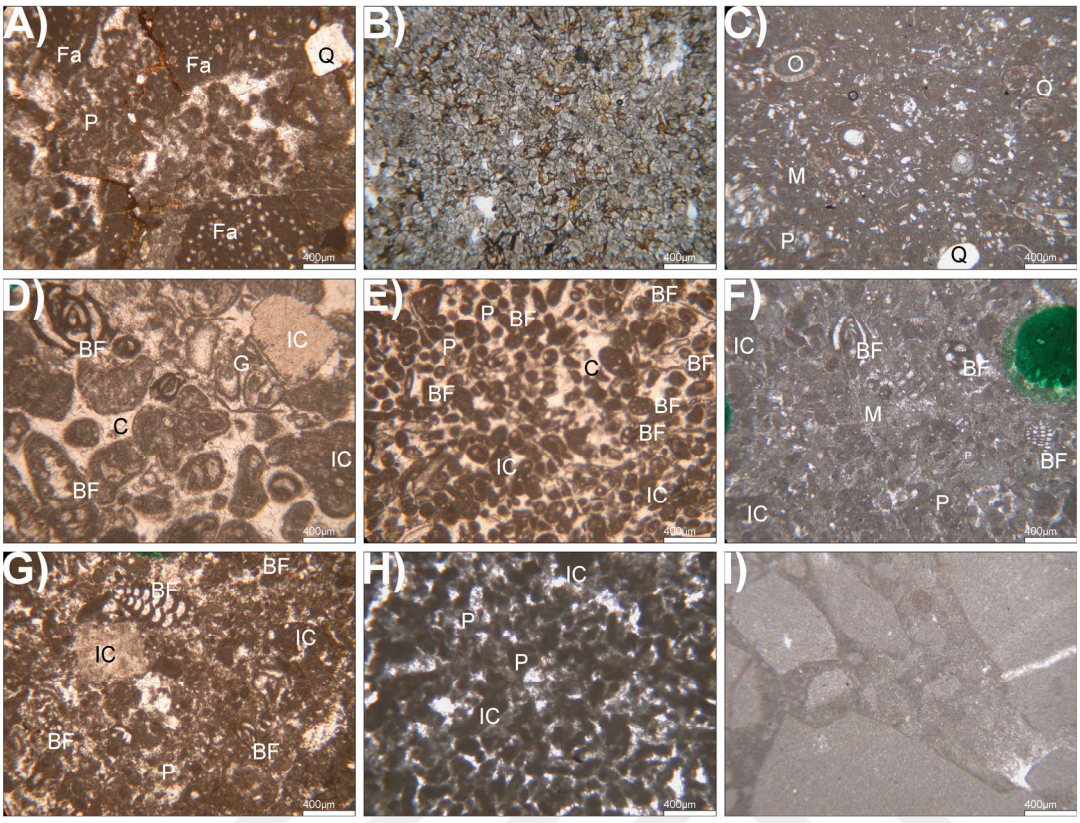

Figure 4.9. Main microfacies types observed in the Nazlıçayır measured section. Berdiga Formation. All scales 400µm. **A)** Favreina wackestone – packstone (MF9/SMF18/FZ7). Sample L62. **B)** Fogged inequigranular dolostone. Sample L66. **C)** Bioclastic ooidal wackestone (MF10/SMF10/FZ7). Sample L72. **D)** Bioclastic intraclastic grainstone (MF9/SMF18/FZ7). Sampel L78. **E)** Bioclastic peloidal intraclastic grainstone (MF9/SMF18/FZ7). Sample L82. **F)** Intraclastic peloidal bioclastic packstone (MF9/SMF18/FZ7). Sample L84. **G)** Peloidal intraclastic bioclastic packstone (MF9/SMF18/FZ7). Sample L106. **H)** Peloidal intraclastic packstone – grainstone (MF9/SMF18/FZ7). Sample L147. **I)** Brecciated calcimudstone at the unconformity surface. Sample L150.

MF10 Bioclastic, ooidal wackestone (SMF10/ FZ7)

This facies again another type of back margin lagoonal facies with relatively less energy with respect to the MF9. Miliolids are the one of the main constituents (Fig. 4.9C). The rest of the grain types are similar to the MF9.

MFCS Lithickwacke (SMF10/ FZ7)

The name of this facies stands for “microfacies clastic shallow”. All shallow marine clastic deposits are grouped under the MFCS. They are confined to the incised valley infill deposits that overly the unconformity surface. Mostly they are composed of lithoclasts floating within a poorly washed matrix (Fig. 4.8G, H, I, J).

Dolomites (SMF10/ FZ7)

They rarely present in the lower portion of the succession (Fig. 4.8C). The strata overlying the unconformity surface is characterized by thick dolomites (Fig. 4.9B).

The lower portion of the Ağören succession is dominated by the deep marine (volcani-)clastics fed by the adjacent platform represented by the Nazlıçayır succession. During the intervals of quiescence pure pelagic carbonate deposits intercalate. The last thick sandstone bed is recorded at the 344 m level in the Ağören section (Fig. 2.3). Following this level, the clastic intercalations get too thin and become very rare. After the final thick slumped interval between the 396 m and 509 m, the porcelaneous pure pelagic limestones with silica bands and nodules dominates the succession. The Ağören region with its clastic turbidites at the bottom levels and the overlying deep marine pelagic carbonates with intercalated clastic intervals represents deep marine mixed depositional setting that recorded carbonate sedimentation and also fed by clastic deep marine fans (Fig. 4.10).

The bottom levels of the OA section in the Ozansu region are represented by the fine grained clastics of the Kelkit Formation. The clastic intervals in the overlying Hozbirikyayla Formation (OB section) are rare and thinner in comparison to the Ağören section. The carbonates of this formation in the Ozansu region represent a carbonate slope environment with its in-situ fine grained pelagic carbonates and intercalated thick carbonate gravity flow deposits shedded from the carbonate platform margin (Fig.4.10).

Based on determined microfacies types and fossil assemblages, a microfacies model for the studied successions is proposed in Figure 4.11.

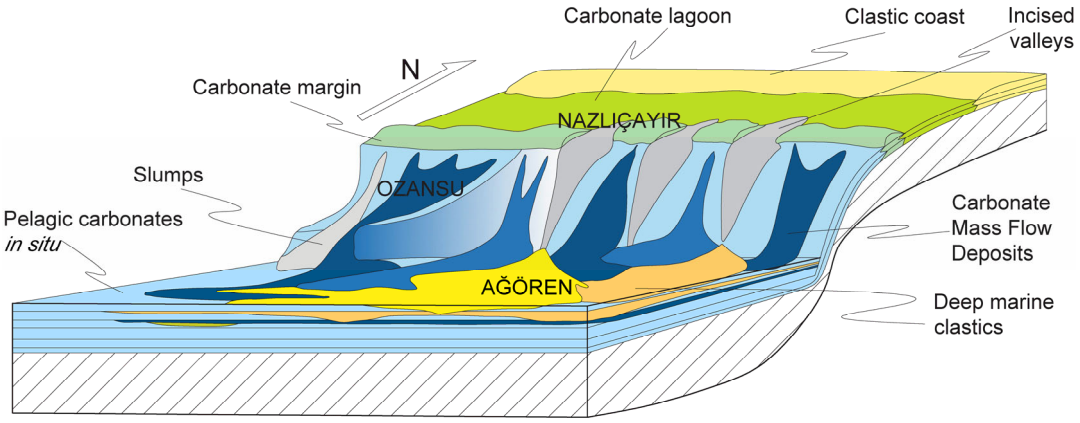

Figure 4.10. A schematic depositional model for the studied region. The Ağören region represents a distal deep marine pelagic depositional environment characterized by clastic gravity flow deposits and in-situ pelagic carbonate deposition. The Ozansu region represents a carbonate slope environment characterized by pelagic carbonate deposition, thick and high frequency carbonate gravity flow deposits and intercalated minor clastic levels. The shallow marine carbonates cropping in the Nazlıçayır region to the north of these slope to basin deposits represent a mixed (carbonate and clastic) shelf environment that was incised by valleys.

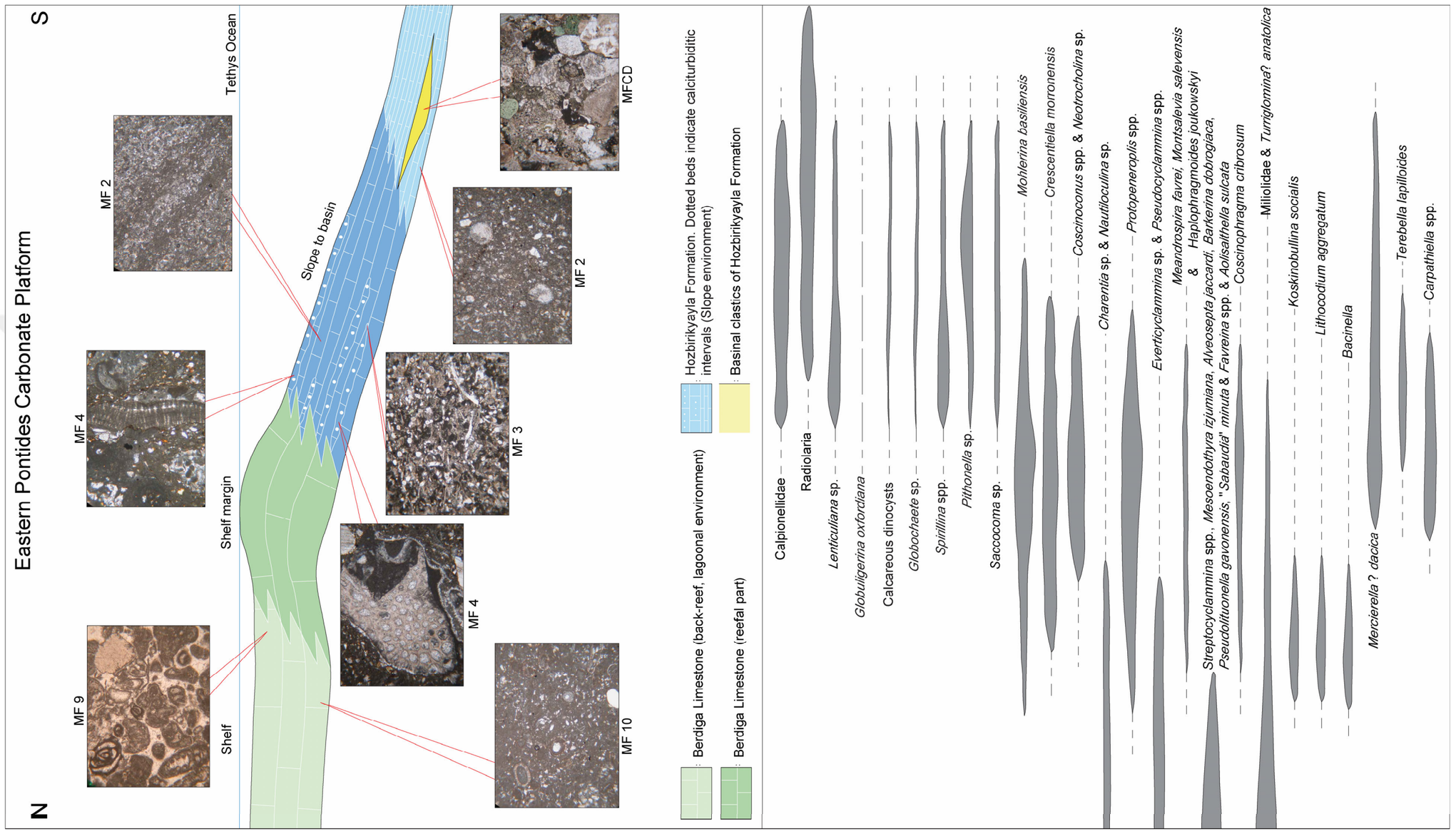

Figure 4.11. Microfacies distribution of the southern platform margin and slope environments of the Eastern Pontides Carbonate Platform during Kimmeridgian – Valanginian interval. There is no direct observation on the reefal parts of this platform, since the studied successions do not reveal such facies. The relationship of the studied formations is illustrated along a model with related facies photomicrographs. Additionally facies distribution of some important microfossils are shown. For microfacies types see the text. Note that fossil distributions in environment are time-dependent (e.g. calpionellids occur in late Tithonian onward). For depositiona model see Figure 4.10

CHAPTER 5

MICROPALEONTOLOGY

The main purpose of this chapter is to clarify the criteria used in the taxonomic classification of the identified fossil assemblages that form the main frame of this study on which all other interpretations based (e.g; biostratigraphy, microfacies evolution etc.). The identifications were carried out on randomly oriented thin sections.

This chapter mainly includes brief descriptions, author's remarks on the morphology and stratigraphic ranges. This chapter is not an attempt to compile all the synonym lists or all the historical background of each taxon. Mainly 3 groups have been studied; calpionellids, foraminifers and *incertae sedis*.

The study of Remane (1985) is mainly used for the generic classification of the calpionellids. For the new genera introduced after this publication and for all the species, the original papers and the more recent ones were used. Loeblich and Tappan (1988), Kaminski (2004) and Pawlowski et al. (2013) are the main reference used in this study for suprageneric and generic classification of the foraminifera. Recent papers were used for the species descriptions. For microproblematica, there is no single complier reference, several papers were used for their classifications. The related papers were listed in the synonym lists. In the following pages information on each fossil group will be given. The related thin section plates are illustrated in Appendix I.

5.1 Calpionellid Taxonomy

FAMILY CALPIONELLIDAE, Bonet 1956

Genus *Crassicollaria* Remane, 1962

Type species: *Crassicollaria brevis* Remane, 1962

C*rassicollaria massutiniana* (Colom, 1948)

Pl. 1, Figs. 1, 2

1948 *Calpionella massutiniana* n. sp., Colom, 243, Fig. 11

1962 *Crassicollaria massutiniana* (Colom) – Remane, p. 15

1971 *Crassicollaria massutiniana* (Colom), Remane, Pl. 3, Figs. 10

1991 *Crassicollaria massutiniana* (Colom), Altıner & Özkan, Pl. 3, Figs. 13, 14

1992 *Crassicollaria remanei* n. sp., Tunç, Pl.1, Figs. 3-5

1995 *Crassicollaria parvula* Remane, Olóriz et al., Pl. 1, Fig. 10

2004 *Crassicollaria massutiniana* (Colom), Marino et al., Pl. 3, Fig.4

2007 *Crassicollaria massutiniana* (Colom), Andreini et al., Pl. 1, Fig. 24

2012 *Crassicollaria massutiniana* (Colom), Petrova et al., Pl. 1, Figs. 24-26

2013 *Crassicollaria massutiniana* (Colom), Lakova & Petrova, Pl.2, Fig.1; Pl.5, Figs. 47, 48

2013 *Crassicollaria massutiniana* (Colom), Krische et al., Figs. 12E, F

2018 *Crassicollaria massutiniana* (Colom), Atasoy et al., Fig. (10) 5, 6

Description & Remarks: The lorica is elongated with a conical aboral pole. The collar is cylindrical. It differs from the *Cr. parvula* by its larger size and massive swelling below the collar. It is distinguished from *Cr. brevis* and *Cr. intermedia* by its cylindrical collar, and the conical aboral pole that does not show caudal appendage. *Cr. massutiniana* appears in the *remanei* subzone, shows increase in abundance in the *massutiniana* subzone and disappears in the lowest levels of the *alpina* subzone just above the J/K boundary (e.g., Michalík & Rehakova, 2011; Lakova & Petrova, 2013). *Cr. massutiniana* specimens were recovered from the latest Tithonian (*massutiniana* subzone) – earliest Berriasian (lowest part of the *alpina* subzone) interval (Figs. 2.15 & 2.17).

Crassicollaria intermedia (Durand-Delga, 1957)

Pl. 1, Figs. 3

1957 *Crassicollaria intermedia* n. sp., Durand-Delga, Pl. 1, Figs. 2, 4

1962 *Crassicollaria intrmedia* (Durand-Delga) – Remane, Figs. 27-34

1971 *Crassicollaria intermedia* (Durand-Delga), Remane, Pl. 3, Figs. 7

1991 *Crassicollaria intermedia* (Durand-Delga), Altıner & Özkan, Pl. 3, Figs. 9-12

1992 *Crassicollaria intermedia* (Durand-Delga), Tunç, Pl. 2, Fig. 1

1992 *Crassicollaria intermedia* (Durand-Delga), Bucur, 572, Fig. 4b

1995 *Crassicollaria intermedia* (Durand-Delga), Olóriz et al., Pl. 1, Figs. 6, 7

1995 *Crassicollaria colomi* (Durand-Delga), Olóriz et al., Pl. 1, Fig. 8

2004 *Crassicollaria intermedia* (Durand-Delga), Marino et al., Pl. 3, Fig. 1

2007 *Crassicollaria intermedia* (Durand-Delga), Andreini et al., Pl. 1, Figs. 28, 29

2012 *Crassicollaria intermedia* (Durand-Delga), Petrova et al., 58, Figs. 22-24

2013 *Crassicollaria intermedia* (Durand-Delga), Lakova & Petrova, Pl. 1, Figs. 32, 33; Pl.5, Figs. 44-46

2018 *Crassicollaria intermedia* (Durand-Delga), Atasoy et al., Fig. (10) 3, 4

Description & Remarks: It is a scaled-up version of *Cr. brevis* with cylindrical lorica wall rather than general conical shape of *Cr. brevis*. Its first occurrence is in the *remanei* subzone of the *Crassicollaria* Zone (late Tithonian) and disappears at the J/K boundary in coherence with *Cr. brevis* (e.g., Lakova & Petrova, 2013; Figs. 2.15 & 2.17). Specimens were recovered from the *massutiniana* subzone in this study due to the facies-controlled arrival of calpionellid-rich facies.

Crassicollaria brevis Remane, 1962

Pl. 1, Figs. 4, 5

1962 *Crassicollaria brevis* n. sp.; Remane, 16, Figs. 19-26

1971 *Crassicollaria brevis* Remane, Remane, Pl. 3, Figs. 5-6

1991 *Crassicollaria brevis* Remane, Altıner & Özkan, Pl. 3, Figs. 6-8

1991 *Crassicollaria brevis* Remane, Tunç, Pl. 3, Fig. 1

1992 *Crassicollaria brevis* Remane, Tunç, Pl. 2, Fig. 3

1995 *Crassicollaria brevis* Remane, Olóriz et al., Pl. 1, Fig. 9

1999 *Crassicollaria brevis* Remane, Lakova et al., Pl. 1, Fig.6

2001 *Crassicollaria brevis* Remane, Ciborowski & Kołodziej, 345, Fig. 4

2004 *Crassicollaria brevis* Remane, Marino et al., Pl. 3, Fig. 3

2007 *Crassicollaria brevis* Remane, Andreini et al., Pl. 1, Figs. 19, 20

2012 *Crassicollaria brevis* Remane, Petrova et al., 58, Figs. 28, 29

2013 *Crassicollaria brevis* Remane, Lakova & Petrova, Pl. 2, Figs. 2,3; P. 6, Figs. 18, 19

2018 *Crassicollaria brevis* Remane, Atasoy et al., Fig. (10) 1, 2

Description & Remarks: The lorica is hyaline. The transition from the collar to the body of lorica is rather smooth in *Crassicollaria* when compared with the *Calpionella* genus. *Crassicollaria* has a wider opening due to the lack of shoulders present in *Calpionella*. It has swelling below the collar and a caudal appendage in the aboral part. This species was observed from the *massutiniana* (Late Tithonian) subzone to *elliptica* (middle Early Berriasian) subzone in this study (Figs. 2.15 & 2.17).

Calpionella elliptalpina Nagy, 1986

Pl. 1, Figs. 6, 7

1985 *Calpionella alpina* Lorenz, Remane, 570, Fig (18) 1

1986 *Calpionella elliptalpina* n. sp., Nagy, Pl. 1, Fig. 4

1991 "Homeomorph" of *Calpionella* elliptica Cadisch, Altıner & Özkan, Pl. 1, Fig.19

1992 *Calpionella elliptica* Cadisch, Tunç, Pl. 2, Fig. 9

1995 *Calpionella alpina* (ejampler grande con ragos proximos a las formas de transicion a C. elliptica) Lorenz, Olóriz et al., Pl. 1, Figs. 15

1999 *Calpionella elliptalpina* Nagy, Lakova et al., Pl. 1, Fig. 8

2006 *Calpionella alpina* Lorenz, Grabowski & Pszczółkowski, 405, Figs. 7D

2012 Calpionella *elliptalpina* Nagy, Petrova et al., 58, Fig. (4) 40, 41

2013 *Calpionella elliptalpina* Nagy, Lakova & Petrova, Pl. 2, Figs. 10, 11; Pl. 6, Fig. 2

2018 *Calpionella elliptalpina* Nagy, Atasoy et al., Fig. (10) 19

Description & Remarks: This species had generally been defined as the "homeomorph" of *Calpionella elliptica* (Remane, 1985; Altıner & Özkan, 1991) and recently the *C. elliptalpina* name has been introduced (Nagy, 1986). Its range is restricted to a limited interval at the uppermost parts of the *massutiniana* subzone just below the J/K boundary (e.g., Petrova et al. 2012; Lakova & Petrova, 2013). The individuals of this species were recoverd in the uppermost part of the *massutiniana* subzone (latest Tithonian) in this study (Figs. 2.15 & 2.17).

Calpionella grandalpina Nagy, 1986

Pl. 1, Figs. 8, 9

1986 *Calpionella grandalpina* n. sp., Nagy, Pl. 1, Fig. 3, 8

1991 *Calpionella alpina* (large form) Lorenz, Altıner & Özkan, Pl. 1, Figs. 1, 2

1999 *Calpionella grandalpina* Nagy, Lakova et al., Pl. 1, Fig. 7

2012 *Calpionella grandalpina* Nagy, Petrova et al., 58, Figs. (4) 37-39

2013 *Calpionella grandalpina* Nagy, Lakova & Petrova, Pl 2, Figs. 8, 9; Pl.5, Figs. 53, 54; Pl. 6, Fig. 1

2015 *Calpionella grandalpina* Nagy, Lopez-Martinez et al., 586, Fig. 5g

2018 *Calpionella grandalpina* Nagy, Atasoy et al., Fig. (10) 9-11

Description & Remarks: This species is the scaled-up version of *C. alpina*, known as the "large form" in literature. It may be confused with the *C. elliptalpina*. It appears in the upper levels of the *massutiniana* subzone, and its abundance greatly

decreases at the J-K boundary synchronously with the bloom of the *C. alpina* (e.g., Remane et al., 1986; Lakova et al., 1999; Petrova et al., 2012; Lakova & Petrova, 2013). The representatives of this species were recoverd from the upper levels of the *massutiniana* subzone (latest Tithonian) and the lowest levels of the *alpina* subzone just above the J/K boundary (Figs. 2.15 & 2.17). The presence of this species in the OB measured section is in accordance with Benzaggagh (2020), however GCM suggests that these records should represent reworked individuals.

Calpionella alpina Lorenz, 1902

Pl. 1, Figs. 10, 11

1902 *Calpionella alpina* n. sp., Lorenz, Pl. 6, Fig. 1

1971 *Calpionella alpina* Lorenz, Remane, Pl. 3, Figs. 1-2

1991 *Calpionella alpina* (spherical form) Lorenz, Altıner & Özkan, Pl. 1, Figs. 3-8

1992 *Calpionella alpina* Lorenz, Tunç, Pl. 2, Fig. 4

1992 *Calpionella alpina* Lorenz, Bucur, 572, Fig. 4e

1995 *Calpionella alpina* Lorenz, Olóriz et al., Pl. 1, Figs. 12, 13

1997 *Calpionella alpina* Lorenz, Grün & Blau, Pl. 1, Figs. 11, 12

1999 *Calpionella alpina* Lorenz, Lakova et al., Pl. 1, Fig. 9

2001 *Calpionella alpina* Lorenz, Ciborowski & Kołdziej, 345, Fig. (2) 3

2004 *Calpionella alpina* Lorenz, Marino et al., Pl. 3, Fig. 9

2007 *Calpionella alpina* Lorenz, Andreini et al., Pl. 1, Figs. 12, 13

2012 *Calpionella alpina* Lorenz, Petrova et al., 60, Figs. (5) 1-7

2015 *Calpionella alpina* Lorenz, López-Martinez et al., 586, Fig. 5I; 288; Fig. 7C, D

2016 *Calpionella alpina* Lorenz, Maalaoui & Zargouni, 50, Figs. (4) 1-3

2018 *Calpionella alpina* Lorenz, Atasoy et al., Fig. (10) 12-16

Description & Remarks: This species is characterized by spherical hyaline lorica with restricted oral end, well-developed shoulder, cylindrical collar and rounded aboral part. The acme of this species defines the base of the *alpina* subzone and the J/K boundary. *C. alpina* ranges from the *massutiniana* subzone (latest Tithonian) to the *oblonga* subzone (late Berriasian). Similiarly, this species was observed from the *massutiniana* subzone to the *oblonga* subzone in this study (Figs. 2.15 & 2.17). The acme of this species was used as the indicator of the J/K boundary following the suggestions of Wimbledon (2011), Michalik and Rehakova (2011), Lakova and Petrova (2012), Lakova and Petrova (2013), Frau et al. (2016).

Calpionella elliptica Cadisch, 1932

Pl. 1, Figs. 12-14

1932 *Calpionella elliptica* n. sp., Cadisch, 249, Fig (3) 10, 11, 17

1971 *Calpionella elliptica* Cadisch, Remane, Pl. 3, Figs. 3, 4

1985 *Calpionella elliptica* Cadisch, Remane, 570, Fig (18) 4

1991 *Calpionella elliptica* Cadisch, Altıner & Özkan, Pl. 1, Fig. 11-18

1992 *Calpionella elliptica* Cadisch, Bucur, 572, Fig. (4) g-j

1995 *Calpionella elliptica* Cadisch, Olóriz et al., Pl. 1, Fig. 17

1997 *Calpionella elliptica* Cadisch, Grün & Blau, Pl. 1, Figs. 17, 18

1999 *Calpionella elliptica* Cadisch, Lakova et al., Pl. 1, Fig. 11

2006 *Calpionella elliptica* Cadisch, Grabowski & Pszczółkowski, 405, Fig. 7G

2007 *Calpionella elliptica* Cadisch, Andreini et al., Pl. 2, Figs. 1, 2

2010 *Calpionella elliptica* Cadisch, Fözy et al., 537, Fig. 9U

2012 *Calpionella elliptica* Cadisch, Petrova et al., 60, Figs. (5) 13-17

2013 *Calpionella elliptica* Cadisch, Lakova & Petrova, Pl. 2, Figs. 36, 37; Pl. 3, Figs. 1, 2; Pl. 6, Fig. 14

2015 *Calpionella elliptica* Cadisch, Boorovå et al., 103, Fig. (6) I, J

2015 *Calpionella elliptica* Cadisch, López-Martinez et al., 588, Fig. 7N

2016 *Calpionella elliptica* Cadisch, Maalaoui & Zargouni, 50, Fig. (4) 4-6

2018 *Calpionella elliptica* Cadisch, Atasoy et al., Fig. (10) 20, 21

Description & Remarks: It differs from all other species of the *Calpionella* genus by its elongated, cylindrical lorica. Its first occurrence defines the basal boundary of the *elliptica* subzone. The oblique sections of this species may be confused with *C. alpina*. Remane (1963, 1964, 1985) offers a length (without collar) to width (largest portion) ratio for their differentiation; all sections with ratio larger than 1.35 should be named as *C. elliptica*, ratio smaller than 1.25 indicates *C. alpina* and individuals with intermediate values should be named as *Calpionella sp.*, regardless of whether they are real transitional forms between *C. alpina* and *C. elliptica* or not. The individuals observed in this study range from the base of the *elliptica* subzone (middle Berriasian) to the base of the *oblonga* subzone (late Berriasian; Figs. 2.15 & 2.17).

In general, there is a tendency towards smaller sizes in the genus *Calpionella* from latest Jurassic to earliest Cretaceous (e.g., Kowal-Kasprzyk & Reháková, 2019) except the species *Calpionella elliptica*.

Genus *Tintinnopsella* Colom, 1948

Type species: *Calpionella carpathica* Murgeanu and Filipescu, 1933

Tintinnopsella carpathica (Murgeanu & Filipescu, 1933)

Pl. 1, Figs. 15-24

1933 *Calpionella carpathica* n. sp., Murgeanu & Filipescu, Pl. 1, Figs. 20-23

1948 *Tintinnopsella carpathica* (Murgeanu & Filipescu) – Colom, Pl. 19, Figs. 4, 5

1969 *Tintinnopsella carpathica* (Murgeanu & Filipescu), Borza, Pl. 78, Figs. 1-16; Pl. 79, Figs. 1-8

1971 *Tintinnopsella carpathica* (Murgeanu & Filipescu), Remane, Pl. 3, Figs. 11, 12

1991 *Tintinnopsella carpathica* (Murgeanu & Filipescu), Altıner & Özkan, Pl. 2, Figs. 1-12

1991 *Tintinnopsella longa* Colom, Tunç, Pl.3, Fig. 9

1992 *Tintinnopsella carpathica* (Murgeanu & Filipescu), Tunç, Pl. 2, Fig. 7

1992 *Tintinnopsella carpathica* (Murgeanu & Filipescu), Bucur, 572, Figs. (4) l, m

1994a *Tintinnopsella carpathica* (Murgeanu & Filipescu), Pop, Pl. 2, Fig. 15

1995 *Tintinnopsella carpathica* (Murgeanu & Filipescu), Olóriz et al., Pl. 1, Figs. 21-23

1997 *Tintinnopsella carpathica* (Murgeanu & Filipescu), Grün & Blau, Pl. 1, Figs. 15, 16

2004 *Tintinnopsella carpathica* (Murgeanu & Filipescu), Marino, Pl. 3, Fig. 15

2007 *Tintinnopsella carpathica* (Murgeanu & Filipescu), Andreini et al., Pl. 1, Figs. 16-18; Pl. 2, Figs. 5, 14, 15

2012 *Tintinnopsella carpathica* (Murgeanu & Filipescu), Petrova et al., 58, Fig. (4) 19; 62, Fig. (6) 14-22

2013 *Tintinnopsella carpathica* (Murgeanu & Filipescu), Lakova & Petrova, Pl. 1, Figs. 35, 36; Pl. 2, Fig. 34; Pl. 3, Figs. 41-44; Pl. 4, Figs. 47-49; Pl. 5, Figs. 38-41; Pl. 6, Fig. 32; Pl. 7, Figs. 36-41

2013b *Tintinnopsella carpathica* (Murgeanu & Filipescu), López-Martinez et al., 6, Fig. 5K; 7, Fig. 6H

2013 *Tintinnopsella carpathica* (Murgeanu & Filipescu), Krische et al., 39, Figs. (12) A, B

2015 *Tintinnopsella carpathica* (Murgeanu & Filipescu), Boorovå et al., 103, Fig. (6) K

2015 *Tintinnopsella carpathica* (Murgeanu & Filipescu), López-Martinez et al., 588, Figs. (7) E, J, K

2016 *Tintinnopsella carpathica* (Murgeanu & Filipescu), Maalaoui & Zargouni, 50, Figs. (4) 8, 9

2018 *Tintinnopsella carpathica* (Murgeanu & Filipescu), Atasoy et al., Fig. (10) 24-26

Description & Remarks: This species is characterized by ovoid or cylindrical lorica with a pronounced caudal prolongation at the conical aboral pole and by its distinctive, somewhat right angle, funnel-shaped collar that may show upward deflection at the outer parts. It differs from the *T. remanei* with its larger size and aboral prolongation.

This species has the longest stratigraphic range amongst the calpionellids that spans

from the *remanei* subzone until the extinction of the calpionellids (F Zone of Altıner & Özkan, 1991; Trejo, 1980; Remane, 1985; Altıner & Özkan, 1991; Lakova et al., 1999; Petrova et al., 2012; Lakova & Petrova, 2013). The representatives of this species were recovered from *alpina* subzone (earliest Berriasian) to *darderi* subzone (earliest Valanginian) interval (Figs. 2.15 & 2.17).

Genus *Remaniella* Catalano, 1965

Type species: *Tintinopsella cadsichiana* Colom, 1948

Remaniella ferasini (Catalano, 1965)

Pl. 1, Figs. 25-29

1965 *Calpionellites ferasini* n. sp., Catalano, Pl. 2, Figs. 1-5; Pl. 3, Figs. 5-7

1969 *Remaniella cadischiana* Colom, Borza, Pl. LXXXI, Fig.4

1971 *Remaniella ferasini* (Catalano) – Catalano & Liguori, Pl. 3, Figs. 1-5

1986 *Remaniella ferasini* (Catalano), Borza & Michalík, Pl. 4, Fig. 4

1991 *Remaniella ferasini* (Catalano), Altıner & Özkan, Pl. 5, Figs. 1, 2

1991 *Remaniella ferasini* (Catalano), Tunç, Pl. 3, Fig. 6

1994a *Remaniella ferasini* (Catalano), Pop, Pl. 1, Figs. 5, 6

1996 *Remaniella ferasini* (Catalano), Grün & Blau, Pl. 1, Figs. 12-15; Pl. 3, Fig. 7

1998 *Remaniella ferasini* (Catalano), Rehåková, Pl. 1, Figs. 1, 2

1999 *Remaniella ferasini* (Catalano), Lakova et al., Pl. 1, Fig. 10

2004 *Remaniella ferasini* (Catalano), Marino, Pl. 3, Fig. 5

2007 *Remaniella ferasini* (Catalano), Andreini et al., Pl. 1, Figs. 30, 31

2012 *Remaniella ferasini* (Catalano), Petrova et al., 60, Figs. 37-39

2013 *Remaniella ferasini* (Catalano), Lakova & Petrova, Pl.2, Figs. 23-25; Pl. 6, Figs. 36-41

2013b *Remaniella ferasini* (Catalano), López-Martinez et al., 7, Figs. (6) F, G

2015 *Remaniella ferasini* (Catalano), López-Martinez et al., 587, Fig. 7H

2016 *Remaniella ferasini* (Catalano), Maalaoui & Zargouni, 50, Fig. (4) 11

2018 *Remaniella ferasini* (Catalano), Atasoy et al., Fig. (10) 35-37

Description & Remarks: It has a small ovoid lorica with bipartite detached collars. The collars are nearly equal in dimension and have triangular shaped profiles (in longitudinal sections). The inner collar is inwardly deflected, and the outer one is little bit divergent in orientation; more or less upwardly directed two triangles in thin sections. The inner on show extinction at 45° under polarized light. Its first occurrence defines the basal boundary of the *Remaniella* subzone. The specimens of this species were identified from *Remaniella* (middle Early Berriasian), *elliptica* (late Early Berriasian) and *simplex* (early Late Berriasian) subzones (Figs. 2.15 & 2.17).

Remaniella duranddelgai Pop, 1996

Pl. 1, Figs. 30-35

1969 *Remaniella cadischiana* Colom, Borza, Pl. LXXXI, Figs. 2, 3, 5-7

1991 *Remaniella cadischiana* Colom, Altıner & Özkan, Pl. 5, Fig. 3

1992 *Remaniella cadischiana* Colom, Bucur, 572, Fig. 4o

1996 *Remaniella duranddelgai* n. sp., Pop, Pl. 2, Figs. 1-6

1996 *Remaniella duranddelgai* Pop, Grün & Blau, Pl. 1, Fig. 11

1997 *Remaniella duranddelgai* Pop, Grün & Blau, Pl. 2, Fig. 9

1998 *Remaniella duranddelgai* Pop, Rehåková, Pl. 1, Fig. 6, 7

2004 *Remaniella duranddelgai* Pop, Marino, Pl. 3, Fig. 7

2007 *Remaniella duranddelgai* Pop, Andreini et al., Pl. 2, Figs. 3, 6

2010 *Remaniella colomi* Pop, Fözy et al., 537, Fig. 9P

2012 *Remaniella duranddelgai* Pop, Petrova et al., 60, Fig. (5) 40-43

2013 *Remaniella duranddelgai* Pop, Lakova & Petrova, Pl. 2, Figs. 26-28; Pl. 3, Fig. 12; Pl. 6, Figs. 42-49

2015 *Remaniella duranddelgai* Pop, Boorová et al., 103, Fig. 6D

2015 *Remaniella duranddelgai* Pop, López-Martinez et al., 589, Fig. 8I

2018 *Remaniella duranddelgai* Pop, Atasoy et al, Fig. (10) 38

Description & Remarks: It is characterized by bell-shaped to slightly ovoid lorica. The aboral pole is conical with a short caudal appendage. The bipartite collar is inequal in size and shape. The inner one is more or less in the direction of the lorica wall and has triangular shape. The other one has a lenticular shape. Its first occurrence observed in the middle part of the *Remaniella* subzone (middle early Berriasian) in accordance with the Rehåková (1998) and Lakova and Petrova (2012). Some authors (Lakova & Petrova, 2013) suggest nearly synchronous first occurrence of it with the *R. ferasini* at the base of the *Remaniella* subzone. The specimens of this species were identified from *elliptica* (late Early Berriasian) and *simplex* (early Late Berriasian) subzones (Figs. 2.15 & 2.17).

Remaniella colomi Pop, 1996

Pl. 1, Figs. 36, 41

1991 *Remaniella cadischiana* Colom, Altıner & Özkan, Pl. 5, Fig. 7

1994a *Remaniella cadischiana* Colom, Pop, Pl. 1, Fig. 4

1996 *Remaniella colomi* n. sp., Pop, Pl. 2, Figs. 7-9

1996 *Remaniella colomi* Pop, Grün & Blau, Pl. 1, Figs. 8-9, ?10

1997 *Remaniella colomi* Pop, Grün & Blau, Pl. 2, Fig. 2

1998 *Remaniella colomi* Pop, Rehåková, Pl. 1, Figs. 8, 9

2007 *Remaniella colomi* Pop, Andreini et al., Pl. 2, Fig. 9

2012 *Remaniella colomi* Pop, Petrova et al., 62, Fig. (6) 1-3

2013 *Remaniella colomi* Pop, Lakova & Petrova, Pl. 2, Figs. 29-32; Pl. 3, Figs. 13-16; Pl. 6, Figs. 50, 51

2015 *Remaniella filipescui* Pop, Boorová et al., 103, Fig. 6E

2015 *Remaniella colomi* Pop, López-Martinez et al, 589, Fig. 8G

2016 *Remaniella ferasini* Catalano, Maalaoui & Zargouni, 50, Fig. (4) 10

2018 *Remaniella colomi* Catalano, Atasoy et al., Fig. (10) 39

Description & Remarks: *Remaniella colomi* differs from *R. duranddelgai* by its cylindrical lorica shape. The other properties are nearly the same. The outer collar is more developed than the inner one. *R. colomi* was observed from the *elliptica* (late Early Berriasian), *simplex* (early Late Berriasian) and *oblonga* (late Late Berriasian) subzones (Figs. 2.15 & 2.17).

Remaniella cadischiana (Colom, 1948)

Pl. 1, Figs. 42, 43

1948 *Tintinnopsella cadischiana* n. sp., Colom, Pl.12, Figs. 34-35

1965 *Remaniella cadischiana* (Colom) – Catalano, Pl. 1, Figs. 6, 7, 11-14; Pl. 3, Fig. 1

1994a *Remaniella cadischiana* (Colom), Pop, Pl. 1, Figs. 1-4

1996 *Praecalpionellites dadayi* Knauer, Grün & Blau, Pl. 1, Figs. 1-3

1996 *Remaniella cadischiana* (Colom), Grün & Blau, Pl. 1, Figs. 4-7

1997 *Remaniella cadischiana* (Colom), Grün & Blau, Pl. 2, Fig. 1

1997 *Praecalpionellites dadayi* Knauer, Grün & Blau, Pl. 2, Fig. 5

1998 *Remaniella cadischiana* (Colom), Rehåková, Pl. 1, Figs. 16, 17

2004 *Praecalpionellites dadayi* Knauer, Marino et al., Pl. 3, Fig. 13

2006 *Remaniella cadischiana* (Colom), Grabowski & Pszczółkowski, 405, Fig. 7H

2007 *"Praecalpionellites" dadayi* Knauer, Andreini et al., Pl. 2, Fig. 21

2010 *Praecalpionellites dadayi* Knauer, Fözy et al., 537, Fig. 9C

2010 *Remaniella cadischiana* (Colom), Fözy et al., 537, Fig. 9K

2012 *Remaniella cadischiana* (Colom), Petrova et al., 62, Figs. (6) 7, 8

2013 *Remaniella cadischiana* (Colom), Lakova & Petrova, Pl. 3, Fig. 18; Pl. 7, Figs. 23, 24

2015 *Remaniella cadischiana* (Colom), Boorová et al., 103, Fig. 6F

2016 *Remaniella cadischiana* (Colom), Maalaoui & Zargouni, 50, Figs. (4) 13, 14

2018 *Remaniella cadischiana* (Colom), Atasoy et al., Fig. (10) 45. 46

Description & Remarks: It differs from the *R. filipescui* by its cylindrical, elongated lorica with acute aboral part that has caudal appendage. The collar configuration is

similiar with the *R. filipescui*. The specimens of *R. cadischiana* were recovered from the *elliptica* (late Early Berriasian), *simplex* (early Late Berriasian) and *oblonga* (late Late Berriasian) subzones (Figs. 2.15 & 2.17).

Generally, after the emendations on the genus *Remaniella* (Pop, 1994; Grün & Blau, 1996), revisions have been made to the previously published biozonation schemes with introduction of more subdivisions, although the main zonal boundaries have remained the same with the Remane's 1971 scheme. Among them, Grün and Blau (1997)'s scheme proposed an unusual first occurrence for the *Remaniella catalanoi* in the *Crassicollaria* zone. They introudced a *catalanoi* subzone as the equivalent of the previously defined *colomi* subzone. Then it was understood that the late Tithonian *Crassicollaria* zone is missing and *elliptica* subzone (of *Calpionella* zone) is in direct contact with the *remanei* subzone (of *Crassicollaria* zone) in the Rau Stau section on which Grün and Blau (1997) based their biozonation (Rehåková, 1998). Additionally, the definition of the genera *Remaniella* and *Praecalpionelllites* in the studies of Grün and Blau (1996, 1997) were very unusual that differentiates them mainly according to the shape of the lorica instead of the collar partitions. They eliminated the tripartite collar definition. This emendation had introduced additional problems in the identification of the remaniellid calpionellids and the determination of their stratigraphical ranges. In this study, Pop (1994, 1996)' s emendations were followed for the identification of them. In recent studies, these definitions have mainly been followed as the synonymy lists indicate. More recently, Lakova and Petrova (2012, 2013) tried to synthesize a global standard calpionellid zonation scheme. In order to achieve this aim, they discarded taxa with controversial vertical ranges and morphologies and subzones that are not recognized globally. They dismissed all zonation based on the controversial taxa like *R. borzai*, *R. colomi*, *R. catalanoi*, and *R. cadischiana*. So, the identification of remaniellid calpionellids are not so important in terms of biostratigraphy, except from the *Remaniella ferasini* that defines the lower boundary of the *Remaniella* subzone.

Remaniella catalanoi Pop, 1996

Pl. 1, Figs. 44-46

1995 *Remaniella cadischiana* Colom, Olóriz et al., Pl. 1, Fig. 25

1996 *Remaniella catalanoi* n. sp., Pop, 320, Figs. 10-15

1997 *Remaniella catalanoi* Pop, Grün & Blau, Pl. 1, Figs. 13, 14

1998 *Remaniella catalanoi* Pop, Rehåková, Pl. 1, Figs. 3-5

2007 *Remaniella catalanoi* Pop, Andreini et al., Pl. 2, Fig. 4

2007 *Remaniella cadischiana* Colom, Andreini et al., Pl. 2, Figs. 7, 8

2012 *Remaniella catalanoi* Pop, Petrova et al., 62, Figs. (6) 4-6

2013 *Remaniella catalanoi* Pop, Lakova & Petrova, Pl. 6, Figs. 52-55

2016 *Remaniella catalanoi* Pop, Maalaoui & Zargouni, 50, Fig. (4) 16

2018 *Remaniella catalanoi*? Pop, Atasoy et al., Fig. (10) 40

Description & Remarks: The lorica is similiar to the *R. duranddelgai*, bell-shaped to ovoid with conical aboral pole that include a short caudal appendage. It differs from it by the configuration of the collar. The outer collar is similiar but the inner one is filiform seen as two symmetrical points in thin section.

The representatives of this species were identified from the *elliptica* (late Early Berriasian), *simplex* (early Late Berriasian) and *oblonga* (late Late Berriasian) subzones (Figs. 2.15 & 2.17). Although the lorica shape is easy to recognize and differentiates them from *R. filipescui* and *R. cadischiana*, taking a good photograph that clearly show the inner collar is very hard.

Remaniella borzai Pop, 1994

Pl. 1, Fig. 47-51

1994a *Remaniella borzai* n. sp., Pop, Pl. 1, Figs. 13-16

1998 *Remaniella borzai* Pop, Rehåková, Pl. 1, Figs. 11-12

2007 *Remaniella borzai* Pop, Andreini et al., Pl. 2, Fig. 19

2013 *Remaniella borzai* Pop, Lakova & Petrova, Pl. 7, Fig. 22

2016 *Remaniella borzai* Pop, Maalaoui & Zargouni, 50, Fig. (4) 18

2018 *Remaniella borzai* Pop, Atasoy et al., Fig. (10) 41

Description & Remarks: It differs from the *R. catalanoi* by its elongated cylindrical lorica. The collars are similiar, again the inner one is filiform and the outer collar is divergent, lenticular. It may be hard to differentiate this species with *Tintinopsella longa* when the inner collar is hard to recognize. Individual of this species were identified from the *elliptica* (late Early Berriasian) and *simplex* (early Late Berriasian) subzones (Figs. 2.15 & 2.17).

Remaniella filipescui Pop, 1994

Pl. 1, Figs. 52, 53

1965 *Remaniella cadischiana* Colom, Catalano, Pl.1, Fig. 13

1985 *Remaniella cadischiana* Colom, Remane, 570, Fig. (18) 19

1991 *Remaniella cadischiana* Colom, Altıner & Özkan, Pl. 5, Figs. 4-6, 8, 9

1994a *Remaniella filipescui* n. sp., Pop, Pl. 1, Figs. 7-12

1996 *Praecalpionellites filipescui* Pop, Grün & Blau, Pl. 2, Figs. 7, 10.

1997 *Praecalpionellites filipescui* Pop, Grün & Blau, Pl. 2, Fig. 4

1998 *Remaneialla filipescui* Pop, Rehåková, Pl. 1, Figs. 13-15

1999 *Praecalpionellites filipescui* Pop, Grün & Blau, 207, Fig. 3

2006 *Praecalpionellites filipescui* Pop, Grabowski & Pszczółkowski, 405, Fig. 7K

2007 *Remaniella filipescui* Pop, Andreini et al., Pl. 2, Figs. 20, 22

2010 *Praecalpionellites filipescui* Pop, Fözy et al., 537, Figs. 9N, ?9T

2013 *Remaniella filipescui* Pop, Lakova & Petrova, Pl. 3, Fig. 17; Pl. 4, Fig. 10

2015 *Remaniella filipescui* Pop, Boorová et al., 103, Fig. 6E

2018 *Remaniella filipescui* Pop, Atasoy et al., Fig. (10) 42-44

Description & Remarks: It differs from the *R. cadischiana* by its bell-shaped lorica with conical aboral part that show caudal appendage. It has two unequal, divergent collars that are oblique in position with respect to the lorica wall. This configuration of the collar differs this species from the other members of *Remaniella*. Its maximum with is near the oral part (in axial sections, oblique sections will reveal convex lorica walls that may give a view of slight restriction at the oral end).

It ranges from the *elliptica* (late Early Berriasian) subzone to *simplex* (early Late Berriasian) subzone (Figs. 2.15 & 2.17).

Genus *Lorenziella* Knauer & Nagy, 1963

Type species: *Lorenziella hungarica* Knauer & Nagy, 1963

Lorenziella hungarica Knauer & Nagy, 1963

Pl. 1, Fig. 54-56

1963 *Lorenziella hungarica* n. sp., Knauer & Nagy, Pl. 1, Figs. 1, 4, 7, 8

1985 *Lorenziella hungarica* Knauer & Nagy, Remane, 570, Figs. (18) 16-18

1991 *Lorenziella hungarica* Knauer & Nagy, Altıner & Özkan, Pl. 5, Figs. 17-18

1991 *Lorenziella hungarica* Knauer & Nagy, Tunç, Pl. 4, Fig. 1

1992 *Lorenziella hungarica* Knauer & Nagy, Tunç, Pl. 2, Fig. 12

1996 *Lorenziella hungarica* Knauer & Nagy, Grün & Blau, Pl. 2, Fig. 5

1997 *Lorenziella hungarica* Knauer & Nagy, Grün & Blaue, Pl. 2, Figs. 6, 7

1999 *Lorenziella hungarica* Knauer & Nagy, Lakova et al., Pl. 1, Fig. 5

2006 *Lorenziella hungarica* Knauer & Nagy, Grabowski & Pszczółkowski, 405, Fig. 7L

2010 *Lorenziella hungarica* Knauer & Nagy, Főzy et al., 537, Fig. 9F

2012 *Lorenziella hungarica* Knauer & Nagy, Petrova et al., 60, Figs. (5) 18-21

2013 *Lorenziella hungarica* Knauer & Nagy, Lakova & Petrova, Pl. 3, Figs. 5-8; Pl. 7, Figs. 9-12

2018 *Lorenziella hungarica* Knauer & Nagy, Atasoy et al., Fig. (10) 48

Description & Remarks: *Lorenziella hungarica* is characterized by a small test with a rounded aboral pole and suboral constriction. The funnel-shaped collar is reduced in size seen as inwardly convex symmetric crescentic shapes at the oral part in thin sections. There is no shoulder or swelling below the collar. It may be confused with oblique sections of smaller forms of *T. carpathica*. This species was recovered from the *elliptica* (late Early Berriasian) and *simplex* (early Late Berriasian) subzones (Figs. 2.15 & 2.17).

Lorenziella plicata Le Hégarat & Remane, 1968

Pl. 1, Fig. 57

1968 *Lorenziella plicata* n. sp., Le Hégarat & Remane, Pl. 9, Figs. 16, 20

2013 *Lorenziella plicata* Le Hégarat & Remane, Lakova, Petrova, Pl. (3) 9-11; Pl. (4) 8, 9; Pl. (7) 14

2017b *Lorenziella plicata* Le Hégarat & Remane, López-Martínez et al., Fig. 3C

Description & Remarks: *Lorenziella plicata* differs from *L. hungarica* in having conical aboral pole and rather elongated lorica with somewhat less convex walls overall and pronounced oral constriction. The individuals of this specimens were recovered from the *elliptica* (middle Berriasian) subzone to *darderi* (Calpionellites – *oblonga*, E1, Early Valanginian) subzone. However, they occur sporadically.

Genus *Calpionellopsis* Colom, 1948

Type species: *Calpionella thalmanni* Colom, 1939

Calpionellopsis simplex (Colom, 1939)

Pl. 1, Figs. 59-63

1939 *Calpionella simplex* n. sp., Colom, Pl. 2, Fig. 11; Pl. 3, Fig. 9

1948 *Calpionellopsis simplex* (Colom) – Colom, 256, Fig. (11) 10

1985 *Calpionellopsis simplex* (Colom), Remane, 570, Fig. (18) 9, 10

1991 *Calpionellopsis simplex* (Colom), Altıner & Özkan, Pl. 4, Figs. 1-10

1991 *Calpionellopsis simplex* (Colom), Tunç, Pl. 4, Fig. 2

1992 *Calpionellopsis simplex* (Colom), Tunç, Pl. 2, Fig. 10

1992 *Calpionellopsis simplex* (Colom), Bucur, 572, Fig. (4) t-v

1994a *Calpionellopsis simplex* (Colom), Pop, Pl. 2, Fig. 1

1996 *Calpionellopsis simplex* (Colom), Grün & Blau, Pl. 2, Figs. 14, 15

1999 *Calpionellopsis simplex* (Colom), Lakova et al., Pl. 1, Fig. 12

2006 *Calpionellopsis simplex* (Colom), Grabowski & Pszczółkowski, 405, Fig. 7I

2007 *Calpionellopsis simplex* (Colom), Andreini et al., Pl. 2, Figs. 10, 11

2010 *Calpionellopsis simplex* (Colom), Özy et al., 537, Fig. 9S

2012 *Calpionellopsis simplex* (Colom), Petrova et al., 60, Figs. (5) 22-26

2013 *Calpionellopsis simplex* (Colom), Lakova & Petrova, Pl. 3, Figs. 19-26; Pl. 7, Fig. 1, 2

2015 *Calpionellopsis simplex* (Colom), López-Martinez et al., 589, Fig. 8D

2018 *Calpionellopsis simplex* (Colom), Atasoy et al., Fig. (10), 29-31

Description & Remarks: *Calpionellopsis simplex* is characterized by cylindrical lorica with parallel lateral walls (curved in oblique sections), subrounded aboral pole and an internal cylindrical collar that show extinctions between crossed nicols at 45°. The collar looks like two symmetrical nodes superimposed on the lorica wall. Its first occurrence defines the basal boundary of the *Calpionellopsis* Zone and the *simplex* subzone. The representatives of this species were recovered from simplex subzone (earliest late Berriasian) to the base of the *darderi* subzone (earliest Valanginian).

Calpionellopsis oblonga (Cadisch, 1932)

Pl. 1, Figs. 64-67

1932 *Calpionella oblonga* n. sp., Cadisch, 251, Figs. 20, 21

1948 *Tintinnopsella oblonga* Cadisch, Colom, Pl. 33, Fig. 5; 256, Fig. 13; 258, Fig. 57; 260, Fig. 5

1964 *Calpionellopsis oblonga* (Cadisch) – Catalano & Lima, Pl. 1, Figs. 7-9

1985 *Calpionellopsis oblonga* (Cadisch), Remane, 570, Fig. (18) 7, 8

1991 *Calpionellopsis oblonga* (Cadisch), Altıner & Özkan, Pl. 4, Figs. 11-20

1991 *Calpionellopsis oblonga* (Cadisch), Tunç, Pl. 4, Fig. 3

1992 *Calpionellopsis oblonga* (Cadisch), Tunç, Pl. 2, Fig. 11

1992 *Calpionellopsis oblonga* (Cadisch), Bucur, 572, Fig. (4) x, y

1994a *Calpionellopsis oblonga* (Cadisch), Pop, Pl. 2, Fig. 2

1999 *Calpionellopsis oblonga* (Cadisch), Lakova et al., Pl. 1, Fig. 15

2004 *Calpionellopsis oblonga* (Cadisch), Marino et al., Pl. 3, Fig. 10

2006 *Calpionellopsis oblonga* (Cadisch), Grabowski & Pszczółkowski, 405, Fig. 7J

2007 *Calpionellopsis oblonga* (Cadisch), Andreini et al., Pl. 2, Figs. 12, 1

2010 *Calpionellopsis oblonga* (Cadisch), Fözy et al., 537, Figs. (9) H, O

2012 *Calpionellopsis oblonga* (Cadisch), Petrova et al., 60, Figs. (5) 27-29

2013 *Calpionellopsis oblonga* (Cadisch), Lakova & Petrova, Pl. 3, Figs. 27-33; Pl. 4, Figs. 1-3; Pl. 7, Figs. 3-6

2013b *Calpionellopsis oblonga* (Cadisch), López-Martinez et al., 202, Fig. 7G

2015 *Calpionellopsis oblonga* (Cadisch), Boorová et al., 103, Fig. 6Q

2015 *Calpionellopsis oblonga* (Cadisch), López-Martinez et al., 589, Fig. 8E

2018 *Calpionellopsis oblonga* (Cadisch), Atasoy et al., Fig. (10) 32-34

Description & Remarks: It differs from the *Calpionellopsis simplex* by its convergent lorica walls rather than parallel ones and conical aboral part. This gave rise to the largest portion being in the lower parts of the lorica near the aboral area. The collar is similar to *Cs. simplex*. The first occurrence of this species defines the lower boundary of the *oblonga* subzone. The specimens were observed from the *oblonga* (latest Berriasian) and the *darderi* (earliest Valanginian) subzones (Fig.2.15 & 2.17).

Genus *Calpionellites* Colom, 1948

Type species: *Calpionella darderi* Colom, 1934

Calpionellites darderi (Colom, 1934)

Pl. 1, Fig. 68

1934 *Calpionella darderi* n. sp., Colom, Pl. 31, Fig. 3

1948 *Calpionellites darderi* (Colom) – Colom, 258, Fig. (12) 1-15

1985 *Calpionellites darderi* (Colom), Remane, 570, Fig. (18) 5, 6

1991 *Calpionellites darderi* (Colom), Altıner & Özkan, Pl. 5, Figs. 11-16

1991 *Calpionellites darderi* (Colom), Tunç, Pl. 4, Figs. 4, 5

1994a *Calpionellites darderi* (Colom), Pop, Pl. 2, Figs. 7, 8

1997 *Calpionellites darderi* (Colom), Grün & Blau, Pl. 2, Fig. 12

2004 *Calpionellites darderi* (Colom), Marino et al., Pl. 3, Fig. 16

2007 *Calpionellites darderi* (Colom), Andreini et al., Pl. 3, Fig. 5

2010 *Calpionellites darderi* (Colom), Fözy et al., 537, Fig. 9A-B

2013 *Calpionellites darderi* (Colom), Lakova & Petrova, Pl. 4, Figs. 20-24; Pl. 7, Figs. 25, 26

2015 *Calpionellites darderi* (Colom), Boorovå, 103, Fig. 6S

2018 *Calpionellites darderi* (Colom), Atasoy et al., Fig. (10) 47

Description & Remarks: *Cts. darderi* is characterized by oral restriction resulted from an inward deflection of a collar just below the end of the lorica wall. It differs from the *Cts. major* by its bell-shaped shorter lorica and from other species (*Cts. coronatus* and *Cts. caravacaensis*) of this genus by its simple conical collar. The first occurrence of this species determines the basal boundary of the *Calpionellites* Zone/ *darderi* subzone and the Berriasian – Valanginian boundary (Fig. 2.15).

Calpionellites caravacaensis Allemann, 1975

Pl. 1, Fig. 69

1975 *Calpionellites caravacaensis* n. sp., Allemann, Pl. 2, Figs. 10-15

2013 *Calpionellites caravacaensis* Allemann, Lakova & Petrova, Pl. 4, Fig. 44; Pl. 7, Figs. 33-35

Description & Remarks: *Cts. caravacaensis* has subcylindrical to cylindrical lorica with short aboral appendix (cannot be seen in our specimen due to deformation). Side- walls are subparallel to parallel. The diagnostic horn-like (s-shaped) collar bifurcates near the oral end of the lorica. The collar is thick near the oral end and thins out towards upward. This thin outer segment swings around the oral opening.

It was observed from the *darderi* subzone of the the Ağören section (Fig. 2.15).

5.2 Foraminiferal Taxonomy

PHYLUM FORAMINIFERA d'Orbigny 1826

?FAMILY ROSALINIDAE REISS 1963

Genus *Mohlerina* Bucur, Senowbari-Daryan and Abate, 1996

Type species: *Conicospirillina basiliensis* Mohler, 1938

Mohlerina basiliensis (Mohler, 1938)

Pl. 2, Figs. 43-44; Pl. 5, Figs. 11-13

1938 *Conicospirillina basiliensis* n. sp., Mohler, Pl. 28-28; Pl. 4, Fig.5

1990 *Archaeosepta basiliensis* (Mohler), Taslı, Pl. 22, Figs. 1-6

1991 "*Conicospirillina*" *basiliensis* Mohler, Altıner, Pl. 3, Figs. 8, 9; Pl. 7, Figs. 6-8

1996 *Mohlerina basiliensis* (Mohler) – Bucur et al., Pl. 3, Figs. 3-6; Pl. 4, Figs. 2, 3, 5-9

2004 *Mohlerina basiliensis* (Mohler), Bucur et al., Pl. 1, Fig. 2

2005 *Mohlerina basiliensis* (Mohler), Schlagintweit et al., Figs. (16) a-e

2010 *Mohlerina basiliensis* (Mohler), Ivanova & Kolodziej, Pl. 5, Figs. 12-18

2012 *Mohlerina basiliensis* (Mohler), Schlagintweit, 639, Figs. (2) a-j; 640, Figs. (3) a-d; 641, Figs. (4) a-f; 642, Figs. (5), (6) a-e; 643, Fig. 7d

2015 *Mohlerina basiliensis* (Mohler), Pleş et al., 51, Figs. (4) g, h

2016 *Mohlerina basiliensis* (Mohler), Okay & Altıner, Fig. (5) 9

2018 *Mohlerina basiliensis* (Mohler), Atasoy et al., Fig. (8) 8-10

2020b *Mohlerina basiliensis* (Mohler), Granier, Fig. (3) 2-15

Description & Remarks: The test wall consits of two layers; inner microgranular and outer hyaline. The test is large, trochospirally coiled. It may fix itself to any substratum (any type of sediment grains or other fossils) via a basal cement layer. With these characteristics it presents great similarities with Paleozoic foraminifera *Tetrataxis* that has the layers of the test in the other way around (inner hyaline, outer microgranular; for more discussion see Schlagintweit, 2012). In our material no specimen was observed in encrusting position. Individuals of this species were recovered from the slope and carbonate platform environments in this study and generally represented by resedimented individuals. The reported wide range of test dimensions most probably a function of the encrusting processes (depending on the shape of the substratum to which organism attached itself; Schlagintweit, 2012). It ranges from Middle Jurassic to Early Cretaceous and recorded from the Kimmeridgian to early Berriasian interval in this study (Fig. 2.15, 2.17 & 2.19). Most of the examples identified here represents the transported, resedimented individuals.

FAMILY VENTROLAMINIDAE WEYNSCHENCK 1950

Genus *Protopeneroplis* Weynschenk, 1950

Type species: *Protopeneroplis striata* Weynschenk, 1950

Protopeneroplis ultragranulata (Gorbatchik, 1971)
Pl. 2, Figs. 1-15; Pl. 9, Figs. 12-13

1971 *Hoeglundina* (?) *ultragranulata* n. sp., Gorbatchik, Pl. V, Figs. (2) a-c

1974 *Protopeneroplis trochangulata* n. sp., Septfontaine, Pl. 1, Figs. 1-18

1991 *Protopeneroplis trochangulata* Septfontaine, Altıner, Pl. 7, Figs. 1-5

1993 *Protopeneroplis ultragranulata* (Gorbatchik) – Bucur, Pl. 2, Figs. 1, 2, 5, 8, 11, 12

1996 *Protopeneroplis ultragranulata* (Gorbatchik), Bucur et al., Pl. 3, Figs. 14-17

1997 *Protopeneroplis ultragranulata* (Gorbatchik), Bucur, Pl. 1, Figs. 13-16; Pl. II, Figs. 1-14; Pl. III, Figs. 1-3

2004 *Protopeneroplis* sp. (Gorbatchik), Bucur et al., Pl. 1, Figs. 7, 8

2010 *Protopeneroplis ultragranulata* (Gorbatchik), Ivanova & Klodziej, Pl. 5, Figs. 1-6

2012 *Protopeneroplis ultragranulata* (Gorbatchik), Petrova et al., 66, Fig. (8) 28

2016 *Protopeneroplis ultragranulata* (Gorbatchik), Okay & Altıner, Fig. (5) 1-5

2018 *Protopeneroplis ultragranulata* (Gorbatchik), Atasoy et al., Fig, (8) 3-6

2019 *Protopeneroplis ultragranulata* (Gorbatchik), Granier, Fig. (12) Y-AD

Description & Remarks: It differs from the *P. striata* by its trochospiral coiling. It ranges from Late Tithonian to Early Valanginian. *P. ultragranulata* were recovered from the latest Tithonian to Early Berriasian in this study. The first occurrence of this species within the studied slope to basin deposits of the Hozbirikyayla Formation is facies controlled, but since it appears within the *Saccocoma* subzone there should not be any question about its proposed stratigraphic position in this study. This taxon is also observed in the Berriasian – Valanginian strata of the Berdiga Limestone.

Protopeneroplis striata Weynschenk, 1950

Pl. 5, Fig. 8

1950 *Protopeneroplis striata* n. sp., Weynschenk, Pl. 2, Figs. 12-14

1974 *Protopeneroplis striata* Weynschenk, Septfontaine, Pl. 2, Figs. 1-15

1990 *Protopeneroplis striata* Weynschenk, Taslı, Pl. 22, Figs. 7-13

1991 *Protopeneroplis striata* Weynschenk, Altıner, Pl. 3, Figs. 1-7

1997 *Protopeneroplis striata* Weynschenk, Bucur, Pl 1, Figs. 1-12

2004 *Protopeneroplis striata* Weynschenk, Bucur et al., Pl. 1, Figs. 3, 4

2010 *Protopeneroplis striata* Weynschenk, Ivanova & Klodziej, Pl. 5, Figs. 7, 8

2015 *Protopeneroplis striata* Weynschenk, Pleş et al., 48, Fig. 3o

2018 *Protopeneroplis striata* Weynschenk, Atasoy et al., Fig. (8) 1, 2

Description & Remarks: The test is involute, planispirally or slightly trochospirally coiled with double wall; inner layer microgranular and outer layer hyaline. This double layering form striation in this species and differentiates it from *Protopeneroplis ultragranulata*.

Some studies (Bucur et al., 1993; Bucur, 1997) extends the range of *P. striata* into Berriasian but generally Aalenian – Late Tithonian interval is accepted for its range (e.g., Loeblich & Tappan, 1988; Velic, 2007; Ivanova & Kolodziej, 2010). The represntatives of this species were only recovered from the Kimmeridgian platform succession (Berdiga Limestone) in this study.

FAMILY MESOENDOTHYRIDAE VOLOSHINOVA, 1958

Genus *Mesoendothyra* Dain, 1958

Type species: *Mesoendothyra izjumiana* Dain, 1958

Mesoendothyra izjumiana Dain 1958

Pl. 4, Figs. 22-28

1958 *Mesoendothyra izjumiana* n. gen. n. sp., Dain in Bykova et al., Pl. 4, Figs. 7-9

1991 *Mesoendothyra izjumiana* Dain, Altıner, Pl. 4, Figs. 1-3

2010 *Mesoendothyra izjumiana* Dain, Olszewska, Pl. IV, Figs. 4, 5

2014 *Mesoendothyra izjumiana* Dain, Kaya, Pl. 1, Figs. 1, 2

2018 *Mesoendothyra*?, Atasoy et al., Fig. (8) 26

Description & Remarks: The semi-spherical and biumblical test is sterptospirally coiled in the early stage, then planispiral (involute). Periphery is rounded. Sutures are depressed. Wall is microgranular and alveolar, septa are nonalveolar. Aperture is an equatorial slit at the base of the septa. There is no uncoiled stage.

The individuals of this species were observed from the *Mesoendothyra izjumiana – Alveosepta jaccardi* subzone (*Crescentiella morronensis* Zone, Kimmeridgian) of the shallow marine carbonates of the Nazlıçayır measured section (Fig. 2.18).

Mesoendothyra cf. *croatica* Gušić 1969

Pl. 4, Figs. 29-31

1966 *Endothyra* sp., Radoičić, Pl. 95, Fig. 2; Pl. 96, Fig. 1; Pl. 112, Fig. 2

1969 *Mesoendothyra croatica* n.sp., Gušić, Pl. XI-XII

1977 *Mesoendothyra croatica* Gušić, Furrer & Septfontaine, Pl. 2, Figs. 4-7

1980-81 *Mesoendothyra croatica* Gušić, Septfontaine, Pl. 3, Fig. 6

1990 *Mesoendothyra croatica* Gušić, Taslı, Pl. 5, Figs. 1-5; Fig. (4.3) a-d

Description & Remarks: *M. croatica* differs from *M. izjumina* with its involute planipiral/ streptospiral to undoiled coiling type. The aperture at the base of septa in

the early stages of coiling and in a central position in the uncoiled part. Wall is alveolar while septa are nonalveolar.

This species was recorded from the *Mesoendothyra izjumiana – Alveosepta jaccardi* subzone (*Crescentiella morronensis* Zone, Kimmeridgian) of the shallow marine carbonates of the Nazlıçayır measured section (Fig. 2.18). They are relatively rare with respect to *M. izjumiana*. Since the speciemens recovered do not reveal fully developed uncoiled part species name with "cf." abbreviation is used.

FAMILY HAURANIIDAE SEPTFONTAINE, 1988

Genus *Pseudocyclammina* Yabe & Hanzawa, 1926

Type species: *Cyclammina lituus* Yokoyama, 1890

Pseudocyclammina lituus (Yokoyama, 1890)
Pl.4, Fig. 36; Pl. 5, Figs. 20, 21, 24-28; Pl. 6, Figs. 2, 3

1890 *Cyclammina lituus* n. sp., Yokoyama, Pl. 5, Fig. 7

1926 *Pseudocyclammina lituus* (Yokoyama) – Yabe & Hanzawa, Pl. 2, Figs. 3-6

1948 *Pseudocyclammina lituus* (Yokoyama), Henson, Pl. IX, Figs. 2, 3; Pl. XIII, Fig. 7

1990 *Pseudocyclammina lituus* (Yokoyama), Taslı, Pl. 10, Figs. 8-11; Pl. 11, Figs. 1, 2

1991 *Pseudocyclammina lituus* (Yokoyama), Altıner, Pl. 4, Fig. 10; Pl. 7, Fig. 14

1991 *Pseudocyclammina lituus* (Yokoyama), Banner & Whittaker, Pl. 5, Figs. 8-11; Pl. 6, Fig. 5

2005 *Pseudocyclammina lituus* (Yokoyama), Schlagitnweit, et al., 38, Figs. 22a-d

2007 *Pseudocyclammina lituus* (Yokoyama), Krajewski & Olszewska, 301, Fig. 6F

2010 *Pseudocyclammina lituus* (Yokoyama), Ivanova & Kolodziej, Pl. 4, Figs. 1-10

2016 *Pseudocyclammina lituus* (Yokoyama), Okay & Altıner, Fig. (5) 24

2018 *Pseudocyclammina lituus* (Yokoyama), Atasoy et al., Fig. (8) 24, 25

2018 *Pseudocyclammina lituus* (Yokoyama), Okay et al., Fig. (8) 14, 16

2019 *Pseudocyclammina lituus* (Yokoyama), Granier, Fig. (4) Z, Figs. (8) J, K

Description & Remarks: This species is characterized by an early involute planipiral stage, later uncoiled and by its coarsely alveolar wall and septa. Aperture is cribrate. Test outline is rounded and somewhat laterally compressed. In our material none of the thin sections we assign to this species is a characteristic section of the taxon. Mostly longitudinal, tangential and oblique-transverse sections were encountered in which the recognition of the planispiral stage is not easy. *Pseudocyclammina lituus* ranges from Oxfordian to Hauterivian (Ivanova & Kolodziej, 2010). In this study, it was recovered from the Tithonian of Hozbirikyayla Formation and the middle Berriasian of Berdiga Limestone.

Pseudocyclammina sphaeroidalis Hottinger, 1967

Pl. 5, Figs. 22, 23

1967 *Pseudocyclammina sphaeroidalis* n. sp., Hottinger, Pl. 10, Figs. 11-13; Figs. (29) a, b

1990 *Pseudocyclammina lituus* (Yokoyama), Taslı, Pl. 10, Figs., 7, 11

1991 *Pseudocyclammina lituus* (Yokoyama), Altıner, Pl. 7, Fig. 9

2005 *Pseudocyclammina sphaeroidalis* Hottinger, Schlagintweit et al., Figs. (23) a, b

2018 *Pseudocyclammina sphaeroidalis* Hottinger, Okay et al., Figs. (8) 11-13

2018 *Pseudocyclammina lituus* (Yokoyama), Okay et al., Fig. (8) 15

Description & Remarks: This taxon differs from *P. lituus* in having a single radial opening of very large caliber located at the center of the apertural face that creates the characteristic star-like appearance in equatorial section (like *Everticyclammina*), sub-spherical outline of the test and absence of the uncoiled stage.

This taxon, relatively rare compared to *P. lituus*, was observed from the Kimmeridgian strata of the Berdiga Limestone.

Genus *Alveosepta* Hottinger, 1967

Type species: *Cyclammina jaccardi* Schrodt, 1894

Alveosepta jaccardi (Schrodt, 1894)
Pl. 4, Figs. 1-14 & 21

1894 *Cyclammina jaccardi* n.sp., Schrodt, p. 734, tfs.

1926 *Cyclammina* (*Choffatella*) *sequana* Merian, Tobler

1928 *Pseudocyclammina personata* Tobler, Pl. 24, Figs. 1-3

1938 *Pseudocyclammina sequana* (Merian) var. *minor*, Mohler, Pl. 1, Figs. 5, 6

1938 *Pseudocyclammina sequana* (Merian) var. *major*, Mohler, Pl. 1, Figs. 3, 4

1958 *Pseudocyclammina jaccardi* (Schrodt) – Maync

1964 *Pseudocyclammina jaccardi* (Schrodt), Redmond, Pl.1, Figs. 2-4; Pl.2, Figs. 3, 4

1967 *Alveosepta jaccardi* (Schrodt), Hottinger, Pl. 15, Figs. 9-13; Pl. 16, Figs. 1-9; Text Fig. 40

1981 *Alveosepta jaccardi* (Schrodt), Septfontaine, Figs. 5, 6

1990 *Alveosepta jaccardi* (Schrodt), Taslı, Pl. 7, Figs. 1-9; Pl. 8, Figs. 1, 3, 4

1991 *Alveosepta* gr. *jaccardi* (Schrodt), Altıner, Pl.3, Figs. 11-16

2001 *Alveosepta jaccardi* (Schrodt), Noujaim Clark & Boudagher-Fadel, Pl. 1, Figs. 3, 6, 9

2018 *Alveosepta jaccardi* (Schrodt), Okay et al., Fig, (8) 22

Description & Remarks: This genus is characterized by involute planispiral coiling, and an agglutinated wall that bears exoskeleton beams and rafters forming subepidermal network. Septa are also alveolar as they are the continuation of the test wall. The main aperture is interiomarginal - equatorial at the base of the septa (Pl.4; Fig. 8), and accessory ones are cribrate. Test periphery is acute and slightly rounded. It ranges from Oxfordian – Kimmeridgian (e.g., Loeblich & Tappan, 1988). This taxon is recorded from the Kimmeridgian strata of the Berdiga Limestone.

FAMILY SPIROCYCLINIDAE MUNIER-CHALMAS, 1887

Genus *Streptocyclammina* Hottinger, 1967

Type species: *Pseudocyclammina* (*Streptocyclammina*) *parvula* Hottinger, 1967

Streptocyclammina gr. *parvula-muluchensis* Hottinger, 1967

Pl.6, Figs. 1, 7-9

1967 *Pseudocyclammina* (*Streptocyclammina*) *muluchensis* n. subgen., n. sp., Hottinger, Fig. 31; Pl. 11, Figs. 29-42

1967 *Pseudocyclammina* (*Streptocyclammina*) *parvula* n. subgen., n. sp., Hottinger, Fig. 31; Pl. 11, Figs. 1-22

1990 *Pseudocyclammina parvula* Hottinger, Taslı, Pl. 9, Figs. 1-7

2004 *Streptocyclammina parvula* Hottinger, Mikhalevich, Pl. III, Fig. 13

2018 *Alveosepta jaccardi* (Schrodt), Okay et al., Fig. (8) 23

2019 *Streptocyclammina* gr. *parvula-muluchensis* Hottinger, Granier & Clavel, Fig. (3) A

2020b *Streptocyclammina parvula-muluchensis* Hottinger, Granier, Fig. (2) 13-15; Fig. (4) 14-16

Description & Remarks: Early stage is streptospirally coiled, later involute and planispiral. Whorls enlarging rapidly, final stages are peneropliform. Periphery of the test is rouded. Wall is finely agglutinated. The exoskeleton consists of imperforate outer layer and very fine subepidermal network. The solid septa (without alveolar structure) are perforated by numerous apertures. This description was originally applied to Kimmeridgian taxon of *P.* (*Streptocyclammina*) *parvula*. The evolutive addition of pillars in the median plane during Late Kimmeridgian enabled differentiation of the sister taxon of *P.* (*Streptocyclammina*) *muluchensis*. Originally being introduced as a subgenus of *Pseudocyclammina* by Hottinger (1967), Loeblich and Tappan (1988) elevated *Streptocyclammina* to generic rank.

Since it is not always possible to observe the pillars in true *S. muluchensis* in randomly oriented thin sections and it is difficult to differentiate *S. parvula* and *S. muluchensis* as stated by Septfontaine (1980-81), *S.* gr. *parvula-muluchensis* nomenclature was used in this study for the recorded individuals. The individuals having the characteristic properties listed above were recorded from the Kimmeridgian strata of the Berdiga Limestone.

Streptocyclammina hottingeri Schlagintweit, Gawlick & Lein, 2005

Pl.6, Figs. 4, 5

1990 *Rectocyclammina* sp., Taslı, Pl. 9, Figs. 8, 9

2003a Lituolidae indet, Schlagintweit et al., Pl. 4, Fig. 13

2005 *Streptocyclammina hottingeri* n. sp., Schlagintweit, Gawlick & Lein, Figs. (27) a-o

2015 *Streptocyclammina hottingeri* Schlagintweit, Gawlick & Lein, Ivanova et al., Fig. 8L

2020b Indeteminate Lituolid, Granier, Fig. (4) 18

Description & Remarks: A streptocyclamminid with a prominent (more than 2/3 of the test) unrolled adult stage that follows a short streptospiral stage. Aperture is interio-marginal basal slit in the coiled stage. The septa in the uncoiled portion are perforated in the adult stage. In the uncoiled stage, the chambers gradually increase in width and show a crescent shape in axial sections.

FAMILY CYCLAMMINIDAE MARIE 1941

Genus *Bramkampella* Redmond, 1964

Type species: *Bramkampella arabica* Redmond, 1964

Bramkampella arabica Redmond, 1964

Pl.4, Fig. 15

1964 *Bramkampella arabica* n. gen., n. sp., Redmond, Pl. 1, Figs., 26-29; Pl. 2, Figs. 19, 20

1991 *Bramkampella arabica* Redmond, Banner & Whittaker, Pl. 2, Figs. 1-7

1997 *Bramkampella arabica* Redmond, Gorbachik & Mohamad, Pl. 2, Figs. 1-7

2001 *Bramkampella arabica* Redmond, Noujaim Clark & Boudagher-Fadel, Pl. 2, Figs. 13, 14; Pl. 3, Figs. 2, 5, 6, 8

2005 *Bramkampella arabica* Redmond, Bucur & Šašaran, Pl. 2, Figs. 6, 7

2023 *Bramkampella arabica* Redmond, Bucur & Lazăr, Figs. (5) a-i

Description & Remarks: The test has initial short planispiral stage that passes into a prominent uncoiled uniserial stage. Chambers increasing rapidly in volume (increase in width rather than volume) in the uncoiled part. The test wall is thick alveolar (choffatellid) that has beams projecting into the central zone (as in *Haurania*); no pillars. This monospecific genus is very similar to *Haurania*; a version of the latter to which the subepidermal cellules have been added. Aperture is cribrate.

B. arabica was firstly described from Upper Jurassic – basal Cretaceous deposits of Arabia (Redmond, 1964). There are several records from Berriasian – Valanginian strata (Gorbachik & Mohamd, 1997; Clark & Boudagher-Fadel, 2001). A single specimen was recorded from the Kimmeridgian neritic strata of the Berdiga Limestone in this study with other 2 questionable records from Berriasian – Valanginian strata.

FAMILY EVERTICYCLAMMINIDAE SEPTFONTAINE, 1988

Genus *Everticyclammina* Redmond, 1964

Type species: *Everticyclammina hensoni* Redmond, 1964

Everticyclammina sp.

Pl. 5, Figs. 2-4

Description & Remarks: It differs from *Pseudocyclammina* by its short, non-alveolar septa that seen as triangular to rectangular thickened prolongation at the base of the septal face in the equatorial section. In comparision to the cribrate aperture of *Pseudocyclammina*, *Evericyclammina* has simple, short vertical areal slit. It ranges from Middle Sinemurian to Aptian (e.g., Banner & Highton, 1990). The representatives of this genus were recorded from the Kimmeridgian strata of the Berdiga Limestone.

Everticyclammina kelleri (Henson, 1948)

Pl. 5, Fig. 5

1948 *Pseudocyclammina kelleri* n. sp., Henson, Pl. 9, Figs. 4, 5, 7

1964 *Everticyclammina eccentrica* n. gen., n. sp., Redmond, Pl. 1, Figs. 16-18; Pl. 2, Figs. 12, 13

1964 *Everticyclammina elegans* n. gen., n. sp., Redmond, Pl. 1, Figs. 19, 20; Pl. 2, Figs. 14-16

1990 *Everticyclammina kelleri* (Henson) – Banner & Highton, Pl. 1, Figs. 2-6; Pl. 2, Figs. 1-4; Pl. 3, Figs. 1, 2

1991 *Everticyclammina kelleri* (Henson), Banner & Whittaker, Pl. 4, Figs. 4-11; Pl. 5, Figs. 1-4

1991 *Everticyclammina* sp., Altıner, Pl. 7, Figs. 10-13

2001 *Everticyclammina kelleri* (Henson), Noujam Clark & Boudagher-Fadel, Pl. 2, Figs. 1-4; Pl. 3, Figs. 1, 3

2004 *Everticyclammina* cf. *kelleri* (Henson), Bucur et al., Pl. IV, Fig. 3, 7

Description & Remarks: Thick walled *Everticyclammina* with involute to uncoiled chamber arrangement. Septa is short due to elongated slit aperture in the direction of

coiling that gives rise to characteristic star-like inner whorls in equatorial sections. Alveolae are much finer and regularly formed than *E. praekelleri*. The test outline is pronouncedly biconvex (diamond shaped) in axial sections with sub-acute periphery. Although, Hottinger (1967) synonymized the type specimen of *E. kelleri* (Henson, 1948) with *E. virguliana* (Koechlin, 1942), Banner and Highton (1990) differentiate these two species based on configurations of their alveolar division; i.e, *E. virguliana*, confined to the Kimmeridgian – Tithonian strata, with smaller and regularly labyrinthic hypodermis that form a distinctive row of subcircular spaces in axial section.

The individuals of this taxon were recorded from Valanginian strata of the Berdiga Limestone.

FAMILY COSCINOPHRAGMATATIDAE THALMANN, 1951

Genus *Coscinophragma* Thalmann, 1951

Type species: *Lichenopora cribrosa* Reuss, 1846

Coscinophragma cribrosum (Reuss, 1846)
Pl. 2, Fig. 38

1846 *Lichenopora cribrosa* n. sp., Reuss, Pl. 14, Fig. 10; Pl. 24, Figs. 3-5

1954 *Coscinophragma cribrosum* (Reuss) - Pkornỳ, Fig. 107

1957 *Coscinophragma cribrosum* (Reuss), Maync, 184, Figs. 1-3; 185, Fig. 4

1996 *Coscinophragma cribrosum* (Reuss), Bucur et al., Pl. 1, Figs. 1, 5, 6; Pl. 6, Figs. 1-3, 5

1999 *Coscinophragma cribrosum* (Reuss), Schlagintweit & Ebli, Pl. 5, Fig. 6

2010 *Coscinophragma cribrosum* (Reuss), Bucur et al., Pl. 3, Fig. 13

2010 *Coscinophragma cribrosum* (Reuss), Ivanova & Kolodziej, 27, Figs. 1-4

2014 *Coscinophragma cribrosum* (Reuss), Kaya, Pl. 4, Figs, 12-18; Pl. 5, Figs. 1-8

2018 *Coscinophragma cribrosum* (Reuss), Atasoy et al., Fig. (9) 1

Description & Remarks: The test is more or less cylindrical or curved tube. The anastomosing character of the irregular internal projections forms a coarsely cellular structure. It was recorded from the Tithonian – Early Berriasian interval of slope to basin deposits and from the Kimmeridgian neritic strata in this study.

FAMILY LITUOLIDAE BLAINVILLE, 1827

Genus *Lituola* Blainville, 1827

Type species: *Lituola nautiloidea* (Lamarck, 1804)

Lituola baculiformis Schlagintweit & Gawlick, 2009
Pl. 8, Fig. 27

1991 Unidentified foraminifera, Altıner, Pl. 8, Fig. 20

1992 *Bullophragmium*? sp., Bodeur, Pl. 23, Figs. 9-11

1996 ?*Cribratina* sp., Bucur et al., Pl. 1, Fig. 4

1996 *Bullophragmium* sp., Bucur et al., Pl. 5, Figs. 1, 2

2006 *Everticyclammina virguliana* (Koechlin, 1943), Krajewski & Olszewska, Fig. 5c

2008 *Ammobaculites celatus* Arnaud-Vanneau 1980, Ivanova et al., Fig. 7V

2009 *Lituola* ? *baculiformis* n. sp., Schlagintweit & Gawlick, Figs. (4) a-d; Figs. (5) a-o

2018 Unidentified foraminifera, Atasoy et al., Fig. (8) 29

Description & Remarks: The initial short spire is followed by a long rectilinear adult stage. The coiling type of the initial stage is not clear (streptospiral or planispiral). This is the reason in the original description the generic name includes a question mark. The wall is simple, non-labyrinthic. The aperture is single within the coiled portion lying close to the base of the septum and cribrate in central part of the chambers in the uncoiled stage. In tangential-longitudinal sections, however, only one main aperture between chambers or no connection may be observed as in the case of our only sample.

This taxon is very rare. It was recorded from the Valanginian strata of the neritic Berdiga Limestone.

FAMILY MAYNCINIDAE LOEBLICH & TAPPAN, 1985

Genus *Freixialina* Ramalho, 1969

Type species: *Freixialina planispiralis* Ramalho, 1969

Freixialina planispiralis Ramalho, 1969
Pl. 6, Figs. 17, 18

1969 *Freixialina planispiralis* g. gen., n. sp., Ramalho, Pl. 1, Figs. 1-4

1990 *Mayncina gediki* n. sp., Taslı, Pl. 2, Figs. 1, 2, 6, 7

1991 *Freixialina planispiralis* Ramalho, Altıner, Pl. 12, Fig. 1

1999 *Freixialina planispira* Ramalho, Figs. 2c, d; Pl. 4, Figs. 1-15; Pl. 5, Figs.55-64; Pl. 9, Figs. 20-23

2004 *Freixialina planispiralis* Ramalho, Bucur et al., Pl. IV, Figs. 10-12, 14

2006 *Freixialina planispiralis* Ramalho, Kobayashi & Vuks, Figs. (4) 5-10

2008 *Freixialina planispiralis* Ramalho, Omaña & Arreola, Fig. 9g

2010 *Freixialina planispiralis* Ramalho, Ivanova & Kołodziej, Pl. 2, Fig. 1

2015 *Freixialina planispiralis* Ramalho, Ivanova et al., Fig. 8C

2018 *Freixialina planispiralis* Ramalho, Okay et al., Figs. (8) 3, 4

Description & Remarks: The test is discoidal in axial section, partly evolute and slightly depressed umbilicus. The spire increases in height rapidly. Chambers are broad and low. Aperture is a single areal slit. The periphery is sharp.

The individuals of this taxon were recorded from the Berriasian – Valanginian strata of the Berdiga Limestone.

FAMILY CHARENTIIDAE LOEBLICH and TAPPAN, 1985

Genus *Charentia* Neumann, 1965

Type species: *Charentia cuvillieri* Neumann, 1965

Charentia spp.

Pl. 5, Figs. 7-10

Description & Remarks: Test is lenticular and early stage is planispiral involute to uncoiled. The aperture is an equatorial slit. Septa is getting thinner towards the aperture. The base of the apertural face is thickened and may be seen as a chomota-

like small triangular swellings at the base of the septa. Wall is microgranular. It is hard to differentiate the axial sections of *Charentia* and *Nautiloculina*, however capture of sections of septa within a chamber lumen can provide hint for the presence of the thin septa of *Charentia*. *Nautiloculina* does not have such a configuration since the septa are even two times thicker than the wall. *Charentia* sp. was observed from the Kimmeridgian strata of the neritic Berdiga Limestone and from the Lower Berriasian of the pelagic carbonates of the Hozbirikyayla Formation.

Genus *Melathrokerion* Brönnimann and Conrad, 1967

Type species: *Melathrokerion valseriensis* Brönnimann and Conrad, 1967

Melathrokerion sp.
Pl. 6, Figs. 16, 19, 20

Description & Remarks: The nautiloid test has rounded periphery and biumblical. The agglutinated wall is thick. The wall and septa are simple in the early stage, later becoming thick. The wall becomes pseudo-alveolar (keriotheca-like; Pl. 6, Figs. 16, 19) in the later stage. There are chomata-like swells the bottom of the septa, like *Charentia*, due to wide crescentic slit aperture. Septa are always simple. The initial whorls can be streptospiral.

The individuals of this taxon were recovered from the Berriasian – Valanginian strata of the Berdiga Limestone.

FAMILY NAUTILOCULINDAE LOEBLICH and TAPPAN, 1985

Genus *Nautiloculina* Mohler, 1938

Type species: *Nautiloculina oolithica* Mohler, 1938

Nautiloculina spp.

Pl. 6, Figs. 10-15

Description & Remarks: Previously, debate on the wall type (whether the wall is microgranular or porcelaneous) gave rise to placement of this genus into different taxonomic levels (into lituloids by Arnaud-Vanneau & Peybernes, 1978; Loeblich & Tappan, 1988; into miliolines by Loeblich & Tappan, 1964 and Boudagher-Fadel, 2008). Recently, Kaminski (2004) has grouped Nautiloculunidae under suborder Nezzazatina that is characterized by trochospiral to planispiral test with simple microgranular wall.

The shape of the test is nautiliform, planispirally coiled, involute. The inner and outer wall is simple without any exoskeletal and endoskeletal structure. In thin section it may be easily confused with *Charentia*. *Nautiloculina* differs from the *Charentia* by the absence of chomata-like, basal septal projections and in having blunt septa characteristicly seen in equatorial sections (see *Charentia* description above for the axial section differences).

The individuals of this genus were recovered from the Kimmeridgian and Valanginian strata of the Berdiga Limestone.

FAMILY PFENDERINIDAE SMOUT & SUGDEN 1962

Genus *Kurnubia* Henson, 1948a

Type species: *Kurnubia palastiniensis* Henson, 1948a

Kurnubia palastiniensis Henson, 1948a

Pl. 5, Figs. 15-19

1948a *Kurnubia palastiniensis* n. gen., n. sp., Henson, Pl. XVI, Figs. 8, 11; Pl. XVIII, Figs. 10, 11

1962 *Kurnubia jurassica* (Henson), Smout & Sugden, Pl. 73, Fig. 19

1962 *Kurnubia palastiniensis* Henson, Smout & Sugden, Pl. 73, Fig. 16

1966 *Kurnubia palastiniensis* Henson, Maync, Pl. V, Figs. 1-7

1967 *Kurnubia palastiniensis* Henson, Hottinger, Fig. 45, 49, 47; Pl. 19, Figs. 30-34, 38-48

2005 *Kurnubia palastiniensis* Henson, Schlagintweit et al., Figs. (12) a-c

2008 *Kurnubia* ex. gr. *palastiniensis* Henson, Taslı et al., Pl. 5, Figs. 1-6

2012 *Kurnubia palastiniensis* Henson, Michetiuc et al., Fig. (4) 3

Description & Remarks: The test is elongated. Early stage with throchospiral coiling and later uncoiled, uniserial and rectilinear. Outer wall has subepidermal network and the central part with endoskeletal pillars. Pillars continue from chamber to chamber. Secondary fill between the pillars forms a central column. The umbilical has a plate with numerous small apertures between the pillars.

Rare individuals of this taxon were recovered from the Kimmeridgian strata of the Berdiga Limestone.

FAMILY HAUERINIDAE SCHWAGER, 1876

Genus *Quinqueloculina* d'Orbigny, 1826

Type species: *Serpula seminulum* Linné, 1758

Quinqueloculina spp.

Pl. 2, Figs. 16-26; Pl. 9, Figs. 19-23, 26, 27

Description & Remarks: Porcelaneous test is ovate in outline. It shows quinqueloculine coiling that is coiling axis shift 72° in each half of coiling resulted in 144° gap between successive chambers in transverse sections. In axial sextions, it is not possible to trace all chambers from the proloculus to the final chamber without coming across wtih the wall material as a result of shift in coiling axis. The individuals of this genus were identified from the Kimmeridgian to early Valanginian interval in this study.

FAMILY TROCHOLINIDAE KRISTAN-THOLMANN, 1963

Genus *Coscinoconus* Leupold *in* Leupold and Bigler, 1936

Type species: *Coscinoconus alpinus* Leupold *in* Leupold and Bigler, 1936

Coscinoconus spp.

Pl. 2, Figs. 49-59; Pl. 9, Figs. 1-11

Description & Remarks: It is characterized by reduced lamellae on the spiral side. The aragonitic test is low to high trochospirally coiled, proloculus followed by second chamber. The stratigraphical range includes Bathonian – Cenomanian interval (Rigaud et al., 2013). The representatives of the genus were recovered from Kimmeridgian – lower Valanginian strata in this study.

FAMILY SPIRILLINIDAE REUSS & FRITSCH, 1861

Genus *Neotrocholina* Reichel, 1956

Type species: *Neotrocholina valdensis* Reichel, 1956

Neotrocholina spp.

Pl. 2, Figs. 8, 49, 56-59

Description & Remarks: The most characteristic feature of this trochospirally coiled form is the presence of well-defined umbilical pillars. The outer wall is thicker when compared with *Coscinoconus*. Rigaud et al. (2013) discarded this genus from Trocholinidae due to the calcitic wall material. Individuals of this genus were identified from the the Tithonian – Valanginian interval in the slope to basin carbonates of Kelkit and Hozbirikyayla Formations and the Berriasian – Valanginian neritic strata of the Berdiga Formation.

FAMILY VAGINULINIDAE REUSS, 1860

Genus *Lenticulina* Lamarck, 1804

Type species: *Lenticulina rotulatus* Lamarck, 1804

Lenticulina sp.

Pl. 2, Fig. 46; Pl. 9, Fig. 14

Description & Remarks: The hyaline test is planispirally coiled, involute. The test is biconvex. Chambers somewhat rapidly increasing in size as new chambers added. *Lenticulina* sp. was recorded from the Kimmeridgian – Valanginian interval.

FAMILY HAPLOPHRAGMOIDIDAE MAYNC, 1952

Genus *Haplophragmoides* Cushman, 1910

Type species: *Nonionina canariensis* (d'Orbigny, 1839)

Haplophragmoides joukowskyi Charollais, Brönnimann & Zaninetti, 1966

Pl. 7, Figs. 7-12

1966 *Haplophragmoides joukowskyi* n. sp., Charollais, Brönnimann & Zaninetti, Pl. 2, Figs. 1, 5, 7; text-fig. 2, 3

1990 *Haplophragmoides joukowskyi* Charollais, Brönnimann & Zaninetti, Taslı, Pl. 1, Figs. 5-13

1991 *Haplophragmoides joukowskyi* Charollais, Brönnimann & Zaninetti, Altıner, Pl. 8, Figs. 1-16

2004 *Haplophragmoides joukowskyi* Charollais, Brönnimann & Zaninetti, Bucur et al., Pl. II, Figs. 13-17

2005 *Haplophragmoides joukowskyi* Charollais, Brönnimann & Zaninetti, Bucur & Sásáran, Pl. 4, Figs. 1, 2

2008 *Haplophragmoides joukowskyi* Charollais, Brönnimann & Zaninetti, Ivanova et al., 72, Fig.7I

2012 *Haplophragmoides joukowskyi* Charollais, Brönnimann & Zaninetti, Olszewska et. al., Pl. 2, Fig. 3; Pl. 10, Fig. 1

2014b *Haplophragmoides joukowskyi* Charollais, Brönnimann & Zaninetti, Bucur et al., 75, Figs. (8) u-v

2018 *Haplophragmoides joukowskyi* Charollais, Brönnimann & Zaninetti, Atasoy et al., Figs. (9) 19-22

Description & Remarks: Small agglutinated tests are planispirally coiled and involute. Test shows umbilical depressions on both sides. Aperture is an elongated equatorial slit at the base of the apertural face, can be recognized in the equatorial sections by the absence of wall material near the base of the septa. It has been

reported from the Berriasian – Valanginian interval (e.g., Altıner, 1991; Ivanova, 2000; Olszewska et al., Atasoy et al., 2018). *H. joukowskyi* were identified form the Middle Berriasian pelagic carbonates of the Hozbirikyayla Formation and the Berriasian – Valanginian strata of the neritic Berdiga Limestone.

FAMILY CORNUSPIRIDAE SCHULTZE, 1854

Genus *Meandrospira* Loeblich & Tappan, 1964

Type species: *Meandrospira washitensis* Loeblich & Tappan, 1946

Meandrospira favrei (Charollais, Brönnimann & Zaninetti), 1966

Pl. 7, Figs. 1-6

1966 *Citaella*? *favrei* n. sp., Charollais, Brönnimann & Zaninetti, Pl. 2, Figs. 3, 4; Pl. 3, Figs. 1-5; Pl.5, Figs. 1, 2; text-figs. 4-6

1988 *Meandrospira favrei* (Charollais, Brönnimann & Zaninetti), Bucur, Pl. 2, Figs. 1-3

1991 *Meandrospira favrei* (Charollais, Brönnimann & Zaninetti), Altıner, Pl. 13, Figs. 1-5

1995 *Meandrospira favrei* (Charollais, Brönnimann & Zaninetti), Bucur et al., Pl. 5, Figs. 13-15

1999 *Meandrospira favrei* (Charollais, Brönnimann & Zaninetti), Schlagintwiet & Ebli, Pl. 4, Figs. 8, 11

2004 *Meandrospira favrei* (Charollais, Brönnimann & Zaninetti), Bucur et al., Pl. 2, Figs. 18-23

2007 *Meandrospira favrei* (Charollais, Brönnimann & Zaninetti), Krajewski, Olszewska, Fig. 7B

2008 *Meandrospira favrei* (Charollais, Brönnimann & Zaninetti), Ivanova et al., Figs. (7) N, O

2010 *Meandrospira favrei* (Charollais, Brönnimann & Zaninetti), Ivanova & Kołodziej, Pl. 2, Figs. 8, 9

2012 *Meandrospira favrei* (Charollais, Brönnimann & Zaninetti), Olszewska et al., Pl. 2, Figs. 4a, b; Pl. 10, Fig. 3

2015 *Meandrospira favrei* (Charollais, Brönnimann & Zaninetti), Ivanova et al., Figs. (11) M, N

2018 *Meandrospira favrei* (Charollais, Brönnimann & Zaninetti), Atasoy et al., Figs. (9) 16, 17

Description & Remarks: Porcelaneous test is composed of a proloculus which is followed by a second undivided tube that bends back and forth in involute zigzag bends (meandering second tube). Exact equatorial sections give an impression of planispiarlly coiled multilocular specimen. Slight obliquity in a section is enough to reveal zigzag bends. The specimens were identified from the Berriasian – Valanginian and ?Hauterivian neritic strata of the Berdiga Limestone.

Genus *Turriglomina* Zaninetti in Limongi et al., 1987

Type species: *Turritellella mesotriasica* (Koehn-Zaninetti, 1969)

Turriglomina anatolica Altıner, Rettori, Zaninetti & Martini, 2001

Pl. 7, Figs. 25-28

1991 *Meandrospiranella* sp., Atıner, Pl. 13, Figs. 6-8

1991 *Meandrospiranella* n. sp., Altıner et al., p. 32 (not figured)

2001 *Turriglomina*? *anatolica* n. sp., Altıner et al., Pl. 1, Figs. 1-16

2012 *Turriglomina*? *anatolica* Altıner, Rettori, Zaninetti & Martini, Petrova et al., Fig. (8) 16

2017 *Turriglomina*? *anatolica* Altıner, Rettori, Zaninetti & Martini, Fekete et al., Fig. 5C

Description & Remarks: The meandrospirid spherical initial stage is followed by a second undivided tubular chamber that shows a helicoidal and close-coiled high spire (forming a columella). The wall is porcelaneous. The aperture is simple, at the end of tube.

FAMILY CUNEOLINIDAE SAIDOVA 1981

Genus *Akcaya* Özdikmen, 2009

Type species: *Textulariella minuta* Hofker, 1965

Akcaya minuta (Hofker, 1965)
Pl. 7, Figs. 13, 14

1965 *Textulariella minuta* n. sp., Hofker, Pl. III, Figs. 5, 6; Pl. IV, Figs. 1-9

1965 *Sabaduia minuta* n. gen., comb. (Hofker), Charollais & Brönnimann, Figs. 1-4

1965 *Sabaduia minuta* (Hofker), Charrollais et al., Pl. 1, Figs. 1-7

1980 *Sabaduia minuta* (Hofker), Arnaud-Vanneau, Figs. 191, 192; Pl. 8, Figs. 15, 16; Pl. 16, Figs. 6-13

2004 *Sabaduia* cf. *minuta* (Hofker), Bucur et al., Pl. III, Fig. 21

2013 *Sabaduia minuta* (Hofker), Schlagintweit, Fig. 2i

2016 *Akcaya minuta* (Hofker), Schlagintweit et al., Figs. (6) G, J

Description & Remarks: The test is conical with flattened base. Small initial trochospiral stage is double-walled, inner microgranular and outer hyaline. Later it passes into biserial stage. Biserial chambers are partially divided by numerous vertical subepidermal partitions (beams), secondary horizontal partitions (rafters) are also present. The wall of the biserial stage is agglutinated and imperforate. Aperture is interiomarginal slit.

Rare individuals of this taxon were recovered from the Valanginian strata of the Berdiga Limestone.

FAMILY BARKERINIDAE FRIZZELL & SCHWARTZ 1950

Genus *Barkerina* Frizzell & Schwartz, 1950

Type species: *Barkerina barkerensis* Frizzell & Schwartz, 1950

Barkerina dobrogiaca Neagu, 2000
Pl. 7, Figs. 16-20

1987 *Barkerina* sp., Bergougnan, Figs. 83, 85, 86

1990 *Barkerina barkerensis* Frizzell & Schwartz, Taslı, Pl. 3, Figs. 1-6

2000 *Barkerina dobrogiaca* n. sp., Neagu, Figs. 3e-g; Pl. 7, Figs. 1-33; Pl. 9, Fig. 4

2002 *Barkerina* cf. *barkerensis* Frizzell & Schwartz, Taslı & Eren, Figs. (9) A1, A2

2004 ?*Barkerina* sp. 1, Bucur et al., Pl. 2, Figs. 1-12

2008 *Barkerina*? sp., Koch et al., Fig. (11) 8 pars.

2019 *Barkerina dobrogiaca* Neagu, Schlagintweit et al., Figs. 3, 4

2020b *Barkerina dobrogiaca* Neagu, Granier, Figs. (4) 19-22, 23 pars., 24-27, 41-43

Description & Remarks: The test outline is globular (oval), compressed vertically (axial diameter>equatorial diameter) and biumblicate. Coiling is involute, planispiral. Aperture consists of row of openings near the base of septa. Wall is simple, microgranular. Thin septula are present with preseptal passages.

The individuals of this taxon were recovered from the Berriasian – Valanginian strata of the Berdiga Limestone.

FAMILY MONTSALEVIIDAE ZANINETTI, SALVINI-BONNARD, CHAROLLAIS & DECROUEZ, 1987

Genus *Montsalevia* Zaninetti, Slavini-Bonnard, Charollais & Decrouez, 1987

Type species: *Montsalevia elavata* Zaninetti, Salvini-Bonnard, Charollais & Decrouez, 1987

Montsalevia salevensis (Charollais, Brönnimann & Zaninetti, 1966)
Pl. 17, Figs. 21-34; 29, 30

1966 *Pseudotextularia salevensis* n. sp., Charollais, Brönnimann & Zaninetti, Pl. 1, Figs. 1-5; Pl. 2, Figs. 2, 6; text-fig. 1

1987 *Montsalevia salevensis* n. gen. (Charollais, Brönnimann & Zaninetti), Zaninetti, Salvini-Bonnard & Decrouez, p. 166

1990 *Cuneolina hensoni* Dalbiez, Taslı, Pl. 15, Fig. 18

1990 *Pseudotextulariella salevensis* Charollais, Brönnimann & Zaninetti, Taslı, Pl. 16, Figs. 1, 3-6, Figs. 9-11

1991 *Montsalevia salevensis* (Charollais, Brönnimann & Zaninetti), Altıner, Pl. 11, Figs. 1-23

1995 *Montsalevia salevensis* (Charollais, Brönnimann & Zaninetti), Bucur et al., Pl. IV, Figs. 11-15

2004 *Montsalevia salevensis* (Charollais, Brönnimann & Zaninetti), Bucur et al., Pl. III, Figs. 1-5

2005 *Montsalevia salevensis* (Charollais, Brönnimann & Zaninetti), Bucur & Sásáran, Pl. 4, Figs. 3-8

2007 *Montsalevia salevensis* (Charollais, Brönnimann & Zaninetti), Krajewski & Olszewska, 298, Fig. 5K

2010 *Montsalevia salevensis* (Charollais, Brönnimann & Zaninetti), Ivanova & Kolodziej, Pl. 2, Fig. 10

2014 *Montsalevia salevensis* (Charollais, Brönnimann & Zaninetti), Bucur et al., 78, Figs. (8) j-r

2018 *Montsalevia salevensis* (Charollais, Brönnimann & Zaninetti), Atasoy et al., Fig. (9) 23

2019 *Montsalevia* gr. *salevensis* (Charollais, Brönnimann & Zaninetti), Granier, Figs. (4) H-M; Figs. (5) D-F; Figs. (9) H-K; Figs. (16) J-N, O, P; Figs. 19R

2020b *Montsalevia* gr. *salevensis* (Charollais, Brönnimann & Zaninetti), Granier, Figs. (4) 28-40.

Description & Remarks: Test is conical, small. Trochospiral initial stage is followed by biserially arranged portion. Chambers additionally are subdivided by exoskeletal beams that can be easily seen in transverse sections, and tangential sections. These beams only appear in the adult chambers. Aperture is an

interiomarginal slit. Wall is microgranular. The specimens of this taxon were recovered from the Valanginian strata of the Berdiga Limestone.

FAMILY COSKINOLINIDAE MOULLADE 1965

Genus *Pseudolituonella* Marie, 1954

Type species: *Pseudolituonella reicheli* Marie, 1954

Pseudolituonella gavonensis Foury, 1968
Pl. 8, Figs. 13, 20-24

1968 *Pseudolituonella gavonensis* n. sp., Foury, Pl. 19, Figs. 11-15

1980 *Pseudolituonella gavonensis* Foury, Arnaud-Vanneanu, Pl. 55, Fig. 7; Pl. 84, Figs. 5, 7

1990 *Pseudolituonella* sp.A, Taslı, Pl. 17, Figs. 9-12

1995 *Pseudolituonella gavonensis* Foury, Bucur et al., Pl. V, Figs. 1, 2

2004 *Pseudolituonella gavonensis* Foury, Bucur et al., Pl. IV, Figs. 4, 8

Description & Remarks: The test is elongated conical. Early stage includes a short trochospiral portion, later stage with broad and low uniserial chambers. Wall is microgranular, imperforate. Aperture is cribrate, consisting of numerous large circular pores in the center of the apertural face.

This taxon was observed from the Valanginian strata of the Berdiga Limestone.

FAMILY TROCHAMMINIDAE SCHWAGER 1877

Genus *Patellovalvulina* Neagu, 1975

Type species: *Patellovalvulina patruliusi* Neagu, 1975

Patellovalvulina patruliusi Neagu, 1975
Pl. 8, Figs. 28-38

1975 *Patellovalvulina patruliusi* n. sp., Neagu, Fig. 10; Pl. XVI, Figs. 1-11; Pl. XVII, Figs. 1-13; Pl. XXVI, Figs. 1, 2

1980 *Patellovalvulina patruliusi* Neagu, Arnaud-Vanneau, Fig. 168; Pl. 54, Fig. 6; Pl. 83, Figs. 1-5, 6?;

1990 "*Valvulammina*" sp.A, Taslı, Pl. 18, Figs. 2-9

1995 *Patellovalvulina patruliusi* Neagu, Bucur et al., Pl. 5, Fig. 16

2015 *Patellovalvulina patruliusi* Neagu, Ivanova et al., Figs. (9)

2020b *Patellovalvulina patruliusi* Neagu, Granier, Fig. (4) 6

Description & Remarks: The test covexo-concave trochospire. Few chambers per whorl. Chambers are low and broadly arcuate, strongly overlapping at the periphery. Chamber interior is simple, undivided. Wall is finely agglutinated. Aperture is interiomarginal slit.

This taxon was observed from the Valanginian strata of the Berdiga Limestone.

5.3 4.3. Taxonomy of *Incertae sedis*, annelids and crinoids

INCERTAE SEDIS (Microproblematica)

Genus *Lithocodium* Elliott, 1956

Type species: *Lithocodium aggregatum* Elliott, 1956

Lithocodium aggregatum Elliott, 1956

Pl. 3, Figs. 3-6; Pl. 10, Figs. 10, 15, 16

1956 *Lithocodium aggregatum* n. sp., Elliott, Pl. 1, Figs., 2, 4, 5

1971 *Lithocodium aggregatum* Elliott, Basson & Edgell, Pl. 1, Fig. 1

1996 *Lithocodium aggregatum* Elliott, Schmid & Leinfelder, 22, Figs. 1, 2; 27, Fig. 3; 28, Fig. 4; Pl. 1, Fig.d 1-6; 36, Fig. 6; Pl. 2, Figs. 1-5

2007 *Lithocodium aggregatum* Elliott, *Bacinella irregularis* Radoičić – *Lithocodium aggregatum* Elliott, Bucur et al., Pl. 3, Fig. 4; Pl. 7, Fig. 3

2010 *Lithocodium aggregatum* Elliott, Bucur et al., Pl. 1, Figs. 4, 5

2013 *Lithocodium aggregatum* Elliott, Pleş et al., 36, Figs. (11) a-d

2014 *Lithocodium aggregatum* Elliott, Kaya & Altıner, Pl. 3, Fig. 3

2015 *Lithocodium aggregatum* Elliott, Kaya & Altıner, Figs. (5) d-f

2015 *Lithocodium aggregatum* Elliott, Pleş et al., 51, Fig. (4) i

2018 *Lithocodium aggregatum* Elliott, Atasoy et al., Figs. (11) 19, 20

Description & Remarks: This encrusting organism is characterized by micritic crust that bears cavities along it that look like alveolar structures. *Lithocodium aggregatum* is mostly found in association with *Troglotella incrustans* and bacinellid structures. This encruster was identified from the Kimmeridgian and Berriasian pelagic successions (Kelkit Formation and Hozbirikyayla Formation) and from the Kimmerdgian and Berriasian – Valanginian neritic carbonates (Berdiga Limestone) in this study.

Genus *Koskinobullina* Cherchi & Schroeder, 1979

Type species: *Koskinobullina socialis* Cherchi & Schroeder, 1979

Koskinobullina socialis Cherchi & Schroeder, 1979

Pl. 3, Figs. 16-17

1979 *Koskinobullina socialis* n. sp., Cherchi & Schroeder, Pl. 1

1991 *Koskinobullina socialis* Cherchi & Schroeder, Altıner, Pl. 5, Figs. 30, 31

1999 *Koskinobullina socialis* Cherchi & Schroeder, Schlagintweit & Ebli, Pl. 5, Fig. 7; Pl. 11, Fig. 10

2007 *Koskinobullina socialis* Cherchi & Schroeder, Schlagintweit & Gawlick, Fig. 7l

2013 *Koskinobullina socialis* Cherchi & Schroeder, Pleş et al., 34 ,Fig. 10 e-h

2014 *Koskinobullina socialis* Cherchi & Schroeder, Kaya & Altıner, Pl. 3, Fig. 5

2015 *Koskinobullina socialis* Cherchi & Schroeder, Kaya & Altıner, Figs. (4) n, o

2018 *Koskinobullina socialis* Cherchi & Schroeder, Atasoy et al., Figs. (11) 21, 23

Description & Remarks: *Koskinobullinas socialis* is characterized by superimposed assemblages of hemispherical chambers with calcitic walls that bear irregular pores. It was recoderd from the Tithonian – lower Berriasian pelagic rocks of the Hozbirikyayla Formation in this study.

Genus *Crescentiella* Senowbari-Daryan, Bucur, Schlagintweit, Săsăran & Matyszkiewicz 2008

Type species: *Tubiphytes morronensis* Crescenti, 1969

Crescentiella morronensis (Crescenti, 1969)

Pl. 3, Figs. 7-9; Pl. 4, Fig. 20

1969 *Tubiphytes morronensis* n. sp., Crescenti, 35-37, Figs. 10, 20-22

1991 *Tubiphytes morronensis* Crescenti, Altıner, Pl. 6, Figs. 4-8

2008 *Crescentiella morronensis* (Crescenti), Senowbari-Daryane et al., Pl. 1, Figs. a-i; 193, Figs. a-h; Pl. 3, Figs. a-g; Pl. 3, Figs. a-h; Pl. 5, Figs. a-h; Pl. 6, Figs. a-h; Pl. 7, Figs. l-e

2012 *Crescentiella morronensis* (Crescenti), Olszewska et al., Pl. 6, Fig. 1; Pl. 16, Fig. 2

2013 *Crescentiella morronensis* (Crescenti), Pleş et al., 26, Figs. (6) d, e; 28, Fig. 7a; 34, Figs. (10) a-d

2015 *Crescentiella morronensis* (Crescenti), Kaya & Altıner, Figs. (4) g-l

2016 *Crescentiella morronensis* (Crescenti), Okay & Altıner, Fig. (5) 29

2018 *Crescentiella morronensis* (Crescenti), Atasoy et al., Figs. (8) 11-15

2023 *Crescentiella morronensis* (Crescenti), Bucur & Lăzar, Figs. (8) a-i

Description & Remarks: The most characteristic feature of *C. morronensis* is the dark micritic envelopes and the general outline having a tube-like shape. This encruster may have foraminifera with amphorellid chambers or any other type of clasts in the cortex. The envelope may include any kind of encrusted clasts.

The stratigraphic range covers the Oxfordian – Berriasian interval and this species shows an acme in the Kimmeridgian – Tithonian inteval (Pleş et al. 2013). Altıner (1991) used this taxon as a Kimmeridgian-base index fossil in his biozonations. It was recorded from the Kimmeridgian – Berriasian interval in the slope to basin deposits (Hozbirikyayla Formation) and from the Kimmeridgian strata in the platform carbonates (Berdiga Limestone).

Genus *Perturbatacrusta* Schlagintweit & Gawlick, 2011

Type species: Perturbatacrusta leini Schlagintweit & Gawlick, 2011

Perturbatacrusta leini Schlagintweit & Gawlick, 2011
Pl. 3, Fig. 18

2011 *Perturbatacrusta leini* n. sp., Schlagintweit & Gawlick, 129, Figs. (5) c, d, g, h; 132, Figs. (7) a-g

2013 *Perturbatacrusta leini* Schlagintweit & Gawlick, Pleş et al., 26, Fig. 6d; 38, Figs. (12) a-d

2014 *Perturbatacrusta leini* Schlagintweit & Gawlick, Kaya & Altıner, Pl. 3, Fig. 7

2015 *Perturbatacrusta leini* Schlagintweit & Gawlick, Kaya & Altıner, Figs. (5) g, h

Description & Remarks: *Perturbatacrusta leini* differs from *Radiomura cautica* by its interconnected tubes and lateral closed tubes. *P. leini* was identified from the Tithonian – Berriasian interval in this study in the slope to basin successions (Hozbirikyayla Formation).

Genus *Iberopora* Granier & Berthou, 2002

Type species: *Iberopora bodueri* Granier & Berthou, 2002

Iberopora bodueri Granier & Berthou, 2002
Pl. 3, Figs. 1, 11-15

2002 *Iberopora bodueri* n. gen., n. sp., Granier & Berthou, Pl. 2, Figs. 2-4

2003 *Iberopora bodueri* Granier & Berthou, Uta & Bucur, Pl. 3, Fig. 4

2004 *Iberopora bodueri* Granier & Berthou, Schlagitnweit, Pl. 1, Figs. 1-6; Pl. 2, Figs. 4-7

2005 *Iberopora bodueri* Granier & Berthou, Bucur et al., Pl. 5, Figs. 6-8, 11, 12

2013 *Iberopora bodueri* Granier & Berthou, Pleş et al., Figs. 10f, 14h

2014 *Iberopora bodueri* Granier & Berthou, Kaya, Pl. 17, Figs. 1, 2

2015 *Iberopora bodueri* Granier & Berthou, Kaya & Altıner, Fig. 4m

Description & Remarks: The tiny, bubble-like superimposed cells of *Iberopora bodeuri* are arranged in layers parallel to the substrate, forming the organism's skeleton. Each cell is surrounded by a thin micritic envelope, with no connections between neighboring or overlapping cells. Thin sparitic layers, which are more or less regularly interspersed with the skeleton, are also observed.

The broken individuals of this taxon were observed from the Tithonian – Lower Berriasian slope to basin successions of the Hozbirikyayla Formation in this study.

Genus *Globochaete* Lombard, 1945

Type species: Globochaete alpina Lombard, 1945

Globochaete sp. Lombard, 1945
Pl. 1, Figs. 80-81

Description & Remarks: *Globochaete* is characterized by kidney-shaped, spherical calcite bodies that has micritic nucleus. They may show serial arrangement, occur in clusters. They may attach to calcitic plates. They are abundant in Late Jurassic deep waters (Brönnimann, 1965; Skompski 1982; Altıner, 1991; Flügel, 2010) and attributed to a planktonic single-celled green algae (Skompski 1982). *Globochaete*

is observed from the Kimmeridgian – Valanginian interval in this study in the slope to basin successions.

Genus *Cayeuxia* Frollo, 1938

Type species: Cayeuxia piae Frollo, 1938

Cayeuxia sp. Frollo, 1938
Pl. 3, Fig. 10, Pl. 10, Fig. 7

Description & Remarks: *Cayeuxia* is characterizd by parallel tubes showing radial branching in longitudinal sections. This taxon has been attributed to calcareous algae and calcimicrobes (Basson & Edgell, 1971; Flügel, 2010). Representative individuals were recovered from the Kimmeridgian – Tithonian interval in this study in the slope to basin successions.

PHYLUM ANNELIDA LAMARCK, 1802

FAMILY TEREBELLIDAE JOHNSTON, 1846

Genus *Terebella* Linnaeus, 1767

Type species: *Terebella lapidaria* Linnaeus, 1767

Terebella lapilloides Münster, 1833
Pl. 3, Figs. 26-28

1833 *Terebella lapilloides* n. sp., Münster, Pl. 71, Fig. 16

1993 *Terebella lapilloides* Münster, Leinfelder et al., Pl. 41, Figs. 1, 3

1996 *Terebella lapilloides* Münster, Schmid, 204 – 205, Fig. 74

1999 *Terebella lapilloides* Münster, Schlagintweit and Ebli, Pl. 1, Fig. 5; Pl. 2, Fig. 6; Pl. 12, Figs. 6-11

2008 *Terebella lapilloides* Münster, Schlagintweit & Gawlick, Fig. 13a

2011 *Terebella lapilloides* Münster, Krajewski et al., Fig. 4B

2014 *Terebella lapilloides* Münster, Kaya & Altıner, Pl. 1, Figs. 1-16; Pl. 2, Figs. 1-8; Pl. 3, Fig. 1

2018 *Terebella lapilloides* Münster, Atasoy et al., Figs. (11) 5-10

2020 *Terebella lapilloides* Münster, Kietzmann & Llanos, Figs. (8) a-i

2023 *Terebella lapilloides* Münster, Bucur & Lăzar, Figs. (8) j-n

2024 *Terebella lapilloides* Münster, Kołodziej et al., Figs. (13) A-L

Description & Remarks: *Terebella lapilloides* is an annelid with an agglutinated tube that is common in Late Jurassic reefal, fore-reef and slope environments (Leinfelder et al., 1993; Kaya & Altıner, 2014). The worm tubes belong to this species were identified from the latest Tithonian – earliest Berriasian interval in this study in the slope to basin successions.

FAMILY SERPULIDAE Rafinesque, 1815

Genus *Mercierella* Fauvel, 1923

Type species: *Mercierella enigmatica* Fauvel, 1923

Mercierella ? *dacica* Münster, 1833

Pl. 3, Fig. 24-25; Pl. 10, Fig. 12

(For synonyms before the year 1998 see Mišík et al. 1999)

1966 *Mercierella* ? *dacica* n. sp., Dragastan, 148, Fig. 1; 149, Fig. 2

1991 *Mercierella* ? *dacica* Dragastan, Altıner et al., not illustrated

1999 *Mercierella* ? *dacica* Dragastan, Mišík et al. 1999, Pl. 1, Figs. 1-11

2001 *Mercierella* ? *dacica* Dragastan, Såsåran et al., Pl. 10, Fig. 1

2005 *Mercierella* ? *dacica* Dragastan, Dragastan et al., not illustrated

2010 *Mercierella* ? *dacica* Dragastan, Bucur et al., not illustrated

2018 *Mercierella* ? *dacica* Dragastan, Atasoy et al., Figs. (11) 1-4

Description & Remarks: *Mercierella dacica* is characterized by a microgranular tube, open at both ends, with unequally spaced collars (3 collars according to Mišík et al. 1999). The generic name has a question mark in the literature (and here) due to the fact that Fauvel (1923) described this genus from brackish water limestones however, *M. dacica* has been found in generally platform margin environments (fore-reef, slope, outer shelf), associated with calpionellids, *Crescetiella morronensis* and *Mohlerina basiliensis* (Dragastan, 1966; Miík et al., 1999; Såsåran et al., 2001; Dragastan et al., 2005; Bucur et al., 2010) which is the same case in this study.

It is nearly impossible to differentiate oblique sections and incomplete tubes of *M. dacica* from *Aeolisaccus* or *Earlandia* in thin sections. Unlike *Earlandia*, *Aeolisaccus* and *Mericierella* do not have a proloculus and a second tubular chamber. They are characterized by a microgranular tube with open ends. *Mercierella* differs from *Earlandia* in having collars diverging from the wall of the tube in irregularly spaced intervals.

This species has been identified from the Kimmeridgian – Berriasian interval (Miík et al., 1999; Dragastan et al., 2005). In this study *Mercierella* ? *dacica* was identified

from the Kimmeridgian to lowermost Valanginian strata of the slope to basin successions.

Genus *Carpathiella* Mišík, Soták, & Ziegler, 1999

Type species: *Carpathiella triangulata* Mišík, Soták, & Ziegler, 1999

Carpathiella perforata Mišík, Soták, & Ziegler, 1999

Pl. 3, Fig. 19

1995 Worm tube, Mišík, Pl. III, Figs. 5, 6

1999 *Carpathiella perforata* n. gen., n. sp., Mišík, Soták, & Ziegler, Pl. III, Figs. 1-3

2003 *Carpathiella perforata* Mišík, Soták, & Ziegler, Schlagintweit et al., Fig. 4; Pl. 4., Figs. 1-3

2018 *Carpathiella* sp. Mišík, Soták, & Ziegler, Atasoy et al., Fig. (11) 12

Description & Remarks: Thick calcitic tube. Triangular outline with rounded corners in transverse sections that reveal 1 to 3 voids in the tube wall other than the main central void.

This taxon was observed as resedimented bioclasts within the Tithonian and Berriasian slope-to-basin deposits in this study.

Carpathiella triangulata Mišík, Soták, & Ziegler, 1999

Pl. 3, Fig. 20, 21, 23

1981 Worm tube, Mišík & Sỳkora, Pl. IX, Fig. 9

1999 *Carpathiella triangulata* n. gen., n. sp., Mišík, Soták, & Ziegler, Pl. II, Figs. 3-9

2003 *Carpathiella triangulata* Mišík, Soták, & Ziegler, Schlagintweit et al., Figs. 2, 3; Pl. 4., Figs. 4-12

2018 *Carpathiella* sp. Mišík, Soták, & Ziegler, Atasoy et al., Fig. (11) 11, 15

Description & Remarks: The triangular tube, with two rounded corners and a more acute corner, consists of one layer and sometimes a thin dark micritized rim on its outer and rarely also in its inner side. In some specimens the wall can exhibit alternating dark and light layering.

This taxon was recorded as resedimented bioclasts within the Tithonian and Berriasian slope-to-basin deposits in this study.

Carpathiella plassenensis Schlagintweit & Gawlick, 2002

Pl. 3, Fig. 22

2002 *Carpathiella plassenensis* n. sp., Schlagintweit & Gawlick, Figs. (1) 1, 2

2003 *Carpathiella plassenensis* Schlagintweit & Gawlick, Schlagintweit et al., Fig. 5; Pl. 1., Figs. 1, 2, 4-6, 8; Pl. 2, Figs. 1-12; Pl. 3, Figs. 1-8

2018 *Carpathiella* sp. Mišík, Soták, & Ziegler, Atasoy et al., Fig. (11) 14

Description & Remarks: Thick, U-shaped, calcareous unilocular tube appears as two ovel (to elongated) separate tubes in transverse sections. The calcitic wall can exhibit dark layers as in the case with *C. triangulata*.

This taxon was recorded as resedimented bioclasts within the Tithonian and Berriasian slope-to-basin deposits in this study.

ClASS CRINOIDAE MILLER, 1821

FAMILY SACCOCOMIDAE D'ORBIGNY, 1852

Genus *Saccocoma* Agassiz, 1853

Saccocoma sp.

Pl. 2, Figs. 61-68

Description & Remarks: In thin sections, they are recognized by their characteristic antler-shaped calcitic structures (facetalia and brachilia). This pelagic crinoid was placed under different genera by several authors like *Eothrix* (by Lombard, 1945) and *Lombardia* (by Brönniman, 1965). They range from Middle Oxfordian to latest Tithonian (Nicosia & Parisi, 1979; Kroh & Lukeneder, 2009). *Saccocoma* shows important abundance in the Tithonian which was used as a possible base-Tithonian marker event in several studies (Nicosia & Parisi, 1979; Altıner, 1991; Skourtis-Coroneou & Solakius, 1999). This pelagic crinoid has generally been considered as Middle to Late Jurassic – confined taxon that did not extend into the Berriasian in the literature, but *Saccocoma* was identified from Tithonian – earliest Berriasian interval in this study. This anomaly can be explained by the different interpration of the J-K boundary.

CHAPTER 6

DISCUSSION AND CONCLUSION

The Eastern Pontides with its Upper Jurassic – Lower Cretaceous neritic and pelagic carbonate successions cropping out in close proximity to each other provides a suitable geological setting for research on the problematic Upper Jurassic – Lower Cretaceous chronostratigraphy spanning the only unstandardized Mesozoic system boundary, i.e. the Jurassic/ Cretaceous (J/K) boundary. The study area is composed of 3 main regions located on different tectonic units broadly representing different depositional environments on the eastern part of the Pontides Carbonate Platform (PCP).

In the Ağören region, a continuous stratigraphic section was measured and sampled at regular intervals, located on the İmalıdağ thrust sheet. A total of 294 samples were collected along the 589-meter-long section. This succession represents the basinal clastic and carbonate deposits of the eastern PCP. In the Ozansu region, located in the Aşutka thrust sheet, two stratigraphic sections were logged (OA & OB measured sections). The OA section is measured 236 m long, with 201 samples were taken along the section. These succesions are located on the slope to basin depositional environment of the eastern PCP. Another section was measured in the Nazlıçayır region located in the relative autochthonous unit of the Eastern Pontides. Throughout this shallow marine sequence of the eastern PCP, a total of 6 stratigraphic sections were measured. Abundant key beds (e.g., basalt levels, counting layers above and below this basalt and checking facies for lateral shifts, tracking thick characteristic dolomitic intervals or distinctive limestone layers laterally), which allow for lateral shifts at levels where outcrop conditions worsen in the region, thereby facilitating reliable correlation and continuous measurements in more accessible outcrop areas,

have enabled the production of a composite stratigraphic section with a total thickness of 350 meters. Along this section, a total of 161 rock samples were collected. Fossil content and constituent composition of each sample were documented and in the light of obtained data, biostratigraphical framework was constructed and microfacies types and depositional environments were determined.

A variety of fossil groups (e.g., foraminifers, calpionellids, microencrusters, crinoids) were used for the construction of the biostratigraphical zonations. 7 zones and 9 subzones were differentiated for the deep marine succsessions of the Ağören and Ozansu measured sections: *Crescentialla morronensis* Zone (Kimmeridgian – lower Tithonian), *Saccocoma* subzone (lower Tithonian), *Protopeneroplis ultragranulata* Zone (middle – upper Tithonian), *Crassicollaria* Zone (uppermost Tithonian), *massutiniana* subzone (uppermost Tithonian), *Calpionella* (*alpina*, *Remaniella* and *elliptica* subzones) Zone (lower Berriasian), *Calpionellopsis* (*simplex* and *oblonga* subzones) Zone (upper Berriasian), and *Calpionellites* (*Calpionellites – oblonga* E1 subzone) Zone and an overlying "Radiolaria" Zone (?Hauterivian). 4 zones and 2 subzones were differentiated in the shallow marine strata of the Nazlıçayır Section: *Crescentiella morronensis* (*Mesoendothyra izjumiana – Alveosepta jaccardi* subzone) Zone (Kimmeridgian), *Meandrospira favrei – Haphlophragmoides joukowskyi – Protopeneroplis ultragranutala* Zone (upper Berriasiabn – lowermost Valanginian), *Barkerina dobrogiaca* subzone (lower Valanginian), *Montsalevia salavensis* (middle – upper Valanginian) and *Meandrispira favrei – Haphlophragmoides joukowksyi* Zone (lower Hauterivian).

Additionally, a fossil data from 17 stratigraphical sections with basinal, marginal-slope and shallow marine facies from the PCP is synthesized to construct a comprehensive dataset that ranges the Oxfordian–Hauterivian interval which is dominated by unstandardized stages and includes the only remaining Mesozoic system boundary without a GSSP i.e., the J/K boundary. This dataset is composed of 69 taxa (and 139 bioevent datums) from varieties of depositional environments (i.e., benthic and planktonic foraminifers, calpionellids, algae, microencrusters and crinoids). To eliminate facies controlled bioevents and local ranges and to calibrate

pelagic and shallow marine fossil datums from unrelated lineages, the quantitative biostratigraphical approaches of the Graphic Correlation Method (GCM) and the Unitary Association Method (UAM), corresponding to two classical biostratigraphical approaches; the zonations based on first occurrence (FO)/ last occurrence (LO) events (i.e., interval zones) and the zonations based on assemblages (i.e., Oppel zones), respectively, are used for data treatment. Calibrated to the Geological Time Scale 2020 (GTS 2020), the Pontides Carbonte Platform Composite Standard Reference Section (PCP-CSRS) obtained from the GCM provide correlation lines with wide lateral traceability regardless of the facies present as long as a number of common taxa, that allow reliable correlation with the PCP-CSRS, is present. The order and relative positions of the bioevent datums from deep and shallow marine deposits are calibrated with respect to the stage boundaries. The UAM provides 15 unitary associatons (UAs) which are differentiated by fossil assemblages. To strengthen lateral applicability, some of the UAs are merged according to their fossil assemblage similarities and resulted in 12 unitary association zones (UAZs) of strictly different maximal sets of fossil assemblages with solid superpositional control.

Correlation among the GCM and the UAM shows important diachronism. Having zonation philosophy of Oppel in its algorithm, the UAM tries to construct assemblage zones that are not subsets of the bounding assemblages without any concern regarding the order of bioevents within each UAZs. This creates many disagreements with the correlation lines from the bioevent-datum-based GCM. The UAM seems to have drawbacks in applications with mixed fauna from varieties of facies and unrelated lineages. The UAZs with the highest lateral traceability are composed of taxa from platform margins that can be readily intercalated with shallow marine and slope to basin deposits.

The important key fossils for calibration of the deep and shallow marine succession of the Late Jurassic–Early Cretaceous interval include *Alveosepta jaccardi*, *Coscinoconus alpinus*, *C. campanellus*, *C. cherchiae*, *C. delphinensis*, *C. elongatus*, *C. sagittarius*, *Coscinophragma cribrosum*, *Haplophragmoides joukowskyi*,

Labyrinthina mirabilis, *Meandrospira favrei*, *Mesoendothyra izjumiana*, *Mohlerina basiliensis*, *Montsalevia salevensis*, *Protopeneroplis striata*, *P. ultragranulata*, and *Pseudocyclammina lituus* among the benthic foraminifers and the microencruster *Crescentiella morronensis* (Fig. 6.1). Placing the Pontides stratigraphical sections in a chronostratigraphic chart obtained from the GCM reveals major diachronisms for most of the FOs of index fossils within individual successions. *P. ultragranulata* has the most stable chronostratigraphic position for its base both in the pelagic and the shallow marine sections from the Pontides compared to other benthics.

The base of the Kimmeridgian can be approximated by the FOs of *Kastamonina abanica* and *Labyrinthina mirabilis* shallow marine foraminifers (Fig. 6.1). The FO of *Campbelliella striata* algae provides a good approximation for the Upper Kimmeridgian in neritic environments (Fig. 6.1).

The LO of *Alveospeta jaccardi* presents bioevent datum as indicator of the Tithonian base in shallow marine settings (Fig. 6.1). The onset of the second acme of saccocomids can provide an approximation for this level in pelagic successions (Fig. 6.1). *Anchispirocyclina lusitanica*, considered as a good marker for the base of Tithonian, has elevated first appearance in the Pontides.

Coscinophragma cribrosum and *Protopeneroplis ultragranulata* successively appeared in the mid-Tithonian well below the base of the latest Tithonian Chitinoidellid Zone (Fig. 6.1). *Mesoendothyra izjumiana* has LO level just below this zone. *Protopeneroplis striata* disappeared within the highest level of the Chitinoidellid Zone (Fig. 6.1). *Coscinoconus delphiniensis* has a FO datum in the middle part of this same zone. These benthic foraminifers can be found both in the back-reef shallow marine and the fore-reef slope deposits (Fig. 6.1). *Kastamonina abanica* has LO within the lowest part of the Chitinoidellid Zone in the shallow marine deposits (Fig. 6.1).

Calpionella alpina acme is the marker for the T/B boundary in the pelagic successions. *Crassicollaria intermedia* and *Calpionella elliptalpina* have successive LOs just below the T/B boundary. *Calpionella grandalpina*, *Crassicollaria brevis*

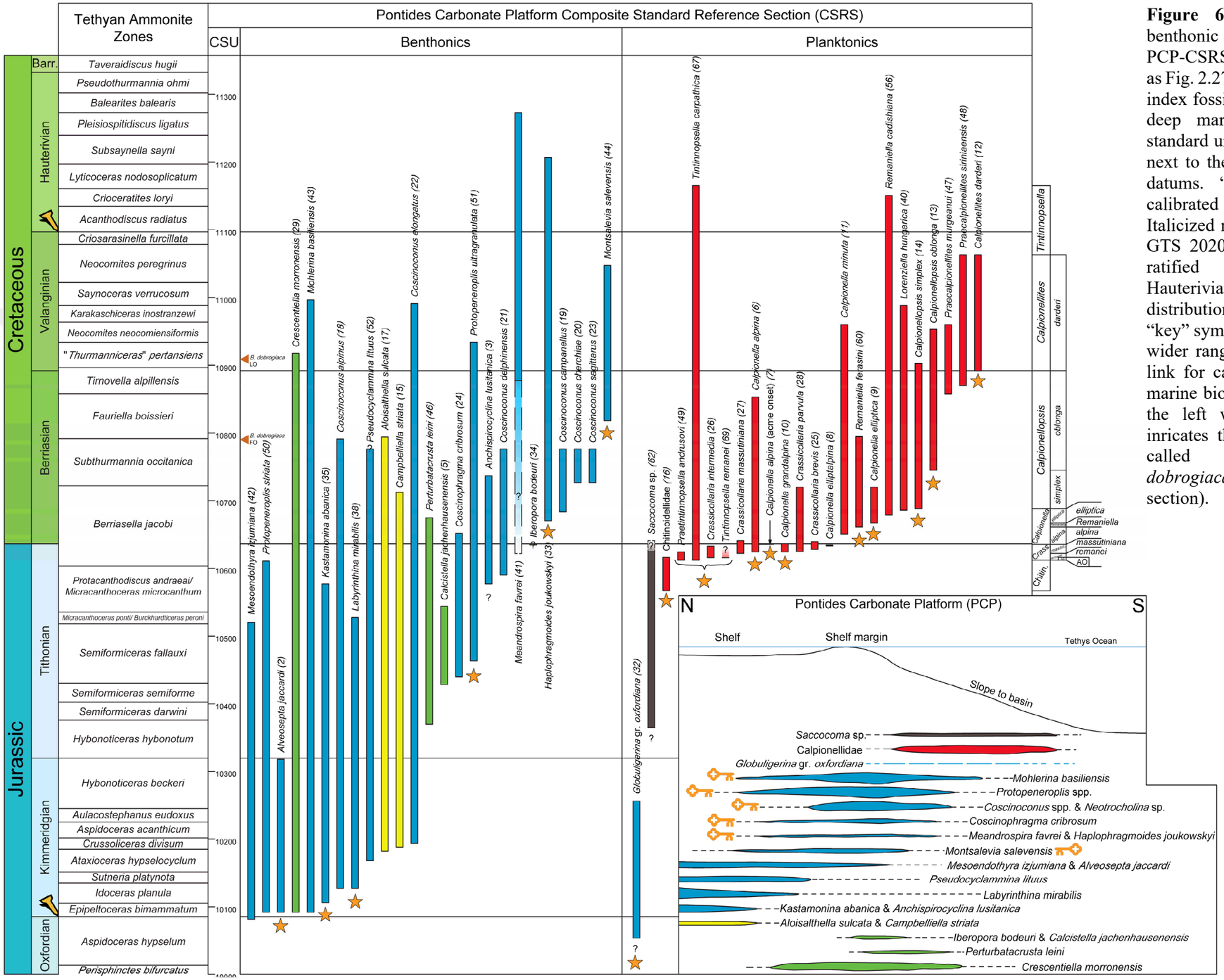

Figure 6.1. Summary of the important benthonic and planktonic fossil ranges in the PCP-CSRS. Colors and taxa codes are the same as Fig. 2.27. Stars below the range bars indicate index fossils used in the previous shallow and deep marine zonations. CSU: Composite standard units. Calpionellid zonations inserted next to the range chart based on calpionellid datums. "Tethyan Ammonite Zones" are calibrated from the GTS 2020 and TSC 8.0. Italicized names are used as suggested by the GTS 2020. The "Golden Spikes" marks the ratified bases of Kimmeridgian and Hauterivian. The inlet illustrates the facies distribution of the taxa along the PCP. The "key" symbol indicates the critical taxa having wider range of occurrence and providing the link for calibration of the shallow and deep marine bioevents. The small orange arrows at the left wall of the "Benthonic" column inricates the FO and LO datums of the so-called Valanginian-marker *Barkerina dobrogiaca* in the Eastern Pontides (Nazlıçayır section).

and *Crassicollaria massutiniana* crossed the boundary with major decline in population and got extinct in the earliest Berriasian (Fig. 6.1). The saccocomid facies is replaced by the calpionellid facies toward the T/B boundary in basinal successions. Among the microencrusters, the LOs of *Perturbatacrusta leini* and *Iberopora bodeuri* seem to provide biohorizons close to the T/B boundary in marginal carbonates and can provide datums for slope and peri-reefal deposits (Fig. 6.1). *Campbelliella striata* seems to have crossed the T/B boundary and disappeared in the early Berriasian. *Aloisalthella sulcata* has LO datum in the middle Berriasian. These two algae provide LO datums indicating the early – middle Berriasian interval in the shallow marine deposits (Fig. 6.1). The FO of *Haplophragmoides joukowskyi* and the LO of *Anchispirocyclina lusitanica* are in the earliest and early Berriasian, respectively. Both benthic foraminiferal biohorizons can provide approximations for the early Berriasian in the shallow marine deposits (Fig. 6.1). *H. joukowskyi* is also present in the marginal to slope carbonates and can also provide criterion in those relatively deeper marine strata. *Meandrospira favrei*, with similar wide facies distribution, seems to appear in the mid-late Berriasian. Among trocholinids, the FOs of *Coscinoconus campanellus*, *C. cherchiae* and *C. sagittarius*, with further studies, have potential to provide good chronostratigraphical control in the early Berriasian (Fig. 6.1). *Pseudocyclammina lituus* seems to have lower tops in the studied successions with middle Berriasian LO (Fig. 6.1). Only the Nazliçayır section recorded the LO datum of this foraminifer within upper Valanginian.

The base of the Valanginian is defined by the FO of *Calpionellites darderi* in the pelagic deposits. *Montsalevia salevensis*, having facies distribution from shallow marine to slope deposits, has FO below this zone and provides an approximation for the Valanginian base both in slope and neritic environments (Fig. 6.1). *Barkerina dobrogiaca* has potential as a Valanginian-marker in neritic deposits, however its FO datum needs further calibration. This so-called Valanginian-marker seems to have FO in the middle Berriasian in the Eastern Pontides (FO and LO datums of this taxon are also labelled in Fig. 6.1). Its LO can present a lowered top in the Nazlıçayır region due to facies control and sample-bias. The LO of *Montsalevia salevensis* and

Calpionellites can provide markers for the approaching V/H boundary (Fig. 6.1). *Coscinoconus elongatus*, *Mohlerina basiliensis* and *Protopeneroplis ultragranualta* show LOs within the *darderi* subzone below the V/H boundary (Fig. 6.1). *Haplophragmoides joukowskyi* and *Meandrospira favrei* disappears in the Hauterivian (Fig. 6.1).

Both canditates for the J/K boundary (i.e., the T/B and B/V boundaries) can be confidently delineated within pelagic deposits on the basis of calpionellid bioevents (Fig. 6.1). There is no direct FO/LO indicator for both boundaries in the shallow marine deposits of the Pontides Carbonate Platform (Fig. 6.1). Diversity increases toward the Berriasian, followed by a decline in the middle Berriasian that continues into the Hauterivian. Increased turnover rates over the Tithonian/ Berriasian transition and in the middle Berriasian resulted in bioevents of calpionellids, foraminifers and algae clustering around these related time intervals. As the difference between origination and extinction converges to zero, turnover rates decrease toward Hauterivian, minor extinctions become enough to create prominent decline in diversity. This diversity drop is in consensus with the general trend toward lower sea levels through the late Tithonian into the Valanginian that reduced the shallow marine platform areas and carbonate production rates, characterizing a drowning phase on the margins of the Tethys Ocean for the Valanginian – Hauterivian interval. This drowning phase resulted in disappearance-dominated bioevents in the shallow marine environments and lack of reliable origination biohorizons. The differentiation from the European foraminiferal and algal associations also limits the direct applicability of the shallow marine European zonations on the southern Laurasian margin carbonate platforms (Fig. 3.2).

The correlation of the measured pelagic and shallow marine sections from the Eastern Pontides with this PCP-CSRS revealed the chronostratigraphic distribution of the recorded neritic and deep marine bioevents in the region and the age spans of the hiatuses present in the shallow marine successions. As opposed to previously suggested Barremian or even Aptian-Albian ages for the uppermost levels of the Nazlıçayır section, it is shown that there is no demonstratable post-Valanginian

shallow marine strata in the region. The unconformity interrupting the shallow marine deposition in the Nazlıçayır section is interpreted to span Tithonian (and probably uppermost Kimmeridgian) – lower (or lowermost) Berriasian. The age of the basalt level in the Nazlıçayır section is dated as middle Kimmeridgian. The Tithonian/ Berriasian boundary is missing in the region. No shallow marine bioevent can confidently delineate also the V/B boundary in the shallow marine strata. In contrast, both the T/B and the B/V boundaries are delineated relatively easily in the pelagic succession based on calpionellid bioevents. The correlation of these pelagic successions with the PCP-CSRS also confirms the stratigraphic positions of these stage boundaries on the measured sections that provide secondary control. These observations also show the impossibility of dating the J/K boundary with unconformity based zonations, e.g. J/K boundary of Granier (2019), in the shallow marine strata since these zonations inherently include time gaps that is hard to judge the geological time lost over the sequence boundaries at which their basal boundaries are located, especially if we are dealing with amalgamated unconformity surfaces (that include several overprinted unconformities or tectonically enhanced stratigraphic gaps as in the case of Nazlıçayır succession).

Based on the microfacies analyses 6 microfacies types for the slope to basin succession and 7 microfacies types for the shallow marine successions were differentiated. A depositional model is produced that visualizes the location of the measured sections in a paleo-depositional setting of the Eastern PCP. While the Ağören section (located in the southernmost tectonic unit – İmalıdağ slice) represents the deepest basinal setting that fed by clastics (transported down to the basin from the shallow marine environments, i.e. the Nazlıçayır succession to the north, through incised valleys) which created intercalated clastic turbidites within the pelagic carboanates, the Ozansu measured sections (located in the Aşutka thrust sheet) reprents a carbonate slope depositinal settings that fed by calciturbidites shedded from the carbonate platform to the north (the Nazlıçayır succession) and rarely with clastic input. A chart that shows the microfacies and fossil distribution over the Eastern PCP is also produced.

REFERENCES

Adamia, S.A., 1975. Plate tectonic and the evolution of the Alpine System: Discussion. Geological Society of America Bulletin, 86(5), 719-720.

Ager, D.V., 1973. The nature of the stratigraphical record. John Wiley, New York, 114.

Agassiz, L., 1853. Principles of zoölogy. Gould and Lincoln. 250 p.

Agterberg, F.P., Nel, L.D., 1982a. Algorithms for the ranking of stratigraphic events. Computers and Geosciences, 8, 69-90.

Agterberg, F.P., Nel, L.D., 1982b. Algorithms for the scaling of stratigraphic events. Computers and Geosciences, 8, 163-189.

Agterberg, F.P., Gradstein, F.M., 1999. The RASC method for ranking and scaling of biostratigraphic events. Earth-Science Reviews, 46, 1-25.

Aguado, R., Company, M., Tavera, J.M., 2000. The Berriasian/Valanginian boundary in the Mediterranean region: new data from the Caravaca and Chegín sections, SE Spain. Cretaceous Research, 21, 1-21.

Ağar, Ü. 1977. Demirözü (Bayburt) ve Köse (Kelkit) bölgesinin jeolojisi, Doktora Tezi, İstanbul Üniversitesi Fen Fakültesi, 59 p.

Ağralı, B., Akyol, E., Konyalı, Y., 1965. Preuves palynologiques de l'existence du Dogger dans la region de Bayburt. Bulletion of the Mineral Research and Exploration, 65, 45-57.

Akdeniz, N. 1988. Demirözü Permo-Karboniferi ve bölgesel yapı içindeki yeri, Türkiye Jeoloji Bülteni, 31, 71-80.

Akdeniz, N., 1989. 1/25000 Ölçekli Sayısal Jeolojı Haritaları, Tortum H45-d2 Paftası. Türkiye Jeoloji Veri Tabanı, Jeoloji Etütleri Dairesi Başkanlığı, Maden Tetkik Arama Genel Müdürlüğü, Ankara.

Akdeniz, N., 2011. Tortum – H45 PAftası, 1:100000 Ölçekli Türkiye Jeoloji Haritaları, Maden Tektik ve Arama Genel Müdürlüğü, No:153.

Akdoğan, R., Okay, A.İ., Dunkl, I., 2018. Triassic-Jurassic arc magmatism in the Pontides as revealed by the U-Pb detrital zircon ages in the Jurassic sandstones of northestern Turkey. Turkish Journal of Earth Sciences, 27, 89-109.

Akdoğan, R., Hu, X., Okay, A.İ., Topuz, G., Xue, W., 2021. Provenance of the Paleozoic to Mesozoic Siliciclastic Rocks of the Istanbul Zone Constrains the Timing of the Rheic Ocean Closure in the Eastern Mediterranean Region. Tectonics, 40, e2021TC006824.

Akkemik, Ü., Kandemir, R., Philippe, M., Güngör, Y., Köroğlu, F., 2022. Palaeobiogeographical implications of the first wood flora from the Jurassic of Turkey. Acta Palaeontologica Polonica, 67(3), 745-766.

Akın, H. 1978. Geologie, Magmatismus und Lagerstaettenbildung im ostpontischen Gebirge-Türkei aus der Sicht der Plattentektonik, Geologische Rundschau, 68, 253-283.

Akyürek, B., Bilginler, E., Dağer, Z., Sunu, O., 1979. Hacılar (Kuzey Çubuk-Ankara) bölgesinde Alt Triyasın varlığı. Türkiye Jeoloji Kurumu Bülteni, 22, 169-174.

Alkaya, F., Meister, C., 1995. Liassic ammonites from the central and eastern Pontides (Ankara and Kelkit areas, Turkey). Revue de Paléobiologie, 14 (1), 125-193.

Allemann, F., Trejo, M., 1975. Two New Species of *Calpionellites* from the Valanginian of Mexico and Spain. Eclogae Geologicae Helvetiae, 68(2), 457-460.

Alleman, F., Catalano, R., Farès, F., Remane, J., 1971. Standard calpionellid zonation (Upper Tithonian – Valanginian) of the Western Mediterranean province. In: Farinacci, A. (Eds.), Proceedings of the II Planktonic Conference, Roma, 1970, 2, 1337-1340.

Allemann, F., Grün, W., Wiedmann, L., 1975. The Berriasian of Caracava (Prov. of Murcia) in the Subbetic zone of Spain and its importance for defining this stage and the Jurassic-Creteceous boundary. Mémoires du Bureau de Recherches Géologiques et Miniéres, 86, 14-22.

Alp, D., 1972. Amasya yöresinin jeolojisi. İstanbul Üniversitesi Fen Fakültesi Monografileri, İstanbul, 22, 101.

Al-Rifaiy, I.A., Lemone, D., 1987. Calpionellids and the late Jurassic and early Cretaceous stratigraphy of Kuwait and the Gulf region. Marine Micropaleontology, 12, 383-388.

Altıner, D., 1991. Microfossil biostratigraphy (mainly foraminifers) of the Jurassic – Lower Cretaceous carbonate successions in North-Western Anatolia, Turkey. Geologica Romana, 27, 167-213.

Altıner, D., Özkan, S., 1991. Calpionellid zonation in North-Western Anatolia (Turkey) and calibration of the stratigraphic ranges of benthic Foraminifera at the Jurassic-Cretaceous boundary. Geologica Romana, 27, 215-235.

Altıner, D., Özkan-Altıner, S., Koçyiğit, A., 2000. Late Permian foraminiferal biofacies belts in Turkey: palaeogeographic and tectonic implications, In: Bozkurt, E., Winchester, J.A., Piper, J.D.A. (Eds). Tectonic and Magmatism in Turkey and the Surrounding Area. Geological Society, London Special Publication, 173, 83-96.

Altıner, D., Rettori, R., Zaninetti, L., Martini, R., 2001. *Turriglomina*? *anatolica*, n. sp. (Foraminiferida) from the Cretaceous of North-Western Anatolia (Turkey): Remarks on the evolution of Mesozoic meandrospirids. Rivista Italiana di Paleontologia e Stratigrafia, 107(3), 477-482.

Altıner, D., Koçyiğit, A., Farinacci, A., Nicosia, U., Conti, M.A., 1991. Jurassic-Lower Cretaceous stratigraphy and paleogeographic evolution of the southern part of North-Western Anatolia (Turkey). Geologica Romana, 28, 13-80.

Altıner, D., Yılmaz, İ.Ö., Özgül, N., Akçar, N., Bayazıtoğlu, M., Gaziulusoy, Z.E., 1999. High–resolution sequence stratigraphic correlation in the Upper Jurassic (Kimmeridgian)–Upper Cretaceous (Cenomanian) peritidal carbonate deposits (Western Tauride, Turkey). Geological Journal, 34, 139-158.

Altınlı, İ. E. 1973a. Orta Sakarya jeolojisi. Cumhuriyet' in 50. yılı Yerbilimleri Kongresi, MTA Enstitüsü, Ankara, 159-191.

Altınlı, İ. E. 1973b. Bilecik Jurasiği. Cumhuriyet' in 50. yılı Yerbilimleri Kongresi, MTA Enstitüsü, Ankara, 103-111.

Amodio, S., Ferreri, V., d'Argenio, B., Weissert, H., Sprovieri, M., 2008. Carbon-isotope stratigraphy and cyclostratigraphy of shallow-marine carbonates: the case of San Lorenzello, Lower Cretaceous of southern Italy. Cretaceous Research, 29, 803-813.

Andreini, G., Caracuel, J.E., Parisi, G., 2007. Calpionellid biostratigraphy of the Upper Tithonian-Upper Valanginian interval in Western Sicily (Italy). Swiss Journal of Geosciences, 100, 179-198.

Anstey, R., Pachut, J.F., 2004. Cladistic and phenetic recognition of species in the Ordovician bryozoan genus Peronopora. Journal of Paleontology, 78 (4), 651-674.

Arkad'ev, V.V., Fedorova, A.A., Savel'eva, Yu.N., Tesakova, E.M., 2006. Biostratigraphy of Jurassic-Cretaceous boundary sediments in the Eastern Crimea. Stratigraphy and Geological Correlation, 14 (3), 302-330.

Arkell, W.J., 1956. Jurassic Geology of the World. Oliver and Boyd, Edinburgh, 806 p.

Arnaud-Vanneau, A., 1980. Micropaléontologie, paléoécologie, et sédimentologie d'une plate-forme carbonatée de la marge passive de la Téthys: l'Urgonien du Vercors septentrional et de la Chartreuse (Alpes occidentales). Géologie Alpine, 11(3, Mémoire), 874 p.

Arnaud-Vanneau, A., 1998. 'Lower Cretaceous larger benthic Foraminifera' column in the Cretaceous Biochronostratigraphy Chart. In: Hardenbol, J.H., Thierry, J., Farley, M.B., Jacquin, T., de Graciansky, P-C., Vail, P.R., Mesozoic and Cenozoic Sequence Stratigraphy of European Basins, Mesozoic and Cenozoic Sequence Chronostratigraphic Framework of European Basins. Society for Sedimentary Geology, Special Publication, 60.

Arnaud-Vanneau, A., Peybernès, B., 1978. Les représentants éocrétacés du genre *Nautiloculina* Mohler, 1938 (Foraminifera, Fam. Lituolidae?) dans les chaines subalpines septentrionales (Vercors) et les pyrénées Franco-Espagnoles. Geobios, 11(1), 67-81.

Arnaud-Vanneau, A., Arnaud, H., Adatte, Th., Argot, M., Rumley, G. & Thieuloy, J.-P. 1987, The Lower Cretaceous from the Jura Platform to the Vocontian Basin (Swiss Jura, France). Field trip guidebook, Excursion D, III International Cretaceous Symposium, Tuebingen, 1-128.

Atasoy, S.G., 2017. Foraminiferal and calpionellid biostratigraphy, microfacies analyses and tectonic implications of the Upper Jurassic–Lower Cretaceous carbonate platform to slope successions in Sivrihisar region (Eskişehir, NW Turkey). Unpublished MSc thesis, Middle East Technical University, Ankara, 256 p.

Atasoy, S.G., Altıner, D., Okay, A.İ., 2018. Reconstruction of a Late Jurassic – Early Cretaceous carbonate platform margin with composite biostratigraphy and microfacies analysis (western Sakarya Zone, Turkey): Paleogeographic and tectonic implications. Cretaceous Research, 92, 66-93.

Atasoy, S.G., Altıner, D., Özkan-Altıner, S., 2022. Calibrating the Late Jurassic – Early Cretaceous shallow and deep marine bioevents by quantitative biostratigraphy: a synthesis from the Pontides Carbonate Platform (Turkey). Earth-Science Reviews, 231 (2022), 104071.

Aubry, M-P., 1991. Sequence stratigraphy: eustasy or tectonic imprint? Journal of Geophysical Research, 96 (B4), 6641-6679.

Aubry, M-P., 1995. From chronology to stratigraphy: interpreting the Lower and Middle Eocene stratigraphic record in the Atlantic Ocean. Geochronology Time Scales and Global Stratigraphic Correlation, Society for Sedimentray Geology, Special Publication, 54, 213-274.

Aubry, M-P., Quda, K., Dupuis, C., Berggren, W.A., van Couvering, J.A., Ali, J., Brinkhuis, H., Gingerich, P.R., Heilmann-Clausen, C., Hooker, J., Kent, D.V., King, C., Knox, R.W.O.'B., Laga, P., Molina, E., Schmitz, B., Steurbaut, E., Ward, D.R., 2007. The Global Standard Stratotype-section and Points (GSSP) for the base of the Eocene Series in the Dababiya section (Egypt). Episodes, 30 (4), 271-286.

Aygül, M., Okay, A.İ., Oberhänsli, R., Sudo, M., 2016. Pre-collisional accretionary growth of the southern Laurasian active margin, Central Pontides, Turkey. Tectonophysics, 671, 218-234.

Azimi, R., Seyed-Emami, K., Sadeghi, A., 2008. Introducing of Calpionellid Zonation at the Jurassic-Cretaceous Boundary in the Shal Section (South-East of Khalkhal). Geosciences Scientific Quarterly Journal, 68, 16-25 [in Persian].

Azema, J., Chabrier, G., Fourcade, E., Jaffrezo, M., 1977. Nouvelles donnees micropaleontologiques, stratigraphiques et paleogeographiques sur le Portlandien et le Neocomien de Sardaigne. Revue de Micropaleontologie 20 (3), 125e139.

Bacella, L., Bosellini, A., 1965. Diagrammi per la stima visive della composizione percentuale nelle rocce sedimentarie. Annali della Universitå di Ferraram Sezione IX, Science Geologische e Paleontologische 1, 59-62.

Bailey, E., McCallien, W.J., 1950. The Ankara Melange and the Anatolian Thrust. Nature, 166, 938-940.

Bailey, R.J., 2009. Cyclostratigraphic reasoning and orbital time calibration. Terra Nova, 21 (5), 340-351.

Bakalova, D., 1977, La succession a calpionelles de la coupe pres du village de Ginci, Bulgarie du Nord-Ouest. Comptes Rendus de l'Academie Bulgare des Sciences, 30, 423–426

Bakalova-Ivanova, D., 1986, Peculiarities of the calpionella zone in Bulgaria, Acta Geologica Hungarica, 29, 89–92

Bakhmutov, V.G., Halásová, E., Ivanova, D.K., Józsa, Š., Reháková, D., Wimbledon, W.A.P., 2018. Biostratigraphy and magnetostratigraphy of the uppermost Tithonian-Lower Berriasian in the Theodosia area of Crimea (southern Ukraine). Geological Quarterly, 62 (2), 197-236.

Banner, F.T., Desai, D., 1988. A review and revision of the Jurassic-Early Cretaceous Globigerinina, with special reference to the Aptian assemblages of Speeton (North Yorkshire, England). Journal of Micropalaeontology, 7 (2), 143-185.

Banner, F.T., Highton, J., 1990. On *Everticyclammina* Redmond (Foraminifera), especially *E. kelleri* (Henson). Journal of Micropalaeontology, 9(1), 1-14.

Banner, F.T., Whittaker, J.E., 1991. Redmond's "New Lituolid Foraminifera" from the Mesozoic of Saudi Arabia. Micropaleontology, 37 (1), 41-59.

Barrell, J, 1917. Rhythms and the measurements of geologic time. Geological Society of America Bulletin, 28, 745-904.

Barrier, E., Vrielynck, B., Brouillet, J.F., Brunet, M.F., 2018. Paleotectonic reconstruction of the central Tethyan Realm: Tectono-sedimentary-palinspastic maps from Late Permian to Pliocene. Commission for the Geological Maps of the World (CGMW/ CCGM), 20 Maps.

Basilone, L., 2021. Valanginian cold/warm climatic oscillation and synsedimentary tectonic interaction for drowning the carbonate platform of Southern Tethys (Sicily). Sedimentary Geology, 423, 105991.

Basilone, L., Sulli, A., 2016. A facies distribution model controlled by a tectonically inherited sea bottom topography in the carbonate rimmed shelf of the Upper Tithonian-Valanginian Southern Tethyan continental margin (NW Sicily, Italy). Sedimentary Geology, 342, 91-105.

Basson, P. W., Edgell, H. S., 1971. Calcareous algae from the Jurassic and Cretaceous of Lebanon. Micropaleontology, 17(4), 411-433.

Bassoullet, J-P., 1997. Foraminifères – Les grands foraminifères. In: Groupe Français d'Étude - Cario, E., Hantzpergue, P. (Eds.), Biostratigraphie du Jurassique ouest-européen et méditerranéen: zonations parallèls et distribution des invertébrés et microfossiles, Bulletin des Centres de Recherches Exploration-Production elf-Aquitaine, Mémoires, 17, 293-304.

Bassoullet, J.P., Bergougnan, H., 1981. Faune et faciès typiques du domaine sud-téthysien: le Lias du Munzur Dağ (Anatolie orientale). Bulletin de la Société Géologique de France, S7-XXIII (1), 83-93.

Bassoullet, J.P., Bergougnan, H., Enay, R., (1975). Répartition des faunes et faciès liasiques dans l'Est de la Turquie (region du Haut-Euphrate). Comptes Rendus de l'Académie des Sciences, Paris, 280(D), 583-586.

Baumgartner, P.O., Bartolini, A., Carter, E.S., Conti, M., Cortese, G., Danelian, T., De Wever, P., Dumitrica, P., Dumitrica-Jud, R., Gorican, S., Guex, J., Hull, D.M., Kito, N., Marcucci, M., Matsuoka, A., Murchey, B., O'Dogherty, L., Savary, J., Vishnevskaya, V., Widz, D., Yao, A., 1995. Middle Jurassic to Early Cretaceous radiolarian biochronology of Tethys based on unitary association. In: Baumgartner, P.O. et al. (Eds.), Middle Jurassic to Lower Cretaceous Radiolaria of Tethys: Occurences, systematics, biochronology. Mém. Géol. (Lausanne), 23, 1013-1048.

Bektaş, O., Çapkınoğlu, S., Akdag, K. 2001. Successive extensional tectonic regimes during the Mesozoic as evidenced by neptunian dikes in the Pontide

Magmatic Arc, Norheast Turkey. International Geology Review, 43, 840-849.

Bektaş, O., Yılmaz, C., Taslı, K., Akdağ, K., Özgür, S., 1995. Cretaceous rifting of the eastern Pontide carbonate platform (NE Turkey): the formation of carbonate breccias and turbidites as evidence of a drowned platform. Giornali di Geologia, 57, 233-244.

Benzaggagh, M., 2020. Discussion on the calpionellid biozones and proposals of a homogenous calpionellid zonation for the Tethyan Realm. Cretaceous Research, 114, 1-24.

Benzaggagh, M., 2021. Systematic revision and evolution of the Tithonian family Chitinoidellidae Trejo, 1975. Carnets Geol., 21 (2), 27-53.

Benzaggagh, M., Atrops, F., 1995. Données nouvelles sur la succession des calpionelles du Berriasien dans le Prérif et le Mésorif (Rif, Maroc). Comptes Rendus de l'Académies des Sciences Paris, t. 321, Série II a, 681-688.

Benzaggagh, M., Cecca, F., Rouget, I., 2010. Biostratigraphic distribution of ammonites and calpionellids in the Tithonian of the internal Perif (Msila area, Morocco). Palaontologische Zeitschrift, 84, 301-315.

Benzaggagh, M., Cecca, F., Schnyder, J., Seyed-Emami, K., Majidifard, M.R., 2012. Calpionelles et microfaunes pélagiques du Jurassique supérieur – Crétacé inférieur dans les Formations Shal et Kolur (Montagnes du Talesh, chaîne de l'Elbourz, Nord-Quest Iran). Répartition stratigraphique, espèces nouvelles, révision systématique et comparaisons régionales. Annales de Paléontologie, 98, 253-301.

Benzaggagh, M., Homberg, C., Schnyder, J., Razgallah, S., Hssaida, T., 2015a. Intérêt des kytes de dinoflagellés calcaires et du biomicrofaciès pélagiques dans la datation des terrains du sommet du Jurassique et de la base du Berriasian dans le domaine téthysien occidental. Annales de Paléontologie, 101, 251-263.

Benzaggagh, M., Homberg, C., Schnyder, J., Abdesselam-Mahdaoui, S.B., 2015b, Description et biozonation des sections de crinoïdes saccocomidés du Jurassique supérieur (Oxfordien-Tithinien) du domaine téthysien occidental. Annales de Paléontologie, 101, 95-117.

Bergougnan, H., 1975. Relations entre les édifices pontique et taurique dans le Nord-Est de l'Anatolie. Bulletin de la Société Géologique de France, XVII (7), 1045-1057.

Bergougnan, H., 1976. Structure de la Chaîne pontique dans le Haut-Kelkit (Nord-Est de l'Anatolie). Bulletin de la Société Géologique de France, 7-t. XVIII (3), 675-686.

Bergougnan, H. 1987. Etudes geologiques dans I'est- Anatolien. These de Doctorat d'etat ès Sciences Naturelles. Paris, à l'Université Pierre et Marie Curie, Paris 6, 606 p.

Bergougnan, H., Fourquin, C. 1982. Remnants of a pre-Late Jurassic ocean in northern Turkey: Fragments of Permian-Triassic Paleo-Tethys?: Discussion and reply: Discussion, Geological Society of America Bulletin, 93, 929-931.

Bernier, P., 1974. *Campbelliella striata* (Carozzi): Algue dasycladacée? une nouvelle interprétation de l' "organisme c" Favre et Richard, 1927. Géobios, 7(2), 155-175.

Bernoulli, D., Jenkyns, H.C., 1974. Alpine, Mediterranean, and Central Atlantic Mesozoic facies in relation to the early evolution of the Tethys. In: Dott, R.H., Shaver, R.H. (Eds.), Modern and ancient geosynclinal sedimentation, SEPM Special Publication, 19, 129-160.

Bingöl, E., Akyürek, B., Korkmazer, B., 1973. Biga Yarımadası'nın Jeolojisi ve Karakaya Formasyonu'nun bazı özellikleri. Cumhuriyet'in 50. Yılı Yerbilimleri Kongresi Tebliğleri, Maden Tetkik ve Arama Enstitüsü, Ankara, 70-77.

Blainville, H.M.D., 1825-1827. Manuel de malacologie et de conchyliologie. Paris, Levrault 1-647 [1825], 649-664 + 109 pl. [1827]. (available online at http://www.biodiversitylibrary.org/item/43891)

Blumenthal, M., 1950. Orta ve Aşağı Yeşilırmak bölgelerinin jeolojisi hakkında. Maden Tetkik ve Arama Enstitüsü. Yayınları, Ankara, D4, 153.

Bodeur, Y., 1992. Microfaciès et micro-organismes du Kimméridgien et du Tithonien au Sud des Cévennes. Université de Nantes, 80 p.

Bodin, S., Petitpierre, L., Wood, J., Elkanouni, I., Redfern, J., 2010. Timing of early to mid-cretaceous tectonic phases along North Africa: New insights from the Jeffara escarpment (Libya-Tunisia). Journal of African Earth Sciences, 58, 489-506.

Boorová, D., Skupien, P., Vašiček, Z. and Lobitzer, H., 2015. Biostratigraphy of the Lower Cretaceous Schrambach Formation on the classical locality of Schrambachgraben (Northern Calcareous Alps, Salzburg Area). Bulletin of Geosciences, Czech Geological Survey, Prague, 90(1), 89-131.

Bornemann, A., Aschwer, U. Mutterlose, J., 2003. The impact of calcareous nannofossils on the pelagic carbonate accumulation across the Jurassic-Cretaceous boundary. Palaeogeography, Palaeoclimatology, Palaeoecology, 199, 187-228.

Borza, K., 1969. Die mikrofazies und mikrofosilien des Oberjuras und der Unterkreide der Klippen-Zone der West-karpatien. Verlag der Slowakischen Akademie der Wissenschaften, Bratislava, 302 p.

Borza, K., 1984. The Upper Jurassic-Lower Cretaceous parabiostratigraphic scale on the base of Tintininae, Cadosinidae, Stomiosphaeridae, Calcisphareulidae and other microfossils from the West Carpathians. Geologicky Zbornik – Geologica Carpathica, 3, 539-550.

Borza, K., Michalík, J., 1986. Problems with delimination of the Jurassic/Cretaceous boundary in the western Carpathians. Acta Geologica Hungarica, 29 (1-2), 133-149.

Boughdiri, M., Sallouhi, H., Maâlaoui, K., Soussi, M., Cordey, F., 2006. Calpionellid zonation of the Jurassic-Cretaceous transition in North-Atlasic Tunisia. Updated Upper Jurassic stratigraphy of the 'Tunisian trough' and regional correlations. Comptes Rendus Géosciences, 338, 1250-1259.

Bozkurt, E., Winchester, J.A., Yiğitbaş, E., Ottley, C.J., 2008. Proterozoic ophiolites and mafic-ultramafic complexes marginal to the İstanbul Block: An exotic terrane of Avalonian affinity in NW Turkey, 461, 240-251.

Bozkuş, C. 1992. Olur (Erzurum) Yöresinin Stratigrafisi, Türkiye Jeoloji Bülteni, 35, 103-119.

Brosse, M., Bucher, H., Goudemand, N., 2016. Quantitative biochronology of the Permian-Triassic boundary in South China based on conodont unitary associations. Earth-Science Reviews, 155, 153-71.

Brönnimann, P., 1965. Microfossils incertae sedis from the Upper Jurassic and Lower Cretaceous of Cuba. Micropaleontology, 1(1), 28-51.

Buckman, S.S., 1893. On the Bajocian of the Sherbourne district: its relation to subjacent and superjacent strata. Geological Society of London, Quarterly Journal, 49, 479-522.

Bucur, I.I., 1988. Les foraminiféres du Crétacé inférieur (Berriasien-Valanginien) de la zone de Reşiţa-Moldova Nouă (Carpathes Méridionales, Roumanie), Remarques biostratigraphiques. Revue de Paléobiologie, Genéve, vol. spéc. no. 2 (Benthos '86), 379-389.

Bucur, I.I., 1992. Calpionellids and calcispheres from the Upper Jurassic – Lower Cretaceous deposits in the Resita-Moldova Noua zone, Southern Carpathians, Romania. Cretaceous Research, 13, 565-576.

Bucur, I. I., 1993. Les représentants du genre Protopeneroplis Weynschenk dans les dépôts du Crétacé inférieur de la zone de Resita-Moldova Nouă (Carpathes Méridionales, Roumanie). Revue de Micropaléontologie, Paris, 36(3), 213-223.

Bucur, I.I., 1997. Representatives of the genus Protopeneroplis (Foraminifera) in the Jurassic and Lower Cretaceous deposits in Romania. Comparisons with other regions of the Tethyan Area. Acta Palaeontologica Romaniae, 1, 65-71.

Bucur, I.I., Săsăran, E., 2005. Micropaleontological assemblages from the Upper Jurassic-Lower Cretaceous deposits of Trascău Mountains and their biostratigraphic significance. Acta Paleontologica Romanie, 5, 27-38.

Bucur, I.I., Lazăr, I., 2023. Upper Jurassic to Lowermost Cretaceous microfossils from the Hăghimaş Mountains (Eastern Carpathians, Romania). Acta Palaeontologica Romaniae, 19(1), 13-26.

Bucur, I.I., Conrad, M.A., Radoicic, R., 1995. Foraminifers and calcareous algae from Valanginian limestones in the Jerma River Canyon, Eastern Serbia. Revue de Paléobiologie, 14(2), 349-377.

Bucur, I.I., Senowbari-Daryan, B., Abate, B., 1996. Remarks on some foraminifera from the Upper Jurassic (Tithonian) reef limestone of Madonie Mountains (Sicily). Bollettino della Società Paleontologica Italiana, 35 (1), 65-80.

Bucur, I.I., Hofmann, M., Kołodziej, B., 2005. Upper Jurassic-Lowermost Cretaceous Benthic Algae from Tethys and the European Platform: A case study from Poland. Revista Espanola de Micropaleontologia, 37(1), 105-129.

Bucur, I.I., Piteiu, M.A., Săsăran, E., 2007. The Mesozoic carbonate deposits from the borehole 6042 Deleni (Transylvanian Depression). Studia Univ. Babeş-Bolyai, Geol., XLIX, 27-48.

Bucur, I.I., Granier, B., Krajewski, M., 2014a. Calcareous algae, microbial structures and microproblematica from Upper Jurassic-Lowermost Cretaceous

limestones of Southern Crimea. Acta Paleontologica Romaniae, 10 (1-2), 61-86.

Bucur, I.I., Koch, R., Kımracı, Z.M., Taslı, K., 2000. Les algues Dasycladales du Crétacé inférieur (Calcaire de Berdiga) de Kırcaova (région de Kale-Gümüşhane, NE Turquie). Revue de Paléobiologie, 19 (2), 435-463.

Bucur, I. I., Koch, R., Kırmacı, Z. M., Taslı, K. 2004. Foraminifères du Jurassique supérieur et du Crétacé inférieur (Calcaire de Berdiga) de Kırcaova (région de Kale-Gümüşhane, NE Turquie). Revu de Paléobiologie, 23 (1), 209-225.

Bucur, I.I., Beleš, D., Săsăran, E., Balica, C., 2010. New data on facies development and micropaleontology of the eastern margin of the Getic Carbonate Platform (South Carpathians, Romania): case study of the Mateiaş Limestone. Studia Universitatis Babeş-Bolyai, Geologia 55(2), 33-41.

Bucur, I.I., Grădinaru, E., Lazăr, I., Grădinaru, M., 2014b. Early Cretaceous micropaleontological assemblages from a condensed section of the Codlea area (Southern Carpathians. Romania). Acta Palaeontologica Romaniae, 9 (2), 67-84.

Bulot, L., Blanc, E., Company, M., Gardin, S., Hennig, S., Hoedemaeker, P.J., Leereveld, H., Magniez-Jannin, F., Mutterlose, J., Pop, G., Rawson, P.F., 1996. The Valanginian Stage. Bulletin de l'Institut Royal des Sciences Naturelles de Belgique, Sciences de la Terre, Supp. 66, 11-18.

Burşuk, A., 1981. Calpionellid biozones in the Aşkale-Bayburt region (NW Erzurum). Karadeniz Teknik Üniversitesi Yer Bilimleri Dergisi, Jeoloji, 1, 21-28.

Burşuk, A., 1992. Bayburt ve Kop Dağları (KB Erzurum) Yöresindeki Calpionellid Biyozonları (Üst Jurasik-Alt Kretase). Türkiye Jeoloji Bülteni, 35, 127-140.

Birkelund, T., Hancock, J.M., Hart, M.B., Rawson, P.F., Remane, J., Robaszynski, F., Schmid, F., Surlyk, F., 1984. Cretaceous stage boundaries – Proposals. Bulletin of the Geological Society of Denmark, 33, 3-20.

Biju-Duval, B., Dercourt, J., Le Pichon, X., From the Tethys ocean to the Mediterranean seas: a plate tectonic model of the evolution of the western Alpine system. In: Biju-Duval, B., Montadert, L. (Eds.), International Symposium on the Structural History of the Mediterranean Basins. Split, Yugoslavia, Edition Technip, Paris, 143–164.

Bykova, N.K., Balakhmatova, V.T., Vasilenko, V.P., Voloshinova, N.A., Grigelis, A., Dain, l.G., Ivanova, L.V., Kuzina, V.I., Kuznetsova, Z.V., Kozyreva, V.F., Morozova, V.G., Myatlyuk, E.V., Subbotina, N.N., 1958. New genera and species of foraminifera. Microfauna of the USSR, Proceedings of the Oil Research Geological Institute, 9(115), 5-106. (available online at https://books.google.pt/books?id=ujYhN1nVcYgC). [in Russian]

Cadisch, J., 1932. Ein Beitrag zum Calpionellen-Problem. Geologische Rundschau, 23, 241-257.

Calloman, J.H., 1995. Time from fossils: S.S. Buckman and Jurassic high-resolution geochronology. In: Le Bas, M.J. (Eds.), Milestones in Geology. Geological Society, London, Memoir No. 16, 127-150.

Calloman, J.H., 2001. Fossils as geological clocks. In: Lewis, C.L.E., Knell, S.J. (Eds.), The Age of the Earth: from 4004 BC to AD 2002. Geological Society, London, Special Publications, 190, 237-252.

Campbell, C.V., 1967. Lamina, laminaset, bed and bedset. Sedimentology, 8, 7-26.

Carney, J.L., Pierce, R.W, 1995. Graphic correlation and composite standard databases as tools for the exploration biostraigrapher. In: Mann, K.O., Lane, H.R., Scholle, P.A. (Eds.), Graphic correlation, Society for Sedimentary Geology, Special Publication, 53, 23-43.

Carras, N., Conrad, M.A., Radoičić, R., 2006. *Salpingoporella*, a common genus of Mesozoic Dasycladales (calcareous green algae). Revue de Paléobiologie, Genève, 25(2), 457-517.

Casellato, C.E., 2008. Causes and consequences of calcareous nannoplankton evolution in the Late Jurassic: implications for biocalcification and ocean chemistry. PhD Thesis, Università degli Studi di Milano, 113 p.

Casellato, C.E., 2010. Calcareous nannofossil biostratigraphy of Upper Callovian – Lower Berriasian successions from the southern Alps, north Italy. Rivista Italiana di Paleontologia e Stratigrafia, 116 (3), 357-404.

Casellato, C.E., Erba, E., 2021. Reliability of calcareous nannofossil events in the Tithonian-early Berriasian time interval: Implications for a revised high resolution zonation. Cretaceous Research, 117, 1-30.

Catalano, R., 1965. Calpionelle di Calabianca (Castellammare, Sicilia). Atti della Società Toscana di Scienze Naturali (A), 72, 1-26.

Catalano R., Lima N., 1964. Distribuzione di alcune Calpionelle nel Malm e nel Neocomiano di Castellammare del Golfo. Rivista Mineraria Siciliana XIV(82-84), 1-8.

Catalano, R., Liguori, V., 1971. Facies a calpionelle della Sicilia occidentale. In: Farinacci, A., Tecnoscienza (Eds.), Proceeding of the II Planktonic Conference, Roma 1970, 1, 167-210.

Cattò, S., Cavazza, W., Zattin, M., Okay, A.I., 2018. No significant Alpine tectonic overprint on the Cimmerian Strandja Massif (SE Bulgariea and NW Turkey). International Geology Review, 60 (4), 513-529.

Catuneanu, O., 2019. Model-independent sequence stratigraphy. Earth-Science Reviews, 188, 312-388.

Cecca, F., Énay, R., Le Hégarat, G., 1989. L'Ardescien (Tithonique supérieur) de la région stratypique: séries de référence et faunes (ammonites, calpionelles) de la bordüre ardéchoise. Documents Laboratoires de Géologie, Lyon, 107, 1-115.

Celestino, R., Wohlwend, S., Reháková, D., Weissert, H., 2017. Carbon isotope stratigraphy, biostratigraphy and sedimentology of the Upper Jurassic – Lower Cretaceous Rayda Formation, Central Oman Mountains. Newsletters on Stratigraphy, 50 (1), 91-109.

Channell, J.E.T., Grandesso, P., 1987. A revised correlation of Mesozoic polarity chrons and calpionellid zones. Earth and Planetary Science Letters, 85, 222-240.

Charollais, J., Brönnimann, P., 1965. Première note sur !es foraminifères du Crétacé inférieur de Ia région genèvoise. *Sabaudia* Charollais et Brönnimann n. gen. Archives des Sciences, Genève, 18(3), 615-624.

Charollais, J., Brönnimann, P., Neumanni M., 1965. Deuxième note sur les foraminifères du Crétacé inférieur de la région genevoise : signification stratigraphique et extension géographique de Sabaudia minuta (Hofker). Archives des Sciences, Genève, 18(3), 623-642.

Cherchi, A., Schroeder, R., 1979. *Koskinobullina* n. gen., microorganism en colonie incertae sedis (Algues?) du Jurassique-Crétacé de la region méditerranéenne; note préliminaire. Bulletin du Centre Recherches Elf Exploration Production, 3, 519-523.

Ciborowski, T. and Kołodziej, B., 2001. Tithonian-Berriasian calpionellids from the Štramberk-type Limestones, Polish Flysch Carpathians. Geologica carpathica, 52(6), 343-348.

Charollais, J., Brönnimann, P., Zaninetti, L., 1966. Troisiëme note sur les foraminiféres du Crétacé inférieur de la région genevoise, Remarques stratigraphiques et description de *Pseudotextulariella salevensis*, n.sp.; *Haplophragmoides joukowskyi*, n. sp., *Citaella ? favrei*, n. sp. Archives des Sciences, Genève, 19(1), 23-48.

Chen, Y., Richoz, S., Krystyn, L., Zhang, Z., 2019. Quantitative stratigraphic correlation of Tethyan conodonts across the Smithian-Spathian (Early Triassic) extinction event. Earth-Science Reviews, 195, 37-51.

Chiocchini, M., Chiocchini, R.A., Didaskalou, P., Potetti, M., 2008. Microbiostratigrafia del Triassico superiore, Giurassico e Cretacio in facies di piattaforma carbonatica del Lazio centro-meridionale e Abruzzo: revisione finale. In: Chiocchini, M. (Eds.), Ricerche micropaleontologiche e biostratigrafiche sul Mesozoico della piattaforma carbonatica laziale-abruzzese (Italia centrale). Memorie Descrittive Della Carta Geologica D'Italia, LXXXIV, 5-65.

Cody, R.D., Levy, R.H., Harwood, D.M., Sadler, P.M., 2008. Thinking outside the zone: High-resolution quantitative diatom biochronology for the Antartic Neogene. Palaeogeography, Palaeoclimatology, Palaeoecology, 260, 92-121.

Colom, G., 1934. Estudio sobre las calpionelas. Boletin de la Real Sociedad Espaňola de Historia Natural, 34, 371-391.

Colom, G., 1939. Tintinnidos fósiles (Infusorios oligótricos), Las Ciencias, Madrid, 4(4), 815-825.

Colom, G., 1948. Fossil tintinnids: loricated infusoria of the order of the Oligotricha, Journal of Paleontology, 22, 233-263.

Cope, J. C. W., 1991, Ammonite faunas of the ammonitico rosso of the Pontide Mountains, northern Anatolia, 27, 303-325.

Cope, J.C.W., 2008. Drawing the line: the history of the Jurassic-Cretaceous boundary. Proceedings of the Geologists' Association, 119, 105-117.

Cowie, J.W., Ziegler, W., Boucot, A.J., Bassett, M.G., Remane, J., 1986. Guidelines and statutes of the International Commission on Stratigraphy (ICS). Courier Forschungsinstitut Senckenberg, 83, 1-14.

Crescenti, U, 1969, Biostratigrafia delle facies mesozoiche dell'Appennino centrale, Corelazioni. Geologica Romana, 8, 15-40.

Cushman, J. A., 1910. A monograph of the Foraminifera of the North Pacific Ocean. Part I. Astrorhizidae and Lituolidae. Bulletin of the United States National Museum. 71(1), 1-134. (available online at https://www.biodiversitylibrary.org/page/7878332)

Cuvier, G., 1796. Mémoire sur les espèces d'éléphans tant vivantes que fossiles, lu à la séance publique de l'Institut national le 15 germinal, an IV. Magasin encyclopédique, 2. e année, 3, 440-445.

Çapkınoğlu, Ş. 2003. First records of conodots from the Permo-Carboniferous of Demirçzü (Bayburt), Eastern Pontides, NE Turkey, Turkish Journal of Earth Sciences, 12, 199-207.

Çimen, O., Göncüoğlu, M.C., Simonetti, A., Sayit, K., 2018. New zircon U-Pb LA-ICP-MS ages and Hf isotope data from the Central Pontides (Turkey): Geological and geodynamic constraints. Journal of Geodynamics, 116, 23-36.

d'Orbigny, A., 1826. Tableau méthodique de la classe des Céphalopodes. Annales des Sciences Naturelles, 7(96-169), 245-314.

d'Orbigny, A., 1839. Foraminifères des îles Canaries. Histoire naturelle des Iles Canaries. 2(2), 120-146. (available online at https://archive.org/stream/HistoirenaturelIIWebb#page/n375/)

d'Orbigny, A., 1840. Paléontologie français. Terrains crétacés. 1. Céphalopodes. Paris. 622 p.

d'Orbigny, A., 1842-1851. Paléontologie français. Description zoologique et géologique de tous les animaux mollusques et rayonnés fossiles de France Terrains oolitiques ou jurassiques l Céphalopodes. Paris, Masson, 642 p.

d'Orbigny, A., 1852. Cours élémentaire de paléontologie et de géologie stratigraphique. Paris, Masson, 2, 383-847.

Dalbiez, F., 1958. *Cuneolina hensoni*, a New Lowermost Cretaceous Marker in Southwestern France. Micropaleontology, 4(1), 97-101.

Davies, H.J., von Blanckenburg, F., 1995. Slab breakoff: a model of lithosphere detachment and its test in the magmatism and deformation of collisional orogens. Earth and Planetary Science Letters, 129 (1-4), 85-102.

Delikan, A., Orhan, H., 2020. Sedimentology of Jurassic pelagic carbonate platforms in the Ankara region (central Anatolia-Turkey). Facies, 66 (19), 1-21.

Derman, A. S., Sayılı, A., 1995. İnaltı Formation: a key unit for regional geology. In: A. Erler, T. Ercan, E. Bingöl and S. Örçen (Eds.), Geology of the Black Sea Region. General Directorate of Mineral Research and Exploration, and Chamber of Geological Engineers, Ankara - Turkey, 99-103.

Dokuz, A., 2000. Yusufeli (Artvin) Yöresinin Jeolojisi, Jeotektoniği, Magmatik-Metamorfik Kayaçlarının Jeokimyası ve Petrojenezi. Doktora Tezi, Karadeniz Teknik Üniversitesi, Jeoloji Mühendisliği Ana Bilim Dalı, 327 p.

Dokuz, A., Sünnetçi, K., 2019. Jurassic acidic magmatism in a back-arc setting, eastern Sakarya Zone Turkey: Geochemical constraints and an evolutionary model. Lithos, 332-333, 312-327.

Dokuz, A., Uysal, İ., Kaliwoda, M., Karslı, O., Ottley, C.J., Kandemir, R., 2011. Early abyssal- and late SSZ-type vestiges of the Rheic oceanic mantle in the Variscan basement of the Sakarya Zone, NE Turkey: Implications for the sense of subduction and opening of the Paleotethys. Lithos, 127, 176-191.

Dokuz, A., Aydınçakır, E., Kandemir, R., Karslı, O., Siebel, W., Derman, A.S., Turan, M., 2017. Late Jurassic Magmatism and Stratigraphy in the Eastern Sakarya Zone, Turkey: Evidence for the Slab Brakeoff of Paleotethyan Oceanic Lithosphere. The Journal of Geology, 125, 1-31.

Dollo, L., 1893. Les Lois de l'évolution. Bulletin de la Société Belge de Géologie de Paléontologie et d'hydrologie, 7, 164-166.

Dott, R.H.Jr., 1983. 1982 SEPM Presidential address: Episodic sedimentation – how normal is average? How rare is rare? Does it matter? Journal Sedimentary Petrology, 53 (1), 5-23.

Dragastan, O., 1966. A new serpulid species in the Upper Jurassic of Rumania, Paläont. Z., Stuttgart, 40(½), 147-150.

Dragastan, O., Popescu, I. S. and Popescu, A., 2005. Early Cretaceous microfacies and algae from the central-eastern sectors of the Moesian Carbonate Platform. Acta Palaeontologica Romaniae, 5, 141-162.

Dragastan, O.N., Antoniade, C., Stoica, M., 2014. Biostratigraphy and zonation of the Lower Cretaceous carbonate succession from Cernavodă-Lock section, soutg Dobrogea, eastern part of the Moesian Platform (Romania). Carpathian Journal of Earth and Environmental Sciences, 9 (1), 231-260.

Dunham, R.J., 1962. Classification of carbonate rocks according to depositional texture. In: Ham, W.E., (Eds.), Classification of carbonate rocks. American Association of Petroleum Geologists, Memoir 1, 108-121.

Durand-Delga, M., 1957. Une nouvelle forme de Calpionelles. Publications du Service géologique de l'Algérie (nouvelle série), 13, 165-170.

Ebli, O., Schlagintweit, F., 1998. On some biostratigraphically important microfossils (benthic Foraminifera, Dascyladales) from subsurface Late Jurassic-Early Cretaceous shallow water limestone of S-Germany. Miltteilungen der Bayerischen Staatssammlung für Paläontologie und Historische Geologie.

Edwards, L.E., 1984. Insights on why graphic correlation (Shaw's Method) works. Journal of Geology, 92, 583-597.

Eker, Ç.S., Arı, U.V., 2023. Geochemical characterization of late Jurassic – early Cretaceous age limstones from Gümüşhane (NE-Türkiye): identification of the source of organic matter and paleo-environmnet conditions. Carbonates and Evaporites, 38, 12.

Elbra, T., Bubík, M., Reháková, D., Schnabl, P., Čížková, K., Pruner, P., Kdýr, Š., Svobodová, A., Švábenická, L., 2018. Magneto- and biostratigraphy across the Jurassic-Cretaceous boundary in the Kurovice section, Western Carpathians, Czech Republic. Cretaceous Research, 89, 211-223.

Eldredge, N., Gould, S.J., 1977. Evolutionary models and biostratigraphy strategies. In: Kauffman, E.G., Hazel, J.E. (Eds.), Concepts and methods of biostratigraphy. Dowden, Hutchinson & Ross, Stroudsburg PA, 25-40.

Elliot, G. F., 1956. Further records of fossil calcareous algae from the Middle East. Micropaleontology, 2, 327-334.

Ellwood, B.B, Wardlaw, B.R., Nestell, M.K., Nestell, G.P., Lan, L.T.P., 2017. Identifying globally synchronous Permian-Triassic boundary levels in successions in China and Vietnam using Graphic Correlation. Palaeogeography, Palaeoclimatology, Palaeoecology, 485, 561-571.

Elmas, A., 1994. Doğu Pontidler'de (Kop Dağı kuzeyi) Geç Kretase-Tersiyer dönemindeki nap yerleşimlerinin stratigrafik verileri. Proceedings of the 10th Petroleum Congress of Turkey, p. 276-289.

Embry, A.F.III, and Klovan, J.S., 1971. A Late Devonian reef tract on northeastern Banks Islands, N.W.T. Bulletin of Canadian Petroleum Geology, 4, 730-781.

Énay, R., 1997. Le Jurassique supérieur. In: Cariou E., Hantzpergue, P. (coord.), Groupe Français d'Étude du Jurassique – Biostratigraphie du Jurassique ouest-européen et méditerranéen: Zonations parallèles et distribution des invertébrés et microfossiles. Bulletin du Centre Recherches Elf Exploration Production Mémoire, 17, 363-369.

Énay, R., 2020. The Jurassic/Cretaceous system boundary is an impasse. Why do not go back to Oppel's 1856 original and historic definition of the Tithonian? Cretaceous Research, 106, 1-20.

Erba, E., Parente, M., 2024. The resilience of Tethyan planktonic and benthic calcifying algae to Early Cretaceous perturbations: comparison between the

Valanginian Weissert Event and the Early Aptian Oceanic Anoxic Event 1a. In: Hart, M.B., Batenburg, S.J., Huber, B.T., Price, G.D., Thibault, N., Wagreich, M., Walaszczyk, L. (Eds.), Cretaceous Project 200 Volume 2: Regional Studies. Geological Society, London, Special Publications, 545 (published online, in press).

Erdem, Z., Schönfeld, J., Glock, N., Dengler, M., Mosch, T., Sommer, S., Elger, J., Eisenhauer, A., 2016. Peruvian sediments as recorders of an evolving hiatus for the last 22 thousand years. Quarternary Science Review, 137, 1-14.

Eren, M., Taslı, K. 2002. Kilop Cretaceous Hardground (Kale, Gümüşhane, NE Turkey): description and origin, Journal of Asian Earth Sciences, 20, 433-448.

Erol, O., 1956. Ankara güneydoğusundaki Elma Dağı ve çevresinin jeoloji ve jeomorfolojisi üzerinde bir araştırma. Maden Tetkik ve Arama Enstitüsü Yayınları, Ankara, D9, 99 p.

Escarguel, G., Bucher, H., 2004. Counting taxonomic richness from discrete biochronozones of unkown duration: a simulation. Palaeogeography, Palaeoclimatology, Palaeoecology, 202, 181-208.

Fauvel, P., 1923. Un nouveau serpulien d'eau saumatre Merceriella n.g., enigmatica n.sp. Bulletin de la Sociét. Zoologique de France. 47, 424-430. (available online at https://www.biodiversitylibrary.org/page/3043518)

Fekete, K., Soták, J., Boorová, D., Lintnerová, O., Michalík, J., Grabowski, J., 2017. An Albian demise of the carbonate platform in the Manín Unit (Western Carpathians, Slovakia). Geologica Carpathica, 68, 385-402.

Flügel, E., 2004. Microfacies of carbonate rocks: analysis, interpretation and application. Springer, 976 p.

Flügel, E., 2010. Microfacies of carbonate rocks: analysis, interpretation and application (2nd ed.). Springer, Verlag Berlin Heidelberg,1006 p.

Flügel, E., Kiessling, W., 2002. Patterns of Phanerozoic reef crises. In: Kiessling, W., Flügel, E., Golonka, J. (Eds.), Phanerozoic reef patterns. Society for Sedimentary Geology Special Publication No. 72, 691-732.

Frau, C., Bulot, L. G., Rehåková, D., Wimbledon, W. A. P., Ilfirm, C., 2016. Revision of the ammonite index species *Berriasella jacobi* Mazenot, 1939 and its consequence for the biostratigraphy of the Berriasian Stage, 66, 94-114.

Frizzell, D.L., Schwartz, E., 1950. A new lituolid foraminiferal genus from the Cretaceous, with an emendation of *Cribrostomoides* Cushman. Bulletin of the University of Missouri School of Mines and Metallurgy, 76, 1-12.

Frollo, M.M., 1938. Sur un nouveau genre de Codiacée du Jurassique supérieur des Carpates Orientales. Bulletin de la Société Géologique de France, 5(8), 269-271.

Fourquin, C., 1975. L'Anatolie du nord-quest, marge meridionale du continent european, histoire paleogeographique, tectonique et magmatique durant le Secondaire et le Tertiaire. Bulletin de la Société Géologique de France, S7-VII (6), 1058-1070.

Foury, G., 1968. Le Crétacé inférieur des Alpilles. Contribution à l'étude stratigraphique et micropaléontologique. Geobios, 1(1), 119-163.

Föllmi, K.B., Godet, A., Bodin, S., Linder, P., 2006. Interactions between environmental change and shallow water carbonate buildup along the northern Tethyan margin and their impact on the Early Cretaceous carbon isotope record. Paleoceanography and Paleoclimatology, 21 (4), 1-16.

Főzy, I., Janssen, N.M.M., Price, G.D., Knauer, J., Pálfy, J., 2010. Integrated isotope and biostratigraphy of a Lower Cretaceous section from the Bakony Mountains (Transdanubian Range, Hungary): A new Tethyan record of the Weissert event. Cretaceous Research, 31, 525-545.

Galster, F., Guex, J., Hammer, Ø., 2010. Neogene biochronology of Antartic diatoms: A comparision between two quantitative approaches, CONOP and UAgraph. Palaeogeography, Palaeoclimatology, Palaeoecology, 285, 237-247.

Gani, M.R., 2017. Mismatch between time surface and stratal surface in stratigraphy. Journal of Sedimentary Research, 87, 1226-1234.

Genç, Ş.C., Tüysüz, O., 2010. Tectonic setting of the Jruassic bimodal magmatism in the Sakarya Zone (Central and Western Pontides), Northern Turkey: A geochemical and isotopic approach. Lithos, 118 (1-2), 95-111.

Gorbatchik, T. N., 1971. On Early Cretaceous foraminifera of the Crimea. Akad. Nauk, Voprosi Micropaleontol., Moskwa, 14, 125-139 [in Russian].

Gorbachik, T.N., Mohamad, G.K., 1997. New species of Lituolida (Foraminifera) from the Tithonian and Berriasian of the Crimea. Paleontologicheskii Zhurnal, 4, 3-9.

Göncüoğlu, M.C., Turhan, N., Şentürk, K., Özcan, A., Uysal, Ş., Yalınız, M.K., 2000. A geotraverse across northwestern Turkey: tectonic units of the Central Sakarya region and their tectonic evolution. Geological Society, London, Special Publication, 173 (1), 139-161.

Göncüoğlu, M.C., Marroni, M., Sayit, K., Tekin, U.K., Ottria, G., Pandolfi, L., Ellero, A., 2012. The Aylı Dağ ophiolite sequence (central-northern Turkey): a fragment of Middle Jurassic oceanic lithosphere within the intra-Pontide suture zone. Ofioliti, 37 (2), 77-92.

Görög, Á, Wernli, R., 2004. A rare protoglobigerinid association (Foraminifera) from the Tithonian of Gerecse Mts, Hungary. In: Kázmér, M. (Eds.), Shallow Tethys 6 Symposium Proceedings, 25-29 August 2003, Budapest. Hantkeniana, 4, 37-45.

Görür, N., 1988. Timing of opening of the Black Sea basin. Tectonophysics, 147, 247-262.

Görür, N., Şengör, A.M.C., Akkök, R., Yılmaz, Y., 1983. Pontidlerde Neo - Tetis'in kuzey kolunun açılmasına ilişkin sedimentolojik veriler. Türkiye Jeoloji Kurumu Bülteni, 26, 11-20.

Görür, N., Monod, O., Okay, A.İ., Şengör, A.M.C., Tüysüz, O., Yiğitbaş, E., Sakınç, M., Akkök, R., 1997. Palaeogeographic and tectonic position of the Carboniferous rocks of the wetern Pontides (Turkey) in the frame of the Variscan belt. Bulletin de la Société Géologique de France, 168, 197-205.

Grabowski, J., Haas, J., Márton, E., Pszczółkowski, A., 2010a. Magneto- and Biostratigraphy of the Jurassic/Cretaceous Boundary in the Lókút Section (Transdanubian Range, Hungary). Studia Geophysica et Geodaetica, 54, 1-26.

Grabowski, J., Michalík, J., Pszczółkowski, A., Lintnerovái O., 2010b. Magneto-, and isotope stratigraphy around the Jurassic/Cretaceous boundary in the Vysoká Unit (Malé Karpaty Mountains, Slovokia): correlations and tectonic implications. Geologica Carpathica, 61 (4), 309-326.

Grabowski, J., Pszczółkowski, A., 2006. Magneto- and biostratigraphy of the Tithonian-Berriasian pelagic sediments of the Tatra Mountains (central Western Carpathians, Poland): sedimentary and rock magnetic changes at the Jurassic/Cretaceous boundary. Cretaceous Research, 27, 398-417.

Grabowski, J., Bakhmutov, V., Kdýr, Š., Krobicki, M., Pruner, P., Reháková, D., Schanbl, P., Stoykova, K., Wierzbowski, H., 2019. Integrated stratigraphy and paleoenvironmental interpretation of the Upper Kimmeridgian to Lower Berriasian pelagic sequences of the Velykyi Kamianets section (Pieniny Klippen Belt, Ukraine). Palaeogeography, Palaeoclimatology, Palaeoecology, 532, 1-29.

Gradstein, F., Waskowska, A., 2021. New insights into the taxonomy and evolution of Jurassic planktonic foraminifera. Swiss Journal of Palaeontology, 140 (1), 1-12.

Gradstein F., Waskowska, A., Glinskikh, L., 2021. The first 40 million years of planktonic Foraminifera. Geosciences, 11 (85), 1-25.

Gradstein, F. M., Ogg, J.G., Schmitz, M.D., Ogg, G.M., 2020. Geologic Time Scale 2020. Elsevier, Amsterdam, 1357 pp.

Gradstein, F. M., Ogg, J.G., Schmitz, M.D., Ogg, G.M., 2021a. Time Scale Creator 8.0. Based on Geologic Time Scale 2020, Elsevier. https://timescalecreator.org/

Gradstein, F., Gale, A., Kpaevich, L., Waskowska, A., Grigelis, A., Glinskikh, L., Görög, Á., 2017. The planktonic Foraminifera of the Jurassic. Part II: Stratigraphy, palaeoecology and palaeobiogeography. Swiss Journal of Palaeontology, 136, 259-271.

Gradstein, F., Waskowska, A., Kopaevich, L., Watkins, D.K., Friis, H., Panera, J.P., 2018. Berriasian planktonic foraminifera and calcareous nannofossils from Crimea Mountains, with reference to microfossil evolution. Swiss Journal of Palaeontology, 138, 213-236.

Grandesso, P., 1977. Gli strata a Precalpionellidi del Titoniano e i loro rapporti conil Rosso-Ammonitico Veneti. Memorie di Scienze geologiche. Universita Padova 32, 3-14.

Granier, B. 2019. Dual biozonation scheme (benthic foraminifera and calcareous green algae) over the Jurassic-Cretaceous transition. Another plea to revert the system boundary to its historical Orbigny's and Oppel's definition. Cretaceous Research, 93, 245-274.

Granier, B., 2020a. Introduction to thematic issue, The transition of the Jurassic to the Cretaceous: an early XXIth century holistic approach. Cretaceous Research, 114, 1-8.

Granier, B., 2020b. Discussion of the paper by Vincent et al., 2018, entitled "Age constraints on intra-formational unconformities in Upper Jurassic-Lower Cretaceous carbonates in northeast Turkey; geodynamics and hydrocarbon implications" (Marine and Petroleum Geology, 91, 639-657). Marine and Petroleum Geology, 112, 1-9.

Granier, B., Deloffre, R., 1994. Invertaire critiques des algues dasycladales fossiles II° Partie - Les algues dasycladales du Jurassique et du Cretace. Revue de Paléobiologie, 12 (1), 19-65.

Granier, B., Berthou, P.-Y., 2002. Algues calcaries fossiles, nouvelles ou peu connues, du Portugal. 1ère partie – New or little known fossil calcareous algae from Portugal. Part 1. In: Bucur, I.I., Filipescu, S. (Eds.), Research advances in calcareous algae and microbial carbonates. Proceedings of the 4th IFAA Regional Meeting (Cluj-Napoca, August 29 – September 5, 2001), Presa Universitara Clujeana, Cluj-Napoca, 117-126.

Granier, B., Bucur, I.I., 2011. Stratigraphic ranges of some Tithonian-Berriasian benthic foraminifers and Dasycladales. Re-evaluation of their use in identifying this stage boundary in carbonate platform settings. Boletin del Instituto de Fisiografia y Geologia, 79 (81), 9-10.

Granier, B., Clavel, B., 2019. Revised dating of the major earliest Cretaceous transgression in S Aquitaine (SW) France. Cretaceous, 99, 246-254.

Granier, B., Énay, R., Charollais, J., 2020a. Discussion of the paper by Wimbledon et al., 2020b, entitled The proposal of a GSSP for the Berriasian Stage (Cretaceous System): Part 1 [Volumina Jurassica, XVIII(1)]. Volumina Jurassica, 18 (2), 1-14.

Granier, B., Ferry, S., Benzaggagh, M., 2020b. A critical look at Tré Maroua (Le Saix, Hautes-Alpes, France), the Berriasian GSSP candidate section. Carnets de géologie, 20 (1), 1-17.

Granier, B., Virgone, A., Busnardo, R., Bulot, L. G. 1995. Des calpionelles dans l'Hauterivien supérieur. Découverte exceptionelle à Busot (Alicante, Espagne). Comptes Rendus de l'Académies des Sciences, t. 321, Série II a, 1179-1186.

Granit, Y., Tintant, H. 1960. Observation préliminaires sur le Jurassique de la region de Bilecik (Turquie). Comptes Rendus de l'Académie des Sciences, 251, 1807-1803.

Grădinaru, M., Lazar, I., Bucur, I.I., Grădinaru, E., Săsăran, E., Ducea, M.N., Andrăşanu, A., 2016. The Valanginian history of the eastern part of the Getic Carbonates Platform (Southern Carpathians, Romania): Evidence for emergence and drowning of the platform. Cretaceous Research, 66, 11-42.

Grün, B., Blau, J., 1996. Phylogenie, systematik und biostratigraphie der Calpionellidae Bonet, 1956: neue daten aus dem rosso ammonitico superiore und dem biancone (Oberjura/ Unterkreide: Tithon-Valangin) von Ra Stua (Prov., Belluno, Italien). Revue de Paléobiologie, 15(2), 571-595.

Grün, B., Blau, J., 1997. New aspects of calpionellid biochronology: proposal for a revised calpionellid zonal and subzonal division. Revue de Paléobiologie, Genève, 16 (1), 197-214.

Grün, B., Blau, J., 1999. On *Praecalpionellites* Pop (Calpionellidae Bonet) and description of *Praecalpionellites hillebrandti* n.sp. (Lower Cretaceous, Italy). Neues Jahrbuch für Geologie und Paläontologie - Abhandlungen, Stuttgart, 211 (1/2), 201-212.

Guex, J., 1977. Une nouvelle méthode d'analyse biochronologique. Bulletin de la Société Vaudoise des Sciences Naturelles, 224, 309-322.

Guex, J., 1991. Biochronological correlations. Springer, Berlin, 250.

Guex, J., 2011. Some recent 'refinements' of the unitary association method: a short discussion. Lethaia, 44, 247-249.

Guex, J., Galster, F., Hammer, Ø., 2016. Discrete biochronological time scales. Springer, 160 p.

Gušić, I., 1969. Some new and inadequately known Jurassic foraminifers from central Croatia. Geološki vjesnik. 22, 55-87.

Frau, C., Bulot, L.G., Reháková, D., Wimbledon, W.A.P., Ifrim, C., 2016. Revision of the ammonite index species Berriasella jacobi Mazenot, 1939 and its

consequences for the biostratigraphy of the Berriasian Stage. Cretaceous Research, 66, 94-114.

Furrer, U., Septfontaine, M., 1977. Nouvelles données biostratigraphiques (à l'aide des foraminifères) dans le Dogger à faciès brianconnais des Préalpes medians romandes (Suisse). Eclogae Geologicae Helvetiae, 70(3), 717-737.

Hamaoui, M., 1973. Barkerina et formes voisines (Foraminifères). Bulletin du Centre de Recherches Pau-SNPA, 7 (2), 337-359.

Hammer, Ø., Guex, J., Savary, J., 2015. The UAgraph program. Retrieved from http://folk.uio.no/ohammer/uagraph.

Hammer, Ø., Harper, D.A.T., 2006. Paleontological data analysis. Blackwell Publishing, 351p.

Hammer, Ø., Harper, D.A.T., 2024. Paleontological data analysis. (2nd Ed.). John Wiley & Sons Ltd., 376p.

Hammer, Ø., Harper, D.A.T., Ryan, P.D., 2001. PAST: Paleontological statistics software package for education and data analysis. Palaeontologica Electronica, 4 (1), 1-9.

Haq, B.U., 2014. Cretaceous eustasy revisited. Global and Planetary Change, 113, 44-58.

Haq, B.U., 2017. Jurassic sea-level variations: A reappraisal. Geological Society of America Today, 28 (1), 4-10.

Heinz, R.A., Isenschmid, C., 1988. Mikrofazielle und stratigraphische Untersuchungen im Massivkalk (Malm) der Préalpes médianes. Eclogae Geologicae Helvetiae, 81 (1), 1-62.

Henson, F.R.S., 1948. Larger Imperforate Foraminifera of South-Western Asia. British Museum (Natural History), XI, 1-127.

Henson, F.R.S., 1948a. New Trochamminidæ and Verneuilinidæ from the Middle East. Journal of Natural History Series 11, 14(117), 605-630. (available online at https://doi.org/10.1080/00222934708654671)

Hesselbo, S.P., Ogg, J.G., Ruhl, M., 2020. The Jurassic Period. In: Gradstein, F.M., Ogg, J.G., Schmitz, M.D., Ogg, G.M. (Eds.), Geologic Time Scale 2020. Elsevier, Amsterdam, 955-1022.

Hilgen, F., Aziz, H.A., Bice, D., Iaccarino, S., Krijgman, W., Kuiper, K., Montanari, A., Raffi, I., Turco, E., Zachariasse, W-J., 2005. The Global boundary Stratotype Section and Point (GSSP) of the Tortonian Stage (Upper Miocene) at Monte Dei Corvi. Episodes, 28 (1), 6-17.

Hippolyte, J.C., Müller, C., Kaymakçı, N., Sangu, E., 2010. Dating the Black Sea Basin: new nannoplankton ages from its inverted margin in the Central Pontides (Turkey). In: Sosson, M., Kaymakçı, N., Stephenson, R.A., Bergerat, F., Starostenko, V., (Eds.), Sedimentary Basin Tectonics from the Black Sea and Caucasus to the Arabian Platform. Geological Society, London, Special Publications, 340, 113-136.

Hippolyte, J.C., Murovskaya, A., Volfman, Y., Yegorova, T., Gintov, O., Kaymakçı, N., Sangu, E., 2018. Age and geodynamic evolution of the Black Sea Basin: Tectonic evidence of rifting in Crimea. Marine and Petroleum Geology, 93, 298-314.

Hippolyte, J.C., Müller, C., Sangu, E., Kaymakçı, N., 2017. Stratigraphic comparison along the Pontides (Turkey) based on new nannoplankton age determinations in the Eastern Pontides: geodynamic implications. In: Sosson, M., Stephenson, R.A., Adamia, S.A., (Eds.), Tectonic Evolution of the Eastern Black Sea and Caucasus. Geological Society, London, Special Publications, 428, 323-358.

Hoedemaeker, P.J., Janssen, N.M.M., Casellato, C.E., Gardin, S., Reháková, D., Jamrichová, M., 2016. Jurassic/Cretaceous boundary in the Río Argos

succession (Caravaca, SE Spain). Revue de Paléobiologie, Genève, 35 (1), 111-247.

Hoedemaeker, P.J., Company, M., Aguirre-Urreta, M.B., Avram, E., Bogdanova, T.N., Bujtor, L., Bulot, L., Cecca, F., Delanoy, G., Ettachfini, M., Memmi, L., Owen, H.G., Rawson, P.F., Sandoval, J., Tavera, J.M., Thieuloy, J.P., Tovbina, S.Z., Vasicek, Z., 1993. Ammonite zonation for the Lower Cretaceous of the Mediterranean region; basis for the stratigraphic correlations within IGCP-Project 262. Revista Espanola de Paleontologia, 8 (1), 117-120.

Hoedemaeker, P.J., Reboulet, S., Aguirre-Urreta, M.B., Alsen, P., Aoutem, M., Atrops, F., Barragan, R., Company, M., Arreola, C.G., Klein, J., Lukeneder, A., Ploch, I., Raisossadat, N., Rawson, P.F., Ropolo, R., Vašiček, Z., Vermeulen, J., Wippich, M.G.E., 2003, Report on the 1st International Wokshop of the IUGS Lower Cretaceous Ammonite Working Group, the 'Kilian Group' (Lyon, 11 July 2002). Cretaceous Research, 24, 89-94.

Holbrook, J.M., Bhattacharya, J.P., 2012. Reappraisal of the sequence boundary in time and space: Case and considerations for an SU (subaerial unconformity) that is not a sediment bypass surface, a time barrier, or an unconformity. Earth-Science Reviews, 113 (3-4), 271-302.

Hollister, C.D., Nowell, A.R.M., Jumars, P.A., 1984. The dynamic abyss. Scientific American, 250 (3), 42-53.

Hottinger, L., 1967. Foraminifères imperforés du Mésozoique marocain. Notes du Service Géologique du Maroc, 209, 1-169.

Hottinger, L., 2013. Micropalaeontology in Basel (Switzerland) during the twentieth century: the rise and fall of one of the smaller fields of the life sciences. In: Bowden, A.J., Gregory, F.J., Henderson, A.S. (Eds), Landmarks in Foraminiferal Micropalaeontology. The Micropalaeontological Society Special Publications by the Geological Society, London, 317-335.

Houša, V., Krs, M., Krsová, M., Man, O., Pruner, P., Venhodová, D., 1999. High-resolution magnetostratigraphy and micropalaeontology across the J/K

boundary strata at Brodno near Žilina, western Slovakia: summary of results. Cretaceous Research, 20, 699-717.

Houša, V., Krs, M., Man, O., Pruner, P., Venhodová, D., Cecca, F., Nardi, G., Piscitello, M., 2004. Combined magnetostratigraphic, palaeomagnetic and calpionellid investigations across Jurassic/Cretaceous boundary strata in the Bosso Valley, Umbria, central Italy. Cretaceous Research, 25, 771-785.

Houša, V., Pruner, P., Zakharov, V.A., Kostak, M., Chadima, M., Rogov, M.A., Šlechta, S., Mazuch, M., 2007. Boreal-Tethyan correlation of the Jurassic-Cretaceous boundary interval by magneto- and biostratigraphy. Stratigraphy and Geological Correlation, 15 (3), 297-309.

Huang, C., 2018. Astronomical time scale for the Mesozoic. Stratigraphy and Timescales, 3, 81-150.

Hudson, W., Hart, M.B., Smart, C.W., 2009. Palaeobiogeography of early planktonic Foraminifera. Bulletin de la Société Géologique de France, 180 (1), 27-38.

Hughes, G.W., 2008. Biofacies and palaeoenvironments of the Jurassic Shaqra Group of Saudi Arabia. Volumina Jurassica, VI, 33-45.

Huxley, T.H., 1862. The anniversary address. Quarterly Journal of the Geological Society, 18, xl-liv.

Ivanova, D., 1997. Upper Jurassic zonation on cadosinids, stomiosphaerids and calpionellids of the Central Forebalkan, Bulgaria. Geologica Balcanica, 27, 33-47.

Ivanova, D., 1999, Middle Callovian to Valanginian microfossil biostratigraphy in the West Balkan Mountain, Bulgaria (SE Europe). Acta Paleontologica Romaniae, 2, 231-236.

Ivanova, D., Kołodziej, B., 2010. Late Jurassic-Early Cretaceous forarminifera from Štramberk-type limestones, Polish Outer Carpathians. Studia Universitatis Babeş-Bolyai, Geologia, 55(2), 3-31.

Ivanova, D., Bonev, N., Chatalov, A., 2015. Biostratigraphy and tectonic significance of lowermost Cretaceous carbonate rocks of the Circum-Rhodope Belt (Chalkidhiki Peninsula and Thrace region, NE Greece). Cretaceous Research, 52, 25-63.

Ivanova, D., Kołodziej, B., Koleva-Rekalova, E., Roniewicz, E., 2008. Oxfordian to Valanginian paleoenvironmental evolution on the western Moesian Carbonate Platofrm: a case study from SW Bulgaria. Annales Societatis Geologorum Poloniae, 78, 65-90.

Jiménez-López, J.C., López-Martinez, R.A., Barragán, R., Buitrón-Sánchesz, B.E., 2021. Calpionélidos de la transición Berriasiano-Valanginiano en la Sección Padhi, centro-este de Hidalgo, México: sistemática y bioestratigrafía. Revista Mexicana de Biodiversidad, 92, e923376.

Johnson, J.G., 1979. Intent and reality in biostratigraphic zonation. Journal of Paleontology, 53 (4), 931-942.

Johnston, G., 1846. An index to the British Annelides [sic]. Annals and Magazine of Natural History, 1(16) (supplement to vol 16), 433-462. (available online at https://www.biodiversitylibrary.org/page/22069506)

Kalvoda, J., Bábek, O., 2010. The margins of Laurussia in central and southeast Europe and southwest Asia. Gondwana Research, 526-545.

Kaminski, M. A., 2004. The year 2000 classification of the agglutinated foraminifera In: M. K. Bubik, Ma (ed.) Proceedings of the sixth international workshop on agglutinated foraminifera, Grzybowski Foundation Special Publicaiton, 237-255.

Kandemir, R., Yılmaz, C. 2009. Lithostratigraphy, facies, and deposition environment of the Lower Jurassic Ammonitico Rosso type sediments

(ARTS) in the Gümüşhane area, NE Turkey: Implications for the opening of the northern branch of the Neo-Tethys Ocean. Journal of Asian Earth Sciences, 34, 586-598.

Kandemir, R., Lerosey-Aubril, R., 2011. First Report of a Trilobite in the Carboniferous of Eastern Pontides, NE Turkey. Turkish Journal of Earth Science. 20, 179-183.

Kandemir, R., Özyurt, M., Karslı, O., 2022. Sedimentological and geochemical characteristics of Lower Jurassic Sandstones from Gümüşhane, NE Turkey: implications for source to sink processes, paleoenvironmental conditions, provenance and tectonic settings. International Geology Review, 64(12), 1719-1742.

Kandemir, R., Özyurt, M., Demir, Y., Karslı, O., 2024. Large Fe-Mn oncoids from Early Jurassic Ammonitico Rosso Facies (eastern Sakarya Zone, NE Turkey): new insights into palaeogeographic conditions of Tetyhs Ocean. International Geology Review, no volume data (published online), 1-23.

Karslı, O., Caran, Ş., Dokuz, A., Çoban, H., Chen, B., Kandemir, R., 2012. A-type granitoids from the Eastern Pontides, NE Turkey: Records for generation of hybrid A-type rocks in a subduction-related environment. Tectonophysics, 530-531, 208-224.

Kaya, M.Y., 2014. Micropaleontological and stratigraphic analyses of the Upper Jurassic-Lower Cretaceous İnaltı Formation (Bürnük, Central Pontides, Turkey): Remarks on the Facies Evolution. MSc. Thesis, Middle East Technical University, 288 pp.

Kaya, M. Y., Altıner, D., 2014. *Terebella lapilloides* Münster, 1833 from the Upper Jurassic-Lower Cretaceous İnaltı carbonates, northern Turkey: Its taxonomic position and paleoenvironmental – paleoecological significance. Turkish Journal of Earth Sciences, 23, 166-183.

Kaya, M.Y., Altiner, D., 2015. Microencrusters from the Upper Jurassic – Lower Cretaceous İnaltı Formation (Central Pontides, Turkey): Remarks on the development of reefal/peri-reefal facies. Facies, 61 (18), 1-25.

Keller, G., Herbert, T., Dorsey, R., D'Hondt, S., Johnsson, M., Chi, W.R., 1987. Global distribution of late Paleogene hiatuses. Geological Society of America, 15, 199-203.

Kemp, D.B., 2012. Stochastic and deterministic controls on stratigraphic completeness and fidelity. International Journal of Earth Sciences, 101, 2225-2238.

Kemple, W.G., Sadler, P.M., Strauss, D.J., 1989. A prototype constrained optimization solution to the time correlation problem. In: Agterberg, F.P., Bonhan-Carter, G.F., (Eds.), Statistical applications in the Earth sciences. Geological Society of Canada, Paper 89-9, 417-425.

Kemple, W.G., Sadler, P.M., Strauss, D.J., 1995. Extending graphic correlation to many dimensions: stratigraphic correlation as constrained optimization. In: Mann, K.O., Lane, H.R., Scholle, P.A. (Eds.), Graphic correlation, Society for Sedimentary Geology, Special Publication, 53, 65-82.

Keskin, İ, Korkmaz, S., Gedik, İ., Ateş, M., Gök, L., Küçümen. Ö., Erdal, T., 1989. Bayburt dolayının jeolojisi. Mineral Research and Exploration Report, 8995 (unpublished).

Ketin, İ. 1951. Bayburt Bölgesinin Jeolojisi Hakkında, İstambul Üniversitesi Fen Fakültesi Mecmuası, 16 (2B), 113-127.

Ketin, İ., 1966, Tectonic units of Anatolia (Asia Minor), Bulletin of the Mineral Research and Exploration, 66 (66), 20-37.

Ketin, İ., Gümüş, A., 1963. Sinop-Ayancık güneyinde üçüncü bölgeye dahil sahaların jeolojisi hakkında rapor (2. Kısım: Jura ve Kretase formasyonlarının etüdü). TPAO Rap. No. 288.

Kırmacı, M. Z. 1992. Alucra – Gümüşhane - Bayburt yörelerindeki (Doğu Pontid Güney Zonu) Üst Jura - Alt Kretase yaşlı Bedirgs Kireçtaşı'nın sedimentolojik incelemesi, Doktora tezi. Trabzon: Karadeniz Teknik Üniversitesi Fen Bilimleri Enstitüsü, 256 p.

Kırmacı, M. Z. 2000. Geç Jura Yaşlı Karbonat Platformunun Litofasiyes Özellikleri ve Evrimi, Uluçayır Yöresi (Bayburt, Doğu Pontidler), Türkiye Jeoloji Bülteni, 43 (2), 33-47.

Kırmacı, M. Z., Koch, R., Bucur, J. I. 1996. An Early Cretaceous Section in the Kırcaova Area (Berdiga Limestone, NE-Turkey) and its Correlation with Platform Carbonates in W-Slovenia, Facies, 34, 1-22.

Kırmacı, M. Z., Yıldız, M., Kandemir, R., Eroğlu-Gümrük, T. 2018. Multistage dolomitization in Late Jurassic – Early Cretaceous platform carbonates (Berdiga Formation), Başoba Yayla (Trabzon), NE Turkey: Implications of the generation of magmatic arc on dolomitization, Marine and Petroleum Geology, 89, 515-529.

Kiessling, W., Flügel, E., Glonka, J., 2003. Patterns of Phanerozoic carbonate platform sedimentation. Lethia, 36, 195-225.

Kietzmann, D.A., Llanos, M.P.I., 2020. Middle Jurassic crustacean microcoprolites and their association with terebellid polychaetes in prodelta deposits from the Nequén Basin, Argentina. Journal of South American Earth Sciences, 100, 102622.

Kietzmann, D.A., Llanos, M.P.I., Tomassini, F.G., Noguera, I.L., Vallejo, D., Reijenstein, H., 2021. Upper Jurassic – Lower Cretaceous calpionellid zones in the Neuquén Basin (Southern Andes, Argentina): correlation with ammonite zones and biostratigraphic synthesis. Cretaceous Research, 127, 104950.

Knauer, J. and Nagy, I., 1963. Lorenziella nov. gen. uj Calpionellidae nemzetség, Lorenziella nov. gen. nouveau genre des Calpionellidés. Foldt. Földtani Intézet Evi Jelentése, Budapest, 1961, 143-153.

Kobayashi, F., Vucks, J.V., 2006. Tithonian-Berriasian foraminiferal faunas from the Torinosu-type calcareous blocks of the southern Kanto Mountains, Japan: their implications for post-accretionary tectonics of Jurassic to Cretaceous terranes. Geobios, 39, 833-843.

Koch, R., Bucur, I. I., Kırmacı, M. Z., Eren, M., Taslı, K. 2008. Upper Jurassic and Lower Cretaceous carbonate rocks of the Berdiga Limestone – Sedimentation on an onbound platform with volcanic and episodic siliciclastic influx. Biostratigraphy, facies and diagenesis (Kırcaova, Kale-Gümüşhane area; NE-Turkey), Neues Jahrbuch für Geologie und Paläontologie Abhandlungen, 247 (1), 23-61.

Kocsis, Á, Scotese, C.R., 2021. Mapping paleocoastlines and continental flooding during the Phanerozoic. Earth-Science Reviews, 213, 103463.

Koçyiğit, A., 1979. Tekneli bölgesinin (Tokat güneyi) tektonik özelliği. TÜBiTAK Proje raporu (unpublished), TBAG-262, 63 p.

Koçyiğit, A., 1991. An example of an accretionary forearc basin from northern Central Anatolia and its implications for the history of subduction of Neo-Tethys in Turkey. Geological Society of America Bulletin, 103, 22-36.

Koçyiğit, A., Altiner, D., 2002. Tectonostratigraphic evolution of the North Anatolian Palaeorift (NAPR): Hettangian-Aptian passive continental margin of the northern Neo-Tethysi Turkey. Turkish Journal of Earth Sciences, 11, 169-191.

Koçyiğit, A., Özkan, S., Rojay, B.F., 1988. Examples from the forearc basin remnants at the active margin of northern Neo-Tethys; development and emplacement ages of the Anatolian Nappe, Turkey. METU Journal of Pure and Applied Sciences, 21 (1-2), 183-210.

Koechlin, E., 1942. *Pseudocyclammina virguliana*, n. sp., aus der *virgula*-Mergeln des Berner Jura. Eclogae Geologicae Helvetiae, 35, 195-199.

Koehn-Zaninetti, L., 1969. Les foraminifères du Trias de la région de l'Almtal (Haute-Autriche). Jahrbuch Austria Geol. Bundesanstalt, 14 (special volume), 1-155.

Kołodziej, B., Lazăr, I., Bucur, I.I., Coman, M., Uchman, A., 2024. Hybrid nature of a new Jurassic-Cretaceous worm burrow indicated by microbial mediation of its wall formation. Palaios, 39, 1-20.

Konak, N., Okay, A. I., Hakyemez, Y. 2009. Tectonics and stratigraphy of the Eastern Pontides, 2nd Internationl Symposium on the geology of the Black Sea Region, Field Trip Guide Book. Maden Tetkik ve Arama Genel Müdürlüğü ve TMMOB Jeoloji Mühendisleri Odası, Ankara, 120 p.

Konak, N., Hakyemez, Y. H., Bilginç, T., Bilgin, Z. R., Hepşen, N., Ercan, T. 2001. Kuzeydoğu Pontidlerin (Oltu-Olur-Şenkaya-Narman-Tortum-Uzundere-Yusufeli) Jeolojisi. Ankara: MTA Raporu, 10489, 355 p.

Korkmaz, S., 1984. 1/25000 Ölçekli Sayısal Jeolojı Haritaları, Trabzon H44-d4 Paftası. Türkiye Jeoloji Veri Tabanı, Jeoloji Etütleri Dairesi Başkanlığı, Maden Tetkik Arama Genel Müdürlüğü, Ankara.

Kowalewski, M., Bambach, R.K., 2008. The limits of paleontological resolution. In: Harries, P.J. (Eds.), High-resolution approaches in stratigraphica paleontology, Springer, 1-48.

Kowal-Kasprzyk, J., Reháková, D., 2019. A morphometric analysis of loricae of the genus *Calpinella* and its significance for the Jurassic/Cretaceous boundary interpretation. Newsletters on Stratigraphy, 52 (1), 33-54.

Kowal-Kasprzyk, J., Krajewski, M., Gedl, P., 2020. The oldest stage of the Outer Carpathian evolution in the light of Oxfordian – Kimmeridgian exotic clast studies (southern Poland). Facies, 66:11.

Krajewski, M., Olszewska, B., 2006. New data about microfacies and stratigraphy of the Late Jurassic Aj-Petri carbonate build-up (SW Crimea Mountains, S Ukraine). Neues Jahrbuch für Geologie und Paläontologie, 5, 298-312.

Krajewski, M., Olszewska, B., 2007. Foraminifera from the Late Jurassic and Early Cretaceous carbonate platform facies of the southern part of the Crimea

Mountains, southern Ukraine. Annales Societatis Geologorum Poloniae, 77, 291-311.

Krajewski, M., Matyszkiewicz, J., Król, K., Olszewska, O., 2011. Facies of the Upper Jurassic–Lower Cretaceous Deposits from the Southern part of the Carpathian foredeep basement in the Kraków-Rzeszów area (Southern Poland). Annales Societatis Geologorum Poloniae, 81, 269–290.

Krische, O., Bujtor, L. and Gawlick, H-J., 2013. Calpionellid and ammonite biostratigraphy of uppermost Jurassic to Lower Cretaceous sedimentary rocks from the Leube Quarry (Northern Calcareous Alps, Salzburg, Austria). Austrian Journal of Earth Sciences 106(1), 26-45.

Kristan-Tollmann, E., 1963. Entwicklungsreihen der Trias-Foraminiferen. Paläontologische Zeitschrift, 37(1-2), 147-154. (available online at https://doi.org/10.1007/BF02989607)

Kroh, A., Lukender, A., 2009. Crinoids from the Late Jurassic of the Nutzhof section (Lower Austria, Gresten Klippenbelt). Annalen des Naturhistorischen Museums in Wien, 110A, 383-399.

Kuznetsova, K.I., Bragin, N.Yu., 1999. Cosmopolitan foraminiferal assemblages from Jurassic deposits of central Turkey. Stratigraphy and Geological Correlation, 7 (6), 606-610.

Kuznetsova (ed.) 1985. Stratigrafiya i Korrelyatsiya Verkhnei Yury SSSR po Foraminferam (Stratigraphy and Correlation of the Upper Jurassic of the USSR by Foraminifera). GIN AN SSSR, Micropaleontological Commission, Moscow, 126 p. [in Russian].

Kuznetsova, K.I., Bragin, N.Yu., Voznesenskii, A.I., Tekin, U.K., 2003. Jurassic planktonic and benthic cosmopolitan foraminiferal communities of central Turkey. Stratigraphy and Geological Correlation, 11 (5), 450-567.

Kuznetsova, K.I., Grigelis, A.A., Adjamian, J., Jarmakani, E., Hallaq, L., 1996. Zonal Stratigraphy and Foraminifera of the Tethyan Jurassic (Eastern Mediterranean). Gordon and Breach Publishers, 256 p.

Kuznetsov, N.B., Belousova, E.A., Griffin, W.L., O'Reilly, S.Y., Romanyuk, T.V., Rud'ko, S.V., 2019. Pre-Mesozoic Crimea as a scontinuation of the Dobrogea paltform: insights from detrital zircons in Upper Jurassic conglomerates, Mountainous Crimea. International Journal of Earth Sciences. 108, 2407-2428.

Lakova, I., 1993. Middle Tithonian to Berriasian praecalpionellid and calpionellid zonation of the Western Balkanides, Bugaria. Geologica Balcanica, 23 (6), 3-24.

Lakova, I. and Petrova, S., 2012. Towards a standard calpionellid zonation of the Mediterranean Realm (Tithonian to Valanginian). Bulgarian Geological Society National Conference with international participation "GEOSCIENCES 2012", Abstract, 89-90.

Lakova, I., Petrova, S., 2013. Towards a standard Tithonian to Valanginian calpionellid zonation of the Tethyan Realm. Acta Geologica Polonica, 63 (2), 201-221.

Lakova, I., Stoykova, K., Ivanova, D., 1997. Tithonian to Valanginian bioevents and integrated zonation on calpionellids, calcareous nannofossils and calcareous dinocysts from the Western Balcanides, Bulgaria. Mineralica Slovaca, 29, 301-303.

Lakova, I., Stoykova, K., Ivanova, D., 1999. Calpionellid, nannofossil and calcareous dinocyst bioevents and integrated biochronology of the Tithonian to Valanginian in the western Balkanides, Bulgaria. Geologica Carpathica, 50 (2), 151-168.

Lakova, I., Grabowski, J., Stoykova, K., Petrova, S., Reháková, D., Sobień, K., Schnabl, P., 2017. Direct correlation of Tithonian/Berriasian boundary calpionellid and calcareous nannofossil events in the frame of

magnetostratigraphy: new results from the west Balkan Mts., Bulgaria, and review of existing data. Geologica Balcanica, 46 (2), 47-56.

Lamarck, J.B.P.A., 1802. Discours d'Ouverture, Prononcé le 27 floréal An 10, au Muséum dHistoire naturelle. Recherches sur l'organisation des corps vivans. Bulletin Scientifique de la France et de la Belgique. 5(40), 483-517. (available online at https://www.biodiversitylibrary.org/page/10730977)

Lamarck, J.B.P.A., 1804. Suite des mémoires sur les fossiles des environs de Paris. Annales du Muséum d'Histoire Naturelle. 5, 28-36; 91-98; 179-188; 237-245; 349-367; pl. 59-62 [plates published in 1806 in vol. 8]. (available online at https://www.biodiversitylibrary.org/page/3496912)

Le Hégarat, G., Remane, J., 1968. Tithonique supérieur et Berriasian de la bordüre cévenole. Corrélation des Ammonites et des Calpionelles. Geobios, 1, 7-69.

Leinfelder, R.R., 1994. Karbonatplattformen und Korallenriffe innerhalb siliziklastischer sedimentationsbereiche (Oberjura. Lusitanisches Becken, Portugal). Profil, 6, 1-207.

Leinfelder, R. R., Nose, M., Schmid, D. U., Werner, W., 1993. Microbial crusts of the Late Jurassic: composition, palaeoecological significance and importance in reef construction. Facies, 29, 195-230.

Less, G., 1998. The zonation of the Mediterranean Upper Paleocene and Eocene by orthophragminae. Dela – Opera Sazu, 4 (34/2), 21-43.

Less, G., Kovács, L.Ó., 2009. Typological versus morphometric separation of orthophragminid species ioin single samples – a case study from Horsarrie (upper Ypresian, SW Aquitaine, France). Revue de micropaléontologie, 52, 267-288.

Leupold, W., Bigler, H., 1936. Coscinoconus eine neue Foraminiferenform aus Tithon-Unterkreide-Gesteinen der Helvetischen Zone der Alpen. Eclogae Geologicae Helvetiae, 28, 606–624. (available online at https://www.e-periodica.ch/digbib/view?pid=egh-001:1935:28#668).

Limongi, P., Panzanelli-Fratoni, R., Ciarapica, G., Cirilli, S., Martini, R., Salvini-Bonnard, G., Zaninetti, L., 1987. *Turriglomina* Zaninetti, n. gen., un nouveau nom pour "*Turritellella*" *mesotriasica* Koehn-Zaninetti, 1968 (Foraminifère, Trias moyen) avec remarque sur la présence de l'espèce dans le Ladinien de l'Apennin méridional. Archives des Sciences, Genève, 40, 13-32.

Linnaeus, C., 1758. Systema Naturae per regna tria naturae, secundum classes, ordines, genera, species, cum characteribus, differentiis, synonymis, locis. Editio decima, reformata [10th revised edition], vol. 1: 824 pp. Laurentius Salvius, Holmiae. (available online at https://biodiversitylibrary.org/page/726886)

Linnaeus, C., 1767. Systema naturae per regna tria naturae: secundum classes, ordines, genera, species, cum characteribus, differentiis, synonymis, locis. Ed. 12. 1., Regnum Animale. 1 & 2. Holmiae [Stockholm], Laurentii Salvii. pp. 1-532 [1766] pp. 533-1327 [1767]. (available online at http://www.biodiversitylibrary.org/item/83650#5)

Loeblich, A. R., Tappan, H., 1985. Some new and redefined genera and families of agglutinated foraminifera; I. The Journal of Foraminiferal Research, 15(2), 91-104.

Loeblich, A.R., Tappan, H., 1946. New Washita Foraminifera. Journal of Paleontology, 20, 238-258.

Loeblich, A.R.Jr. and Tappan, H., 1988. Foraminiferal genera and their classification, von Nostrand Reinhold Company, New York, 2 volumes, 970 p.

Lokier, S.W., Junaibi, M.A., 2016. The petrographic description of carbonate facies: are we all speaking the same language? Sedimentology, 63, 1843-1885.

Lombard, A., 1945. Attribution de microfossiles du Jurassique supérieur alpin à des chlorophycées (Proto- et Pleurococcacéees). Eclogae Geologicae Helvetiae 38(1), 163-173.

Loutit, T.S, Hardenbol, J., Vail, P.R., 1988. Condensed sections: The key to age determination and correlation of continental margin sequences. In: Wilgus, C.K., Hastings, B.S., Psamentier, H., van Wagoner, J., Ross, C.A., Kendall, C.G.St.C. (Eds.), Sea-level changes: an intergrated approach, Society for Sedimentary Geology, 42, 183-213.

López-Martínez, R., Barragán, R., Reháková, D., 2013a. The Jurassic/Cretaceous boundary in the Apulco area by means of calpionellids and calcareous dinoglagellates: An alternative to the classical Mazatepec section in eastern Mexico. Journal of South American Earth Sciences, 47, 142-151.

López-Martínez, R., Barragán, R., Reháková, D., 2015. Calpionellid biostratigraphy across the Jurassic/Cretaceous boundary in San José de Iturbide, Nuevo León, northeastern Mexico. Geological Quarterly, 59 (3), 581-592.

López-Martínez, R., Barragán, R., Reháková, D., Cobiella-Reguera, J.L., 2013b. Calpionellid distribution and microfacies across the Jurassic/Cretaceous boundary in western Cuba (Sierra de los Órganos). Geologica Carpathica, 64 (3), 195-208.

López-Martínez, R., Aguirre-Urreta, B., Lescano, M., Concheyro, A., Vennari, V., Ramos, V.A., 2017a. Tethyan calpionellids in the Neuquén Basin (Argentine Andes), their significance in defining the Jurassic/Cretaceous boundary and pathways for Tethyan-Eastern Pacific conections. Journal of South American Earth Sciences, 78, 116-125.

López-Martínez, R., Barragán, R., Bernal, J.P., Reháková, D., Gómez-Tuena, A., Martini, M., Ortega, C., 2017b. Integrated stratigraphy and isotopic ages at the Berriasian – Valanginian boundary at Tlatlauquitepec (Puebla, Mexico). Journal of South American Earth Sciences, 75, 1-10.

Lorenz, Th., 1902. Geologische Studien im Grenzgebiet zwischen helvetischer und ostalpiner Fazies. II Der südliche Rhätikon, Berichte der Naturforschenden Gesellschaft zu Freiburg, 12, 35-95.

Lucas, S.G., 2018. The GSSP method of chronostratigraphy: a critical review. Frontiers in Earth Science, 6 (191), 1-18.

Lukeneder, A., Halásová, E., Kroh, A., Mayrhofer, S., Pruner, P., Reháková, D., Schnabl, P., Sprovieri, M., Wagreich, M., 2010. High resolution stratigraphy of the Jurassic-Cretaceous boundary interval in the Gresten Klippenbelt (Austria). Geologica Carpathica, 61 (5), 365-381.

Maalaoui, K. and Zargouni, F., 2016. The lower and middle Berriasian in Central Tunisia: integrated ammonite and calpionellid biostratigraphy of the Sidi Kralif Formation. Acta Geologica Polonica, 66(1), 43-58.

Maalaoui, K., Zargouni, F., 2017. Biostratigraphical study around the Jurassic/Cretaceous boundary in Central Tunusia zonal schemes and correlation. Journal of African Earth Sciences, 125, 166-176.

MacLeod, N., Keller, M., 1991. How complete are Cretaceous/Tertiary boundary sections? A chronostratigraphic estimate based on graphic correlation. Geological Society of America Bulletin, 103, 1439-1457.

Macquaker, J.H.S., Howell, J.K., 1999. Small-scale (<5.0 m) vertical heterogeneity in mudstones: implications for high-resolution stratigraphy in siliciclastic mudstone successions. Journal of the Geological Society, 156, 105-112.

Mailliot, S., Mattioli, E., Guex, J., Pittet, B., 2006. The Early Toarcian anoxia, a synchronous event in the Western Tethys? An approach by quantitative biochronology (Unitary Associaiton), applied on calcareous nannofossils. Palaeogeography, Palaeoclimatology, Palaeoecology, 240, 562-586.

Makarieva, S.F., 1974. Significance of fossil Tintinnidae (Infusoria) for substantiation of the Jurassic-Cretaceous boundary in the Chechnya-Ingushetia SSR (Assa river). In: Geology and oil-and-gas bearing of Eastern Peri-Caucasus, 20, 15-20 [in Russian].

Makarieva, S.F., 1979. Mesozoic Tintinnids from the North Caucasus, and the Jurassic-Cretaceous boundary. In: Upper Jurassic and the boundary to the Cretaecous system. Acad. Nauk. USSR, Siberian branch, Institute for Geology and Geophysics, Novosibirsk, 168-171 [in Russian].

Magniez, F., 1974. *Novalesia*, nouveau nom pour le genre de foraminifères des formations para-urgoniennes cantrabriques (Espagne). Revista espanola de Micropaleongologia, 4, 179-198.

Marie, P., 1941. Les Foraminifères de la craie à Belemnitella mucronata du Bassin de Paris. Mémoires du Muséum National d'Histoire Naturelle de Paris, Nouvelle Série, 12, 1-296.

Marie, P., 1954. Quelques genres nouveaux de foraminifères du Crétacé à facies récifal. Compte Rendu 19ème Congrès Géologique International, Alger 1952, 13(15), 117-124.

Marino, M. C., Andreini, G., Baldanza, A., D'Arpa, C., Mariotti, N., Pallini, G., Parisi, G., and Petti, F. M., 2004. Middle Jurassic-Early Cretaceous integrated biostratigraphy (ammonites, calcareous nannofossils and calpionellids) of the Contrada Diesi Section (south-western Sicily, Italy). Rivista Italiana di Paleontologia e Stratigrafia, 110(1), 357-372.

Marroni, M., Göncüoğlu, M.C., Frassi, C., Sayit, K., Pandolfi, L., Ellero, A., Ottria, G., 2020. The intra-Pontide ophiolites in northern Turkey revisited: From birth to death of a Neotethyan oceanic domain. Geoscience Frontier, 11, 129-149.

Masse, J-P., 1998. 'Calcareous Algae' column in the Cretaceous Biochronostratigraphy Chart. In: Hardenbol, J.H., Thierry, J., Farley, M.B., Jacquin, T., de Graciansky, P-C., Vail, P.R., Mesozoic and Cenozoic Sequence Stratigraphy of European Basins, Mesozoic and Cenozoic Sequence Chronostratigraphic Framework of European Basins. Society for Sedimentary Geology, Special Publication, 60.

Maync, W., 1957. *Coscinophragma cribrosum* (Reuss) in a lower Cretaceous limestone from Switzerland. Micropaleontology, 3(2), 183-186.

Maync, W., 1958. Note sur *Pseudocyclummina jaccardi* (Schrodt) ct sa synonymic. Revue de Micropaléontologie, 1, 9-16.

Maync, W., 1966. Microbiostratigraphy o the Jurassic of Israel. Geological Survey of Israel Bulletin, 40, 56 p.

Mayr, E., 1963. Animal species and evolution. The Belknap Press of Harvard University Press, Cambridge, Massachusetts, 797.

Memmi, L., Donze, P., Combémorel, R., Le Hégarat, G., 1989. The transition from Jurassic to Cretaceous in northeast Tunisia: biostratigraphic details and distribution of facies. Cretaceous Research, 10, 137-151.

McLaren, D.J., 1970. Presidential address: Time, life and boundaries. Journal of Paleontology, 44, 801-813.

McLaren, D.J., 1977. The Silurian-Devonian Boundary Committee: A final report. In: Martinsson, A. (Eds.), The Silurian-Devonian boundary. International Union of Geological Sciences, 1-34.

Meijers, M. J. M., Langereis, C. G., van Hinsbergen, D. J. J., Kaymakci, N., Stephenson, R. A., Altiner, D. 2010. Jurassic-Cretaceous low paleolatitudes from the circum-Black Sea region (Crimea and Pontides) due to True Polar Wander. Earth and Planetary Science Letters, 296 (3–4), 210–226.

Mekik, F.A., Yi Ling, H., Özkan-Altiner, S., Altiner, D., 1997. Preliminary radiolarian biostratigraphy across the Jurassic-Cretaceous boundary from Northwestern Turkey. Geodiversitas, 21 (4), 715-738.

Miall, A.D., 1992. Exxon global cycle chart: An event for every occasion? Geology, 20, 787-790.

Miall, A.D., 2004. Empricism and model building in stratigraphy: The historical roots of present-day practices. Stratigraphy, 1 (1), 3-25.

Miall, A.D., 2010. Chronostratigraphy, correlation, and modern tests for global eustasy. In: Miall, A.D., The Geology of Stratigraphic Sequences, Springer, 391-459.

Miall, A.D., 2015. Updating uniformitarianism: Stratigraphy as just a set of 'frozen accidents'. In: Smith, D.G., Bailey, R.J., Burgess, P.M., Fraset, A.J. (Eds.), Strata and Time: Probing the gaps in our understanding. Geological Society, London; Special Publications, 404, 11-36.

Miall, A.D., 2016. The valuation of unconformities. Earth-Science Reviews, 163, 22-71.

Miall, A.D., Miall, C.E., 2004. Empricism and model-building in stratigraphy: Around the hermeneutic circle in the pursuit of stratigraphic correlation. Stratigraphy, 1 (1), 27-46.

Michalík, J., Reháková, D., Grabowski, J., Lintnerová, O., Svobodová, A., Schlögl, J., Sobien, K., Schnabl, P., 2016. Stratigraphy, plankton communities, and magnetic proxies at the Jurassic/Cretaceous boundary in the Pieniny Klippen Belt (Western Carpathians, Slovakia). Geologica Carpathica, 67 (4), 303-328.

Michalík, J., Grabowski, J., Lintnerová, O., Reháková, D., Kdýr, Š., Schnabl, P., 2021. Jurassic – Cretaceous boundary record in Carpathian sedimentary sequences. Cretaceous Research, 118, 1-19.

Michalík, J., Reháková, D., Halásová, E., Lintnerová, O., 2009. The Brodno section – a potential regional stratotype of the Jurassic/Cretaceous boundary (Western Carpathians). Geologica Carpathica, 60, 213-232.

Michetituc, M., Catincuţ, C., Bucur, I.I., 2012. An Upper Jruassic-Lower Cretaceous carbonate platform from the Vâlcan Mountains (Southern Carpathians, Romania): paleoenvironmental interpretation. Geologica Carpathica, 63(1), 33-48.

Mikhalevich, V., 2004. On the new understanding of the Order Lituolida Lankester, 1885 (Foraminifera). Acta Palaentological, 4, 247-267.

Miller, J.S., 1821. A natural history of the Crinoidea or lily-shaped animals, with observations on the genera Asteria, Euryale, Comatula, and Marsupites. C.

Frost. Bristol. 150 p. (available online at https://doi.org/10.5962/bhl.title.32130)

Miller, F.X., 1977. The graphic correlation method in biostratigraphy. In: Kauffman, E.G., Hazel, J.E. (Eds.), Concepts and methods of biostratigraphy. Hutchinson & Ross, Stroudsburg, Pa., Dowden, 165-186.

Mircescu, C.V., Bucur, I.I., Săsăran, E., 2013. Dasycladalean algae from Upper Jurassic-Lower Cretaceous limestones of Piatra Craiului Massif (South Carpathians, Romania) and their relationship to paleoenvironment. Studia UBB Geologia, 59 (1), 5-27.

Mišík, M., 1995. Selective silicification of calcitic fossils and bioclasts in the West-Carpathian limestones. Geologica Carpathica, 46(3), 151-159.

Mišík, M., Sỳkora, M., 1981. Der pieninische exotische Rücken rekonstruiert aus Geröllen karbonatischer Gesteine kretazischer Konglomerate der Klippen zone und der Manín-Eingeit. Západ. Karpaty, Sér. Geol., 7, 7-111

Mišík, M., Soták, J. and Ziegler, V., 1999. Serpulid worms Mercierella Fauvel, Durandella Dragastan and Carpathiella Nov. Gen. from the Upper Jurassic, Cretaceous and Paleogene of the Western Carpathians. Geol. Carp., 50(4), 305-312.

Mohler, W., 1938. Mikropaläontologische Untersuchungen in der nordschweizerischen Juraformation. Abhandlungen der Schweizerischen Paläontologischen Gesellschaft, 60, 1-53.

Molina, E., Algret, L., Arenilla, I., Arz, J.A., Gallala, N., Hardenbol, J., von Salis, K., Steurbaut, E., Vandenberghe, N., Zaghbib-Turki, D., 2006. The Global Boundary Stratotype Section and Point for the base of the Danian Stage (Paleocene, Paleogene, "Tertiary", Cenozoic) at El Kef, Tunisia — Original definition and revision. Episodes, 29 (4), 263-273.

Moullade, M., 1965. Contribution au problème de la classification des Orbitolinidae (Foraminiferida, Lituolacea). Comptes rendus hebdomadaires des séances de l'Académie des sciences, 260, 4031-4034.

Munier-Chalmas, E., 1887. Sur la Cyclolina et trois nouveaux genres de foraminifères des couches à rudistes: *Cyclopsina*, *Dicyclina* et *Spirocyclina*. Compte Rendu des Séances de la Société géologique de France, 4(7), 30-31.

Monnet, C., Klug, C., Goudemand, N., De Baets, K., Bucher, H., 2011. Quantitative biochronology of Devonian ammonoids from Morocco and proposals for a refined unitary association method. Lehaia, 44, 469-489.

Monod, O., 1977. Recherches geologiques dans le Taurus occidental au sud de Beyşehir (Turquie). Thése de doctorat, Université de Paris-Sud Orsay, 442 p.

Monty, C.L.V., 1968. d'Orbigny's concepts of stage and zone. Journal of Paleontology, 42 (3), 689-701.

Morales, C., Gardin, S., Schnyder, J., Spangenberg, J., Arnaud-Vanneau, A., Arnaud, H., Adatte, T., Föllmi, K.B., 2013. Berriasian and early Valanginian environmental change along a transect from the Jura Platform to the Vocontian Basin. Sedimentology, 60, 36-63.

MTA, 2002. 1/500000 ölçekli jeoloji haritaları serisi, Samsun, Trabzon ve Erzurum paftaları. Ankara, Maden Tetkik ve Arama Genel Müdürlüğü.

MTA, 2011. 1/100000 ölçekli jeoloji haritaları serisi, Tortum – H45 paftası. Ankara, Maden Tetkik ve Arama Genel Müdürlüğü.

MTA, 2015. 1/1000000 ölçekli Türkiye jeoloji haritası. Ankara, Maden Tetkik ve Arama Genel Müdürlüğü.

MTA, 2016a. 1/100000 ölçekli jeoloji haritaları serisi, Giresun – H41 paftası. Ankara, Maden Tetkik ve Arama Genel Müdürlüğü.

MTA, 2016b. 1/100000 ölçekli jeoloji haritaları serisi, Trabzon – H43 paftası. Ankara, Maden Tetkik ve Arama Genel Müdürlüğü.

MTA, 2016c. 1/100000 ölçekli jeoloji haritaları serisi, Trabzon – H44 paftası. Ankara, Maden Tetkik ve Arama Genel Müdürlüğü.

MTA, 2018. 1/100000 ölçekli jeoloji haritaları serisi, Trabzon – H42 paftası. Ankara, Maden Tetkik ve Arama Genel Müdürlüğü.

Murgeanu, G., Filipescu, M. G., 1933. Calpionella carpathica n. sp. dans les Carpathes roumaines. Notationes Biologicae, 1(2), 63-64.

Murphy, M.A., 1977. On time-stratigraphic units. Journal of Paleontology, 51 (2), 213-219.

Murphy, M.A., Salvador, A., 1999. International stratigraphic guide – An abridged version. Episodes, 22 (4), 255-272.

Muttoni, G., Erba, E., Kent, D.V., Bachtadse, V., 2005. Mesozoic Alpine facies deposition as a result of past latitudinal plate motion. Nature, 434, 59-63.

Münster, G.V., 1833. Verzeichnis der Versteinerungen, welche in der Kreis-Naturalien-Sammlung zu Bayreuth vorhanden sind: Bayreuth, published anonymously, 116 p.

Nagy, I., 1986. Investigation of Calpionellides from the Mecsek Mountains (S. Hungary). Acta Geologica Hungarica, 29(1-2), 45-64.

Neagu, T., 1975. Monographie de la faune des Foraminifères éocrétacés du couloir de la Dimbovicioara, de Codlea et des Monts Persani (Couches de Carhaga). Memoriile Institutului Geologic al României - Mémoires de l'Institut de Géologie et Géophysique, Bucarest, 25, 141 p. (available online at https://igr.ro/wp-content/uploads/2021/06/Mem_v25_Compressed.pdf)

Neagu, T., 2000. Lower Cretaceous calcareous agglutinated Foraminifera from Southern Dobrogea – Romania Part IV. Miscelianea (Litulolacea, Biokovinacea and Loftusiacea – Some new taxa). Acta Palaeontologica Romaniae, 2, 287-304.

Neamţu, O., Bucur, I.I., Ungureanu, R., Mircescu, C.V., 2019. Upper Jurassic-Lower Cretaceous limestones from the Hăghimaş Massif (Eastern Carpathians, Romania): Microfacies, microfossils and depostional environments. Carnets Geol., 19 (16), 345-368.

Nebert, K. 1961. Kelkit Çayı ve Kızılırmak (Kuzey Anadolu) nehirleri mecra bölgelerinin jeolojik yapısı, Maden Tetkik ve Arama Dergisi, 57, 1-49.

Nebert, K. 1964. Zur Geologie des Kelkit Çay – Oberlaufs Südwestlich von Şiran (Nordostanatolien), Maden Tetkik ve Arama Enstitüsü Dergisi, 62, 41-59.

Neumann, M., 1965. Contribution à l'étude de quelques lituolidés du Cénomanien de l'Ile Madame (Charente-Maritime). Revue de Micropaléontologie, 8, 90-95.

Nicosia, U. and Parisi, G., 1979, *Saccocoma tenella* (Goldfus) – Distribuzione stratigrafica e geografica, Bollettino della Società Paleontologica Italiana, 18 (2), 320-326.

Nikishin, A.M., Okay, A.İ., Tüysüz, O., Demirer, A., Wannier, M., Amelin, N., Petrov, E., 2015. The Black Sea basins structure and history: New model based on new deep penetration regional seismic data. Part 2: Tectonic history and paleogeography. Marine and Petroleum Geology, 59, 656-670.

Norman, T., 1976. Bayburt güneyindeki Alt Tersiyer havzasında paleo-akıntı yönleri. Türkiye Jeoloji Kurumu Bülteni, 19, 23-30.

Noujaim Clark, G., Boudagher-Fadel, M.K., 2001. The Larger Benthic Foraminifera and Stratigraphy of the Upper Jurassic/Lower Cretaceous of Central Lebanon. Revue de Micropaléontologie, 44 (3), 215-232.

Ocakoğlu, F., Hakyemez, A., Açıkalın, S., Özkan-Altiner, S., Büyükmeriç, Y., Licht, A., Demircan, H., Şafak, Ü., Yıldız, A., Yilmaz, İ.O., Wagreich, M., Campbell, C., 2019. Chronology of subduction and collision along the İzmir-Ankara suture in Western Anatolia: Records from the Central Sakarya Basin. International Geology Review, 61, 1244-1269.

Odin, G., Lamaurelle, M., 2001. The global Campanian-Maastrichtian Stage Boundary. Episodes, 24, 229-238.

Okay, A.İ. 1983. The geology of the Ağvanis metamorphic rocks and neighbouring formations, Maden Tetkik ve Arama Dergisi, 99/100, 16-36.

Okay, A.İ. 1984. Distribution and characteristics of the north-west Turkish blueschists. Geological Society of London, 17, 455-466.

Okay, A.İ. 1989. Tectonic Units and Sutures in the Pontides, Northern Turkey. In: Şengör. A.M.C. (Eds.), Tectonic Evolution of the Tethyan Region. NATO ASI Series, Series C: Mathematical and Physical Sciences, 259, 109-116.

Okay, A.İ., 1996. Granulite Facies Gneisses from the Pulur Region, Eastern Pontides, Turkish Journal of Earth Sciences, 5, 55-61.

Okay, A. İ., Leven, E. 1996. Stratigraphy and Paleontology of the Upper Paleozoic Sequence in the (Bayburt) Region, Eastern Pontides, Turkish Journal of Earth Sciences, 5, 145-155.

Okay, A.İ., Şahintürk, Ö., 1997. Geology of the Eastern Pontides. In: Robinson, A.G. (Eds.), Regional and petroleum geology in the Black Sea and surrounding region. American Associaiton of Petroleum Geologists, Memoir 68, 291-311.

Okay, A.İ., Tüysüz, O., 1999. Tethyan sutures of northern Turkey. Geological Society, London, Special Publications, 156, 475-515.

Okay, A.İ., Göncüoğlu, M.C., 2004. The Karakaya Complex: a review of data and concepts. Turkish Journal of Earht Sciences, 13, 77-95.

Okay, A.İ., Nikishin, A.M., 2015. Tectonic evolution of the southern margin of Laurasia in the Black Sea region. International Geology Review, 57, 1051-1076.

Okay, A.İ., Altiner, D., 2016. Carbonate sedimentation in an extensional active margin: Cretaceous history of the Haymana region, Pontides. International Journal of Earth Sciences, 105 (7), 2013-2030.

Okay, A.İ, Topuz, G., 2017. Variscan orogeny in the Black Sea region. International Journal of Earth Sciences. 106, 569-592.

Okay, A. İ., Siyako M., Bürkan K.A., 1990. Geology and tectonic evolution of the Biga Peninsula. Bulletin of Technical University of Istanbul, 44 (1-2), 191-256.

Okay, A.İ., Şengör, A.M.C., Görür, N., 1994. Kinematic history of the opening of the Black Sea and its effect on the surrounding regions. Geology, 22(3), 267-270.

Okay, A.İ., Şahintürk, Ö., Yakar, H., 1997. Stratigraphy and tectonics of the Pulur (Bayburt) region in the Eastern Pontides. Bulletin of the Mineral Research and Exploration, 119, 1-24.

Okay, A.İ., Altiner, D., Kılıç, A.M., 2015. Triassic limestones, turbidites and serpentinite–the Cimmeride orogeny in the Central Pontides. Geological Magazine, 152 (3), 460-479.

Okay, A.İ., Altiner, D., Kylander-Clark, A.R.C., 2019. Major Late Cretaceous mass flows in Central Turkey recording the disruption of the Mesozoic continental margin. Tectonics, 38 (3), 960-989.

Okay, A.İ., Zattin, M., Özcan, E., Sunal, G., 2020a. Uplift of Anatolia. Turkish Journal of Earth Sciences, 29, 696-713.

Okay, A.İ., Altıner, D., Özcan, E., Hakyemez, A., 2024. Significance of the Paleocene olistostrome-turbidite belt (Abant Formation) along the Intra-Pontide Sutude, northern Turkey. Journal of the Geological Society, 181(5), jgs2023-191.

Okay, A.İ., Satır, M., Tüysüz, O., Akyüz, S., Chen, F., 2001. The tectonics of the Strandja Massif: late-Variscan and mid-Mesozoic deformation and metamorphism in the northern Aegean. International Journal of Earth Sciences, 90, 217-233.

Okay, A.İ., Sunal, G., Sherlock, S., Kylander-Clark, A.R.C, Özcan, E., 2020b. İzmir-Ankara suture as a Triassic to Cretaceous plate boundary – data from central Anatolia. Tectonics, 39 (5), 1-21.

Okay, A.İ., Bozkurt, E., Satır, M., Yiğitbaş, E., Cowley, Q.G., Shang, C.K., 2008. Defining the southern margin of Avalonia in the Pontides: geochronological data from the Late Proterozoic and Ordivician granitoids from NW Turkey. Tectonophysics, 461, 252-264.

Okay, A. I., Sunal, G., Tüysüz, O., Sherlock, M., Keskin, M., Kylander-Clark, A. R. C. 2014. Low-pressure-high-temperature metamorphism during extension in a Jurassic magmatic arc, Central Pontides, Turkey. Journal of Metamorphic Geology, 32, 49-69.

Okay, A.İ., Sunal, G., Sherlock, S., Altiner, D., Tüysüz, O., Kylander-Clark, A.R.C., Aygül, M., 2013. Early Cretaceous sedimentation and orogeny on the active margin of Eurasia: southern Central Pontides, Turkey. Tectonic, 32, 1247-1271.

Okay, A.İ, Altiner, D., Sunal, G., Aygül, M., Akdoğan, R., Altiner, S., Simmons, M., 2018. Geological evolution of the Central Pontides. In: Simmons, M.D., Tari, G.C., Okay, A.İ. (Eds.), Petroleum Geology of the Black Sea. Geological Society, London, Special Publications, 464, 33-68.

Olóriz, F., Caracuel, J. E., Marques, B. and Rodriguez-Tovar, F. J., 1995. Associaciones de tintinoides en facies ammonitico rosso de la Sierrar Norte (Mallorca). Revista Espaňola de Paleontologia, 77-93.

Olszewska, B., 2010. Microfossils of the Upper Jurassic – Lower Cretaceous formations of the Lublin Upland (SE Poland) based on thin section studies. Polish Geological Institute Special Paper, 26. Warszawa, 54 p.

Olszewska, B., Matyszkiewicz, J., Król, K., Krajewski, M., 2012. Correlation of the Upper Jurassic-Cretaceous epicontinental sediments in southern Poland and southwestern Ukraine based on thin sections. Biuletyn Państwowego Instytutu Geologicznego, 453, 29-80.

Omaña, L., Arreola, C.G., 2008. Late Jurassic (Kimmeridgian) larger benthic Foraminifera from Santiago Coatepec, SE Puebla, Mexico. GEOBIOS, 41, 799-817.

Oppel, A.C., 1856-1858. Die Juraformation Englands, Frankreichs und des Südwestlichen Deutschlands. Württemberger Naturforschende Jahreshefte, 12-14, 857 p.

Önal, M., Helvacı, C., İnci, U., Yağmurlu, F., Meri, E., Tansel, İ., 1988. Çayırhan, Kuzeybatı Ankara Kuzeyindeki Soğukçam Kireçtaşı, Nardin Formasyonu ve Kızılçay Grubu'nun Stratıgrafisi, Yaşı, Fasiyesi ve Depolanma Ortamları. Türkiye Petrol Jeologları Derneği Bülteni, 1–2, 152-163.

Özcan, A., Erkan, A., Keskin, A., Oral, A., Özer, S, Sümengen, M., Tekeli, O., 1980. Kuzey Anadolu Fayı-Kırşehir Masifi arasının temel jeolojisi. Maden Tetkik ve Arama Enstitüsü, Rapor 6722 (yayımlanmamış/ unpublished).

Özdikmen, H., 2009. Substitute names for some unicellular animal taxa (Protozoa). Munis Entomology & Zoology, 4(1), 233-256.

Özkan, S., 1993. Calcareous nannofossils from the Late Jurassic – Early Cretaceous of northwest Anatolia, Turkey. Geological Journal, 28, 295-307.

Özkaya, İ., 1982. Origin and tectonic setting of some mélange units in Turkey. The Journal of Geology, 90(3), 269-278.

Özgül, N., 1976. Toroslar'ın bazı temel jeoloji özellikleri. Türkiye Jeoloji Kurumu Bülteni, 19, 65-78.

Özgül, N., 2012. Stratigraphy and some structural features of the İstanbul Paleozoic: Turkish Journal of Earth Sciences, 21, 817-866.

Özyurt, M., Kırmacı, M.Z., 2024. Microfacies and geochemistry of Kimmeridgian limestone strata in the Eastern Pontides (North-East Turkey): Palaeoclimate and palaeoenvironmental influence on organic matter enrichment. The Depositional Record, 2024;00, 1–18.

Özyurt, M., Kırmazı, M. Z., Al-Aasm, I., 2018. Geochemical characteristics of Late Jurassic – Early Cretaceous platform carbonates in Hazine Mağara, Gümüşhane (NE Turkey): Implications for dolomitization and recrystallization. Canadian Journal of Earth Sciences, 56 (3), 306-320.

Özyurt, M., Kandemir, R., Yıldızoğlu, S., 2023. Geochemistry of the Turonian-Coniacian strata: New insight into paleoenvironmental conditions of the Tethys, Eastern Pontides, NE Türkiye. Journal of Asian Earth Sciences, X (10), 100156.

Özyurt, M., Kırmacı, M.Z., Al-Aasm, I.S., Kandemir, R., 2024. Geochemistry of the Massive Dolomites in Eastern Black Sea Region: REE Implications for Dolomite Petrogenesis. Geochemistry International, 62 (2), 184-207.

Özyurt, M., Kırmacı, M.Z., Yılmaz, İ.Ö., Kandemir, R., Taslı, K., 2022. Sedimentological and geochemical approaches for determination of the palaeoceanographic and palaeoclimatic conditions of Lower Cretaceous marine deposits in the eastern part of Sakarya Zone, NE Turkey. Carbonates and Evaporites, 37, 25.

Page, K.N., 1995. Biohorizions and zonules: Intra-subzonal units in Jurassic ammonite stratigraphy. Palaeontology, 38 (4), 801-814.

Page, K.N., 2008. The evolution and geography of Jurassic ammonoids. Proceedings of Geologists' Association, 119, 35-57.

Page, K.N., 2017. From Oppel to Calloman (and beyond): Building a high-resolution ammonite-based biochronology for the Jurassic System. Lethia, 50 (3), 336-355.

Paul, R.K., 1983. Evolution of a biostratigraphic zonation: Lessons from Lower Triassic conodonts, U.S. Cordillera. Transactions of the Wisconsin Academy of Sciences, Arts and Letters, 71, 68-78.

Pawlowski, J., Holzmann, M., Tyszka, J., 2013, New supraordinal classification of Foraminifera: Molecules meet morphology. Marine Micropaleontology, 100, 1-18.

Pelin, S., 1977. Alucra (Giresun) Güneydoğu yöresinin petrol olanakları bakımından jeolojik incelenmesi. Doçentlik tezi, Trabzon, Karadeniz Üniversitesi, 103 p.

Petrova, S., Lakova, I., Ivanova, D., 2011. Berriasian-Valanginian boundary in Bulgaria. Review of the Bulgarian Geological Soceity, 72 (1-3), 91-97.

Petrova, S., Koleva-Rekalova, E., Ivanova, D., Lakova, I., 2019. Biostratigraphy and microfacies of the pelagic carbonate formations in the Yavorets section (Tithonian–Berriasian), Western Balkan Mts, Bulgaria. Geologica Balcanica, 48 (2), 51-73.

Petrova, S., Rabrenović, D., Lakova, I., Koleva-Rekalova, E., Ivanova, D., Metodiev, L., Malešević, N., 2012. Biostratigraphy and microfacies of the pelagic carbonates across the Jurassic/Cretaceous boundary in eastern Serbia (Stara Planina-Poreč Zone). Geologica Balcanica, 41 (1-3), 53-76.

Pettijohn, F.J. 1975. Sedimentary Rocks, 3rd Edition. Harper and Row, New York, 628 p.

Peybernès, B., 1998. 'Jurassic larger benthic Foraminifera' column in the Cretaceous Biochronostratigraphy Chart. In: Hardenbol, J.H., Thierry, J., Farley, M.B., Jacquin, T., de Graciansky, P-C., Vail, P.R., Mesozoic and Cenozoic Sequence Stratigraphy of European Basins, Mesozoic and Cenozoic

Sequence Chronostratigraphic Framework of European Basins. Society for Sedimentary Geology, Special Publication, 60.

Pignatti, J.S., 1998. The philosophy of larger foraminiferal biozonation – a discussion. Dela – Opera Sazu, 34 (2), 15-20.

Pignatti, J., Papazzoni, C.A., 2017. Oppelzones and their heritage in current larger foraminiferal biostratigraphy. Lethaia, 50, 369-380.

Platonov, E., Lakova, I., Petrova, S., Arkadiev, V., Tithonian and Lower Berriasian calpionellid against ammonite biostratgraphy of the Dvuyakornaya Formation in eastern Crimea. Geologica Balcanica, 43 (1-3), 63-76.

Pleş, G., Mircescu, C.V., Bucur, I.I., Săsăran, E., 2013. Encrusting micro-organisms and microbial structures in Upper Jurassic limestones from the Southern Cartpathians (Romania). Facies, 59, 19-48.

Pleş, G., Bucur, I.I., Păcurariu, A., 2015. Foraminiferal assemblages and facies associations in the Upper Jurassic Carboantes from Ardeu Unit (Metaliferi Mountains, Romania). Acta Paleontologica Romaniae, 11 (2), 43-57.

Pleş, G., Oprişa, A., Bucur, I.I., Săsăran, E., Mircescu, C.V., Oltean, G., Iacob, R.G., 2019. The central-western Getic Carbonate Platform: Upper Jurassic to Lower Cretaceous biostratigraphy and sedimentary evolution of the Cioclovina-Băniţa sector (Southern Carpathians, Romania). Facies, 65 (32).

Plotnick, R.E., 1986. Geological notes. Journal of Geology, 94, 885-890.

Pkornỳ, V., 1954. Základy zoologické mikropalentologie. Prague, 54-287.

Pop, G., 1974. Les zones de Calpionellides tithonique–valanginiennes du sillon de Reşiţa (Carpate méridionales). Revue Roumaine de Géologie, Géophysique et Géographie, Série de Géologie, 18, 109-125.

Pop, G., 1976. Tithonian – Valanginian calpionellid zones from Cuba. Dări de Seamă ale Ședințelor Institutul de Geologie și Geofizică, 3. Paleontologie, 62, 237-266.

Pop, G., 1986. Calpionellids and correlation of Tithonian-Valanginian formations. Acta Geologica Hungarica, 29, 93-102.

Pop, G., 1994. Calpionellid evolutive events and their use in biostratigraphy. Romanian Journal of Stratigraphy, 76, 7-24.

Pop, G., 1994a, Systematic revision and biochronology of some Berriasian – Valanginian calpionellids (Genus Remaniella), Geologica Carpathica, 45(6), 323-331

Pop, G., 1996. Trois nouvelles espéces du genre Remaniella (Calpionellidae Bonet, 1956). Comptes Rendus de I'Académie des Sciences Paris, 332, 317-323.

Pop, G., 1997. Révision systématique des chitinoïdelles tithoniennes des Carpathes méridionales (Roumanie). Comptes Rendus de l'Académies des Sciences, t. 324, Série II a, 931-938.

Pop, G., 1998. Stratigraphic distribution and biozonation of Tithonian praecalpionellids and calpionellids from the South Carpathians. Romanian Journal of Stratigraphy, 77, 3-25.

Price, G.D., Fözy, I., Pálfy, J., 2016. Carbon cycle history through the Jurassic-Cretaceous boundary: a new glocal δ13C stack. Palaeogeography, Palaeoclimatology, Palaeoecology, 451, 46-61.

Pruner, P., Houša, V., Olóriz, F., Košták, M., Krs, M., Man, O., Schnabl, P., Venhodová, D., Tavera, J.M., Mazuch, M., 2010. High-resolution magnetostratigraphy and biostratigraphic zonation of the Jurassic/Cretaceous boundary in the Puerto Escaño section (southern Spain). Cretaceous Research, 31, 192-206.

Pszczółkowski, A., 1996. Calpionellid stratigraphy of the Tithonian-Berriasian pelagic limestones in the Tatra Mts (Western Carpathians). Studia Geologica Polonica, 109, 103-130.

Pszczółkowski, A., Myczyński, R., 2004. Ammonite-supported microfossil and nannoconid stratigraphy of the Tithonian-Hauterivian limestones in selected sections of the Branisko Succession, Pieniny Klippen Belt (Poland). Studia Geologica Polonica, 123, 133-197.

Pszczółkowski, A., Myczyński, R., 2010. Tithonian-Early Valanginian evolution of deposition along the proto-Caribbean margin of North America recorded in Guaniguanico successions (western Cuba). Journal of South American Earth Sciences, 29, 225-253.

Purdy, E.G., 2008. Comparision of taxonomic diversity, strontium isotope and sea-level patterns. International Journal of Earth Sciences, 97, 651-664.

Radoičić, R., 1966. Microfacies du Jurassique des Dinarides extemes de la Yougoslavie. Geologija, 9, 5-23.

Rafinesque, C.S., 1815. Analyse de la nature ou Tableau de l'univers et des corps organisés. 1-224, (self-published) Palermo. (available online at http://gallica.bnf.fr/ark:/12148/bpt6k98061z.r=rafinesque.langEN)

Ravizza, G.E., Zachos, J.C., 2003. Records of Cenozoic Ocean Chemistry. Treatise on Geochemistry, 6, 551-581.

Rea, D.K., Lyle, M.W., Liberty, L.M., Hoň, S.A., Bolyn, M.P., Gleason, J.D., Hendy, I.L., Latimer, J.C., Mıurphy, B.M., Owen, R.M., Paul, C.F., Rea, T.H.C., Stancin, A.M., Thomas, D.J., 2006. Broad region of no sediment in the southwest Pacific Basin. Geological Soceity of America, 34 (10), 873-876.

Reboulet, S., Szives, O., Aguirre-Urreta, B., Barragán, R., Company, M., Frau, C., Kakabadze, M.V., Klein, J., Moreno-Bedmar, J.A., Lukeneder, A., Pictet, A., Ploch, I., Raisossadat, S.N., Vašíček, Z., Baraboshkin, E.J., Mitta, V.V.,

2018. Report on the 6th international meeting of the IUGS Lower Cretaceous Ammonite Working Group, the Kilian Group (Vienna, Austria, 20th August, 2017). Cretaceous Research, 91, 100-110.

Redmond, C.D., 1964. Lituolid foraminifera from the Jurassic and Cretaceous of Saudi Arabia. Micropaleoatology, 10, 405-414.

Reháková, D., 1995. Calpionellid distribution in Upper Jurassic and Lower Cretaceous sequences of the Western Carpathians. Mineralica Slovoca, 27, 308-318.

Reháková, D., 1998. Calpionellid genus Remaniella Catalano 1956 in Lower Cretaceous pelagic deposits of Western Carpathians. Mineralia Slovaca, 30, p. 443-452.

Reháková, D., Michalík, J., 1997. Evolution and distribution of calpionellids—the most characteristic constituents of Lower Cretaceous Tethyan microplankton. Cretaceous Research, 18, 493-504.

Reháková, D. and Michalik, J. 1997a, Calpionellid associations versus Late Jurassic and Early Cretaceous sea – level fluctuations. Mineralia Slovaca, 29, 306–307.

Reháková, D., Michalík, J., Ožvoldová, L., 1996. New Microbiostratigraphical Data from Several Lower Cretaceous Pelagic Sequences of the Northern Calcareous Alps, Austria (Preliminary Results). Geologisch-Paläontologische Mitteilungen, Inssbruk, 4, 57-81.

Reháková, D., Halásová, E., Lukeneder, A., 2009. The Jurassic-Cretaceous boundary in the Gresten Klippenbelt (Nutzhof, Lower Austria): Implications for Micro- and Nannofacies analysis. Annalen des Naturhistorischen Museums in Wien, 110 (A), 345-381.

Reháková, D., Matyja, B.A., Wierzbowski, A., Schlögl, J., Krobicki, M., Barski, M., 2011. Stratigraphy and microfacies of the Jurassic and lowermost Cretaceous

of the Veliky Kamenets section (Pieniny Klippen Belt, Carpathians, Western Ukraine). Volumina Jurassica, IX, 61-104.

Reichel, M., 1956. Sur une Trocholine du Valanginien d'Arzier. Eclogae Geologicae Helvetiae. 48, 396-408.

Remane, J., 1962. Zur Calpionellen-Systematik, Neus Jahbuch für Geologie und Paläontologie, Monatshefte, 1, 8-24.

Remane, J., 1963. Les Calpionelles dans les couches de passage jurassique-crétacé de la foss vocontienne. Travaux du Laboratoire de Géologie de la Faculté des Sciences de Grenoble, 39, 25-82.

Remane, J., 1971. Les Calpionelles, Protozoaires planctoniques des mers mésogéennes de l'époque secondaire. Annales Guébhard, 47, 369-432.

Remane, J., 1985. Calpionellids, In: Bolli, H. M., Saunders, J. B. and Perch-Nielsen, K. (Eds.): Plankton stratigraphy, Cambridge Earth Science Series, Cambridge University Press, 555-572.

Remane, J., 1991. The Jurassic-Cretaceous boundary: Problems of definition and procedure. Cretaceous Research, 12, 447-453.

Remane, 1998. Calpionellids. In: Hardenbol, J.H., Thierry, J., Farley, M.B., Jacquin, T., de Graciansky, P-C., Vail, P.R., Mesozoic and Cenozoic Sequence Stratigraphy of European Basins, Mesozoic and Cenozoic Sequence Chronostratigraphic Framework of European Basins. Society for Sedimentary Geology, Special Publication, 60.

Remane, J., 2003. Chronostratigraphic correlations: their importance for the definition of geochronologic units. Palaeogeography, Palaeoclimatology, Palaeoecology, 196, 7-18.

Remane, J., Bakalova-Ivanova, D., Borza, K., Knauer, J., Nagy, I., Pop, G., and Tardi-Filacz, E., 1986. Agreement on the subdivision of the standard

calpionellid zones defined at the II planktonic conference, Rome 1970, Acta Geolocia Hungarica, 29, 5-14.

Remane, J., Bassett, M.G., Cowie, J.W., Gohrbandt, K.H., Lane, H.R., Michelsen, O., Naiwen, W., 1996. Revised guidelines for the establishment of global chronostratigraphical standards by the International Commission on Stratigraphy (ICS). Episodes, 19 (3), 77-81.

Reuss, A.E., 1846. Die Versteinerungen der böhmischen Kreideformation. E. Schweizerbart, Stuttgart, 148 p.

Reuss, A.E., 1860. Die Foraminiferen der westphälischen Kreideformation. Sitzungsberichte der mathematisch-naturwissenschaflichen Classe der kaiserlichen Akademie der Wissenschaften, 40(8), 147-238. (available online at https://www.biodiversitylibrary.org/page/644236)

Reuss, A.E., Fritsch, A., 1861. Verzeichniss von 100 Gypsmodellen von Foraminiferen, welche unter der Leitung des Prof. A. Reuss und Dr Anton Fritsch gearbeitet wurden. Ausgegeben von W. Frič. Naturalienhändler in Prag, Karl Seyfried, Wassergasse Nro. 736-II.

Rigaud, S., Blau, J., Martini, R., Rettori, R., 2013. Taxonomy and phylogeny of the Trocholinidae (Involutinina). Journal of Foraminiferal Research, 43(4), 317-339.

Robertson, A.H.F., Ustaömer, T., 2012. Testing alternative tectono-stratigraphic interpretations of the Late Paleozoic-Early Mesozoic Karakaya Complex in NW Turkey: Support for and accretionary origin related to northward subduction of Palaeotethys. Turkish Journal of Earth Sciences, 21, 961-1007.

Robinson, A.G., Banks, C.J., Rutherford, M.M., Hirst, J.P.P., 1995. Stratigraphic and structural development of the Eastern Pontides, Turkey. Journal of the Geological Society, London, 152, 861-872.

Rojay, B.F., 1985. The tectonostratigraphic characteristics of the Kelkit Valley subzone of the North Anatolian Fault. M.Sc. Thesis, Middle East Technical University, Ankara, 105 p.

Rojay, B.F., 1993. Tectonostratigraphy and Neotectonic Characteristics of the southern margin of Merzifon-Suluova Basin (Central Pontides, Amasya). Ph.D Thesis, Middle East Technical Universitym Ankara, 216 p.

Rojay, B.F., 1995. Post-Triassic evolution of central Pontides: evidence from Amasya region, northern Anatolia. Geologica Romana, 31, 329-350.

Rojay, B.F., 2013. Tectonic evolution of the Cretaceous Ankara Ophiolitic Mélange during the Late Cretaceous to pre-Miocene interval in Central Anatolia, Turkey. Journal of Geodynamics, 65, 66-81.

Rojay, B.F., Süzen, M.L., 1997. Tectonostratigraphic evolution of the Cretaceous dynamic basins on accretionary ophiolitic melange prism, SW of Ankara region. The Bulletin of Turkish Association of Petroleum Geologists, 9 (1), 1-12.

Rojay, B.F., Altiner, D., 1998. Middle Jurassic – Lower Cretaceous Biostratigraphy in the Central Pontides (Turkey): Remarks on paleogeography and tectonic evolution. Rivista Italiana di Paleontologia e Stratigrafia, 104 (2), 167-180.

Roth, P.H., 1983. Jurassic and Lower Cretaecous calcareous nannofossil in the Western North Atlantic (site 534); biostratigraphy, preservation, and some observation on biogeography and paleoceanography. Initial Reports of the Deep Sea Drilling Project 76, 587-621.

Sadler, P.M., 1981. Sediment accumulation rates and the completeness of stratigraphic sections. Journal of Geology, 89, 569-584.

Saddler, P.M., 1999. The influence of hiatuses on sediment accumulation rates. GeoResearch Forum, 5, 15-40.

Sadler, P.M., 2020. Global composite sections and constrained optomization. In: Gradstein, F. M., Ogg, J.G., Schmitz, M.D., Ogg, G.M. (Eds.), Geologic Time Scale 2020. Elsevier, Amsterdam, 424-438.

Sadler, P.M., Cooper, R.A., Melchin, M., 2009. High-resolution, early Paleozoic (Ordovician-Silurian) time scales. Geological Societ of America Bulletin, 121 (5/6), 887-906.

Saidova, K.M., 1981. О современном состоянии системы надвидовых таксонов кайнозойских бентосных фораминифер - [On an up-to-date system of supraspecific taxonomy of Cenozoic benthonic foraminifera]. Akademiya Nauk SSSR. 79 p. (available online at https://books.google.pt/books?id=h-jxnSjjmhQC)

Sallouhi, H., Boughdiri, M., Cordey, F., 2011. Tithonian chitinoidellids of the South-Tetyhan margin of the Maghreb: New data from northern Tunisia. Comptes Rendus Palevol, 10, 641-653.

Salvador, A. (Eds.), 1994. International Stratigraphic Guide, A Guide to Stratigraphic Classification, Terminology, and Procedure, 2nd ed. International Union of Geological Sciences, Geological Society of America, 214 p.

Saner, S., 1980. Mudurnu – Göynük havzasının Jura ve sonrası çökelim nitelikleriyle paleocoğrafik yorumlaması. Türkiye Jeoloji Kurumu Bülteni, 23, 39-52.

Sarjeant, W.A.S., Wimbledon, W.A.P., 2000. The terminal Jurassic stage: history of a controversy in stratigraphy. Modern Geology, 24, 125-158.

Sayit, K., Göncüoğlu, M.C., 2013. Geodynamic evolution of the Karakaya mélange complex, Turkey: A review of geological and petrological constraints. Journal of Geodynamics, 65, 56-65.

Săsăran, E., Bucur, I. I. and Prica, I., 2001. Microfacies and microfossils in Upper Jurassic Limestones from Cheile Turenilor. Studia Universitatis Babeş-Bolyan, Geologica, XLVI (2), 35-52.

Schlager, W., 2010. Ordered hierarchy versus scale invariance in sequence stratigraphy. International Journal of Earth Sciences, 99, S139-S151.

Schlager, W., Marsal, D., van der Geest, P.A.G., Sprenger, A., 1998. Sedimentation rates, observation span, and the problem of spurious correlation. Mathematical Geology, 30 (5), 547-556.

Schlagintweit, F., 2004. *Iberopora bodeuri* Granier & Berthou 2002 (*incertae sedis*) from the Plassen Formation (Kimmeridgian – Berriasian) of the Tethys Realm. Geologica Croatica. 57 (1), 1-13.

Schlagintweit, F., 2011. The dasycladalean algae of the Plassen Carbonate Platform (Kimmeridgian – Early Berriasian): taxanomic inventory and palaeogeographical implications within the platform-basin-system of the Northern Calcareous Alps (Austria, p.p. Germany). Geologica Croatica, 64 (3), 185-206.

Schlagintweit, F., 2013. Taxanomic review of some Late Jurassic – Early Cretaceous benthic foraminifera established by Gollestaneh (1965) from the Zagros Fold and Thrust Belt of Iran. Acta Palaeontologica Romaniae, 9(2), 27-31.

Schlagintweit, F, 2012. *Mohlerina basiliensis* (Mohler, 1938): a Middle Jurassic-Early Cretaceous facultative (?) epilithic benthic foraminifera. Facies, 58, 637-647.

Schlagintweit, F., Ebli, O., 1999. New results on microfacies, biostratigraphy and sedimentology of Late Jurassic-Early Cretaceous platform carbonates of the Northern Calcareous Alps. Part I: Tressenstein Limestone, Plassen Formation. Abhandlungen der Geologischen Bundesanstalt, 56 (2), 379-418.

Schlagintweit, F., Gawlick, H.-J., 2002. The genus *Carpathiella* MISÍK, SOTÁK & ZIEGLER, 1999 (Serpulidae), its representatives from the Alpine Plassen Formation (Kimmeridgian – Berriasian) and description of *Carpathiella plassenensis* n. sp. Geologica Carpathica, Special Issue 2002, Carpato-Balkan Congress, supplement, 5 pages, Bratislava.

Schlagintweit, F., Gawlick, H.-J., 2007. Analysis of Late Jurassic to Early Cretaceous algal debris-facies of the Plassen carbonate platfrom in the Northern Calcareous Alps (Germany, Austria) and in the Kurbnesh area of the Mirdita zone (Albania): a tool to reconstruct tectonics and palaeogeography of eroded platform. Facies, 53, 209-227.

Schlagintweit, F., Gawlick, H.-J., 2008. The occurrence and role of microencrusters frameworks in Late Jurassic to Early Cretaceous platform margin deposits of the Northern Calcareous Alps (Austria). Facies, 54, 207-231.

Schlagintweit, F., Gawlick, H.-J., 2009. *Lituola*? *baculiformis* n. sp., a new benthic foraminifer from Late Jurassic peri-reefal carbonates of the Western Tethyan domain. Journal of Alpine Geology, 51, 39-49.

Schlagitnweti, F., Gawlick, H-J., 2011. Perturbatacrusta leini n. gen., n. sp. a new microencruster incertae sedis (? sponge) from Late Jurassic to earliest Cretaceous platform margin carbonates of the Northern Calcareous Alps of Austria. Facies, 57; 123-135.

Schlagintweit, F., Bucur, I.I., 2021. The late Berriasian early evolutionary burst of the Orbitolinidae: New insights into taxonomy, origin, diversification and phylogeny of the family based on data from eastern Serbia. Carnets Geol., 21 (15), 343-382.

Schlagintweit, F., Gawlick, H-J., Sanders, D., 2003. Serpulid tubes of the genus *Carpathiella* Mišík, Soták, & Ziegler, 1999 from the Upper Jurassic to Paleogene of the Northern Calcareous Alps (Austria, Germany). Mitt. Ges. Geol. Bergbaustud. Österr., 46, 91-110.

Schlagintweit, F., Gawlick, H.-J., Lein, R., 2003a. Die Plassen-Formation der Typlokalität (Salzkammergut, Österreich) – neue Daten zur Fazies, Sedimentologie und Stratigraphie. - Mitt. Ges. Geol. Bergbaustud. Österr., 46, 1-34.

Schlagintweit, F., Gawlick, H-J., Lein, R., 2005. Mikropaläontologie und Biostratigraphie der Plassen-Karbonatplattform der Typlokalität (Ober-Jura

bis Unter-Kreide, Salzkammergut, Österrich). Journal of Alpine Geology (Mitt. Ges. Geol. Bergbaustud. Österr.), 47, 11-112.

Schlagitnweit, F., Rosales, I., Najarro, M., 2016. *Glomospirella cantabrica* n. sp., and other benthic foraminifera from Lower Cretaceous Urgonian-type carbonates of Cantabria, Spain: Biostratigraphic implications. Geologica Acta, 14(2), 113-138

Schlagintweit, F., Bucur, I. I., Granier, B., Koch, R. 2019. *Barkerina dobrogiaca* Neagu, 2000, a Valanginian marker taxon from the northern Neotethysian margin, Cretaceous Research, 101, 76-83.

Schmid, D.U.,1996. Marine Mikrobiolithe und Mikroinkrustierer aus dem Oberjura. Profil, 9, 101–251.

Schmid, D. U., Leinfelder, R. R., 1996. The Jurassic *Lithocodium aggregatum* – *Troglotella incrustans* foraminiferal consortium. Palaeontology, 39(1), 21-52.

Schrodt, F., 1894. Das Vorkommen der Foraminiferen-Gattung Cyclammina im oberen Jura. Zeitschrift der Deutschen Geologischen Gesellschaft, 45, 733-735.

Schroeder, R., 1968. Sobre algunos foraminiferos del Valanginense de la Sierra de Valdancha (provincial de Castellon). Boletin de la Real Sociedad Espanola de Historia Natural 66, 311e318.

Schultze, M. J. S., 1854. Über den Organismus der Polythalamien (Foraminiferen), nebst Bemerkungen über die Rhizopoden im allgemeinen. Ingelmann, Leipzig. 68 p. (available online at https://books.google.pt/books?id=o7rk00_xueQC)

Schwager, C., 1876. Saggio di una classificazione dei foraminiferi avuto riguardo alle loro famiglie naturali, Bolletino R. Comitato Geologico d'Italia, 7, 475-485. (available online at https://biodiversitylibrary.org/page/53477189)

Schwager, C., 1877. Quadro del proposto sistema di classificazione dei foraminiferi con guscio. Bolletino R. Comitato Geologico d'Italia, 8, 18-27. (available online at https://biodiversitylibrary.org/page/53535675)

Scott, G.H., 2013. Biostratigraphy: Interpretations of Oppel's zones. Earth-Sciences Reviews, 126, 266-274.

Scott, R.W., 2019. Jurassic-Cretaceous boundary bioevents and magnetochrons: A stratigraphic experimen. Cretaceous Research, 100, 97-104.

Senowbari-Daryan, B., Bucur, I.I., Schlagintweit, F., Săsăran, E., Matyszkiewicz, J., 2008. *Crescentiella*, a new name for "*Tubiphytes*" *morronensis* CRESCENTI, 1969: an enigmatic Jurassic-Cretaceous microfossil. Geologica Croatica, 61(2-3), 185-214.

Sepkoski, J.J.Jr., Koch, C.E., 1996. Evaluating paleontological data relating to bio-events. In: Walliser, O.H. (Eds.), Global events and event stratigraphy, Springer, Berlin, 21-34.

Septfontaine, M., 1974. Présence de Protopeneroplis trochangulata sp. nov. (Foraminifère) dans le Crétacé inférieur du Jura méridional et révision de Protopeneroplis Weynschenk, 1950. Eclogae Geologicae Helvetiae, 67 (3), 605-628.

Septfontaine, M., 1980-81. Les foraminifères imperforés des milieux de plate-forme au Mésozoïque: Détermination pratique, interprétation phylogénétique et utilisation biostratigraphique. Revue de Micropaléontologie, 23 (3/4), 169-203.

Septfontaine, M, 1988. Vers une classification évolutive des Lituolidés (Foraminiféres) jurassiques en milieux de plate-forme carbonatée, Revue de Palébiologie, Vol. Spéc. 2 (Benthos '86), 229-256.

Septfontaine, M., 1991. Les foraminifères imperforés des plates-formes carbonatées jurassiques: État des connaissances et perspectives d'avenir. Bulletin de la Société vaudoise des Sciences naturelles, 80 (3), 255-277.

Septfontaine, M., 2020. Steps of morphogenesis and iterative evolution of imperforate larger Foraminifera in shallow carbonate shelves during Mesozoic times: Possible relations to symbiotic and abiotic factors. In: Guex, J., Torday, J.S., Miller Jr., W.B. (Eds.), Morphogenesis, environmental stress and reverse evolution, Springer, 129-174.

Serra-Kiel, J., Hottinger, L., Caus, E., Drobne, K., Ferràndez, C., Jauhri, A.K., Less, G., Pavlovec, R., Pignatti, J., Samsó, J.M., Schaub, H., Sirel, E., Strougo, A., Tambareau, Y., Tosquella, J., Zakrevskaya, E., 1998. Larger foraminiferal biostratigraphy of the Tethyan Paleocene and Eocene. 169 (2), 281-299.

Seymen, İ., 1975. Kelkit vadisi kesiminde Kuzey Anadolu Fay Zonunun tektonik özelliği. İstanbul Teknik Üniversitesi, İstanbul, 192.

Shaw, A.B., 1964. Time in stratigraphy. McGraw-Hill, New York, 365.

Silva, P., McNulty, C.L., 1984. Planktonic Foraminifers and Calpionellids From Gulf of Mexico Sites, Deep Sea Drilling Project Leg 77. DSDP Reports and Publications, LXXVII, 22, 547-584.

Sinnesael, M., De Vleeschouwer, D., Zeeden, C., Batenburg, S.J., Da Silva, A-C., de Winter, N.J., Dinarès-Turell, J., Drury, A.J., Gambacorta, G., Hilgen, F.J., Hinnov, L.A., Hudson, A.J.L., Kemp, D.B., Lantink, M.L., Laurin, J., Li, M., Liebrand, D., Ma, C., Meyers, S.R., Monkensbusch, J., Montanari, A., Nohl, T., Pälike,H., Pas, D., Ruhl, M., Thibault, N., Vahlenkamp, M., Valero, L., Wouters, S., Wu, H., Claeys, P., 2019. The Cyclostratigraphy Intercomparison Project (CIP): Consistency, merits, and pitfalls. Earth-Science Reviews, 199, 1-16.

Simmons, M.D. 1994. Micropalaeontological biozonation of the Kahmah Group (Early Cretaceous), Central Oman Mountains. In: Simmons, M.D. (Eds.), Micropalaeontology and hydrocarbon exploration in the Middle East. Chapman & Hall, London, New York, 177-206.

Sirel, E., 1993. Kastamonina abanica, n.gen. n.sp., a Complex Lituolid (Foraminiferida) from the Upper Jurassic Limestone of the Kastamonu Area (North Turkey). Geologica Croatica, 46(1), 1-7.

Skompski, S., 1982. The nature and systematic position of the microfossils *Globochaete alpina* Lombard, 1945. Acta Geologioa Polonica, 32,(1-2), 47-59.

Skourtsis-Coroneou, V. and Solakius, N. 1999, Calpionellid zonation at the Jurassic/Cretaceous boundary within the Vigla Limestone Formation (Ionian Zone, western Greece) and carbon isotope analysis, Cretaceous Research, 20, 583–595.

Smith, W., 1815. A memoir to the map and delineation of the strata of England and Wales, with part of Scotland. London, John Carey, x + 51 p. + 1 p. of errata.

Smith, A.G., Barry, T., Bown, P., Cope, J., Gale, A., Gibbard, P., Gregory, J., Hounslow, M., Kemp, D., Knox, R., Marshall, J., Oates, M., Rawson, P., Powell, J., Waters, C., 2015. GSSPs, global stratigraphy and correlation. In: Smith, D.G., Bailey, R.J., Burgess, P.M., Fraset, A.J. (Eds.), Strata and Time: Probing the gaps in our understanding. Geological Society, London; Special Publications, 404, 37-67.

Smout, A.H., Sugden, W., 1962. New information on the foraminiferal genus *Pfenderina*. Palaeontology, 4, 581-591.

Senowbari-Daryan, B., Bucur, I.I., Schlagintweit, F., Săsăran, E., Matyszkiewicz, J., 2008. *Crescentiella*, a new name for "*Tubiphytes*" *morronensis* CRESCENTI, 1969: an enigmatic Jurassic – Cretaceous microfossil. Geologica Croatica, 61(2-3), 185-214.

Soycan, H., 2017. Doğu Pontidler (Trabzon, Bayburt, Erzurum ve Artvin) Orta Jura ve Üst Kretase Volkano-sedimanter İstiflerinin Radyolarya Taksonomisi, Biyostratigrafisi ve Çökel Ortamları. Doktora Tezi, Ankara, Hacettepe Üniversitesi, 514 p.

Soycan, H., Hakyemez, A., 2018. The first calibration of radiolarian biochronology with Late Cretaceous (latest Coniacian – Santonian to early Campanian) planktonic foraminifera in the volcano-sedimentary sequences of the Eastern Pontides, NE Turkey. Cretaceous Research, 85, 319-348.

Speijer, R.P., Pälike, H., Hollis, C.J., Hooker, J.J., Ogg, J.G. Paleogene biostratigraphy. In: Gradstein, F. M., Ogg, J.G., Schmitz, M.D., Ogg, G.M. (Eds.), Geologic Time Scale 2020. Elsevier, Amsterdam, 1105-1123.

Stampfli, G.M., Hochard, C., 2009. Plate tectonics of the Alpine realm. Geological Society, London, Special Publication, 327, 89-111.

Steininger, F.F., Aubry, M.P., Berggren, W.W., Biolzi, M., Borsetti, A.M., Carlidge, J.E., Cati. F., Corfield, R., Gelati, R., Jaccarino, S., Napoleone, C., Ottner, F., Rögl, F., Roetzel, F., Spezzaferri, S., Tateo, F., Villa, G., Zevenboom, D., 1997. The Global Stratotype Section and Point (GSSP) for the base of the Neogene. Episodes, 20, 23-28.

Strasser, A. 2016. Hiatuses and condensations: An estimation of time lost on a shallow carbonate platform. The Journal of the International Association of Sedimentologists, 1 (2), 91-117.

Strauss, D., Sadler, P.M., 1989. Stochastic models for the completeness of stratigraphic sections. Mathematical Geology, 21 (1), 37-59.

Sunal, G., Satır, M., Natal'in, B., Topuz, G., von der Schmidt, O., 2011. Metamoprhism and diachronous cooling in a contractional orogen: the Strandja Massif, NW Turkey. Geological Magazine, 148, 580-596.

Svobodová, A., Košťák, M., 2016. Calcareous nannofossils of the Jurassic/Cretaceous boundary strata in the Puerto Escaño section (southern Spain) – biostratigraphy and palaeoecology. Geologica Carpathica, 67 (3), 223-238.

Svobodová, A., Švábenická, L., Reháková, D., Svobodová, M., Skupien, P., Elbra, T., Schnabl, P., 2019. The Jurassic/Cretaceous boundary and high resolution biostratigraphy of the pelagic sequences of the Kurovice section (Outer Western Carpathians, the northern Tethyan margin). Geologica Carpathica, 70 (2), 153-182.

Ślączka A., Bąk, M., Pfersmann, C., Koukal, V., Wagreich, M., Kowalik, S., Maslo, M., 2018. Jurassic-Cretaceous radiolarian-bearing strata from the Gresten Klippen Zone and the St. Veit Klippen Zone (Wienerwald, Eastern Alps, Austria): Implications for stratigraphy and paleogeography. Austrian Journal of Earth Sciences, 111 (2), 204-222.

Şen, C. 2007. Jurassic volcanism in the Eastern Pontides: is it rift related or subduction related?, Turkish Jourmal of Earth Sciences, 16, 523-539.

Şengör, A.M.C., 1979. Mid-Mesozoic closure of Permo-Triassic Tethys and its implications. Nature, 279, 590-593.

Şengör, A.M.C., 1990. A new model for the late Paleozoic-Mesozoic tectonic evolution of Iran and implications for Oman. In: Robertson, A.H.F., Searle, M.P., Ries, A.C. (Eds.), The Geology and Tectonics of the Oman Region. Geological Society Special Publication, 49, 797-831.

Şengör, A.M.C., 2016. What is the use of the history of geology to a practicing geologist? The propaedeutical case of stratigraphy. The Journal of Geology, 124 (6), 643-698.

Şengör. A.M.C., Yılmaz, Y., 1981. Tethyan evolution of Turkey: Plate tectonic approach. Tectonophysics, 75, 181-241.

Şengör, A. M. C., Yılmaz, Y., Ketin, İ. 1980. Remnant of a pre-Late Jurassic ocean in northern Turkey: Fragments of Permian-Triassic Paleo-Tethys?, 91, 599-609.

Şengör, A.M.C., Atayman, S., Özeren, S., 2008. A scale of greatness and causal classification of mass extinctions: Implications for mechanisms. PNAS, 105 (37), 13736-13740.

Şengör, A.M.C., Altiner, D., Cin, A., Ustaömer, T., Hsü, K.J., 1988. Origin and assembly of the Tethyside orogenic collage at the expense of Gondwana Land. In: Audley-Charles, M.G., Hallam, A. (Eds.), Gondwana and Tethys. Geological Society, London, Special Publication, 37, 119-181.

Taslı, K. 1984. İkisu (Gümüşhane) ile Hamsiköy (Trabzon) yörelerinin jeolojisi ve Berdiga Formasyonu'nun biyostratigrafik deneştirmesi. Yüksek lisans tezi, Trabzon, Karadeniz Teknik Üniversitesi, 120 p.

Taslı, K. 1990. Gümüşhane ve Bayburt Yörelerindeki Üst Jura-Alt Kretase Karbonat İstiflerinin Stratigrafik, Paleocoğrafik ve Mikropaleontolojik İncelenmesi, Doktora Tezi. Trabzon, Karadeniz Teknik Üniversitesi, 223 p.

Taslı, K., 1993. Micropaléontologie, stratigraphie et environnement de dépôt des séries Jurassiques à faciès de plate-forme de la région de Kale-Gümüşhane (Pontides Orientales, Turquie), Revue de Micropaléontologie, 36 (1), 45-65.

Taslı, K., 1997. Stratigraphical and paleontological data on the Malm volcanism in the Eastern Pontides (NE Turkey). İstanbul Üniversitesi, Earth Sciences Bulletin, 8/1-3, 95-101.

Taslı, K., Özsayar, T. 1997. Stratigraphy and paleoenvironmental setting of the Albian-Campanian deposits within the Gümüşhane Province (Eastern Pontides, NE Turkey). Türkiye Petrol Jeologları Derneği Bülteni, 9, 13-29.

Taslı, K., Özer, E., Yılmaz, C. 1999. Biostratigraphic and Environmental Analysis of the Upper Jurassic – Lower Cretaceous Carbonate Sequence in the Başoba Yayla Area (Trabzon, NE Turkey). Turkish Journal of Earth Sciencis, 8, 125-135.

Taslı, K., Altıner, D., Koç, H., Eren, M., 2008. Benthic foraminiferal biostratigraphy of the Jurassic carbonate succession in the Bolkar Mountains (southern Turkey). Micropaleontology, 54(5), 425-444.

Teichert, C., 1958. Some biostratigraphical concepts. Bulletin of the Geological Society of America, 69, 99-120.

Tekeli, O., 1981. Subduction complex of pre-Jurassic age, Northern Anatolia, Turkey. Geology, 9, 68-72.

Thalmann, H.E., 1951. *Coscinophragma* n. nom. Für Polyphragma Reuss, 1871 (non Quatrefages, 1865). Eclogae Geologicae Helvetiae, 40 (2), 221.

Timur, E., 1997. Yeşirçöl Dağı (Aşkale, Erzurum) Dolayının Jeolojisi ve Sedimenter Özellikleri. Doktora Tezi, İstambul, İstanbul Üniversitesi, Jeoloji Mühendisliği Anabilim Dalı, 204 p.

Timur, E., 2000, Yesirçöl Dağı (Aşkale, Erzurum) ve Dolayının Stratigrafisi, İstanbul Üniversitesi Mühendilsik Fakültesi Yerbilimleri Dergisi, 13 (1-2), 85-99.

Tipper, J.C., 1983. Rates of sedimentation, and stratigraphical completeness. Nature, 302, 696-698.

Tipper, J.C., 2015. The importance of doing nothing: stasis in sedimentation systems and its stratigraphic effects. In: Smith, D.G., Bailey, R.J., Burgess, P.M., Fraset, A.J. (Eds.), Strata and Time: Probing the gaps in our understanding. Geological Society, London; Special Publications, 404, 105-122.

Tobler A., 1928. Über Pseudocyclammina und *Choffatella* im Sehweizerischen Juragebirge. Eclogae Geologicae Helvetiae, 21, 212-216.

Toker, V., 1976. Stratigraphical studies of the area located between Nallıhan and Bozyaka villages along the Sorgun River. Communications de la Faculté de Sciences de l'Université d'Ankara, C 1, Géologie, 19, 1-63.

Topuz, G., Altherr R., Satır M., Schwarz, M., 2004. Low grade metamorphic rocks from the Pulur complex, NE Turkey: Implications for pre-Liassic evolution of the Eastern Pontides. International Journal of Earth Sciences 93, 72–91.

Topuz, G., Altherr, R., Schwartz, W. H., Dokuz, A., Meyer, H. P. 2007. Variscan amphibolite-facies rocks from Kurtoğlu metamorphic complex (Gümüşhane area, Eastern Pontides, Turkey). International Journal of Earth Science, 96, 861-873.

Topuz, G., Okay, A. I., Altherr, R., Schwarz, W. H., Sunal, G., Altınkaynak, L. 2014. Triassic warm subduction in northeast Turkey: Evidence from the Ağvanis metamorphic rock, Island Arc, 23, 181-205.

Topuz, G., Candan, O., Okay, A.İ., von Quadt, A., Othman, M., Zack, T., Wang, J., 2019. Silurian anorogenic basic and acidic magmatism in Northwest Turkey: Implications for the opening of the Paleo-Tethys. Lithos, 356-357, 1-14.

Topuz, G., Altherr, R., Candan, O., Wang, J.M., Okay, A.İ., Wu, F.Y., Zack, T., Siebel, W., Shangh, C.K., Schwarz, W.H., Meyer, H.P., Satır, M., 2023. Carboniferous mafic-ultramafic intrusions in the Eastern Pontides (Pulur Complex): Implications for the source of coeval voluminous granites. Lithos, 436-437, 106946.

Torrens, H.S., 2002. Some personal thoughts on stratigraphic precision in the twentieth century. In: Oldroyd, D.R. (Eds.), The Earth inside and out: some major contributions to geology in the twentieth centruy. Geological Society, London, Special Publications, 192, 251-272.

Trabucho-Alexandre, J., 2015. More gaps than shale: Erosion of mud and its effect on preserved geochemical and palaeobiological signals. In: Smith, D.G., Bailey, R.J., Burgess, P.M., Fraset, A.J. (Eds.), Strata and Time: Probing the gaps in our understanding. Geological Society, London; Special Publications, 404, 251-270.

Trejo, M., 1975. Los Tintínidos mesozoicos de México. In: Colloque International sur la limite Jurassique–Crétacé, Lyon-Neuchâtel, 1973. Mémoires du Bureau de Recherches Géologiques et Minières 86, 95–104.

Trejo, M., 1980. Distribución estratigráfica de los tintínidos Mesozoicos Mexicanos. Revista del Instituto Mexicano del Petroleo, 12, 4-13.

Tunç, M., 1991, Aktaş (Kızılcahamam) yöresinin pelajik kireçtaşlarının biyostratigrafisi, Türkiye Jeoloji Bülteni, 34, 27-42

Tunç, M. 1992. Olur (Erzurum) yöresindeki Üst Jura – Akt Kretase yaşlı kireçtaşlarının biyostratigrafisi, Türkiye Jeoloji Bülteni, 35, 121-130.

Tüysüz, O., 1999. Geology of the Cretaceous sedimentary basins of the Western Pontides. Geological Journal, 34, 75-93.

Tüysüz, O., Yiğitbaş, E., Yılmaz, Y., Serdar, H., S., 1990. Orta Pontidlerde Üst Jura – Alt Kretase stratigrafisi ve tektonik anlamı. Türkiye 8. Petrol Kongresi Bildirileri, 340-350.

Ustaömer, T., Robertson, A.H.F., 2010. Late Palaeozoic – Early Cenozoic tectonic development of the Eastern Pontides (Artvin area), Turkey: stages of closure of Tethys along the southern margin of Eurasia. In: Sosson, M., Kaymakcı, N., Stephenson, R.A., Bergerat, F., Starostenko, V. (Eds.), Sedimentary Basin Tectonics from the Black Sea and Caucasus to the Arabian Platform. Geological Society, London, Special Publications, 340, 281-327.

Ustaömer, P.A., Mundil, R., Renne, P.R., 2005. U/Pb and Pb/Pb zircon ages for arc-related intrusions of the Bolu Massif (W Pontides, NW Turkey): Evidence for Late Precambrian (Cadomian) age. Terra Nova, 17 (3), 215-223.

Uta, A., Bucur, I.I., 2003. Microbil structures and microencrusters in the Upper Jurassic-Lower Cretaceous deposits from Buila-Vânturarita Massif (South Carpathians). Studia Universitatis Babeş-Bolyai, XLVIII (2), 3-14.

van Hinsbergen, D.J.J., Torsvik, T.H., Schmid, S.M., Maţenco, L.C., Maffione, M., Vissers, R.L.M., Gürer, D., Spakman, W., 2020. Orogenic architecture of the Mediterranean region and kinematic reconstruction of its tectonic evolution since the Triassic. Gondwana Research, 81, 79-229.

Vaňková, L., Elbra, T., Pruner, P., Vašíček, Z, Skupien, P., Reháková, D., Schnabl, P., Košťák, M., Švábenická, L., Svobodová, A., Bubík, M., Mazuch, M., Čížková, K., Kdýr, Š., 2019. Integrated stratigraphy and palaeoenvironment of the Berriasian peri-reefal limestones at Štramberk (Outer Western Cartpathians, Czech Republic). Palaeogeography, Palaeoclimatology, Palaeoecology, 532, 109256.

Varol, B., Gökten, E., 1994. The facies properties and depositional environments of nodular limestones and red marly limestones (Ammonitico Rosso) in the Ankara Jurassic sequence, central Turkey. Terra Nova, 6, 64-71.

Vaughan, S., Bailey, R.J., Smith, D.G., 2011. Detecting cycles in stratigraphic data: Spectral analysis in the presence of red noise. Paleoceanography, 26 (PA4211), 1-15.

Vörös A., Kandemir, R., 2011. A new Early Jurassic brachiopod fauna from the Eastern Pontides (Turkey). Neues Jahrbuch für Geologie und Paläontologie – Abhandlungen, 260(3), 343-363.

Vulpius, S., Kiessling, W., 2018. New constraints on the last aragonite-calcite sea transition from early Jurassic ooids. Facies, 64(3), 1-9.

Vincent, S. J., Guo, L., Flecker, R., BouDagher-Fadel, M. K., Ellam, R. M., Kandemir, R. 2018. Age constraints on intra-formational unconformities in Upper Jurassic-Lower Cretaceous carbonates in northeast Turkey; geodynamic and hydrocarbon implications. Marine and Petroleum Geology, 91, 639-657.

Wade, B.S., Pearson, P.N., Berggren, W.A., Pälike, H., 2011. Review and revision of Cenozoic tropical planktonic foraminiferal biostratigraphy and calibration to the geomagnetic polarity and astronomical time scale. Earth-Science Reviews, 104, 111-142.

Wedding, H. 1963. Kelkit Hattı Jeolojisine Ait Düşünceler ve Kelkit-Bayburt (Gümüşhane) Çevresindeki Jura Stratigrafisi, Maden Tetkik ve Arama Dergisi, 61, 30-36.

Weissert, H., Lini, A., Föllmi, K.B., Kuhn, O., 1998. Correlation of Early Cretaceous carbon isotope stratigraphy and platform drowning events: a possible link? Palaeogeography, Palaeoclimatology, Palaeoecology, 138, 189-203.

Wernli, R., 1988. Les protoglobigérines (foraminifères) du Toarcien et de l'Aalénien du Domuz Dag (Taurus Occidental, Turquie). Eclogae Geologicae Hlevetiae, 81 (3), 661-668.

Weynschenk, R., 1950, Die Jura-mikrofauna und –flora des Sonnwendgebirges (Tirol), Schlern-Schr., 83, 1-32.

Wilson, J. L., 1975, Carbonate facies in geologic history, Springer-Verlag, NewYork, 471 p.

Wimbledon, W.A.P., 1997. The Jurassic-Cretaceous boundary: An age-old correlative enigma. Episodes, 31 (4), 423-428.

Wimbledon, W.A.P., 2017. Developments with fixing a Tithonian/Berriasian (J/K) boundary. Volumina Jurassica, XV, 181-186.

Wimbledon, W.A.P., Mohialdeen, I.M.J., Andreini, G., Rehakova, D., Stoykova, K., 2016. The Jurassic/Cretaceous boundary beds in Kurdistan – a preliminary note on wider correlations. Special Issue, GeoKurdistan II, 269-276.

Wimbledon, W.A.P., Reháková, D., Pszczółkowski, A., Casellato, C.E., Halásová, E., Frau, C., Bulot, L.G., Grabowski, J., Sobień, K., Pruner, P., Schnabl, P., Čížková, K., 2013. An account of the bio- and magnetostratigraphy of the Upper Tithonian – Lower Berriasian interval at Le Chouet Drôme (SE France). Geologica Carpathica, 64(6), 437-460.

Wimbledon, W.A.P., Reháková, D., Svobodová, A., Elbra, T., Schnabl, P., Pruner, P., Šifnerová, K., Kdýr, Š., Dzyuba, O., Schnyder, J., Galbrun, B., Košťák, M., Vaňková, L., Copestake, P., Hunt, C.O., Riccardi, A., Poulton, T.P., Bulot, L.G., Frau, C., de Lena, L., 2020a. The porposal of a GSSP for the Berriasian Stage (Cretaceous System): Part 1. Volumina Jurassica, 18 (1), 53-160.

Wimbledon, W.A.P., Reháková, D., Svobodová, A., Schnabl, P., Pruner, P., Elbra, T., Šifnerová, K., Kdýr, Š., Frau, C., Schnyder, J., Galbrun, B., 2020b. Fixing a J/K boundary: A comparative account of key Tithonian-Berriasian profiles

in the departments of Drôme and Hautes-Alpes, France. Geologica Carpathica, 71 (1), 24-26.

Winterer, E.L., Bosellini, A., 1981. Subsidence and sedimentation on Jurassic passive continental margin, southern Alps, Italy, The American Association of Petroleum Geologists, 65, 394-421.

Woodburne, M.O., Swisher, C.C.III, 1995. Land mammal high-resolution geochronolgy, intercontinental overland dispersals, sea level, climate, and vicariance. In: Berggren, W.A., Kent, D.V., Aubry, M-P., Hardenbol, J. (Eds.), Geochronolgy Time Scales and Global Stratigraphic Correlation, Socity of Petroleum Geologists Special Publications, 54, 335-364.

Wu, K., Tong, J., Metcalfe, I., Liang, L., Xiao, Y., Tian, L., 2020. Quantitative stratigraphic correlation of the Lower Triassic in South China based on conodont unitary associations. Earth-Science Reviews, 200, 1-21.

Yabe, H. and Hanzawa, S., 1926. *Choffatella* Schlumberger and *Pseudocyclammina*, a new genus of aranaceous foraminifera. Tohoku University Science Reports, series 2 (Geology), 9(1), 9-11.

Yılmaz, A. 1989. Kafkasya'nın tektonik kuşakları ve bu kuşakların kuzeydoğu Türkiye'deki uzantıları: bir karşılaştırma. Maden Tetkik ve Arama Dergisi, 109, 89-106.

Yılmaz, A., Adamia, S., Chabukiani, A., Chkhotua, T., Erdoğan, K., Tuzcu, S., Karabıyıkoğlut, M. 2000. Structural correlation of the southern Transcaucasus (Georgia) – eastern Pontides (Turkey). In: Bozkurt, E., Winchester, J. A., Piper, J. D. A. (Eds.), Tectonic magmatisim in Turkey and the Surrounding Area. Geological Society, London, Special Publications, 173, 171-182.

Yılmaz, C. 1992. Kelkit (Gümüşhane) Yöresinin Stratigrafisi. Jeoloji Mühendisliği, 40, 50-62.

Yılmaz, C. 1997. The sedimentological records of the Cretaceous platform-basin transition in the Gümüşhane region (NE Turkey). Géologie Méditerranéenne, 24 (1-2), 125-135.

Yılmaz, C., Kandemir, R. 2006. Sedimentary records of the extensional tectonic regime with temporal cessation: Gümüşhane Mesozoic Basin (NE Turkey). Geologica Carpathica, 57 (1), 3-13.

Yılmaz, H. U. 1985. Olur (Erzurum) yöresinin stratigrafi. Karadeniz Üniversitesi Dergisi, Jeoloji, 4 (1-2), 23-41.

Yılmaz, İ.Ö., Altıner, D., 2001. Use of sedimentary structures in the recognition of sequence boundaries in Upper Jurassic–Upper Cretaceous peritidal carbonates of the Western Taurides, Turkey. International Geology Review, 43, 736-753.

Yilmaz, İ.Ö., Altiner, D., Ocakoğlu, F., 2016. Upper Jurassic – Lower Cretaceous depositional environments and evolution of the Bilecik (Sakarya Zone) and Tauride carbonate platforms, Turkey. Palaeogeography, Palaeoclimatology, Palaeoecology, 449, 321-340.

Yilmaz, İ.Ö., Altiner, D., Tekin, U.K., Ocakoğlu, F., 2012. The first record of the "Mid-Barremian" Oceanic Anoxic Event and the Late Hauterivian platform drowning of the Bilecik platform, Sakarya Zone, western Turkey. Cretaceous Research, 38, 16-39.

Yılmaz, Y. 1976. Geology of the Gümüşhane granite (petrography). İstanbul Üniversitesi Fen Fakültesi Mecmuası, 39 (B), 157-172.

Yılmaz, Y., Tüysüz, O., 1984. Kastamonu – Boyabat – Vezirköprü - Tosya arasındaki bölgenin jeolojisi (Ilgaz - Kargı masiflerinin etüdü). MTA Raporu, 7883, 275 p.

Yılmaz, Y., Tüysüz, O., Gözübol, A. M., and Yiğitbaş, E., 1981. Abant (Bolu) – Dokurcan (Sakarya) arasındaki Kuzey Anadolu Fay Zonunun kuzey ve

güneyinde kalan tektonik birliklerin jeolojik evrimi. İstanbul Üniversitesi Yerbilimleri, 1, 239-261.

Yılmaz, Y., Tüysüz, O., Yiğitbaş, E., Gen., Ş. C., Şengör, A. M. C. 1997. Geology and Tectonic Evolution of the Pontides. In: Robinson, A. G. (Ed.), Regional and petroleum geology of the Black Sea and surrounding region. American Association Petroleum Geologists, Memoir 68, 183-226.

Yokoyama, M., 1890. Foraminiferan aus dem Kalksteine von Torinosu und Kompira, In: Naumann, E. & Neumayr, M. (Hrsg.), Zur Geologie und Paläntologie von Japan. Denkschriften der Kaiserlichen Akademie der Wissenschaften, Wien, Mathematisch-Naturwissenschaftliche, 57, 26-27.

Zaninetti, L., Salvini-Bonnard, G., Charollais, J., Decrouez, D., 1987. Montsalevia, n. gen. (Montsaleviidae, n. fam., foraminifères) dans le Crétacé inférieur (Berriasian moyen-Valanginien) du Mont Salève et du Jura méridional (Haute-Savoie, France); note préliminaire. Revue de Paléobiologie, 6 (1), 165-168.

Zeller, E.J., 1964. Cycles and psychology. In: Merriam, D.F. (Ed.), Symposium on cyclic sedimentation. Kansas Geological Survey, Bulletin, 169, 631-636.

Zeiss, A., 2003. The Upper Jurassic of Europe: its subdivision and correlation. Geological Survey of Denmark and Greenland Bulletin, 1, 75-114.

APPENDICES

A. Measured Stratigraphic Sections

CD

B. Sample-by-Sample Fossil Assemblages and Microfacies Types

CD

C. Simplified Biostratigraphic Range Charts

CD

D. CSRS Cycles and Section Data

CD

E. Graphic Correlations_Building the Pontides CSRS

CD

F. Calibration Points, Biostratigraphic Literature, Calibrated Fossil Datums and CSRS Ranges

CD

G. Unitary Association Matrix

CD

H. Graphic Correlation of the sections with the Pontides CSRS

CD

I. Fossil Plates

PLATE 1

Calpionellid and calcareous dinoflagellate photographs from the slope to basin successions. Scale is 500μm.

1, 2) *Crassicollaria massutiniana*, 1-A90, 2-A94, *massutiniana* subzone

3) *Crassicollaria intermedia*, A117, *massutiniana* subzone

4, 5) *Crassicollaria brevis*, 4-A148, 5-A106, *massutiniana* and *Remaniella* subzone

6, 7) *Calpionella elliptalpina*, 6, 7-A96, *massutiniana* subzone

8, 9) *Calpionella grandalpina*, 8-A96, 9-A114, *massutiniana* subzone

10, 11) *Calpionella alpina*, 10-A101, 11-A125, *massutiniana* and *alpina* subzone

12-14) *Calpionella elliptica*, 12-A162, 13-A198, 14-A245, *elliptica* and *simplex* subzone

15-24) *Tintinnopsella carpathica*, 15-A148, 16-A188, 17-A189, 18,19-A220, 20-A222, 21,22-OB178, *Remaniella* and *elliptica* subzones, 23-A239, 24-A264, *elliptica* and *darderi* subzones

25-29) *Remaniella ferasini*, 25,26-A189, 27-A211, 28-OB125, 29-OB130, *elliptica* subzones

30-35) *Remaniella duranddelgai*, 30-A193, 31-A201, 32-A217, 33-OB107, 34,35-OB126, *elliptica* subzones

36-41) *Remaniella colomi*, 36,37-A192, 38-A199, 39-OB173, 40-OB189, 41-A254, *elliptica* and *oblonga* subzones

42, 43) *Remaniella cadischiana*, 42-A231, 43-A249, *elliptica* and *simplex* subzones

44-46) *Remaniella catalanoi*, 44-A213, 45-OB107, 46-OB127, *elliptica* subzone

47-51) *Remaniella borzai*, 47,50-A199, 48-A249, 49-A220, 51-OB-178, *elliptica* and *simplex* subzones

52, 53) *Remaniella filipescui*, 52-A231, 53-A249, *elliptica* and *simplex* subzones

54-56) *Lorenziella hungarica*, 54-A213, 55-A214, 56-A239, *elliptica* subzone

57) *Lorenziella plicata*, 57-A214, *elliptica* subzone.

58) *Sturiella oblonga*, 58-OB173, *elliptica* subzone

59-63) *Calpionellopsis simplex*, 59-A245, 60-A253, 61-A254, 62-A260, 63-OB199, *simplex* and *oblonga* subzones

64-67) *Calpionellopsis oblonga*, 64-A253, 65,66-A254, 67-A260, *darderi* subzones

68) *Calpionellites darderi*, 68-A264, *darderi* subzone

69) *Calpionellites caravacaensis*, 69-A264, *darderi* subzone

70-79) Calcareous dinoflagellates, 70-A23, 71,72-A26, 73-A57, 74-A61,75-A69, 76,77-A77, 78,79-A245, *Crescentialla morronensis* Zone – *darderi* subzone

80, 81) *Globochaete alpina*, 80,81-A77, *Saccocoma* subzone

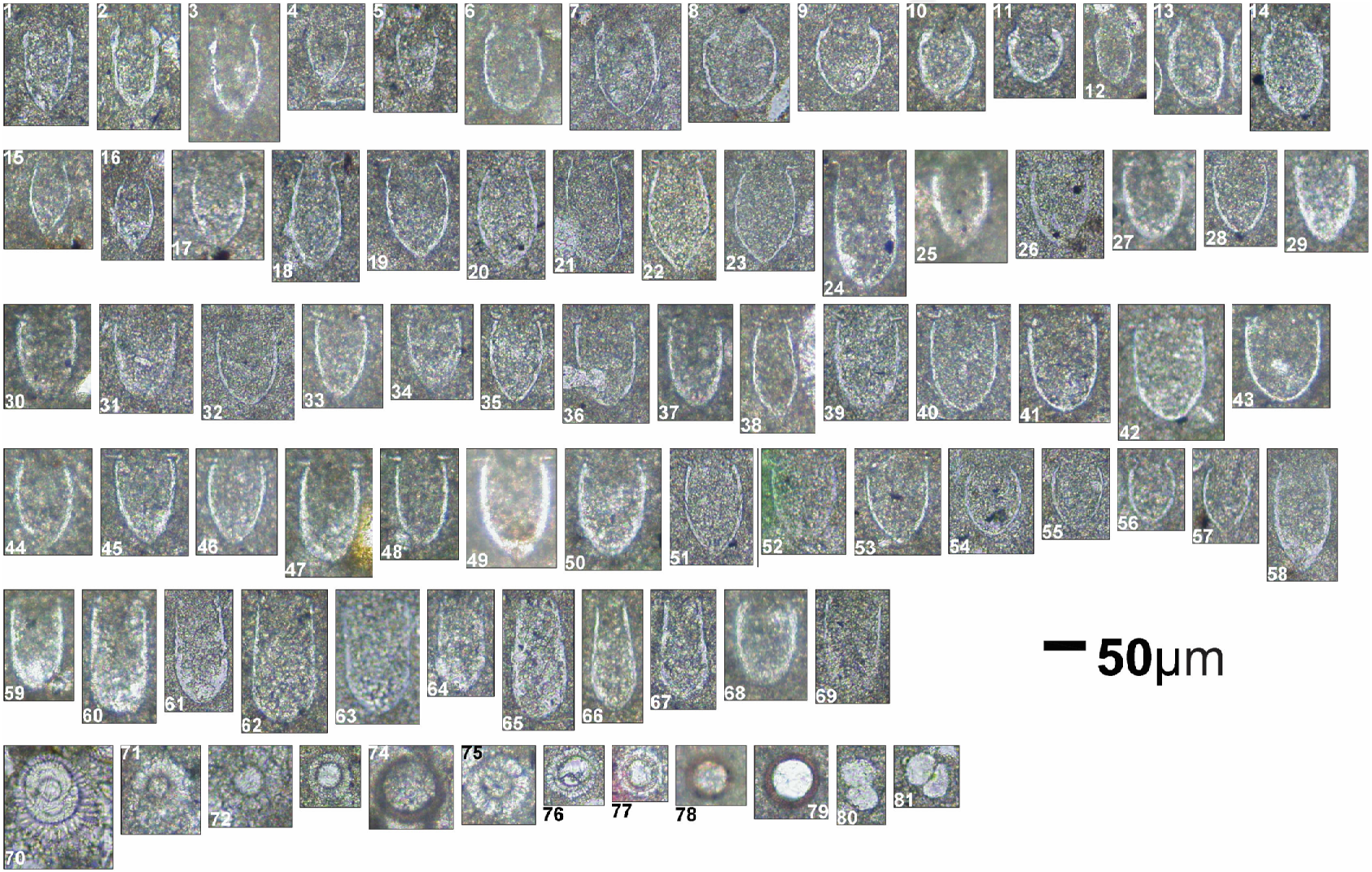
50µm

PLATE 2

Microphotographs of the major foraminifers and pelagic crinoids from the slope to basin successions.

The scale is common to all photographs. For the photographs 27, 28, 36, 38, 45, 50, 52, 53, 54, 55 scale is 500µm. For the photographs 25 and 39 scale is 100µm. For the rest, scale is 200µm.

1-15) *Protopeneroplis ultragranulata*, 1,2-A262, 3-OB16, 4-OB83, 5,6,7-OB94, 8,9,10-OB110, 11,12-OB113, 13-A85, 14,15-OB122, *Protopeneroplis ultragranulata* Zone – *oblonga* subzone.

16-21, 25-26) *Quinqueloculina* spp., 16,21-A63, 17,26-OB110, 18-A123, 19-A136, 20-A34, 25-OA9, 26-OB110, *Crescentiella morronensis* Zone – *elliptica* subzone

22-24) *Ophthalmidium* sp., 22,23-A34, 24-A72, *Saccocoma* subzone

27, 28) *Verneuilinoides*? sp., 27-A19, 28-A85, *Crescentiella morronensis* and *Protopeneroplis ultragranulata* Zones

29) *Haghimashella*? sp., 29-A61, *Saccocoma* subzone

30) Verneulinid foraminifer, 30-A18, *Crescentiella morronensis* Zone

31) *Textularia* sp., 31-A18, *Crescentiella morronensis* Zone

32, 33) *Meandrospira* spp., 32-A19, 33-A18, *Crescentiella morronensis* Zone

34, 35) *Siphovalvulina* sp., 34-A34, 35-A63, *Saccocoma* subzone

36) *Pseudocyclammina lituus*, 36-OA9, *Saccocoma* subzone

37) *Protomarsonella* sp., 37-A63, *Saccocoma* subzone

38) *Coscinophragma cribrosum*, 38-OB83, *elliptica* subzone

39-42) *Spirillina* spp., 39-A26, 40-A111, 41-A148, 42-A19, *Crescentiella morronensis* Zone – *elliptica* subzone

43, 44) *Mohlerina basiliensis*, 43,44-A85, *Protopeneroplis ultragranulata* Zone

45, 46) *Lenticulina* spp., 45-A63, 46-A58, *Saccocoma* subzone

47) *Patellina* sp., 47-A123, *massutiniana* subzone

8, 49, 56-59) *Neotrocholina* spp., 48-A123, 49-OB122, 56-A264, 57-A46, 58-A58, 59-OB110, *Saccocoma* subzone – *darderi* subzone

50-55) *Coscinoconus* spp., 50-OB122, 51,53,54,55-OB110, 52-OB111, *elliptica* subzone

60) Aptychus, 60-A46, *Saccocoma* subzone

61-68) *Saccocoma* sp., 61, 62-A57, 63,64,65,68-A87, 66-A34, 67-A63, *Saccocoma* subzone and *Protopeneroplis ultragranulata* Zone

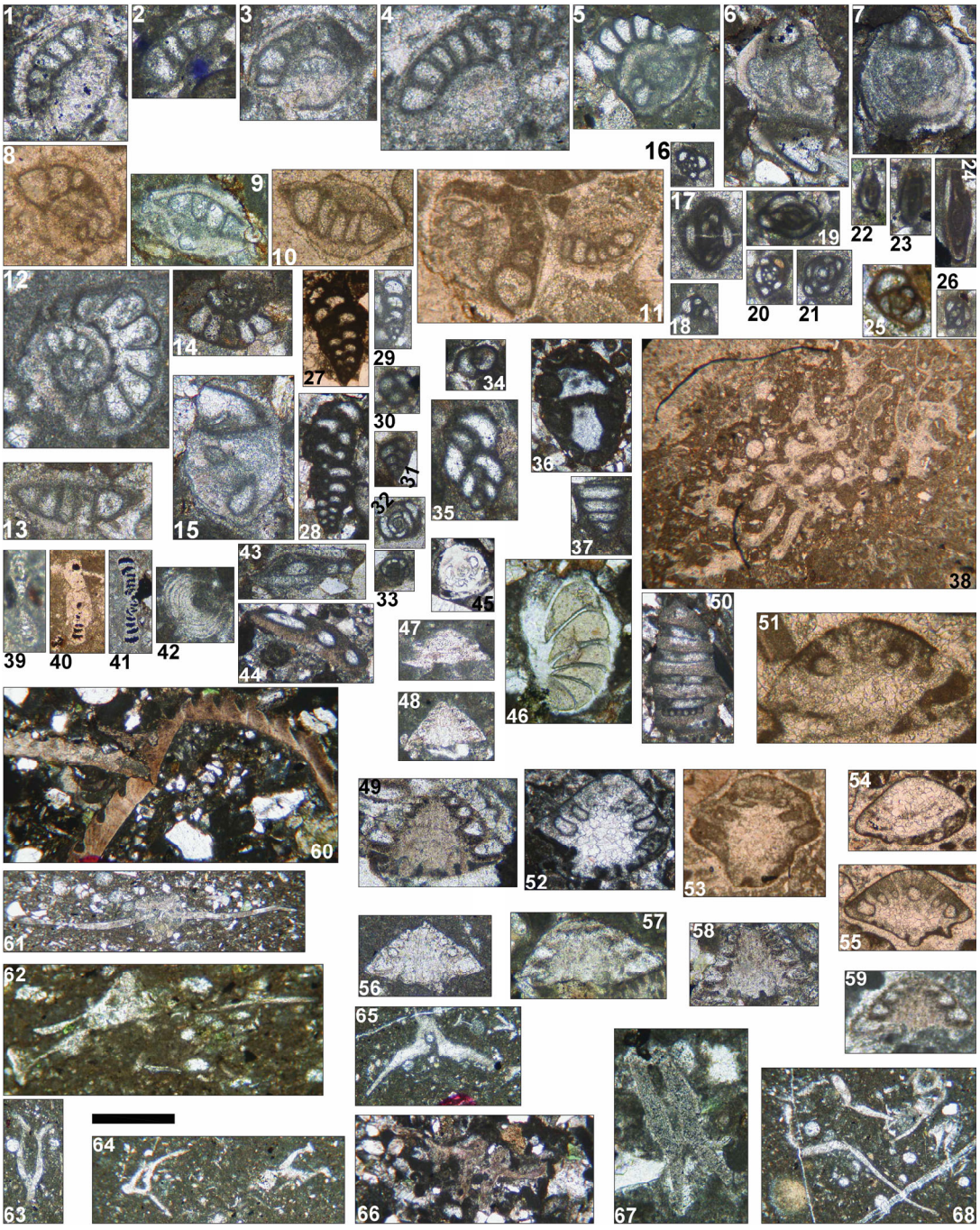
1
2
3
4
5
6
7
8
9
10
11
12
13
14
15
16
17
18
19
20
21
22
23
24
25
26
27
28
29
30
31
32
33
34
35
36
37
38
39
40
41
42
43
44
45
46
47
48
49
50
51
52
53
54
55
56
57
58
59
60
61
62
63
64
65
66
67
68

PLATE 3

Microphotographs of the major microencrusters and worm tubes from the slope to basin successions.

The scale is common to all photographs. For the 14 and 24 photographs, the scale is 200µm. For the rest, the scale is 500µm.

1, 2) Bryozoa (B) and *Iberopora bodueri* (I), 1-OB113, 2-OB110, *elliptica* subzone

3-6) *Lithocodium aggregatum*, 3-OB110, 4-A44, 5-OB110 (L: *Lithocodium aggregatum*, Tr: *Trogrotella incrustans*), 6-OB83, *Saccocoma* and *elliptica* subzones

7-9) *Crescentiella morronensis*, 7-A44, 8,9-OB83, *Saccocoma* and *elliptica* subzones

10) *Cayeuxia* sp., 10-A19, *Crescentiella morronensis* Zone

11-15) *Iberopora bodueri*, 11-OB110, 12-OB113 (T: *Terebella lapilloides*, CM: *Crescentiella morronensis*), 13-OB122, 14-A85, 15-OB110, *Protopeneroplis ultragranulata* Zone and *elliptica* subzone

16, 17) *Koskinobullina socialis*, 16-OB110, 17-A81 (T: *Terebella lapilloides*, K: *Koskinobullina socialis*), *Saccocoma* subzone and *elliptica* subzone

18) *Perturbatacrusta leini*, 18-OB110, *elliptica* subzone

19) *Carpathiella perforata*, 19-A46, *Saccocoma* subzone

20, 21, 23) *Carpathiella triangulata*, 20-A72, 21-OB110, 23-A46, *Saccocoma* subzone and *elliptica* subzone

22) *Carpathiella plassenensis*, 22-OB110, *elliptica* subzone

24, 25) *Mercierella*? *dacica,* 24-A61, 25-OB115, *Saccocoma* and *elliptica* subzones

26-28) *Terebella lapilloides*, 26-A45, 27-OB110, 28-A72, *Saccocoma* and *elliptica* subzones

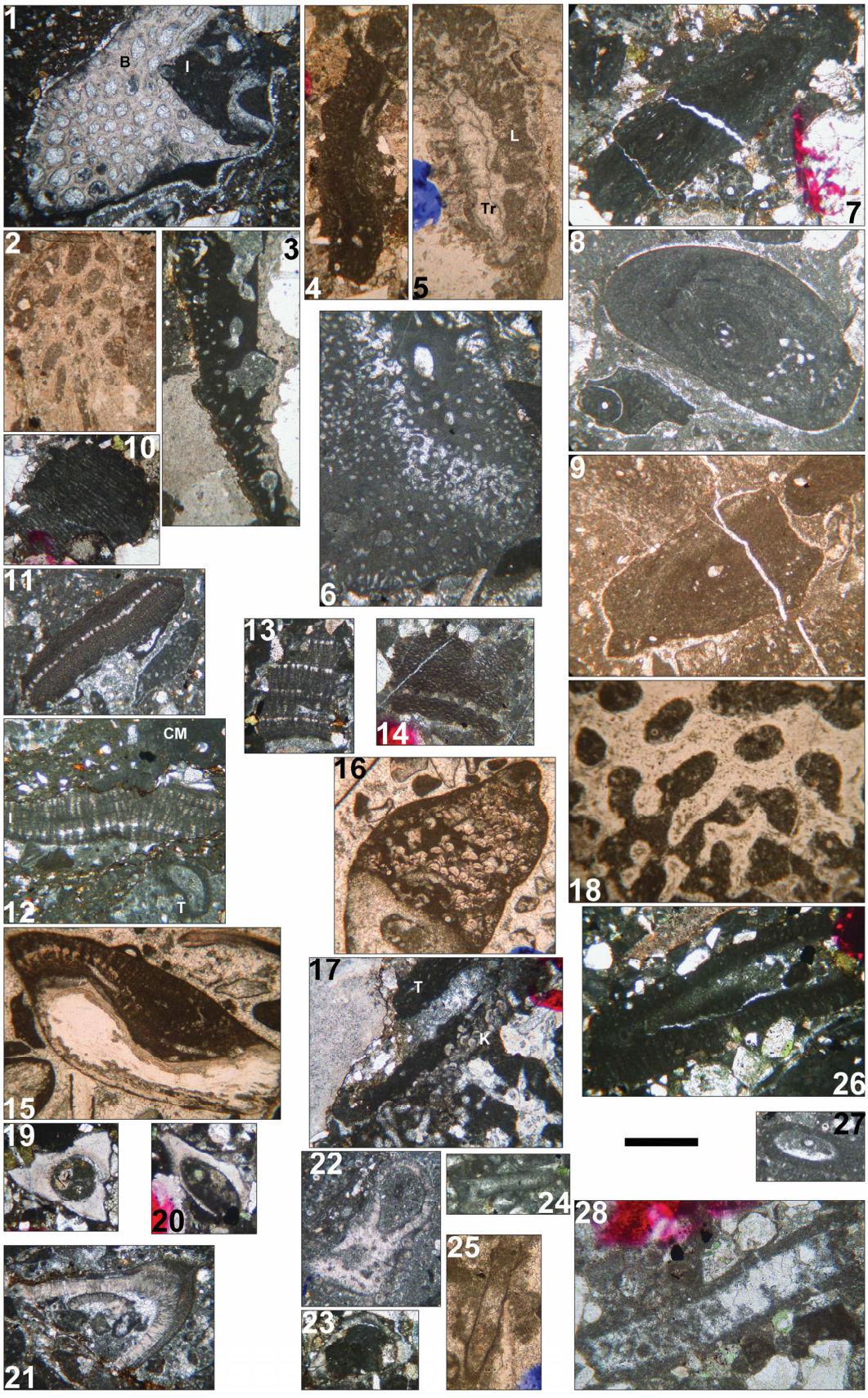
1
B
I
2
3
4
5
L
Tr
6
7
8
9
10
11
12
CM
I
T
13
14
15
16
17
T
K
18
19
20
21
22
23
24
25
26
27
28

PLATE 4

Microphotographs of the major foraminifers, algae and microencrusters from the neritic carbonates.

The scale is common to all photographs. Scale is 200μm.

1-14, 21) *Alveosepta jaccardi*, 1,2,3,4-L15, 5,6-L20, 7-L21, 8,9,10,11-L21, 12-L34, 13-L35, 14-L40, 21-L54 (*Crescentiella morronensis* Zone; *Mesoendothyra izjumiana – Alveosepta jaccardi* subzone)

15, 15a) *Bramkampella arabica*, 15-L55 (*Crescentiella morronensis* Zone; *Mesoendothyra izjumiana – Alveosepta jaccardi* subzone); 15a-L84 (*Montsalevia salevensis* Zone)

16-19) *Aolisalthella sulcata*, 18-L5 (*Crescentiella morronensis* Zone; *Mesoendothyra izjumiana – Alveosepta jaccardi* subzone); 16,19-L65 (unzoned dolomitic interval); 17-L85 (*Montsalevia salevensis* Zone)

20) *Crescentiella morronensis*, L5 (*Crescentiella morronensis* Zone; *Mesoendothyra izjumiana – Alveosepta jaccardi* subzone)

22-28) *Mesoendothyra izjumiana*, 22,23-L5, 24,25,26,27,28-L23(*Crescentiella morronensis* Zone; *Mesoendothyra izjumiana – Alveosepta jaccardi* subzone)

29-31) *Mesoendothyra* cf. *croatica*, 29-31-L5 (*Crescentiella morronensis* Zone; *Mesoendothyra izjumiana – Alveosepta jaccardi* subzone)

32) *Mesoendothyra croatica*?, L108 (*Montsalevia salevensis* Zone)

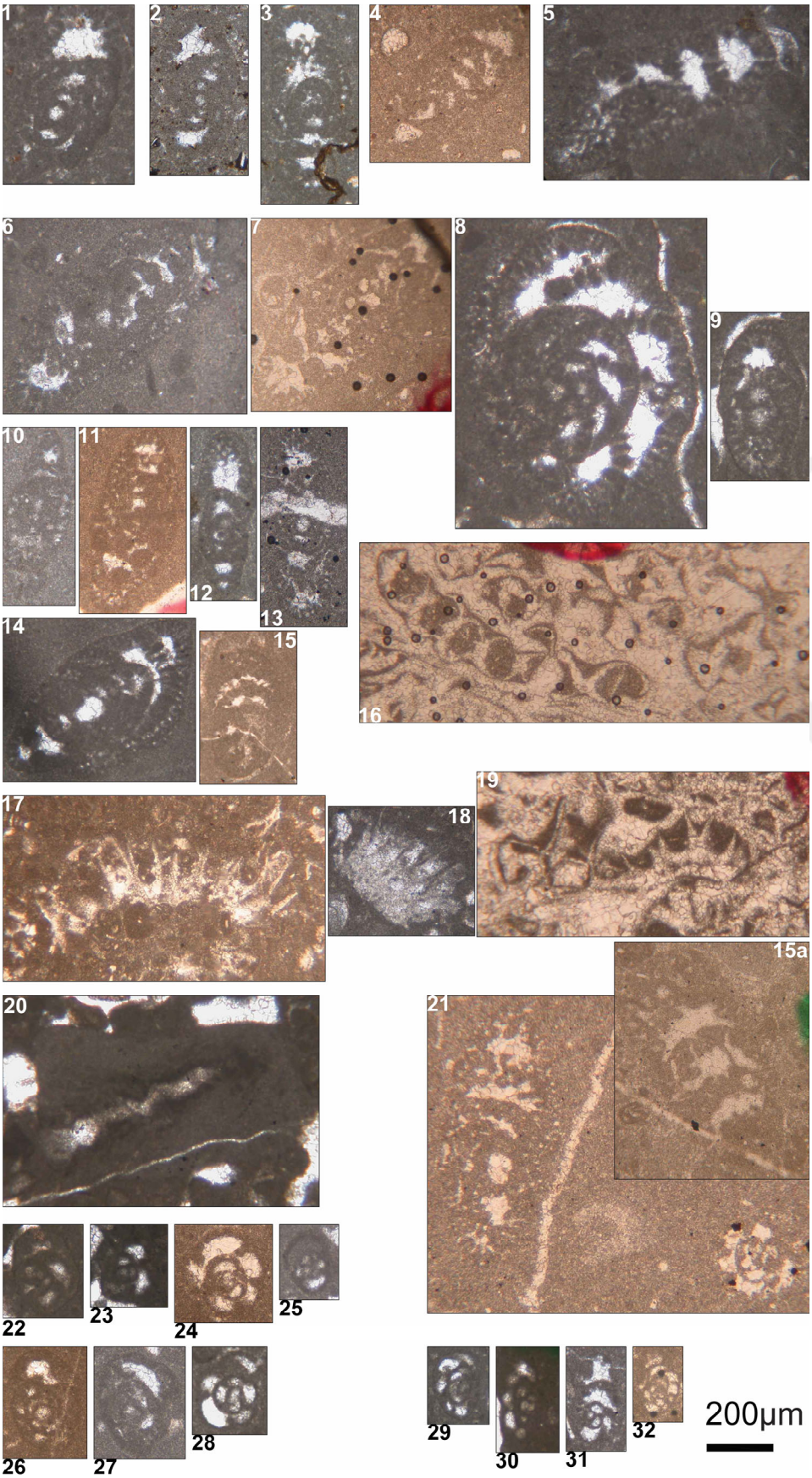
1
2
3
4
5
6
7
8
9
10
11
12
13
14
15
16
17
18
19
15a
20
21
22
23
24
25
26
27
28
29
30
31
32
200µm

PLATE 5

Microphotographs of the major foraminifers and algae from the neritic carbonates.

The scale is common to all photographs. Scale is 200μm.

1) *Campbelliella striata*, L4 (*Crescentiella morronensis* Zone; *Mesoendothyra izjumiana – Alveosepta jaccardi* subzone)

2-4) *Everticyclammina* sp, 2,3-L4, 4-L5 (*Crescentiella morronensis* Zone; *Mesoendothyra izjumiana – Alveosepta jaccardi* subzone)

5) *Everticyclammina kelleri*, L105 (*Montsalevia salevensis* Zone)

6) *Protopeneroplis striata*, L5 (*Crescentiella morronensis* Zone; *Mesoendothyra izjumiana – Alveosepta jaccardi* subzone)

7-10) *Charentia* spp., 7,8-L4, 9,10-L5 (*Crescentiella morronensis* Zone; *Mesoendothyra izjumiana – Alveosepta jaccardi* subzone)

11-13) *Mohlerina basiliensis*, 11-L5, 12,13-L4 (*Crescentiella morronensis* Zone; *Mesoendothyra izjumiana – Alveosepta jaccardi* subzone)

14-19) *Kurnubia palastiniensis*, L30 (*Crescentiella morronensis* Zone; *Mesoendothyra izjumiana – Alveosepta jaccardi* subzone)

20, 21, 24-28) *Pseudocyclammina lituus*, 20-L30, 21-L5, 24-L22, 25-27-L54, 28-L55 (*Crescentiella morronensis* Zone; *Mesoendothyra izjumiana – Alveosepta jaccardi* subzone)

22, 23) *Pseudocyclammina sphaeroidalis*, 22-L23, 23-L21 (*Crescentiella morronensis* Zone; *Mesoendothyra izjumiana – Alveosepta jaccardi* subzone)

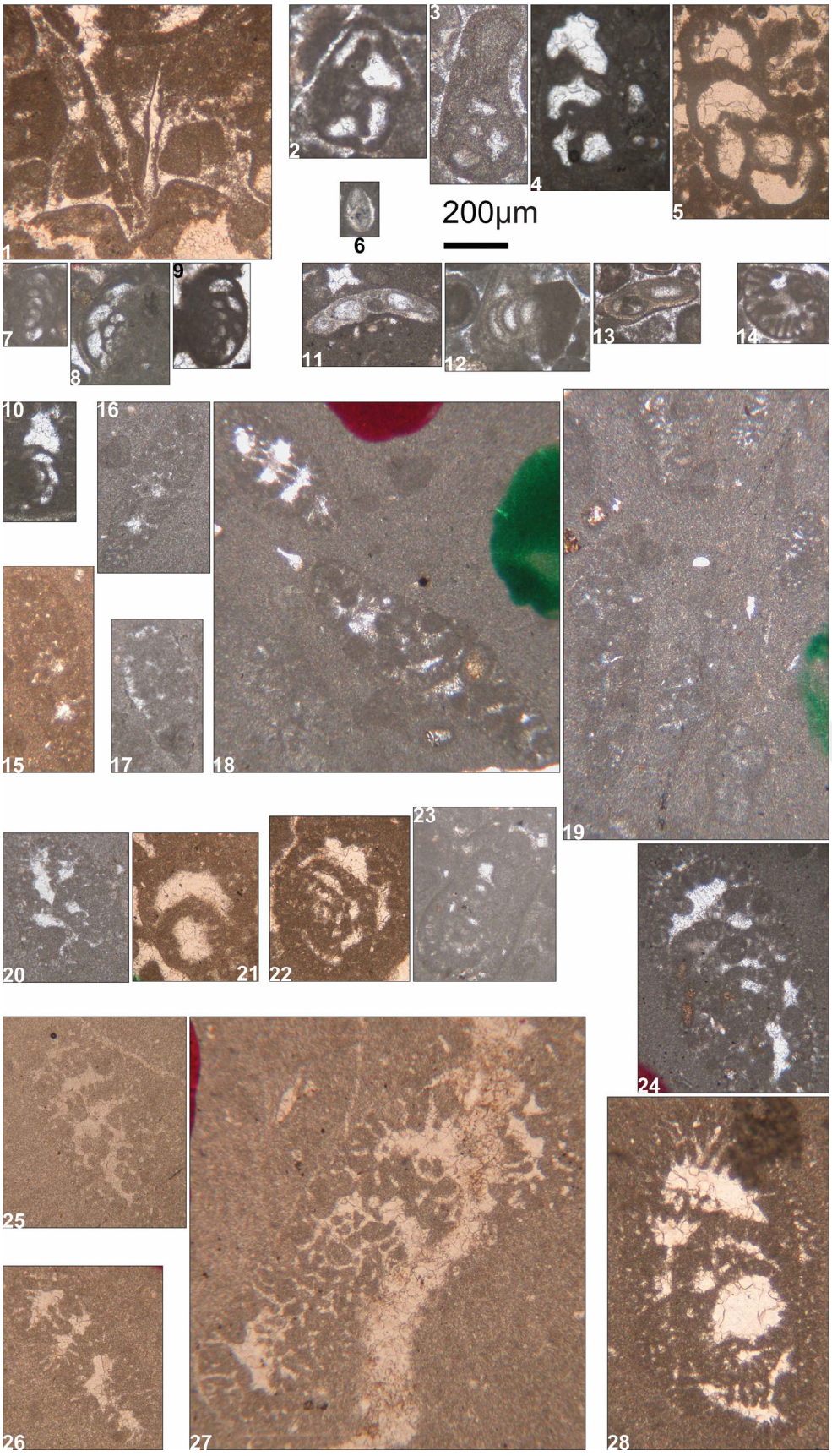
200µm

PLATE 6

Microphotographs of the major foraminifers from the neritic carbonates.

The scale is common to all photographs. Scale is 200μm.

1, 7-9) *Streptocyclammina* gr. *parvula-muluchensis*, 1,9-L55, 7-L15, 8-L21 (*Crescentiella morronensis* Zone; *Mesoendothyra izjumiana – Alveosepta jaccardi* subzone)

2, 3) *Pseudocyclammina lituus*, 2-L122 (*Montsalevia salevensis* Zone); 3-L55 (*Crescentiella morronensis* Zone; *Mesoendothyra izjumiana – Alveosepta jaccardi* subzone)

4, 5) *Streptocyclammina hottingeri*, 4-L85 (*Montsalevia salevensis* Zone); 5-L21 (*Crescentiella morronensis* Zone; *Mesoendothyra izjumiana – Alveosepta jaccardi* subzone)

6, 22) *Reophax* spp., 6-L4 (*Crescentiella morronensis* Zone; *Mesoendothyra izjumiana – Alveosepta jaccardi* subzone); 22-L132 (*Montsalevia salevensis* Zone)

10-15) *Nautiloculina* spp., 10-L5, 11-L4 (*Crescentiella morronensis* Zone; *Mesoendothyra izjumiana – Alveosepta jaccardi* subzone); 12-L102, 13-L134, 14-L116, 15-L133 (*Montsalevia salevensis* Zone)

16, 19, 20) *Melathrokerion* sp., 16-L100, 19-L136, 20-L138 (*Montsalevia salevensis* Zone)

17. 18) *Freixialina planispiralis*, 17-L79 (*M. favrei – H. joukowskyi – P. ultragranulata* Zone; *Barkerina dobrogiaca* subzone); 18-L113 (*Montsalevia salevensis* Zone)

23-26) *Textularia* spp., 23-L106, 24-L90, 25-L91 (*Montsalevia salevensis* Zone); 26-L4 (*Crescentiella* morronensis Zone; *Mesoendothyra izjumiana – Alveosepta jaccardi* subzone)

27) Verneulinid foraminifer, L4 (*Crescentiella morronensis* Zone; *Mesoendothyra izjumiana – Alveosepta jaccardi* subzone)

28) *Belorussiellas* sp., L141 (*Montsalevia salevensis* Zone)

29) *Redmondoides* sp., L113 (*Montsalevia salevensis* Zone)

30) Undetermined foraminifer, L125 (*Montsalevia salevensis* Zone)

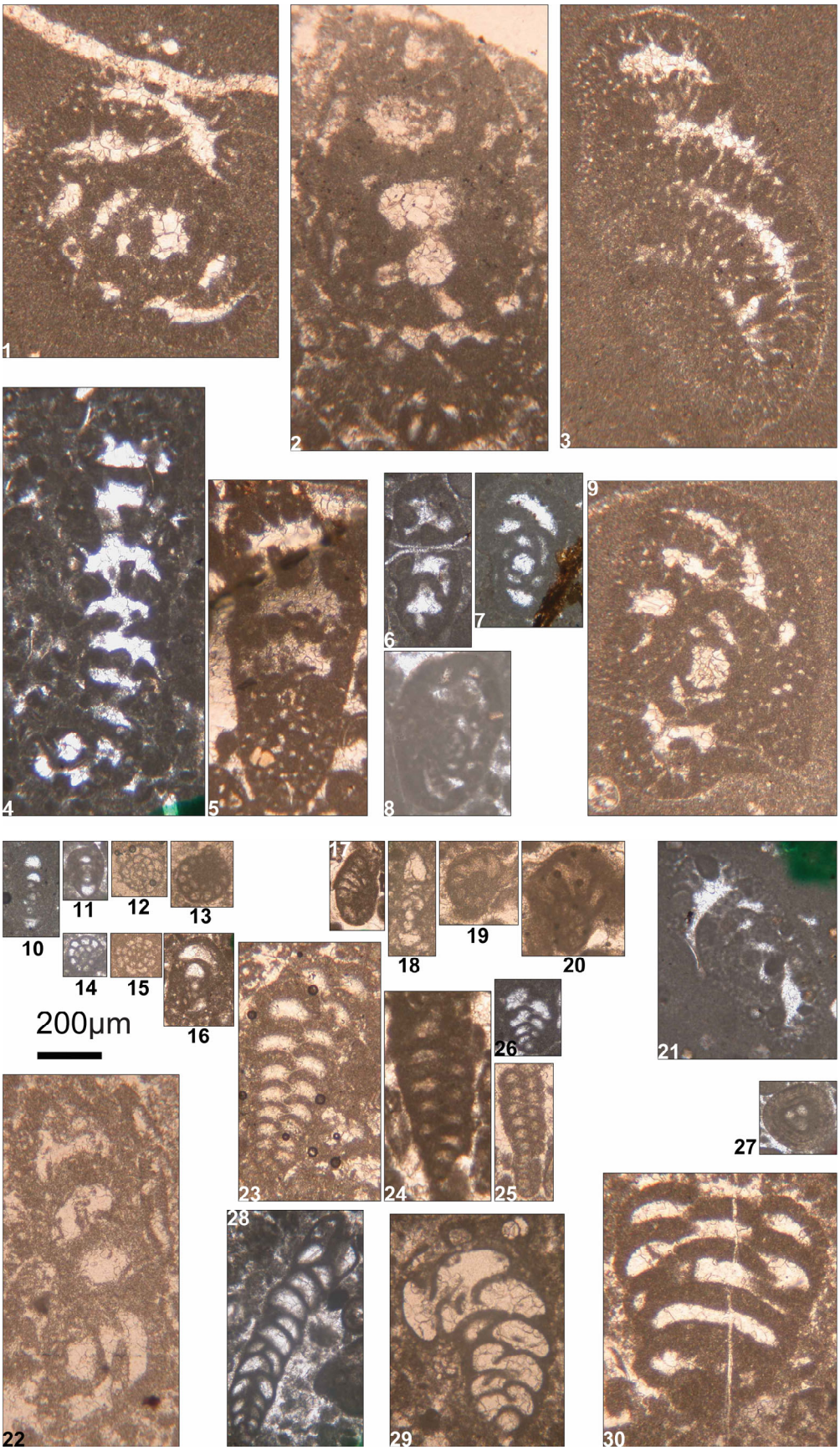
1
2
3
4
5
6
7
8
9
10
11
12
13
14
15
16
200µm
17
18
19
20
21
22
23
24
25
26
27
28
29
30

PLATE 7

Microphotographs of the major foraminifers from the neritic carbonates.

The scale is common to all photographs. Scale is 200μm.

1-6) *Meandrospira favrei*, 1-L79 (*M. favrei – H. joukowskyi – P. ultragranulata* Zone; *Barkerina dobrogiaca* subzone); 2-L138, 3-L108, 4-L85, 5-L86, 6-L112 (*Montsalevia salevensis* Zone)

7-12) *Haplophragmoides joukowskyi*, 7-L76 (*M. favrei – H. joukowskyi – P. ultragranulata* Zone); 10-L79 (*M. favrei – H. joukowskyi – P. ultragranulata* Zone; *Barkerina dobrogiaca* subzone); 8-L81a, 9-L138, 11-L122, 12-L82 (*Montsalevia salevensis* Zone)

13, 14) *Akcaya minuta*, L85, L113 (*Montsalevia salevensis* Zone)

15) *Meandrospira* sp., 15-L103 (*Montsalevia salevensis* Zone)

16-20) *Barkerina dobrogiaca*, L79 (*M. favrei – H. joukowskyi – P. ultragranulata* Zone; *Barkerina dobrogiaca* subzone)

21-24, 29, 30) *Montsalevia salevensis*, 21,22-L82, 23-L138, 24,29-L85, 30-L86 (*Montsalevia salevensis* Zone)

25-28) *Turriglomina anatolica*, 25-L144, 26-L90; 27-L95, 28-L109 (*Montsalevia salevensis* Zone)

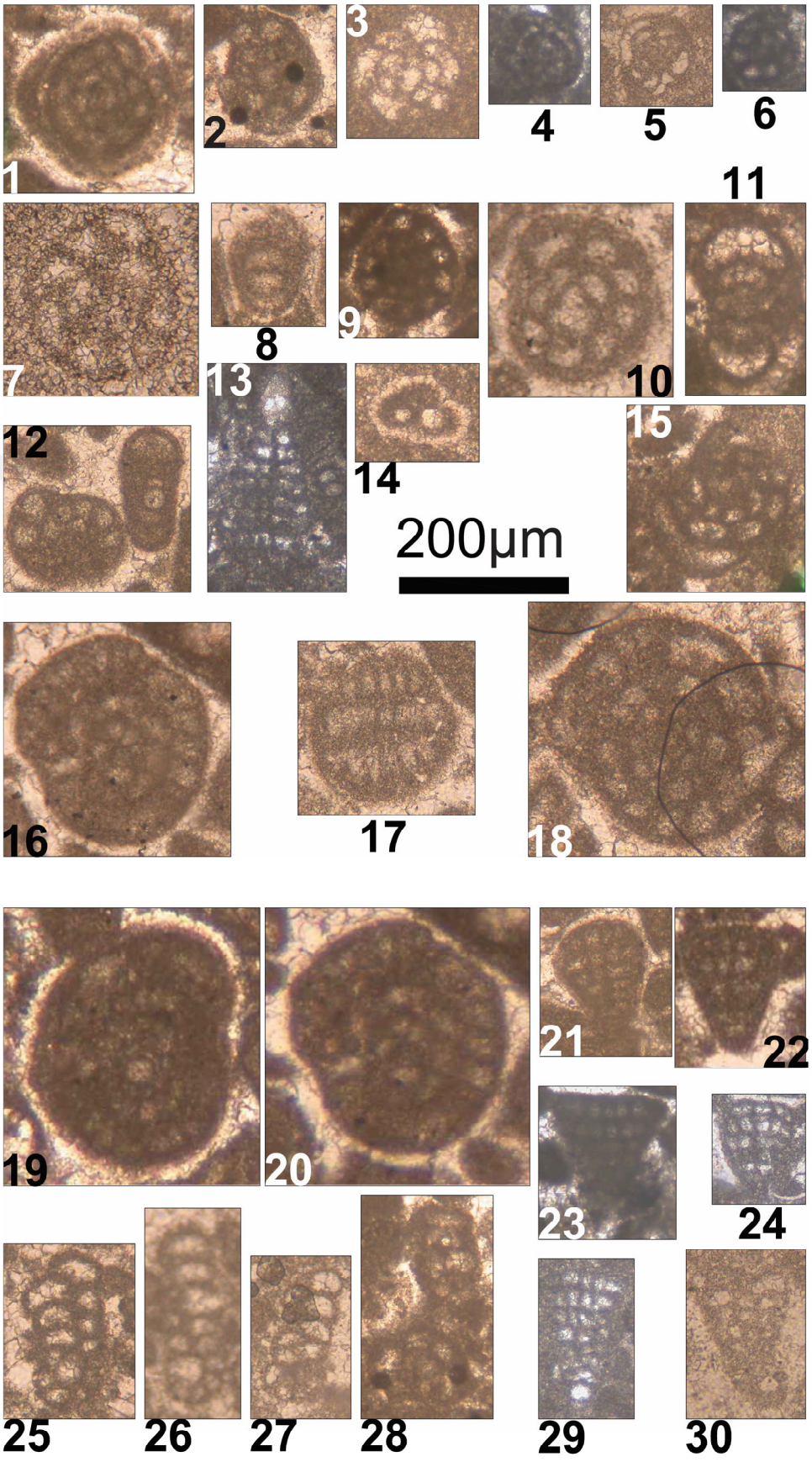
1
2
3
4
5
6
7
8
9
10
11
12
13
14
15
200µm
16
17
18
19
20
21
22
23
24
25
26
27
28
29
30

PLATE 8

Microphotographs of the major foraminifers from the neritic carbonates.

The scale is common to all photographs. Scale is 200μm.

1-12) *Vercorsella* spp., 1,2,9,12-L112, 3-L84, 4-L85, 5,10-L99, 6,7-L113, 8-L91, 11-L105 (*Montsalevia salevensis* Zone)

13, 20-24) *Pseudolituonella gavonensis*, 13,24-L124, 20-L90, 21,22-L96, 23-L112 (*Montsalevia salevensis* Zone)

25, 26) *Ammobaculites* sp., 25-L85, 26-L97 (*Montsalevia salevensis* Zone)

27) *Lituola baculiformis*, L109 (*Montsalevia salevensis* Zone)

28-32, 33-38) *Patellovalvulina patruliusi*, 28-L84, 29,31-L141, 30-L86, 32 (on the right),33-L91, 34-L105, 35,36-L99, 37,38-L124 (*Montsalevia salevensis* Zone)

32) *Haghimashella* sp. (on the left), L-91 (*Montsalevia salevensis* Zone)

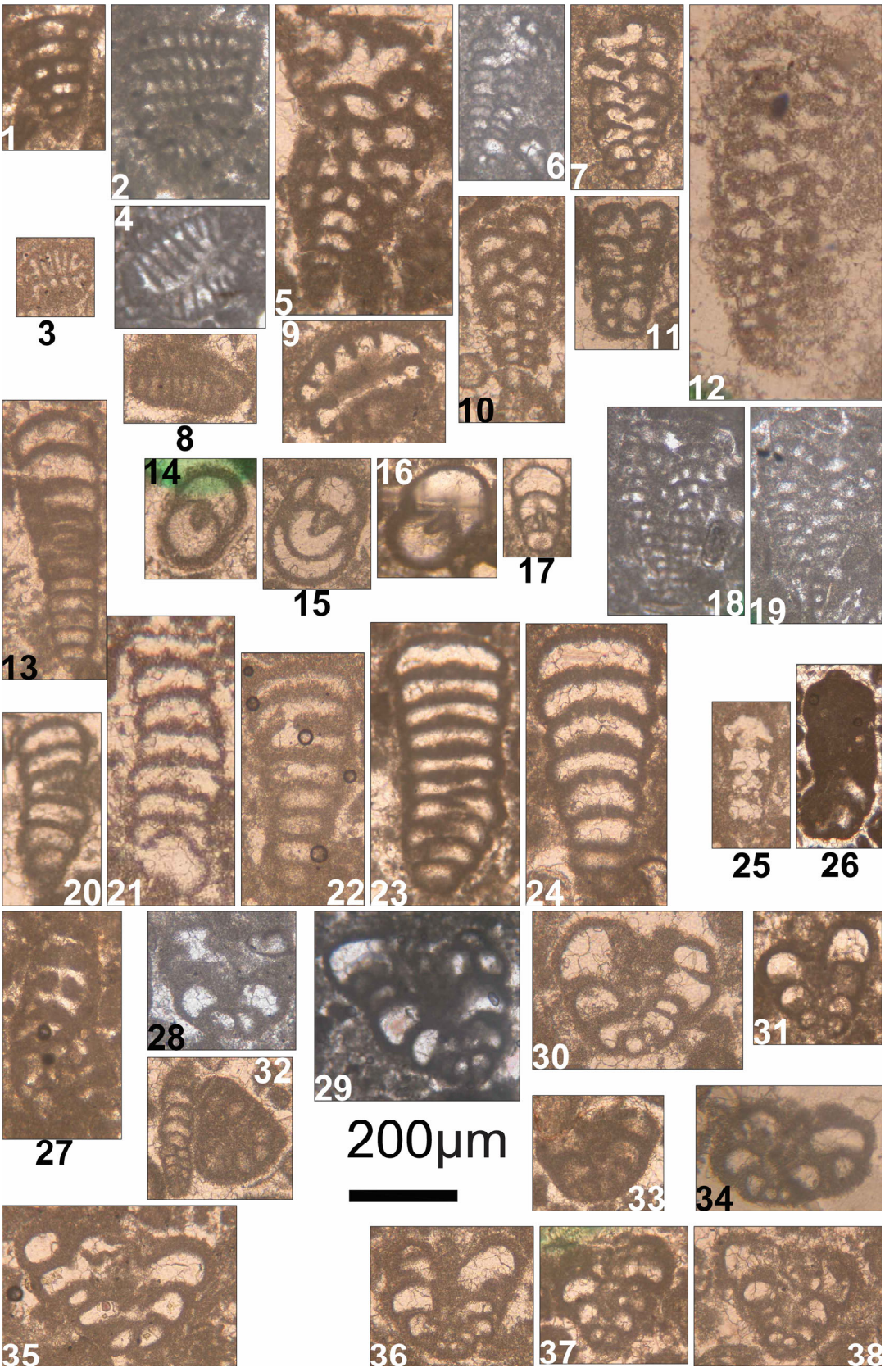
1
2
3
4
5
6
7
8
9
10
11
12
13
14
15
16
17
18
19
20
21
22
23
24
25
26
27
28
29
30
31
32
33
34
35
36
37
38
200µm

PLATE 9

Microphotographs of the major foraminifers from the neritic carbonates.

The scale is common to all photographs. Scale is 200μm.

1-11) *Coscinoconus* spp., 1-6,10,11-L78 (*M. favrei – H. joukowskyi – P. ultragranulata* Zone); 7,9-L4, 8-L7 (*Crescentiella morronensis* Zone; *Mesoendothyra izjumiana – Alveosepta jaccardi* subzone)

12, 13) *Protopeneroplis ultragranulata*, 12-L101, 13-L91 (*Montsalevia salevensis* Zone)

14) *Lenticulina*, L137 (*Montsalevia salevensis* Zone)

15) *Troglotella incrustans*, L8 (*Crescentiella morronensis* Zone; *Mesoendothyra izjumiana – Alveosepta jaccardi* subzone)

16-18) *Istriloculina* sp., 16-L4, 17,18-L5 (*Crescentiella morronensis* Zone; *Mesoendothyra izjumiana – Alveosepta jaccardi* subzone)

19) *Glomospira* sp. (on the left), 19-L102 (*Montsalevia salevensis* Zone)

19-23, 26, 27) *Quinqueloculina* spp., 19 (on the right)-L102, 26-L84, 27-L87 (*Montsalevia salevensis* Zone); 20-L4 (*Crescentiella morronensis* Zone; *Mesoendothyra izjumiana – Alveosepta jaccardi* subzone); 21-23-L78 (*M. favrei – H. joukowskyi – P. ultragranulata* Zone)

24, 25) *Moesiloculina* sp., 24-L106, 25-L99 (*Montsalevia salevensis* Zone)

28, 29) *Ophthalmidium* sp., 28-L138, 29-L134 (*Montsalevia salevensis* Zone)

30-34) *Hechtina*? sp., 30-33-L78, 34-L79 (*M. favrei – H. joukowskyi – P. ultragranulata* Zone)

35-37) *Massilina*? sp., 35-L79 (on the left), 36,37-L79 (*M. favrei – H. joukowskyi – P. ultragranulata* Zone)

38, 39) *Derventina*? sp., L136 (*Montsalevia salevensis* Zone)

40-47) Indeterminate lituolids, 40-L113, 41,42,46,47-L134, 43,44,45-L138 (*Montsalevia salevensis* Zone)

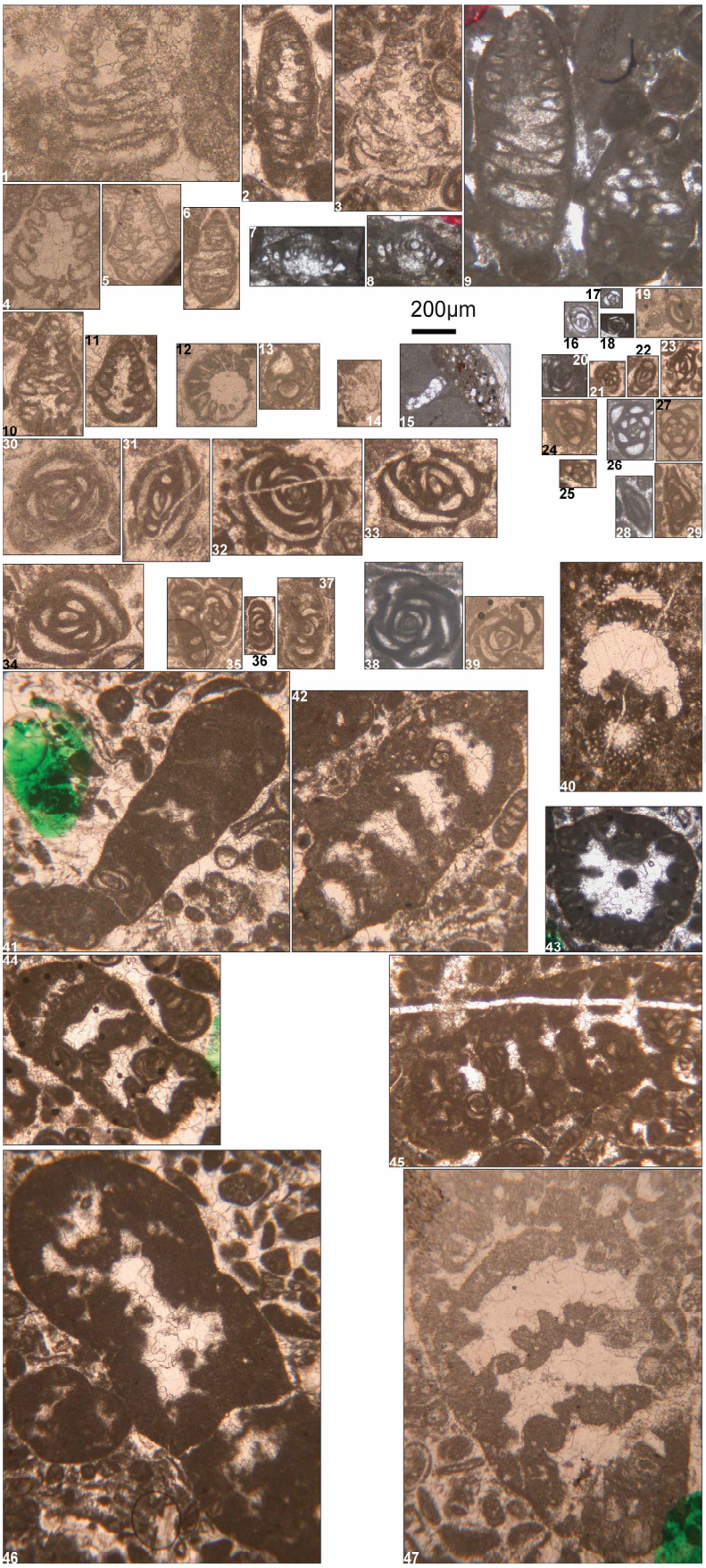
200µm

PLATE 10

Microphotographs of *incertae sedis*, bryozoa, bivalvesm gastropods, coral and echinoids from the neritic carbonates.

The scale is common to all photographs. Scale is 200μm.

1-6) *Favreina* spp., 1-L58, 2,3-L62 (Unzoned-dolomites); 4,6-L22, 5-L24 (*Crescentiella morronensis* Zone; *Mesoendothyra izjumiana – Alveosepta jaccardi* subzone)

7) *Cayeuxia* sp., L4 (*Crescentiella morronensis* Zone; *Mesoendothyra izjumiana – Alveosepta jaccardi* subzone)

8, 11) Bryozoa fragments, L79 (*M. favrei – H. joukowskyi – P. ultragranulata* Zone; *Barkerina dobrogiaca* subzone); 11-L5 (*Crescentiella morronensis* Zone; *Mesoendothyra izjumiana – Alveosepta jaccardi* subzone)

9) Bivalve fragment, L84 (*Montsalevia salevensis* Zone)

10, 15, 16) *Lithocodium aggregatum*, 10-L4, 15-L8 (*Crescentiella morronensis* Zone; *Mesoendothyra izjumiana – Alveosepta jaccardi* subzone); 16-L100 (*Montsalevia salevensis* Zone)

12) *Mercierella*? *dacica*, L143 (*Meandrospira favrei – Haplophragmoides joukowskyi* Zone)

13) Ostracod, L15 (*Crescentiella morronensis* Zone; *Mesoendothyra izjumiana – Alveosepta jaccardi* subzone)

14, 17-20) Gastropods, 14-L4, 17,18-L15 (*Crescentiella morronensis* Zone; *Mesoendothyra izjumiana – Alveosepta jaccardi* subzone); 19-L65 (unzoned-dolomites), 20-L78 (*M. favrei – H. joukowskyi – P. ultragranulata* Zone)

21) Echinoid spine, L8 (*Crescentiella morronensis* Zone; *Mesoendothyra izjumiana – Alveosepta jaccardi* subzone)

22) Coral fragment, L113 (*Montsalevia salevensis* Zone)

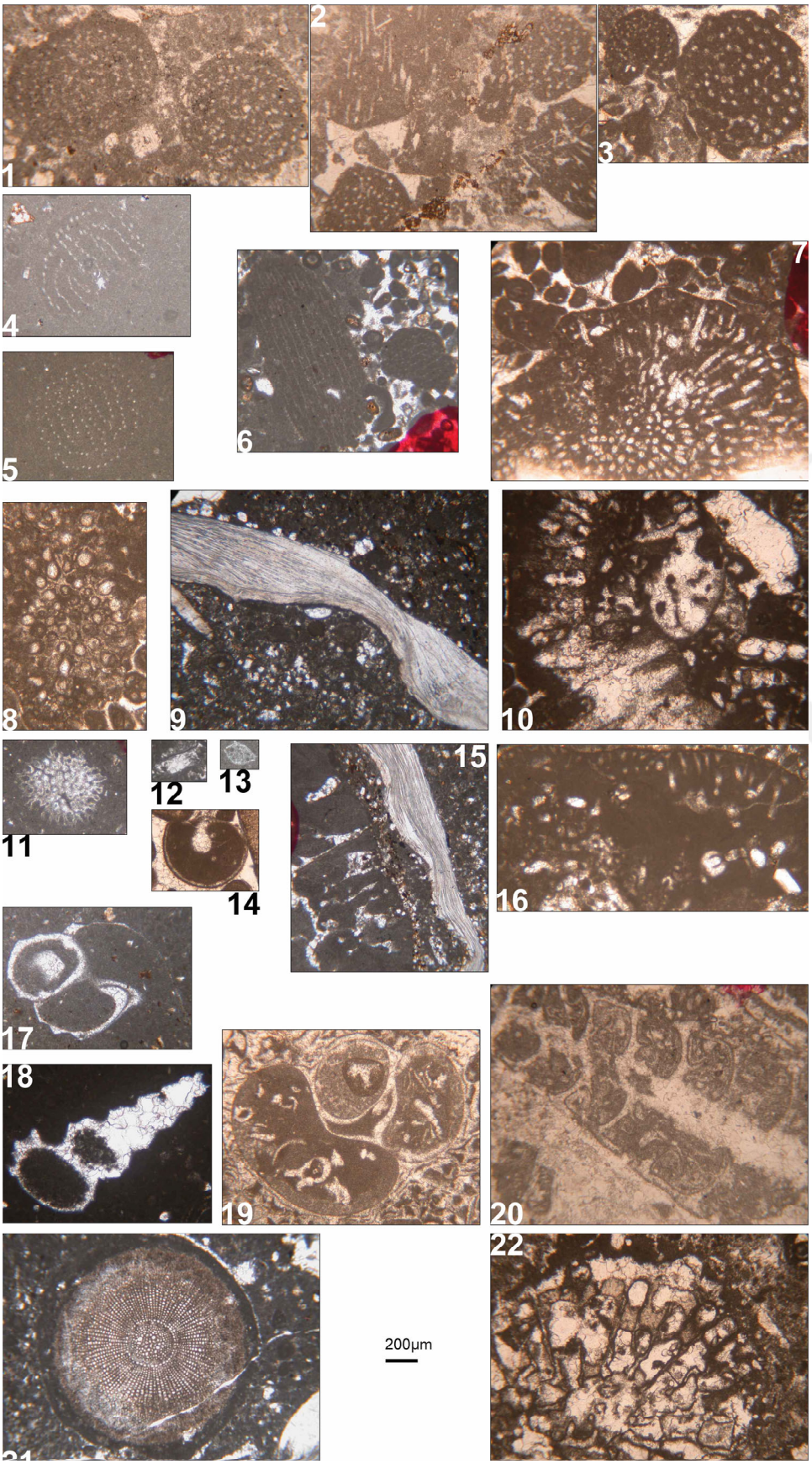
1
2
3
4
5
6
7
8
9
10
11
12
13
14
15
16
17
18
19
20
21
22
200µm

PLATE 11

Microphotographs of undetermined algae from the neritic carbonates.

The scale is common to all photographs. Scale is 200μm.

1-3, 12, 13) *Salpingoporella annulata*?, 1-3, 12,13-L79 (*M. favrei – H. joukowskyi – P. ultragranulata* Zone; *Barkerina dobrogiaca* subzone)

4) Undetermined alga, L5 (*Crescentiella morronensis* Zone; *Mesoendothyra izjumiana – Alveosepta jaccardi* subzone)

5, 6) Red alge, L8 (*Crescentiella morronensis* Zone; *Mesoendothyra izjumiana – Alveosepta jaccardi* subzone)

7) *Campbelliella striata*?, L79 (*M. favrei – H. joukowskyi – P. ultragranulata* Zone; *Barkerina dobrogiaca* subzone)

8-24) Undetermined algae, 8-L140, 9,24-L132, 11-L91, 14,15,22-L138, 16-L123, 17,18-L127, 20-L92, 21-L133, 23-L100 (*Montsalevia salevensis* Zone); 10 (on the left)-L58 (unzoned-dolomites); 19-L79 (*M. favrei – H. joukowskyi – P. ultragranulata* Zone; *Barkerina dobrogiaca* subzone)

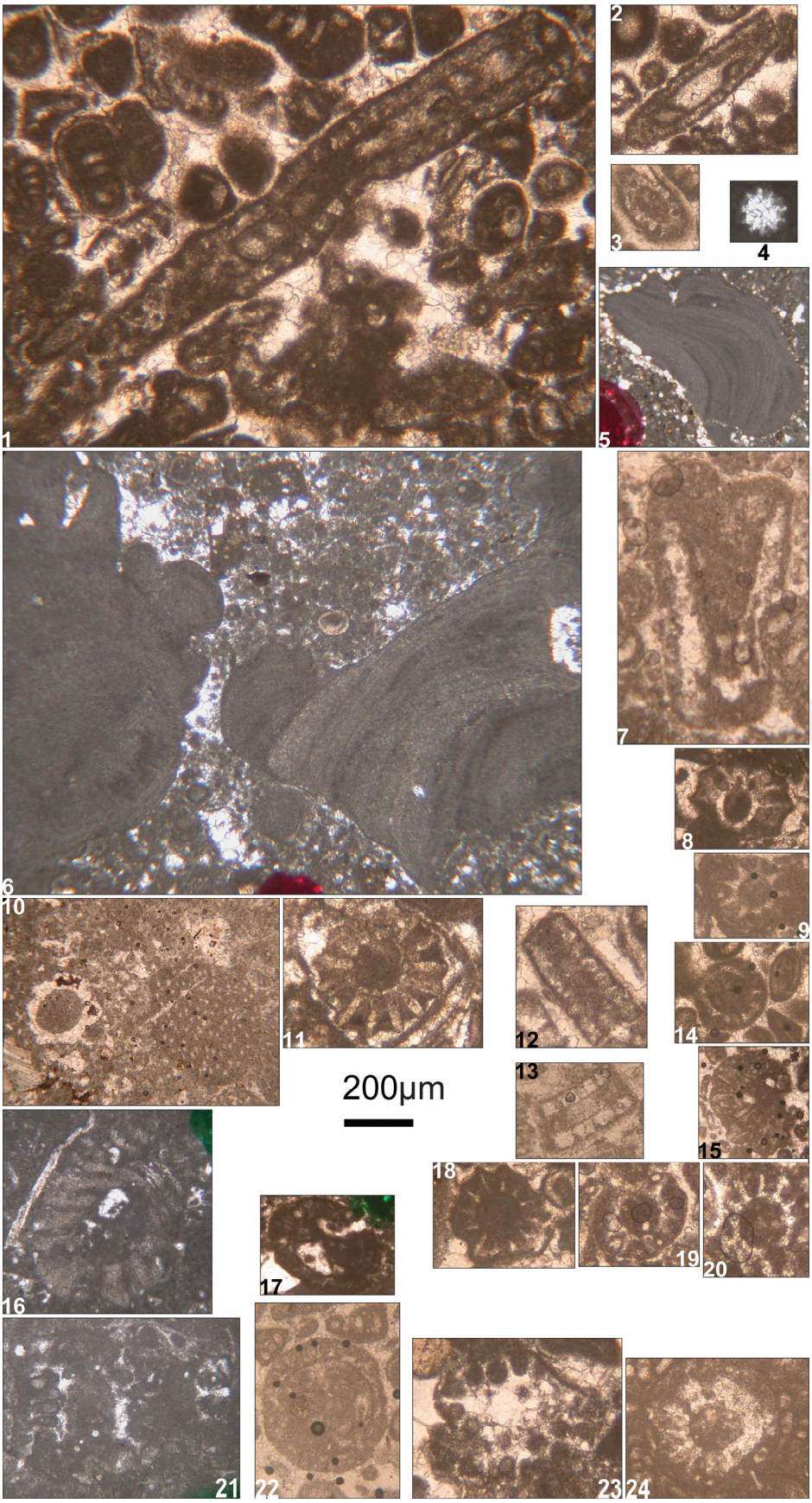
1
2
3
4
5
6
7
8
9
10
11
12
13
14
15
16
17
18
19
20
21
22
23
24
200µm

CURRICULUM VITAE

Surname, Name: Atasoy, Serdar Görkem

EDUCATION

Degree	Institution	Year of Graduation
MS	METU Geological Engineering	2017
BS	METU Geological Engineering	2013
High School	Nermin Mehmet Çekiç (Batıkent) High School, Ankara	2007

FOREIGN LANGUAGES

Advanced English

PUBLICATIONS

1. **Atasoy, S.G.**, Altıner, D., Altıner-Özkan, S., 2022. Calibrating the Late Jurassic – Early Cretaceous shallow and deep marine bioevents by quantitative biostratigraphy: A synthesis from the Pontides Carbonate Platform (Turkey). Earth-Science Reviews, 231, 104071.

2. Altıner, D., Altıner-Özkan, S., **Atasoy, S.G.**, Şahin, N., 2021. *Paynita Permotaurica* n.Gen., n.Sp. and the other dagmaritin foraminifera from the Changhsingian (Permian) of southern Turkey: review of dagmaritin phylogeny. Journal of Foraminiferal Researhe 51, 14-31.

3. **Atasoy, S.G.**, Altıner, D., Okay, A.İ., 2018. Reconstruction of a Late Jurassic – Early Cretaceous carbonate platform margin with composite biostratigraphy and microfacies analysis (western Sakarya Zone, Turkey): Paleogeographic and tectonic implications. Cretaceous Research, 92, 66-93.

Motor Sports, Horology, Diecast, History and Philosophy of Science